# The Institute of Paper Science and Technology

Atlanta, Georgia

## Doctor's Dissertation

**The Influence of Drying Rate on the Pore Volume Distribution of Clay Coatings**

**Daniel Thomas Bunker**

**October, 1991**

# THE INFLUENCE OF DRYING RATE ON THE PORE VOLUME DISTRIBUTION OF CLAY COATINGS

A Thesis Submitted by

Daniel Thomas Bunker

B. S. 1985, Western Michigan University

M. S. 1987, Lawrence University (Institute of Paper Chemistry)

In partial fulfillment of the requirements
for the degree of Doctor of Philosophy
from The Institute of Paper Science and Technology
Atlanta, Georgia



October 1991

TABLE OF CONTENTS

Table of Contents, Continued

Table of Contents, Continued

TABLE OF FIGURES

List of Figures, Continued

page

List of Figures, Continued

List of Figures, Continued

List of Figures, Continued

List of Figures, Continued

LIST OF TABLES

## ABSTRACT

To gain insight into the role of drying strategy on the printability of coated paper, the influence of drying rate on coating structure was investigated. Experiments executed in a low velocity hot air drier were designed to determine the effect of the drying rate on the pigment packing structure of coating films. Delaminated clay coatings were applied to plastic film at 50 $g/m^2$ and dried at various rates between 0.5 and 17 $kg/m^2hr$.

Electron microscopy and image analysis were employed to measure the z-directional pore volume distribution of coating films. This is a new technique to quantify coating structure and yielded results within 5% of oil absorption techniques. Accurate results were obtained when a minimum magnification of 5000X and a maximum cross-section thickness of 120 nm were employed.

The void volume through the coating thickness was not distributed uniformly. The coatings were characterized by dense regions near the surfaces which were separated by a bulky region. Coatings with 43% relative pore volume had differences in pore volume between the dense and bulky regions of 5% to 8%.

Temperature did not seem to affect the packing structure when the coating was dried at constant rate.

Up to a point, increasing drying rate at constant temperature resulted in increases in total pore volume and altered the pore volume distribution of coating films. The changes in pore volume distribution consisted of a narrowing of the dense regions near the boundaries and a broadening of the bulky region. The difference between the void volumes at the surfaces and the interior increased with drying rate.

At slow drying rates, the forces resulting from particle interactions during consolidation probably make a significant contribution to the coating packing structure. Increasing the drying rate lessens the influence of consolidation forces on packing structure by limiting the time for particle reorientation.

At drying rates greater than 3 $kg/m^2hr$ the effect of drying rate on packing structure was much less than at slower drying rates. Extrapolation of results to industrial drying rates would lead to a conclusion that packing structure is not greatly influenced by drying rate.

# INTRODUCTION

Pigmented coatings are applied to paper to improve its optical and printing properties. Coating colors are spread in excess on paper as an aqueous suspension. The amount of coating color is metered to the desired weight via pressure, using a blade or a nip, or it is metered volumetrically by wire wound rods(1). Subsequently, the water from the coating is evaporated to produce a coated sheet. Coating properties such as gloss(2,3), print density(4), light scattering ability(5), and print gloss(6) are dependent upon the bulk structure and the surface structure of the coating film(7). An understanding of how coating structure develops and how process variables affect the structure plays an important role in the ability to continually improve coated paper quality, increase production efficiency, and produce new products to meet the demands of the customer.

In recent years, a considerable effort has been made to understand coating consolidation mechanisms(2,8-11) and to understand how process parameters affect the coating structure. Coating structure has been shown to be influenced by the type of binder(12,13), the pigment size, shape and composition(14-16), the flow properties of the coating suspension(17-19), the method of application(20-22), the rate of drying(23,24), and the type of finishing operation(25,26). Lepoutre has written an excellent review of the knowledge that has been obtained thus far(27,28).

Considerable knowledge has been gained concerning the effect coating structure has on the physical properties of a coating film. However, little emphasis has been placed on pigment packing structure or on how the process variables affect the packing structure. The objective of this work was to investigate how the rate at which a coating is dewatered by evaporation from a single surface affects the packing structure of the pigment. Some challenges included: development of a method for quantifying the packing structure, production of coatings in which the evaporation rate was the only process variable influencing the coating structure, and formulation of a consolidation mechanism which predicted the effect of evaporation rate on the packing structure of a coating film.

# BACKGROUND

In order to understand possible effects which drying rate may have on the packing structure of pigment films, it is necessary to review the current knowledge of the mechanism of consolidation and factors affecting it. The following literature review includes what is known about consolidation of coatings. Further, the review describes the factors affecting the coating structure with emphasis on the influence of drying rate on coating properties.

## CONSOLIDATION OF A COATING

The mechanism of the consolidation of a coating layer has been addressed by several researchers. The work of Lepoutre and co-workers(7,6,8,29) describes the physical changes taking place during consolidation on non-porous media. Hagen(30,31) describes the mechanism of consolidation on paper coatings applied to porous media. The conclusions of these researchers lead to a viable description of the mechanism of consolidation.

Watanabe and Lepoutre(7), working with clay films applied to non-porous media, found three characteristic physical changes which occurred in coating films during drying. At a specific solids volume concentration (First Critical Concentration-FCC) the coating gloss begins a rapid decrease (Fig. 1a). It is theorized that the largest of the

pigment particles are forced close enough together that the van der Waals attractive force between them dominates. The dominant attractive force causes the particles to form a network of capillaries which are filled with smaller particles and the remaining suspending medium. At this point in the drying process the dispersion is broken; menisci form between particles at the surface and the capillaries begin draining.

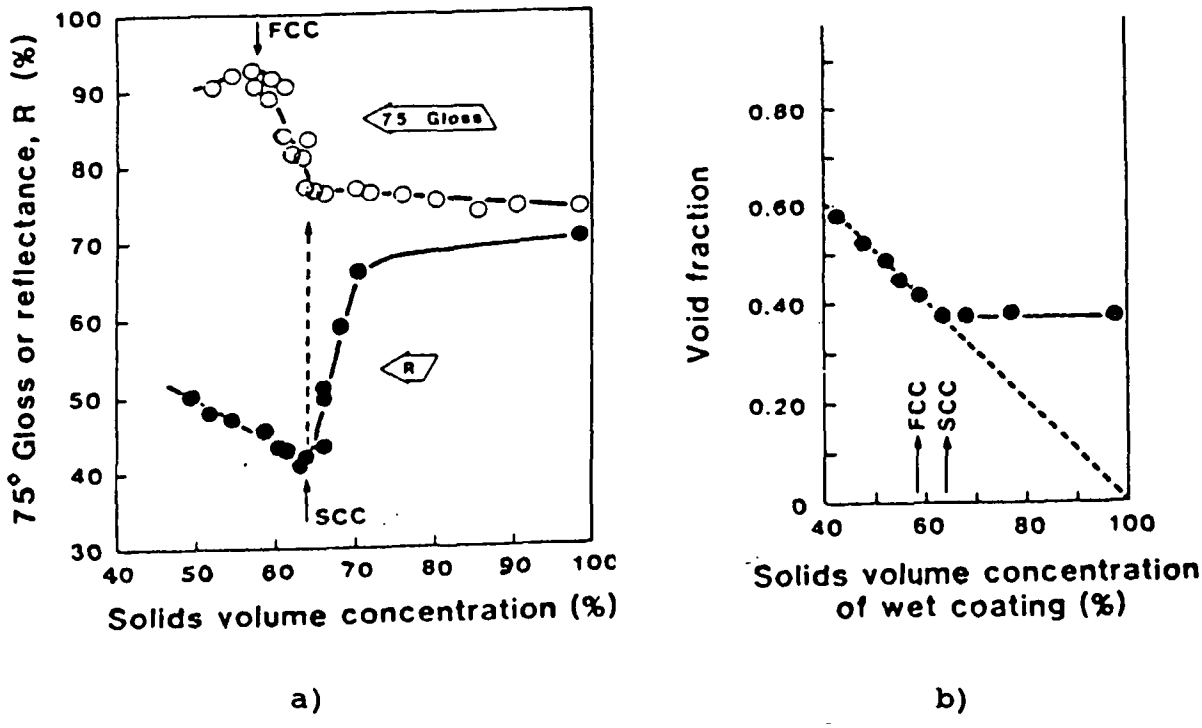


Figure 1. a) Plot of the gloss and reflectance of coating VS solids concentration. b) void volume VS drying time for the coatings in (a). FCC-First Critical Concentration, SCC-Second Critical Concentration. From reference 7.

After a small gain in solids concentration (Second Critical Concentration-SCC), the reflectance of the wet coating begins to increase and the rapid drop in coating

gloss ends. The gain in reflectance results from the formation of air pockets in the coating. The additional interfaces thus created between materials of different refractive index cause an increase in the coating's ability to scatter light. Figure 1b shows that the structure of the coating ceases to consolidate at the solids volume concentration where reflectance begins to increase (SCC). Thus, once the dispersion is broken and the capillary transport of liquid begins to leave voids, the structure of the coating is fixed. As a result, the coating structure can only be affected prior to the SCC. Thus, the initial drying rate and all the process variables up to immobilization at the SCC are important to the formation of the dry packing structure.

## PARTICLE PACKING

Understanding the packing arrangements of model particles may give some insight into the possible packing densities (complement of the relative void volume) of clay coatings. Knowing the possible packing densities for a coating is useful for determining the effect that drying rate may have on coating structure.

### Model Particles

Numerous investigators have examined packings of model particles. Scott(32-35) used steel balls poured into rough-

sided cannisters to simulate random packing of hard spheres. Bernal *et al.*(36) built an instrument for removing the steel balls while simultaneously recording the position in 3-dimensional space. Hagemeyer(37,14) used large plastic models of clay and carbonates to simulate packing structures consisting of particles of different geometries. More recently, Schneider and Rippin(38) built an optical device which employed transmission images to study packing structures of spheres in radial flow. Cook(39) worked with mixtures of polystyrene particles of different diameters in order to determine the influence of particle size on packing density. To test the practicality of a packing model, Leskinen(40) measured the void volume of coatings made from combinations of different size polystyrene spheres. The above researchers have discovered a wide range of packing densities (0.56 to 0.64) is possible for spheres. Because of the wide range of possible densities, it may be possible to change particle packing structures during the coating process enough to change a coating's physical properties.

The expected packing density of either hexagonal close-packed or face-centered cubic packing of equal-size spheres is 0.7405(41). Scott(32,35) has shown for uniform hard spheres that the maximum density obtainable in a randomly packed structure is 0.6366. This result has been supported in other experiments, simulations, and models. Scott and Kilgour(35) also measured the density of a loosely packed

structure, and found it to be about 0.603. Problems in defining the boundary conditions for loose packing has resulted in only limited support for this value from packing simulations. Obviously, there are significant differences between random and regular packing structures. In a coating film composed of uniform spheres, one might expect to find either random or ordered packing. The fraction of regular packing in a coating film depends on the quality of the suspension and how well the particles retain their shape (like the hard spheres used by Scott(32,35)).

Leskinen(40) measured the void fraction of coating films containing various ratios of two different sized latex spheres and eight parts per hundred binder (on pigment). For coatings containing a single sphere size, the packing densities were found to be 0.64 for 100% large spheres and 0.56 for 100% smaller spheres. Results near and slightly lower than the 0.6366 obtained by Scott are surprising for several reasons: 1. polystyrene spheres do not behave as hard spheres; 2. polystyrene spheres obtained commercially are not monodispersed and the polydispersity usually increases with particle size; and 3. binder has been shown to affect the total pore volume of clay coatings(7,42). Each of these factors would tend to make the coating denser than the random dense packing results reported by Scott(32,35). It can be concluded that Leskinen's films had random and ordered

regions which when averaged had a density near that of an ideal random packing.

Cook(39), in a similar study which did not include an adhesive binder, found densities of about 0.684 for each of three coatings made from three different size polystyrene latex spheres (0.12 μm, 0.2 μm, and 0.67 μm). This result is predictable from Scott's analysis(32,35) in which he measured a maximum packing density of 0.6366 for dense random packing of hard spheres. Cook reported that visual inspection of the coating surfaces showed regions of random and regular packing. He also reported that similar structures were found on the surface of loosely packed and densely packed steel balls. Cook believed that the regular packings were those of cubic and rhombohedral geometries (Fig. 2). These structures have a difference in void volume of about 21%. The surface structures were found to have about 3% less void volume than the overall coating void volume, suggesting that the rhombohedral packing is the dominant surface structure. A computer simulation designed to model packing structures(43) of a bed of monodispersed spheres yielded results similar to Cook's experimental results. The higher surface packing density accounts, in part, for the overall density being higher than that of random close packings (0.684 versus 0.637).

The results of experiments using monodispersed spheres indicate that a coating film bounded by two surfaces tends to

be more ordered than a particle packing not influenced by boundaries(39,40). Coatings composed of monodispersed spheres are expected to be denser than dense random packings.

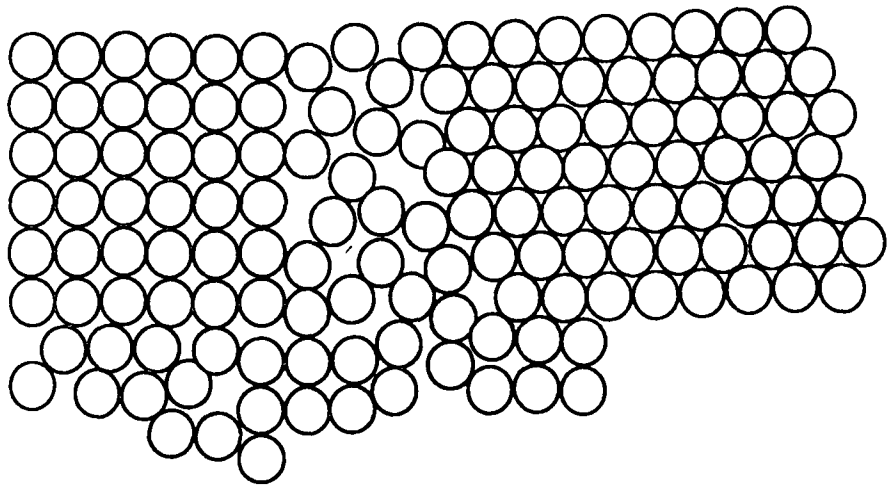

Figure 2. Schematic of the surface of monodispersed spheres as described by Cook(39). Coatings contained regions of regular packing separated by zones of random packing.

Packing Simulations

Studies of packings of spherical particles have ranged from intentionally random to regularly packed to nearly real systems; however, no packing model has been developed to suitably predict the void volumes obtained experimentally.

Two approaches using principles of statistical geometry have been used extensively in efforts to describe how particles will pack. The first approach is that used by Bernal(44,45), Finney(46,47) *et al.*(48), who used variable geometric structures to describe packing structures. Voronoi polyhedra were used to describe the geometry of Scott's steel

balls. Polyhedra were constructed about the center of mass of each ball, the number of faces, edges and vertices were tabulated for each and a statistical representation was calculated. Using computer-simulated packing structures, the method has been used to characterize many different configurations including short range order in random structures and systems where gaps between particles were present. The method is useful for describing structures, but has limited value for predicting changes in structures when forces other than gravity are incorporated during the construction of particle beds.

The second approach is that used by Wise(49), Hogendijk(50), and Dodds(51). By choosing a single geometry to represent sphere packing, the density of the packing can be described from the sphere sizes and the relative concentrations in the system. For example, assuming gapless packing and that packed spheres form tetrahedrons, there are five different tetrahedrons that can be formed from two sphere sizes. Each type of tetrahedron has a statistical frequency related not only to the number of possible tetrahedrons formed but also to the fraction of each particle size in the system. Dodds found solutions for systems containing up to nine different sphere sizes. Wise derived the equations for determining the packing density for a log normal distribution of particle sizes but was unable to solve them. Hogendijk later developed a numerical method to solve

Wise's equations. In general, their studies show that densities of binary mixtures are most sensitive to mixture composition. Figure 3 shows the calculated density of a bed of hard spheres as smaller particles are added to the bed. The asymmetrical "V-shape" is typical. The depth of each curve is dependent upon the ratio of sphere diameters making up the structure. Dodds reported that increasing the number of components (different size spheres) in a structure reduces the effect of composition on porosity(51).

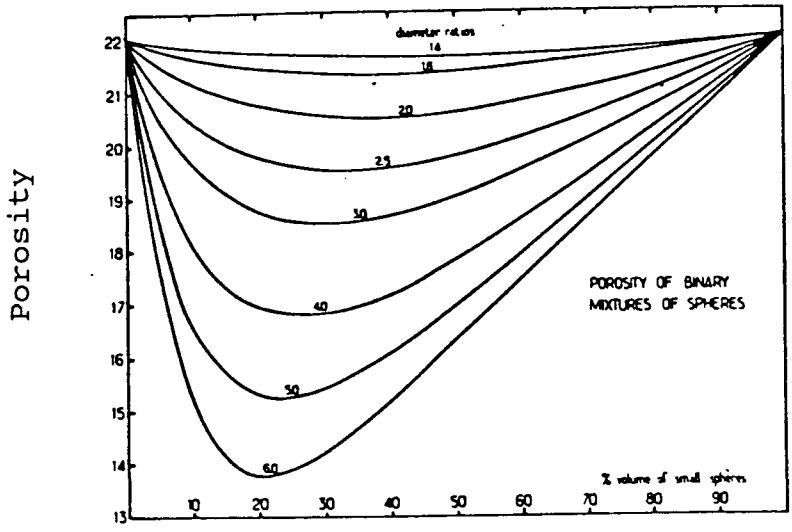


Figure 3. Results from Dodd's model of tetrahedral packing of spheres. Porosity of binary mixtures of spheres. Reproduced from ref. #51.

This technique is not satisfactory for predicting absolute packing densities but is useful in predicting changes in density which occur as the components change. Dodds' results were supported by the work of Cook(39) and Leskinen(40) for cases where two and three particle size

classes were used. This method provides only a method for quantifying a structure. Other than changes in the pigment composition, differences in packing density which result from alterations in the method of film production can not be predicted using this method.

Dynamic Models

Because calculations describing how particles behave in solution are complex, few dynamic models have been developed. Bousfield's work(11) is the only model found that simulates drying of a suspension. He presented a case in which the upper boundary to a particle suspension moved at a fixed rate toward the lower boundary. The lower boundary was allowed to pass fluid but not particles. If a particle was supported by other particles it was allowed to pass through the upper boundary. These conditions are not a complete representation of real drying systems in that colloidal forces have been neglected and dewatering occurs only by drainage. However, this type of simulation may be useful in predicting the changes in packing at different drying rates. Figure 4 is an example of the formation of the packing structure for spherical particles as predicted by Bousfield's model.

In the simulation presented in Fig. 4, the packing density increases from the base up. In coatings applied to porous media, there would be a significant filtration effect

on the structure of the coating. The simulation did not include evaporation as a parameter.

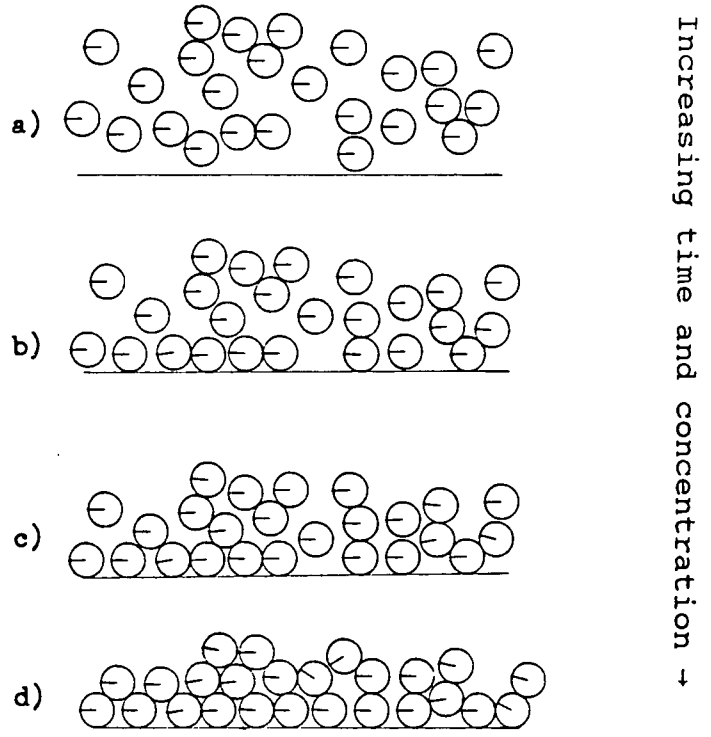


Figure 4. Two-dimensional consolidation by filtration of monodispersed spheres as predicted by Bousfield's model. (a-d) Structure as a function of time during the consolidation. Reproduced from ref. #11.

Brady, Bossis, and co-workers have presented a technique called Stokesian Dynamics for simulation of the motion of a large number of particles in flow fields(52-56). Using a supercomputer for the calculations, they were able to incorporate Brownian motion, interparticle forces, long-range lubrication forces and short-range lubrication forces. Their model is considerably more complex and more representative of the actual suspension than Bousfield's model. Unfortunately,

no simulation results have been found for any model which resembles a drying pigment suspension.

Summary of Model Particle Packing

There has been a considerable effort to produce a mathematical representation of the packing of spheres. Success has been good for random dense packing of spheres, in that various models have yielded the same packing density as experiments. Success has also been good for regular packings where structures can be represented by relatively simple geometric figures. Geometrical descriptions fail in situations where packings are combinations of random and regular structures. Unfortunately, this type of packing occurs in coatings composed of spherical pigments.

Dynamic models which predict the behavior of particles influenced by fluid flow or certain boundaries are a recent development which require the use of supercomputers to perform the calculations. However, the results obtained from simpler models will be useful for qualitatively predicting the packing of particles in dynamic systems.

From the results of studies of model systems, it can be concluded that boundaries have a significant influence on structure, and that the mechanisms of dewatering, filtration and evaporation also affect the packing structure.

## PACKING IN A COLLOIDAL DISPERSION

During the time interval between application and immobilization of a coating, the pigment film can be viewed as a suspension. Therefore, a review of the structures which exist in colloidal dispersions and the effect on the resultant packing structure is relevant.

Coating structure has been shown to be affected by dispersion properties(14,28,57). Hoy(41) suggested that a coating should be expected to have a number of properties which are directly related to the structure of the pigment suspension. A considerable amount of research has been directed toward the relation of colloidal properties to properties of suspensions under flow(58,59). As a result of this effort, there exists a large body of literature on typical structures present in suspensions. Recently, Tadros presented a review of this subject(60).

Van Olphen(61) explained clay particle interactions in suspension in terms of structures which depend on the nature of interparticle interaction forces. Because the magnitude of the van der Waals attractive forces acting between particles is dependent on the relative orientation of the particles, the energy of interaction depends on the geometry of contact. There are three basic geometries with which clay particles approach one another: face-to-face, edge-to-face, and edge-to-edge. The relative populations of these three structures will differ due to differences in the energy of

interaction and in the rates of diffusion of the particles. Figure 5 shows potential structures. Flocculation of a dispersion results in different rheological and structural behavior. Spherical particles form similar structures which also affect rheological and structural behavior of the suspension(60).

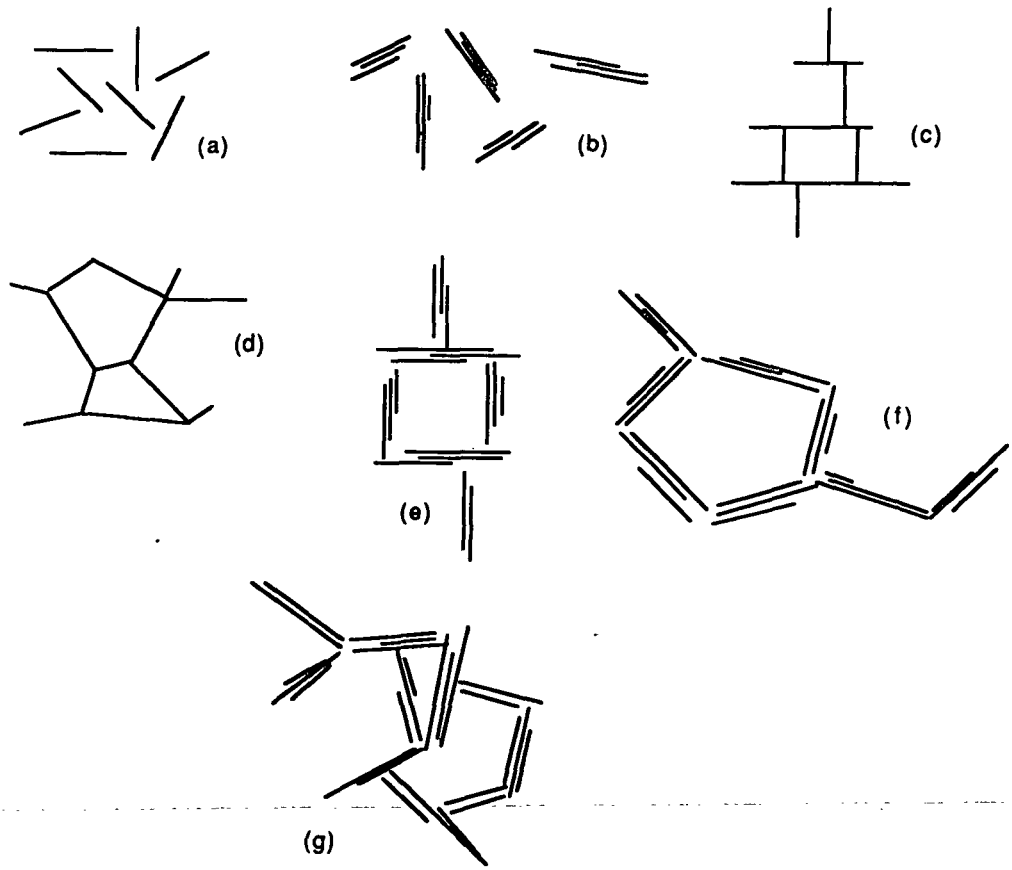


Figure 5. Modes of particle association in clay suspensions. a) dispersed (random) b) aggregated but dispersed c) edge-to-face floc d) edge-to-edge floc e) aggregated edge-to-face floc f) edge-to-edge aggregated floc and g) aggregated edge-to-edge and edge-to-face flocs. Redrawn from reference 61.

In Fig. 5 there are corresponding figures for agglomerated and single particle structures. Figure 5b shows a dispersed aggregate randomly orientated. The energy necessary to disperse the other flocculated structures is less than that for the face-to-face floc; therefore, the face-to-face structures are considered aggregates. In a clay suspension, it is not known whether single particles exist or if clay suspensions are made up of face-to-face aggregates. Aggregates can flocculate forming structures similar to those formed by single particles. Therefore, the structures of dispersions are similar for suspensions consisting of either aggregate or individual clay particles.

## Experimental Determination of Colloidal Structure

Sheehan and Whalen-Shaw(10), using cryogenic scanning electron microscopy (Cryo-SEM), demonstrated that clay suspensions contain structures predicted by van Olphen(61). In concentrated suspensions, Sheehan and Whalen-Shaw(10) discovered that crowding of the platelets resulted in considerable parallel alignment as hypothesized by Lepoutre(28). Micrographs of suspensions contained in Sheehan and Whalen-Shaw's work showed that much of the clay in their suspensions was in the form of aggregates.

Liu *et al.*(62) studied the structure of suspensions of small particles (colloidal gold) using a transmission electron microscope (TEM). In untreated samples considerable

agglomeration started at the points of contact, resulting in "bead-like" structures of low density. Treating the particles with a surfactant which coated their surfaces, resulted in a dispersion structure which was uniform and dense. Particle separation was discovered to be about twice the size of the surfactant. Because the addition of the surfactant resulted in a uniform surface charge and because it provided some steric hindrance to close approach, the particles formed a random/dispersed structure.

Hiltner and Krieger(63) used the Bragg diffraction of visible light to determine the structure of a monodispersed suspension of latex particles. They discovered a packing density of 0.74, implying that the structures were either face-centered-cubic or hexagonal-close-packed. By changing the salt concentration of the solution, they varied the interparticle distance. At high salt concentrations the interparticle separation was significantly less than the diameter of a particle. At very low salt concentrations particles were separated by nearly four particle diameters. In dilute solutions, regular packing was not limited to the air interface but was present throughout the solution. In concentrated solutions, only the first few surface layers could be analyzed. Some doubt exists as to whether the surface structure was present throughout the solution. Figure 6 shows a schematic of the results.

Two important conclusions can be drawn from the work of Hiltner and Krieger(63). First, particles in a stagnant colloidal suspension tend toward lattice type structures. This conclusion lends support to the observations made by Cook(39). Second, the particle/particle interactions are significantly affected by salt concentration.

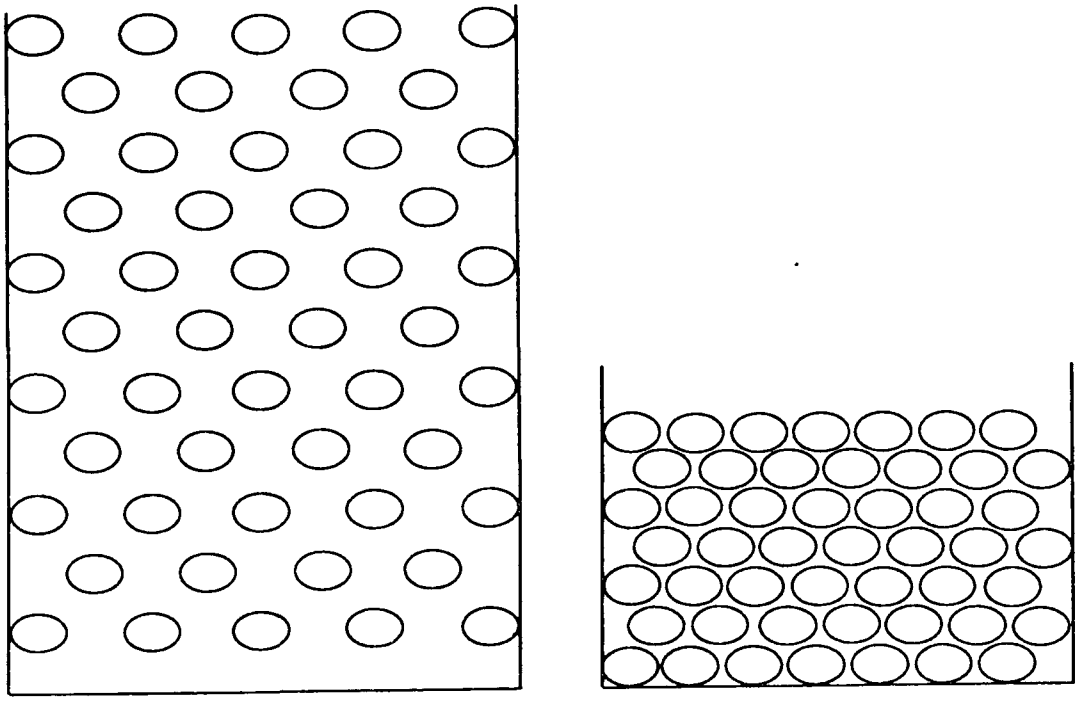

a) b)

Figure 6. Schematic of suspension structures at two salt concentrations(63). a) packing structure of a dilute, low salt concentration dispersion. b) same dispersion as a at high salt concentration.

Hoy(41), in a review of the structure of concentrated coatings, predicted that ordered structures near a surface extend about 10 diameters into the film before random packing dominates the structure. He also hypothesized that ordered

packing structures at and near surfaces result from particle interaction with the surface. Hoy stated that boundaries limit the number of nearest neighbors a particle may have, resulting in a more open structure as compared to ordered packings. Further, he predicted that when two boundaries are near one another they severely limit the packing ability of the film, resulting in a loosely packed structure. This view is the opposite of the results discovered in the earlier experiments of Hiltner and Krieger(63).

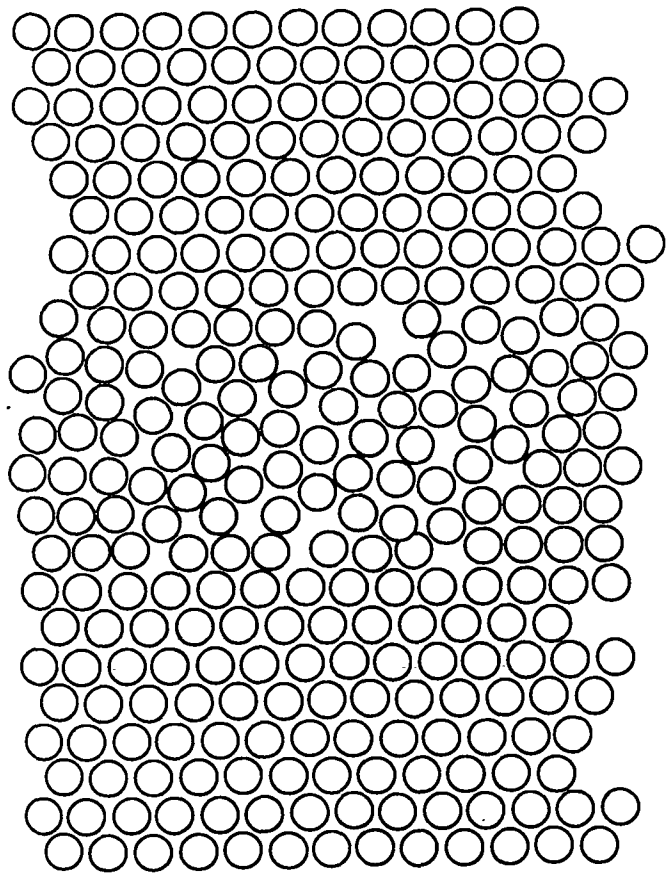

Figure 7. Schematic of a dispersion of uniform spheres bounded on two sides.

Combining the results of Hiltner and Krieger(63) and parts of the model hypothesized by Hoy(41), a description of the structure of dispersion in a film can be inferred. Figure 7 is a schematic of the author's interpretation of the knowledge available on colloidal structures in a film.

## Effect of Suspension Properties on Coating Structure

The results of Sheehan and Whalen-Shaw's work(10) indicate that at high solids content, 50% to 70% by weight, the arrangement of clay particles in suspension is nearly a face-to-face configuration. Mechanically or chemically reducing the amount of flocculation in a suspension tends to dissociate face-to-face aggregates therefore increasing the particle-particle separation. Flocculation of a dispersion causes suspended particles to form edge-to-face and edge-to-edge structures. Flocculated suspensions appear to be less conformable and have bulkier particle structures relative to an unflocculated dispersion of the same concentration.

The statement above has been supported by the work of several researchers. Hagemeyer(37) used sediment volumes of dispersions as a measure of packing structure. He discovered that mixing particles of different materials and identical shape gave a non-additive sediment volume. The difference in surface properties between the different pigments resulted in a change of dispersion properties, thus causing a change in the packing structure.

Hemstock and Bergmann(17) correlated dispersant level with sediment volume and dry film void volume for binderless coatings. They found that the dry film void volume was directly related to, but smaller than, the sediment volume. In addition, both the void volume and sediment volume initially decreased and subsequently passed through a minimum as the level of dispersant was increased (Fig. 8a). Addition of dispersant reduced flocculation; however, after a minimum flocculation was achieved additional dispersant induced flocculation.

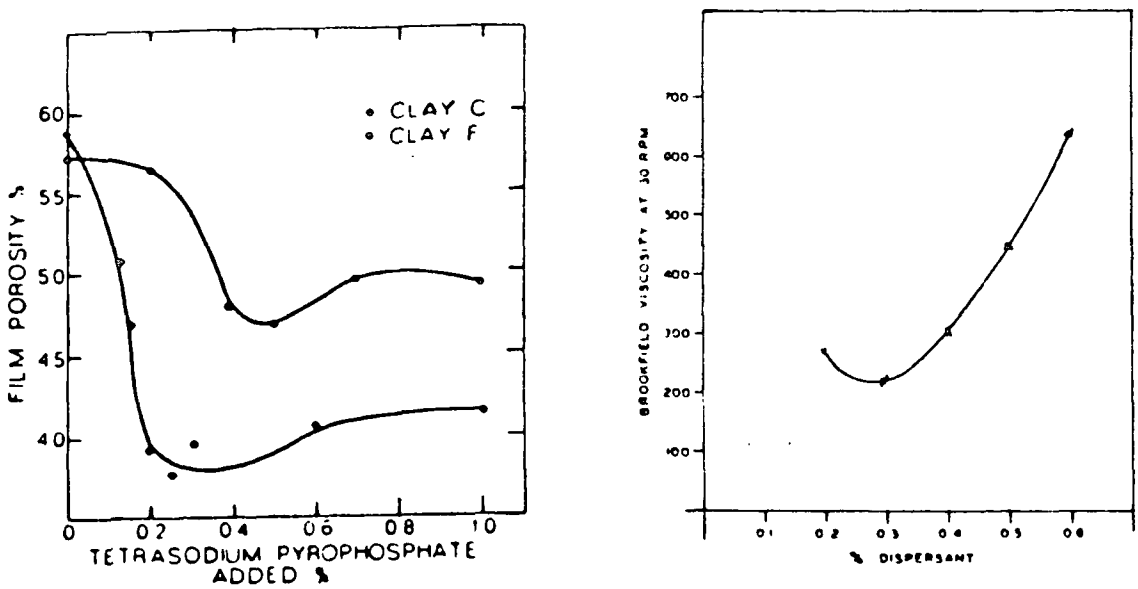


a b

Figure 8. a) Relationship between void volume of the dry film and dispersant level. From ref. 17 with permission. b) Relationship between Brookfield viscosity and level of dispersant for a plate-like pigment at 70% solids. From ref. 37.

Hagemeyer(37) had previously shown that the viscosity of the coating suspension is dependent on the level of dispersant (Fig. 8b). The relationship was the same as that

found by Hemstock and Bergmann(17) for the effect of dispersant level on the sediment volume and void volume of dry coating films. It is also known that the viscosity of a solution is dependent on the dispersion structure(58-60). Therefore, the combined work of Hagemeyer(37) and Hemstock and Bergmann(17) indicate that the degree of flocculation in a dispersion is important to the resultant coating structure.

## EFFECT OF DRYING STRATEGY

### Introduction

As coating speed has increased and coat weights have dropped in industrial practice, the incidence of printing problems has risen. Print mottle, or the variation in optical density, results from variations in ink coverage. Ink coverage is a function of several properties of the coating, of which absorbency is one. High drying rates and variations in drying strategy have affected print quality. Print mottle is believed to result from uneven deposition of binder at or near the coating surface. Therefore, ink absorption may be used as one measure of the effect of drying strategy on coating structure and/or binder migration. Gate and Windle(64) reported the rate of oil absorption to be related to the void volume; denser coatings have lower oil absorption rates. Many studies have used the above relation as an index for measuring coating structure.

The presumed relation between ink absorption and coating structure may not be correct. Lepoutre(27), in a review of the current knowledge of coating structure, commented on ink absorption tests:

> Because of its simplicity the K&N ink absorbancy test continues to be used to characterize the absorbency of paper and board coatings. The test consists of measuring the drop in reflectance of the coating after two minutes contact with the grey colored test ink. However, relationships between oil absorption rate and K&N stain reflectance remain elusive (Lepoutre, DeGrace(65)). Hattula and Oittinen(66) made a thorough investigation of the test and concluded in a remarkable understatement that "the K&N test may not give a true picture of the absorption performance of coatings in printing."...

Further doubt is cast by Kent and Lyne(67) on Gate and Windle's conclusions(64) concerning the absorption of ink into coatings. In a paper which discusses theoretical aspects of capillary movement through non-cylindrical, discontinuous capillaries, Kent and Lyne(67) have shown that flow through capillaries is dependent on capillary geometry. Gate and Windle defined an effective pore radius for a coating, r, and assumed that coatings behave as a collection of parallel capillaries having a length of $h\delta/\varepsilon$, where h is the average coating thickness, $\varepsilon$ is the ratio of pore volume to total apparent volume (packing density) and $\delta$ is a tortuosity factor. The tortuosity factor is the ratio of the real distance travelled by an element to the distance $h/\varepsilon$. The above definition of capillary length was used in the Washburn equation to determine the rate of oil absorption according to the following:

$$\left(\frac{h\delta}{\varepsilon}\right)^2 = \frac{\gamma(\cos\theta)rt}{2n} \qquad (1)$$

Rearranging and assuming complete wetting, i.e., $\cos\theta \rightarrow 1$:

$$h^2 = \left(\frac{\gamma}{2n}\right)\left(\frac{\varepsilon}{\delta}\right)^2 rt \qquad (2)$$

where $\gamma$ = surface tension of the oil
$t$ = time
$\theta$ = contact angle between the oil and the coating
$n$ = viscosity of the oil
$\varepsilon$ = porosity (void volume/total volume)

Experimentally they found that the time of penetration is proportional to both the square of the film thickness and to the square of the inverse of the porosity. Figure 9 is the plot presented by Gate and Windle(64) of 10 different clay coatings as a function of $1/\varepsilon^2$.

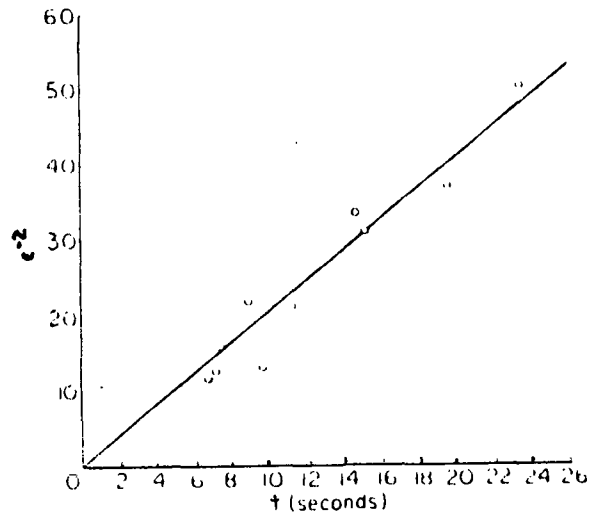


Figure 9. Oil absorption time of 10 different clay coatings containing 15 pph binder as a function of $1/\varepsilon^2$. From ref. 64.

Kent and Lyne(67) developed a model to find the effect of discontinuities in capillaries on capillary transport. They applied Gibbs' inequality to the three phase contact point of a liquid in a capillary at a discontinuity and calculated the pressure difference across the meniscus, $\Delta P$, from the Young-Laplace Equation:

$$\Delta P = \gamma_{LV}(1/r_1 + 1/r_2) \qquad (3)$$

where $r_1$ and $r_2$ are the principle radii of curvature of the meniscus. They calculated the pressure difference for the three model geometries of capillary intersections shown in Fig. 10. The results of their calculations are shown in Fig. 11-13.

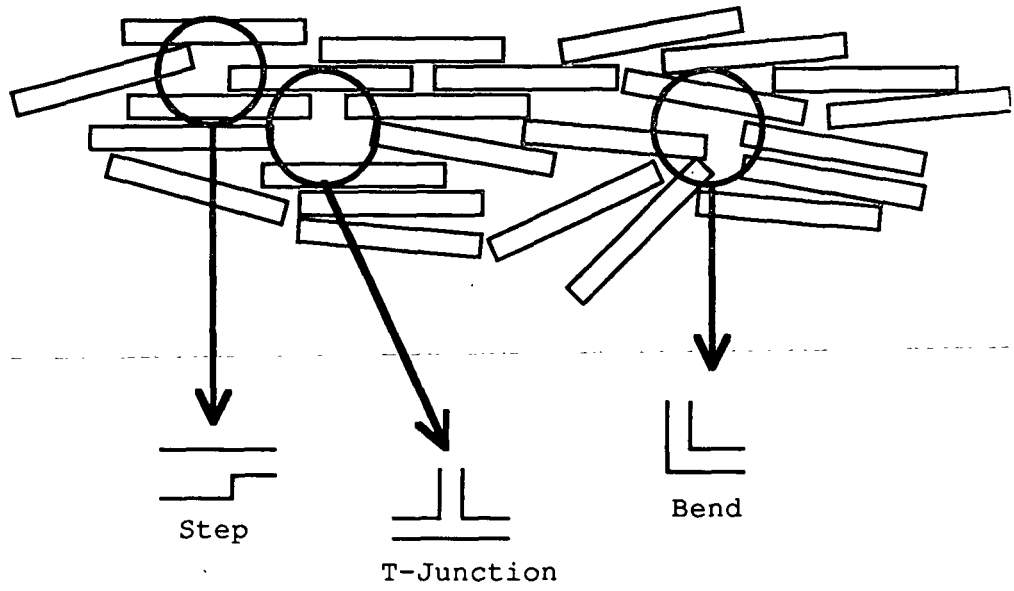


Figure 10. Representation of a coating film comprised of plate-like pigments whose orientation is nearly parallel to the x-y plane. Sketch shows three typical capillary geometries (redrawn from ref. 67).

Figure 11a shows that a significant change occurs in the pressure driving the fluid as it enters the Step junction; however, the jump in $\Delta P$ is not great enough to stop fluid flow. Similar results were obtained for the Bend intersection. The T-junction had a $\Delta P$ that passed through zero, indicating that external pressure, $P_e$, would be necessary to drive the fluid through the intersection. Therefore, the extent and rate at which liquid absorption occurs is dependent on pore geometry as well as film porosity and surface tension and the viscosity of the absorbing fluid.

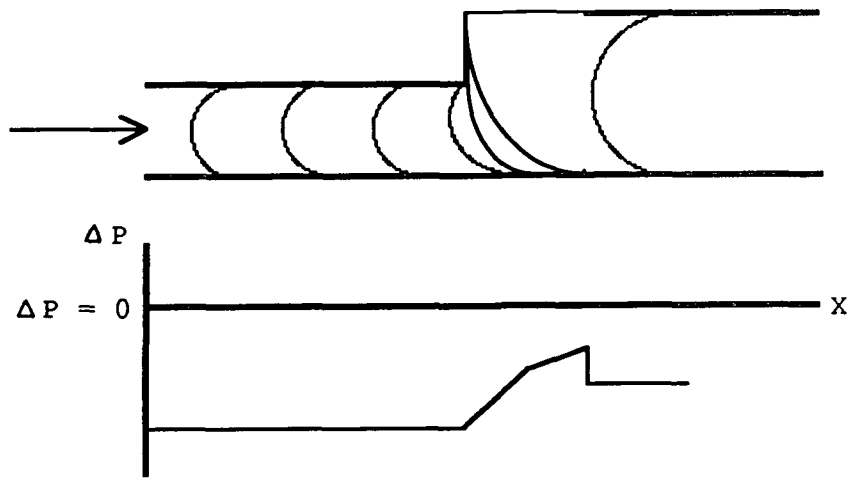


Figure 11a. Sketch of the contact angle of a liquid passing through a Step junction and the calculated pressure difference driving the fluid (redrawn from ref. 67).

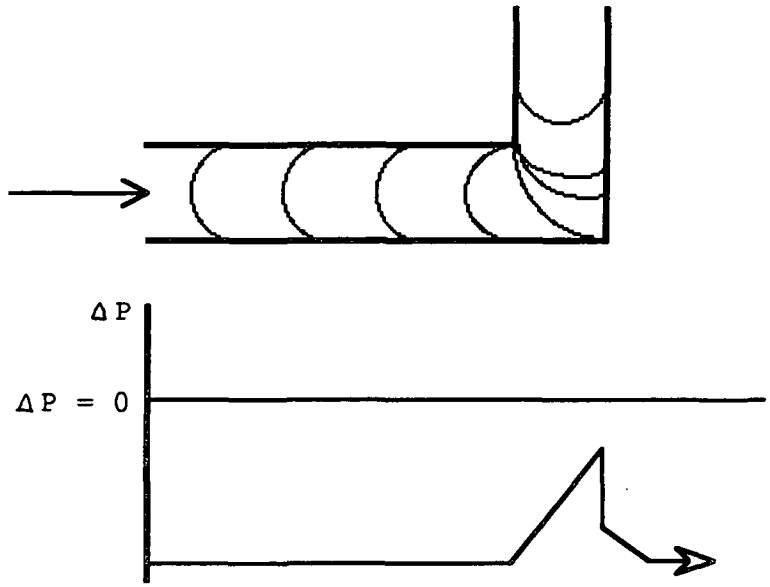


Figure 11b. Sketch of the contact angle of a liquid passing through a Bend junction and the calculated pressure difference driving the fluid (redrawn from ref. 67).

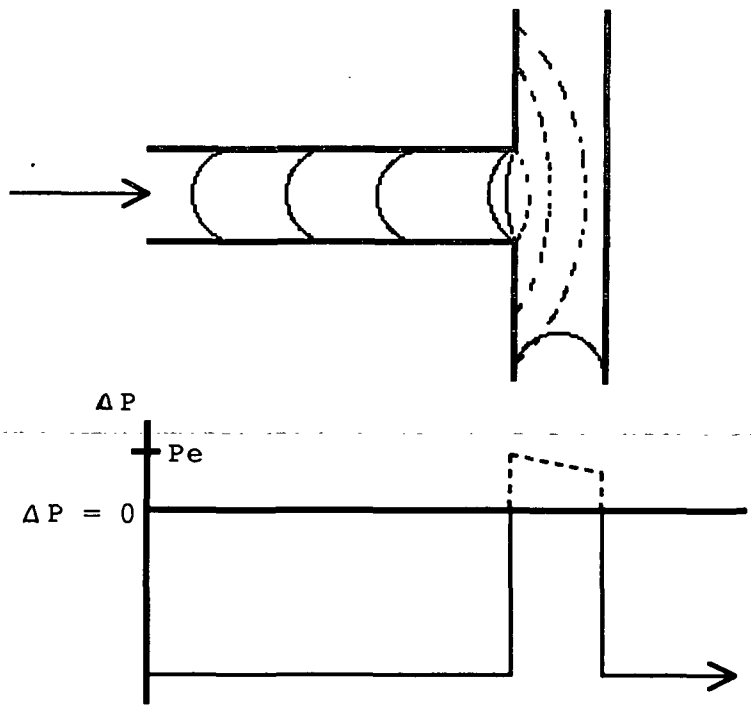


Figure 11c. Sketch of the contact angle of a liquid passing through a T-junction and the calculated pressure difference driving the fluid (redrawn from ref. 67).

The predictions of Kent and Lyne have been only recently applied to coatings (1989) whereas the work of Gate and Windle, the use of the Washburn equation, and ink absorption tests have been discussed for some time. A majority of the studies of the effects of drying rate on coating structure have employed indirect tests such as ink absorption or print density variation to measure changes in coating structure. Conflicting results (presented below) may be a consequence of the methodologies used to determine coating properties.

Drying Studies

Engstrom *et al.*(68,69) studied the effects of drying rate on print mottle and ink absorption of coated plastic and coated paper. Using the K&N ink test, they found that the ink absorption decreases if the high drying rates are employed during coating immobilization. The differences in ink absorption between coatings dried by different strategies were not detected at high coat weights. The effect of drying rate on ink absorption was also found to be influenced by the type of binder in the system. Coatings applied to paper and dried by different strategies were examined for print mottle after printing on a Prufbau press. Results were similar to the coatings that were applied to plastic. These results suggest that a high drying rate during immobilization causes lower void volume and an ordered structure. In addition, the effect of binder type may have been caused by differences in

"binder migration" (non-uniform deposition of binder) within the coating layer. Variation in binder concentration at the coating surface may cause variation in ink absorption (appearing as print mottle). However, because ink absorption is primarily a surface phenomenon, the results may indicate that high drying rates during immobilization cause an increase in surface density. Increased surface density may result from increased packing order and/or binder migration.

Heiser and Baker(70) performed a study of binder migration. They controlled binder migration on a pilot coater by gelling the latex binder immediately after application in one half of the coating by exposing half of the sheet to ammonia. Drying was performed with hot air driers employing the same conditions on both halves of the sheet. The result was one coating whose structure and binder distribution at application were preserved and another coating whose structure was dominated by the consolidation process via filtration and evaporation.

The experiment was designed to produce binder migration; however, the distribution of binder through the thickness of the coating was found to differ only in degree between the coatings. The shape of the binder distributions for the gelled and ungelled coatings were the same. This result suggests that perhaps some quantity of binder was transferred to the base paper and no alteration of the distribution was achieved. K&N ink absorption was significantly greater for

the gelled coating. Greater ink absorption was thought to result from greater void volume or less binder migration. The calendered gloss and pick strength were greater for the ungelled system, while the opacity of the gelled coating was slightly greater than that of the ungelled coating. Pick failure, in both coatings, was reported to be by coating pick and not fiber pull. The print gloss was lower for the gelled coating, and particle orientation relative to the coating axis was greater for the ungelled coating.

Using stereoimaging, thin cross-sections and scanning electron microscopy (SEM), Heiser and Baker(70) also studied the microstructure of the coatings. The stereoimages showed that the surface pores of the gelled coating had considerable depth and were more abundant than the surface pores in the ungelled coating. SEM analysis confirmed these results and also showed a difference in the smoothness and the particle size distribution near the surface. Heiser and Baker observed that the gelled coating was noticeably rougher than the ungelled coating and that it had a wide variation of particle sizes at the surface. The ungelled coating appeared to be covered with a layer of fine particles (possibly latex) with only a few larger particles present. Cross-sections of the coatings were fragmented as a result of the embedding and cross-sectioning process. Each coating showed similar features. Each coating contained clusters of clay particles separated by a matrix composed of latex.

The observed differences between samples (i.e., ink absorption, print gloss, etc.) were tentatively attributed to non-uniform binder distribution within the coating layer. Property differences may have also resulted from packing structure differences between coatings. The ungelled coating consolidated, packing the particles while the gelled coating essentially preserved the structure of the particles in the bulk dispersion. The greater random orientation and greater void volume of the ungelled coating may explain differences in properties of the gelled and ungelled coatings.

Aschan(71), in a pilot plant study concerning the effects of drying strategy on coating structure, showed that print mottle was critically dependent upon the drying rate over a specific solids range (about 71%-78% solids). The drying rate before and after the critical range had little effect on print quality. He theorized that the critical solids content for a coating begins when the surface has both dry and wet places (as the last of the free water is removed - 71 to 74% solids) and ends when there are no wet places left on the surface(74-78% solids). The described critical solids content range falls between the first and second critical concentrations described by Lepoutre(7) (Fig. 1).

Aschan(71) reported that, for coatings of equal coat weight, increasing the drying rate during the critical solids range resulted in a slight increase in roughness and drop in ink absorption. He also reported that pick strength

increased as drying rate was increased. These results are not entirely consistent with those of Heiser and Baker(70). If Heiser's and Baker's gelled and ungelled coatings are considered in terms of changes in the drying rate, the gelled coating (dried rapidly) had greater ink absorption than the ungelled (slowly dried) coating. The differences between Heiser's and Baker's results and Aschan's results can be attributed to two factors: first, the distribution of binder in Aschan's coatings may have been different than those of Heiser and Baker, and, secondly, changes in drying rates of Aschan's coatings were later in the drying process, creating the possibility of a wholly different packing structure than the Heiser and Baker coatings.

In another pilot coater drying study, Engstrom *et al.*(72) performed trials using drying strategies similar to those of Aschan(71). They also found that slower drying rates through a critical solids range produced less print mottle. In addition, they measured the relative binder content of the surface of the coating using ESCA. Surprisingly, a drying strategy characterized by high initial drying rates and no forced drying (gap between driers) near the critical solids range (between the gloss and reflectance points) yielded coatings which had high surface binder to pigment ratios. The high surface binder concentration is an indication of extensive binder migration, yet the coating exhibited insignificant print mottle. This result

contradicted previous work which found decreased ink absorption and increased mottle for coatings prepared using high drying rates during immobilization(70,71). Engstrom *et al.*(72) theorized that the amount of water available during the high drying rate period was more critical for production of print mottle than was the overall drying rate. Furthermore, they thought that other structural properties might be responsible for ink mottle as well.

Gane(73) supported the notion that print mottle does not result from binder migration. Through analysis of the variation in base sheet roughness and coating roughness, he found that print mottle resulted from surface inhomogeneity of smoothness and fiber coverage. He also noted that if binder migration occurs, leading to variations in surface concentration, then it is apparent only in regions where variations in coat weight occur. Experimentally supported relations between base sheet properties and packing structure are scarce, but those data which exist support the above findings. Base sheet roughness disrupts the parallel alignment of particles causing greater disorder in the coating layer which results in greater pore volume(42). High base sheet absorption rates result in rougher coatings and variations in base sheet absorbancy cause variations in coat weight, ink absorbancy and packing structure(23).

Recently, Norrdahl(74) reported that the extent of print mottle is dependent on the drying rate used over a particular

solids content range and not on the type of drier used. The critical solids range begins at a concentration which is about 4% lower than the concentration where immobilization occurs and extends to the solids content where the reflectance of the coating begins to increase (the SCC as defined by Watanabe and Lepoutre(2)). When drying rates greater than 5 kg/$m^2$hr were employed during the critical solids concentration range, an increase in the incidence of print mottle was observed. Deterioration of other coating properties paralleled the mottle response. Gloss, print gloss, and IGT pick decreased as the rate of drying over the critical solids concentration was increased. Tests of surface binder concentration and distribution(75) showed no sign of binder migration or mottle. Norrdahl did report significant effects of base sheet temperature and base sheet formation on print mottle.

In a study of the causes of print mottle, Engstrom *et al.*(76) discovered relationships between print mottle and the average evaporation rate. As part of the study, the binder and coat weight distributions were determined as well as the X-Y variation of each. Varying the evaporation rate resulted in only small variations in the surface content of latex binder. The effect on coat weight distribution was not reported in detail other than "...the mass of the coating layer is evidently redistributed during its consolidation process."

The correlations that Engstrom *et al.*(76) drew between print mottle and evaporation rate are suspect. They have shown relationships between mottle and binder distribution and between mottle and coat weight distribution; however, mottle, binder distribution, and coat weight distribution appear to have a greater dependency on the base sheet properties than the evaporation rate. This suggests that the relative contributions of the different mechanisms of dewatering (absorption and evaporation) are important. Apparently in cases where water removal by absorption into the base sheet is dominant, evaporation rate has little effect on the properties of the coating. Engstrom *et al.*(76) also pointed out that the type of absorption, capillary or diffusion, has an effect on the coating properties. Therefore, the hypothesis can be made that coating structure must be affected differently by each mechanism.

In none of the studies discussed above were the z-direction properties of the coatings examined.

## Examination of Coating Cross Sections

Heiser *et al.*(22) used light and electron microscopy to relate gloss, print mottle, and sorption characteristics to the coating morphology. Coatings consisting of 88% clay, 12% $CaCO_3$, and 16 pph latex binder (on pigment) were applied by roll, metered with an air knife and dried at two different rates: 300 ft/min. at 300°F and 700 ft/min. at 550°F. Two

trials were run, one with a latex of 0.45 to 0.55 μm and the second with a latex binder of 3.0 μm. In the first case the binder was presumed to follow the liquid phase and in the second case it was presumed to behave as a pigment. Microscopic analysis of the surfaces of coatings containing the smaller latex showed that coatings dried at the lower rate contained more large voids than the coatings dried at the higher rate. The coating dried at the lower rate was also reported to have greater internal void volume.

Heiser *et al.*(22) believed that differences in void volume were due to surface tension forces present during evaporative drying. They believed that at high drying rates, where evaporative drying was dominant, surface tension forces caused more platelet alignment and a denser pigment packing structure. However, surface tension forces predominate after immobilization and result in a loss in platelet orientation(42). Watanabe and Lepoutre(7) have shown that little consolidation occurred after immobilization in coatings which were applied to plastic film. The findings of Heiser *et al.*(22) contradict the ink absorption data reported in other studies(71-76). Others(64,68,69) found that high drying rates reduced ink absorption and thus pore volume. One possible explanation for the discrepancy may be the change in the speed of the coater to achieve the change in the drying rates. Engstrom and Rigdahl(24) have shown that the speed of the coater has an effect on the structure.

Regardless of the chosen drying method, Heiser *et al.*(22) have shown that when higher average drying rates are used the coating had a higher packing density than the same coating dried at a lower rate.

For coatings of large binder size, Heiser *et al.*(22) found results similar to those given above, except that the total void volume was larger. This is probably because the larger latex particles caused greater disruption of the regular packing structure of the clay than the small particles. The researchers did not discuss the distribution of void volume through the thickness except to state that, for the large particle size latex, the surface of the coating dried at the faster rate was quite dense above a more friable internal structure.

Hattula and Aschan(77) observed from coating cross-sections that clay platelets were oriented parallel to the surface. The parallel orientation was disrupted in the bulk of the coating by occasional large anisometric particles. Cross-sections published in other studies showed similar disorder around large particles(22,70,78).

Cross-sections of mechanically compacted and dried clays(79-81) have shown packets of face-to-face flocculated particles aligned parallel to one another. In systems compacted at moisture contents above the immobilization point, the face-to-face packets exhibited considerably more

parallel alignment than systems compacted at solids near the immobilization solids content(79,81). In the later case, particles were less ordered and packets were aligned at various angles with respect to one another. Diamond(81) discovered that clays compacted at low solids experienced significantly more shrinkage than those consolidated from higher solids concentration during drying. These results indicate that the ability of particles to reorient in the dispersion is dependent on the solids concentration.

## SUMMARY OF BACKGROUND

The influence of coating structure on the physical characteristics of coatings and the effects of coating processes on coating structure are discussed in the literature. Many studies report correlations of coating structure and coating properties using indirect methods for evaluation of coating structure. One study reported that the average pore diameter is related to the scattering coefficient of the coating. As a result, different coating pigments have been used to change the opacity of a coating by changing the pore size distribution of the coating. Furthermore, scientists have studied how to change the coating structure in order to produce the best coating for a particular purpose. For example, if a smooth, glossy surface is desired, highly anisometric clay particles are used in the coating, and the dry coating is super calendared to further

improve the gloss and smoothness. The mechanisms which produce a given structure are reasonably well understood. However, the knowledge of the relationship of coating structure to print quality is not well understood.

The factors affecting absorption of oil and ink into a coating were thought to be influenced primarily by the density of a coating and the relative amount of adhesive present at the coating surface. Recently, pore geometry has been shown theoretically to affect absorption. The absorption rate of a fluid into the surface of a coating is dependent upon geometry of the pore structure, the surface density, and the wettability.

It has been established that the rate at which a coating is dried influences the absorptive properties and the uniformity of the coating. Furthermore, studies have shown that the drying rate during immobilization has the greatest influence on coating properties. The mechanism describing how drying rate effects absorption and absorption uniformity has not been elucidated. Until recently, it was believed that high drying rate through the critical drying stages resulted in the deposition of additional binder at or near the coating surface, and several mechanisms were proposed to explain binder migration.

Variations in ink absorption, exhibited as print mottle, were thought to result from micro-variations in the drying

rate within the coating layer. These drying rate variations are caused by the existence of thick and thin areas of coating coverage which correspond to valleys and hills present in the paper. Therefore, the differences in ink absorption of coatings dried at different rates may be caused by differences in the degree of binder surface concentration which, in turn, affect the density of the coating surface. Furthermore, variations in ink absorption rate across the surface of a coating may be the result of differences in surface density and wettability caused by different levels of local binder concentration. The micro-area variation is caused by roughness and/or density variations in the base sheet.

The discussed mechanisms and effects have been a subject of debate in the literature for several years. Recently, new techniques for measuring the surface properties of the coating, including roughness and binder concentration have been developed. Direct determination of the surface binder concentration has not, in some cases, been consistent with the mechanisms used previously to explain print quality problems. In other studies, variations in surface binder concentration have been correlated to variations in print density. In any case, some doubt remains as to whether binder migration occurs and, if it does, whether it is primarily responsible for observed print quality problems. Additionally, the effects of pore geometry and packing

structure on the absorption properties of coatings have not been explored. Little is known about the differences in coating structure which result from the use of different drying strategies.

# PROBLEM STATEMENT

Problems of print quality have accompanied the increased production speeds in the coating industry in the past 15 years. These print quality concerns have led to research on the mechanisms for ink transfer and ink absorption. Recent theoretical analysis of fluid flow in discontinuous capillaries has suggested that further complexities exist in ink absorption mechanisms. This analysis may suggest a solution to inconsistencies among studies concerning the effect of drying strategy on print quality. Unfortunately, little is known about the actual packing structure of particles in a coating.

To clarify the effects of drying strategy on binder deposition at the coating surface and on print quality, several questions about coating structure must be answered. For example, what are the relative contributions of pore geometry, density and wettability to coating absorptivity? What fraction of coating dewatering occurs by evaporation and what fraction occurs by absorption into the base paper? How does the drying strategy affect the packing structure of a coating layer?

This dissertation is concerned with the last question. The specific objectives include: (1) Development of a technique for quantifying the packing structure of a pigment through the thickness of the coating; (2) Production of

coating films whose process of consolidation is dependent only on the rate at which they are dried; and (3) Formulation of a consolidation mechanism which predicts the effect of drying rate on the coating structure.

# THEORETICAL APPROACH

An analysis of the forces acting on the particles during consolidation is necessary in order to describe the effects of drying rate on coating structure. Understanding the nature of interaction forces between particles under conditions of suspension consolidation may lead to a hypothesis which is able to describe the effect of increasing the evaporation rate on the packing structure of the dry coating film.

The following discussion will consider dewatering by evaporation only; filtration and sorption into the substrate will be considered functions of the substrate and not part of the drying process.

## PROXIMITY OF PARTICLES

Consider a coating color at 50% solids made up of uniform hard spheres whose specific gravity is 1.0. If the particle radius is 0.5 micrometer, the volume of the sphere is 0.5236 $\mu m^3$. The volume of solution associated with each sphere is also 0.5236 $\mu m^3$; the equivalent spherical sheath around each particle is 0.13 μm thick. Each particle is, at most, 0.26 μm from its nearest neighbors. Table I contains the data for the same particles at higher concentrations. Particle separation distance is a significant factor for

determination of the energy of particle/particle interaction at different points during coating consolidation.

TABLE I

Separation Distances for 0.5 Micron Particles at Various Concentrations

| Solids Concentration (vol. %) | Maximum Separation Distance (μm) | Separation to Diameter Ratio |
|---|---|---|
| 40 | 0.38 | 0.76 |
| 50 | 0.26 | 0.52 |
| 60 | 0.18 | 0.36 |
| 65 | 0.16 | 0.32 |
| 70 | 0.12 | 0.24 |
| 75 | 0.10 | 0.20 |
| 80 | 0.08 | 0.16 |
| 85 | 0.06 | 0.12 |
| 90 | 0.04 | 0.08 |

In a typical coating suspension, consisting of clay (sp. gr. = 2.62) at 60% solids content, the pigment occupies about 36.4% of the total volume. At immobilization, there is no longer enough water present in the coating film to maintain particle dispersion. The immobilization solids content of a delaminated clay coating is approximately 78%. In a typical coating suspension 55% of the aqueous phase is necessary to maintain the suspension. The remaining 45% of the water volume is excess, providing some volume for particle motion. The amount of movement is restricted by interactions between particles. The limited motion of suspended particles allows them to react to disturbances occurring in the system.

## PARTICLE MOTION

### Rotational Diffusion

The rate at which clay particles change orientation in solution is important, in that it partially determines the rate at which particles will recover a random orientation after being stressed. Such stresses occur during drying of a coating. When a coating is applied to a non-porous medium, it is essentially a thin layer of the coating suspension spread onto the surface of the substrate. As water is evaporated from the coating surface, the surface recedes, concentrating the particles and aligning the particles parallel to the surface. The concentration gradient caused by evaporation and the forced particle orientation at and below the surface are counteracted by diffusion and repulsive interaction forces between particles. The rate of recovery (recovery of random orientation and uniform concentration) is defined by the above forces.

Particles suspended in solution normally undergo translational motion as a result of Brownian motion(82). Suspended particles also randomly rotate during Brownian motion. The net rotation is known as rotational diffusion. In dilute solutions, absent of external forces, the orientation of a clay platelet at a fixed moment in time is a function of its rotational diffusion. In concentrated solutions, rotational diffusion is limited by interactions with neighboring particles.

Assuming that no external electrical or magnetic fields are applied to a dilute solution, the suspended particles will rotate at a rate inversely proportional to the cube of the particle radius and the solvent viscosity(83-85). For oblate disks, the relationship between particle size and the rotational diffusion coefficient is:

$$D_R = 3kT/(na^3) \qquad (4)$$

where $k$ = Boltzman's constant (J/K)
$T$ = Absolute temperature (K)
$n$ = Solvent viscosity (kgm/s)
$a$ = Semi-major particle axis (m)
$D_R$ = Rotational diffusion coefficient (radians/s)

Examination of equation 4 leads to several conclusions about rotational diffusion: 1) The rate of rotational diffusion drops rapidly as the size of the particle increases; 2) Increasing the temperature of the solution increases the diffusion rate; and, 3) Increased temperature causes an increase in molecular motion and a decrease in the viscosity of the suspension medium, resulting in an increase in diffusion rate.

In a dilute clay suspension, for every two-fold increase in particle size there is an eight-fold drop in rotational diffusion. A typical commercial #2 clay has particles whose major axis may vary from 0.1 μm to 2 μm or more. Therefore, a clay suspension will have particles rotating at a wide

range of rates. In a concentrated coating suspension (60% solids content), allowing for the fact that as a particle rotates a substantial volume is swept out, electric double layer (a potential field in the suspending medium induced by the properties of the suspended particle - discussed in detail later) overlap can occur(86). The continuous electric double layer interaction forces acting on the particles in concentrated suspension restrict the motion of the particles. For larger particles, electric double layer interactions are probably the dominant factor affecting the orientation of the particles. For smaller particles, rotational diffusion may be significant to particle orientation.

## Particle Interactions

After application and metering, the coating has the properties of the original coating suspension; it is reasonable to assume that there are no shear forces acting on the coating or fluid flow present after metering. The forces acting on the particles are van der Waals attractive forces, electric double layer repulsion and hydrodynamic forces caused by particle movement.

### Van Der Waals Interaction

Van der Waals forces for spherical particles are dependent upon the separation distance between particles, the

radius of the particles, and the Hamaker constant for the particle composition(87). The following equation is that for a two particle system:

$$V_A = \frac{-A}{12}\left[\frac{y}{x^2+xy+x} + \frac{y}{x^2+xy+x+y} + 2\ln\frac{x^2+xy+x}{x^2+xy+x+y}\right] \qquad (5)$$

Where $a_1$, $a_2$ = Particle radii
A = Hamaker constant
H = Distance of separation
$x = H/a_1+a_2$
$y = a_1/a_2$
$V_A$ = London dispersion interaction energy

In a dynamic situation where particles react to these forces, calculation of the interaction energy between particles is difficult because the position of every particle is a function of the position of all the other particles. Considering radii $a_1$ and $a_2$ to be equal (0.5 μm) and the Hamaker constant, A, to be that of polystyrene ($5 \times 10^{-21}$ J), the energy of attraction between two particles may be calculated relative to H from equation 5. Figure 12 shows the results of the calculations just described. The energy of attraction is large at small separations and trails off rapidly as the distance of separation is increased.

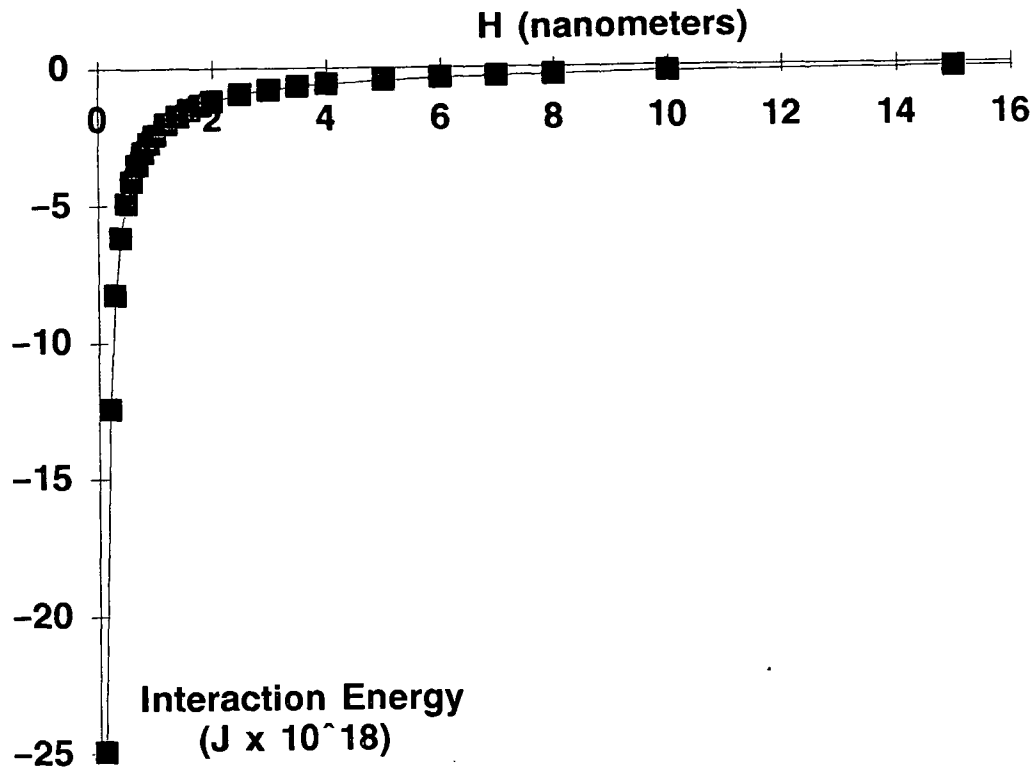


Figure 12. Plot of the energy of attraction due to van der Waals forces for a two polystyrene particles upon close approach. For particles of the same radius, 0.5 μm, and an A of ($5 \times 10^{-21}$ J).

Spherical particles, because of the lack of angular dependance on the potential field, are relatively simple particles to handle in theoretical calculations. Vold(88) has derived equations for anisometric particles and found that for rod- and plate-shaped particles the orientation is an important factor. Calculations of the van der Waals interaction energy for particles in coating suspensions should include factors for particle shape, orientation, composition, and distance of separation. Regardless of

shape, a suspension, where only van der Waals forces are present, the particles would usually form particle agglomerates due to the net attractive nature of van der Waals forces. However, there are cases in which the attraction of the suspending medium for the particle is greater than the particles for each other. In these cases agglomeration will not occur spontaneously.

## Electric Double Layer Interaction

Most substances acquire a surface charge when immersed in a polar medium, and the mechanisms for charge development have been described in textbooks on colloid chemistry(87). Briefly, a particle's surface charge affects the distribution of the ions present about the particle. Ions of opposite charge are concentrated near the surface and like-charged ions are repelled away from the surface. The net result of the attraction and repulsion is the formation of an electric double layer which consists of the charged surface and a diffuse distribution of neutralizing counter-ions and co-ions(87). The electric potential of the diffuse layer surrounding a charged particle was originally modeled by Gouy(89), Chapman(90), and Debye and Huckel(91). Their models are discussed in textbooks on colloidal phenomena.

Verwey and Overbeek(92) have described the role that the electric double layer plays in colloidal stability. The similar charge of the electric double layers of like

particles causes the particles to be repelled when they come into contact in a suspension. In a concentrated suspension the electric double layer repulsion retards flocculation. Equation 6 is used to calculate the energy of interaction of electric double layers from two spherical particles(87):

$$V_R = \frac{64\pi\varepsilon a_1 a_2 k^2 T^2 \gamma_1 \gamma_2}{(a_1+a_2)e^2 z^2} \exp[-DH] \qquad (6)$$

where $\varepsilon$ = permittivity of the medium
$a_1, a_2$ = particle radii
$k$ = Boltzman's constant
$T$ = temperature K
$\gamma_1 = (\exp[ze\mu_{d1}/2kT]-1)/(\exp[ze\mu_{d1}/2kT]+1)$
$\gamma_2 = (\exp[ze\mu_{d2}/2kT]-1)/(\exp[ze\mu_{d2}/2kT]+1)$
$\mu_d$ = Stern Potential
$e$ = fundamental charge
$z$ = counter-ion charge number
$H$ = separation distance
$D = [(2e^2 N_A c z^2)/(\varepsilon kT)]^{0.5}$
$N_A$ = Avogadro's Number
$c$ = electrolyte concentration
$V_R$ = interaction potential

The potential energy of interaction decreases exponentially with separation distance and is dependent on the concentration of electrolyte. Figure 13 is a plot of the interaction energy for the case of two interacting spheres which have the same diameter, 0.5 μm, and where $\varepsilon$ is 78.5, c is 0.01M, z is 1, $\mu_d$ is assumed to be the same as the zeta potential (equal to 50 mV) and T is 25°C.

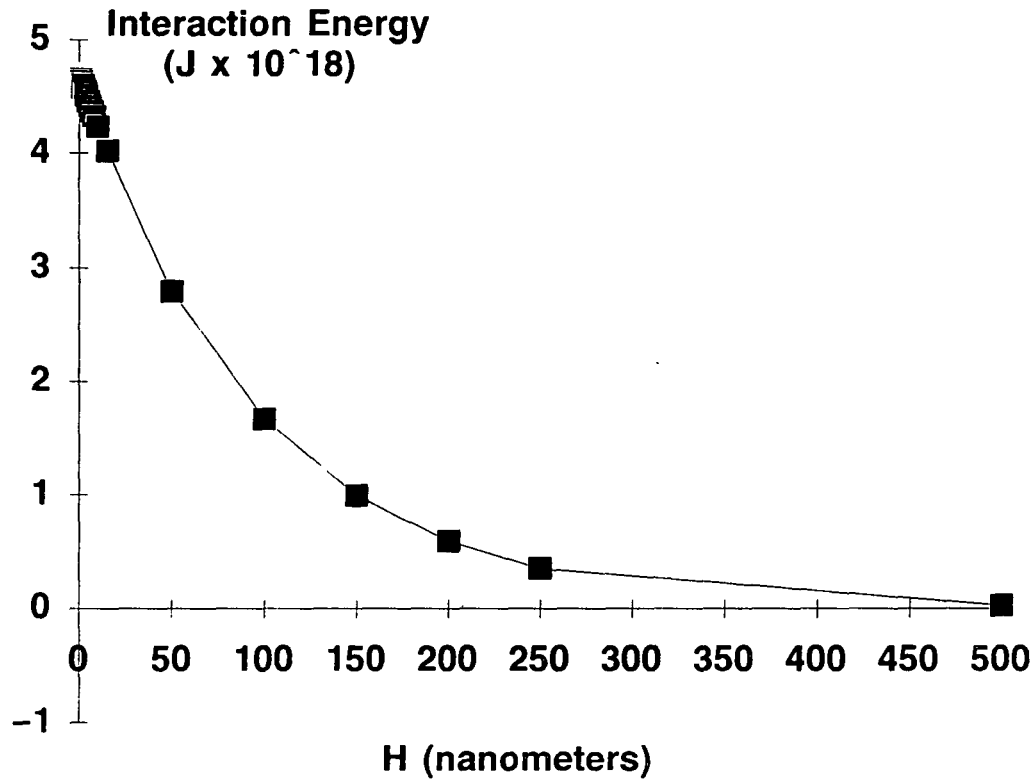


Figure 13. Calculated interaction potential of the electric double layers of a pair of spherical particles at 25°C with a Stern potential of 50 mV in a 0.01M KCl solution.

Total Energy of Interaction

The total energy of interaction is taken as the sum of $V_A$ and $V_R$. Figure 14 is the result of adding the $V_A$ curve of Fig. 12 and the $V_R$ curve of Fig. 13. In this situation, van der Waals attraction dominates only at very close approach (0.5 nanometers) and at relatively large distances (0.5 micrometers - not shown). From the work of Etzler and Drost-Hansen(93), we know that the vicinal water layer is at least 5.0 nanometers. Vicinal water has physical properties which are different from bulk water. The above equations and

theory assume that the properties of water are constant at all points in the suspension. In addition, the Stern potential can not be measured. Because of this, the zeta potential is commonly substituted for the Stern potential in the calculations. Thus the distances and corresponding energies of interaction calculated are approximations. For small particles with high surface charge density, the electric double layer repulsion is believed to be the dominant force in a coating suspension.

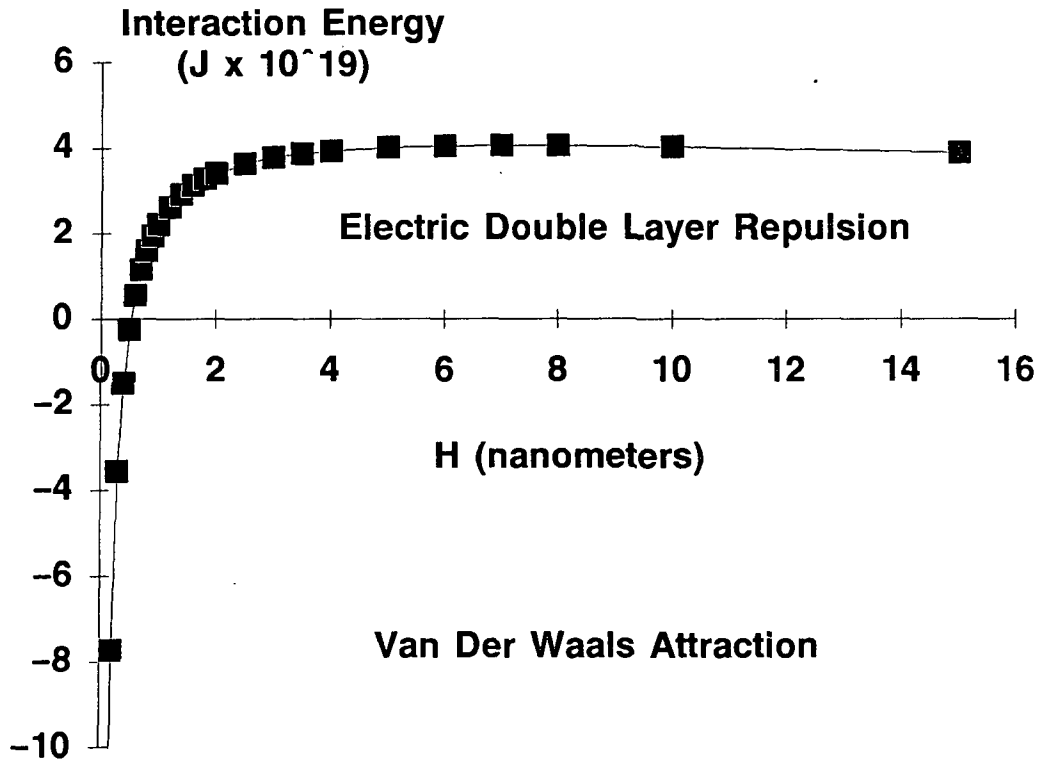


Figure 14. Total potential energy of interaction of the particles described in Figs. 12 and 13.

Diffusion causes particles in solution to have some translational and rotational velocity. Each particle has a quantity of thermal energy of about kT. If two particles were to collide, the collision would be buffered by electric double layer repulsion. However, if the energy barrier, the highest energy in Fig. 14, is small relative to kT, the separation distance may become small enough that the van der Waals attractive forces would dominate and the particles will adhere to each other.

Dilute solution particles interact occasionally, whereas, in a coating suspension, electric double layers continually interact. Generally, the energy barrier for the particles in a coating suspension is high enough to prevent flocculation. During the occasional particle/particle interaction in dilute suspensions, particles move away from one another until the energy of interaction approaches zero via rotational and translational motion. In concentrated suspensions, a particle will reorient relative to its nearest neighbors to minimize the interaction energy.

## Hydrodynamic Forces

The motion of a particle as it passes another particle causes a force to be exerted on the particle and vice versa. Greatly simplified, this is the basis for modeling the behavior of particles in a concentrated particle suspension using the lubrication theory. Bousfield(11) has described

the force on a sphere as it travels toward a second identical sphere:

$$F = 3\pi\mu Ua[1.5\beta\ln(\beta/(\beta-1) + 0.5\beta - 1/4\beta - 1 - \beta^2/(\beta-1)] \quad (7)$$

where $\mu$ = Liquid viscosity
$U$ = Particle velocity
$a$ = Particle radius
$\beta$ = $(h_o + a)/a$
$h_o$ = Half the particle separation distance
$F$ = Force felt by the particle in the presence of another particle

Therefore, as the particles come together ß→1 and the force goes to infinity. Figure 15 shows the decreasing change in force on the particles as the gap distance widens.

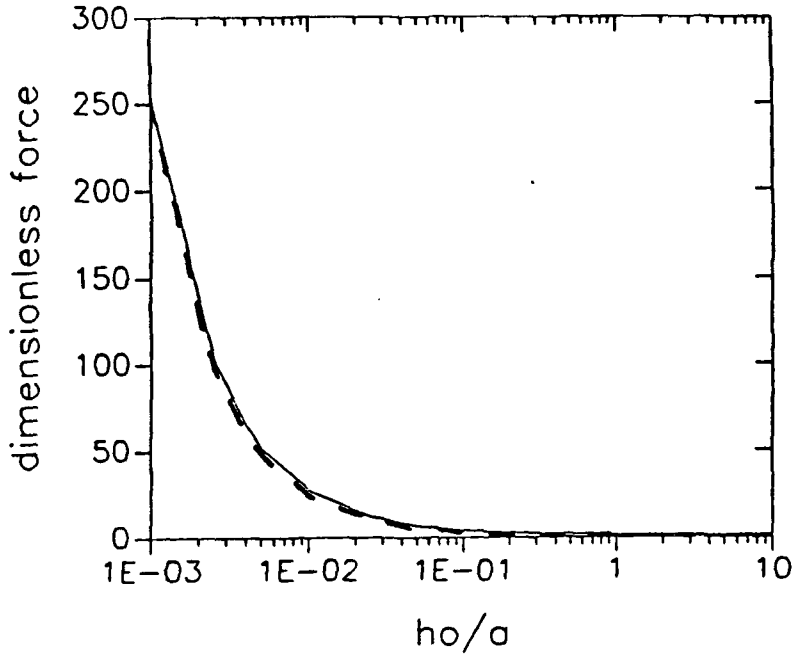


Figure 15. The dimensionless force ($F/6\pi\mu Ua$) on each sphere as a function of the gap distance. From Bousfield(11)

As in the case of van der Waals forces, the motion of every particle in the system has an influence on the motion of every other particle of the system. Simulating the interaction of the hydrodynamic forces on particles in suspension is impossible without some simplifications. Bousfield(11) neglected the colloidal forces and assumed any long range forces to be insignificant in a concentrated suspension. Through the use of a resistance matrix to represent the forces acting on all the particles at any one time and pair-wise calculations, he simulated the motion of several spheres under different boundary conditions (Fig. 4)

In dilute solution, it is convenient to consider particles as if they have a velocity relative to one another, in which case the lubrication forces (forces caused by the velocity difference between particles) may be significant. If, for concentrated suspensions, the shear forces imparted by metering and fluid flow caused by absorption into the substrate are neglected, then the relative velocities of particles may be neglected and lubrication forces are probably not important.

Summary of Particle-Particle Interactions

In order to predict the behavior of a suspension of particles, one must consider van der Waals attractive forces, electric double layer repulsion and hydrodynamic forces induced by relative particle motion. A balance of these

forces is required for dispersion of pigment particles; however, changing the factors affecting any of the forces will cause a change in the suspension properties and potentially cause a change in the packing structure of the dry film.

## HYPOTHESIS - CONSOLIDATION MECHANISM

Lepoutre and co-workers(6,7,8,29) have proposed the existence of two critical concentrations a coating experiences during drying. The first critical concentration is defined as the solids level where surface gloss begins to drop rapidly. This is the point where enough of the excess water has been removed from the coating suspension to break the suspension; the pigment particles have formed a semi-rigid network, which, through restricted consolidation, supports capillary conduction to the evaporation surface. Figure 1a shows that almost all the consolidation occurs prior to the first critical concentration.

The second critical concentration occurs shortly after the first critical concentration. It is defined as the point where the opacity of the coating film begins to increase rapidly. At the second critical concentration, consolidation ceases and the capillaries can no longer shrink to accommodate capillary flow to the coating surface. As a result, the capillaries begin to drain the largest reservoirs (fluid filled spaces between pigment particles) to supply the

surface with liquid for evaporation(30,31). The creation of air/solid interfaces causes an increase in the amount of scattered light, thus increasing opacity.

Because almost all consolidation occurs before the first critical concentration and because particle mobility is highest prior to the second critical concentration, a study of the effects of drying rate needs to consider the forces acting on the particles between metering and the second critical concentration.

Evaporation of liquid from the coating film reduces the volume of water available for particle motion and, through increased electrolyte concentration(61,87,92,94,95), increases the van der Waals contribution of particle/particle interactions. In response to the interparticle forces, the particles change orientation to minimize the interaction energy between particles. At short interparticle distances, van der Waals forces restrict the ability of the particles to react to shear stresses and eventually cause flocculation and immobilization. An underlying assumption is that the electric double layer repulsion between particles dominates van der Waals attractive forces in the initial coating suspension. This assumption appears to be reasonable considering that the coating suspension has been made to be stable; particles are chosen to have high surface charge densities and usually a polymer dispersant is adsorbed onto the surface to provide some steric stabilization as well.

Agglomeration of particles begins near the first critical concentration. As the suspension approaches the first critical concentration, the clay platelets orient with their faces parallel to each other forming face-to-face flocs. Aggregates grow by adding particles in a face-to-face orientation to flocs until a particle becomes bound in a non-parallel orientation. An aggregation about the "new" orientation forms on the "out of plane" particle. The out of plane particle may also act as a bridge between oriented agglomerates. The net result is two types of pores: those within the aggregates and those between the aggregates. The pores between the aggregates are an order of magnitude larger than those within the aggregates(79,81).

The packing phenomenon discussed above helps explain the existence of second critical concentration. The consolidation which occurs between the first and second critical concentrations may result from the compaction of aggregates by capillary forces. As agglomerates slide past one another, capillary volume continues to decrease, enabling the system to support evaporation at the coating surface without draining the large pores. Consolidation ends when the attractive force between agglomerates becomes large enough to fix them in place within the coating.

In summary, coatings consolidate as water is evaporated from the surface. Particles remain in suspension as long as repulsive electric double layer forces and hydrodynamic

forces are dominant over van der Waals attractive forces. Particle packing is determined by the ability of the suspension to react to increased particle interaction caused by compaction as water is removed.

Particles, given time and sufficient space, will reorient to minimize the energy of interaction. Reorientation increases the density of the structure in suspension until, at a given solids concentration, van der Waals forces cause the particles to aggregate. Aggregated particles form a network of capillaries which support liquid flow to the surface for evaporation. At the first critical concentration loss of the continuous liquid film on the surface of the coating occurs.

Consolidation continues as the aggregates are pulled together by capillary forces. When attractive forces prevent any further collapse of the structure, the largest pores of the coating are drained to support surface evaporation. The solids concentration when the voids begin to drain is known as the second critical concentration, and is characterized by a rapid increase in opacity of the coating film. Drying is completed by draining the remaining pores in order from largest to smallest.

HYPOTHESIS - PACKING STRUCTURE

Assuming that the coating behaves as a particle suspension in the form of a film when applied to the substrate, then the colloidal structures discussed in the Background section may be present in the coating film.

In a dilute suspension, particles have enough free volume to rotate about their axis without hindrance from their neighbors. The structure of the suspension will be random at any given moment in time. A schematic is shown in Figure 16a of a plate-like material in an eight per cent suspension by volume. Interactions occur as the particles approach one another; however, there is ample room for response, thus each particle can achieve minimum energy of interaction.

The concentration of a typical clay coating is almost five times that of the above example. As shown in Fig. 16b, the particles have little room to move and are in close proximity so that they strongly interact. They also appear to have regions of organization where particles are oriented parallel to one another. If the suspension volume were reduced by 10%, the particles would move relative to their nearest neighbors to achieve minimum interaction energy. This action results in an increase in parallel orientation. Continuing the consolidation would eventually result in the dominance of attractive forces and immobilization of the suspension. The packing structure would consist of a series

of randomly oriented aggregates made up of several clay platelets in face-to-face orientation.

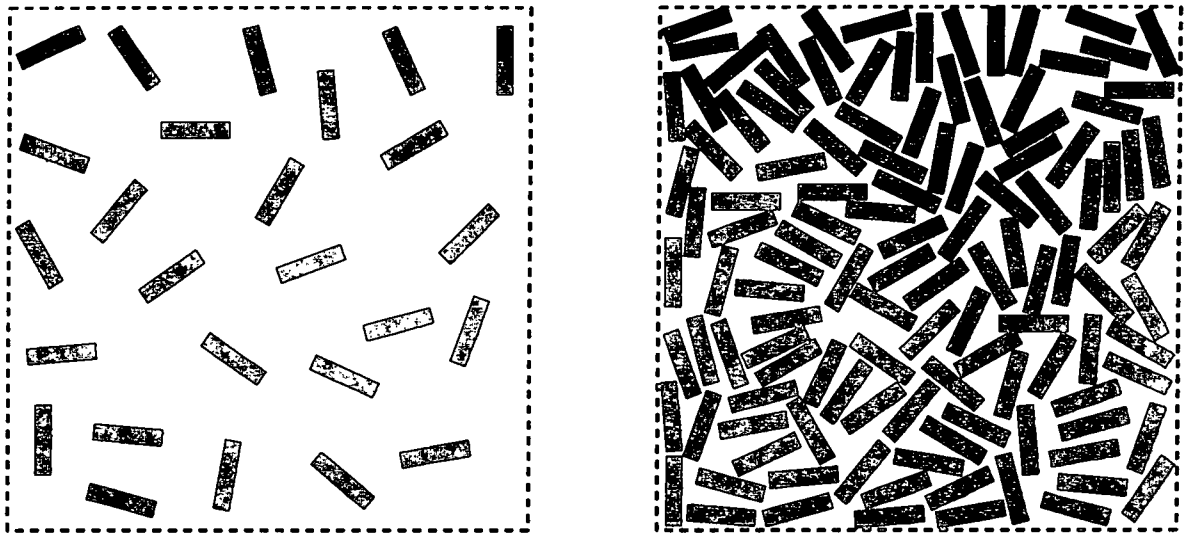

(a) (b)

Figure 16. Schematic of uniform plate-like material in suspension a) 8% by volume. b) 37.5% by volume.

The air interface and the substrate bound the coating dispersion on two sides. The dispersion is assumed to be infinite in the x-y plane. The work of Hiltner and Krieger(63) has demonstrated that the air interface imparts an orienting force on suspended particles, causing them to pack in ordered structures. Schneider and Rippin(38) have observed that solid boundaries also have an influence on the packing structure of the particles near them. Therefore, a hypothesis for describing the packing structure of a thin film must account for the boundary effects.

Plate-like particles near boundaries will be rotationally restricted. As the surface does not repel

particles as other particles do, particles tend to orient with their largest face parallel to the surface. Once in this position, surface particles experience little motion and orientation of subsequent layers will occur with respect to the surface particles. Local parallel organization near the surface will dissipate with depth due to a reduction of rotational restrictions.

The substrate, another boundary, also serves to orient suspended particles. Upon application, some particles adhere to the surface forming a layer of rigidly-held particles which serves as a template for the neighboring particles. The particles which adhere to the substrate have some parallel orientation due to the shear during metering. However, the extent of the parallel orientation will not be as great as at the air interface because the particles are held in place in the orientation that they were applied. The particles at the film surface are able to move to achieve axial orientation. The resultant packing structure near the substrate will mirror the surface structure, except that it will tend to have less organization parallel to the substrate. The resultant structure of the dry film will be made up of particles of greater axial orientation near the boundaries while the bulk of the coating will have more random orientation. Figure 17 is a schematic of the proposed coating structure.

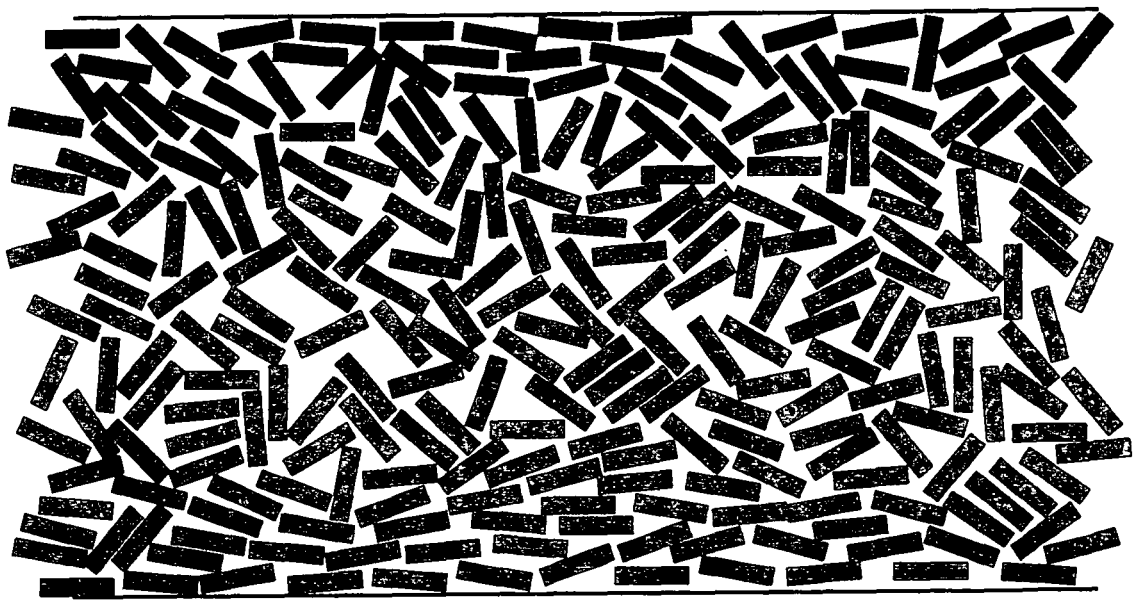

Figure 17. Schematic drawing of the hypothesized structure of a coating of uniform plates.

HYPOTHESIS - EFFECT OF DRYING RATE

For the purpose of this study, it will be assumed that the Gouy-Chapman double layer model is adequate and that the hypotheses for the consolidation mechanism and the structure of a suspension are accurate. Using these earlier models it is assumed that electric double layer forces dominate and that particles may reorient in response to external stresses applied to a coating suspension. The response or reorientation of the particles, being dependent on translational diffusion, rotational diffusion, the magnitude of the double layer repulsion, and gravity (gravity is

significant only at very long times)(96), is a time dependent phenomenon. Therefore, the rate at which a coating is dewatered should affect the packing structure of the coating film.

Drying a coating film at a slow rate will allow sufficient time for the particles to rearrange into dense structures. The time necessary for rearrangement is a function of the rate of rotational diffusion of a particle: approximately 2.5 seconds for a 90° rotation. The density through the z-direction (cross-section) of the coating film will reflect the structures near the boundaries. The surface layer and the layer near the substrate will have a net particle orientation parallel to the coating axis. The inner layers of the film will be less axially oriented but will retain the face-to-face particle orientation.

Fast drying of a coating layer limits the time for particle response to consolidation forces. The resultant coating will be less ordered than the same coating dried at a slow rate. Less order implies greater relative pore volume for the films dried at high rates. The density profile through the cross-section will also reflect the disorder of the structure. It will have dense areas near the boundaries, but the depth of those layers will be smaller than for slowly dried coatings. The bulk of the coating will be more randomly ordered with less face-to-face orientation.

The total pore volume of a coating film will increase as drying rate increases. The pore volume distribution through the thickness of a coating dried at a high rate will have a larger density variation than a coating dried slowly.

# EXPERIMENTAL APPROACH

The preceding hypotheses are based on the dynamic consolidation of a colloidal dispersion. The properties of the dispersion and the changes which occur during consolidation are directly related to the packing structure of the dry pigment film. Evidence for testing the hypotheses can therefore be obtained from the features or characteristics of the structure of the film. Experimental challenges include quantifying the packing structure, and production of coatings dried at different rates without changing other variables that affect coating structure.

## QUANTIFYING COATING STRUCTURE

For the purpose of this study, coating structure is defined as the spatial distribution of the components of the coating film. A spatial description of the components is useful for estimating the effect packing structure may have on the physical properties of a film. The hypotheses describe the coating film as dense near the interfaces and bulky in between; locating the coating components provides the information to test the hypotheses. Experimental techniques used to test the stated hypotheses must be capable of quantifying the packing structure of coating films through a description of the spatial arrangement of the coating components.

For pigment suspensions such as coating colors, the literature describes bulk characteristics of pigment packing structures and changes in those structures which cause changes in coating properties. The literature also describes the packing structures of concentrated suspensions and the physical changes which occur during consolidation. From knowledge of the pigment structure in suspension and the structure of the consolidated suspension, a mechanism describing the consolidation of the suspension can be deduced. A set of experiments which determine the effects of drying rate on coating structure should provide the knowledge necessary to conclude how the structures are formed.

The nature of a coating renders this relatively simple-sounding approach difficult. A coating consists of three basic components: pigment, binder, and air. A simple recording of the position of each part is hindered not only by the size of the components but also by their proximity. Binder and pigment can not be separated without disturbing the position of one or the other. Even if it were possible, one would be unable to tell the difference between voids left by the absent component and voids present prior to component separation. To overcome this problem, bulk properties of coating films are often measured and then related theoretically to the packing structure. For example, the density of a coating is determined from its dimensions and mass. Measured densities and the densities of the components

are used to calculate void volumes of coatings. The void volume has been experimentally related to several physical properties of the coating. However, information on the spatial distribution of the components cannot be derived from the density.

Techniques have been developed that yield information about coating structure besides the void volume. For example, the light scattering ability of the coating has been shown to be a function of pore size(5). Techniques have been developed for quantifying surface topography(2) and pore volume(4,97) in efforts to predict printing quality. In order to predict ink absorption, opacity, and coating strength, techniques for measuring the pore size distributions have been developed(5,98,99). None of these methods, although useful for predicting the desired property, describe the spatial distribution of the coating components.

The technique used to quantify the coating structure for this study must be able to either directly or indirectly determine the relative locations of the coating components. In principle, the coating components could be picked out one at a time and their position in space recorded. In practice this is impossible, but the technology to measure the relative location of the components from planar images is available and has been used to measure pore size distributions in coatings(5) and to determine the density profiles in paper(100).

Areal measurements of the components can be made from planar images. The relative areas obtained are directly related to volumetric features through the principles of stereology(101,102,103). Three-dimensional analysis is insured statistically by analyzing images of coating cross-sections which have been cut at random angles perpendicular to the plane of the coating film. Distributions of components through the thickness of coatings can be determined, thereby producing the density profiles necessary for analysis of the stated hypotheses.

Areal measurements are made optically and are usually incapable of distinguishing between chemically different materials which have nearly the same optical or electron density (In our case, coating binders and epoxy resins used to embed coatings were both carbon-based polymers and have nearly the same electron density). This limitation may be overcome by eliminating all the solid components except one. For example, instead of producing coatings containing two solid components, pigment and binder, a coating could be made using only one solid component - the pigment. Analysis of a cross-section of such a coating would require only differentiation between the pigment and the voids.

COATING FILM PRODUCTION

Every aspect of the coating process has been shown to affect the properties of coatings which relate to their structure(17-26). All variables which affect coating structure during coating production are interrelated; changing variables early in the coating process will affect how subsequent variables influence coating structure. To produce different coating films which are only different in their drying rate requires that all process variables be controlled.

The variables in the coating process can be divided into three groups; materials, metering, and drying. Materials include the coating components, the coating dispersion and the substrate. The substrate roughness and porosity contribute to coating structure and are difficult to quantify. Both can be eliminated by coating a smooth, nonporous material. Other materials can not be eliminated but can be characterized. The effects of pigment chemistry can be avoided by choosing a single pigment. The effects of particle geometry and particle shape can be eliminated by using the same material throughout the study. The coating dispersion can be produced by reproducible methods and, therefore, also be held constant throughout the study.

The shear on coatings which occurs during metering has been shown to align clay particles(20). Quantification of the effect is difficult and, as a result, the variable must

be eliminated or controlled during drying studies. Applicators which employ blades or nips use pressure to control coat weight and impart high shear rates at the point of metering. Pressure devices are not compatible with smooth non-porous substrates because they "scrape" the substrate clean during metering. For these reasons blade and nip applicators may only be used for this type of drying study with difficulty.

Shear during metering cannot be completely eliminated, but it can be significantly reduced by using volumetric metering devices such as Bird bars or Meyer rods. Volumetric applicators control coat weight by allowing a specific thickness or volume of coating color through a gap between the substrate and the metering device. Coating applications using the same device and following the same procedure should yield potentially consistent coat weights and structures.

Drying coating films usually involves heating to aid in evaporation of the liquid phase which is subsequently removed from the coating surface by an air stream. Various factors involved in drying processes may affect coating structure.

Movement of air across the coating surface imparts a shear on the coating and also contributes to heat and mass transfer rates. Changing air flow velocities to control drying rates may result in a change in the shear rate on the coating surface, potentially creating different packing

structures of particles near the surface. Alternatively, the temperature of the drying air may be raised to increase the rate of heat transfer and the evaporation rate. Temperature affects the viscosity of the liquid medium which will in turn affect the hydrodynamic forces acting on the coating particles. Diffusion rates and electric double layer properties are also temperature-dependent. For these reasons increasing the temperature to increase the drying rate may also affect coating structure.

A third method of controlling the drying rate is to control the relative humidity of the drying air. The evaporation rate is dependent upon the relative humidity of the air at the point of evaporation. Increasing the moisture content of the drying air will slow evaporation of the water from the coating. In this case, the only change in the system is the dew point temperature. Because evaporation occurs only at the surface of the coating prior to the immobilization, the temperature should be of minimal consequence to the coating structure. When relative humidity is used to control the drying rate, all the drying factors affecting the coating will remain constant except the rate of consolidation.

Summary

The following steps are necessary to produce coatings that differ only in their respective rates of consolidation:

1) Eliminate the effects of substrate roughness and porosity variations; 2) Hold the coating dispersion and coating materials constant and well-defined; 3) Limit the shear rate during metering and maintain a reproducible coat weight; and, 4) Change the drying rate without altering the drying parameters that influence coating structure.

The use of a non-porous plastic substrate will suffice to eliminate the effects of a non-uniform base sheet. A single, well-characterized pigment in the coating color limits the effect of size and geometry on the coating structure. Coating dispersion preparations need only be reproducible - standard methods have proven reliable. Metering with a volumetric metering device limits the shear rate on the coating and provides a reproducible coat weight. Finally, changing the drying rate by controlling the mass transfer through the relative saturation of the drying air should produce coating films suitable for analysis and for testing the hypotheses put forth in the previous section.

# MATERIALS AND METHODS

The following text contains a description of the materials and equipment used in this project, including details of the procedures for coating, drying and analysis of the coating films.

## COATING PIGMENTS

Researchers have reported that the size, shape and chemistry of the particles used in a coating pigment affect the packing density of coating films(14-16,26,37,57,104-111). The pigment properties must be held constant to determine the effects of drying rate on pigment packing structure independently of pigment properties. Two different types of pigment were chosen for this study. Each pigment was used in an independent set of experiments and the results were compared on a relative basis. One pigment was a delaminated clay (Hydraprint) supplied by J.M. Huber Company and the second was a polystyrene latex (Lytron 2503) supplied by Morton International.

### Clay Pigment

Hydraprint is a mechanically delaminated clay that has been spray dried. Its physical properties as reported by the supplier are shown in Table II(112). Typical coating clays are characterized by small narrowly distributed particle size

distributions (i.e., #1 clay has 95% of the particles below 2 μm and #2 clay has 85% of the particles below 2 μm). A delaminated clay was chosen because of its high aspect ratio (12:1 compared to 8:1 for #1 clay) and broad size distribution (documented below). For detecting changes in packing structure, the large size facilitates visual inspection of the structure. The large particle size distribution increases the range of possible packing geometries, and the high aspect ratio helps to insure that regular packing will not occur.

Table II

Properties of Clay Pigment

| | |
|---|---|
| Tappi Brightness | 87.5% - 89% |
| Surface Area ($m^2/g$) | 14 |
| 325 Mesh Residue | 0.01% |
| Moisture | 1.0% |
| pH (28% solids) | 6.0-7.5 |
| Viscosity (67% Solids) (cP) Brookfield 20rpm | 350 |
| Specific Gravity ($g/cm^3$) | 2.60 |
| Refractive Index | 1.56 |

Because of the high aspect ratio of a Georgia delaminated clay (12:1), equivalent spherical diameter is not normally used to describe the particle size distribution. The clay particle size distribution was determined by three methods. Stokes settling(42) was used to fractionate the clay into two fractions. The equivalent spherical diameter (e.s.d.) of each fraction was measured using a Malvern Zetasizer II. The fractionation method yielded some crude

information about the clay size distribution. Table III shows that two-thirds of the particles had a relatively small mean e.s.d. of 0.67 μm. The remaining third (the heavy fraction) had a mean e.s.d. of 6.14 μm, which is larger than a typical #1 or #2 clay.

Table III

Sedimentation Fractionation of Clay

| Fraction | Weight % | Mean e.s.d. |
|---|---|---|
| A | 68% | 669 nm |
| B | 32% | 6144 nm |

Micrographs of clay platelets were acquired directly from a JEOL JSM-35C SEM into a Tracor Northern TN-8502 image analysis system. After calibration of the images, the longest dimension for 200 particles was measured and recorded. Results from the measured particles are shown in Fig. 18. (Note that the x-axis is not linear.)

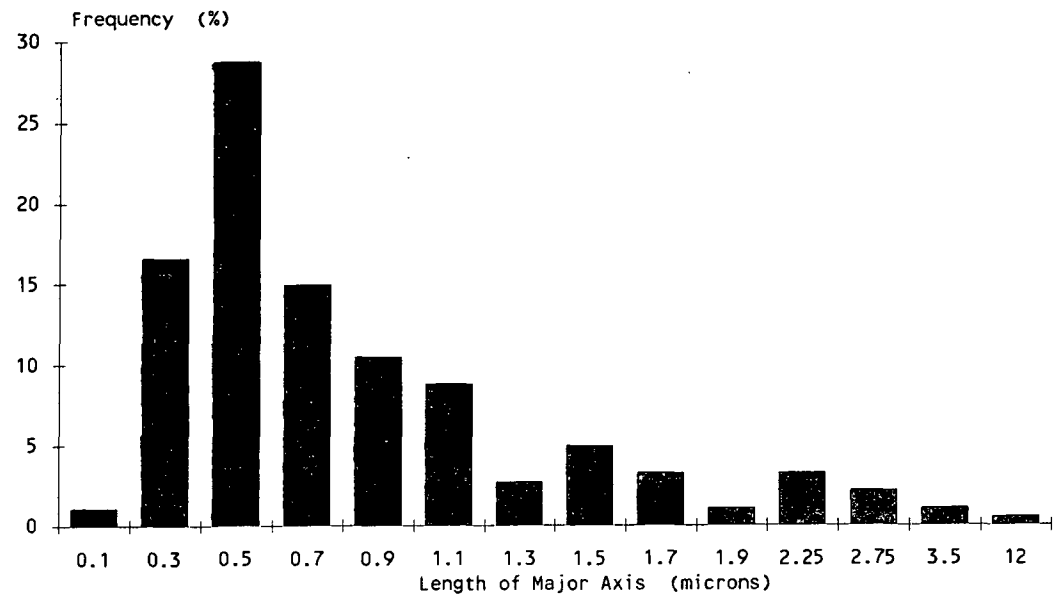


Figure 18. Frequency distribution of the semi-major axis for Hydraprint, a delaminated clay.

The number average semi-major axis of the clay was 0.92 μm, which, from equation (4), has an average rotational diffusion coefficient, $D_R$, of 0.6 rad/s (68°/s) at 25°C.

A third method for documenting the size distribution of the clay involves scanning electron microscopy, in which the area of a face of the particle is measured and the diameter is calculated as the square root of the area. Figure 19 shows that the calculated diameters from this technique were distributed similarly to the previous results. The results indicate that the delaminated clay used in this study had a wide particle size range (0.1 μm to >7 μm) and a relatively large average size, 1 μm, as compared to a #1 or #2 clay.

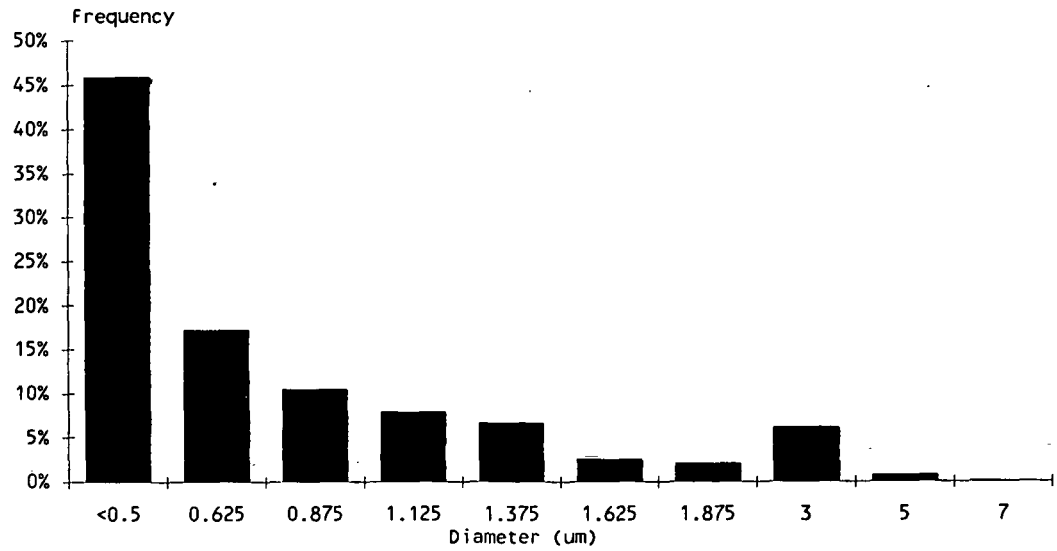


Figure 19. Frequency distribution of particle diameter calculated from 1000 particles as measured automatically from backscatter images via SEM.

Size is not the only clay parameter of importance. The electric double layer thickness and energy of interaction is

dependent upon the surface charge per unit area of the clay. The stability of the suspension and the repulsion forces necessary for the reorientation of the particles during consolidation are dependent on these properties. The zeta potential of a particle, the potential at the slip plane, is a relative indication of the surface potential(87). An extremely positive or negative zeta potential is an indicator of strong repulsion between particles.

The electrophoretic mobility of a particle, the measured velocity of a particle in an electric field, may be calculated from the zeta potential by the Smouluchowski equation(95):

$$u_E = \frac{v_E}{X} = \frac{\phi\varepsilon}{4\pi\mu} \qquad (8)$$

where $u_E$ = electrophoretic mobility ($\mu$m/s per volt/cm)
$v_E$ = electrophoretic velocity ($\mu$m/s)
X = electric field (volt/cm)
$\phi$ = zeta potential (volts)
$\varepsilon$ = permittivity of the medium ($s^4A^2/kgm^3$)
$\mu$ = viscosity of medium (kg/m sec)

The electrophoretic mobility of the clay was measured by a Malvern Zetasizer II at pH 9.0 and 25°C, in 0.01M KCl solution. The average mobility was discovered to be -3.84 $(\mu m\ s^{-1})/(volt\ cm^{-1})$ ± 0.62. The corresponding zeta potential was about -50 millivolts. The zeta potential was sufficiently high that the dispersion was stable and the particles experienced enough electric double layer repulsion to develop dense packing structures during consolidation.

Plastic Pigment

Spherical particles are used most commonly in packing simulations and model systems to determine the packing structure of particle beds or thin films(35,40,43-47,49-51,63,113-116). The use of spheres is primarily due to the relative ease with which their geometry can be mathematically represented and manipulated. In order for the results of this study to be compared to simulations and other coating studies, a set of experiments was performed using a polystyrene latex as the coating pigment. Latex pigments suffer some disadvantages however, and for this reason, they were not chosen as the primary pigment.

Commercially available latexes can be obtained that are relatively monodispersed, allowing models like those of Bernal(44,45) and Dodds(51) to be used. However, electron micrographs show (see Fig. 20) that latex particles do not behave as hard spheres and, therefore, do not satisfy most simulation criteria. In Fig. 20 a visible deviation in the curvature of the particles can be seen where particles are in contact. The hard sphere model requires the particles to remain spherical in all situations. Latex particles have another disadvantage. Monodispersed spherical particles have a limited range of possible packing densities(35). The limited number of conformations available in a system composed of monodispersed particles may limit the ability to detect changes in packing structure.

The spherical particles used in this study were a polystyrene/acrylate copolymer, Lytron 2503, donated by Morton Chemical. Table IV contains the properties of the latex as determined by the supplier(117). Particle size analyses were supplied by Morton Chemical as determined by centrifugation techniques - results are shown in Fig. 21. Lytron 2503 has an average diameter of 0.39 μm with a bimodal particle size distribution having peaks at 0.42 μm and 0.35 μm. Examination of the latex using a SEM qualitatively confirmed the bimodal particle size distribution determined by the centrifugation technique.

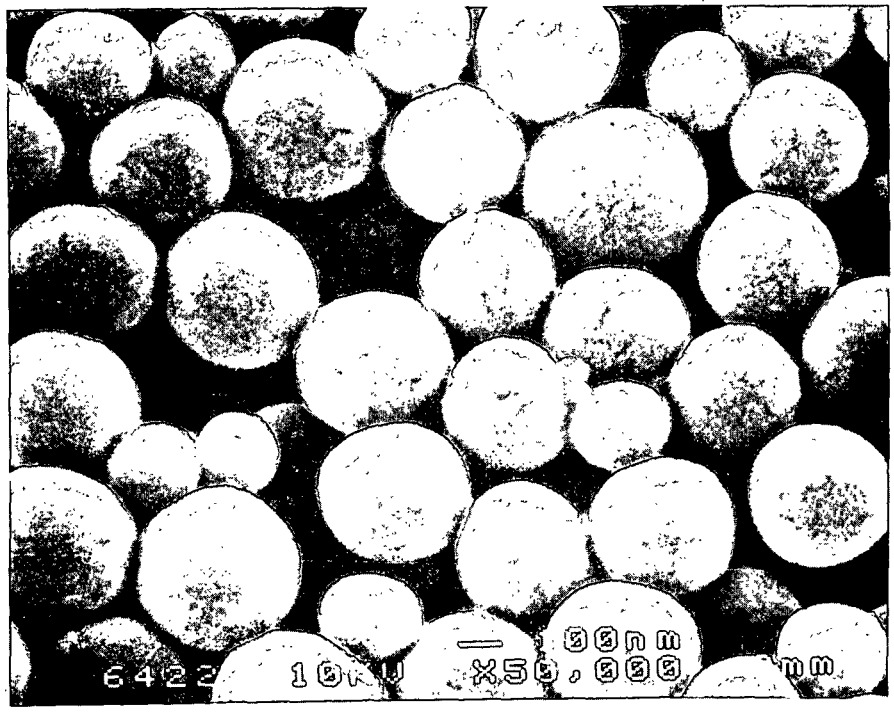


Figure 20. Micrograph of Lytron 2503, polystyrene latex coating on plastic film. Particle surfaces appear flattened at particle contact points. 10 keV, 10,000X.

Table IV

Properties of Plastic Pigment

| | |
|---|---|
| Solids | 48.0% |
| pH | 9.0 |
| Viscosity | 50 cP |
| Surface Tension | 50 dynes/cm |
| Particle Charge | anionic |
| Specific Gravity | 1.05 g/cm$^3$ |
| Fusion Temp. | 102°C |
| Refractive Index | 1.59 |

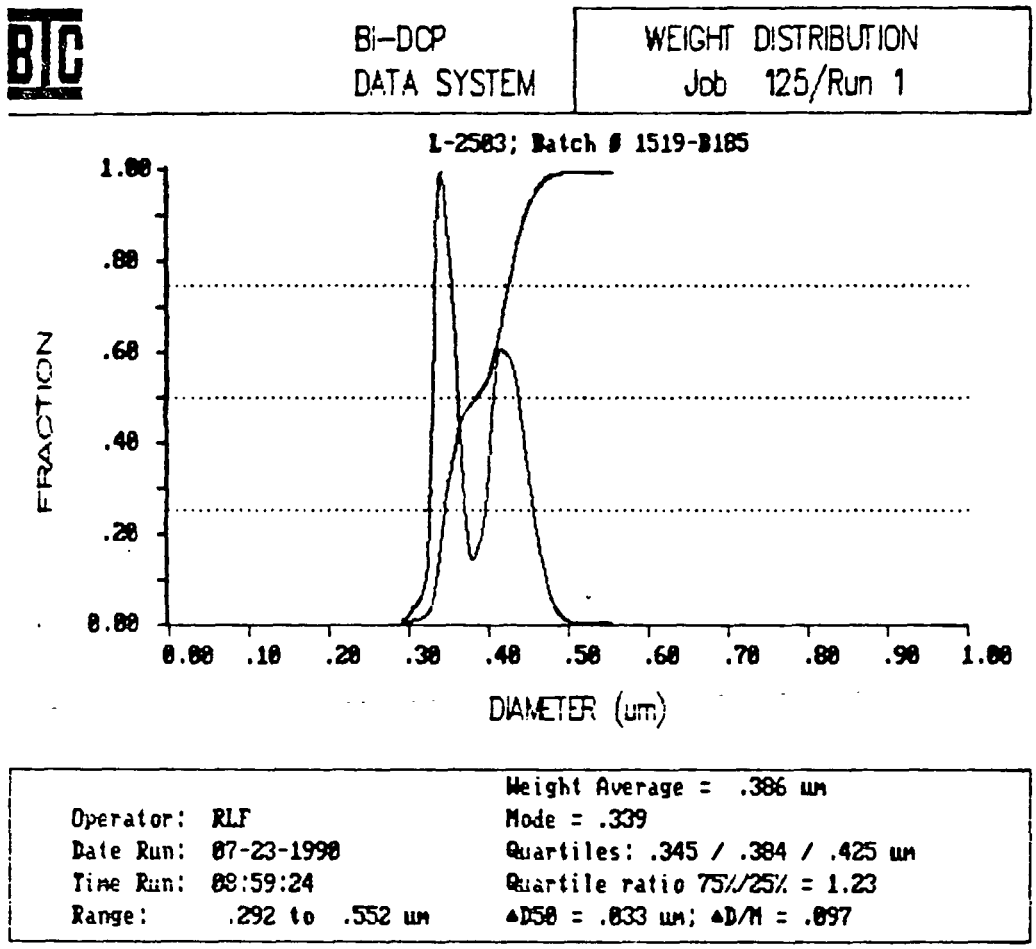


Figure 21. Particle size distribution for Lytron 2503, polystyrene/acrylate pigment as supplied by Morton Chemical.

## COATING DISPERSIONS

Hydraprint, a delaminated Georgia kaolin, was received as a powder. The clay was suspended at 60% solids in distilled water which had been adjusted to a pH of 9 with 0.1N NaOH. Suspensions were made by slowly adding dry clay to the water while mixing at high speed with a dual impeller laboratory mixer. Mixing was continued at high speed for 20 minutes after addition of the dry clay. Brookfield viscosity of the coating was about 350 cP at 20 RPM and 23°C. Solids content was determined from the difference between the mass of the wet coating and the same coating dried by heating to 104°C and maintaining that temperature for eight hours.

Plastic pigment coatings were used as received. Dispersions were at 48.5% solids, pH 9, and a room temperature Brookfield viscosity of 50 cP at 20 RPM.

## COATING SUBSTRATES

### Plastic Film

A non-porous substrate was chosen in order to avoid the effects of local variations in porosity and roughness found in paper systems. Coatings in each experiment were applied to a plastic film (polyethylene terephthalate). The plastic used was a 3M 700 PPC film used in plain paper copiers to produce overhead transparencies. Prior to coating, the plastic was washed with soap and water followed by an

ammonia-based window cleaner. Plastic substrates were attached either to glass or a polished metal plate. The surface tension of a thin film of distilled water between the plastic and the base plate was used to adhere the plastic to the plates. Plastic substrates were taped along the leading and trailing edges to hold them in place.

### Polycarbonate Membrane Filters

To test the effect of dewatering by filtration with simultaneous evaporation, a substrate of uniform porosity and smoothness was necessary. Polycarbonate filters are polycarbonate sheets that have been exposed to radiation and etched with alkali to produce a random distribution of cylindrical capillaries. Sheets 10 μm thick were used having a pore size of 0.2 μm. Other filter properties were: $3 \times 10^8$ pores/$cm^2$, 1.0 mg/$cm^2$, a water bubble point of 82 psi, and a water flow rate at 25°C of 20 ml/min/$cm^2$.

## COATING APPLICATORS

### Meyer Rod

In some experiments coatings were applied and metered with a #10 Meyer rod. A Meyer rod (Fig. 22) is a wire wound rod which controls coat weight volumetrically. The amount of coating that is not "scraped" off by the rod is a function of the coarseness of the wire on the rod. For a clay coating at

60% solids content, the #10 rod yielded a reproducible 20 $g/m^2$ coat weight.

Difficulties with consistent wettability of the plastic substrate were encountered with slow drying strategies for Meyer rod coatings.

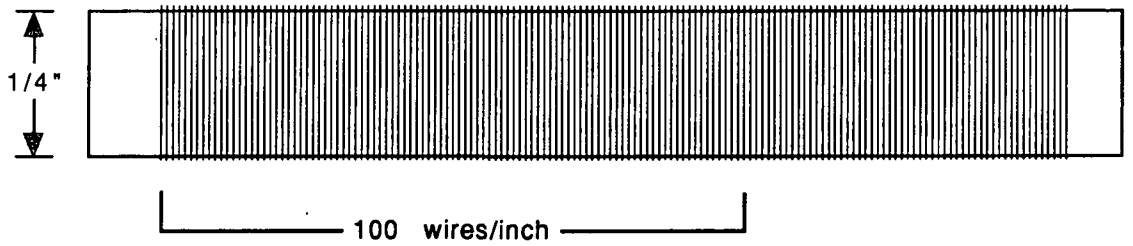


Figure 22. Diagram of a #10 Meyer rod.

Bird Bar Applicator

The majority of coating applications performed during this study were done with a Bird bar applicator (Fig. 23). The Bird bar is a volumetric metering device which controls coat weight by the gap width between the substrate and bar. The #4 bar used in this study yielded coat weights of about 50 $g/m^2$ and 20 $g/m^2$ for 60% solids clay coatings and 50% solids latex coatings respectively. Uniformity of the coating is primarily a function of the uniformity of the metering stroke. The bar must be pulled at a constant speed during the entire stroke to obtain uniform coverage.

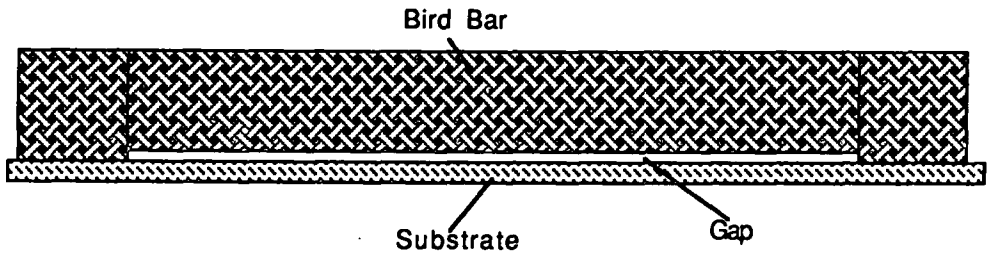


Figure 23. A sketch of the bird bar coating applicator used in this study.

IMMOBILIZATION SOLIDS

Watanabe and Lepoutre(7) have shown that when dried a coating passes through a solids content at which the gloss begins a rapid drop. The solids content at the gloss point is called the first critical concentration (FCC). The consolidation of the coating film is nearly complete at the FCC(7) (Fig. 1b). Because the change in gloss can be easily detected and because the solids content is reproducible for constant coat weight, the time to the gloss point can be used to determine the drying rate of the coating.

The solids concentration at the gloss point was determined for both coating pigments. The analyses were gravimetric. The mass of wet coating and film was recorded immediately after coating by setting the coated substrate and a tared backing plate on a balance. The gloss of the coating was visually monitored. At the gloss point, the mass of the coating system was recorded. The difference in mass between

the initial coating and the coating at the gloss point was assumed to result from water evaporation. A simple calculation involving the coat weight and initial coating solids was performed to determine the solids at the gloss point. Table V shows the results for clay coatings and latex coatings.

Table V

Solids Concentration at the Gloss Point for Coatings Applied by Hand to a Non-Porous Substrate

| Coating Pigment | Initial Solids | Coat Weight | Final Solids | Average |
|---|---|---|---|---|
| Clay | 60.23% | 50.32g/$m^2$ | 77.21% | |
| | 60.23% | 49.70 | 78.15% | |
| | 60.23% | 49.89 | 77.93% | 77.86% |
| | 59.87% | 50.03 | 77.31% | ± 0.51 |
| | 59.87% | 51.17 | 78.55% | |
| | 59.87% | 49.72 | 78.01% | |
| Lytron 2503 | 48.53% | 21.36g/$m^2$ | 61.99% | |
| | 48.53% | 20.54 | 63.20% | |
| | 48.53% | 20.50 | 63.81% | 63.15% |
| | 48.51% | 19.78 | 64.11% | ± 0.76 |
| | 48.51% | 20.39 | 62.73% | |
| | 48.51% | 20.48 | 63.07% | |

Drying Rate Calculation

The drying rate was calculated from the drying time to the gloss point, the immobilization solids, the initial solids and the coat weight (equation 9). It was assumed that, regardless of the drying rate, the gloss point occurred at the same solids content as measured under static

conditions. This assumption is acceptable when the drying rate has no effect on the packing structure of the coating.

$$\text{Drying Rate} = \frac{\text{Mass } H_2O_{\text{ initial}} - \text{Mass } H_2O_{\text{ gloss pt.}}}{\text{Area} * \text{Time to gloss pt.}} \quad (9)$$

## DRYING OF COATING FILMS

### Preliminary Experiments

Coatings were applied to plastic films using a Meyer rod. They were dried in a vacuum oven at room temperature at approximately 0.1 torr. Identical coating formulations were dried in the oven preheated to 120°C. A 100-watt light bulb was mounted in the back of the vacuum oven to facilitate the measurement of the time to the gloss point. The average drying rate for coatings dried at 21°C was 0.12 $kg/m^2hr$ and 1.54 $kg/m^2hr$ for those dried at 120°C.

Each dry coating was visually inspected for coat weight uniformity; nonuniform samples were discarded.

### Drying Experiments and Apparatus

In order to separate the effect of drying rate from the effect of temperature on coating structure, a system for controlling the air temperature and humidity was designed and built. Figure 24 is a schematic of the drying system and Fig. 27 is a photograph of the system used.

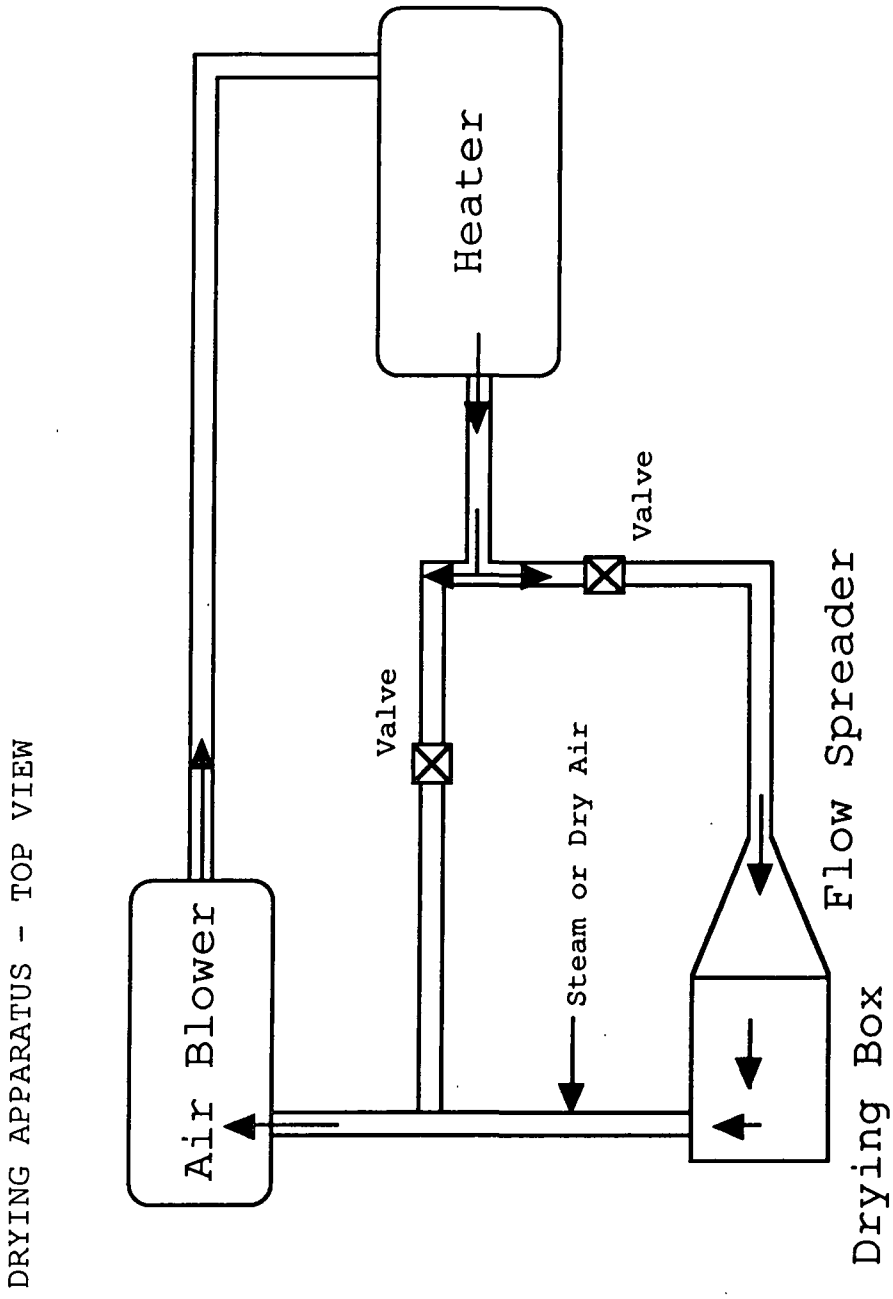


Figure 24. Diagram of the apparatus used to dry hand coatings in a controlled temperature and humidity environment.

An electric heater and blower were used as a hot air source. The hot drying air exiting the electric heater

passed through the flow spreader and then the drying box. The drying box had a false bottom so that wet coatings could be slid into the air stream without disruption of the air flow. Drying air exited the drying box into the feed line of the blower, thus completing a closed air loop.

The pipe leading from the exit side of the drying box to the inlet side of the pump had two access ports. The upper port was used for steam injection to increase humidity and the lower port was used to insert desiccant (Drierite) and/or dry air to lower the humidity. The temperature and humidity of the system was monitored using dry bulb and wet bulb thermocouples mounted in the air stream at the inlet and outlet of the drying box.

## Drying Box

A batch-type drying system was designed and built to control the drying environment and to facilitate the closure of the drying air loop. Figures 25 and 26 are a photograph and a diagram of the drying box respectively. The drying chamber was a tunnel wide enough to contain an 8 x 6 inch coating film. A low velocity (4.1 $ft^3$/min) air stream entered one end of the tunnel through the flow spreader and exited through the conduit at the back end of the tunnel. The coating served as the bottom of the tunnel over which the drying air passed.

The upper boundary of the chamber was a tempered glass plate. The time to the gloss point was determined by observing the coating through the glass window during drying. The bottom of the chamber was one of two metal plates or drawers. Each plate could be slid in and out of the drying box. Only when both drawers were withdrawn was the air loop broken. The top plate (false bottom) was inserted while the system was equilibrating to the desired temperature and humidity. The bottom plate was a tempered steel plate polished to ±0.0005 inch tolerance. The wet coating was applied to the substrate attached to the bottom drawer and slid into the bottom slot (0.3 cm below the upper plate) and the upper drawer was withdrawn. When the upper drawer was removed the bottom drawer was exposed to the air stream.

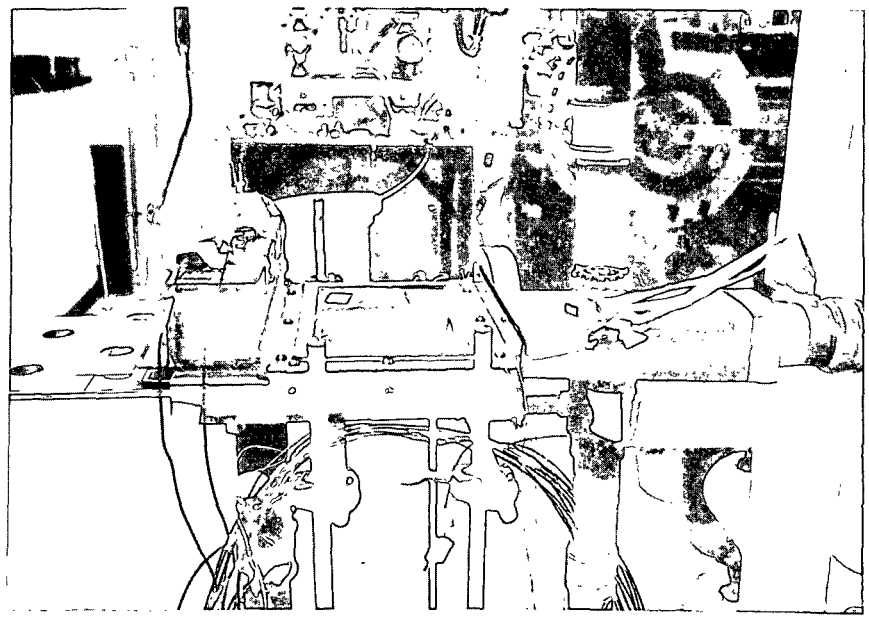

Figure 25. Photograph of the drying box.

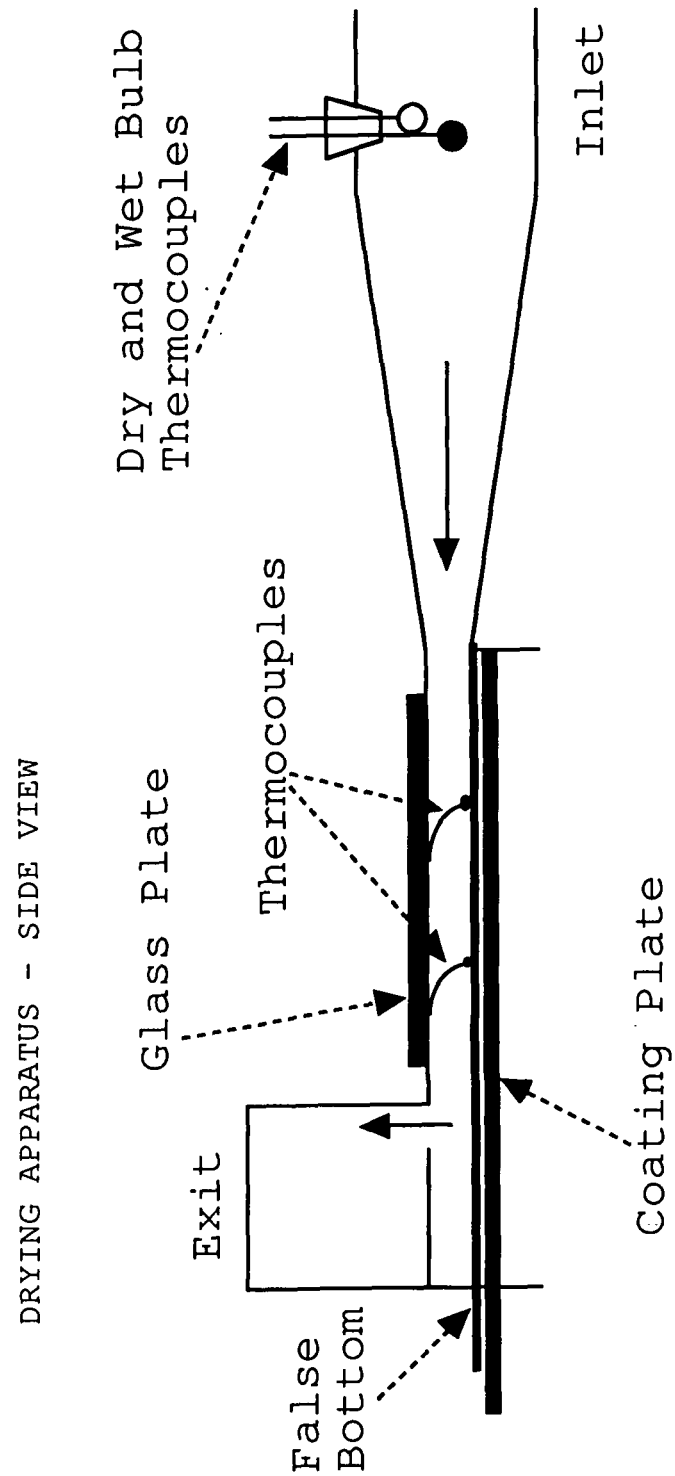


Figure 26. Diagram of the drying box, in which hand applied coatings are dried under controlled temperature and relative humidity.

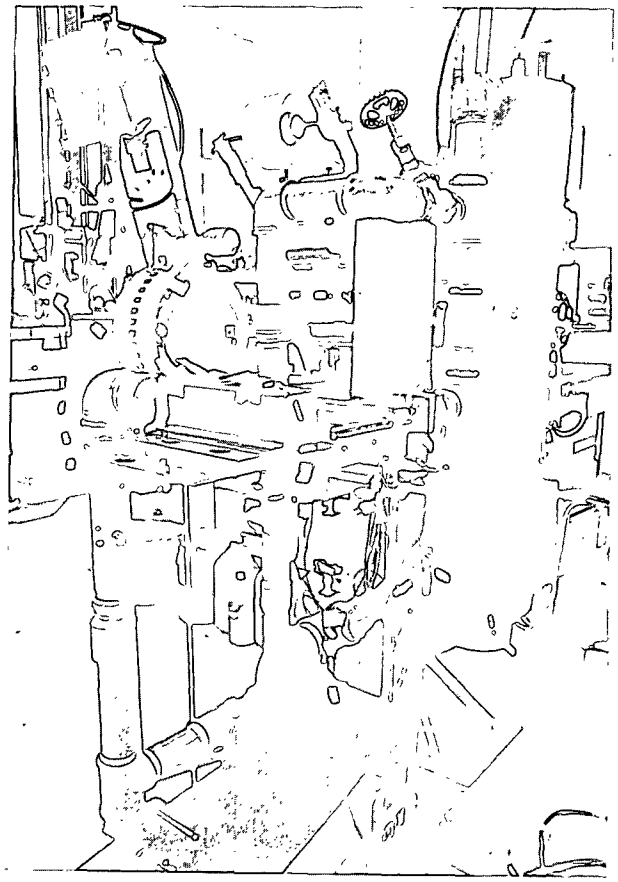

Figure 27. Photograph of the drying system.

To continuously measure the temperature of the drying air and the coating during drying, three thermocouples were mounted inside the drying box. The lead wires for each thermocouple were taped to the inside of the glass plate of the drying box about 1 1/2 inches above the thermocouple. The wires were stiff enough so that when the false bottom was retracted the wires sprang into the coating film. One of the three thermocouples was bent, so that, when the false bottom was opened it fell to within 1/16 inch above the surface of

the coating. Figure 28 is a sketch of the system before and after opening the top drawer.

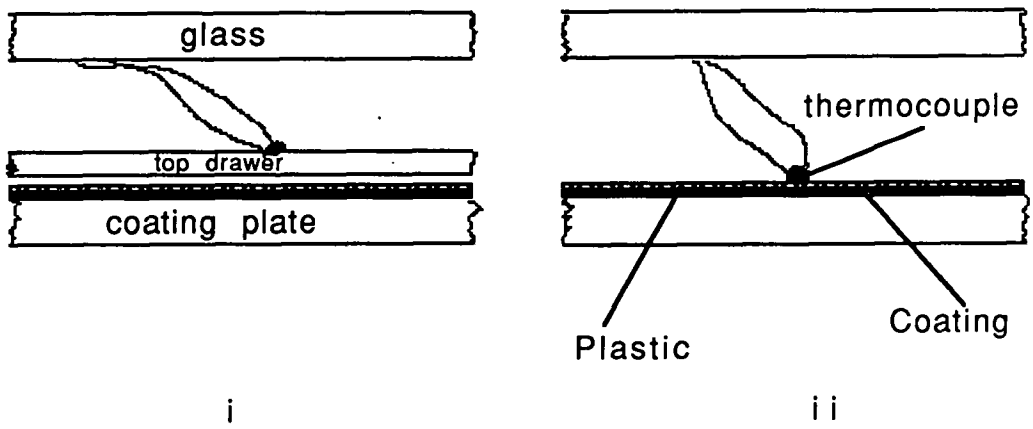


Figure 28. Schematic of the thermocouples mounted inside the drying box i) Before drying ii) During drying.

Continuous temperature acquisition was made using a personal computer connected to the thermocouples through an amplifier (EXP-16 Metrabyte board) and an A to D converter (Das-8 Metrabyte Board). The hardware and software used for temperature acquisition are described in Appendix II.

## Coater Preparation

### Low Humidity

In order to obtain constant temperature and humidity within the drying system, it was necessary for the blower to reach constant temperature and for the heat loss to the room to reach steady state. It was also necessary to purge dust and particulate materials entrained in the air stream from

the system. With the blower and heater running, both drawers of the drying box were retracted and left open for 30 minutes to purge dirt from the system. After 30 minutes, the top drawer of the drying box was closed and a dry air source was connected to the drier line.

Air with a pressure of 5 psig was passed through a flask of desiccant (Drierite) and into the drier line. After 15 minutes, the air in the drying system reached an equilibrium relative humidity (RH) near 15%. The equilibrium RH varied between 12% and 18% RH depending on the temperature of the drying air. Adjustments to relative humidity were made with steam and/or desiccant which could be inserted into the drop leg of the recirculation line.

Medium and High Relative Humidity

Low pressure steam was used to raise the humidity of the drying air. A steam source was attached to the drier line a foot below the drying box exhaust. Steam was injected into the air line until condensation was visible on the glass window in the drying box. After removal of the steam source, leakage of ambient air and a low velocity injection of dry air caused the RH of the system to drop. The drop in relative humidity with time was reproducible, as long as saturation was the starting point. By starting the drying process at different lengths of time after steam injection, it was possible to obtain different levels of relative

humidity. High humidity drying was performed at about five minutes after steam injection. In this case, the relative humidity was 80% to 85%. Medium humidity drying (55% RH) was performed at about 21 minutes after injection.

Coating Application

Preparation of the substrate, coating plate and coating were important to the application process. Condensation of moisture from the drying air onto the coating and backing plate was found to occur when room temperature coatings were dried under high relative humidity. The temperature difference between the coating and the drier air caused the air near the surface of the coating to cool. Cooling the drier air reduced its saturation point and increased the relative humidity to 100% at the coating surface resulting in condensation. Condensation was avoided by heating the coating, coating plate, and substrate to 5°C above the drying air temperature prior to coating.

The coating plate was preheated in a stream of tap water. The substrate was held flat to the plate by laying it down over a thin film of distilled water. It was anchored at the top and bottom with transparent tape. The shims (or tracks) for the Bird bar were attached to the coating plate the same way. The assembled plate was placed in a preheated oven for 15 minutes prior to coating. Figure 29 is a diagram of the assembled coating plate.

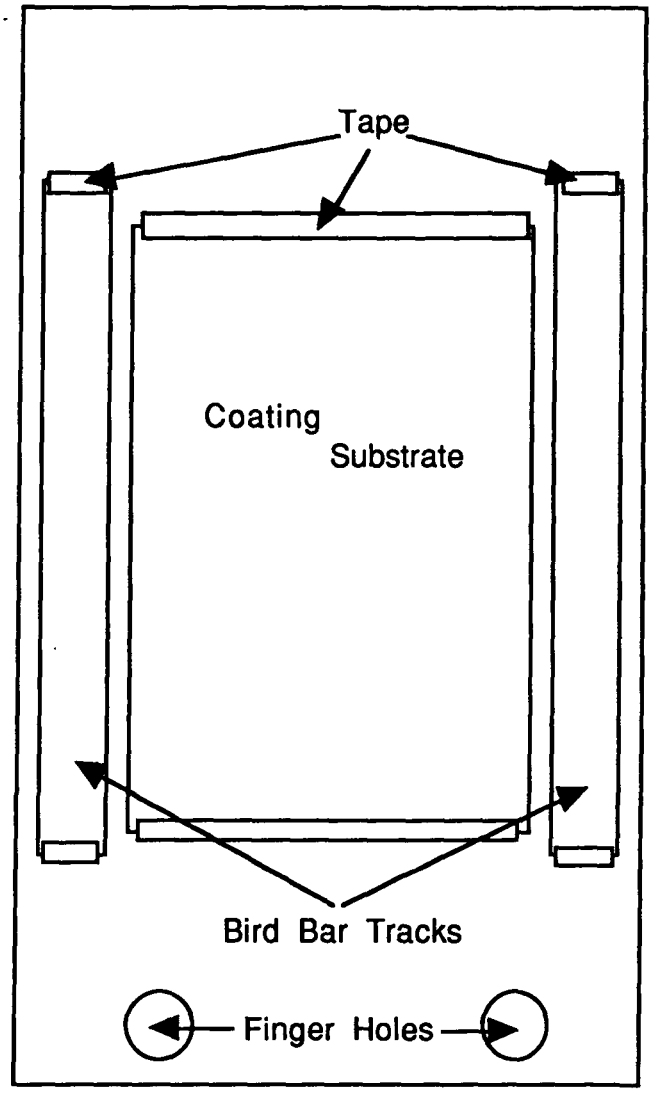


Figure 29. Diagram of the coating plate (bottom drawer) assembled for coating and insertion into the drying box.

The coatings (polystyrene latex and delaminated clay) were heated in a water bath to the desired temperature. Coatings were removed from the bath prior to application; however, the containers were covered to prevent excessive evaporation and changes in solids concentration.

Excess coating was puddled on the transparent tape at the leading edge of the substrate. The bird bar was pulled in an even stroke through the puddle and down the length of the substrate past the transparent tape at the trailing edge. As quickly as possible, the coating plate was inserted into the bottom slot on the drying box and the upper drawer was retracted. Elapsed time from the point where the coating plate was removed from the oven to the point where the coated plate was exposed to drying was about 35 seconds. The time lapse from coating application to the start of drying in the drier was about 7 seconds.

Determination of Drying Rate

The drying rate was determined from the time necessary to reach the gloss point. The gloss point was determined visually. A stop watch was started as the leading edge of the top drawer passed a point 5 inches from the inlet of the drying box as it was retracted. The watch was stopped as the coating, at the 5 inch point, lost its glossy, wet-like appearance. The gloss line was easily detected and the time was reproducible. The average drying rate to the gloss point was calculated using equation 9.

## COATING TEMPERATURE DETERMINATION DURING DRYING

Coating temperature during drying was measured via the thermocouples described earlier. Because the thermocouples,

dropped into the coating from the roof of the drying tunnel, were larger than the coating layer was thick, they were exposed to both the coating and the drier air. As a result, the coating temperatures measured during the coating trials were believed to be inaccurate. The acquisition of the coating temperature during drying was desired to determine if there was a temperature gradient present in the coating layer during drying, and to determine the extent of cooling of the coating layer caused by evaporation from the surface. An alternative method was used to measure the interface temperature between the coating and the substrate.

Thin film resistors have been used to measure temperatures of interfaces and surfaces under a variety of conditions(118-122). Platinum resistors have been used by Bellhouse and Bellhouse to measure the skin friction of air, blood and water(118). Grant *et al.*(119) used platinum thin film resistors to measure the temperature fluctuations in turbulent sea water. Hanson(120), Waterhouse and Scott(121) each used platinum thin film resistors to measure the heat transfer at solid-gas interfaces in a shock wave. Meyer's theories(122), proposed during development of a meter for use with thin film thermometers to measure heat flux, have enabled thin film resistor use in studies of dynamic heat transfer processes.

Thin film resistance thermometers were used to determine the coating temperature and the heat transfer rates during

drying. To avoid disrupting the air flow pattern near the surface of the plate, and to avoid variations in thickness of coating caused by thermometers placed under the coating, thin platinum films were fired into a piece of window glass. The glass plate was of the same dimensions as the polished steel backing plate used to support the coating substrate.

Hanovia #05 platinum ceramic paint (2 grams) was purchased from Dolphin Ceramics in Jacksonville, Florida. The paint was composed of platinum suspended in a camphor-based medium. Platinum paint was brushed onto the surface of the glass plate, previously cleaned with concentrated sulfuric acid followed by acetone, using a #3 artist paint brush. Film shape and dimensions were controlled by masking the glass with tape. The paint was allowed to set and a second coat was painted over the first. The glass plate was then fired in a muffle furnace, while placed atop a flat steel plate on four masonry bricks. The furnace was heated at 100°C/hr to 640°C where it was held for 10 minutes. The glass was cooled slowly in the furnace with the door slightly ajar.

Leads from the resistors to the edge of the glass plate were made of a silver paint applied like the platinum paint and fired at the same time as the platinum films. The silver leads were polished with a number 7 white polishing compound. The resistors and leads on the glass plate were covered with

a thin layer of formvar (polyvinlyformal) to prevent shorting through the wet coating.

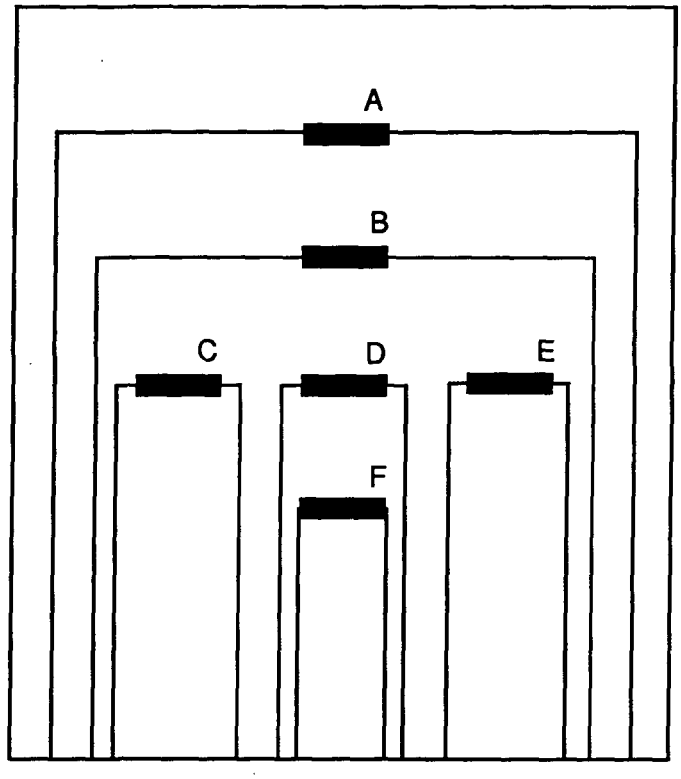


Figure 30. Diagram of the glass plate used to measure interface temperatures in the drying system for hand coatings.

Twenty-two gauge copper wires were soldered to the ends of the silver leads using standard 60/40 rosin core solder. To relieve stress at the solder joints, terminal connectors were glued to the bottom of the glass. The copper leads were threaded through the terminals and pinched in position. The opposite ends of the wires (about six inches from the end of the glass plate) were fitted with male couplers. Female couplers were connected to similar copper wires which connected the resistors to the circuitry necessary for

continuous measurement of the resistance of the platinum films.

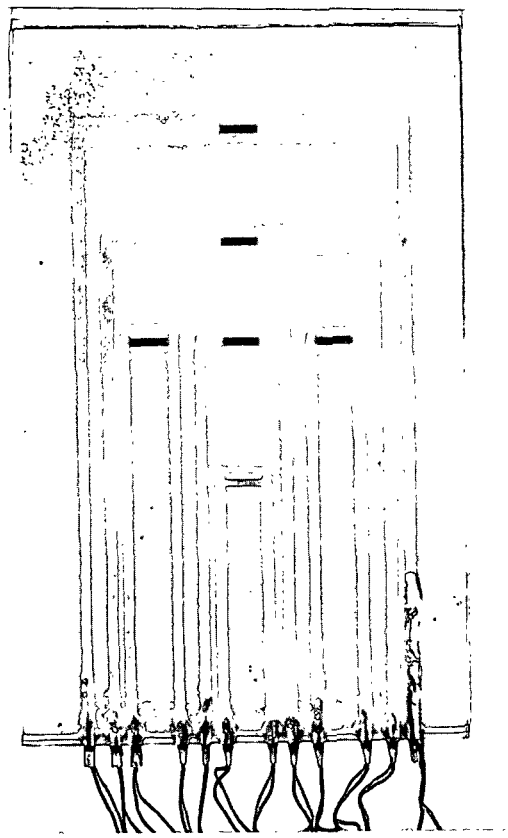

Figure 31. Photograph of the glass plate fitted with thin film resistors used to measure the interface temperature between the coating and the substrate during drying.

Temperature Acquisition System

Each resistor on the glass plate served as one leg of a Wheatstone bridge (Figs. 32 and 33). When a constant current is applied to the bridge the first order change in bridge output with resistance is:

$$\Delta E = i\Delta R \qquad (10)$$

where $\Delta E$ is the change in voltage across the bridge, i is the current and $\Delta R$ is the change in resistance. The resistance of most metals, including thin films, is approximated by(123):

$$R = R_o[1 + \alpha(T-T_o)] \qquad (11)$$

where $R_o$ is the reference resistance at reference temperature $T_o$, R is the resistance of the film at a temperature T, and $\alpha$ is the temperature coefficient of resistance (TCR). The magnitude of the TCR is dependent upon the thickness and composition of the film. It is usually determined from the slope of a temperature resistance curve developed for each resistor. Combining equations 10 and 11 an expression for change in temperature as a function of the change in voltage across the bridge circuit can be derived:

$$\Delta T = \Delta E/(i\alpha R_o) \qquad (12)$$

Using the same acquisition system used to acquire thermocouple data, the voltage across the Wheatstone bridges was measured as a function of time. Therefore, by expressing the change in voltage as a function of time, the change in temperature at the resistor can be calculated as a function of time:

$$T(t) = T_o + [\Delta E(t)]/(i\alpha R_o) \qquad (13)$$

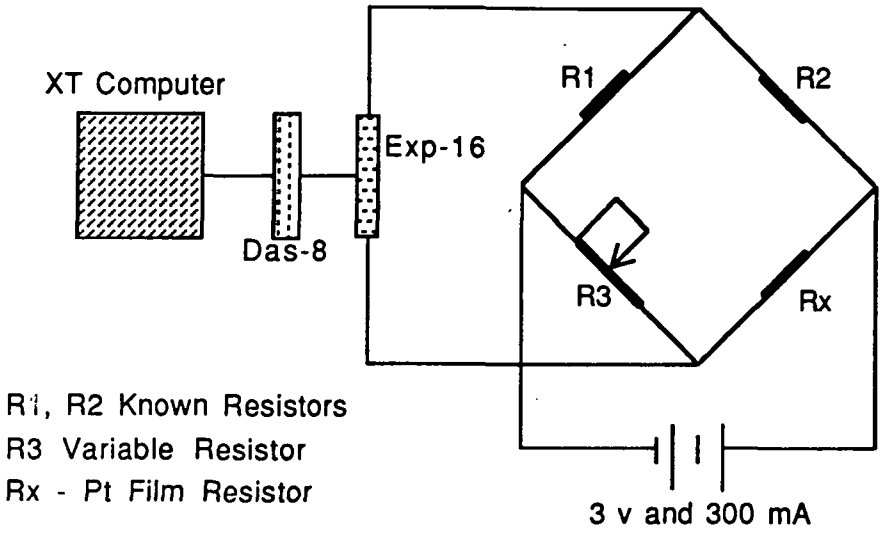


Figure 32. Wheatstone bridge arrangement used for determination of the resistance change of the platinum films on glass.

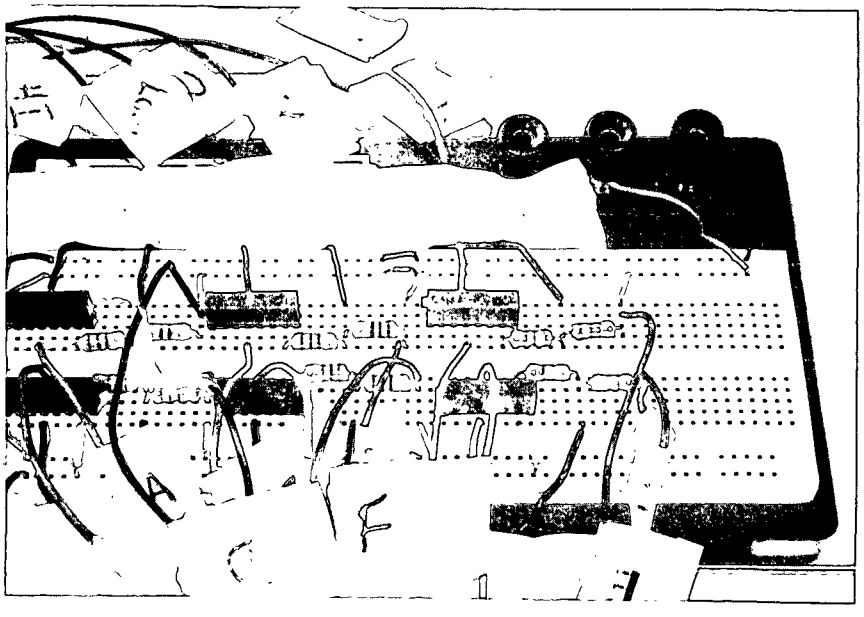

Figure 33. Photograph of the circuit board of Wheatstone bridges used in measuring the resistance of platinum thin film resistors during drying.

A temperature/resistance curve for each resistor was developed by measuring its resistance after equilibrating in an oven held at a known temperature. At the same time, the voltage across the corresponding Wheatstone bridge, previously balanced at 0°C, was measured. A second trial was conducted using an oil bath. The resistors were immersed in oil and held at constant temperature for twenty minutes, at which time the resistance and voltage across each bridge was measured. The TCR was calculated from the resistance data, and $1/i\alpha R_o$ was determined from the voltage data. Table VI contains the properties of the resistors fired into the glass plate.

Table VI

Resistor Properties

| Resistor Code | Resistor Area $mm^2$ | $R_o$ ohms | $\alpha$=TCR 1/°C | $\alpha R_o$ ohm/°C | $1/i\alpha R_o$ °C/volt |
|---|---|---|---|---|---|
| A | 45 | 58.1 | 0.00076 | 0.0442 | 0.000528 |
| B | 45 | 38.6 | 0.00085 | 0.0328 | 0.000528 |
| C | 45 | 81.8 | 0.00078 | 0.0641 | 0.000507 |
| D | 45 | 77.5 | 0.00074 | 0.0572 | 0.000481 |
| E | 45 | 77.3 | 0.00075 | 0.0579 | 0.000509 |
| F | 45 | 45.3 | 0.00075 | 0.0338 | 0.000473 |

Interface Temperature Measurement in Drier

The resistors in the glass plate were used to measure the temperature at the coating/substrate interface during drying. Trials were conducted under various conditions to obtain temperature response curves in the experimental drier.

The glass plate was handled in the same fashion as the coating base plate during the coating trials except that no substrate was used. Table VII contains the conditions of each trial.

Table VII

Parameters Used to Measure Temperature Response During Drying in the Experimental Drier

| Trial Code | Air Temperature (°C) | Application Temperature (°C) | Relative Humidity (%) |
|---|---|---|---|
| PT1-PT4 | 53°C | 23°C | no coating |
| PT5-PT6 | 53°C | 58°C | no coating |
| PT17 | 52°C | 54°C | 15% |
| PT18 | 52°C | 54°C | 15% |
| PT19 | 52°C | 54°C | 15% |
| PT20 | 52°C | 54°C | 25% |
| PT21 | 52°C | 54°C | 85% |
| PT22 | 34°C | 35°C | 15% |
| PT23 | 34°C | 35°C | 15% |
| PT24 | 35°C | 36°C | 15% |
| PT25 | 35°C | 36°C | 85% |
| PT26 | 35°C | 36°C | 85% |
| PT27 | 35°C | 36°C | 85% |
| PT28 | 35°C | 35°C | 55% |

## DRYING EXPERIMENTS

Preliminary drying experiments performed in the vacuum oven were designed to determine if a change in the coating structure could be obtained by changing the drying conditions. Different drying rates were at first obtained by drying at two different temperatures 100°C apart; because of the manner in which the drying rate was changed it was impossible to tell if changes in coating structure were caused by the temperature difference, the change in drying

rate or both. In contrast, by using the drying apparatus described earlier, the temperature and evaporation rate could be controlled independently through control of the relative humidity at a fixed temperature. A set of coating trials was performed using the experimental drier to test the effect of drying rate (only) on coating structure.

The experimental plan involved a $2^3$ factorial design. The two variables were temperature and humidity. Three levels of each variable were chosen to produce mild drying conditions and extreme or harsh drying conditions as well as a level in between. Table VIII contains a summary of the conditions employed in each trial.

Table VIII

Experimental Parameters of Coating Trials

Clay and Latex Coatings on Plastic

| Sample Code | Pig. Type | Air Temp. (°C) | Rel. Humid. (%) | n | Time After Steaming (min.) | Gloss Point (sec.) | Drying Rate $kg/m^2hr$ |
|---|---|---|---|---|---|---|---|
| T75R15 | clay | 73°C | 16% | 4 | -- | 4.2 | 17.05 |
| T75R85 | c | 73°C | 83% | 4 | 2 | 95.2 | 0.75 |
| T55R15 | c | 57°C | 14% | 8 | -- | 6.2 | 11.55 |
| | latex | 56°C | 15% | 4 | -- | 4.2 | 9.11 |
| T55R55 | c | 55°C | 56% | 4 | 21 | 60.7 | 1.19 |
| | l | 55°C | 56% | 4 | 21 | 11.3 | 3.39 |
| T55R85 | c | 56°C | 85% | 8 | 5 | 108.0 | 0.66 |
| | l | 55°C | 86% | 4 | 5 | 50.9 | 0.75 |
| T35R15 | c | 34°C | 16% | 4 | -- | 25.0 | 2.86 |
| | l | 35°C | 15% | 4 | -- | 15.5 | 2.47 |
| T35R55 | c | 34°C | 53% | 4 | 23 | 65.1 | 1.10 |
| | l | 35°C | 54% | 4 | 23 | 27.2 | 1.41 |
| T35R85 | c | 34°C | 86% | 4 | 7 | 128.0 | 0.56 |
| | l | 35°C | 87% | 4 | 7 | 61.0 | 0.63 |

(Table VIII continued)

Clay and Latex Coatings on Membrane Filter

| Sample Code | Pig. Type | Air Temp. (°C) | Rel. Humid. (%) | n | Time After Steaming (min.) | Gloss Point (sec.) | Drying Rate $kg/m^2hr$ |
|---|---|---|---|---|---|---|---|
| T55R15p | c | 55°C | 14% | 1 | -- | 5.0 | 16.26 |
| | l | 56°C | 15% | 1 | -- | 2.2 | 19.18 |
| T55R55p | c | 57°C | 55% | 1 | 21 | 35.7 | 2.28 |
| | l | 55°C | 56% | 1 | 21 | 12.4 | 3.40 |
| T55R85p | c | 56°C | 83% | 1 | 5 | 75.0 | 1.08 |
| | l | 54°C | 86% | 1 | 5 | 38.7 | 1.09 |
| T35R15p | c | 34°C | 15% | 1 | -- | 19.6 | 4.15 |
| | l | 35°C | 16% | 1 | -- | 14.9 | 2.83 |

n = replications, c = clay, l = latex, pig. = pigment

Several problems were encountered during the coating trials. The latex dispersion was discovered to be unstable above 73°C. Above 73°C pigment flocculation made uniform coating impossible. In addition, all the clay coatings dried at 73°C and 55% relative humidity had significant coat weight variability, and thus, were omitted from the analysis. Additional trials under those conditions were not performed because a significant range of drying rates was obtained in other trials. Coatings applied to the porous media were fragile and tended to disintegrate during transport, disrupting the structure of the coating. Several areas with minimal damage were salvaged for analysis, but the statistical significance of these analyses is suspect.

The acceptable coatings from the trials described above were analyzed for pore volume distribution as described in the next section.

# METHODS OF ANALYSIS

## SAMPLE PREPARATION

### Cutting Samples

Samples for coating structure analysis were cut from the coated plastic film with a razor blade. Figure 34 is a sketch of the sample cutting procedure.

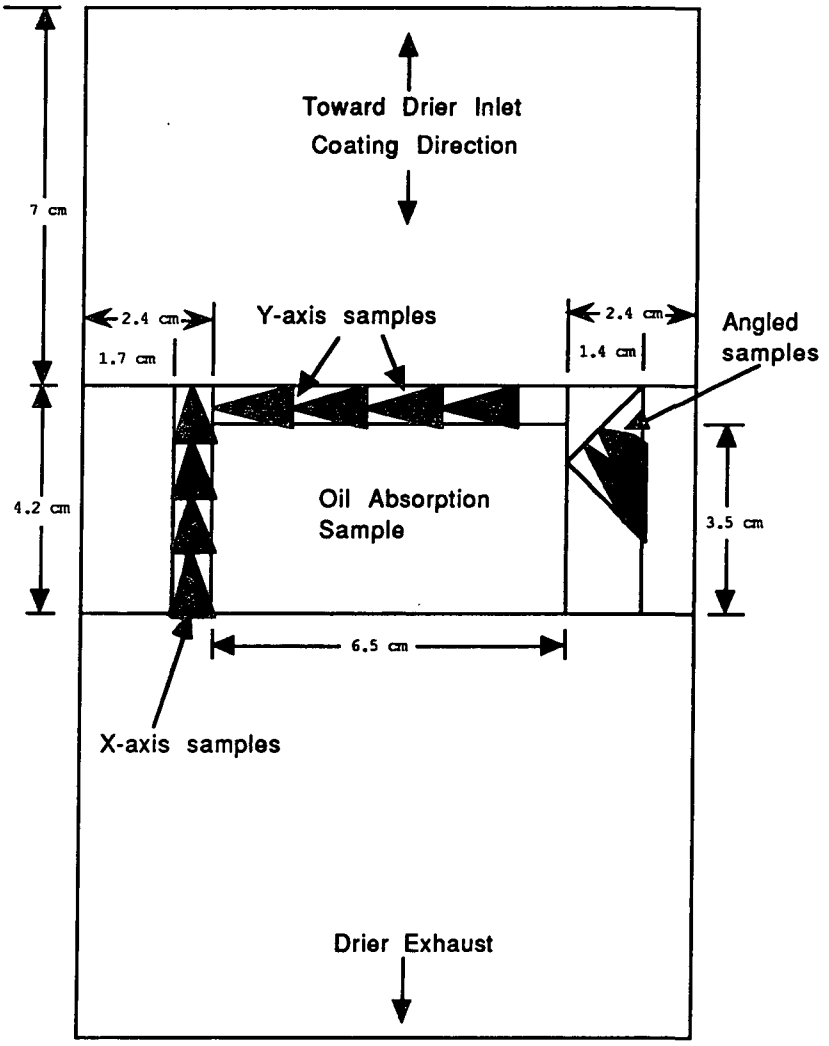


Figure 34. Sketch of the locations from which the samples for embedding and sectioning were cut from a coating applied to plastic.

## Embedding

Samples cut from the coated plastic film were dried under vacuum for three days. Dried samples were placed in embedding capsules and covered with freshly made, ultra low viscosity embedding resin (purchased from Electron Microscopy Sciences). The capsules were returned to the desiccator and placed under a vacuum until the surface of the samples released entrapped air. The capsules were left in the desiccator for two days before beginning polymerization of the resin. Polymerization was accomplished by heating the capsules to 70°C and holding them at that temperature for 12 hours. The embedding capsules were cut away from the embedded samples and discarded.

The latex pigment was found to be soluble in most embedding resins; those in which it was not soluble caused dispersion of the latex particles. No successfully embedded samples were obtained from polystyrene/acrylate coatings.

## Sectioning

Sectioning was performed according to Abad's technique(124). Thin sections (<0.1μm), were made by cutting embedded coatings with a diamond knife, at a sectioning angle of 6°. Sections were floated onto distilled water and compression wrinkles were relieved with 1,2-dichloroethane vapors. Sections were collected on 2000 μm single hole nickel grids and placed face down on a thin formvar film.

Sections were dried under high humidity at 60°C on a hot plate. Grids were punched through the formvar film, collected and stored.

Four sections were cut from at least three embedded samples of each coating. The sections were examined with a stereomicroscope and prioritized by apparent damage for examination by transmission electron microscopy (TEM).

## MICROSCOPY EXAMINATION

### Scanning Electron Microscopy

Samples were examined using a JEOL 35C scanning electron microscope (SEM). Resolution of the surface of a thin coating cross-section was good at low magnification (500X). At the magnifications suitable for resolution of individual clay particles, adequate resolution was not obtained.

### Transmission Electron Microscopy

Microscope time was purchased from the Department of Ultramicrostructural Research at the University of Georgia in Athens (Mark Farmer) and the Department of Biology at Georgia State University (Robert Simmons). Micrograph negatives were developed by the author in the dark rooms provided by the above Universities.

Each grid obtained from the sectioning procedure contained between one and four sections. Each section was

examined for continuity of the coating layer, number of holes and amount of wrinkling. Sections with few holes, no wrinkles and those containing areas which did not show signs of damage prior to embedding, were photographed at 80 keV and 8,000X to 14,000X using a JEOL 100-CX II transmission electron microscope. Because of the high magnification, more than one micrograph was frequently necessary to capture entire coating cross-sections. When more than one photomicrograph was necessary, the photographed areas were overlapped to avoid missing details.

## PORE VOLUME

Total pore volume of a coating layer can be used as a rough measure of the coating structure, and most end-use properties of coated papers have been related to the total void volume of the coating. For these reasons, studies of the void fraction of various coatings can be found in the literature(6,7,64,70). Measurement of the relative void volume of the coatings produced in this study was necessary to ensure that the coatings were comparable to other works and as a method of checking the image analysis technique which was developed to measure the void distribution through the coating thickness.

Mercury Porosimetry

Mercury porosimetry has been employed to measure the pore size distribution of coating films(13,16,98,125). It can also be used to measure the total pore volume. Briefly, mercury is forced into the pores of an evacuated sample. The volume of mercury forced into the pores per change in applied pressure is used to determine the pore size distribution of the sample. The total pore volume of the sample is equivalent to the total volume of mercury intruded.

A large area (20 to 40 $cm^2$) of sample was required for accurate measurement using mercury porosimetry, because of the small volume per unit area of voids in a coating layer. To accommodate the large area, samples were placed side by side in the sample cell. The close proximity of the samples resulted in apparent pores (intersample pores) whose size and total volume were greater than pores usually found within a coating layer (intrasample pores). To compensate for the apparent pores, the void volume was calculated from the difference between the volume of mercury intruded and the volume of mercury in the intersample pores (Fig. 35).

Oil absorption

The oil absorption technique for measuring the total pore volume of coatings applied to non-porous media described by Lepoutre and Rezanowich(6) was modified to handle binderless clay coatings.

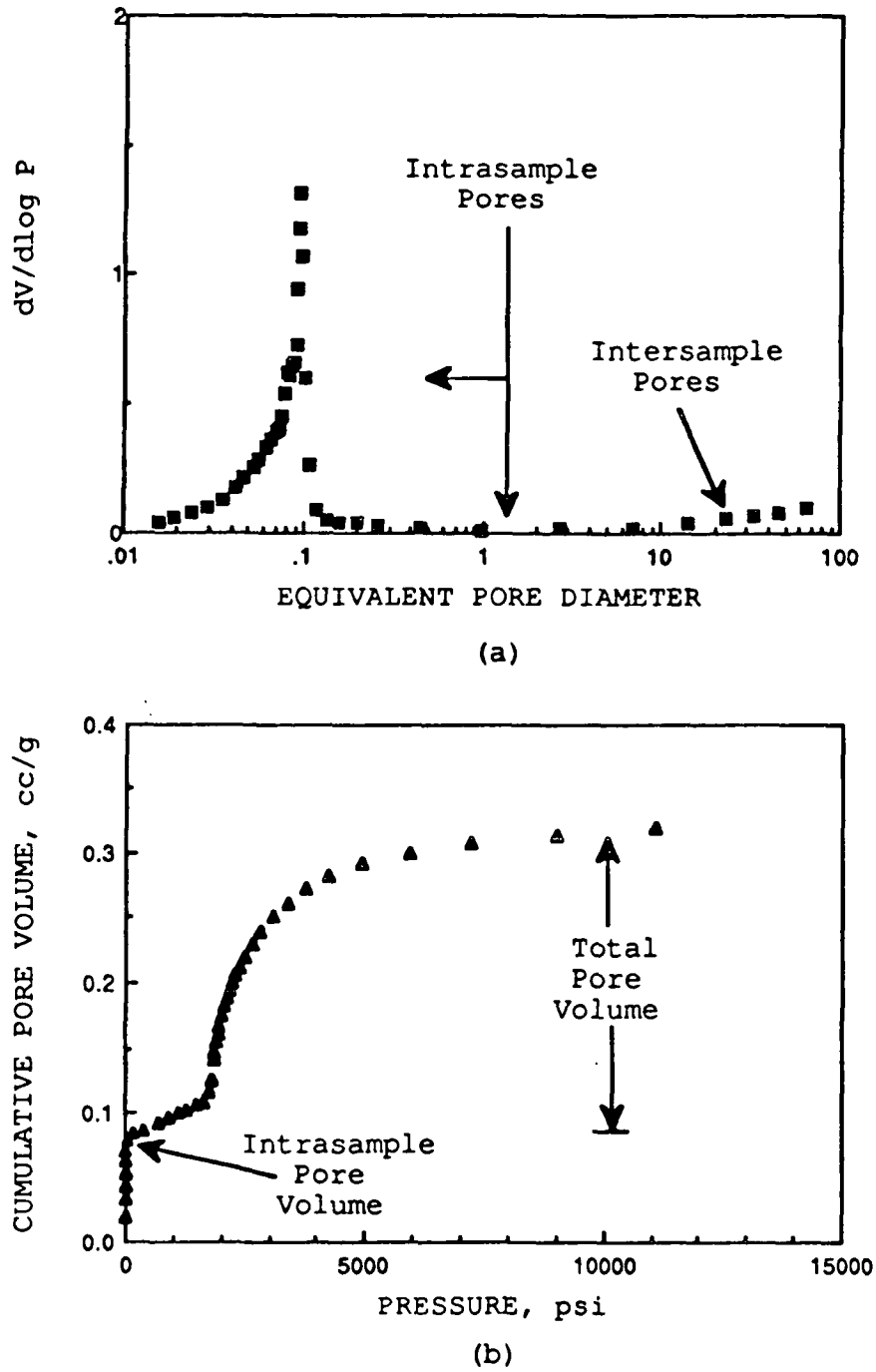


Figure 35. Mercury porosimetry results from a clay coating on non-porous media. a) Pore size distribution showing regions of inter- and intra-sample pores. b) Cumulative pore volume versus pore size showing large volume of intersample pores.

Samples cut from coated plastic were placed coating side up on a piece of Whatman's #41 filter paper. Twenty drops of vacuum pump oil (density 0.868 g/cm$^3$, refractive index 1.4806) were dropped onto the sample. The oil covered sample was placed in a desiccator. A slight vacuum was pulled over the sample for about 30 minutes or until the oil completely spread on the coating surface (Fig. 36). The excess oil, which appeared as a transparent glossy film on the surface, was removed by blotting with filter paper until the translucency of the sample disappeared. Samples were weighed and the pore volume calculated from the coat weight and densities of the clay and oil.

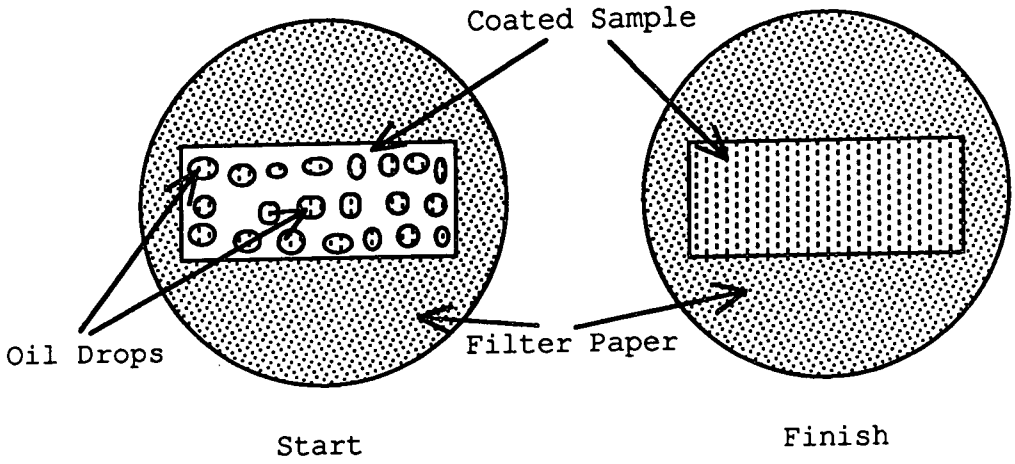


Figure 36. Schematic diagram of oil absorption test before and after exposure to vacuum.

## IMAGE ANALYSIS

Mercury porosimetry and oil absorption provide quantitative information about the bulk structure of the

coating. Different process variables may not affect the bulk structure of the coating but may instead cause changes in the local packing structure. It has been hypothesized here that both the bulk and the local pigment packing are a function of drying rate. Therefore, it was necessary for a technique to be developed to measure the internal structure of coating films.

Climpson and Taylor(5) and Andersson(100) have used image analysis techniques to measure the internal structure of coating films and paper respectively. From micrographs of thin coating cross-sections, Climpson and Taylor measured the pore size distribution using ellipsoid pores as a model. Pore dimensions were calculated from the longest pore projection on the x-y plane. From thin cross-sections of paper, Andersson(100) measured the density distribution through the paper thickness using image analysis.

The technique developed for this study was a combination of the two procedures where both pore characteristics and density distributions of the cross-sections were produced. The information from the analysis was used to test the hypotheses stated earlier.

Technique Overview

Images obtained from the TEM observation of coating cross-sections were used in the analysis. The images were used as either photo positives or photo negatives. The only

processing difference was the type of lighting (reflected or transmitted) used during digitization of the image. Micrograph negatives, although more difficult to use, were preferred because dimensional changes and contrast problems resulting from print making were eliminated.

Digitization of the TEM micrographs was accomplished through an MTI Series 68 video camera. The signal from the camera was received by a (512 x 512) frame grabber housed in a Tracor Northern TN-8502 image analysis system. The frame grabber assigned an intensity value to each pixel of the camera image. The value assigned was between 0 and 255 depending on the magnitude of the signal received; the image analysis computer therefore interpreted the image as a matrix of intensity values. The picture shown in Fig. 37 is an enlarged portion of an image with its corresponding intensity or grey levels.

Once the image is in digital form it can be manipulated mathematically. For instance, the matrix of intensities representing the image can be multiplied or divided by a constant to increase or decrease its brightness. The intensity range can also be converted to a log function, maximizing differences in the darker areas while minimizing differences in the white areas; several other functions can be applied to the intensity scale as well.

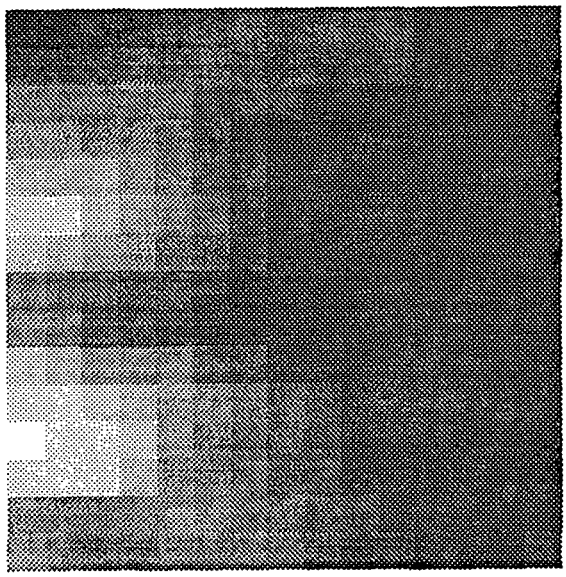

| | | | | | | | | | | | | | | |
|---|---|---|---|---|---|---|---|---|---|---|---|---|---|---|
| 99 | 100 | 101 | 102 | 104 | 106 | 106 | 105 | 105 | 103 | 101 | 99 | 99 | 99 | 98 |
| 106 | 106 | 108 | 109 | 110 | 109 | 107 | 105 | 102 | 101 | 101 | 100 | 100 | 99 | 99 |
| 115 | 115 | 116 | 115 | 113 | 110 | 106 | 102 | 100 | 99 | 100 | 100 | 100 | 100 | 100 |
| 121 | 121 | 120 | 118 | 114 | 109 | 104 | 100 | 99 | 99 | 100 | 100 | 100 | 100 | 99 |
| 129 | 128 | 126 | 121 | 116 | 110 | 105 | 100 | 98 | 97 | 97 | 97 | 97 | 96 | 96 |
| 135 | 134 | 130 | 125 | 119 | 112 | 105 | 100 | 98 | 96 | 95 | 95 | 95 | 95 | 95 |
| 131 | 128 | 125 | 121 | 116 | 110 | 104 | 99 | 97 | 96 | 95 | 94 | 94 | 94 | 95 |
| 119 | 116 | 113 | 110 | 107 | 103 | 100 | 97 | 96 | 95 | 95 | 94 | 94 | 94 | 95 |
| 119 | 114 | 110 | 106 | 103 | 100 | 98 | 97 | 96 | 95 | 95 | 94 | 94 | 95 | 95 |
| 132 | 127 | 123 | 118 | 114 | 109 | 104 | 100 | 98 | 96 | 95 | 94 | 95 | 94 | 95 |
| 139 | 136 | 132 | 128 | 123 | 118 | 112 | 106 | 102 | 99 | 97 | 95 | 95 | 95 | 95 |
| 145 | 143 | 139 | 131 | 126 | 117 | 112 | 107 | 103 | 99 | 97 | 96 | 95 | 95 | 95 |
| 137 | 137 | 134 | 129 | 123 | 117 | 112 | 108 | 103 | 99 | 98 | 96 | 96 | 96 | 96 |
| 119 | 118 | 118 | 118 | 119 | 116 | 113 | 109 | 105 | 101 | 99 | 98 | 97 | 97 | 98 |
| 122 | 117 | 114 | 114 | 115 | 116 | 115 | 112 | 108 | 103 | 101 | 99 | 98 | 99 | 102 |

(a) (b)

Figure 37. a) Grey image. b) Grey (intensity) value assigned to each location (pixel) of image a.

For quantitative analysis of the packing structure of a coating film, it is necessary to differentiate between pigment and pores. For differentiation, the grey level of the pigment must be different from the grey level of the pores; this being the case, the image can be altered (converted to a binary image) to show regions of pores and regions of pigment. A grey level is chosen which divides the pores from the pigment, then every pixel or image element that has a grey level greater than the divider is adjusted to 255 (or an intensity of 100%) and every pixel at or below the level is turned off (or to 0%). The resultant image is black and white, with (for example) the white areas representing pores and the black areas representing pigment. The black and white (binary) image is used to perform quantitative image measurements.

## Procedure Details

### Image Acquisition

Using a copy stand, micrographs of coating cross-sections were illuminated by four quartz lamps positioned two feet above and 15° vertically offset from the micrograph. Micrograph negatives were illuminated by a single quartz lamp from below through a diffusing plastic sheet. Excess light was limited by turning off the room lights and by blocking the non-image areas on the copy stand with heavy corrugated board. This action prevented over saturation of the camera detector. The signal from the MTI Series 68 camera was adjusted for size, focus, brightness and contrast while watching a real time image as acquired by the Tracor image analysis system. The images for processing were produced from an average of one hundred frames received from the camera. Kalman frame averaging was used to minimize random spatial noise in the image. The image was calibrated manually from the micrograph magnification and the known width of the micrograph. For a typical digitized image each micrometer was represented by forty five pixels.

### Image Processing

Due to hardware and computer memory limitations some resolution was lost and some contrast variation was introduced during digitization. Some processing of the image was necessary to facilitate the accurate conversion of the

grey image to a binary image. For example, in Fig. 37, it would be difficult to trace a line exactly separating the pigment (white) from the voids. The pigment particles were made more distinct with enhancement algorithms. For most of the micrographs the edges of the pigment particles were enhanced through the use of a sharpening filter. The sharpening filter is a convolution filter used to adjust the intensity of a pixel based on the intensity of the pixels around it. The operation of convolution filters is described in texts concerning image processing(126). Figure 38 shows an example of the use of a sharpening filter.

| | | |
|---|---|---|
| 0 | -1 | 0 |
| -1 | 10 | -1 |
| 0 | -1 | 0 |

(a)

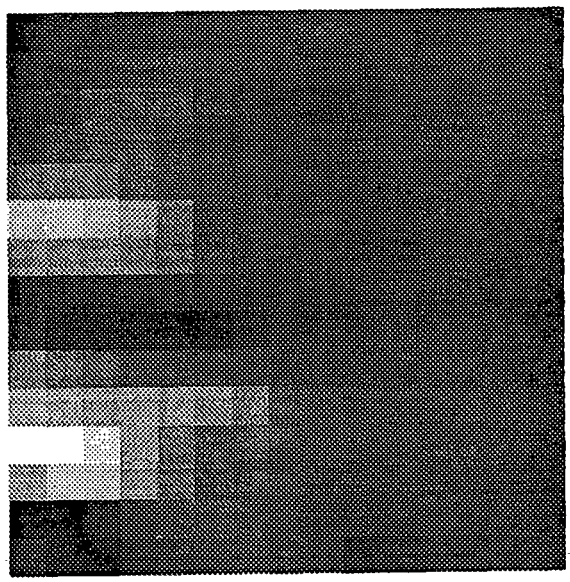

(b)

Figure 38. a) 3 x 3 Sharpening filter. b) Result of applying the sharpening filter to a grey image.

The effect of the filter is dependent upon its size and magnitude. The example in Fig. 38 uses a 3 x 3 sharpening filter. The filter is designed to enhance the contrast along

intensity lines. The size of the filter controls the size of the regions that are separated; a 3 x 3 filter is not efficient for enhancing the contrast differences of particles larger than 15 to 20 square pixels. The smallest areas of interest in the coating cross-sections were about 10 pixels in the x-direction and 5 pixels in the z-direction. A 5 x 5 sharpening filter was used on each micrograph after contrast adjustment.

Depending upon the quality of the micrograph, some images needed contrast smoothing and all the images had significant contrast variations. Contrast variations cause problems in converting the image to a binary. If, for example, in one portion of a micrograph the pigment particles have a 20% higher intensity value than the pigment in another portion, the area that has the higher intensity values could have errors when the intensity level for binary conversion is chosen; the pigment in the region of greater intensity could be mistaken for pores. Figure 39 is a sketch illustrating the potential problem of local contrast variations. In Fig. 39 the background intensity of 75 in the left half of the image requires that intensity values 74 and below be converted to 0 and pixels of intensities 75 and up be converted to 255 for detection of the particles with intensity 40. As shown on the right in Fig. 39, such a conversion would cause the particles of intensity of 80 to be erroneously analyzed as pores.

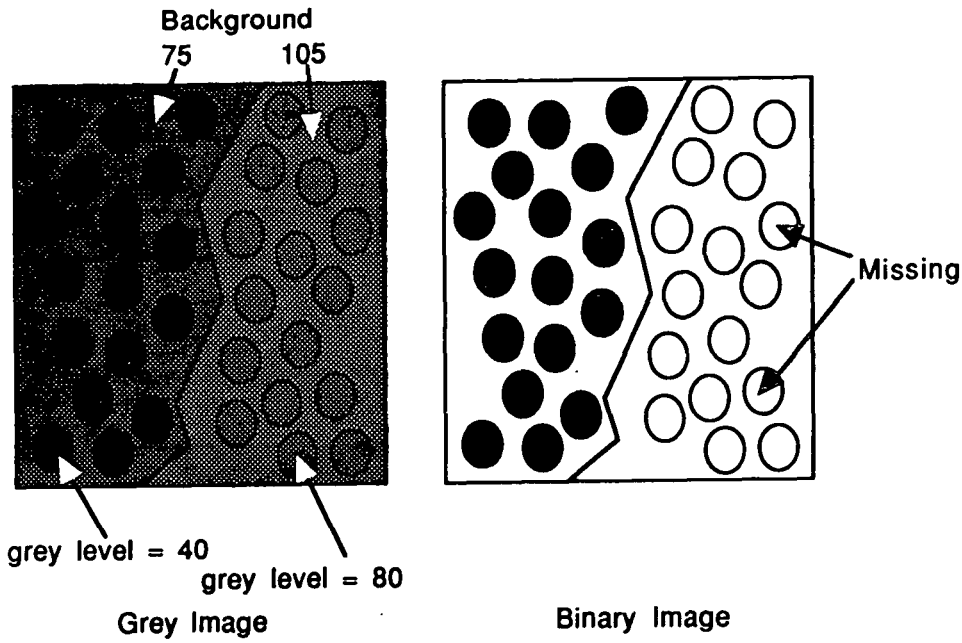


Figure 39. Sketch of problems contrast variations can cause when converting a grey image to a binary image.

Two methods used in combination were employed to overcome contrast variations. Using a 7 x 7 smoothing filter repeated eight times, the images were smoothed until no fine details remained. The operation of the smoothing filter is shown in Fig. 40. The smoothed image was reversed (the dark areas made light) and subtracted from the original image to correct broad variations in contrast.

| | | |
|---|---|---|
| 1 | 1 | 1 |
| 1 | 1 | 1 |
| 1 | 1 | 1 |

Smoothing Filter

| | | | |
|---|---|---|---|
| 100 | 108 | 105 | 102 |
| 102 | 109 | 107 | 109 |
| 111 | 120 | 141 | 138 |
| 122 | 125 | 138 | 140 |

Image

| | | | |
|---|---|---|---|
| 100 | 108 | 105 | 102 |
| 102 | 111 | 115 | 109 |
| 111 | 119 | 125 | 138 |
| 122 | 125 | 138 | 140 |

First Pass Smooth

| | | | |
|---|---|---|---|
| 100 | 108 | 105 | 102 |
| 102 | 110 | 114 | 109 |
| 111 | 118 | 124 | 138 |
| 122 | 125 | 138 | 140 |

After Four Passes

Process [(1*100)+(1*108)+(1*105)+...+(1*141)] = 111

Figure 40. Operation of a smoothing filter.

Contrast variations also existed that were not affected by the smoothing filter. Local contrast variations were handled using a Rank Smoothing filter. This filter is a separable filter allowing independent treatment of the x and y directions. A rank filter may be set to any dimensions and does not necessarily have to be square. The rank of the filter determines the value for replacement. The filter ranks the values masked from highest to lowest; a 50% rank filter would replace the center position with the middle value of the ranking. Assuming a 10 pixel filter, a 20% rank would place the second lowest value in the center position. Subtracting the smoothed images from the originals resulted in less local contrast variation.

Further correction for contrast variations was made by dividing the micrograph into subunits for analysis. The advantage was that the magnitude of the contrast variation was combatted by changing the size of the area to process. The procedure required that areas of parallel sides be digitally cut from the image and pasted into another work area. Conversion to a binary was made on the small pieces, which were reassembled for analysis after conversion. The pieces cut were 1/4 to 1/2 the width of a micrograph (1.5 to 3.5 μm) and one micron thick. When reassembled, single micron thick layers were analyzed to produce distributions of pore properties across the coating thickness. The process is shown in Fig. 41-45.

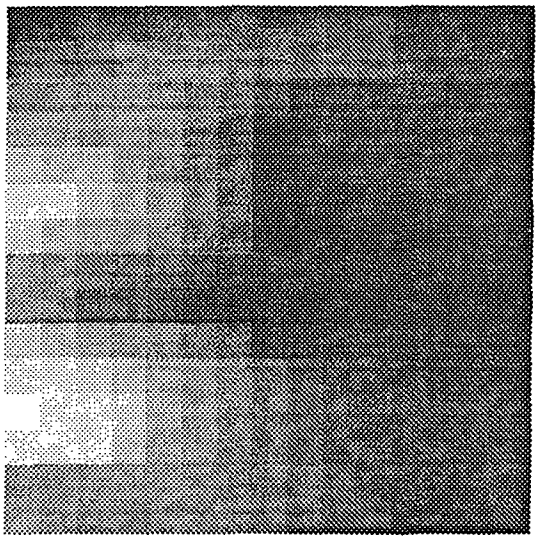

| | | | | | | | | | | | | | | |
|---|---|---|---|---|---|---|---|---|---|---|---|---|---|---|
| 99 | 100 | 101 | 102 | 104 | 106 | 106 | 105 | 105 | 103 | 101 | 99 | 99 | 99 | 98 |
| 106 | 106 | 108 | 109 | 110 | 109 | 107 | 105 | 102 | 101 | 101 | 100 | 100 | 99 | 99 |
| 119 | 119 | 116 | 113 | 113 | 110 | 106 | 103 | 100 | 99 | 100 | 100 | 100 | 100 | 100 |
| 121 | 121 | 120 | 118 | 114 | 109 | 104 | 100 | 99 | 99 | 100 | 100 | 100 | 100 | 98 |
| 129 | 128 | 126 | 121 | 116 | 110 | 105 | 100 | 98 | 97 | 97 | 97 | 97 | 96 | 96 |
| 135 | 134 | 130 | 125 | 119 | 112 | 105 | 100 | 98 | 96 | 95 | 95 | 95 | 95 | 95 |
| 131 | 130 | 129 | 121 | 116 | 110 | 104 | 99 | 97 | 96 | 95 | 94 | 94 | 94 | 95 |
| 119 | 115 | 112 | 110 | 107 | 103 | 100 | 97 | 96 | 95 | 95 | 94 | 94 | 94 | 95 |
| 110 | 114 | 110 | 106 | 103 | 100 | 98 | 97 | 96 | 95 | 95 | 94 | 94 | 95 | 95 |
| 132 | 127 | 123 | 118 | 114 | 109 | 104 | 100 | 98 | 96 | 95 | 94 | 95 | 94 | 95 |
| 139 | 136 | 132 | 128 | 123 | 118 | 112 | 106 | 102 | 99 | 97 | 95 | 95 | 95 | 95 |
| 145 | 143 | 139 | 131 | 124 | 117 | 112 | 107 | 103 | 99 | 97 | 96 | 95 | 95 | 95 |
| 137 | 137 | 134 | 129 | 123 | 117 | 112 | 108 | 103 | 99 | 99 | 96 | 96 | 96 | 96 |
| 119 | 118 | 118 | 118 | 119 | 116 | 113 | 109 | 105 | 101 | 99 | 98 | 97 | 97 | 98 |
| 122 | 117 | 114 | 114 | 115 | 116 | 115 | 112 | 108 | 103 | 101 | 99 | 98 | 99 | 102 |

Figure 41a. Original grey image and intensity values.

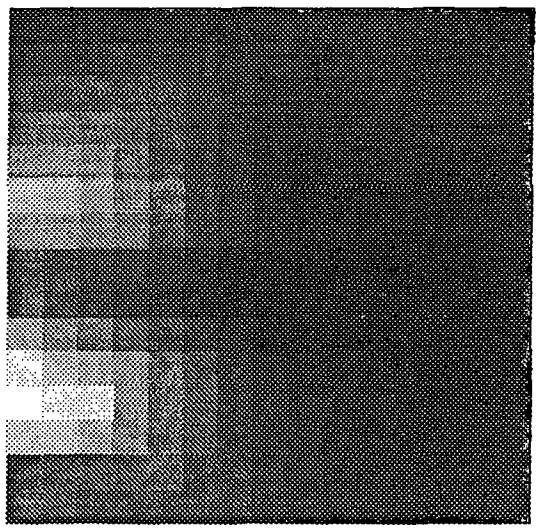

| | | | | | | | | | | | | | | |
|---|---|---|---|---|---|---|---|---|---|---|---|---|---|---|
| 70 | 71 | 73 | 74 | 77 | 80 | 80 | 78 | 78 | 76 | 73 | 70 | 70 | 70 | 68 |
| 80 | 80 | 83 | 84 | 86 | 84 | 81 | 78 | 74 | 73 | 73 | 71 | 71 | 70 | 70 |
| 93 | 93 | 94 | 93 | 90 | 86 | 80 | 74 | 71 | 70 | 71 | 71 | 71 | 71 | 71 |
| 102 | 102 | 100 | 97 | 92 | 84 | 77 | 73 | 70 | 70 | 71 | 71 | 71 | 71 | 71 |
| 113 | 112 | 109 | 102 | 94 | 86 | 78 | 71 | 68 | 67 | 67 | 67 | 67 | 65 | 65 |
| 122 | 120 | 115 | 107 | 99 | 89 | 78 | 71 | 68 | 65 | 64 | 64 | 64 | 64 | 64 |
| 116 | 112 | 107 | 102 | 94 | 86 | 77 | 70 | 67 | 65 | 64 | 63 | 63 | 63 | 64 |
| 99 | 93 | 89 | 86 | 81 | 76 | 71 | 67 | 65 | 64 | 64 | 63 | 63 | 63 | 64 |
| 99 | 92 | 86 | 80 | 76 | 71 | 68 | 67 | 65 | 64 | 64 | 63 | 63 | 63 | 64 |
| 118 | 110 | 103 | 97 | 92 | 84 | 77 | 71 | 68 | 65 | 63 | 63 | 63 | 63 | 64 |
| 120 | 123 | 118 | 112 | 105 | 97 | 89 | 80 | 74 | 70 | 67 | 64 | 64 | 64 | 64 |
| 136 | 134 | 128 | 116 | 106 | 96 | 89 | 81 | 76 | 70 | 67 | 65 | 64 | 64 | 64 |
| 125 | 128 | 120 | 113 | 105 | 96 | 89 | 83 | 76 | 70 | 68 | 65 | 65 | 65 | 65 |
| 99 | 97 | 97 | 97 | 99 | 94 | 90 | 84 | 78 | 73 | 70 | 68 | 67 | 67 | 68 |
| 103 | 96 | 92 | 92 | 93 | 94 | 93 | 89 | 83 | 76 | 73 | 70 | 68 | 70 | 74 |

Figure 41b. Image from (a) after enhancement steps.

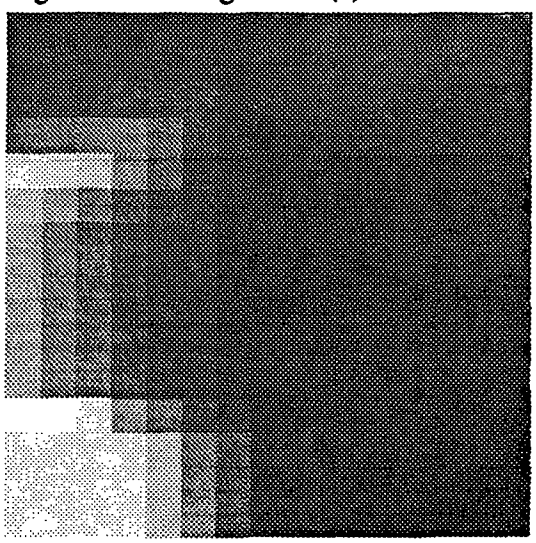

| | | | | | | | | | | | | | | |
|---|---|---|---|---|---|---|---|---|---|---|---|---|---|---|
| 65 | 65 | 65 | 65 | 67 | 67 | 70 | 70 | 70 | 70 | 70 | 70 | 68 | 68 | 68 |
| 67 | 67 | 67 | 77 | 68 | 72 | 70 | 70 | 70 | 70 | 70 | 70 | 68 | 67 | 67 |
| 70 | 70 | 70 | 71 | 73 | 72 | 68 | 67 | 67 | 67 | 67 | 65 | 65 | 64 | 64 |
| 78 | 78 | 80 | 80 | 77 | 72 | 68 | 65 | 64 | 64 | 64 | 64 | 64 | 64 | 64 |
| 93 | 93 | 90 | 84 | 77 | 70 | 67 | 65 | 64 | 63 | 63 | 63 | 63 | 63 | 63 |
| 89 | 86 | 81 | 76 | 71 | 67 | 65 | 64 | 64 | 63 | 63 | 63 | 63 | 63 | 63 |
| 86 | 80 | 76 | 71 | 68 | 67 | 65 | 64 | 64 | 63 | 63 | 63 | 63 | 63 | 63 |
| 86 | 80 | 76 | 71 | 68 | 67 | 65 | 64 | 64 | 63 | 63 | 63 | 63 | 63 | 63 |
| 86 | 80 | 76 | 71 | 68 | 67 | 65 | 64 | 64 | 63 | 63 | 63 | 63 | 63 | 63 |
| 86 | 80 | 76 | 71 | 68 | 67 | 65 | 64 | 64 | 63 | 63 | 63 | 63 | 63 | 63 |
| 86 | 80 | 76 | 71 | 68 | 67 | 65 | 64 | 64 | 63 | 63 | 63 | 63 | 63 | 63 |
| 97 | 97 | 92 | 84 | 77 | 72 | 68 | 65 | 64 | 63 | 63 | 63 | 63 | 63 | 63 |
| 92 | 92 | 92 | 92 | 89 | 80 | 74 | 70 | 67 | 64 | 64 | 64 | 64 | 64 | 64 |
| 92 | 92 | 92 | 92 | 89 | 82 | 76 | 70 | 67 | 65 | 64 | 64 | 64 | 64 | 64 |
| 92 | 92 | 92 | 92 | 89 | 83 | 76 | 70 | 68 | 65 | 65 | 65 | 65 | 65 | 65 |

Figure 41c. Smoothed image and intensities after one pass with a 20% Rank filter.

| | | | | | | | | | | | | | | |
|---|---|---|---|---|---|---|---|---|---|---|---|---|---|---|
| 55 | 56 | 58 | 59 | 59 | 63 | 60 | 58 | 58 | 56 | 53 | 50 | 52 | 52 | 51 |
| 63 | 63 | 66 | 67 | 68 | 64 | 61 | 58 | 54 | 53 | 53 | 51 | 53 | 53 | 53 |
| 73 | 73 | 74 | 72 | 67 | 65 | 62 | 57 | 54 | 53 | 54 | 56 | 56 | 57 | 57 |
| 74 | 74 | 70 | 67 | 65 | 63 | 59 | 56 | 56 | 56 | 57 | 57 | 57 | 57 | 54 |
| 70 | 69 | 69 | 68 | 67 | 66 | 61 | 56 | 54 | 54 | 54 | 54 | 54 | 52 | 52 |
| 83 | 84 | 84 | 81 | 78 | 72 | 63 | 57 | 54 | 52 | 51 | 51 | 51 | 51 | 51 |
| 80 | 82 | 81 | 81 | 76 | 69 | 62 | 56 | 53 | 52 | 51 | 50 | 50 | 50 | 51 |
| 63 | 63 | 63 | 65 | 63 | 59 | 56 | 53 | 51 | 51 | 51 | 50 | 50 | 50 | 51 |
| 63 | 62 | 60 | 59 | 58 | 54 | 53 | 53 | 51 | 51 | 51 | 50 | 50 | 51 | 51 |
| 82 | 80 | 79 | 76 | 74 | 67 | 62 | 57 | 54 | 52 | 51 | 50 | 51 | 50 | 51 |
| 92 | 93 | 92 | 91 | 87 | 80 | 74 | 66 | 60 | 57 | 54 | 52 | 51 | 51 | 51 |
| 90 | 87 | 86 | 82 | 79 | 75 | 71 | 66 | 62 | 57 | 54 | 52 | 51 | 51 | 51 |
| 83 | 83 | 70 | 71 | 66 | 66 | 65 | 63 | 59 | 56 | 54 | 51 | 51 | 51 | 51 |
| 57 | 55 | 55 | 55 | 60 | 63 | 64 | 64 | 61 | 58 | 56 | 54 | 53 | 53 | 54 |
| 61 | 54 | 50 | 50 | 54 | 61 | 67 | 69 | 65 | 61 | 58 | 55 | 53 | 55 | 59 |

Figure 41d. Grey image and Intensity values after subtracting images b and c.

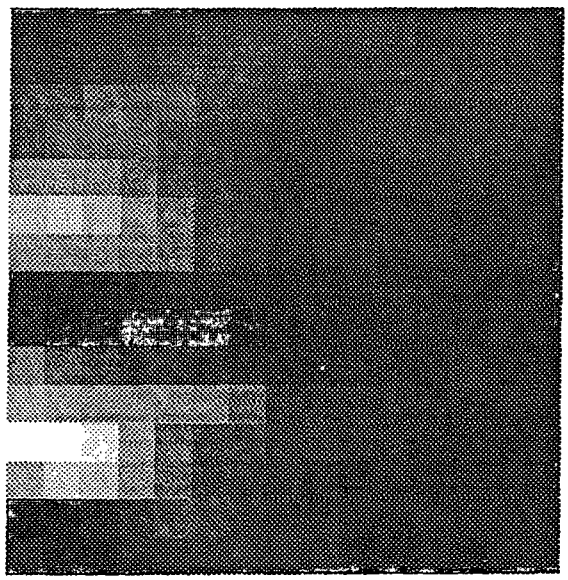

| | | | | | | | | | | | | | | |
|---|---|---|---|---|---|---|---|---|---|---|---|---|---|---|
| 57 | 58 | 58 | 58 | 60 | 62 | 62 | 62 | 62 | 61 | 60 | 58 | 59 | 60 | 59 |
| 60 | 59 | 61 | 62 | 64 | 63 | 63 | 62 | 60 | 60 | 60 | 60 | 60 | 60 | 60 |
| 66 | 66 | 65 | 65 | 64 | 63 | 61 | 59 | 58 | 58 | 60 | 60 | 60 | 61 | 61 |
| 64 | 64 | 65 | 64 | 63 | 61 | 59 | 58 | 59 | 60 | 61 | 61 | 61 | 61 | 60 |
| 60 | 60 | 60 | 65 | 63 | 62 | 60 | 58 | 58 | 58 | 59 | 59 | 59 | 58 | 58 |
| 78 | 73 | 71 | 69 | 67 | 64 | 61 | 59 | 60 | 59 | 60 | 59 | 59 | 59 | 58 |
| 69 | 60 | 60 | 67 | 66 | 64 | 61 | 59 | 59 | 59 | 59 | 59 | 59 | 59 | 59 |
| 80 | 97 | 57 | 59 | 59 | 59 | 59 | 59 | 59 | 59 | 59 | 59 | 59 | 59 | 59 |
| 59 | 56 | 55 | 56 | 56 | 56 | 56 | 57 | 59 | 59 | 59 | 58 | 58 | 59 | 59 |
| 60 | 66 | 65 | 63 | 63 | 61 | 59 | 58 | 59 | 59 | 59 | 58 | 59 | 59 | 58 |
| 71 | 70 | 69 | 69 | 68 | 67 | 65 | 62 | 61 | 60 | 59 | 58 | 59 | 59 | 59 |
| 77 | 76 | 75 | 70 | 66 | 63 | 63 | 61 | 61 | 59 | 59 | 59 | 58 | 58 | 59 |
| 71 | 73 | 72 | 69 | 66 | 63 | 61 | 61 | 59 | 59 | 59 | 59 | 58 | 58 | 57 |
| 55 | 56 | 58 | 61 | 64 | 63 | 62 | 60 | 59 | 58 | 59 | 59 | 58 | 59 | 58 |
| 59 | 56 | 56 | 58 | 60 | 62 | 62 | 60 | 59 | 56 | 57 | 57 | 57 | 58 | 59 |

Figure 41e. Grey image and intensity values after treating image (a) with a sharpening filter.

Figure 41. Sequence of imaging processing for pore distribution analysis. a) Original as acquired. b) After contrast enhancement. c) Smoothed image after one pass with a 20% rank filter. d) Difference between image in b and in c. e) After 1 pass with a 5 x 5 sharpening filter.

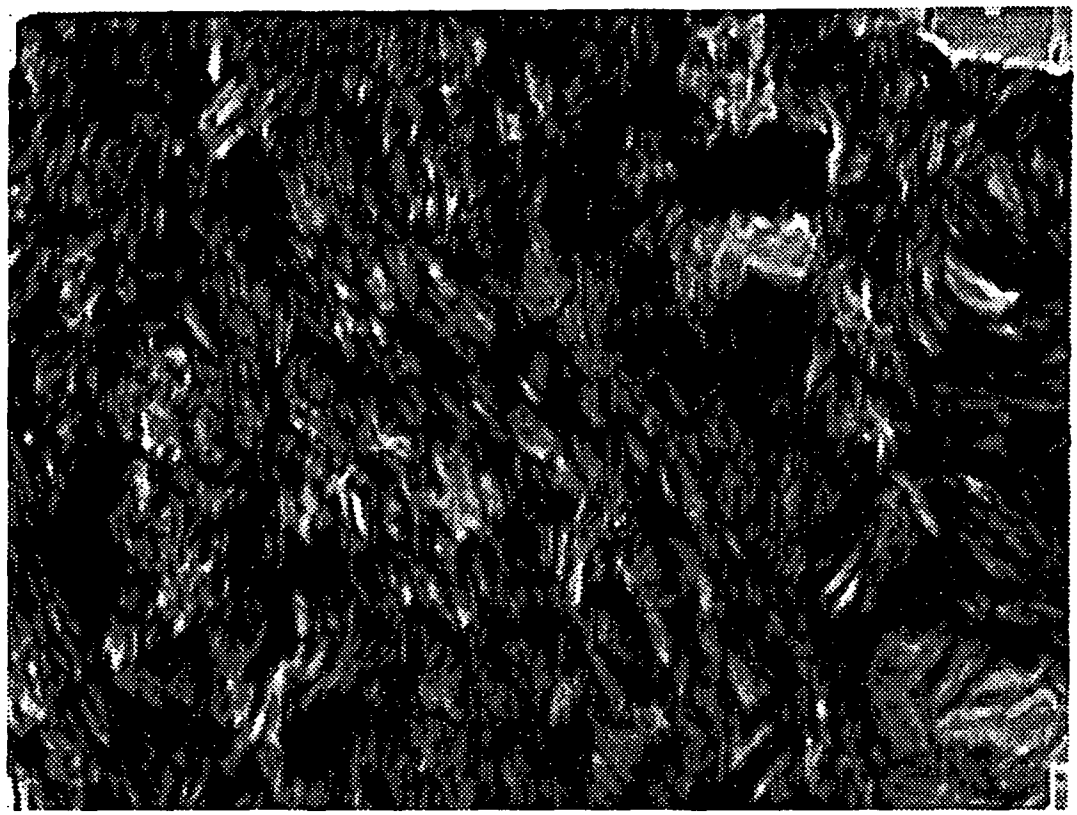

After Contrast Enhancement

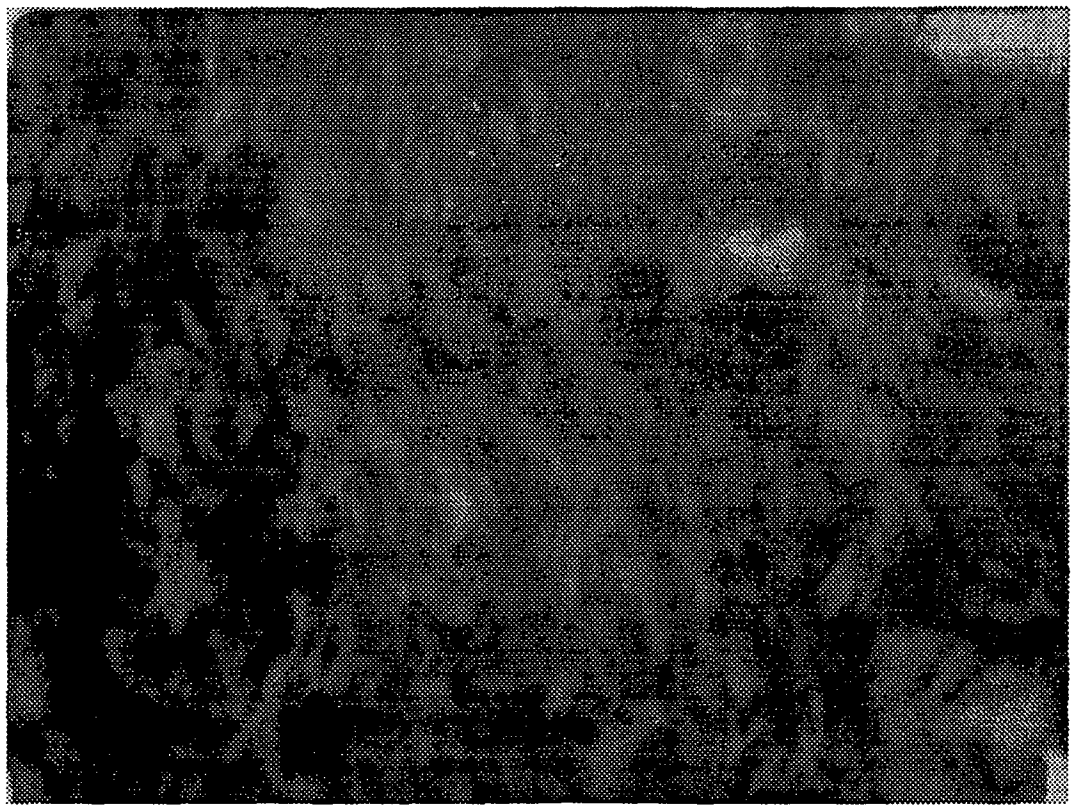

Original Grey Image

Figure 42. Original grey of an entire micrograph and a contrast enhanced version of the same image.

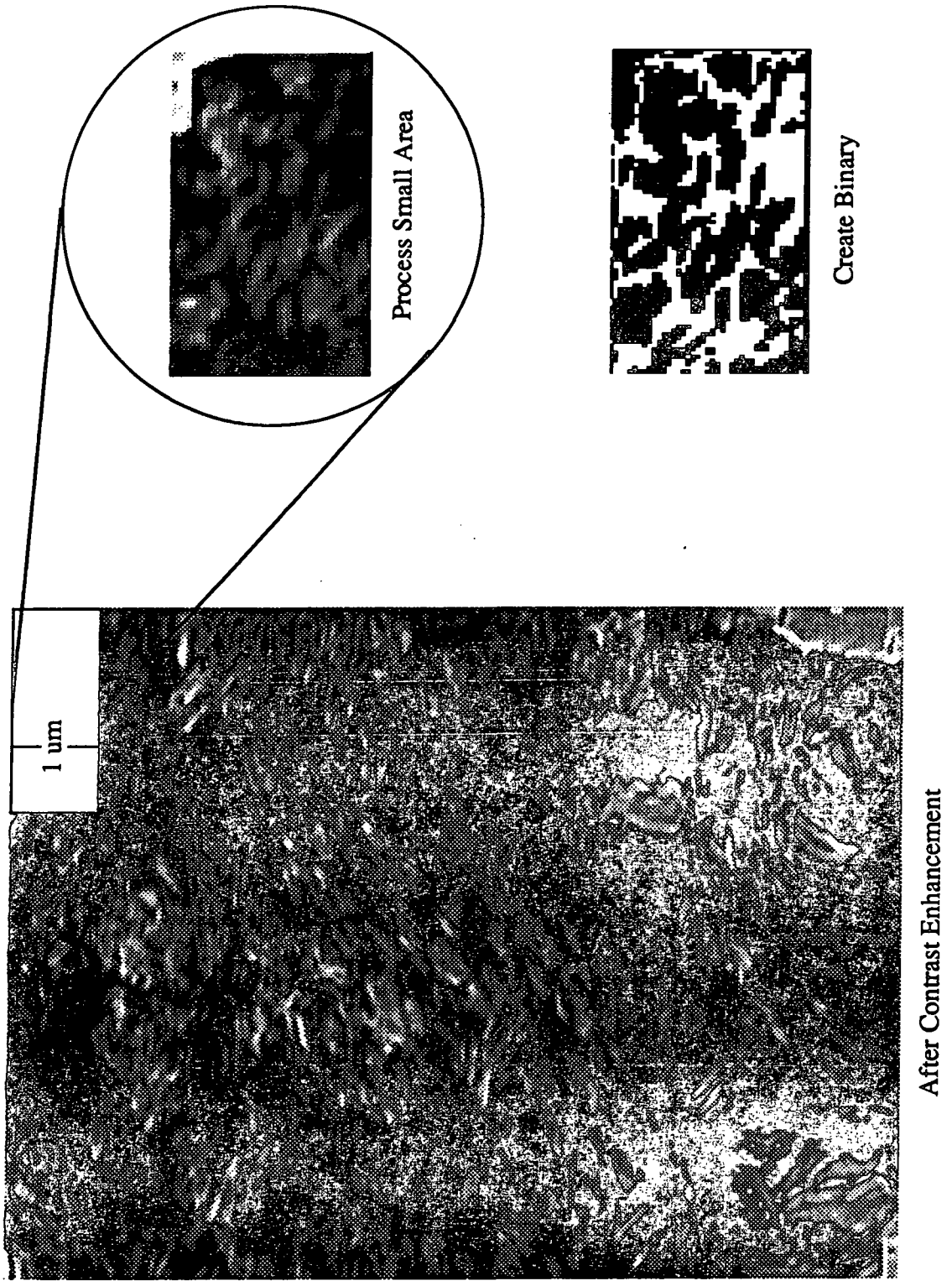


Figure 43. Conversion of a small piece of the grey image to a binary image.

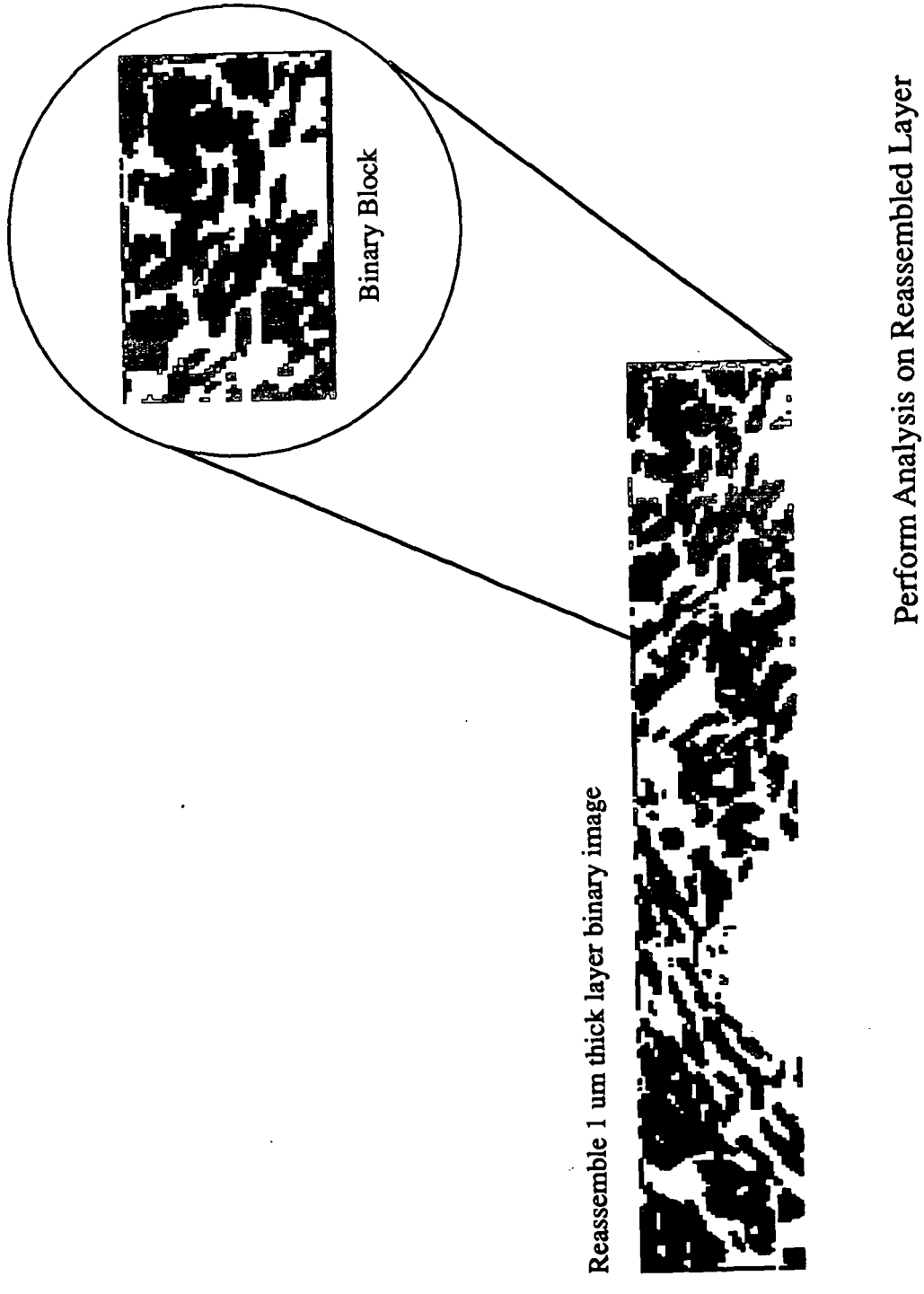


Figure 44. Assembly of the binary image followed by analysis of the 1 micrometer thick slab.

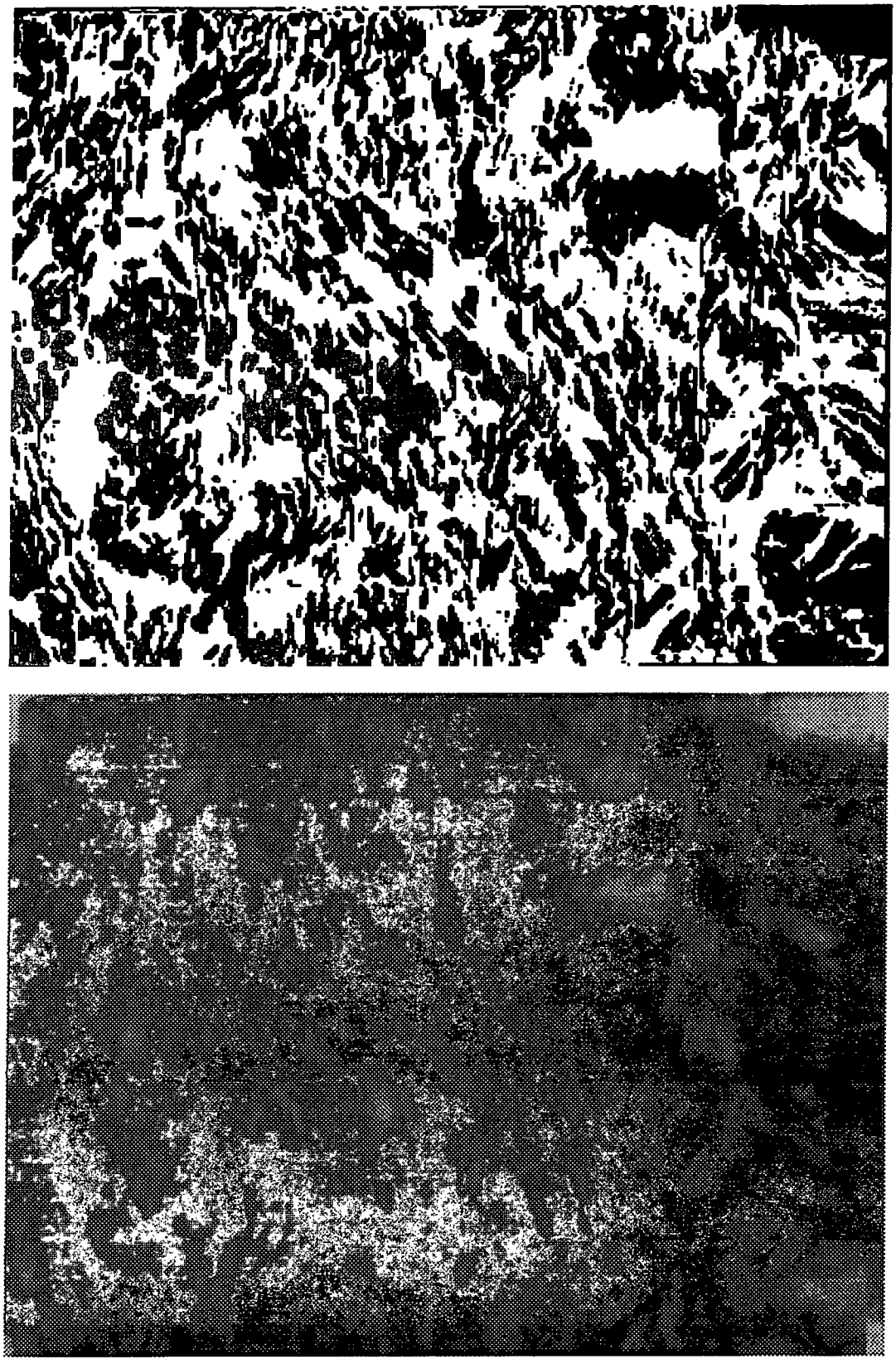


Figure 45. Enhanced grey image with corresponding binary.

Image Analysis

Quantitative data from the coating cross-sections were obtained from binary images. The technique used for measuring pore parameters was pixel counting. Pore characteristics were calculated from the calibrated size of the pixel, the number of pixels in a pore area and a formula relating the pixel quantity to a particular parameter.

The analyses were run on 1 μm thick layers from cross-sections; in this way, the data for the distribution of pore volume through the coating thickness was obtained directly. The pore area was measured and a relative pore area was calculated as the ratio of pore area to the total area analyzed. The ratio of areas was taken to be equivalent to the ratio of volumes for each coating cross-section(103). The process is shown schematically in Fig. 46.

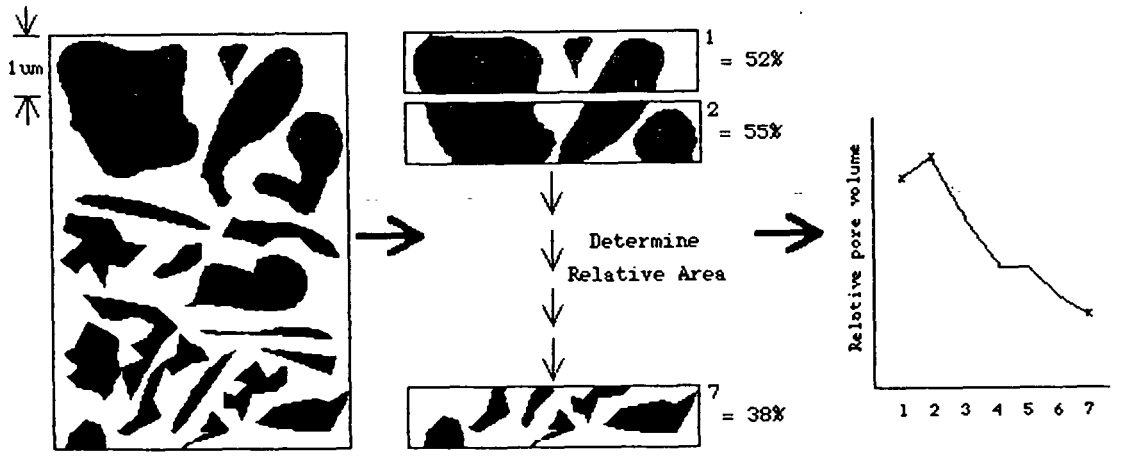


Figure 46. Schematic showing the typical method of analysis for producing profile data of relative pore volume.

Several other pore parameters were determined during analysis. The x and y ferets, which are the longest projections of the pore on the x-axis and y-axis respectively, were determined for each pore. The x and y ferets were used as a crude indication of the shape of the pores. Obviously, a pore that is part of a network of pores is not accurately represented by these factors (Fig. 47). No significant correlation with film thickness was found.

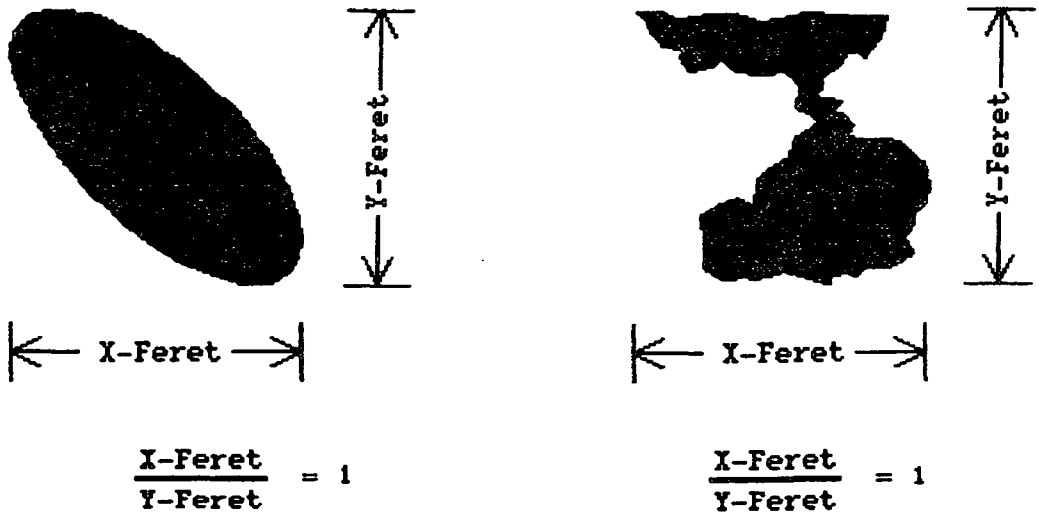


Figure 47. Diagram of the x and y ferets for a symmetrical and an asymmetrical pore.

The external perimeter of each pore was measured by counting the pixels of a pore that were not completely surrounded by pixels of the same pore. Assuming that there are no orientation effects in the x-y plane of the coating, then the external perimeter is a relative measure of the surface area of the pores. As with the x and y ferets, no correlation was found between the external perimeter and the position in the thickness of the coating.

The aspect ratio of each pore was calculated as a ratio of its maximum projection and its width. The aspect ratio also served as an indication of shape. It is different from the x and y ferets in that its value is independent of pore orientation. A pore that is rectangular in shape will have the same aspect ratio regardless of its position relative to the x-axis. However, the x and y ferets are sensitive to direction; if the same pore was placed parallel to the x-axis it will have different x and y ferets than the same pore positioned perpendicular to the x-axis (Fig. 48). Because a majority of the pores were interconnected, no significant length to width variations were detected relative to the coating thickness.

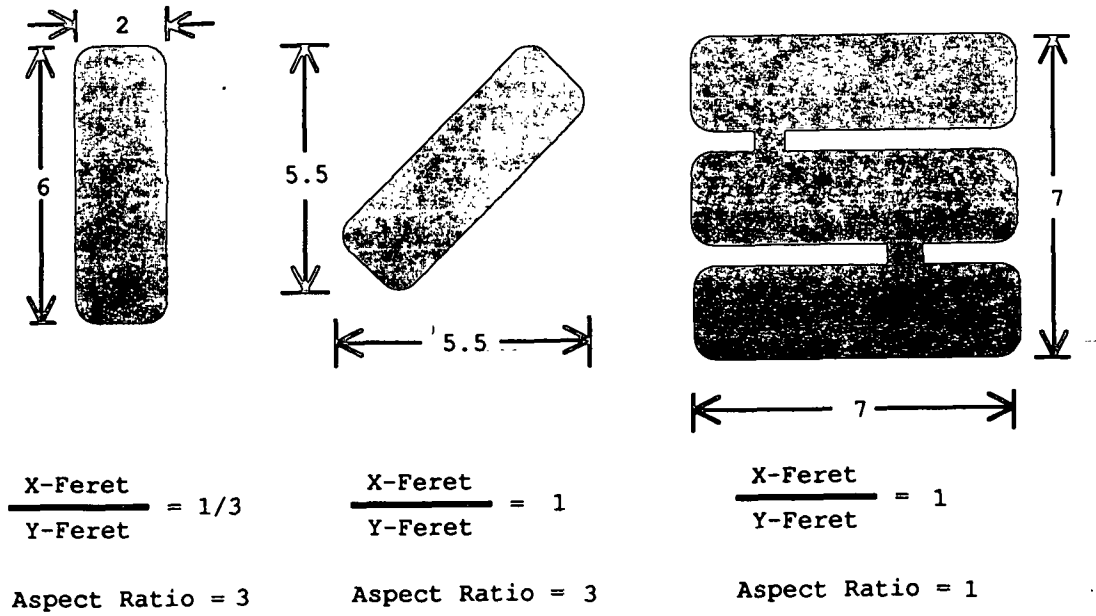


Figure 48. Diagram demonstrating the effect of orientation and interconnection on the ferets and aspect ratio of a pore.

Pore orientation was measured as the angle of the maximum projection of the pore relative to the x-axis. Orientation measurements suffered from the same problems as the aspect ratio, in that networked pores do not have a specific axis from which the orientation can be determined. Pore orientation appeared to have a correlation with the position through the coating thickness. However, statistical treatment showed no positive correlation between pore orientation and coating thickness at a 90% confidence interval.

The results for the six parameter measurements were tabulated for each micrometer-thick layer of the coating film cross-sections. The average and standard deviation were calculated and plotted for each layer in the thickness of the film. Parameters which had significant correlations are discussed later in this text.

## Experiments

Although no measurements of packing structure have been previously reported for the thickness direction, the accuracy of the techniques described above can be checked relative to the oil absorption and mercury porosimetry methods for total pore volume.

To make the comparison among techniques, sixteen cross-sections, oriented parallel to the coating direction, were

analyzed from a single coating. The relative areas of the samples were determined. The average and variance of the total pore volume were then calculated and compared to the results of the other techniques for the same coatings. The results from the 16 samples were also used to determine the number of specimens from a single coating necessary to achieve consistent results.

To check the x-y plane symmetry of the pore structure, eight additional samples from the same coating were cut perpendicular to the coating direction (y-axis) and eight cross-sections were cut at 45° to the coating direction. Relative pore volumes were compared from all the sections.

Two other experimental parameters were analyzed for their effect on the accuracy of the technique: magnification and cross-section thickness. The magnification of the micrograph will affect to the resolution of the pores and particles. Too low a magnification results in pores which are too small to be accurately differentiated via image analysis, because the pigment particles and pores can become as small or smaller than the pixels. Sections from the sixteen samples cut parallel to the coating direction (x-axis), were photographed at various magnifications (1000X, 3000X, 5000X, 8000X, 10,000X and 14,000X). The cross-sections were analyzed for pore volume and the results compared.

The thickness of the cross-section is also important to the technique's accuracy. A section which is sliced too thick will contain pores that cannot be seen by transmission microscopy. Therefore, the maximum section thickness must be no thicker than the individual pore dimensions. For example, if the pores in a coating occurred between 0.1 μm thick plates which were oriented with their faces parallel to the thickness direction (z-direction), and if the cross-section was cut 0.25 μm thick, pores between the plates will be obscured. Figure 49 shows a sketch of the above situation.

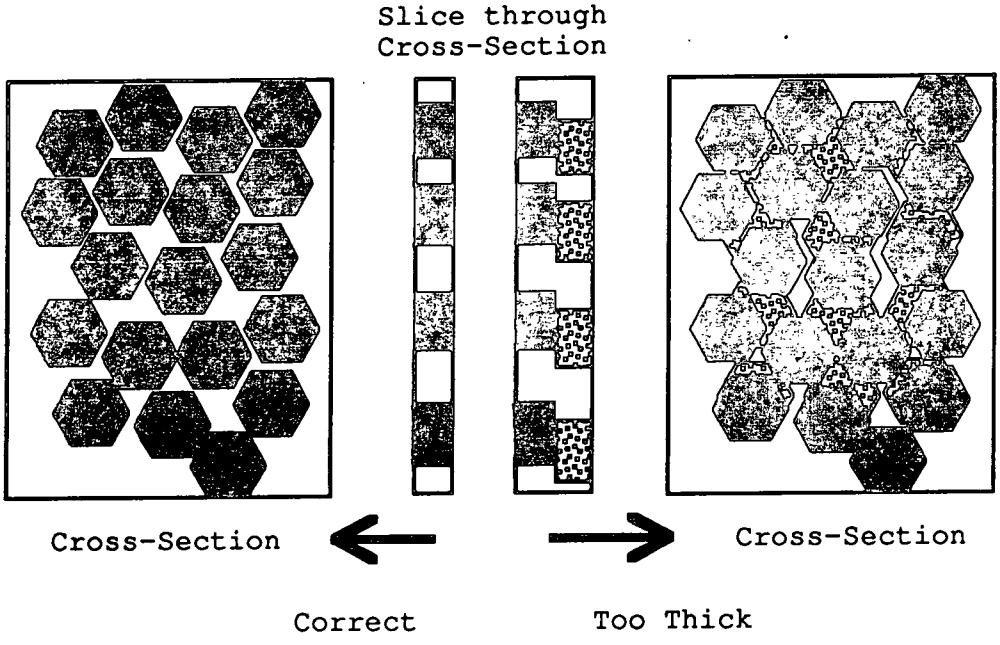


Figure 49. Schematic of blind pores in a cross-section which is too thick.

To determine the maximum thickness for accurate results, cross-sections from the same coating were cut at several

thicknesses. Each section was analyzed and the results compared.

## SUMMARY OF EXPERIMENTS

Polystyrene/acrylate latex and clay coatings were applied to non-porous media using volumetric metering devices, a Meyer rod and a Bird bar. The coatings were dried at different rates using two separate methods. Initially coatings were dried in an oven and drying rates were controlled by the temperature. In later experiments, the coatings were dried in a laminar flow air stream under controlled humidity and temperature, each of which was adjustable for production of a wide range of drying rates.

Total pore volume of dry coatings was tested using oil absorption techniques. Other samples were embedded with an epoxy resin and thin cross-sections were cut with a diamond knife. The cross-sections were micrographed using a TEM and the micrographs were digitized for analysis. The digitized micrographs were first processed to produce sharper images. They were then converted to binary images which separated the pores from the pigment, and sequentially analyzed to quantitatively determine the pore features.

To test the hypotheses about the effects of drying rate on coating structure, analyses were conducted on micrometer-thick layers from consecutive positions through the thickness

of the coatings. Distributions of the relative pore volume through the coating thickness were used to represent the coating structure. The results and their implications are discussed in the next section.

# RESULTS AND DISCUSSION

Before discussing the experimental results, it is appropriate to review the objective of this study. One problem which the coated paper industry faces concerns printing defects associated with increased coating speeds. Specifically, increased drying rates have increased the incidence of print and backtrap mottle. Uneven distribution of binder is often blamed for print mottle, but little direct evidence has been discovered. Research has concentrated on mechanisms of binder migration and has placed little emphasis on the consolidation and structure of the coating. The goal of this work is to discover the influence of drying rate on the packing structure of the coating pigment.

## ANALYSIS OF THE TECHNIQUE FOR MEASURING COATING STRUCTURE

The lack of information on the actual packing structure of a coating is due in part to the size range of coating pigment particles and the thickness of the coating layer. For these reasons, quantitative analysis of the packing structure of the coating is difficult. An objective of this study was to develop a technique for quantitative analysis of the coating structure. Details were discussed previously and the effectiveness of the procedure used will be evaluated in this section. Results of experiments are given to illustrate the limitations of the developed technique.

Comparison of Analytical Techniques

The image analysis technique developed for measuring coating structure was designed to measure the local properties of the coating structure across the coating thickness. The total pore volume of a coating sample could also be measured with this technique. For comparison, two other methods were used to measure the total pore volume of coating films: mercury porosimetry(98) and oil absorption(6). Measurements were made on two coatings, differing only in the particle size of the pigment. Coatings were applied with a Meyer rod and dried at room temperature. Figure 50 shows the results.

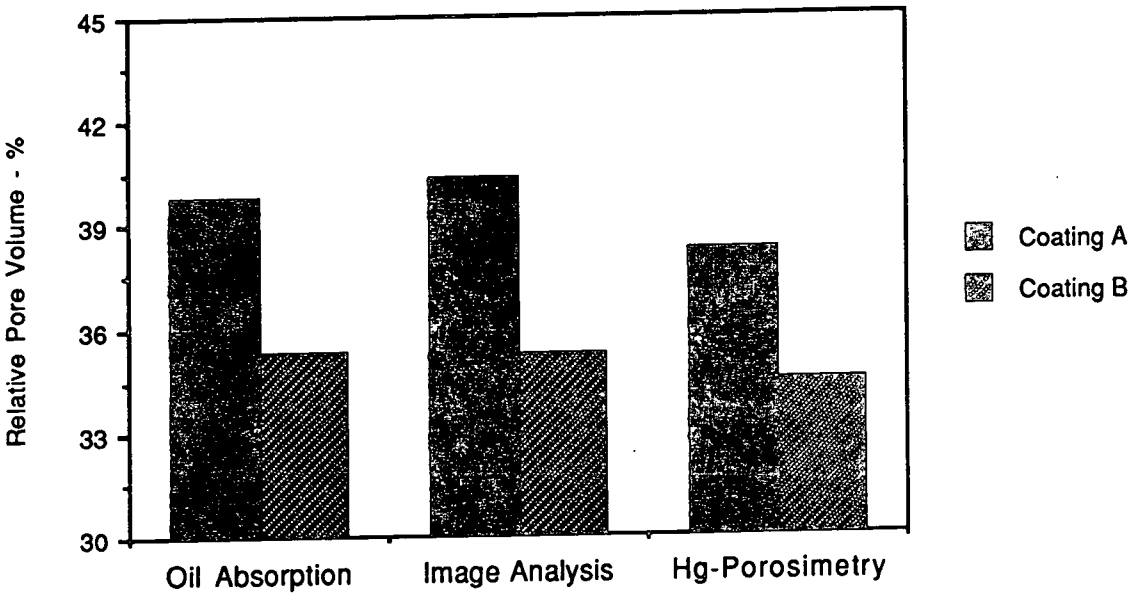


Figure 50. Total pore volume of two different coatings as determined by oil absorption, image analysis and mercury porosimetry. Coating A delaminated clay, coating B #1 clay.

Total pore volumes ranged from 38.2% to 40.3% for the larger pigment A, and pigment B, the smaller particle size, yielded pore volumes between 34.5% and 35.3% depending on the measuring technique. The results indicate that the values obtained by mercury porosimetry were lower (3%-5%) than those of the other methods. The oil absorption and image analysis techniques yielded similar values.

The lower values obtained with mercury porosimetry are possibly an artifact of the interpretation of the test data. As indicated in the Materials and Methods section, the low pore volume to sample area ratio for coating films required a relatively large area of sample to be run in the porosimeter. The crowding of the sample chamber resulted in the apparent formation of pores between coating pieces; these intersample pores were eliminated from the total pore volume calculations. If there were a significant volume of pores of diameter greater than 1 μm, then the interpretation of the data would result in erroneously low values for total pore volume. Surface pores, which potentially have large diameters, are included in the analysis of the other methods but would be eliminated in the interpretation of the mercury porosimetry results. Examination of the results of Climpson and Taylor's(5) work show that they found similar results.

A comparison of literature data shows that all three methods gave results within the range reported in the

literature. Table IX shows some literature values for various binderless coatings applied to non-porous media.

Table IX

Comparison of Literature Values with Results for Total Pore Volume

| Source | Pigment Type | Value |
|---|---|---|
| Climpson(5) | Coarse Clay | 36% |
| | #2 Clay | 38% |
| Lepoutre(6) | Delaminated Clay | 36% |
| Lepoutre(18) | #1 Clay | 43% |
| Trader(128) | Filler Clay | 50.2% |
| | #2 Clay | 31.1% |
| | #1 Clay | 35% |
| Kaliski(129) | Delaminated Clay | 56.5% |
| | #2 Clay | 53.9% |
| | #1 Clay | 53.9% |
| Hemstock(17) | Coarse Clay | 44% |
| | Fine Unfractionated | 46% |
| | #2 Clay | 40% |
| | #1 Clay | 38% |
| | Delaminated Clay | 43% |
| | Fine #1 Clay | 47% |
| Burke(42) | Fine Fraction Clay | 48.5% |
| Lepoutre(130) | #1 Clay | 38.5% |
| Bunker (This Study) | #1 Clay(clay B, Fig. 50) | 35.2% |
| | Delaminated Clay(20 $g/m^2$) | 40.1% |
| | Delaminated Clay(50 $g/m^2$) | 43% |

Effect of Sampling Size

A set of micrographs comprising a coating cross-section at 10,000X may include (on average) about 5 μm of sample length. A single cross-section taken randomly is probably not representative of the entire coating. To determine the number of sections necessary for adequate representation of the coating structure, the total void volumes of sixteen cross-sections, chosen randomly from a single coating, were

determined using the image analysis method. The results are shown in Table X.

Based on the results from the sixteen cross-sections the variance of the population was estimated to be 0.42. In order to detect a 0.5% difference in relative pore volume between samples at the 90% confidence interval, six samples of each coating type were necessary(127). At least seven samples were used in subsequent analyses.

Table X

Error Analysis of Analytical Technique

Coating - 100% Delaminated clay
Applicator - #10 Meyer Rod
Coat Weight - 20 $g/m^2$

| Sample Number | Relative Pore Volume | |
|---|---|---|
| 1 | 39.8% | |
| 2 | 40.3% | |
| 3 | 39.1% | |
| 4 | 40.7% | |
| 5 | 39.9% | Mean = 40.2% |
| 6 | 39.9% | |
| 7 | 41.2% | Std. Dev. = 0.65 |
| 8 | 40.2% | |
| 9 | 40.1% | Variance = 0.42 |
| 10 | 41.5% | |
| 11 | 39.2% | Desired resolution - 0.5 |
| 12 | 40.4% | |
| 13 | 40.6% | Confidence Interval - 90% |
| 14 | 40.1% | |
| 15 | 39.5% | Number of samples - 6[a] |
| 16 | 40.4% | |

[a]Calculations made according to ref. 127 page 86.

Pore properties such as the x and y ferets have a dependence upon orientation. Because coating application is a directional process, it was necessary to determine if

orientation of the coating cross-section had a significant influence on the measured properties of the coating. From the same coating studied in the above test, eight cross-sections were taken perpendicular to the coating direction and eight were taken at 45° to the coating direction. No detectable difference in relative pore volume was found for cross-sections taken at different orientations relative to the coating direction (Table XI). Therefore, it was assumed that the coating structure is symmetric in the x-y plane.

Table XI

Results From a Study of the Influence of Cross-Sectioning Geometry on Relative Pore Volume

| | X-Axis | Y-Axis | 45° |
|---|---|---|---|
| Average | 40.18% | 40.06% | 40.09% |
| Std. Dev. | 0.65 | 0.46 | 0.59 |
| Variance | 0.42 | 0.21 | 0.35 |
| No. Samples | 16 | 8 | 8 |

Analysis of Variance Table

| | Degrees of Freedom | Sum of Squares | Mean Square | F |
|---|---|---|---|---|
| Between Orientations | 2 | 0.093 | 0.046 | 0.132 |
| Error within Sample | 29 | 10.172 | 0.351 | |
| Total | 31 | 10.263 | | |

$F_{(0.05,2,29)} = 3.32$

Effect of Section Thickness

The thickness of the cross-section used in the analysis is critical to the accuracy of the technique. Cross-sections thicker than the smallest dimension of the pores may shield

small pores from the analysis. Electron micrographs were obtained from several cross-sections of different thickness cut from a single coating. The photo negatives were analyzed using image analysis techniques described earlier. A plot of the relative pore volume for each section versus the magnification is shown in Fig. 51. The statistical results are presented in Table XII.

Table XII consists of three sub-tables of information. The first table contains the experimental results, including pore volumes, standard deviations and variance for n number of sections analyzed per section thickness. An analysis of variance was performed on the experimental data and the result is contained in the second sub-table. Comparison of the F values indicates that the hypothesis that the pore volume is independent of each section thickness is rejected. Therefore, it can be concluded that the section thickness has an effect on the results of the analysis technique.

In Fig. 51 there is a point close to 125 nm where the pore volume begins a rapid drop with increasing section thickness. A Student-Newman-Keuls' test(127) was performed to determine if the pore volume results prior to the transition point were the same. The results are presented in the last sub-table of Table XII. The difference between each pair of experimental means was compared to the test statistic at a 95% confidence level.

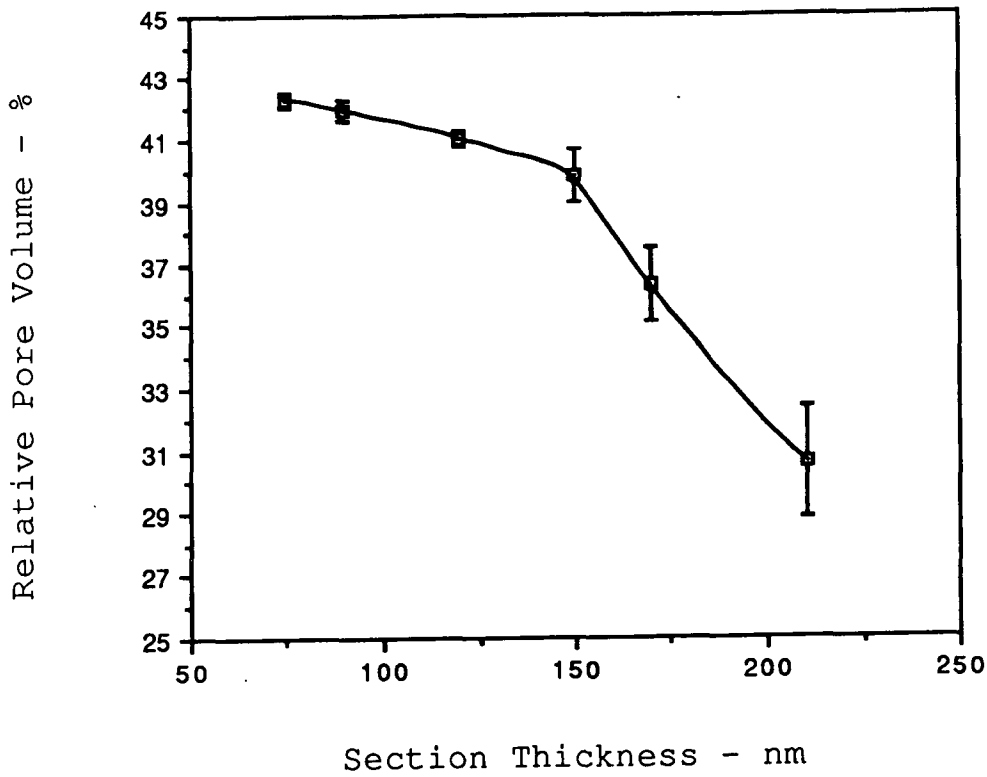


Figure 51. Relative pore volume of a delaminated clay coating as measured by image analysis of cross-sections of various thickness. Error bars are equal to one standard deviation from the mean.

No significant differences were found in pore volumes between samples sectioned up to 120 nm thick. Cross-sections cut thicker than 120 nm yielded pore volumes that were significantly less than values obtained from thinner samples and from oil absorption analysis. In addition, the sample standard deviation was discovered to increase as section thickness increased. Because section thickness does not affect total pore volume analysis below 120 nm, it was assumed that pore obstruction is not significant below that thickness. Therefore, it can be inferred that the smallest pore dimension in the x-z and y-z planes that significantly contributed to pore volume was about 0.1 μm.

Table XII

Results From a Study of the Effect of Cross-Section Thickness on the Accuracy of the Analytical Technique

| Section Thickness (nm)-code | Average Relative Pore Volume | Std. Dev. | Variance | n |
|---|---|---|---|---|
| 75 a | 42.29% | 0.53 | 0.28 | 8 |
| 90 b | 41.94% | 0.59 | 0.35 | 8 |
| 120 c | 41.21% | 0.53 | 0.28 | 8 |
| 150 d | 39.81% | 0.88 | 0.78 | 8 |
| 170 e | 36.24% | 1.03 | 1.06 | 8 |
| 210 f | 30.53% | 1.25 | 1.57 | 8 |

Analysis of Variance Table

| | Degrees of Freedom | Sum of Squares | Mean Square | F |
|---|---|---|---|---|
| Between Orientations | 5 | 830.3 | 166.1 | 230.7 |
| Error within Sample | 42 | 30.2 | 0.72 | |
| Total | 47 | 860.6 | | |

$F_{(0.05,5,42)} = 2.45$

Results of Student-Newman-Keuls' Test

| Mean Pair | Differences Between Means | Pass Fail | |
|---|---|---|---|
| a-b | 0.35 | P | |
| a-c | 1.08 | P | Test Statistic 1.605 |
| a-d | 2.48 | F | |
| a-e | 6.05 | F | Confidence interval 95% |
| a-f | 11.8 | F | |
| b-c | 0.72 | P | |
| b-d | 2.12 | F | |
| b-e | 5.7 | F | |
| b-f | 11.4 | F | |
| c-d | 1.4 | P | |
| c-e | 4.98 | F | |
| c-f | 10.7 | F | |
| d-e | 3.58 | F | |
| d-f | 9.29 | F | |
| e-f | 5.71 | F | |

Mercury porosimetry tests yielded a significant number of pores whose diameter was smaller than 0.1 μm. However, mercury porosimetry is known to yield calculated pore sizes which are smaller than the actual pore size(125). The errant pore sizes result from ink bottle-shaped pores, in which mercury must be forced through a small pore to enter a large one. Climpson and Taylor(5) and Davis and Smith(99), using image analysis and NMR techniques respectively, found that the lower end of the pore size distribution for coating films is about 0.1 μm. Based on the results of this study and the data from the literature, 0.1 μm was used as the section thickness for the structure analysis.

Effect of Sample Magnification

The detection of a pore using the image analysis technique is dependent on several aspects of the procedure. The contrast difference between the pore and the particle is most important. When digitizing the image there is some imprecision at the edges of the pigment particles. Instead of a clean transition from the grey level of the pigment to that of the pores there is a gradual change. For narrow pores, the transition region may occupy significant pore area. If the grey level for separating pores and pigment is part of the fuzzy region, then a significant error will be made in the measured area of that pore.

Because digitization was performed from micrograph negatives and digitization was performed at constant magnification, resolution of pores in a cross-section was dependent upon the TEM magnification. Reducing the magnification reduced the area of the pores on the negative. Smaller areas required fewer pixels to represent them and the percentage of the pore area that is part of the fuzzy region was greater, ultimately increasing the error in the analysis. Increasing the magnification of the sample had the opposite effect.

The results of an experiment to test the limit of useful magnifications are shown in Fig. 52 and the statistical analysis is contained in Table XIII.

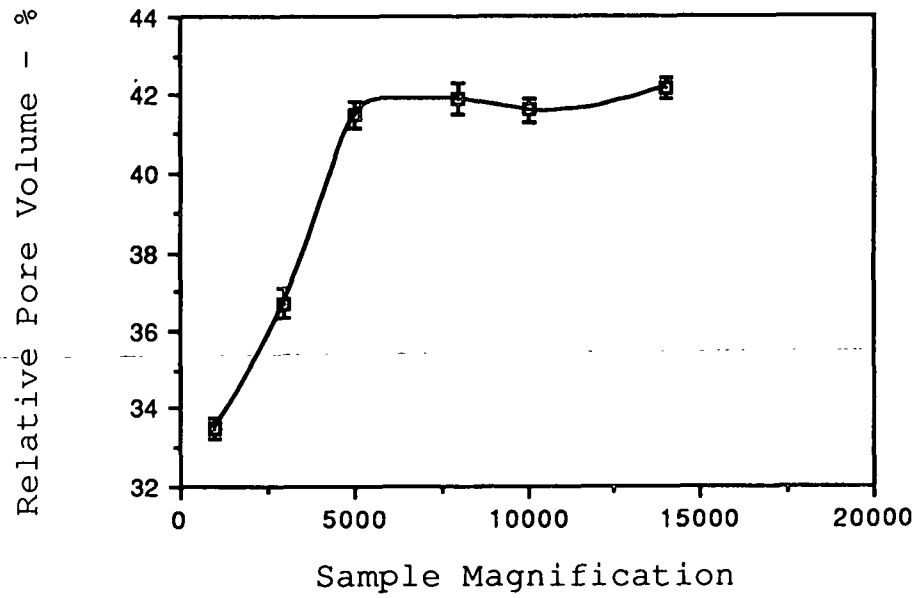


Figure 52. Relative pore volume of a delaminated clay coating applied to plastic film versus micrograph magnification. Error bars are equivalent to one standard deviation from the mean.

Table XIII

Results From a Study of the Influence of Sample Magnification on the Accuracy of the Image Analysis Technique

| Sample Magnification x-code | | Average Relative Pore Volume | Std. Dev. | Variance | n |
|---|---|---|---|---|---|
| 1,000 | a | 33.46% | 0.75 | 0.57 | 7 |
| 3,000 | b | 36.66% | 0.66 | 0.44 | 7 |
| 5,000 | c | 41.51% | 0.62 | 0.38 | 7 |
| 8,000 | d | 41.90% | 0.63 | 0.40 | 7 |
| 10,000 | e | 41.57% | 0.68 | 0.47 | 7 |
| 14,000 | f | 42.06% | 0.63 | 0.40 | 7 |

Analysis of Variance Table

| | Degrees of Freedom | Sum of Squares | Mean Square | F |
|---|---|---|---|---|
| Between Orientations | 5 | 456.7 | 91.3 | 206.4 |
| Error within Sample | 36 | 15.9 | 0.44 | |
| Total | 41 | 472.6 | | |

$F_{(0.05,5,36)} = 2.48$

Results of Student-Newman-Keuls' Test

| Mean Pair | Differences Between Means | Pass Fail | |
|---|---|---|---|
| a-b | -3.20 | F | |
| a-c | -8.06 | F | Test Statistic 1.267 |
| a-d | -8.44 | F | |
| a-e | -8.11 | F | Confidence Interval 95% |
| a-f | -8.6 | F | |
| b-c | -4.86 | F | |
| b-d | -5.24 | F | |
| b-e | -4.91 | F | |
| b-f | -5.4 | F | |
| c-d | -0.39 | P | |
| c-e | -0.06 | P | |
| c-f | -0.54 | P | |
| d-e | 0.33 | P | |
| d-f | -0.16 | P | |
| e-f | -0.49 | P | |

The results support the effects of magnification described above - at least 5000X was required to give reproducible results. By comparison, analyses by Climpson and Taylor(5) were performed on images magnified 4000 times, but with additional processing the images analyzed were magnified 33,000 times. Based on the analysis of the effect of magnification presented here their data should be valid. In this study, samples were magnified 10,000 times for photographing. The typical resolution after digitization was 0.023 μm/pixel.

Analysis Technique Summary

Through a comparison of the results of relative pore volume determinations on like samples and from published values for similar coatings, it has been shown that the image analysis technique is accurate and can be used to determine the relative pore volume of a coating from a thin cross-section. Based on these results, it was assumed that the method was also suitable for measuring the pore characteristics of any portion of the coating thickness providing the sample was thin enough, the magnification was high enough and enough samples were measured to accurately differentiate changes in structure.

## ANALYSIS OF THE COATING DRYING APPARATUS

A second objective of this study was to produce and analyze coating films whose structures were dependent only on their drying rate. The equipment and procedures for the drying system were discussed in the Materials and Methods section. The following text discusses some difficulties with the drying techniques and results of tests to determine the effectiveness of the methods.

### Coating Uniformity

A coating coverage problem occurred when coatings were dried at high temperatures and high humidities. The coating dried slowly and, even at very low air flow rates, the coating was blown toward the bottom edge of the substrate. During these experiments the coating temperature entering the drier was below the dew point of the drying air. Therefore, before drying could occur the coating had to be heated to at least the wet bulb temperature of the drying air. While the coating heated, the drying air near the coating surface was cooled below its dew point. Beads of water were observed on the open portions of the coating plate during drying, indicating that condensation was occurring. The condensation lowered the solids content of the coating and reduced its viscosity, allowing the coating to flow in the air stream.

To quantify the condensation, a coated sample was exposed to the drying air for 15 seconds and then removed.

Once removed, the coating was scraped off the substrate and its solids content was determined. The solids content of the scrapings was 56% - 4% lower than at application. The problem was solved by bringing the coating components and apparatus to the dry bulb temperature of the drying air before drying the coating. This action prevented excessive cooling of the drier air and thus condensation at the coating surface. Because at higher drying temperatures some evaporation occurred prior to insertion into in the experimental drier, heating the coating prior to drying resulted in some loss in accuracy of measured time to the gloss point and therefore in the calculation of the drying rate.

Coating Temperature

Two 0.002 inch thermocouples were dropped into the coating film during each trial. A third thermocouple (0.05 inch) was dropped just above the coating to measure the temperature of the drying air. Figures 53 and 54 show the response curves of the three thermocouples for a latex coating being dried under high and low relative humidity respectively.

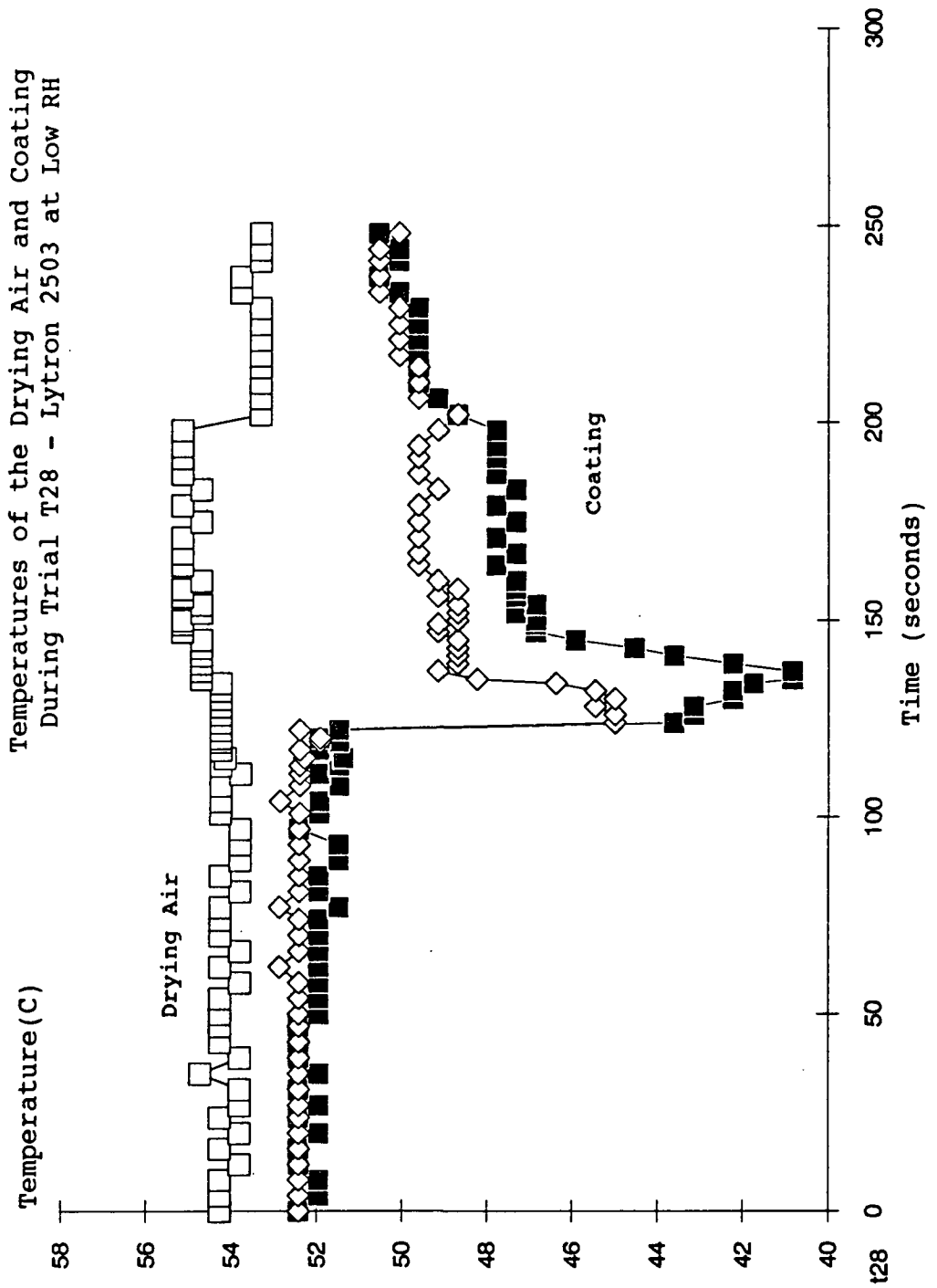


Figure 53. Temperature of the drying air and coating during trial T28 - Latex pigment at 15% relative humidity.

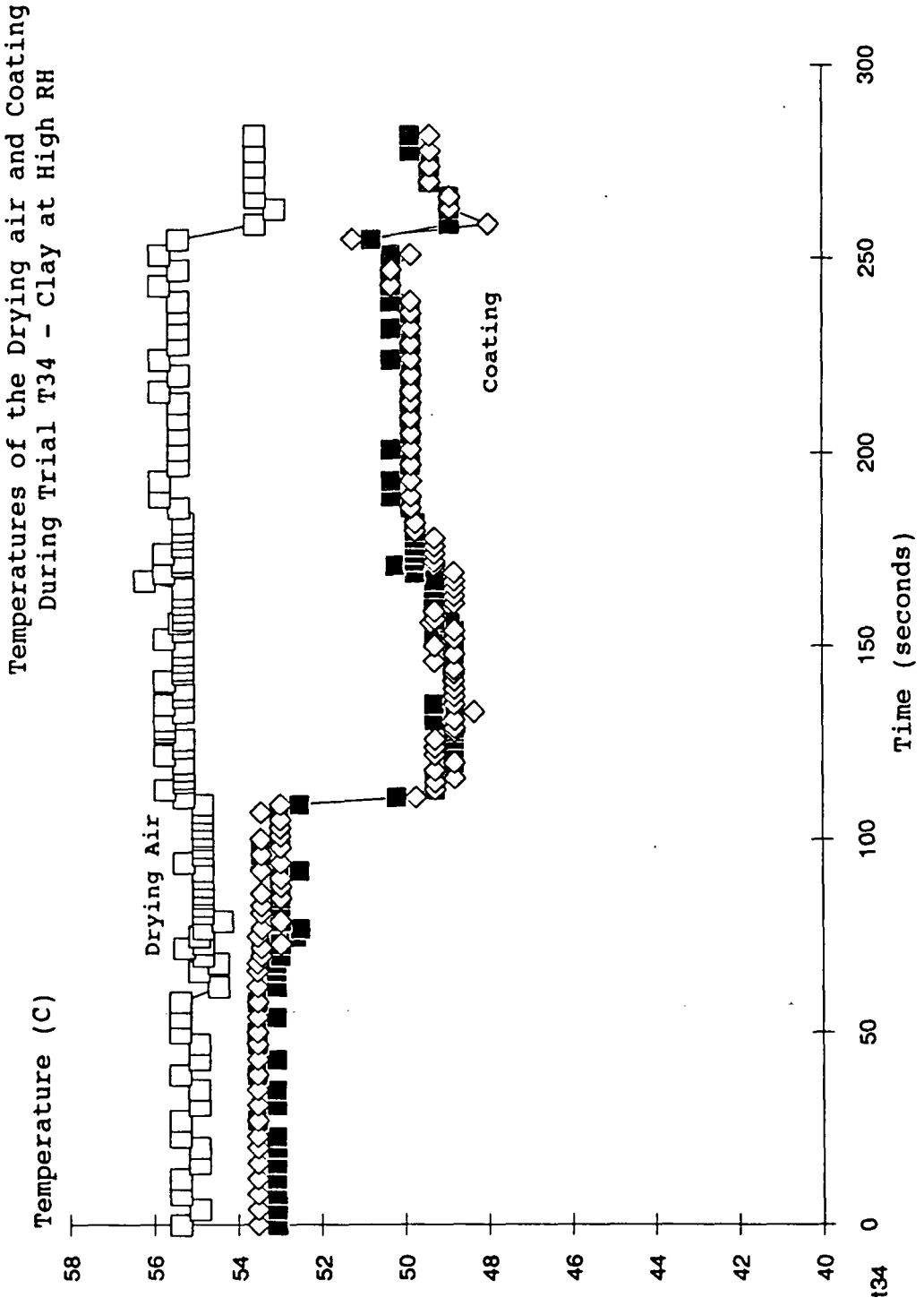


Figure 54. Temperature of the drying air and coating during trial T34 - Lytron 2503 at 86% relative humidity.

As the coating entered the drier there was an immediate temperature drop whose magnitude approached the wet bulb temperature of the drying air. For Figs. 53 and 54, the wet bulb temperatures were 32°C and 46°C respectively and the gloss points were 4.0 and 74.3 seconds respectively. After the gloss point, the temperatures increased to a point at which they remained constant until the coating was dry. The sharp temperature change near the end of each curve was an artifact caused by closing the top drawer of the drying box which had cooled under ambient conditions during drying.

Coating/Substrate Interface Temperatures During Drying

Because the thermocouples which were dropped into the coating during drying were thicker than the coating, the temperatures returned were not purely the temperatures of the coating but a combination of the coating temperature and the drying air near the surface. The glass plate containing platinum thin film resistors (discussed earlier) was used to investigate the temperature profiles of the drying box and to measure the temperature of the coating during drying.

Figures 55 and 56 present the temperature history of the first 100 seconds of a trial designed to measure the heating rate of the glass plate at different locations in the drying box. The glass plate was inserted at room temperature into the drier which was running at about 55°C and 15% RH. The results indicate that the rate of temperature gain was

dependent upon the location within the drier. The temperature change in the first few seconds shows that resistors A and B increased in temperature faster than C, D and E, and resistor F was slower than the others (see Fig. 30 for resistor locations). The results present evidence that a temperature gradient in the direction of the air flow existed in the drier. The maximum gradient discovered occurred at 75 °C and was 1°C/inch along the center line of the drier between resistors A and F.

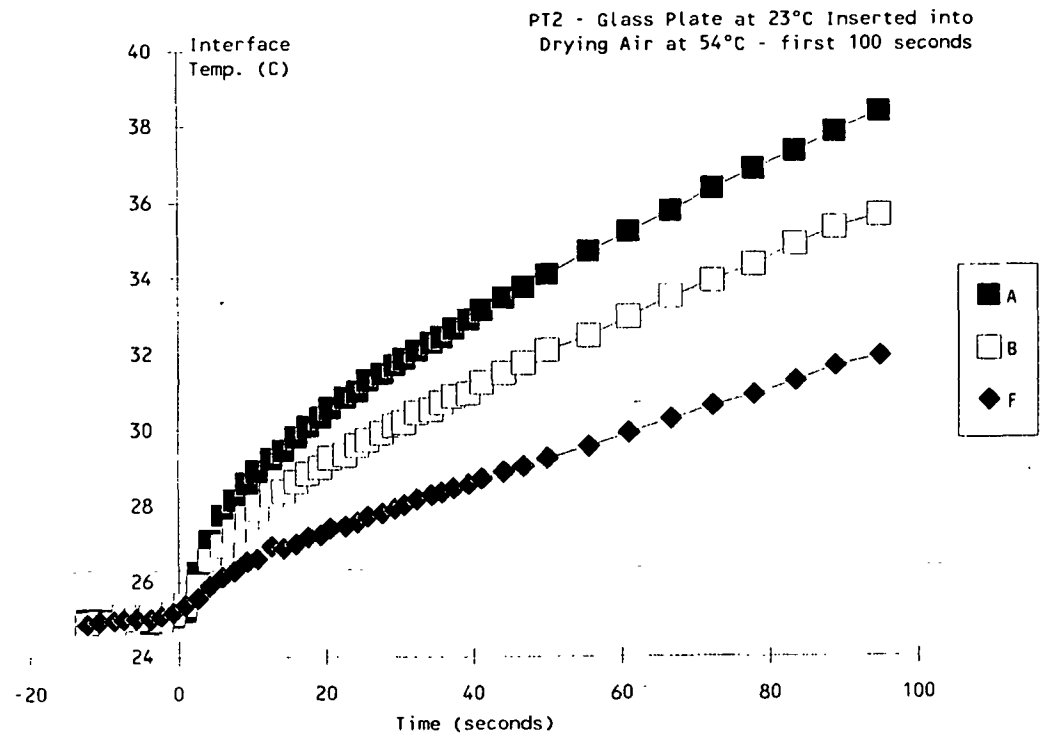


Figure 55. Trial PT2 temperature response of resistors A, B and F mounted in glass under drying conditions without coating.

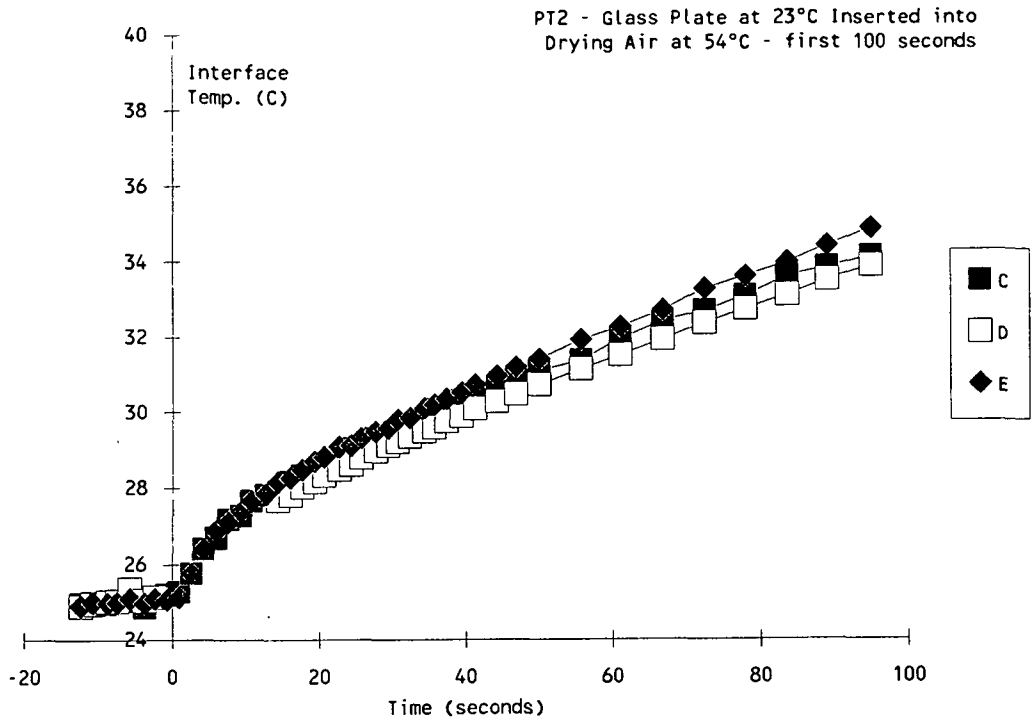


Figure 56. Trial PT2 temperature response of resistors C-E mounted in glass under drying conditions without coating.

The next pair of graphs, Fig. 57, are from a trial in which the plate was heated to a temperature five degrees hotter than the drying air before insertion. The trends were the same as those shown above except they were in the opposite direction. Resistor F experienced the greatest loss in temperature and resistors A and B showed the least. It is difficult to determine if the rate of cooling varied among resistors. The glass reached equilibrium temperature only after a relatively long time in the drier (20 minutes).

The equilibrium temperature difference between positions A and B was small, but between A and F the

difference was about 4°C. Resistors C, D, and E consistently yielded about the same temperature; this was expected because resistors C, D, and E were the same distance from the mouth of the drier. It is also noteworthy that the equilibrium temperatures were about 2°· to 4°C lower than the air temperature in the drier. Thermocouples sitting on the surface of the glass between resistors B and D registered about 1.5°C below that of the drying air. The lower temperatures may be the result of radiative heat loss from the exposed surface of the glass plate.

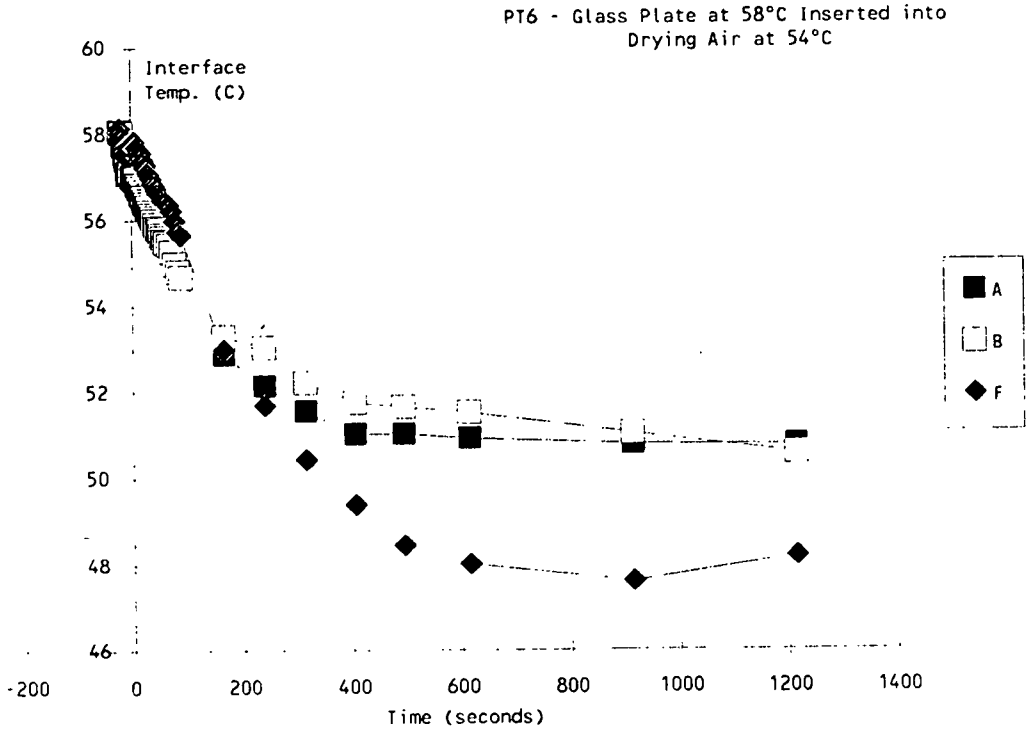


Figure 57a. Trial PT6 - temperature response of heated glass upon exposure to drying conditions without coating application.

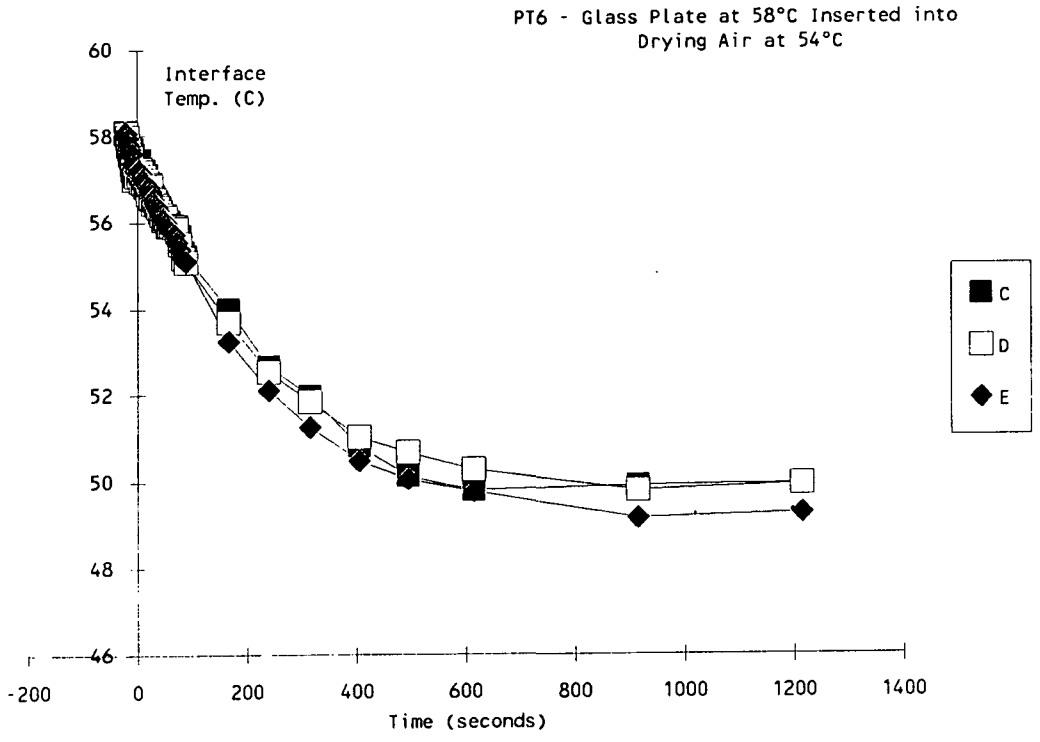


Figure 57b. Trial PT6 - temperature response of heated glass upon exposure to drying conditions without coating application.

## Coating Temperature During Drying

Figures 58-61 on the following pages show the temperature response of the glass surface when coated and dried at 55°C and 15% relative humidity.

When the coating was applied to the plate approximately 30 seconds prior to exposure to the drying air, the rate of cooling at the resistors increased relative to the cooling which occurred under room conditions. The top drawer was opened approximately five seconds after the temperature leveled off. Upon exposure to the drying air, the cooling rate of the coating color increased dramatically. The temperature reached a minimum shortly after the measured gloss point of the coating. After the temperature minimum, the glass surface tended toward a constant temperature slightly lower than that of the drier air. The above results provide evidence that evaporative cooling occurred during drying.

A temperature gradient was discovered in the air flow direction on the glass plate when no coating was applied to the glass (Figs. 56 and 57). Figures 60 and 61 show that there was also a temperature gradient present when a coating was applied. Evidence that the drying rate is different along the gradient can be seen by comparing times at the temperature minimum. For resistor A the gloss point was reached at 10 seconds and the minimum temperature was reached at about 12 seconds. The coating at resistor D, 9 cm down stream from resistor A, reached its gloss point at about 30 seconds, 20 seconds after the coating at resistor A.

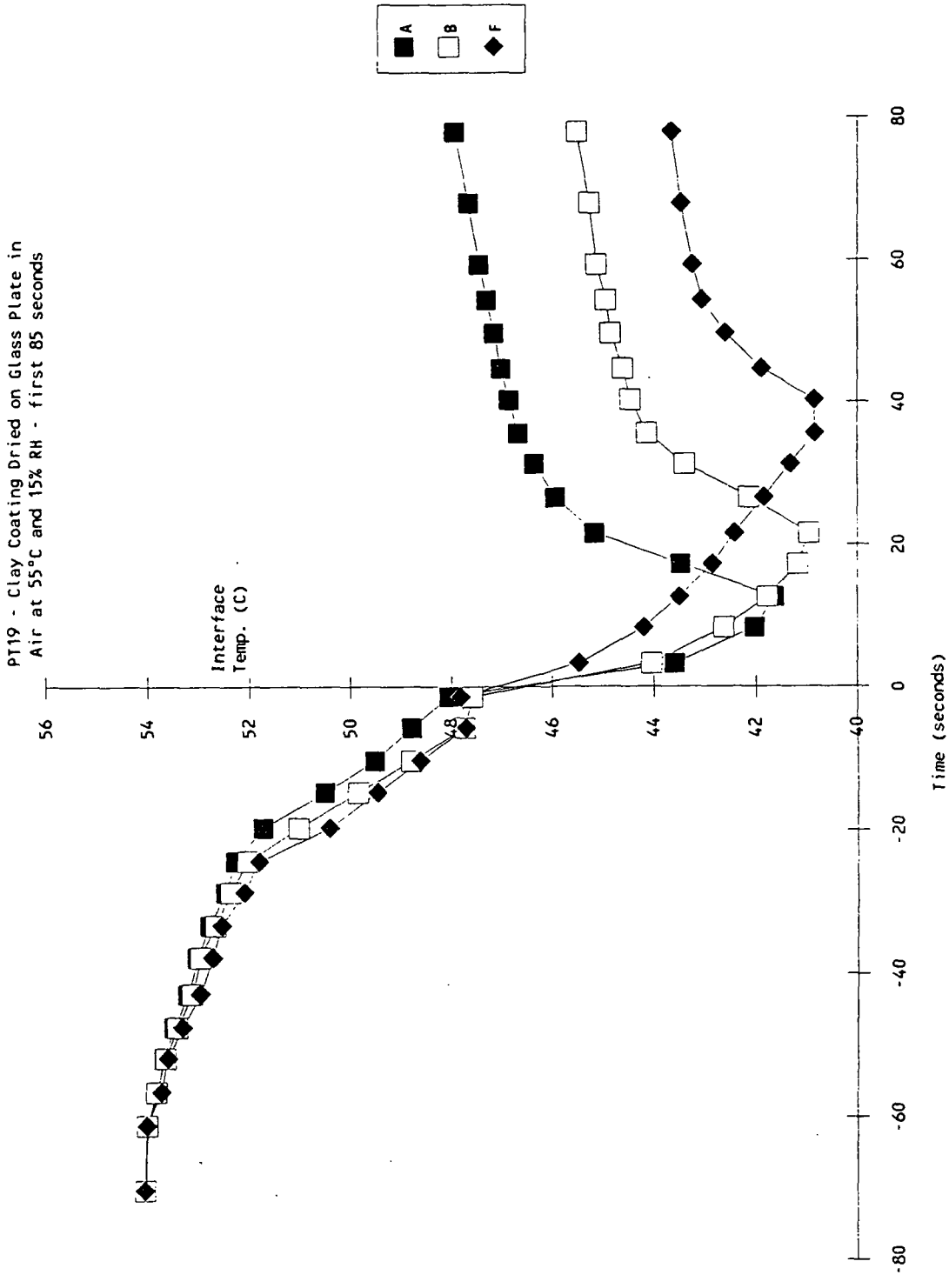


Figure 58. Temperature response for coating trial PT19. Clay coating applied and dried on the glass plate at 55°C and 15% RH. Plot of initial 80 seconds after insertion into the drier for resistors A, B and F.

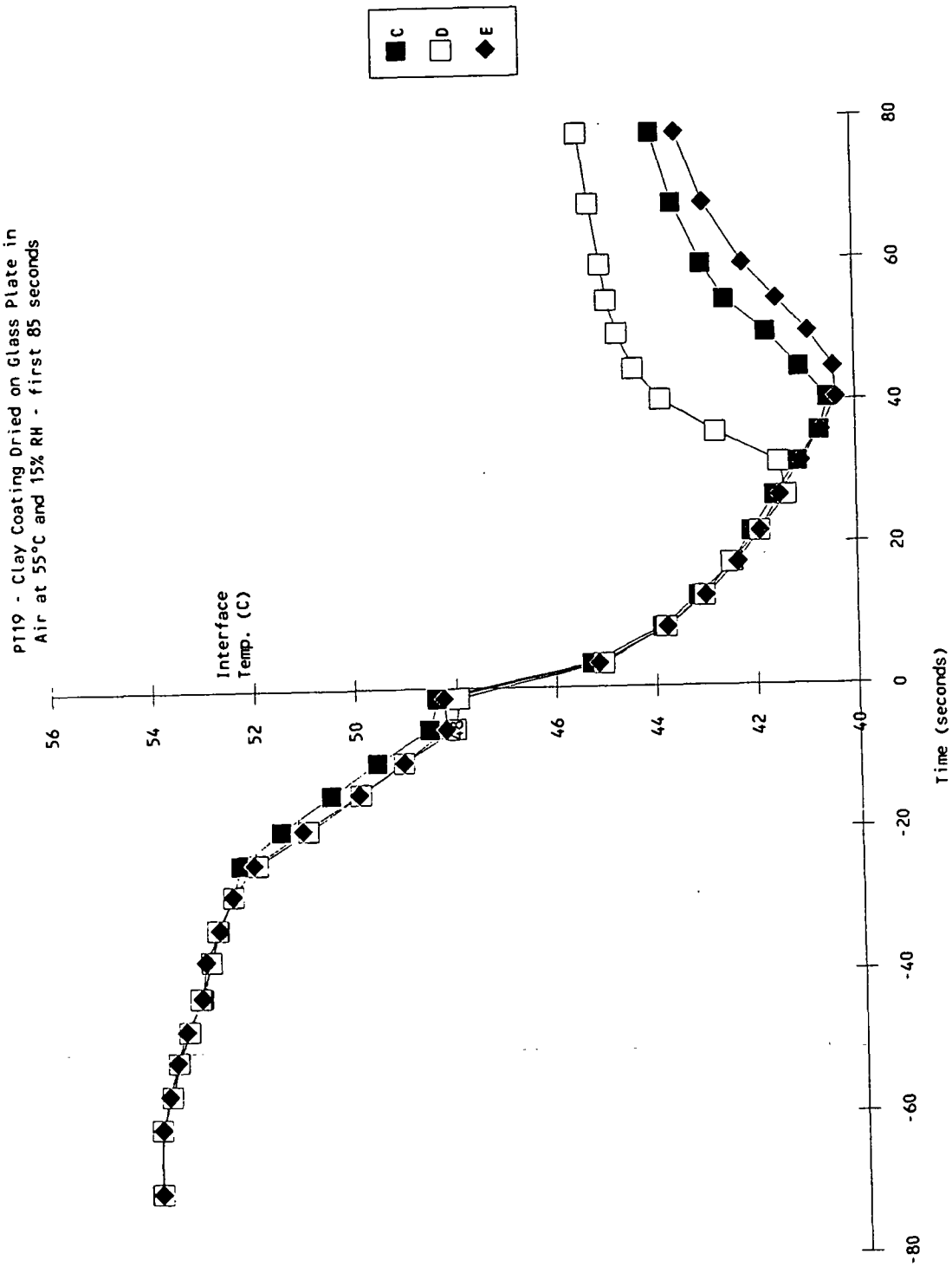


Figure 59. Same plot as Fig. 58 for resistors C, D and E.

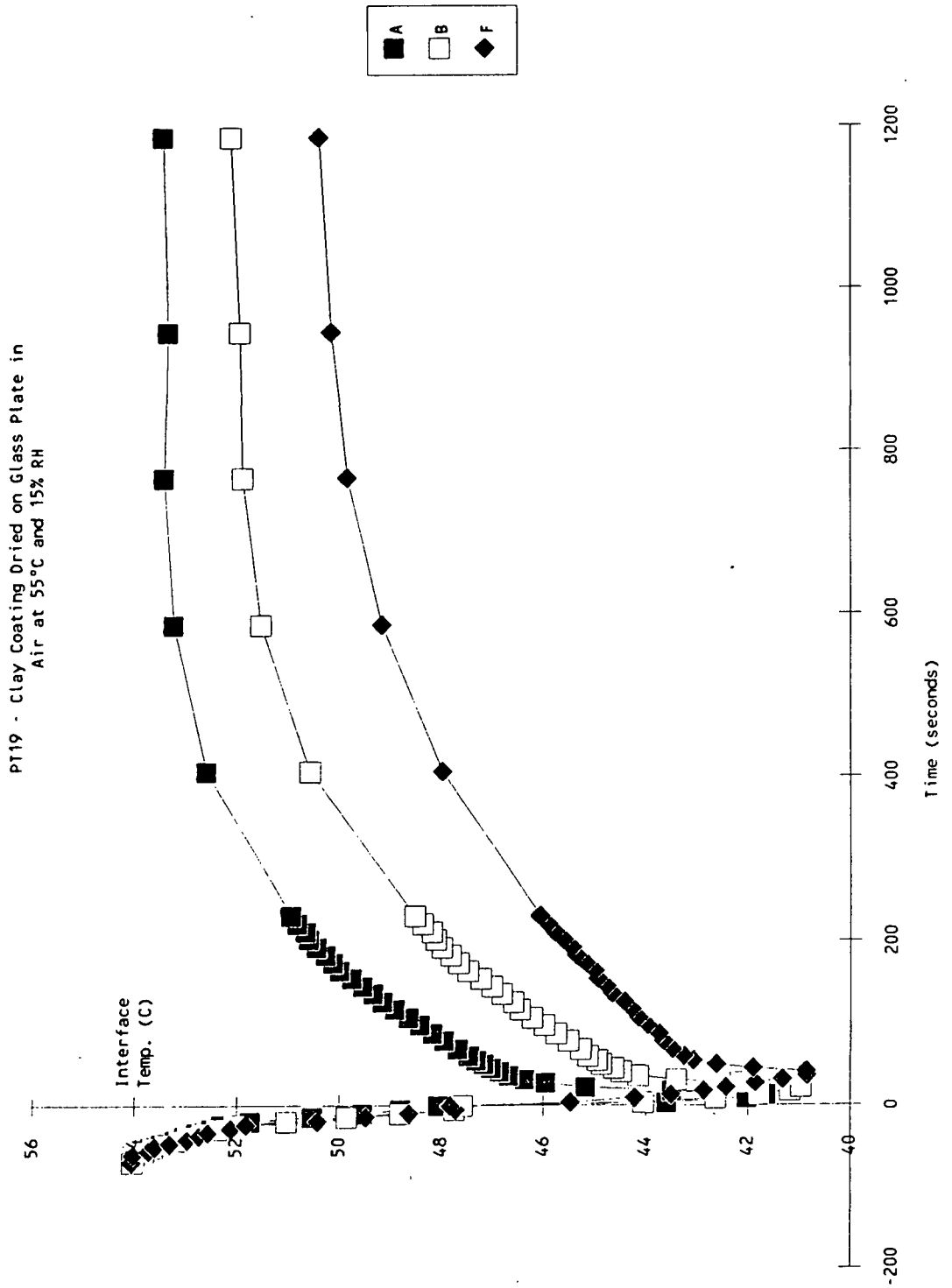


Figure 60. Same plot as Fig. 58 showing the entire trial.

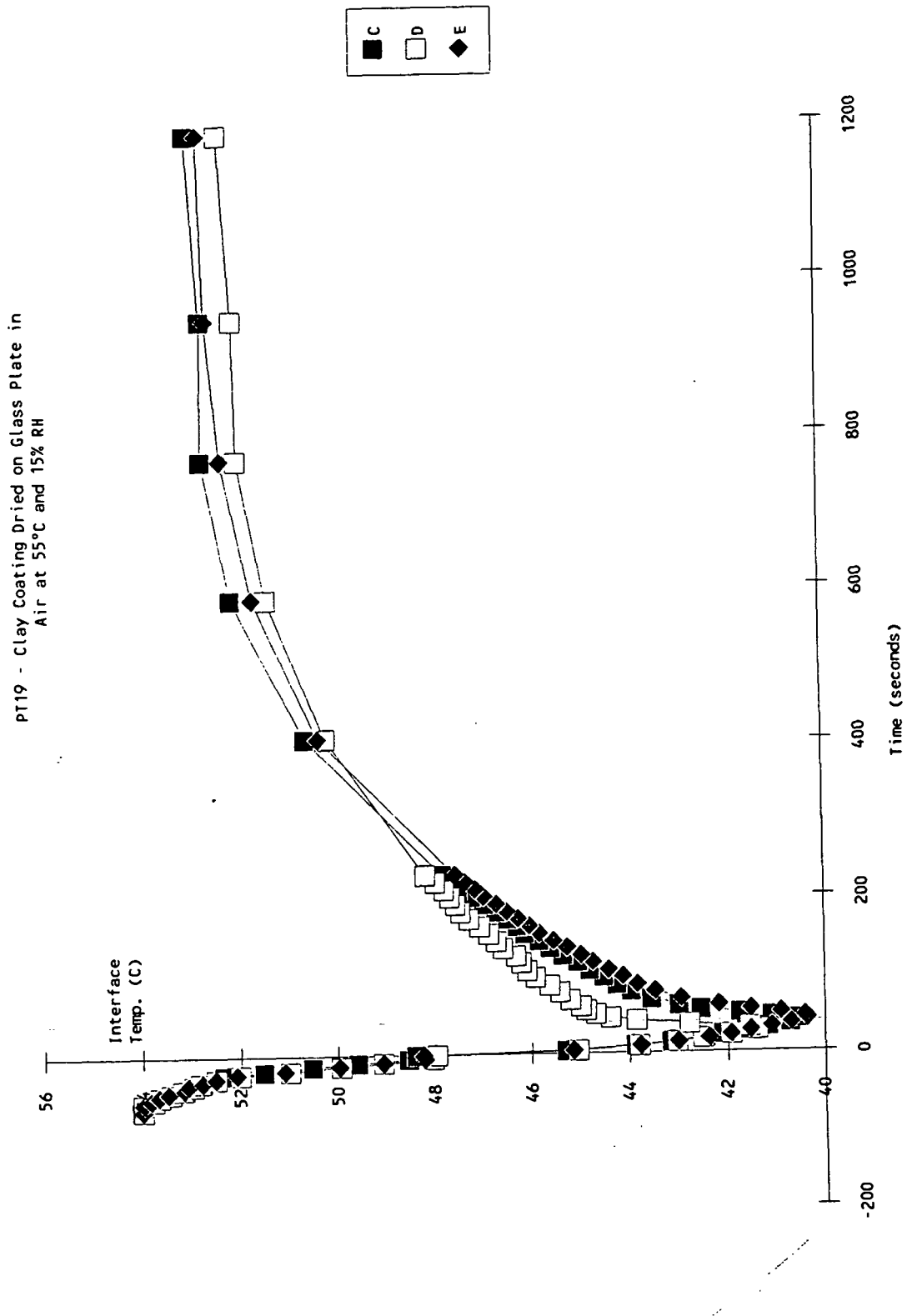


Figure 61. Same plot as Fig. 59 showing the entire trial.

Figures 62-65 (on the following pages) show the temperature response of the glass surface after coating application and drying at 55°C and 85% relative humidity.

Although the curves in Figs. 62-65 are similar to those in Figs. 58-61, two major differences are apparent. First, there was a difference in the rate of temperature change as the coatings entered the drier. For coatings dried at low RH (15%), the rate of cooling increased as the coating entered the drier, while for the coatings dried at high RH (85%) the cooling rate decreased. The decrease in rate of temperature drop as the coating entered the drier was caused by the difference in wet bulb temperatures of the air near the coating. Under ambient conditions the wet bulb temperature was close to 17°C, whereas in the drier it was 45°C. The difference between the wet bulb temperature and the coating bulk temperature was much greater when the coatings were exposed to room conditions, causing rapid cooling before insertion into the drier.

A second difference among the sets of temperature data was the additional time required to reach a minimum temperature (as well as higher observed minimum temperatures) for coatings dried at higher relative humidity. For example, resistor B dropped 1.5°C over 70 seconds under high humidity and 6.5°C in 20 seconds under low humidity.

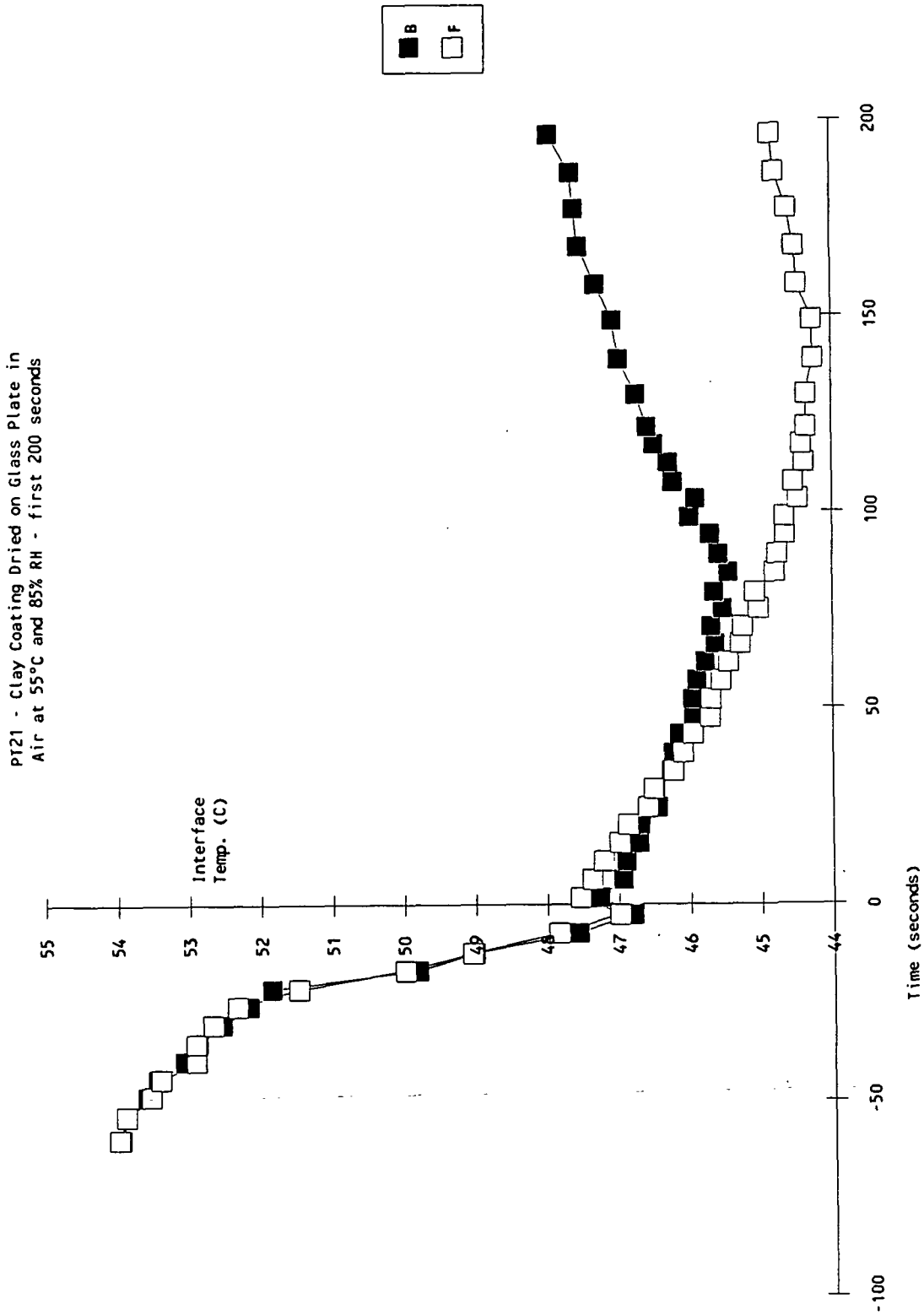


Figure 62. Temperature response for coating trial PT21. Clay coating was applied and dried on the glass plate at 55°C and 85% relative humidity. Plot of 80 seconds after insertion into the drier for resistors B and F.

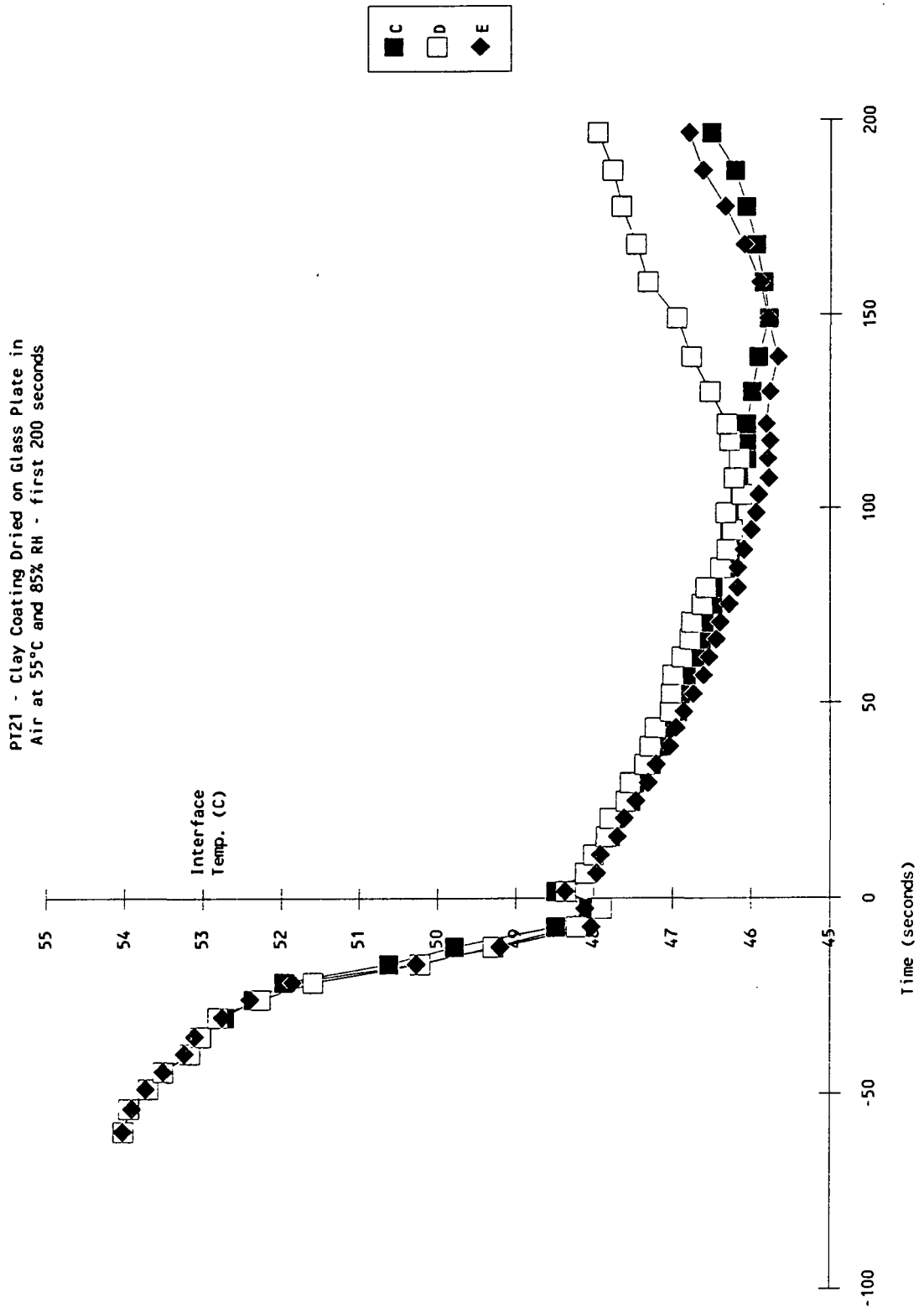


Figure 63. Same plot as Fig. 62 for resistors C, D and E.

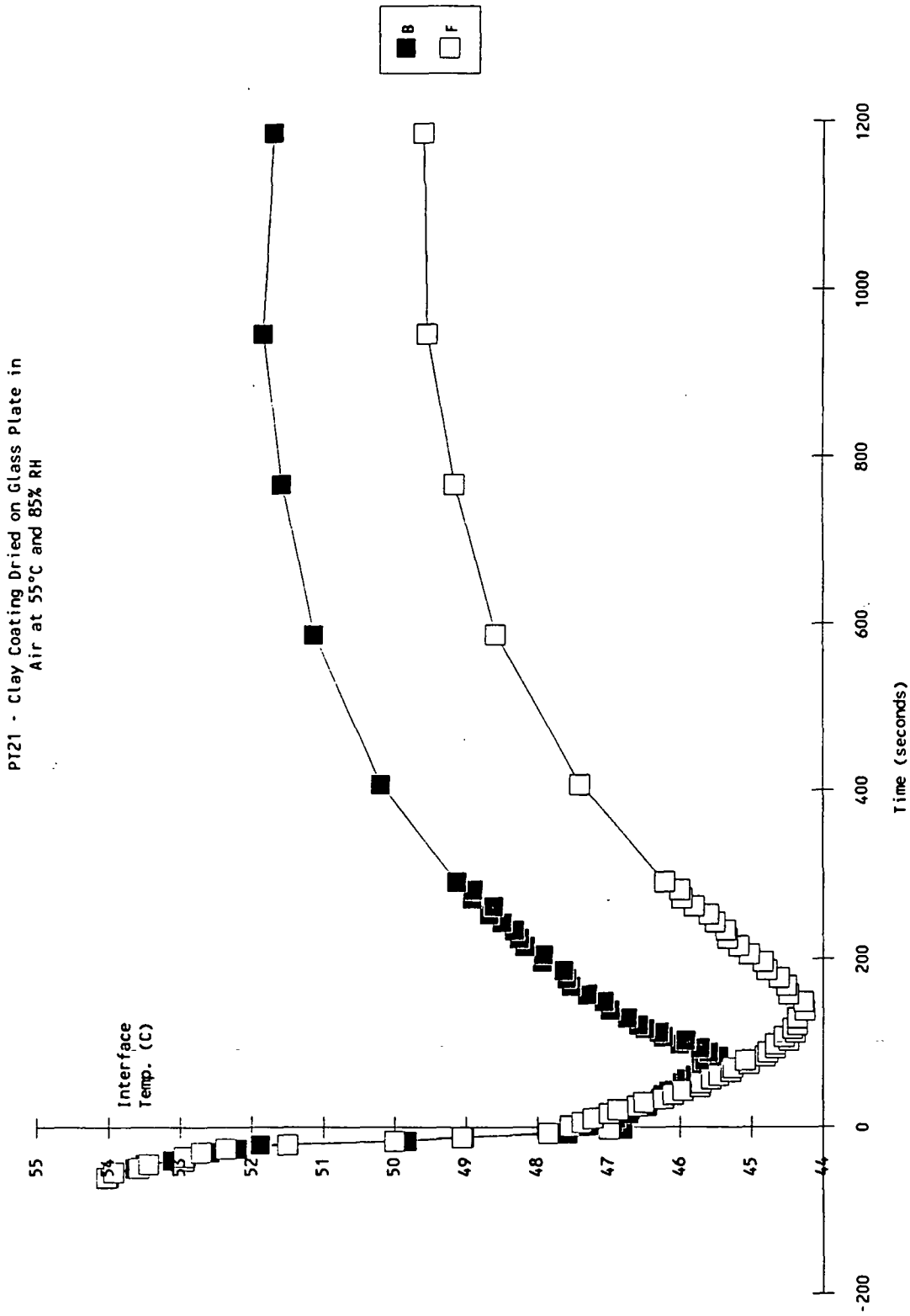


Figure 64. Same plot as Fig. 62 showing the entire trial.

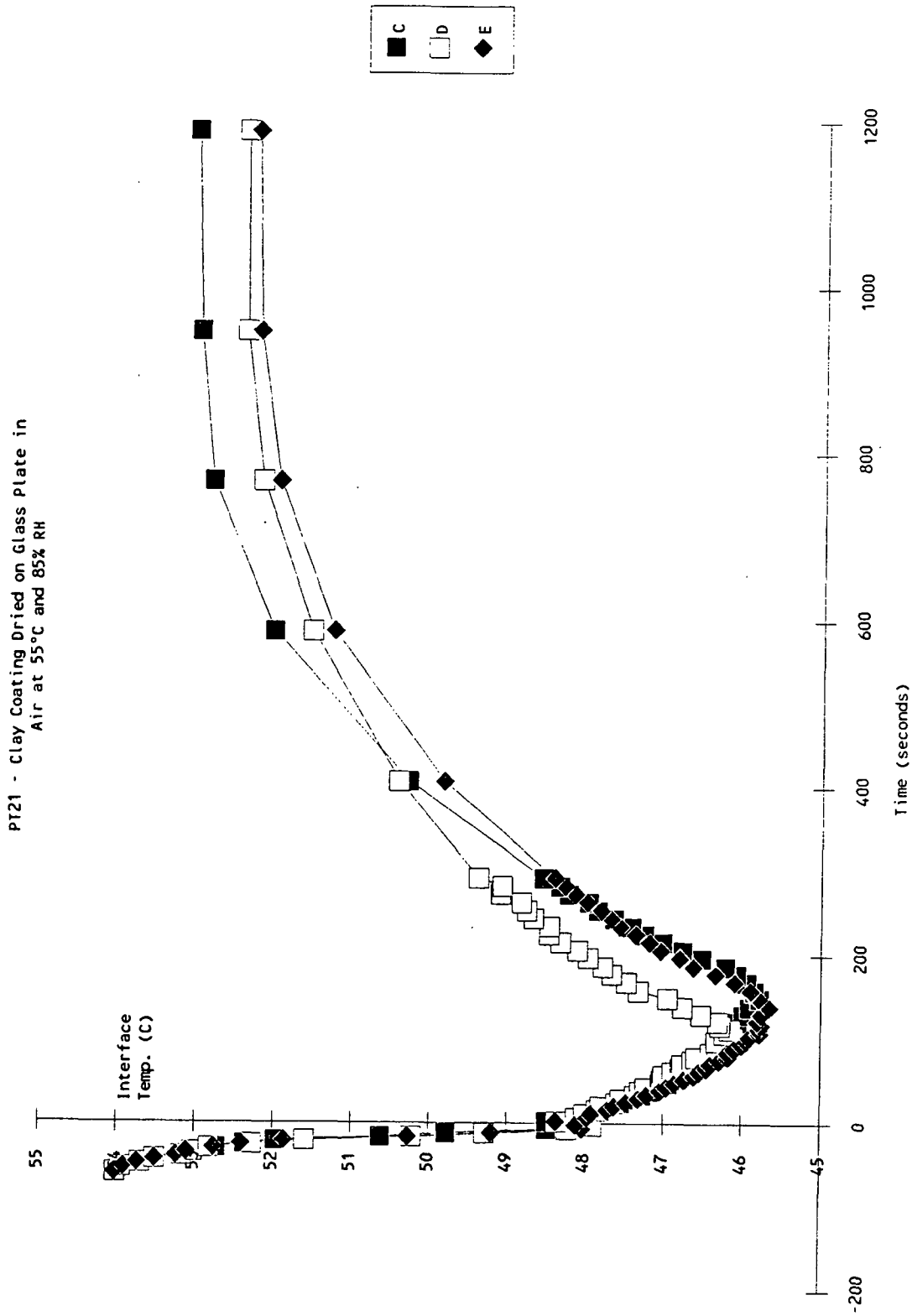


Figure 65. Same plot as Fig. 63 showing the entire trial.

## Interpretation of Results

The wet bulb temperatures of the drier air during the trials whose temperature data are shown in Figs. 58-61 was 29 °C, and 45°C for the curves shown in Figs. 62-65. The temperature minima at resistor B were 41°C and 46°C respectively. Because of the thinness of the coating layer, one would expect that any change in its temperature would be instantaneous within the layer; therefore, the coating temperature should be at the wet bulb temperature of the drying air. Because the minimum temperatures did not always reach the wet bulb temperature of the drying air, initial review of the data led the author to believe there were temperature gradients across the coating films during drying.

There are two possible aspects of the system that could account for the high minimum temperature of the coating glass/interface. Vaporization requires an energy input. The energy sources in the system employed were the drying air, the glass plate and coating layer. For the short time necessary to reach the gloss point during the experiments, both the glass and the drying air are assumed to function as an infinite energy source and remain at constant temperature. Therefore, the energy loss (cooling) that occurs during vaporization is minimal. However, the cooling will be greater for coatings dried at higher rates because the rate of energy consumption is greater.

Alternatively or perhaps simultaneously, the boundary layer adjacent to the coating surface may have been at a different level of saturation than the bulk air flow. The higher the saturation level of the air near the surface the higher the wet bulb temperature will be. Thus, because evaporation occurs at the wet bulb temperature of the air in contact with the coating, the temperature of the coating should be greater than the wet bulb temperature of the drying air. Either of the above mechanisms could account for the discrepancy between the coating temperature and the wet bulb temperature of the drying air.

Employing rough estimates, the help of Dr. Jeff Lindsay(131), and assuming that no temperature gradient existed within the coating layer, calculations were made to determine if the coating temperatures measured were reasonable. The calculations are shown in Appendix III.

It was assumed that: 1. the bottom of the glass had insignificant heat loss, 2. the air temperature was constant, 3. the coating surface remained saturated, 4. the coating and glass had the same thermal properties, and 5. that the air had a zero humidity. The last two assumptions are questionable. To simplify the model and to compensate for the unknown thermal properties of the coating as it dries and the unknown thermal properties of the interface between the coating and the glass, the thermal properties were chosen as the average of the glass, water and clay. Zero humidity

drying air was chosen to be the most drastic case, providing a system with the largest temperature difference between the evaporating surface and the bulk air and glass. Even though dry air was not used experimentally, it would be the case which produced the greatest temperature difference between the wet bulb temperature of the drying air and the wet coating and glass. Using such an extreme might help determine if it were possible, under the assumed conditions, to have a temperature gradient present in the coating film.

The transient heat transfer during drying is governed by the heat equation. The solution is a function of the properties of the materials, the heat transfer coefficient and the evaporative mass flux. The mass flux involves the mass transfer coefficient and the saturation level of the air. The Chilton-Colburn Analogy(132) relating the heat and mass transfer coefficients was used to solve for the coefficients. The Crank-Nicholson(133) numerical method was used to solve the equations with the Crout algorithm(134) for determining the implicit temperatures. Figures 66-68 show the results of the analysis.

Figure 66 (low heat transfer rate) shows that it would take 15 to 20 minutes for the system to reach thermal equilibrium if evaporation could continue that long. Under the short times that the surface of the coating remained saturated at the high drying rates (10 to 20 seconds), Figure 67 shows that a temperature of near 47°C would be achieved.

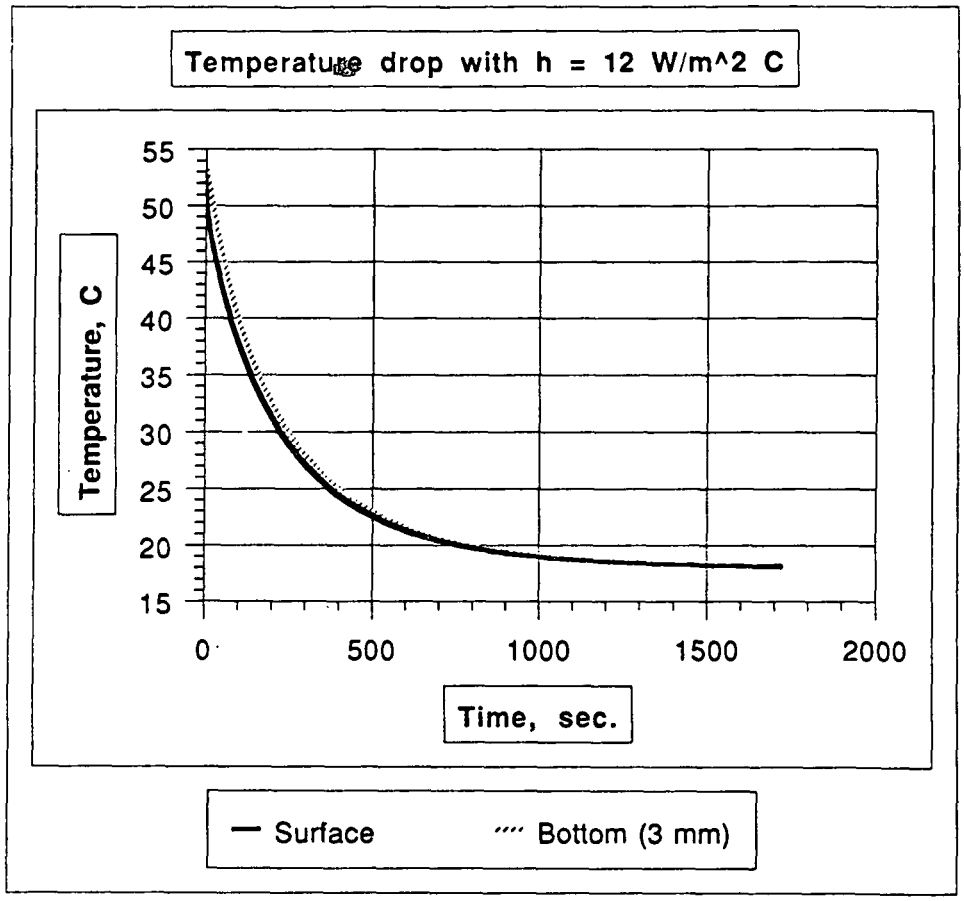


Figure 66. Calculated temperature versus time plot for the coated glass-heat transfer coefficient 12 $W/m^2°C$.

For the actual coating, the initial heat transfer rate could be as high as 69 $W/m^2°C$ (theoretical value for laminar flow over a flat plate), which would drop as the coating dries. The higher heat transfer rate of the actual coating may account for lower measured temperatures relative to values from Figs. 66 and 67. Figure 68 shows that, under the same conditions and with the heat transfer coefficient of 69 $W/m^2°C$, the temperature would be 33°C at 25 seconds. The measured temperature, for the conditions used in the calculations, was 41°C. The difference can be explained by

the fact that the calculated values of 47°C and 35°C for heat transfer rates of 12 and 69 W/m$^2$°C respectively, were calculated as reasonable extremes of heat transfer rates; the actual heat transfer rate and temperature minimum were probably between the calculated extremes. Also, the fact that the temperature difference between the wet bulb temperature of the drying air and drier air temperature was maximized places the calculated temperature slightly higher than the actual value.

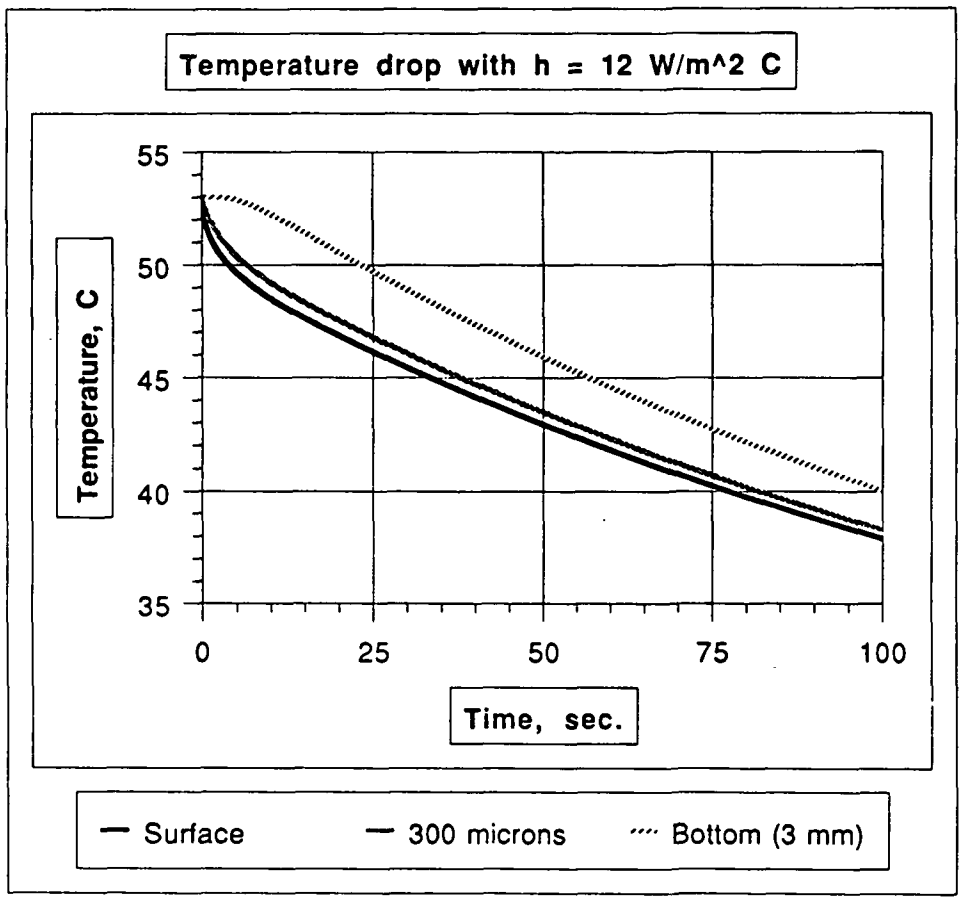


Figure 67. First 100 seconds of Fig. 66 including the temperature at 300 μm into the glass from the coating surface.

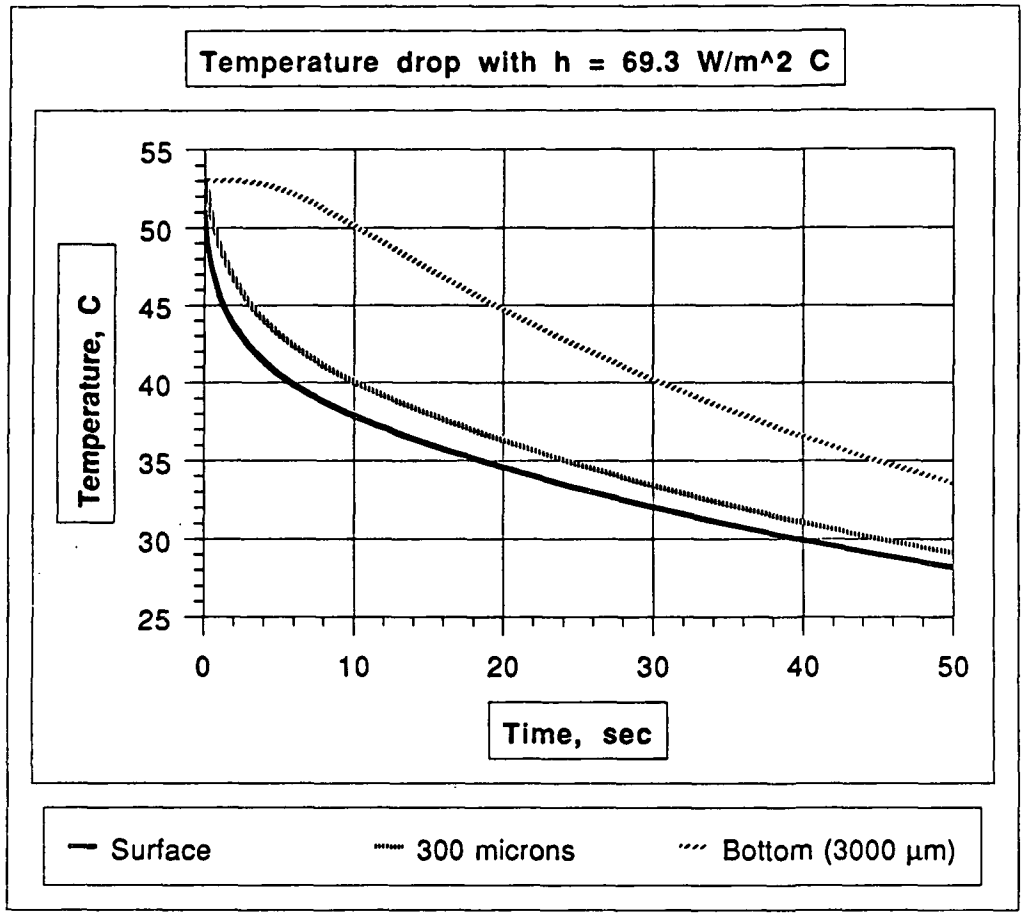


Figure 68. Calculated temperature versus time plot for the coated glass-heat transfer coefficient 69 W/m$^2$°C.

The results of the above calculations show that temperatures measured during drying were reasonable; if it is assumed that there was no temperature gradient in the coating layer, then it can be concluded that there was no convective fluid flow within the coating layer as the result of temperature gradients. It can also be concluded that differences in z-directional pore volume distributions between coatings were not artifacts of temperature gradients present during the consolidation of the coating.

Another implication of the above results is that drying rate is not completely independent of temperature. The coatings dried at slower rates actually dried at slightly higher temperatures than those dried at faster rates. The largest measured temperature difference (at constant drier temperature) was 6°C. This is comparatively small compared to the 100°C difference used in the oven drying experiments which produced changes in both drying rate and coating structure. It was assumed that small temperature differences did not affect the packing structure of the coating films and that the drying system used was adequate to test the effect of drying rate on coating structure.

Variation in Coating Structure with Position in Drier

Coating films dried at high rates were found to have greater total void volume than coatings dried at low rates (discussed later). The local drying rate of coating films dried in the experimental drier varied depending on their position in the drier. The coating near the air inlet dried faster than the coating near the exhaust. For example, a point one inch from the opening and a point five inches downstream may have gloss points which differ by one second or by as much as 13 seconds. To test whether the drying rate gradient caused significant differences in film structure, coating films were tested for total pore volume at different locations along the drying path. Table XIV contains the results of the measurements.

TABLE XIV

Total Pore Volume of Coating Films Dried at
Low Temperature and Medium Relative Humidity

Coating Trial T35R55

Average Drying Rate 1.1 kg/m$^2$hr

| Sample | 1 | 2 | 3 | 4 | Overall |
|---|---|---|---|---|---|
| Image Analysis | 42.90% | 42.95% | 42.93% | 43.17% | 42.93% |
| Std. Dev. | 0.05 | 0.26 | | | 0.18 |
| Oil Absorption | 42.76% | 42.89% | 43.00% | 42.97% | 42.90% |
| Std. Dev. | | | | | 0.11 |
| Near Inlet | 42.55% | 42.93% | 43.18% | 42.70% | 42.84% |
| Std. Dev. | | | | | 0.28 |
| Near Exhaust | 42.35% | 42.88% | 42.89% | 43.23% | 42.84% |
| Std. Dev. | | | | | 0.36 |

Data in Table XIV indicates that there was no detectable difference in total pore volume among different areas of the coatings dried in the experimental drying system. The trial chosen for the analysis had a relatively low drying rate (1.10 kg/m$^2$hr) and the difference in time to gloss point from inlet to exhaust was approximately seven seconds. The time difference corresponds to a difference in drying rate of approximately 0.12 kg/m$^2$hr.

## Viscosity Limitation of Drying Apparatus

The shear forces exerted on the coating surface by the drying air influenced the surface structure of the coating. Coatings were dried under various air velocities to determine the maximum air flow that could be used without damaging the

coating surface. For latex coatings, full drier air velocity (30.1 $ft^3/min$) caused waves which resulted in cracks and visible coat weight variations in the dry coating. The low viscosity of the plastic pigment did not provide enough resistance to flow when it was sheared by the drying air. Tests were run at diminishing flow rates until the coatings showed no visual signs of change during drying. Examination of the coatings using an SEM confirmed the results (Fig. 69). At high magnification, coatings dried with low air flow rates (4.1 $ft^3/min$), appeared to have an uninterrupted uniform packing structure. In Fig. 70 it can be seen that the coatings which were dried at high air flow rates had discontinuities and piles of particles. At low flow rates these defects disappeared and the piling of the pigment ceased.

Similar tests were performed on clay coatings. Clay dispersed to 70% solids was applied to the plastic substrate and dried under full air velocity. No flow during drying was detected. The solids content of the clay solution was reduced and the test repeated. No detectable effect of the air flow was found until coating solids content of 55% was used, at which point, the viscosity of the coating dropped below 300 cP (Brookfield 100 rpm).

All the coatings dried in the experimental drier were dried under the low flow rate conditions.

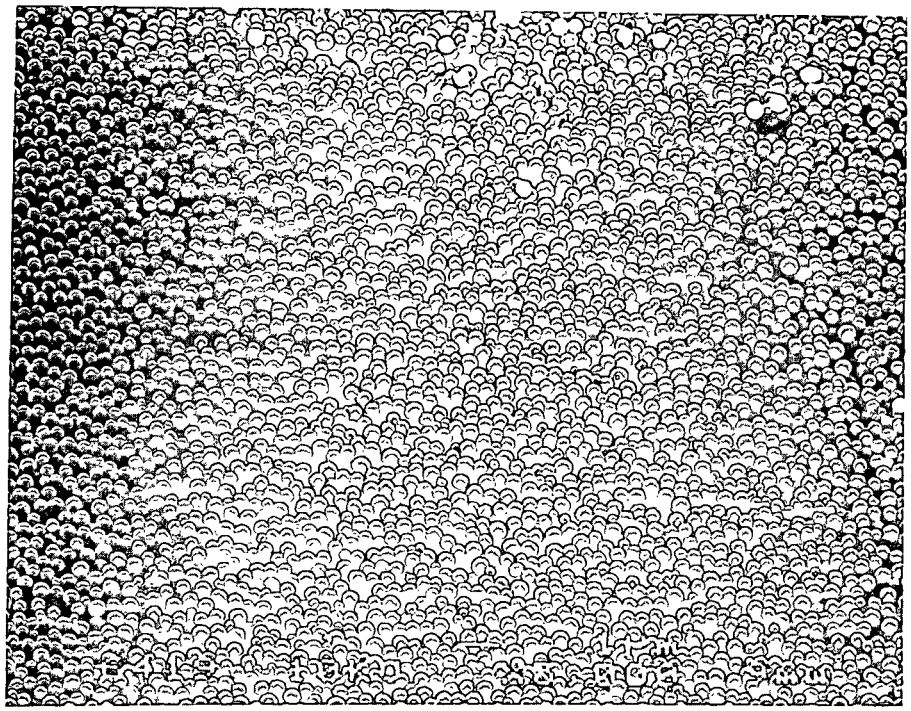

Figure 69. Electron micrograph of the surface of a polystyrene/acrylate latex coating dried at low flow rate. SEM 5,000X.

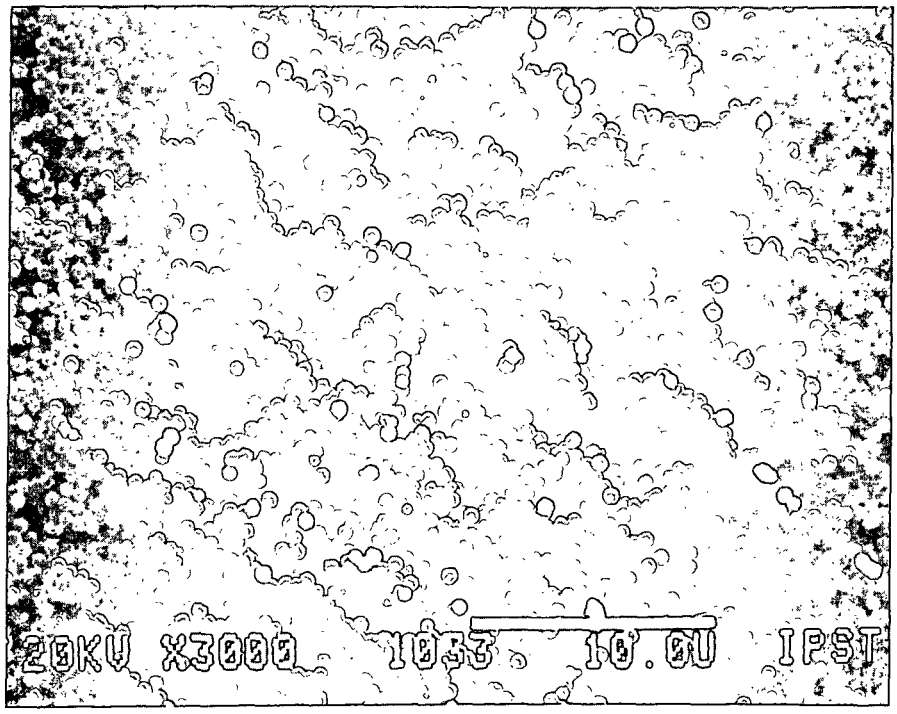


Figure 70. Electron micrograph of the surface of a polystyrene/acrylate latex coating dried at high air flow rate. SEM 3,000X.

Packing Structure of Latex Pigment

In order to determine how the polystyrene spheres pack and to determine if there is a difference between the surface structure and the bulk structure, the latex pigment was poured into a 25 mm diameter, 5 mm deep embedding mold and allowed to air dry. The dry structure was coated with Au-Pd and examined with the SEM. The surface of the dried puddle was flat, with particles packed in a triangular and pentagonal arrangements (Figs. 71-72). A cross-section of the dried puddle was made by freeze fracturing the sample (embedding latex coating was unsuccessful), but the sample did not break cleanly. Figure 73 is a micrograph of the cross-section produced by freeze fracture. The bulk of the structure appeared to be more three-dimensional and have less order than the surface. The depth apparent in Fig. 73 may be an artifact of the sample preparation technique. Because of the difficulty in preparing the polystyrene latex for electron microscopy observation no conclusions about the bulk structure can be drawn. However, the images did show that the surface structure of the latex pigment which had been dried slowly at room temperature was dense and uniform.

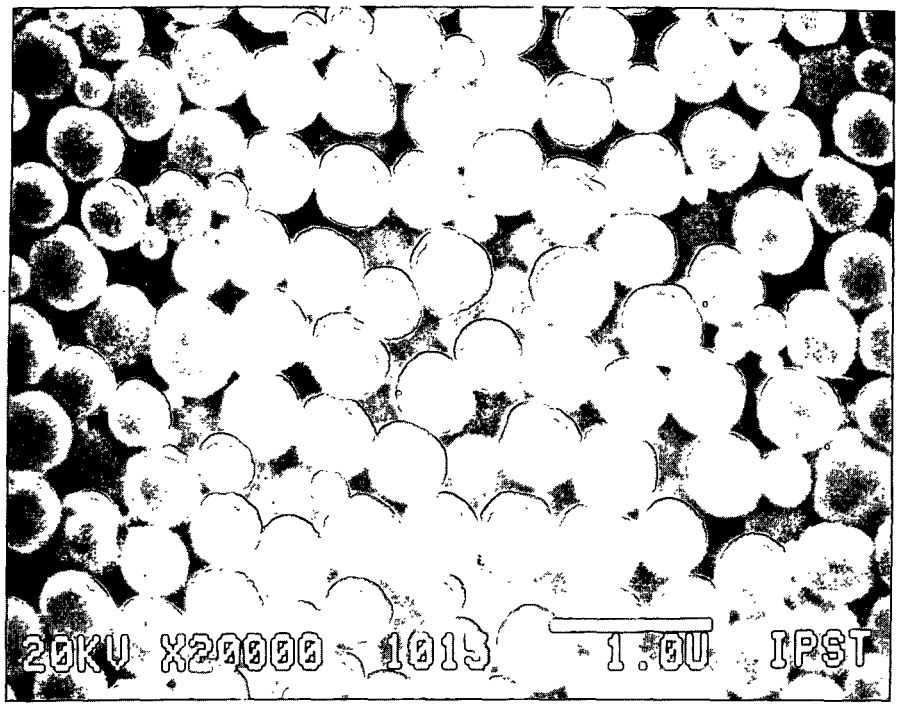


Figure 71. Photomicrograph of the surface of a dry polystyrene latex puddle. Photo taken near the middle of the puddle. SEM 20,000X

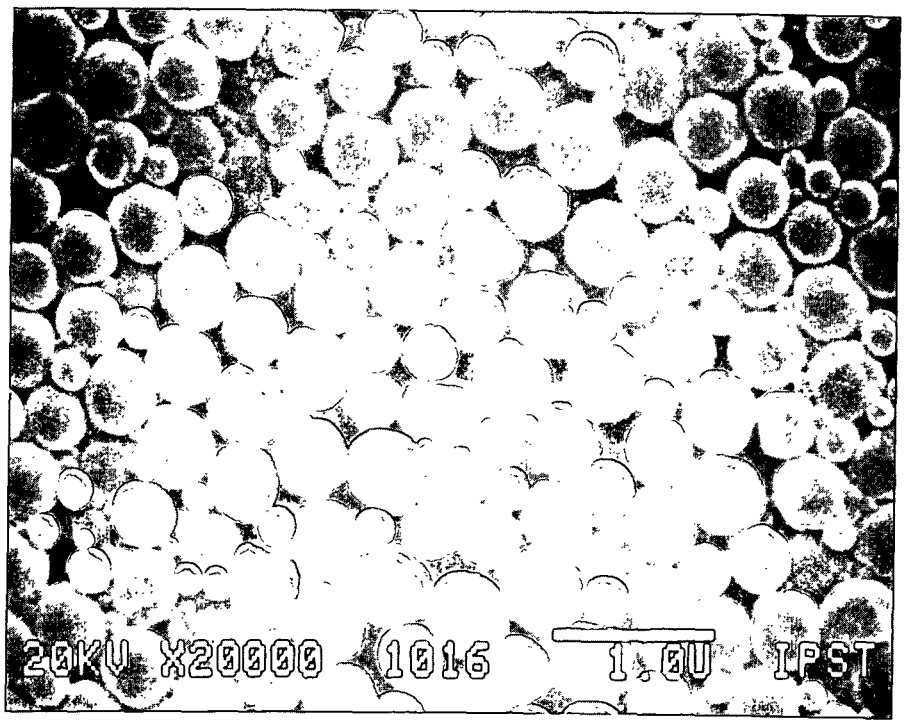


Figure 72. Photomicrograph of a the surface of a dry polystyrene latex puddle. Photo taken near the edge of the puddle. SEM 20,000X

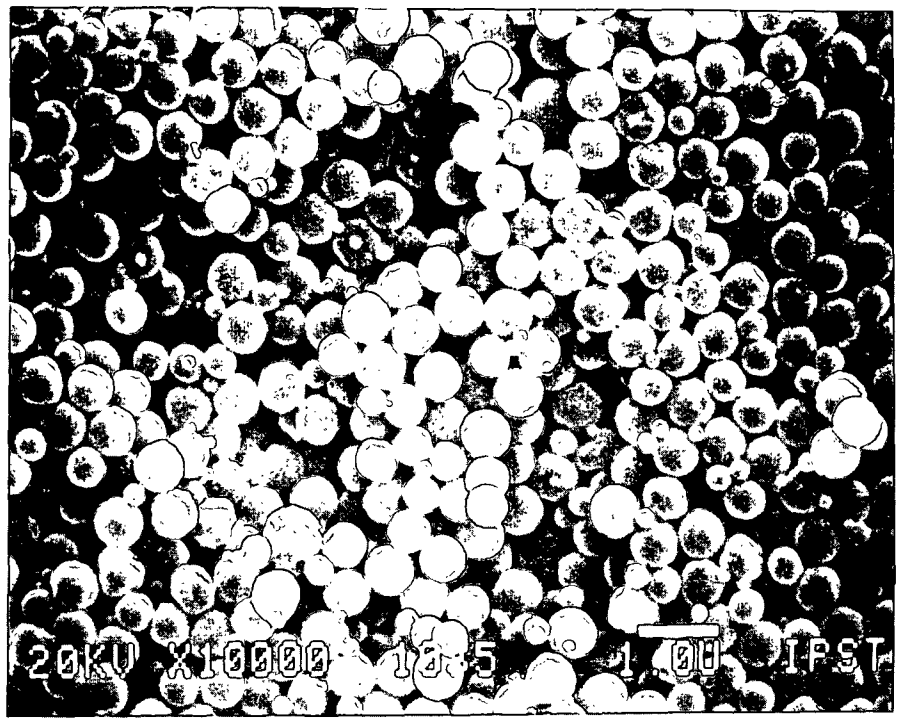


Figure 73. Photomicrograph of a cross-section of a dry polystyrene latex puddle, taken near the middle of the puddle. SEM 10,000X

Figures 71 and 72 show that the structure of the surface layer is dependent upon the location relative to the edge of the coating puddle. The latex dispersion formed a meniscus in the embedding mold and was observed to dry from the edges inward. The pigment packing structure near the rim of the meniscus (Fig. 72) was denser than the packing structure near the bottom of the meniscus (Fig. 71). This implies that surface tension forces, responsible for the formation of the meniscus, affected the packing structure of the surface particles. The surface tension forces are continuous and directed along the curvature of the meniscus. The maximum pressure on the surface particles occurs at the rim where the fluid is bounded by the wall of the mold. The pressure

results in a denser packing arrangement near the rim of the puddle of coating. Because the surface tension of a liquid is inversely related to its temperature, the temperature of application and the drying temperature will have an effect on the packing structure of the coating surface. Because the distribution of the void volume through the coating thickness is hypothesized to depend on the structure of the surface, the void volume distribution would be affected by the variables affecting the surface structure of the coating. Therefore, the importance of temperature control in this study is again emphasized.

Summary of the Drying Apparatus Effectiveness

The drying apparatus used in the experiments was adequate for drying coatings at different rates through control of the drying temperature and the relative humidity of the drying air. Temperature measurements made at the substrate/coating interface showed that no significant temperature gradient exists in the coating thickness. However, temperature and drying rate gradients do exist in the drier. Further, it was also discovered that, even at constant air temperature, the coatings were not dried at exactly the same temperature when relative humidity was changed. The coatings dried at high relative humidity were dried at a maximum of a 6°C higher temperature. It is assumed that the small temperature difference did not affect packing structure to any measurable extent.

The drying system was used as described in the Material and Methods section to produce coatings whose structural differences resulted from changes in the drying rate independently of other process variables.

## PRELIMINARY DRYING EXPERIMENTS

Pairs of coatings, one dried at room temperature and one dried at 120°C in a vacuum oven, were evaluated using oil absorption to measure the relative pore volumes of the coatings. The test was repeated four times for each coating. Results are given in Table XV.

Table XV

Results of Total Pore Volume of Hand Coatings

| | | 21°C | | 120°C | |
|---|---|---|---|---|---|
| Coating Code | vph Binder | Pore Volume | Std. Dev. | Pore Volume | Std. Dev. |
| 4000 | 0 | 38.8% | 0.5 | 39.7% | 0.6 |
| 4001 | 2.94 | 37.7% | 0.3 | 38.5% | 0.3 |
| 4002 | 5.43 | 37.2% | 0.7 | 37.5% | 0.3 |
| 4003 | 7.97 | 36.6% | 0.6 | 37.0% | 0.5 |
| 4004 | 11.09 | 35.4% | 0.4 | 36.2% | 0.3 |
| 4005 | 16.12 | 34.3% | 0.4 | 35.7% | 0.6 |
| 4006 | 22.56 | 28.9% | 0.7 | 31.1% | 0.2 |
| 4007 | 34.11 | 24.2% | 0.6 | 25.0% | 0.7 |
| 4008 | 50.15 | 18.7% | 0.7 | 18.6% | 0.8 |

At a 90% confidence level coatings 4000, 4001, and 4004-4006 dried at 120°C (1.54 $kg/m^2hr$) had pore volumes significantly higher than comparable coatings dried at room temperature (0.12 $kg/m^2hr$). There was no detectable difference between the other pairs of coatings.

The coatings were studied using image analysis techniques. Seven sections from each coating, containing no binder (4000a-21°C and 4000b-120°C), were analyzed for total pore volume and pore volume distribution using image analysis. The results are presented in Table XVI.

Table XVI

Results of Image Analysis Determination of the Pore Volume and Pore Volume Distribution of Coatings Dried at 21°C (4000a) and 120°C (4000b)

| 4000A Sect. NO. | Total Pore Vol | Relative Pore Volume (%) Depth into Coating (μm) 1 | 2 | 3 | 4 | 5 | 6 | 7 | 8 | 9 | base 10 |
|---|---|---|---|---|---|---|---|---|---|---|---|
| 1 | 36.7 | 37.0 | 35.5 | 36.5 | 36.0 | 37.2 | 38.0 | 37.5 | 37.0 | 35.2 | 35.0 |
| 2 | 37.1 | 36.2 | 34.1 | 35.7 | 36.2 | 37.8 | 38.4 | 38.0 | 36.9 | 36.1 | 35.2 |
| 3 | 39.0 | 38.1 | 36.6 | 35.0 | 35.6 | 37.0 | 38.8 | 40.6 | 39.2 | 37.9 | 37.1 |
| 4 | 38.4 | 36.8 | 34.9 | 36.0 | 36.6 | 37.5 | 38.6 | 38.5 | 38.0 | 36.3 | 35.8 |
| 5 | 37.8 | 37.1 | 35.7 | 35.5 | 35.8 | 37.8 | 38.2 | 37.9 | 37.3 | 36.6 | 36.0 |
| 6 | 38.0 | 36.9 | 35.5 | 35.9 | 36.4 | 37.5 | 38.6 | 38.0 | 37.7 | 36.6 | 35.1 |
| 7 | 38.3 | 37.0 | 35.4 | 35.7 | 36.2 | 37.7 | 38.8 | 38.2 | 37.4 | 36.1 | 35.9 |
| avg. | 38.0 | 37.0 | 35.4 | 35.8 | 36.1 | 37.5 | 38.5 | 38.4 | 37.6 | 36.4 | 35.7 |
| std. | 0.8 | 0.6 | 0.8 | 0.5 | 0.3 | 0.3 | 0.3 | 1.0 | 0.8 | 0.8 | 0.7 |
| 4000B | | | | | | | | | | | |
| 1 | 39.2 | 36.2 | 33.4 | 34.2 | 36.7 | 38.1 | 39.7 | 40.3 | 38.2 | 37.8 | 36.4 |
| 2 | 38.6 | 35.9 | 34.5 | 33.9 | 37.2 | 37.9 | 39.4 | 39.7 | 39.1 | 38.1 | 36.4 |
| 3 | 38.7 | 36.9 | 34.2 | 34.6 | 36.5 | 38.3 | 39.6 | 38.9 | 38.8 | 36.9 | 35.3 |
| 4 | 38.9 | 36.5 | 33.1 | 34.0 | 37.9 | 38.5 | 39.5 | 39.3 | 38.5 | 37.3 | 35.9 |
| 5 | 39.2 | 37.1 | 33.9 | 35.2 | 37.2 | 37.8 | 39.6 | 39.7 | 38.7 | 37.9 | 36.7 |
| 6 | 38.6 | 35.8 | 34.2 | 34.7 | 37.0 | 38.0 | 39.2 | 39.4 | 39.2 | 38.0 | 36.4 |
| 7 | 36.3 | 36.3 | 34.3 | 34.1 | 36.6 | 38.0 | 39.3 | 38.9 | 38.9 | 37.9 | 36.1 |
| avg. | 38.9 | 36.4 | 33.9 | 34.5 | 37.0 | 38.1 | 39.5 | 39.5 | 38.8 | 37.7 | 36.2 |
| std. | 0.3 | 0.5 | 0.5 | 0.5 | 0.5 | 0.2 | 0.2 | 0.5 | 0.3 | 0.4 | 0.5 |

Results from Table XVI are shown graphically in Fig. 74. The total pore volumes for coatings dried at 120°C were higher than the coatings dried at room temperature; however, there was no statistical difference between distributions at

a 95% confidence interval. Figure 74 shows that the pore volume distributions follow similar curves. The void volume distribution for the coating dried at 120°C had a greater difference between a extremes in local void volume than the curve for the room temperature-dried coating.

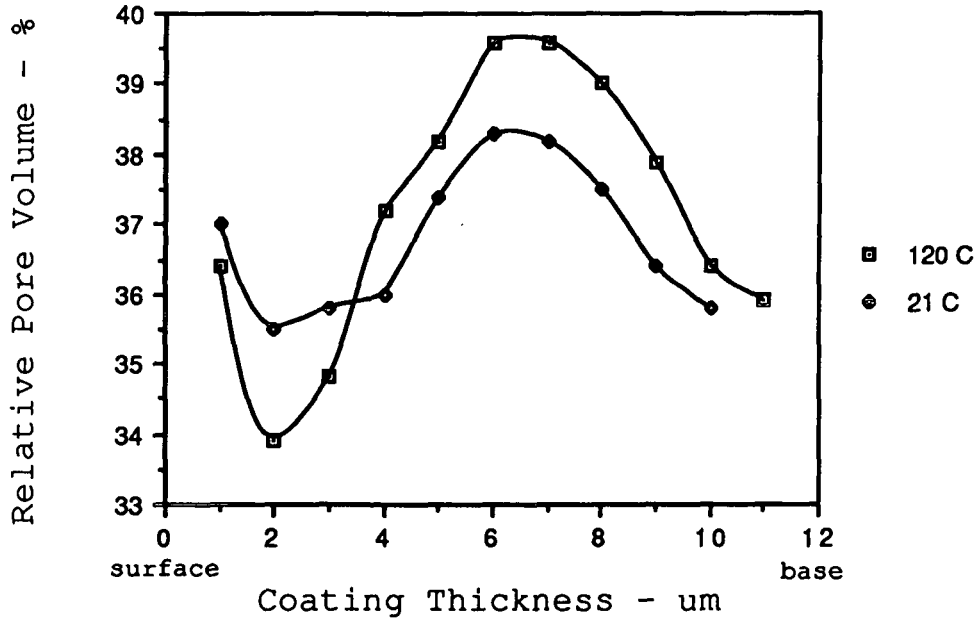


Figure 74. Pore volume distributions for coatings dried under vacuum at 21°C and 120°C.

The density profiles have two other interesting features. Each curve shows a dense region below the surface of the coating and an asymmetrical peak in pore volume. The bulky region at the coating surface may have resulted from an artifact of the measuring technique. The surface layer of the coating, for analysis purposes, was defined as the layer which contained the coating surface beginning at the uppermost peak on the surface and extending one micrometer

into the coating. As a result of this procedure, analysis of some surface subsections may have had included space above the coating surface as pores. The variance of the pore volume from place to place along the surface of the coating serves as an indication of the extent of surface roughness (Figs. 75 and 76).

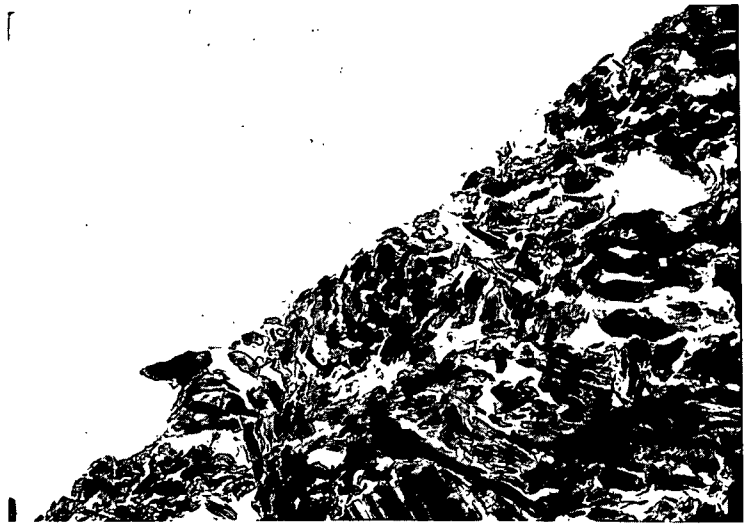

Figure 75. Micrograph of a portion of a coating cross-section which includes the coating surface and shows the microroughness that may account for the increase in measured density beneath the surface.

The second feature of the density profiles which is of interest is the peak in pore volume. Based on the findings of Cook(39), Hiltner and Krieger(63) and the hypotheses of this study, one might expect a coating bounded on two sides would have a symmetric density profile. However, the coatings contained a peak in pore volume closer to the substrate than to the surface. This result implies that the

surface structure of the wet coating film had a greater influence on the internal density than the structure near the substrate.

Figure 76. Composite micrograph of a coating cross-section (TEM 14,000X).

The results of the density profile analysis indicate that changes in coating structure were produced by changing the drying conditions. However, because of the methodology used to dry the coatings, it is not possible to determine if changes were caused by temperature effects or by effects caused directly by evaporation rate. Additional experiments run in the experimental drier system were used to determine whether drying rate influences coating structure.

## STRUCTURE OF COATINGS DRIED AT DIFFERENT RATES

### Total Pore Volume of Coatings Dried at Different Rates

The total pore volume, measured by oil absorption, was determined for each of the coatings dried in the experimental drier. The average results of the tests are shown in Table XVII.

Table XVII

Total Pore Volume Analysis of Experimental Coatings[A]

**Clay Coatings**

| Sample Code | Drying Temp. (°C) | Relative Humidity (%) | Gloss Point (sec.) | Drying Rate $kg/m^2hr$ | Total Pore Volume |
|---|---|---|---|---|---|
| T35R15 | 35 | 15 | 25 | 2.86 | 43.5% |
| T35R55 | 35 | 55 | 65.1 | 1.10 | 42.9% |
| T35R85 | 35 | 85 | 128 | 0.56 | 42.1% |
| T55R15 | 55 | 15 | 6.2 | 11.55 | 43.8% |
| T55R55 | 55 | 55 | 60.7 | 1.19 | 43.1% |
| T55R85 | 55 | 85 | 108 | 0.66 | 42.5% |
| T75R15 | 73 | 15 | 4.2 | 17.05 | 44.2% |
| T75R85 | 73 | 85 | 95.2 | 0.75 | 42.4% |

**Polystyrene Coatings**

| Sample Code | Drying Temp. (°C) | Relative Humidity (%) | Gloss Point (sec.) | Drying Rate $kg/m^2hr$ | Total Pore Volume |
|---|---|---|---|---|---|
| T35R15 | 35 | 15 | 15.5 | 2.47 | 36.3% |
| T35R55 | 35 | 55 | 27.2 | 1.41 | 35.5% |
| T35R85 | 35 | 85 | 61 | 0.63 | 35.4% |
| T55R15 | 55 | 15 | 4.2 | 9.11 | 37.1% |
| T55R55 | 55 | 55 | 11.3 | 3.39 | 36.6% |
| T55R85 | 55 | 85 | 50.9 | 0.75 | 35.8% |

[A]Temperatures and relative humidities are ±3°C and 3%

Examination of the drying rates shown in column 5 of Table XVII shows that, at 15% RH, temperature has a significant effect on drying rate. For the clay coatings the drying rate increased from 2.86 kg/m$^2$hr at 35°C to 11.55 kg/m$^2$hr at 55°C. At 55% RH the effect of temperature is not significant (1.10 kg/m$^2$hr versus 1.19 kg/m$^2$hr for 35°C and 55° C respectively). Increasing the relative humidity at constant temperature influenced the drying rate at all levels. For instance, increasing the RH from 15% to 55% to 85% at 35°C caused the drying rate to drop from 2.86 to 1.10 to 0.56 kg/m$^2$hr respectively. Analyses of the pore volume and pore volume distributions of the coatings consider effects of temperature and effects of relative humidity.

The relative pore volume was plotted against drying rate for the clay films and the latex films. The plots are shown in Figs. 77 and 78 respectively.

The change in total pore volume with drying rate was significant at low drying rates. Examination of the points below 2 kg/m$^2$hr in Fig. 77 shows a 1.5% increase in pore volume, whereas the increase in pore volume beyond 3 kg/m$^2$hr is less than 0.5% for much greater increases in drying rate. Evidently the differences in the packing structure caused by increasing drying rates were most important at low drying rates (<3 kg/m$^2$hr).

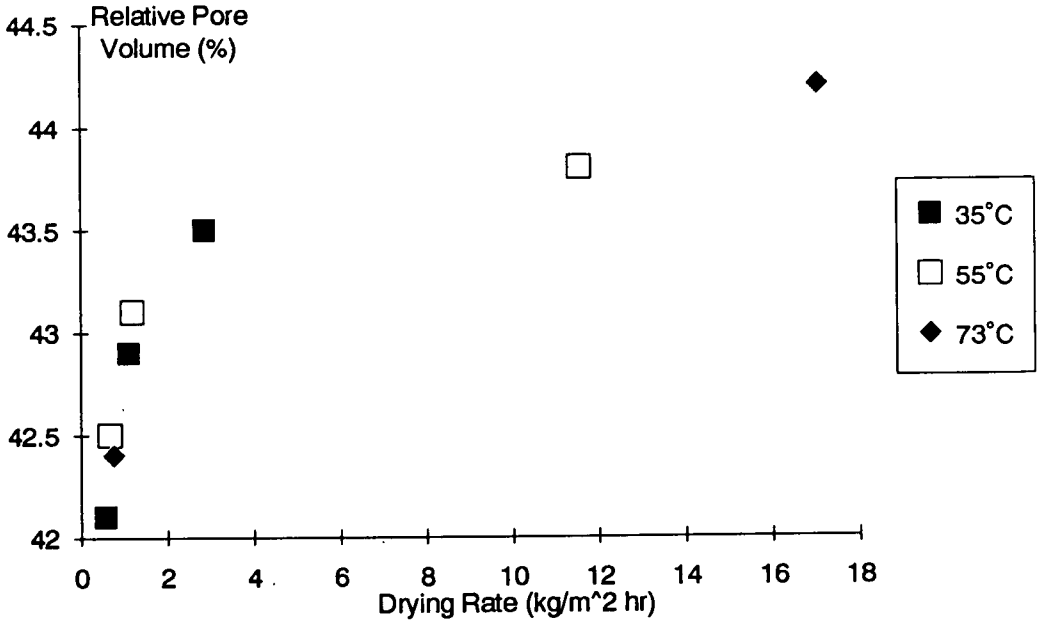


Figure 77. Relative pore volume versus drying rate for clay films dried in a low velocity air stream.

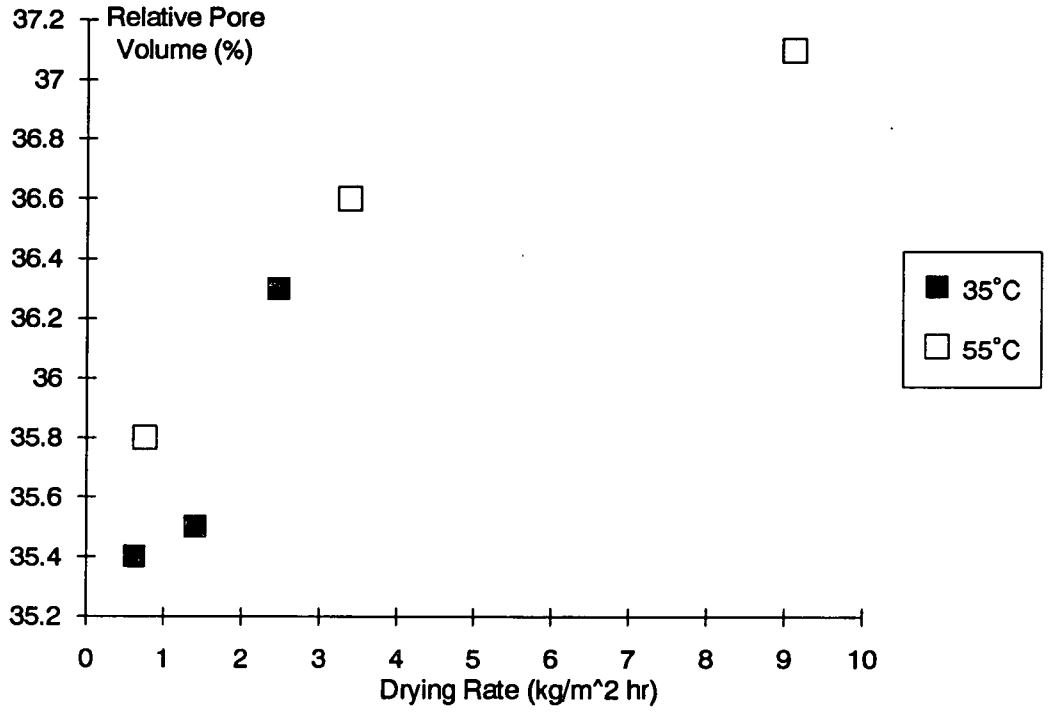


Figure 78. Relative pore volume versus drying rate for latex films dried in a low velocity air stream.

The relationship for the polystyrene latex coatings appears to be the same as that for the clay films; however, the variance of the pore volume determinations for the latex coatings was greater than that for the clay coatings. As a consequence the results were not statistically significant.

## Coating Film Density Profiles

In addressing the role of drying rate in the consolidation of a coating film, one objective was to quantitatively measure changes in the packing structure of the coating. The image analysis technique discussed in an earlier section was used to describe the distribution of pore volume through the coating thickness. Distributions of voids were used to describe the structure of the coatings which had been applied to plastic films and dried at different rates.

Calculations of distributions of pore volume as a function of coating thickness were tabulated and both averaged data and curves for each trial can be found in Appendix IV. For discussion, the results will be presented in two sets of curves. The first, Figs. 79-81, are the void volume distributions for coatings which were dried at the same temperature and different relative humidities. The second set, Figs. 82-84, depicts the void volume distributions of clay films which were dried at different temperatures and constant relative humidity.

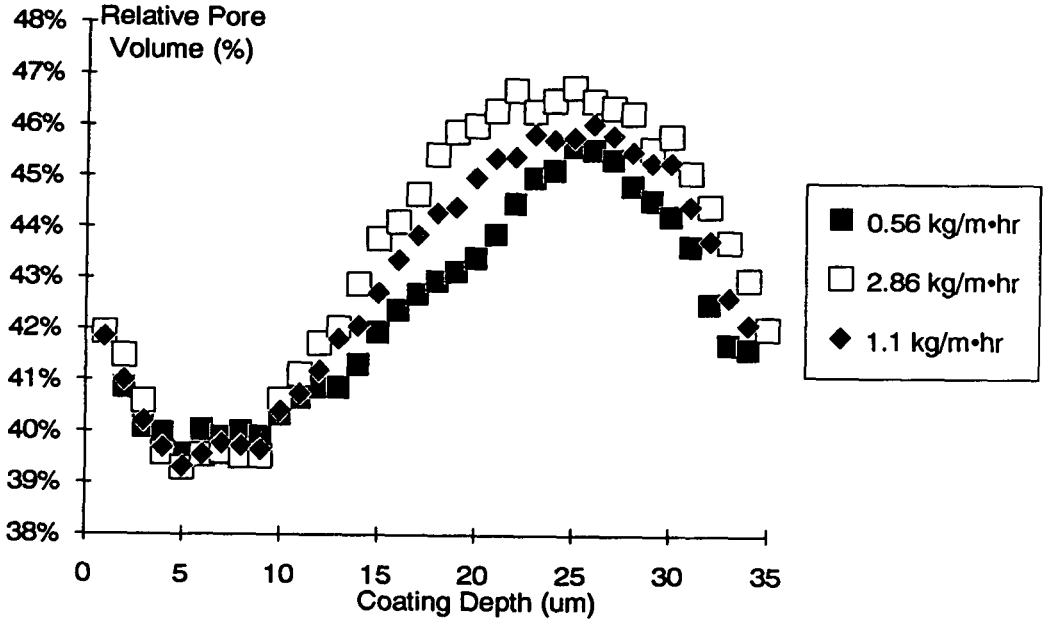


Figure 79. Z-directional pore volume distribution for clay films dried at different rates at 35°C.

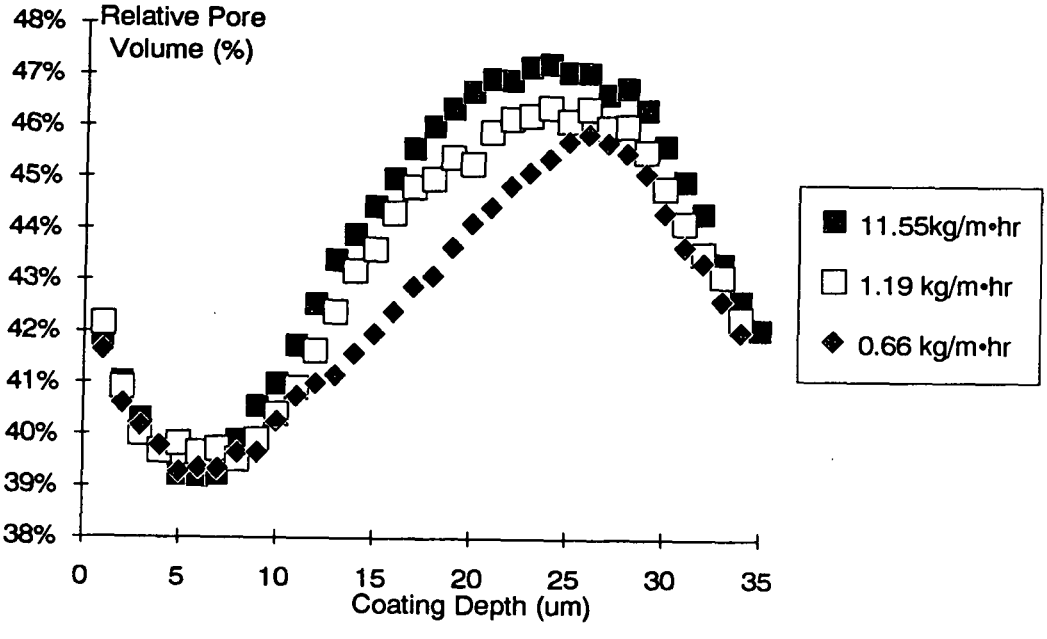


Figure 80. Z-directional pore volume distribution for clay films dried at different rates at 55°C.

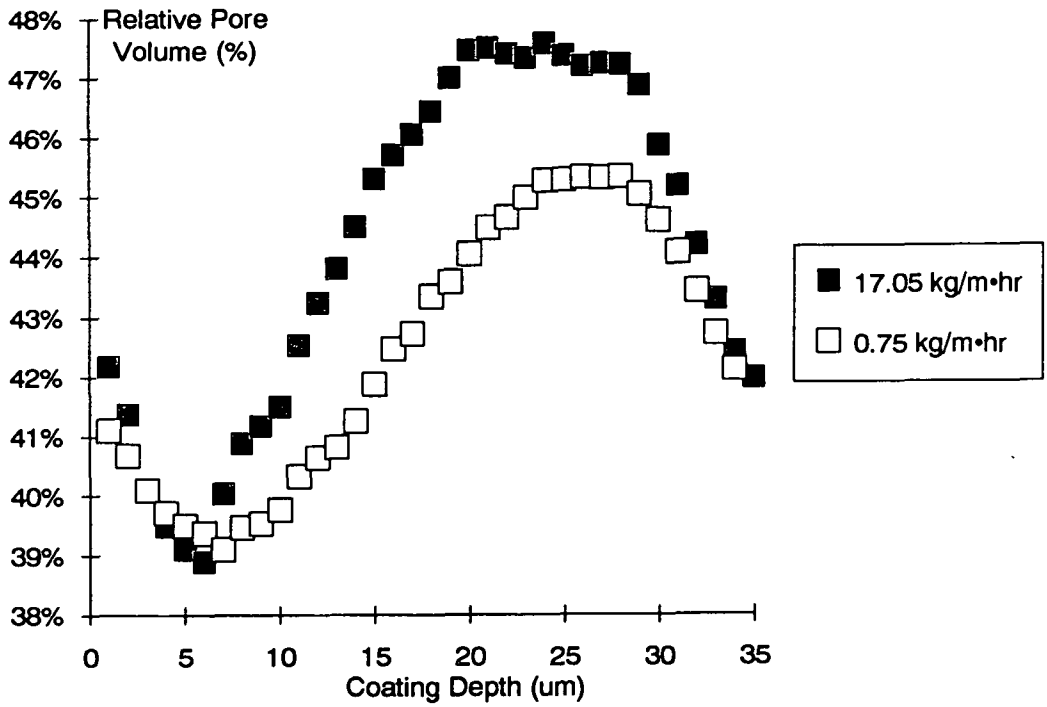


Figure 81. Z-directional pore volume distribution for clay films dried at different rates at 75°C.

The shape of the pore volume distribution for the clay films is not affected by the drying rate. Figures 79-81 show that, even for the coatings with the greatest difference in pore volume and drying rate (Fig. 81, 1.8% and 16.3 kg/m$^2$hr), the shape of the distribution is similar. The difference between the curves occurs at the transitions from constant density areas to rising or falling density areas. The dense region near the surface of coating T75R85 (0.75 kg/m$^2$hr, Fig. 81) begins about three micrometers below the surface and extends to a depth of about 10 μm, whereas the dense zone for coating T75R15 (17.05 kg/m$^2$hr) extends from 3 to 5 micrometers. Similarly, the bulky region of constant density for coating T75R85 extends from about 23 to 27 μm, while the

coating dried at the higher rate has a bulky region 9 μm thick, 18 to 27 micrometers from the surface.

The transition regions between dense and bulky areas were also affected by drying rate. The slope of the pore volume change with thickness between the dense and bulky areas is greater as the drying rate is increased. The same is true for the falling pore volume zone near the base of the coating. It is also important to note that the curves in Figs. 79-81 show that as drying rate was increased the differences between pore volume distributions were diminished.

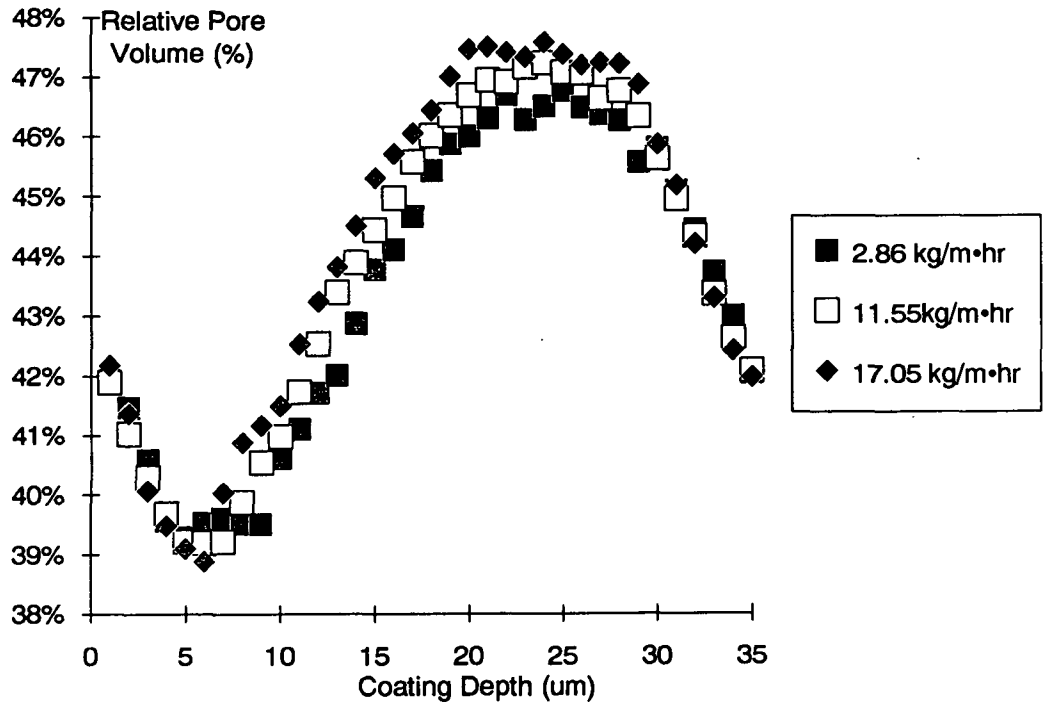


Figure 82. Z-directional pore volume distribution for clay films dried at different rates at 15% RH.

Figures 82-84 illustrate that the temperature had little effect on the pore volume distributions even between coatings with large differences in drying rate beyond 3 kg/m$^2$hr. Figure 82 contains the curves for the fastest drying rates (17.05, 11.55, and 2.86 kg/m$^2$hr for temperatures 75°, 55° and 35°C respectively). Even when the drying rate differed by a large amount, only a minimal change in void volume distribution was produced beyond 3 kg/m$^2$hr. Figure 84 contains the pore volume distributions for coatings which were dried at 35°C, 55°C and 75°C and 85% RH. All three coatings dried at nearly the same rate and analyses showed that they had no significant differences in void volume distribution (95% C. I.). Increasing the temperature of the coating during drying did not affect the void volume distribution of the dry coating films.

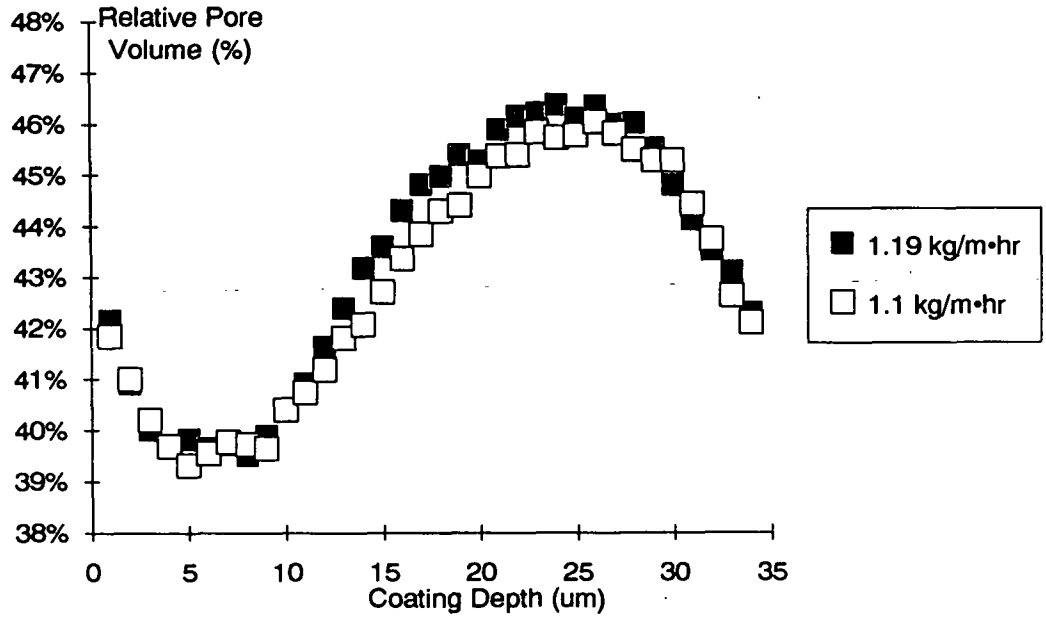


Figure 83. Z-directional pore volume distribution for clay films dried at different rates at 55% RH.

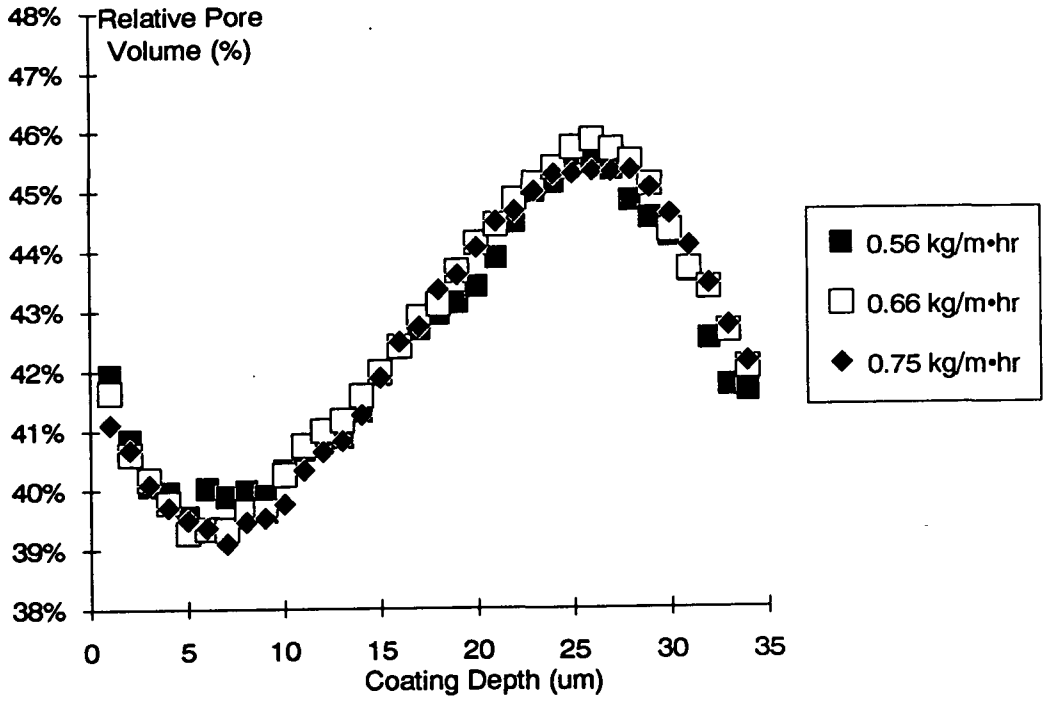


Figure 84. Z-directional pore volume distribution for clay films dried at different temperatures at 85% RH.

Interpretation of Density Profiles

Because models for predicting the packing density of anisometric particles have not been sufficiently developed and because quantitative experimental data on the density distribution of such particles in thin films are not available, it is difficult to determine whether the density profiles in Figs. 79-81 are typical. Assuming the general form is typical, the density distributions and the corresponding changes resulting from changes in the drying rate give some insight as to the role of dispersive forces in defining the packing structure of a coating film.

## Discussion of Particle Size and Rotational Diffusion

Drying under ambient conditions may require five minutes in order to immobilize the solid particles. If particle-particle interactions are ignored, rotational diffusion of particles smaller than 2 μm may be significant (20 s/90° rotation) in defining particle orientation (equation 4). In the experimental drier, immobilization solids were obtained as quickly as two seconds after application. In this case, only the particles less than 0.9 μm in diameter could undergo significant rotation (1.9 s/90° rotation). It becomes obvious that under industrial drying conditions where immobilization is reached in a fraction of a second, the time dependent rotation could only be significant for the particles of fastest rotation (0.7 s/90° rotation for 0.5μm diameter particles). Thus, the influence of rotational diffusion on the coating structure is limited to the smallest of particles. Because of the concentration of a coating suspension, even the smallest particles are continually subjected to colloidal interaction forces which because of their strength probably take precedence over particle rotation by diffusion.

## Colloidal Interactions

Each particle in a coating suspension has associated with it an electric double layer made up ions from the suspending fluid. The electric potential of the ion layer

decreases exponentially from the particle surface(92). As particles approach one another their electric double layers interfere with the approach. However, the electric double layer interaction is only one factor that influences how particles behave in suspension. The total interaction energy is a function of the attractive van der Waals forces(87), the repulsive double layer interaction(92), and steric interactions of absorbed molecules(60). The energy of interaction is the sum of these energies.

Alternatively, Derjaguin, *et al.*(135) describe the interaction of two particles as an interaction of two hydrodynamic layers, which when overlapped have a pressure greater than that of the bulk solution. The pressure difference is known as the disjoining pressure. Derjaguin describes the total energy of interaction as a pressure, but energy terms will be used in this text.

Coating particles have a reasonably high charge density and, therefore, a significant repulsive energy upon close approach. The magnitude of the interaction energy determines how the particles react to the reduced separation distance and increased particle/particle interactions caused by consolidation of the coating film during drying. Particles dispersed in the coating suspension respond to particle interactions in such a way as to reduce the energy of interaction. Upon interaction, electric double layers deform and recover as the particles move to reduce the interaction

energy. The action of the particles is not instantaneous; time is required for the electric double layers to recover their original form(87). Simply stated, interaction with other particles is a time dependent phenomenon.

In concentrated suspensions, particles cannot move without interaction; the interaction of two particles theoretically affects the total interaction energy of all the other particles in suspension. If a particle is fixed in space, the neighboring particles move in such a way as to minimize the energy of interaction. Through the previous argument, reorientation relative to the fixed particle is time dependent.

In coating suspensions the geometry of the clay particles also influence how the particles respond to particle/particle interactions. Through rotational motion and asymmetry, anisometric particles like clay are capable of a greater variety of conformations than spherical particles of similar dimensions. Because their shape allows them to react more efficiently than spheres to reduce interaction energy, anisometric particles tend to be more randomly orientated in solution. However, during sedimentation, anisometric particles align in face-to-face structures as the suspension concentrates to form structures more uniform and more dense than spherical particles.

Consider a concentrated suspension of clay particles in a thin film. The liquid surface of the film, through surface tension forces, imparts an orienting pressure on the particles near the surface. The particles at the surface form regular packing structures instead of the more random structures of the bulk solution(41,63). The particles near the surface respond to the axial orientation of the surface particles, forming a dense layer of particles oriented parallel to one another. The dense packing is disrupted by particles which can not move into parallel orientation and the uniform structures deteriorate into random structures which are present in the bulk of the film.

The bottom surface of the film behaves similarly except that the orienting force on the particles is temporary, occurring as the coating is metered onto the substrate. When the suspension is applied the particles contacting the surface adhere, forming the base for particle reorientation.

Consider the thin film to be new, so that the dense regions near the boundaries are poorly developed. Concentrating the film increases the interaction of the axially oriented surface particles with the particles near the surface. At the same time, the particles have less space to move, making reorientation more difficult. Eventually, the particles will be forced close enough together that van der Waals attractive forces become dominant and the system becomes immobilized. Because the reorientation of the

particles is time dependent, the rate of film consolidation has an effect on the final structure of the coating.

The density distributions shown in Figs. 79-84 reflect the above arguments. All the coatings analyzed contained dense areas near the film boundaries. The roughness of the surface, apparent by the greater density three micrometers below the surface than at the surface, is partially an artifact of the measuring technique and partially caused by collapse of the surface pores. The surface tension of liquid trapped between particles pulls the particles together as the last of the water is removed(42).

Figure 81 shows the effect of increasing the rate of consolidation. The dense regions are reduced and the bulky regions become wider as the rate of evaporative dewatering increases. Increasing the evaporation rate beyond about 3 $kg/m^2hr$ had little effect on the packing structure; however, differences in evaporation rate below that level caused significant changes in the structure. The rate of particle reorientation in response to consolidation forces is limited by the rate of rotational diffusion. For example, a 1.0 μm diameter particle would take greater than three seconds to rotate 90° in a dilute solution unhindered by the presence of other particles. Forces acting on a particle in a coating resulting from electric double layer interaction, van der Waals forces, hydrodynamic forces and gravity hinder rotation and slow the particle response further. As a result, at

higher drying rates there is insufficient time for a significant reorientation of the particles in response to stresses caused by consolidation.

## SUMMARY OF RESULTS

Several experiments were run to test the limits of the image analysis technique used to measure pore volume distributions. Comparison of total void volumes measured by the developed technique and oil absorption techniques showed that there was no statistical difference between the values obtained by the two methods. The image analysis technique has two critical limitations: (1) The minimum sample magnification for accurate results must be at least 5000x; and, (2) The section thickness must be no more than 120 nm to avoid blinding pores to the analysis. The image analysis technique was used within these limits to determine the void volume distributions of coating films produced in subsequent experiments.

The distribution of void volume in coatings was discovered to be non-uniform. Each coating showed a "horizontal S" shaped pore volume distribution. The density was greatest near the coating surface and near the substrate, while the interior was found to be considerably less dense than the boundary layers.

Preliminary drying studies, in which coatings were dried under vacuum at 20°C and 120°C (drying rates of 0.12 kg/$m^2$hr and 1.54 kg/$m^2$hr), showed that simultaneously varying temperature and evaporation rate produced changes in the void volume distribution. Analysis of coating films dried at controlled rates showed that changing the temperature at constant drying rate produced little effect on the total void volume or the void volume distribution. Further, changing the evaporation rate at constant temperature produced changes in both the total void volume and the void volume distribution of coatings dried at low evaporation rates. Increasing the drying rate caused an increase in total void volume and increased the size of the bulky region in interior of a coating film. Changing the drying rate above a certain limiting value was not found to affect the coating structure significantly in the drying system employed.

# CONCLUSIONS

The following conclusions are based on a concentrated suspension of a delaminated clay applied to a non-porous media with a volumetric metering device. The films were dried in a low velocity air stream under controlled temperature and drying rate.

1. Image analysis techniques developed for quantifying coating structure proved comparable to the oil absorption method for measuring total pore volume. This being the case, it is assumed that the technique is also valid for measuring the pore volume distribution for any local region in a coating cross-section.

2. The total void space in a coating film is not evenly distributed through the thickness of the film. The density distribution is characterized by a bulky region sandwiched between two dense regions near the boundaries of the film.

3. Up to a point, increasing the drying rate of the coating film results in an increase in the total void volume of the film, characterized by a reduction in the depth of the dense regions and an increase in thickness of the bulky region (as described above). In addition, increasing the drying rate increases the difference between the density minimum and maximum in the coating.

4. At low drying rates, <3 kg/$m^2$hr, there appears to be sufficient time for coating particles to make a dynamic response to forces acting on the particles as a result of consolidation. The dynamic response of the particles to consolidation forces made a significant contribution to the packing structure of the pigment films. Increasing the drying rate beyond 3 kg/$m^2$hr apparently reduces the time available for particles to react to consolidation forces and thereby limits particle reorientation and makes any effect on packing structure undetectable.

5. The results of this study are significant for coatings dried at low rates. Extrapolating the results to drying rates commonly used in the coating industry would lead to the conclusion that, with all other factors equal, increasing the drying rate would have minimal effect on the resultant particle packing structure of the coating.

# FUTURE RESEARCH

The conclusions drawn from this study and the techniques developed for analysis of coating structure lead to two paths of continued research. First, the effect of drying rate on coating structure should be studied further. Logically, a study of the effect of drying rate on the void volume distribution of coatings applied to porous media should follow this work. The main objective would be to determine the dewatering mechanism which has the greatest influence on structure: filtration into the substrate or evaporation from the surface. Such a study, using paper for a substrate, would complete the picture of the effects which drying strategy could have on packing structure.

A second direction would be to experimentally test the work of Kent and Lyne(67) concerning liquid absorption and capillary geometry. Study of the relative quantities of specific pore geometries in conjunction with a liquid penetration rate study would test Kent and Lyne's model. The analysis technique developed here could be refined to measure the distribution of specific pore geometries through the thickness of the coating. Additional work would include testing the effects of the density distribution on other physical properties such as pick strength and fracture mechanisms as well as opacity and gloss.

## ACKNOWLEDGMENTS

I wish to acknowledge some of the many contributions by others to the completion of this thesis. Dr. Terrance Conners, who served as chairman of my thesis advisory committee, provided guidance, encouragement, friendship and endless enthusiasm for me and the project. Dr. Frank Etzler and Professor John Waterhouse also served as advisory committee members and provided invaluable insight into the results and continually supported me with guidance and friendship throughout the study. Mary Block and Ellen Foxgrover-Sikorski proved to be excellent resources and teachers of SEM and TEM skills. Lisa Detter-Hoskins, Mark Farmer and Janet Woodward gave invaluable help with electron microscopy. Many thanks also go to the members of the shop and the design center - Jerry Kloth, Chris Knerr, Kurt Lorenz, Dexter Evans and Joe Nadeau, who provided help with design and building of the equipment involved in this study. Special thanks go to Dr. Jeff Lindsay for performing the heat and mass transfer analysis for evaporative drying of a thin film. The people in Photography (especially Pam Prouty, who prepared slides, overheads and prints of electron micrographs) and the editorial staff are not forgotten, for they provided irreplaceable support and time saving functions during the thesis.

Others whose contribution consisted of conversations, support and friendship, all of which were intricate parts of

the thesis process, include Tom Spielbauer for philosophy on how to coax the image analyzer to work; Dr. Cyrus Aidun for technical and philosophical discussions during racquetball lessons; Pat Medvecz for keeping reality humorously in check; Dr. Ron Dinus for insurmountable enthusiasm and friendship; Chris Luettgen for tremendous support, friendship and help with zeta potential measurements, and my classmates for their support and friendship.

I would also like to express my gratitude to the Institute of Paper Science and Technology and its member companies for providing the opportunity, space and funding to pursue a thesis not directly related to or associated with any ongoing or funded research.

Finally and with great emphasis I thank Linda Bunker for continued love, support and infinite patience during two moves of a household and a thesis continually behind schedule.

# LITERATURE CITED

1. Booth, G. L. Pigmented Coating Processes for Paper and Board. Tappi Monograph Series No. 28, Easton, PA, Mack Printing Co., 1964:1-90.

2. Kent, H. J.; Climpson, N. A.; Coggon, L.; Hooper, J. J.; Gane, P. A. C. Novel Techniques for Quantitative Characterization of Coating Structure. Tappi Journal 69(5):78-83(May, 1986).

3. Van Den Akker, J. A.; Sears, G. Gloss of Coated Paper and Paperboard. Tappi Journal 47(11):179A-182A(November 1964).

4. Garey, C. L. Surface Porosity of Coated Paper. Tappi Coating Conference (Detroit) Proceedings:117-123(May 23-26, 1982).

5. Climpson, N. A.; Taylor, J. H. Pore Size Distributions and Optical Scattering Coefficients of Clay Structures. Tappi Journal 59(7):89-92(July 1976).

6. Lepoutre, P.; Rezanowich, A. Optical Properties and Structure of Clay-Latex Coatings. Tappi Journal 60(11):86-91(November 1977).

7. Watanabe, J.; Lepoutre, P. A Mechanism for the Consolidation of the Structure of Clay-Latex Coatings. Journal of Applied Polymer Science 27(11):4207-4219(1982).

8. Lepoutre, P. New Concepts Change Traditional Ideas of Coating Processes. Paper Trade Journal:87-90(September 1984).

9. Nowicki, S. C.; Scriven, L. E. On the Physics of Drying and Binder Migration in Coated Papers. Tappi Coating Conference (Boston) Proceedings:49-64(May 13-16, 1990).

10. Sheehan, J. G.; Whalen-Shaw, M. High Magnification Cryo-SEM of Wet Coating Microstructures. Tappi Coating Conference (Boston) Proceedings:49-64(May 13-16, 1990).

11. Bousfield, D. W. The Simulation of Pigment Motion During Blade Coating. Tappi Coating Conference (Boston) Proceedings:49-64(May 13-16, 1990).

12. Dobson, R. L. Effects of Synthetic Binders on Coated Board Properties. Pulp and Paper Magazine of Canada 68(10):T511-T516(October 1967).

13. Garey, C. L.; Leekley, R. M.; Hultman, J. D. Effect of Mixed Binder Systems on the Film Volume and Pore Size Distribution of Isolated Clay Coatings. Tappi Journal 58(5):79-82(May 1975).

14. Hagemeyer, R. W. The Effect of Particle Shape and Chemical Composition on the Packing Characteristics of Pigment Combinations. Tappi Journal 47(2):74-77(February 1964).

15. Watanabe, J.; Kohara, Y.; Takahashi, S. Effects of Clay Properties on Paper Coating Structure-Printability Relations. Tappi Coating Conference (Cincinnati) Proceedings:119-126(May 21-23, 1979).

16. Slepetys, R. A.; Morgan, L. J. Optics and Surface Chemistry of a Chemically Structured Coating Pigment. Tappi Journal 74(1):195-201(January 1991).

17. Hemstock, G. A.; Bergmann, R. J. Studies of Relationships Between Suspension and Paper Coating Film Properties I. Clay-Water Systems. Tappi Journal 51(11):489-496(November 1968).

18. Lepoutre, P.; Lord, D. Destabilized Clay Suspensions: Flow Curves and Dry Film Properties. Journal of Colloid and Interface Science 134(1):66-73(January 1990).

19. Lepoutre, P.; Engstrom, G.; Rigdahl, M. On the Interpretation of Flow Curves of Coating Colors. Nordic Pulp and Paper Research Journal (1):48-50(1989).

20. Gane, P. A. C.; Coggon, L. Coating Blade Geometry: Its Effect on Coating Color Dynamics and Coated Sheet Properties. Tappi Journal 70(12):87-96(December 1987).

21. Hofmann, H. P.; von Raven, A. Production Troubles from Stalagmite Like Buildups of Coating Colors on the Blades of High Speed Coaters. Wochenblatt fur Papierfabrikation 114(8):261-264,266(April 30, 1986).

22. Heiser, E. J.; Baker, E. J.; Herr, J. W. Relationship Between Coating Morphology and Performance. Tappi Journal 53(9):1739-1745(September 1970).

23. Lepoutre, P. Paper Coatings: Substrate Absorbancy and Coating Structure. Tappi Coating Conference (Denver, CO) Proceedngs:61-68(May 1-3, 1978).

24. Engstrom, G.; Rigdahl, M. In-Situ Studies of Water Drainage From Wet Coating Layers. Tappi Journal 69(1):86-89(January 1986).

25. Hunger, G. K. The Influence of Calendering on Sheet and Coating Densification and Final Printability. Tappi Journal 50(7):372-379(July 1967).

26. Brociner, R. E.; Beazley, K. M. The Influence of the Coating Pigment on Missing Dots in LWC Gravure Paper. Tappi Journal 63(5):55-58(May 1980).

27. Lepoutre, P. The Structure of Paper Coatings: An Update. Atlanta, GA, Tappi Press 1989:1-56.

28. Lepoutre, P. Paper Coatings: Structure Property Relationships. Tappi Journal 59(12):70-75(December 1976).

29. Lepoutre, P. The Consolidation of a Paper Coating. Pulp and Paper Magazine of Canada 80(2):98-101(February 1979).

30. Hagen, K. G. A Fundamental Assessment of the Effect of Drying on Coating Quality. Tappi Coating Conference (Atlanta) Proceedings:131-137(May 19-23, 1985).

31. Hagen, K. G. An Assessment of the Use of Infra-Red in Coating Drying. Tappi Coating Conference (Chicago) Proceedings:1-7(May 14-17,1989).

32. Scott, G. D. Nature, London 188:908-909(1960).

33. Scott, G. D. Nature, London 194:956-958(1962).

34. Scott, G. D. Journal of Chemical Physics 40:611-612(1964).

35. Scott, G. D.; Kilgour, D. M. The Density of Random Close Packed Spheres. British Journal of Applied Physics (Journal Physics D) ser. 2, vol. 2:863-866(1969).

36. Bernal, J. D.; Cherry, I. A.; Finney, J. L.; Knight, K. R. An Optical Machine for Measuring Sphere Coordinates in Random Packings. Journal of Physics E 3:388-390(May 1970).

37. Hagemyer, R. W. The Effect of Pigment Combination and Solids Concentration on Particle Packing and Coated Paper Characteristics. Tappi Journal 43(3):277-288(March 1960).

38. Schneider, F. A.; Rippin, D. W. T. Determination of the Local Voidage Distribution in Random Packed Beds of Complex Geometry. Industrial & Engineering Chemistry Research 27:1936-1941(1988).

39. Cook, J. A. The Relationship of Pore Volume and Pore Size Distribution to the Development of Gloss and Scattering Coefficient. Masters Thesis, Western Michigan University, 1988:p 141.

40. Leskinen, A. M. Layer Structure in Model Coatings. TAPPI Coating Conference Proceedings:71-82(May 1987).

41. Hoy, K. L. The Effect of Particle Size Distribution on the Rheology and Film Formation of Latex Coatings. In Organic Coatings Vol. 5. Parfiee, G. D. and Patsis, A. V. eds., New York, NY, Marcel Dekker, Inc., 1983:123-146.

42. Burke, J. An Investigation of the Role of the Adhesive in the Structure of Pigment-Adhesive Films. Doctoral Dissertation. Appleton, WI, The Institute of Paper Chemistry, 1966. p. 140

43. Dickinson, E.; Milne, S. J.; Patel, M. Structure and Porosity of Simulated Sediments of Polydisperse Particles. Industrial & Engineering Chemistry Research 27(10):1941-1946(1988).

44. Bernal, J. D. Geometry of the Structure of Monatomic Liquids. Nature 185:68-70(January 9, 1960).

45. Bernal, J. D.; King, S. V. Random Close-Packed Hard-Sphere Model. I. Effect of Introducing Holes. Discussions of the Faraday Society (43):60-69(1967).

46. Finney, J. L. Random Packings and the Structure of Simple Liquids. I. The Geometry of Random Close Packing. Proceedings of the Royal Society of London A 319:479-493(1970).

47. Gotoh, K.; Finney, J. L. Statistical Geometrical Approach to Random Packing Density of Equal Spheres. Nature 252:202-205(November 15, 1974).

48. Takacs, L. Statistical Geometry of Some Dense Random Packing of Hard Spheres Model Structures. Journal of Non-Crystalline Solids 81:1-11(1986).

49. Wise, M. E. Dense Random Packing of Unequal Spheres. Philips Research Reports 7(5):321-343(October 1952).

50. Hogendijk, M. J. Random Dense Packing of Spheres with a Discrete Distribution of the Radii. Philips Research Reports 18:109-126(1963).

51. Dodds, J. A. The Porosity and Contact Points in Multicomponent Random Sphere Packings Calculated by a Simple Statistical Geometric Model. Journal of Colloid and Interface Science 77(2):317-327(October 1980).

52. Brady, J. F.; Bossis, Annual Review of Fluid Mechanics 20:111-157(1988).

53. Durlofsky, L.; Brady, J. F.; Bossis, G. Journal of Fluid Mechanics 180:21-49(1987).

54. Brady, J. F.; Bossis, G. Journal of Fluid Mechanics 155:105-129(1985).

55. Phillips, R. J.; Brady, J. F.; Bossis, G. Physics of Fluids unpublished.

56. Durlofsy, L. J.; Brady, J. F. Journal of Fluid Mechanics 200:39-67(1989).

57. Sennett, P.; Drexel, R. J. JR; Morris, H. H. Appearance of Anisotropic Pigment Particles in Paper Coatings. Tappi Journal 51(12):567-569(December 1968).

58. Couture, L.; van der Ven, T. G. M. The Effect of Hydrodynamic Interactions on the Rheological Properties of Suspensions of Polymer-Coated Particles. CPPA/TAPPI Symposium on Papercoating Fundamentals, Montreal, Quebec:15-19 (May 17-18, 1991).

59. Krieger, I. M. Structure-Rheology Relations in Dispersions. CPPA/TAPPI Symposium on Papercoating Fundamentals, Montreal, Quebec:15-19 (May 17-18, 1991).

60. Tadros, T. F. Colloidal and Rheological Phenomena in High Solids Dispersions. CPPA/TAPPI Symposium on Papercoating Fundamentals, Montreal, Quebec:1-14 (May 17-18, 1991).

61. van Olphen, H. An Introduction to Clay Colloid Chemistry. 2nd edition. New York, NY, John Wiley & Sons, 1977, pp. 92-109.

62. Liu, J.; Sorikaya, M.; Aksay, I. A. Structural Control with Ultrafine Particles. 46th Annual Meeting EMSA (Milwaukee, WI) Proceedings:716-717(August 7-12, 1988).

63. Hiltner, P. A.; Krieger, I. M. Diffraction of Light by Ordered Suspensions. Journal of Physical Chemistry 73(7):2386-2389(July 1969).

64. Gate, L. F.; Windle, W. Absorption of Oils into Porous Coatings. The Fundamental Properties of Paper Related to Its Uses. Transactions of the Symposium held at Cambridge, England, Bolam, F. ed. vol 2.:438-451(September 1973).

65. Hattula, T.; Oittinen, P. An Analysis of Ink Penetration Into Pigment Coatings. Paperi ja Puu 64(6-7):407-412 (June-July, 1982).

66. Lepoutre, P.; DeGrace, J. H.; Mangin, J. P. Influence of Coating Absorbancy on the Printability of Coated Papers. Tappi Coating Conference (Cincinnati) Proceedings:21-25(May 21-23, 1979).

67. Kent, H. J.; Lyne, M. B. Influence of Paper Morphology on Short Term Wetting and Sorption Phenomena. Fundamentals of Papermaking. Transactions of the Ninth Fundamental Research Symposium Held at Cambridge Vol. 2:895-920(September 1989).

68. Engstrom, G.; Fineman, I.; Persson, A.; Karlsson, I.; Akesson, R. Experiences with Drying of Starch Containing Coating Colors in Air Float Dryers. Wochenblatt fur Papierfabrikation 108(19):793-794,796,798-799(October 15, 1980).

69. Engstrom, G.; Fineman, I.; Persson, A.; Karlsson, I.; Akesson, R. How Ink Mottling in Offset-Printing on Coated Paper is Influenced by the Drying Conditions During Coating-A Comparison Between Starch and CMC/SB-Latex Binders. Tappi Coating Conference (Detroit) Proceedings:109-115(May 23-26, 1982). Tappi Journal 65(11):81-84(November 1982).

70. Heiser, E. J.; Baker, H. M. Effect of Controlled Binder Migration on Coating Structure. Tappi Journal 51(11):528-532(November 1968).

71. Aschan, P. -J. Solving Problems of Print Mottle on Coated Board. Tappi Coating Conference (Washington, D.C.) Proceedings:73-78(May 4-7, 1986). Tappi Journal 6(12):35-38(December 1986).

72. Engstrom, G.; Norrdahl, P.; Strom, G. Studies of Drying and Its Effect on Binder Migration and Offset Mottling. Tappi Coating Conference (Houston) Proceedings:35-43 (May 17-21, 1987).

73. Gane, P. A. C. Mottle and the Influence of Coating and Binder Migration. Paper Technology 30(4):34-41(April 1989).

74. Norrdahl, P. C. Effect of Drying Conditions on the Quality of Wood-Containing Lightweight Coated Paper. Tappi Journal 74(5):73-78(May 1991).

75. Heikkinen, M-L. Masters Thesis. Åbo Akademi, Finland. (Not seen by this author, cited in #74).

76. Engstrom, G.; Rigdahl, M.; Kline, J.; Ahlroos, J. Binder Distribution and Mass Distribution of the Coating Layer - Cause and Consequence. Tappi Journal 74(5):171-179(May 1991).

77. Hattula, T.; Aschan, P. -J. Z-Distribution Analysis of Binder in Board Coatings. Paperi ja Puu 60(11):665-668,671-672,675-677(November 1978).

78. Hellawell, J. M.; Nelson, R. Scanning Electron Microscopy Studies of Paper Coating Structures in Cross Section. Tappi Journal 54(10):1647-1654(October 1971).

79. Foster, R. H.; Der, P. K. Optical and Electron Microscopic Investigation of Shear Induced Structures in Lightly Consolidated (Soft) and Heavily Consolidated (Hard) Kaolinite. Clays and Clay Minerals 19:31-47(1971).

80. Slone, R. L.; Kell, T. R. The Failure of Mechanically Compacted Kaolin. Clays and Clay Minerals Proceedings of the Fourteenth National Conference (Berkeley, CA):289-296(1966).

81. Diamond, S. Microstructure and Pore Structure of Impact-Compacted Clays. Clays and Clay Minerals 19:239-249(1971).

82. Einstein, A. An Investigation on the Theory of the Brownian Movement. Cowper, A. D. and Furth, R., eds. New York, NY, Dover Publications, Inc., 1956:9-35.

83. Kahn, A. Studies on the Size and Shape of Clay Particles in Aqueous Suspension. Sixth National Conference of Clays and Clay Minerals 6:220-236(1959).

84. Kahn, A.; Lewis, D. R. The Size of Sodium Montmorillonite Particles in Suspension from Electo-Optical Birefringence Studies. Journal of Physical Chemistry 58(10):801-804(December 18, 1954).

85. Mark, H.; Tobolsky, A. V. Physical Chemistry of High Polymeric Systems. New York, Interscience Publishers, Inc., 1950:pp. 318-320.

86. Counter, R. The Effect of Pigmentation on the Structure and Performance of a Coating. Preprints of CPPA 61 Annual Meeting, Montreal, Quebec:A51-A57(January 28-31, 1975).

87. Shaw, D. J. Introduction to Colloid and Surface Chemistry, 3rd edition. London, Butterworths, 1980, pp. 183-186.

88. Vold, M. J. Van Der Waals Attraction Between Anisometric Particles. Journal of Colloid Science 9(5):451-459(1954).

89. Gouy, G. J. Physique 9(4):457(1910). also Ann. d. Phys. 7(9):129(1917).

90. Chapman, D. L. Philos. Mag. 25(6):475(1913).

91. Debye, P.; Huckel, E. Phyzik. Z. 24:185(1923) also 25:97(1924).

92. Verwey, E. J. W.; Overbeek, J. TH. G. Theory of the Stability of Lyophobic Colloids. New York, NY, Elsevier Publishing Company, Inc., 1948, pp 1-20, 66-133.

93. Etzler, F. M.; Drost-Hansen, W. A Role for Water in Growth, Metabolism, and Intercellular Organization. Advances in Chemistry Series (188) Bioelectrochemistry: Ion, Surfaces, Membranes ch. 28:485-497(1980).

94. Adamson, A. A. Physical Chemistry of Surfaces. New York, NY, Interscience Publishers, Inc., 1960, pp. 175-179.

95. Shaw, D. J. Electrophoresis. London, England, Academic Press, 1969, pg. 17-18.

96. Callaghan, I. C.; Ottewill, R. H. Interparticle Forces in Montmorillonite Gels. Discussions of Faraday Chemical Society 57:110-129(1975).

97. Lyne, B. Meausrement of the Distribution of Surface Void Sizes in Paper. Tappi Journal 59(7):102-105(July 1976).

98. Garey, C. L.; Leekley, R. M.; Hultman, J. D.; Nagel, S. C. Determination of Pore Size Distribution of Pigment Coatings. Tappi Journal 56(11):134-138(November 1973).

99. Davis, P. J.; Smith. D. M. Using NMR Spectroscopy to Analyze the Pore Structure of Coatings. Tappi Journal 72(5):85-89(May 1989).

100. Andersson, H. Image Analysis in Paper Research at STFI. Scandinavian Conference on Image Analysis (3rd: 1983: Copenhagen, Denmark), Proceedings:194-198(July 12-14, 1983).

101. DeHoff, R. T.; Rhines, F. N., eds. Quantitative Microscopy. New York, NY, McGraw-Hill Book Company, 1968, pp. 32-126.

102. Underwood, E. E. Quantitative Stereology. Reading, MA, Addison-Wesley Publishing Company, 1970, pp. 1-47.

103. Weibel, E. R. Stereological Methods. Vol. 1. London, Academic Press Inc., 1979, pp. 26-31.

104. Bundy, W. M.; Johns, W. D.; Murry, H.H. Physico-Chemical Properties of Kaolinite and Relationships to Paper Quality. Tappi Journal 48(12):688-696(December 1985).

105. Heiser, E. J.; Shand, A. Lightweight Polymeric Pigment. Tappi Journal 56(1):70-73(January 1973).

106. Hollingsworth, R. L.; Jones, J. P. E.; Bonney, C. The Effect of Calcined Clays on the Printability of Coated Rotogravure and Offset Printing Papers. Tappi Coating Conference (San Francisco) Proceedings:9-16(May 15-18, 1983).

107. Lee, D. I. Coating Structure Modification and Coating Hold-Out Mechanisms. Tappi Coating Conference (Houston) Proceedings:143-153(May 17-21, 1981).

108. Reinbold, I.; Ullrich, H. Possibilities and Limitations of High Solids Coating Colors. Tappi Journal 63(1):47-51(January 1980).

109. Sennett, P.; Massey, H. L.; Morris, H. H. Effect of Pigment Particle Size and Shape on Rotogravure Print Quality of Light Weight Coated Paper. Tappi Coating Conference (Detroit) Proceedings:23-33(May 23-26, 1982).

110. VanGilder, R. L.;Purfeerst, R. D. The Effect of Coating Color Solids on Properties and Surface Uniformity. Tappi Journal 69(5):62-68(May 1986).

111. Whalen-Shaw, M.; Coco, C. E. The Effect of Controlled Coating Structure on Offset Printability. Tappi Coating Conference (Atlanta) Proceedings:97-107(May 19-23, 1985).

112. J. M. Huber Corporation Clays for the Paper Industry. Publ. of J. M. Huber Corp. 3pg, (1986).

113. Adams, D. J.; Matheson, A. J. Computation of Dense Random Packings of Hard Spheres. Journal of Chemical Physics 56(5):1989-1994(March 1, 1972).

114. Mason, G. The Structure and Properties of Liquids. Discussions of the Faraday Society (43):75-88(1967).

115. Speedy, R. J. Statistical Geometry of Hard-Sphere Systems. J. C. S. Faraday II 76:693-703(1980).

116. Troy, E. M.; Church, B. H.; Tam, M. K.; Ratne, M. Simulated Random Packing of Equal Spheres. Canadian Journal of Chemical Engineering 51:484-493(August, 1973).

117. Morton International. Lytron Plastic Pigments. Publication of Morton International Speciality Chemicals Group, Chicago, IL, 1990, pg 1.

118. Bellhouse, B. J.; Bellhouse, F. H. Thin-Film Gauges for the Measurement of Velocity of Skin Friction in Air, Water and Blood. Journal of Scientific Instruments (Journal of Physics E) Sr 2 Vol 1:1211-1213(1968).

119. Grant, H. L.; Huges, B. A.; Vogel, W. M.; Moilliet, A. The Spectrum of Temperature Fluctuations in Turbulent Flow. Fluid Mechanics 34(pt.3):432-442(1968).

120. Hanson, R. K. Study of Gas-Solid Interactions Using Shock-Wave Reflection. Shock Tube Research - Proceedings of the Eighth International Shock Tube Symposium (Imperial College, London):58-58/12 (July 5-8, 1971).

121. Waterhouse, J. F.; Scott, E. M. A Progress Report on the Calibration of the H. S. D. 2.9" Shock Tube Tunnel. Hawker Siddeley Dynamics Limited Aerodynamic Research Laboratory, Dec. 1964, pp. 18.

122. Meyer, R. F. A Heat-Flux-Meter for Use with Thin Film Surface Thermometers. National Research Council of Canada Aeronautical Report LR-279, April 1960, pp. 18.

123. Foltz, G. E.; Mesler, R. B. The Measurement of Surface Temperatures With Platinum Films During Nucleate Boiling of Water. AIChE Journal 16(1):44-48(January 1970).

124. Abad, A. A Study of Section Wrinkling on Single-Hole Coated Grids Using TEM and SEM. Journal of Electron Microscopy Technique 8(3):217-222(1988).

125. Smith, D. M.; Stermer, D. L. Mercury Porosimetry: Theoretical and Experimental Characterization of Random Microsphere Packings. Journal of Colloid and Interface Science 111(1):160-168(May 1986).

126. Russ, J. C. Computer Assisted Microscopy. The Measurement and Analysis of Images. Raleigh, North Carolina, North Carolina State University, 1988, pp. 3-20 to 3-21.

127. Steel, R. G. D.; Torrie, J. H. Principles and Procedures of Statistics. New York, McGraw-Hill Book Company, Inc., 1960, pp. 86-87, 110-111.

128. Trader, C. D. Laboratory Studies Relating Coating Structure and Coating Performance. Tappi Journal 54(10):1709-1713(October 1971).

129. Kaliski, A. Performance of Some Commercial Clays in Starch Containing Paper Coating Films. Part I. Black Glass Plates as Model Substrates. Tappi Journal 53(11):2077-2084(November 1970).

130. Lepoutre, P.; Hiraharu, T. On the Cohesion of Clay and $CaCO_3$. Journal of Applied Polymer Science 37(7):2077-2084(March 1989).

131. Lindsay, J. D. Institute of Paper Science and Technology, Personal communication, 1991.

132. Treybal, R. E. Mass-Transfer Operations. New York, NY, McGraw-Hill Book Company, Inc., 1987, pg. 70.

133. Beck, J. V.; Blackwell, B.; St. Clair, C. R. Jr. Inverse Heat Conduction - Ill-posed Problems. New York, NY, John Wiley & Sons, Inc., 1985, pp. 96-102.

134. Maron, M. J. Numerical Analysis: A Practical Approach. New York, NY, Macmillan Publishing Co., Inc., 1982, pp. 116-117.

135. Derjaguin, B. V.; Churaev, N. V.; Muller, V. M. Surface Forces. New York, NY, Consultants Bureau, 1987, pp. 1-51.

# APPENDIX I

## ANALYTICAL METHODS FOR QUANTIFYING COATING STRUCTURE

Morphological analysis in the z-direction of paper is difficult due to paper's thickness relative to its morphological properties. The method employed in this thesis is microscopic examination of cross sections of embedded samples. This method has a major disadvantage, in that any effect of structural formation on strength, elastic moduli, or absorptive properties can not be measured. In addition, x-y analysis is impossible without 3-D reconstruction. Three-dimensional reconstruction techniques have not developed sufficiently to yield quantitative data. Ideally, surface layers could be removed without damaging the remaining structure. Tests could be performed on the remains, followed by removal of another layer and subsequent tests. In this way the morphology of a material through its thickness could be determined and the contribution of the local morphology to the bulk properties of the structure could be determined as well.

### Excimer Laser Ablation

Excimer lasers are pulsed lasers with maximum average output at 248 nm, using a KrF laser, of about 80 watts. The lasers high power output can be used to drill holes in metals, mark or score glass and ceramics, and sculpt organic

materials. The destruction of these materials occurs by ablation(1). The energy transmitted to the material causes its destruction by disrupting the molecular integrity of the material. The products are ejected from the area of ablation at high speed and can be collected and analyzed. Whether the mechanism is purely photochemical, purely thermal or a combination of the two has not been solved. What makes the process of the excimer unique is the lack of detectable thermal damage to the substrate(2).

An excimer is an atom, molecule or ion that exhibits dimer characteristics while in one of its excited states. If one or both of the atoms making up the excimer is a rare gas atom, the excitation energy is large allowing high powered laser emission. The active medium in an excimer laser can be an excited rare gas dimer ($Ar_2^*$, $Kr_2^*$, $Xe_2^*$), a rare gas oxide ($ArO^*$, $KrO^*$, $XeO^*$) or a rare gas atom in combination with a halide atom ($ArF^*$, $KrF^*$, $XeF^*$). The pure rare gas systems and the rare gas halides lase in the Ultraviolet (UV) region while all of the rare gas oxides lase around 558 nm(1).

The penetration of the radiation from an excimer laser follows Beer's Law:

$$I_t = I_o \exp(-\alpha l) \qquad (a1)$$

where $I_o$ and $I_t$ are the beam intensities before and after transmission respectively. The intensity after transmission,

$I_t$, is exponentially related to the sample thickness, l, and the sample's absorptivity, $\alpha$.

If the intensity per unit area or fluence of the laser is above a threshold level ablation will occur. The threshold fluence is a function of the material absorptivity and the power of the laser per pulse. The depth of ablation per pulse is a function of the pulse energy, extent of focus of the beam, energy of the pulse and the ability to remove the ablation products.

Excimer pulsed laser technology could be used to remove thin layers (0.1 μm) of the coating surface, exposing a fresh surface for examination. In this way, the coating film would be physically sectioned in the z-direction. Each ablated surface would represent a successive layer of coating that could be analyzed to determine the pore volume. The products of the ablation could be quantitatively analyzed producing information necessary for measurement of the binder concentration distributions in coatings.

One drawback of the use of excimer laser technology is obtaining a laser of wavelength and lasing power suitable for ablating coating pigment and coating binder at the same rate. Porous media poses another problem. The laser cannot differentiate between the surface and the bottom of a pore, resulting in an uneven ablation front. Analysis of a coating structure that has been ablated nonuniformly would be

difficult to do accurately. A surface consisting of a solid single material would ablate with greater uniformity, allowing the possibility of practical use of the excimer laser as a "surface grinder".

Literature concerning the application of excimer lasers and a business card that had been used to focus an excimer laser beam was obtained from Mike Scaggs of Lambda Physik (an excimer laser manufacturer). The card was discolored where the beam had contacted it and microscopic examination showed evidence of surface damage. The business card was made from a synthetic material and was coated on both sides, making it difficult to decide what happened to the card during exposure to the laser.

Surface examination of the laser etched business card, sent to us by Lambda Physik, showed areas of fiber damage. It was difficult to tell whether fibers had shrunk from dehydration caused by heating, been burned away, or were ablated. A cross-section of the areas of greatest damage showed areas where fibers were loosened from the matt. It was impossible to determine what mechanism was responsible for the disruption of the fiber network.

Excimer laser ablation, as a method of successive layer removal for analysis of coating structure, was not used because of the difficulties that needed to be ironed out of

the technique and because of the limited/costly availability of a laser.

Plasma Etching

Plasma etching of cellulose has been investigated in a large volume plasma generator by Sapieha *et al.*(3). Plasma generated from $CF_4/O_2$ gases contain species that react with polymeric samples producing radical sites. The radicals readily undergo reactions with the source elements O and F to cleave the polymer chains and remove material(3). The apparatus for producing a large volume of cold plasma was introduced by Bosisio, *et al.*(4) in 1973. Lamontagne *et al.*(5) modified the device to include control of sample temperature and gas pressure. They also added a rotational stage to overcome any variations in field strength.

Sapieha *et al.*(3) studied the effects of gas composition (rate of $CF_4$ and $O_2$ inflow) and pressure on the etch rate of several papers and a coated sheet. They discovered that the etch rate was dependent on gas pressure and on the gas composition. They went on to determine the optimal conditions for use on paper.

Etching of the paper surface showed that the plasma preferentially removes microfibrils, small cellulose fragments and other debris(3). The authors also suggested that the plasma etch front extends a significant depth into the paper. This is a result of non-uniform distribution of

mass density through the thickness of the paper. If some way of controlling the penetration of the etch front can be developed, plasma etching may be a suitable way of removing layers of paper.

Under the conditions chosen for the etching of paper, etching of a coated paper was unsuccessful(3). It was discovered that the inorganics were cleaned of organic material and left on the paper. However, under different conditions (i.e., pressure and gas composition), the inorganic fraction can be etched(6). As in the excimer laser, the inability to etch the inorganic and the organic materials at the same rate may limit its applicability to paper coatings. Another limiting factor is the inability to determine where the material has been etched, in that plasma etching appears to show preference to the material of least mass.

Plasma generating systems like that used by Sapieha may be commercially available and their use could be used for paper. However, due to the time frame and budget of this thesis, plasma etching was not pursued further than the above review.

## Literature Cited

1. O'Shea, D. C.; Callan, W. R.; Rhodes, W. T. Introduction to Lasers and Their Application. Addison-Wesley Publishing Company: Reading, Mass., 1978, pp. 146-148.

2. Srinivasan, R. "UV Laser Ablation of Organic Polymers and Biological Tissue" Highlights (a publication of Lambda Physik) (1):2-3(October 1986).

3. Sapieha, S.; Wrobel, A. M.; Wertheimer, M. R. Plasma Assisted Etching of Paper. Plasma Chemistry and Plasma Processing 8(3):331-346(1988).

4. Bosiso, R. G.; Wertheimer, M. R.; Weissfloch, C. F. Generation of Large Volume Microwave Plasmas. Journal of Physics E: Scientific Instruments 6:28-630(1973).

5. Lamontagne, B.; Wrobel, A. M.; Jalbert, G.; Wertheimer, M. R. Large Area Microwave Plasma Etching of Polyimide. J. Phys. D: Appl. Phys. 20:851-857(1987).

6. Peccoud, L.; Laporte, Ph.; Arroyo, J.; Charlet, B. New Trends and Limits in Plasma Etching. J. Phys. D: Appl. Phys. 20:851-857(1987).

# APPENDIX II

## EQUIPMENT AND SOFTWARE FOR TEMPERATURE ACQUISITION

Temperature measurements were made with type-J thermocouples during drying trials in the experimental drier, at the following locations:

1. Room conditions in close proximity to the drier.
2. In the air stream inside the drying box about 1/16" above coating.
3. In the coating, inside the drying box (two thermocouples).
4. In the air stream just prior to mouth of the flow spreader (two thermocouples - dry bulb and wet bulb).
5. In the air stream immediately after the exhaust conduit of the drying box (two thermocouples - dry bulb and wet bulb).

The temperature data was gathered to document the drying conditions for each coating trial. Dry bulb and wet bulb thermocouples were used to measure the relative humidity of the drying air at the inlet and outlet of the drying box and to monitor the temperature of the drying air. The thermocouples in the drying box were used to investigate how the coating and the air in the chamber responded during drying.

The interaction of the two metals which make up a thermocouple result in a potential which is conveyed through the thermocouple lead wires. The magnitude of the voltage is related to the temperature at the thermocouple junction. By

acquiring the voltage output from the thermocouple and comparing it to a known calibration of the specific composition of the thermocouple, the temperature at the junction can be determined. Because of the number of thermocouples and the other tasks required of the operator during drying, an acquisition system was purchased to directly acquire and store the thermocouple data. The following is a list of the components used:

- Swan 10XT IBM compatible portable computer.
- MetraByte Das 8 data acquisition and control interface Board.
- MetraByte Exp-16 universal expansion interface multiplexer/amplifier board

Each pair of thermocouple leads was connected to a separate channel of the Exp-16 board external to the computer. The Exp-16 was housed in a electromagnetic shield to reduce noise generated by stray radiation from the computer monitor or computer itself. The Exp-16 amplified the thermocouple signal 100 times prior to transmission to the Das-8 board. The Das-8 converted the analog thermocouple signal to a digital signal. The digital signals were converted to temperatures through comparison with a calibration table for the J-type thermocouples. The resultant temperatures were stored along with the date, channel and time of acquisition. These functions were all controlled by a computer program written in BASIC. The program, listed below, was a version of acquisition software

supplied by MetraByte which was modified for use in the system described above.

The system was capable of acquiring temperatures at two different speeds. The speed was adjusted by changing the clock speed of the computer. With the computer in standard operating mode, 4.77 Mhz, temperatures were acquired and stored approximately every two seconds. Invoking the turbo on the computer, 10 Mhz, resulted in an acquisition every 0.8 second.

The software, as supplied, stored the data as a binary file which was easily read in basic for manipulation. The program was modified to convert the binary data to ASCII data in a comma separated variable (CSV) format. This format was easily read by most personal computer spreadsheets enhancing the graphing capabilities of the data.

Calibration of the thermocouples at 0°C and 100°C showed them to be accurate to 2°C. The variation in temperature reported by the acquisition system when the thermocouples were held at constant temperature was 0.5°C. Temperatures reported for each coating trial were the result of averaging the recorded data over as long a time as possible with at a minimum of 15 data points.

Software for acquiring and storing thermocouple temperatures.

```
100'*************************************************************
    ************
110'*
    *
120'*   EXAMPLE OF USING ONE EXP-16 WITH DAS-8 AND J
    THERMOCOUPLE        *
130'*  MetraByte Corporation                    Rev. 1.20
    4-5-85     *
140'*************************************************************
    ************
150 SCREEN 0,0,0: KEY OFF : CLS : WIDTH 80
155 GOSUB 2000:CLS
160 'This example performs scanning and measurement of J type
    thermocouples
170 'connected to one EXP-16. The program can be expanded to
    handle multiple
180 'EXP-16's.
190 'Steps are:-
200 '1 - Initialize DAS-8 and load thermocouple look up
    tables
210 '2 - Dimension other arrays and provide set up
    information
220 '3 - Measure temperature of connector block from CJC
    channel
230 '            (CJC = cold junction compensation)
240 '4 - Measure output voltages of thermocouples on EXP-16
250 '5 - Convert, correct and linearize thermocouple outputs
    to degrees
260 '6 - Display output
270 'Note that thermocouple routines J.BAS, K.BAS etc. are in
    ASCII form and
280 'can be MERGE'd with any program and edited in.
290 '
300 'For purposes of example the EXP-16 output channel should
    be connected to
310 'DAS-8 channel #0 and the CJC channel to DAS-8 channel
    #7.
320 '
330 '---- STEP 1: Contract BASIC workspace, load DAS8.BIN and
    initialize -----
340 '
350 'See LOADCALL.BAS for a fuller explanation of Step 1 and
    an alternative
360 'way of loading outside workspace.
370 '
380 CLEAR, 49152!
385 LOCATE 25,1:COLOR 0,7:PRINT"-PLEASE WAIT-";:COLOR
    7,0:PRINT"  Loading DAS-8 I/O address and thermocouple
    lookup table data":LOCATE 1,1
390 DEF SEG = 0
400 SG = 256 * PEEK(&H511) + PEEK(&H510)
410 SG = SG + 49152!/16
```

```
420 DEF SEG = &H4000
430 BLOAD "c:\basic\DAS8.BIN", 0
450 LET BASADR% = 768 'initialize & declare CALL parameters
470 DAS8 = 0
480 FLAG% = 0
490 MD% = 0              'Mode 0 = initialization
500 CALL DAS8 (MD%, BASADR%, FLAG%)
510 IF FLAG% <>0 THEN PRINT"INSTALLATION ERROR"
520 '
530 'Load thermocouple linearizing look up data
540 GOSUB 50000
542 'Get gain setting of EXP-16
545 LET AV = 100
547 CLS
550 '---- STEP 2: Initialize an integer array D%(15) to
     receive data
560 DIM D%(12)  '16 elements, one for each EXP-16 channel
570 'Also initialize a corresponding real array to receive
     temperature data
580 DIM T(12)
585 LET NR = 1
590 INPUT "Name of Data File (e.g. B:MYFILE.DAT)";FILE$
591 INPUT "Name of data file in ASCII form" ;ASKE$
593 CLS
594 OPEN FILE$ AS #1
596 FIELD #1, 10 AS DT$, 8 AS TM$, 5 AS T0$, 5 AS T1$, 5 AS
     T2$, 5 AS T3$, 5 AS T4$, 5 AS T5$, 5 AS T6$, 5 AS T7$, 5
     AS T8$, 5 AS T9$, 5 AS T10$, 5 AS T11$, 5 AS T12$, 5 AS
     CJC$
600 '---- STEP 3: Get cold junction compensation temperature
610 'Output of CJC channel is scaled at 24.4mV/deg.C. This
     corresponds to
620 '0.1 deg.C./bit. Dividing output in bits by 10 yields
     degrees C.
630 '
640 'Lock DAS-8 to channel #7 (CJC channel selected) using
     mode 1
650 MD%=1 : LT%(0)=7 : LT%(1) = 7
660 CALL DAS8 (MD%, LT%(0), FLAG%)
670 IF FLAG% <> 0 THEN PRINT "ERROR IN SETTING CJC CHANNEL" :
     END
680 'Next get CJC data from this channel using Mode 4
690 MD% = 4 : CJ% = 0
700 CALL DAS8 (MD%, CJ%, FLAG%)
710 'Change output in bits to real temperature
720 CJC = CJ%/10
730 '
740 '----- STEP 4: Get the thermocouple data
750 CH% = 0
760 GOSUB 1000
770 'This step is written as a subroutine so you can use it
     in your own
780 'programs by editing it out. Entry parameters are:-
```

```
790 '  CH% - specifies DAS-8 channel that EXP-16 is connected
    to (0-7).
800 '  D%(11) - integer data array to receive data from
    channels.
810 '
820 '----- STEP 5: Convert data to volts and linearize
830 'AV = Gain setting on Dipswitch of EXP-16 (change to
    suit).
840 FOR I = 0 TO 12
850 V = (D%(I)*5)/(AV*2048)
855 IF I=12 THEN GOTO 5000
860 GOSUB 51000  'perform look-up linearization
870 T(I)=TC          '= TF for degrees Fahrenheit
880 NEXT I
890 '
900 '----- STEP 6: Display temperature data
910 LOCATE 1,1
920 FOR I= 0 TO 12
930 PRINT USING "Channel ## temperature = #####.#  deg.
    C.";I;T(I)
940 NEXT I
942 PRINT
944 PRINT USING "Cold junction temperature (CJC) = ###.# deg.
    C.";CJC
950'Converts Data to Binary from for writing to a file
960 LET TI$ = TIME$
962 LET DAT$ = DATE$
964 LSET DT$ = DAT$
966 LSET TM$ = TI$
968 LSET T0$ = MKS$(T(0))
970 LSET T1$ = MKS$(T(1))
972 LSET T2$ = MKS$(T(2))
974 LSET T3$ = MKS$(T(3))
976 LSET T4$ = MKS$(T(4))
978 LSET T5$ = MKS$(T(5))
980 LSET T6$ = MKS$(T(6))
982 LSET T7$ = MKS$(T(7))
984 LSET T8$ = MKS$(T(8))
986 LSET T9$ = MKS$(T(9))
988 LSET T10$ = MKS$(T(10))
989 LSET T11$ = MKS$(T(11))
990 LSET T12$ = MKS$(T(12))
991 LSET CJC$ = MKS$(CJC)
992 PUT #1, NR
994 NR = NR + 1
995 A$=INKEY$: IF A$="" THEN GOTO 600
997 IF ASC(A$)=27 THEN GOTO 3000
999 GOTO 600
1000 '---- Subroutine to convert EXP-16 channels to number of
    bits
1010 'First lock DAS-8 on the one channel that EXP-16 is
    connected to.
1020 LT%(0) = CH% : LT%(1) = CH% : MD% = 1
1030 CALL DAS8 (MD%, LT%(0), FLAG%)
```

```
1040 IF FLAG% <> 0 THEN PRINT "ERROR IN SETTING CHANNEL" :
     END
1050 'Next select each EXP-16 channel in turn and convert it.
1060 'Digital outputs OP1-4 drive the EXP-16 sub-multiplexer
     address, so use
1070 'mode 14 to set up the sub-multiplexer channel.
1080 FOR SUB% = 0 TO 12   'note use of integer index SUB%
1090 MD% = 14
1100 CALL DAS8 (MD%, SUB%, FLAG%)      'address set
1110 IF FLAG% <> 0 THEN PRINT "ERROR IN EXP-16 CHANNEL
     NUMBER" : END
1120 'Now that channel is selected, perform A/D conversion
     using mode 4.
1130 'Transfer data to corresponding array element D%(SUB%)
1140 MD% = 4  'do 1 A/D conversion
1150 CALL DAS8 (MD%, D%(SUB%), FLAG%)
1160 IF FLAG% <> 0 THEN PRINT "ERROR IN PERFORMING A/D
     CONVERSION"
1170 'Now repeat sequence for all other EXP-16 channels
1180 NEXT SUB%
1190 'All done - return from subroutine
1200 RETURN
1210 '
2000 '---- Subroutine to describe operation and connections
     (pre-amble)
2010 CLS
2020 PRINT"    This program  demonstrates  the  operation of
     J thermocouples"
2030 PRINT"with the EXP-16/DAS-8 combination. It performs the
     following:-"
2040 PRINT
2050 PRINT"1.  Acquires the data"
2060 PRINT"2.  Linearizes and performs cold junction
     compensation"
2070 PRINT"3.  Displays data"
2080 PRINT"4.  Repeats display until <Ctrl-Break> is pressed"
2090 PRINT
2100 PRINT"The thermocouples should be  attached to the HI &
     LO's of each"
2110 PRINT"channel on the EXP-16 starting  with channel 0.
     Also  you  should"
2115 PRINT"connect LO to L.L. GND.  on  each  channel.
     Alternatively,  for a"
2120 PRINT"permanent installation, a better method is to fill
     the solder gaps"
2130 PRINT"on the back of the EXP-16 board behind the
     connector  with  solder"
2140 PRINT"so that the  two  semi-circular halves are shorted
     together.  The"
2145 PRINT"thermocouples can then be connected to HI & LO
     only  (no jumper is"
2147 PRINT"required to L.L. GND.)."
2150 PRINT"Set the OUTPUT CHANNEL jumper block to position 0
     and the  CJC"
```

```
2155 PRINT"CHANNEL to position 7."
2160 PRINT"On running the program,  you will be  prompted
     for  the  gain"
2170 PRINT"setting of the EXP-16. Usually a gain of 100,200
     or 1000  is  best"
2180 PRINT"for thermocouples depending on their output and
     measuring range."
2185 PRINT "LIST this program for commented explanation of
     steps."
2190 PRINT:COLOR 0,7:PRINT" - Press any key to continue -
     ";:COLOR 7,0
2200 IF INKEY$="" GOTO 2200
2210 RETURN
2999 ---- Conversion of binary to ASCII file in CSV form
3000 LOCATE 20,5:COLOR 0,7:PRINT "DATA COLLECTION
     TERMINATED";:COLOR 7,0
3005 LET NR = 1
3010 LOCATE 22,5:PRINT "PROCEEDING WITH DATA CONVERSION TO
     ASCII FORM"
3015 LOCATE 24,5:PRINT "TO ABORT THE CONVERSION OF DATA HIT
     THE <Esc> KEY"
3025 OPEN "O", #2, ASKE$
3110 GOSUB 3210
3120 IF EF = 1 THEN GOTO 4600
3125 SP$=" "
3135 WRITE #2,
     DAT$,TI$,T0,T1,T2,T3,T4,T5,T6,T7,T8,T9,T10,T11,T12,CJC
3140 LET NR = NR + 1: ROW = ROW + 1
3150 A$=INKEY$:IF A$="" GOTO 3200
3160 IF ASC(A$)=27 THEN GOTO 4620
3200 GOTO 3110
3210 LET EF = 0
3220 GET #1, NR
3230 DAT$=DT$
3240 TI$=TM$
3250 T0 = CVS(T0$)
3260 T1 = CVS(T1$)
3270 T2 = CVS(T2$)
3280 T3 = CVS(T3$)
3290 T4 = CVS(T4$)
3300 T5 = CVS(T5$)
3310 T6 = CVS(T6$)
3320 T7 = CVS(T7$)
3330 T8 = CVS(T8$)
3340 T9 = CVS(T9$)
3350 T10 = CVS(T10$)
3360 T11 = CVS(T11$)
3370 T12 = CVS(T12$)
3410 CJC = CVS(CJC$)
3420 IF ASC(MID$(DAT$,3,1))=0 THEN EF = 1
3430 DAT$ = LEFT$(DAT$,6)+RIGHT$(DAT$,2)
3450 RETURN
4000 PRINT
4005 CLS
```

```
4010 LOCATE 20,1:COLOR 0,7:PRINT "TERMINATED";:COLOR 7,0
4020 LOCATE 21, 1: CLOSE #1: END
4600 CLOSE #1
4605 CLS
4610 CLOSE #2:LOCATE 20,1:PRINT "END OF FILE":PRINT "  NUMBER
     OF RECORDS = ";INT(NR-1):END
4620 CLOSE #1
4625 CLS
4630 CLOSE #2:LOCATE 20,1:PRINT "BREAK":END
5000 IF V<0 THEN V=0
5002 LET V1=SQR(V)
5004 LET T(I)=22.458+(1005.713*V1)
5010 GOTO 880
5020 PRINT USING "Channel ## Output      = #.#####   mV
     ";I;T(I)
5030 GOTO 940
5040 IF I=12 THEN GOTO 5020
50000 '------- Table lookup data for J type thermocouple
50010 'Run this subroutine only in the initialization section
     of your program
50020 'Number of points, voltage step interval (mV), starting
     voltage (mV)
50030 DATA  257 ,  .2 , -8.2
50040 READ NJ, SIJ, SVJ
50050 'Temperature at -8.2mv, -8.0mV, -7.8mV etc.
50060 DATA -215.0,-205.3,-196.1,-187.7,-179.9,-172.8,-165.9,-
     159.3,-153.1,-147.1
50070 DATA -141.2,-135.6,-130.0,-124.6,-119.3,-114.2,-109.1,-
     104.2, -99.2, -94.4
50080 DATA  -89.7, -85.0, -80.3, -75.8, -71.3, -66.8, -62.4,
     -58.0, -53.7, -49.3
50090 DATA  -45.1, -40.8, -36.7, -32.5, -28.3, -24.2, -20.1,
     -16.1, -12.0,  -8.0
50100 DATA   -4.0,  -0.0,   3.9,   7.9,  11.8,  15.7,  19.6,
     23.5,  27.4,  31.2
50110 DATA   35.1,  38.9,  42.7,  46.5,  50.3,  54.1,  57.8,
     61.6,  65.3,  69.1
50120 DATA   72.8,  76.5,  80.3,  84.0,  87.7,  91.4,  95.1,
     98.7, 102.4, 106.1
50130 DATA  109.8, 113.4, 117.1, 120.7, 124.4, 128.0, 131.7,
     135.3, 139.0, 142.6
50140 DATA  146.2, 149.9, 153.5, 157.1, 160.7, 164.3, 168.0,
     171.6, 175.2, 178.8
50150 DATA  182.4, 186.0, 189.6, 193.2, 196.8, 200.4, 204.0,
     207.6, 211.2, 214.8
50160 DATA  218.4, 222.0, 225.6, 229.2, 232.8, 236.4, 240.0,
     243.6, 247.2, 250.8
50170 DATA  254.5, 258.1, 261.7, 265.3, 268.9, 272.5, 276.1,
     279.7, 283.3, 286.9
50180 DATA  290.5, 294.1, 297.7, 301.4, 305.0, 308.6, 312.2,
     315.8, 319.4, 323.0
50190 DATA  326.7, 330.3, 333.9, 337.5, 341.1, 344.8, 348.4,
     352.0, 355.6, 359.3
```

```
50200 DATA  362.9, 366.5, 370.1, 373.8, 377.4, 381.0, 384.7,
     388.3, 391.9, 395.5
50210 DATA  399.2, 402.8, 406.4, 410.1, 413.7, 417.3, 420.9,
     424.5, 428.2, 431.8
50220 DATA  435.4, 439.0, 442.6, 446.3, 449.9, 453.5, 457.1,
     460.7, 464.3, 467.9
50230 DATA  471.5, 475.1, 478.7, 482.3, 485.9, 489.5, 493.1,
     496.6, 500.2, 503.8
50240 DATA  507.3, 510.9, 514.5, 518.0, 521.6, 525.1, 528.7,
     532.2, 535.7, 539.3
50250 DATA  542.8, 546.3, 549.8, 553.3, 556.8, 560.3, 563.8,
     567.3, 570.8, 574.2
50260 DATA  577.7, 581.2, 584.6, 588.1, 591.5, 594.9, 598.4,
     601.8, 605.2, 608.6
50270 DATA  612.0, 615.4, 618.8, 622.1, 625.5, 628.9, 632.2,
     635.6, 638.9, 642.3
50280 DATA  645.6, 648.9, 652.2, 655.5, 658.8, 662.1, 665.4,
     668.7, 672.0, 675.2
50290 DATA  678.5, 681.7, 685.0, 688.2, 691.5, 694.7, 697.9,
     701.1, 704.3, 707.5
50300 DATA  710.7, 713.9, 717.1, 720.3, 723.5, 726.6, 729.8,
     733.0, 736.1, 739.3
50310 DATA  742.4, 745.6, 748.7, 751.8, 755.0, 758.1, 761.2
50320 DIM TJ(NJ-1)
50330 FOR I = 0 TO NJ-1:READ TJ(I):NEXT I
50340 RETURN
50350 '
51000 '------ Interpolation routine to find J thermocouple
     temperature
51010 'Entry variables:-
51020 ' CJC = cold junction compensator temperature in deg.
     C.
51030 ' V = thermocouple voltage in volts
51040 'Exit variables:-
51050 ' TC = temperature in degrees Centigrade
51060 ' TF = temperature in degrees Fahrenheit
51070 'Execution time on std. IBM P.C. = 46 milliseconds
51080 'Perform CJC compensation for J type
51090 VJ = 1000*V + 1.277 + (CJC-25)*.05155   'VJ in mV
     (corrected 4/5/85)
51100 '
51110 'Find look up element
51120 EJ = INT((VJ-SVJ)/SIJ)
51130 IF EJ<0 THEN TC=TJ(0):GOTO 51170 'Out of bounds, round
     to lower limit
51140 IF EJ>NJ-2 THEN TC=TJ(NJ-1):GOTO 51170 'Out of
     bounds,round to upper limit
51150 'Do interpolation
51160 TC = TJ(EJ) + (TJ(EJ+1) - TJ(EJ))*(VJ-EJ*SIJ-SVJ)/SIJ
     'Centigrade
51170 TF = TC*9/5 + 32   'Fahrenheit
51180 RETURN
```

# APPENDIX III

Transcription of notes made by Dr. Lindsay on the heat and mass transfer calculations for the drying of the coating film in the experimental low velocity air flow drier.

Dan:

My analysis indicates that your measurements are reasonable. There should not be a significant gradient in temperature near the surface. It just takes an awfully long time to reach the wet bulb temperature for a saturated coating on glass. The temperature drops you observe are entirely reasonable, unless I've really goofed

-J. Lindsay

Problem:

Hot air, laminar flow, removes moisture from a coating on a glass substrate. How does the temperature in the coating change with time? Is there a steep gradient in the coating?

Assumptions:

- Back of glass is insulated.
- Air temperature is constant at 53°C.
- Coating surface stays saturated (situation up to the gloss point)
- Coating and glass have the same thermal properties.
- The thermal properties remain constant.
- Drying air has 0% relative humidity.

Governing Equations:

In the coating and glass, transient heat transfer is governed by the heat equation:

$\delta T/\delta t = \alpha(\delta^2 T/\delta x^2)$ $\alpha$ = Thermal diffusivity, $m^2/s$.

At the upper surface, heat in = heat out, or

$$-k(\delta T/\delta x)_{x=0} + h(T_{air} - T_{surf}) = -\underline{m}h_{vap}$$

where k = conductivity of the coating (W/m°C)
h = heat transfer coefficient ($W/m^2$°C)
$h_{vap}$ = heat of vaporization (J/kg)
$\underline{m}$ = evaporative mass flux ($kg/m^2s$)

$$\underline{m} = h_m(C_{H2O,sat} - C_{H2O,air})$$

h = mass transfer coefficient (m/s)
C = concentration ($kg/m^3$)

Let $C_{H2O,air} = 0$ then

$$C_{H2O,sat} = (P_{sat}(T_{surf}) \times MW)/R(T_{surf} + 273.15)$$

MW = molecular weight of water (18 kg/kgmole)
R = Gas Constant (8314 J/kgmole°C)
$P_{sat}$ = Saturation pressure
$T_{surf}$ = Surface temperature in °C

$$P_{sat}(T)=\exp(23.3265-(3802.7/(T+273.15))-(472.7/(T+273.15))^2)$$

[From Chem Eng. Prog., March 1991]

Now all we need are h, $h_m$ and properties.

Chilton-Colburn analogy: $h/h_m = k_{air}/(D_{H2O-air} \times Le^{0.33})$

Le = $\alpha_{air}/D_{H2O-air}$ at 50°C, $D_{H2O-air} = 0.26x10^{-4}$ $m^2/s$
$k_{air} = 0.028$ W/mK
$\alpha_{air} = 2.8x10^{-5}$ $m^2/s$

Le = 1.077 → $h_m = h/1051$ J/$m^3$°C

But what is h? Nu = $hL/k_{air}$, L = Characteristic length

For laminar flow in a pipe,

Nu = 3.66 for constant $T_{surf}$
4.36 for constant heat flux.

For flow over a flat plate,

Nu = $0.332xRe_x^{1/2}xPr^{1/3}$, Re=$vx/\mu_{air}$ $\mu_{air}=17x10^{-6}$ $m^2/s$
v = 0.5 m/s
x = 5 cm

Nu = $0.332 \times (0.5*0.5/(1.7x10^{-6}))^{1/2} \times (0.7)^{1/3} = 11$

I expect Nu to be in the range of 4 to 11

h = (6 x 0.028 W/mK)/0.05m = 3.4 W/$m^2$K

But I think the characteristic length may be closer to 1 cm, in which case we could use Nu≈4.3 to get,

h = (4.3 x 0.028 W/mK)/0.01m = 12 W/$m^2$K

I should look-up actual Nu values for flow between parallel plates, but I think h = 12 W/$m^2$K will be a good estimate.

If h = 12 W/$m^2$K then $h_m$ = 0.011 m/s

Coating/glass Properties:

I'll use intermediate values between clay, glass and water.

k = 0.78 W/m°C, d = 1900 kg/$m^3$, $C_p$ = 2000 J/kg°C,
$\alpha=2.05x10^{-7}$ $m^2$/sec, and $h_{vap} = 2.4x10^6$ J/kg

Finite Difference Approach:

$T_i^\circ$ means the $T_i$ from the previous time step. The last node is insulated, so $T_{N+1} = T_N$.

I'll use the Crank-Nicholson scheme for stability and speed. This means that all $T_i$'s appearing on the r.h.s. are replaced with $0.5(T_i + T_i^\circ)$ -- in other words, it's half implicit and half explicit in time.

The Crout algorithm is used to solve for the implicit temperatures.

I'll use 200 nodes, each 15 μm thick (the upper node is 7.5 μm thick). Temperatures are determined at thicknesses of 0, 15, 30μm,...,etc. and printed out for locations of 0, 15, 30, 45, 60, 300μm and 3000μm (end point).

Fortran Code is Attached and Results follow.

```
      PROGRAM BUNKER
C**** TEST THIS WITH PLAIN WATER TO SEE IF IT GIVES THE
C**** TRUE STEADY STATE TEMPERATURE
C       T is in Celsius
        IMPLICIT NONE
        INTEGER N,NTIME
C       PARAMETER (NX = 200)
        INTEGER J,NOUTLITE,NANS,I,MM,ITER
        INTEGER EVENT,INFO1,INFO2
        REAL ALPHA,K,KAIR,R,MW,DAB,TEST,
     *  CP,CPAIR,RO,ROAIR,DT,DTMAX,H,HM,MDOT,PSAT,
     *  T(2,200),TIME,TINIT,TAIR
        REAL XHEATIN,TOTHEAT,TSURF,L,HVAP,QEVAP,
     *  DX,A(200),B(200),C(200),S(200),X(200),Z
        CHARACTER *16 NAME
        CHARACTER*1 ANS,CR,LF,BEL,TAB
        LOGICAL NEXT     ! If TRUE, go to next time step
$INCLUDE:HLTBI.CON
        DATA TAB/9/

        PSAT(Z)= EXP(23.3265-3802.7/(Z+273.18)-(472.68/(Z+273.18))**2) ! Z is in Celsius
        MDOT(Z,HM) = -HM*18.* EXP(23.3265-3802.7/(Z+273.18)-(472.68
     &      /(Z+273.18))**2)/(8314.*(Z+273.15))
C       PSAT(T)= EXP(23.1964 - 3816.44/(T+227.05) )  ! T is in Celsius
C       MDOT(Z,HM) = -HM*18.* EXP(23.1964 - 3816.44/(Z+227.05) )
C     &      /(8314.*(Z+273.15))
C-------------------------------------------------
C       READ IN INITIAL INFO ABOUT THE CASES TO BE RUN
C       AND INITIALIZE A FEW FIXED TERMS
C-------------------------------------------------
        TEST = PSAT(53.)
        TYPE *,'PSAT(53) = ',TEST
        TEST = MDOT(53.,.012)
        TYPE *,'MDOT(53.,.012) = ',TEST
        TYPE *,'ENTER OUTPUT FILE NAME'
        READ(*,2) NAME  ! NAME
2       FORMAT(A16)

        OPEN(UNIT=13,FILE=NAME,STATUS='NEW')
        WRITE(13,4499)  (TAB,J=1,9)

4499    FORMAT('*',/,'TIME',A1,'HEAT_IN',A1,'QEVAP',A1,'T1',
     * A1,'T2',A1,'T3',A1,'T4',A1,'T5',A1,'T20',A1,
     *'T300')
        CLOSE(UNIT=13)


C---- ALL SI UNITS
        R = 8314. !J/kgmol C
        MW = 18
C---- Properties of the coating/solid section
        K=0.78 !W/m C
        ALPHA = 2.053E-07 !m^2/sec
        RO = 1900 ! kg/m^3
        CP = 2000 ! J/kg C
        HVAP = 2.4E06 ! J/kg ** correct? **
C---- Properties for air
        DAB = 0.26
        H = 12.04 !W/m^2 C
        HM = H/1.051E03
        CPAIR = 1000 !J/kg C
        KAIR = 0.028 ! W/m C
        ROAIR = 1 ! kg/m^3

C----- RUN CONDITIONS
        N = 200
```

```
        TAIR = 53.
        TINIT = 53.
        DO 10 J = 1,N
        T(2,J)=TINIT
10      T(1,J) = TINIT
        L = .003 ! m
        DX = L/N  ! 10 MICRONS  15 μm
        DTMAX = DX**2/(2*ALPHA)
        TYPE *,'DTMAX IS ',DTMAX
        TYPE *,'ENTER DT AND # OF TIME STEPS'
        READ *, DT,NTIME
        NOUTLITE = INT(0.05/DT)  ! number of steps before outputting data - every .05 s
C-------------------------------------
C---- Begin the batch cycle here:
C       ONE CASE AT A TIME
C-------------------------------------

        TIME = 0


        DO 700 MM=2,NTIME !This begins the time stepping loop
C-------------------------------------------------
C----- CHECK FOR EVENTS: A MOUSECLICK OR TYPING TO PAUSE.
C       PERHAPS THE USER WANTS TO CHANGE THE VALUE OF DT
C-------------------------------------------------
        CALL WINDTB(GEVENT,0,EVENT,INFO1,INFO2)
        IF(EVENT.GT.1) THEN !Pause, release control
           TYPE *,'ITERATION, TIME = ',MM,TIME
           TYPE *,'HERE ARE THE UPPER 15 TEMPS:'
           DO 3954 J=1,15
3954       TYPE *,J,T(2,J)
           TYPE *,'CARE TO CHANGE DELT? NOW IT IS',DT
           TYPE *,'TYPE ANY NUMBER TO CONTINUE, 1 TO CHANGE DT'
           READ *,NANS
           IF (NANS.EQ.1) THEN
                TYPE *,'NEW DT AND NOUT:'
                READ *,DT,NOUTLITE
C               NOUTLITE = INT(0.05/DT)
           END IF
        END IF   ! End the block checking for events like a mouse click.
C-------------------------------------------------
C       SEE IF THE CASE IS OVER
C-------------------------------------------------

C----   UPDATE THE CURRENT TIME AND SEND TO SCREEN.
         TIME = TIME + DT
        TYPE *,'TIME, TSURF:',TIME,T(2,1)

C-------------------------------------------------
C       GET THE NEW TEMPERATURES
C       USE THE CRANK-NICHOLSON APPROACH
C-------------------------------------------------

C---    LOWER SURFACE (INSULATED)
        A(N) = 1./DT + 0.5*(ALPHA/(DX*DX))
        B(N) = 0.5*(-ALPHA/(DX*DX))
        C(N) = 0
        S(N) = T(1,N)/DT + 0.5*ALPHA/(DX*DX)*(T(1,N-1)-T(1,N))  ! THE insulated back boundar
y

C---    UPPER SURFACE (EVAPORATIVE COOLING OCCURS HERE)
        A(1) = RO*CP*DX*0.5/DT + 0.5*(K/DX + H)
        B(1) = 0
        C(1) = 0.5*(-K/DX)
        QEVAP =  MDOT(T(1,1),HM)*HVAP ! W/m^2
        S(1) = T(1,1)*(RO*CP*DX*0.5/DT) + H*TAIR +
```

```
     &          QEVAP + 0.5*(K/DX*T(1,2) -(K/DX+H)*T(1,1))

C---     MAIN BODY OF COATING AND SOLID (INTERIOR NODES)
         DO 100 J = 2,N-1
            A(J)=1./DT + ALPHA/(DX*DX)
            B(J) = -ALPHA*0.5/(DX*DX)
            C(J) = -ALPHA*0.5/(DX*DX)
            S(J) = T(1,J)/DT +ALPHA*0.5/(DX*DX)*(T(1,J+1)-2*T(1,J)
     &              +T(1,J-1))
100      CONTINUE

         CALL XCROUT(A,B,C,S,X,N)
         DO 101 J = 1,N
101      T(2,J) = X(J)
          DO 21 J=1,N
21        T(1,J)=T(2,J)

         XHEATIN=H*(TAIR-T(2,1)) !CONVECTION IN
         TOTHEAT=TOTHEAT+XHEATIN*DT

C-------------------------------------------------------
C        OUTPUT RESULTS
C-------------------------------------------------------

           IF(MM.EQ.(INT(MM/NOUTLITE)*NOUTLITE)) THEN
             OPEN(UNIT=13,FILE=NAME,STATUS='OLD',POSITION='APPEND')
             WRITE(13,8339) TIME,TAB,XHEATIN,TAB,QEVAP,TAB,(T(2,J),
     *       TAB,J=1,5),T(2,20),TAB,T(2,N)
8339         FORMAT(10(E12.5,A1))
             CLOSE(UNIT=13)
           END IF
700    CONTINUE  ! DO loop for multiple time steps
9999     CONTINUE ! DO LOOP for multiple cases.
         TYPE *,'ALL DONE, KIMOSABE' !We're outa here.
       STOP
       END


         SUBROUTINE XCROUT(A,B,C,BB,X,N)
C        CROUT reduction solver for tridiag. systems unique solutions:
C        ALG067 from Math 411. Details on p. 312 of Burden, Faires,
C        and Reynolds, Numerical Analysis, 2nd ed., Prindle, Weber and
C        Schmidt, Boston, Mass., 1981,
         DIMENSION A(300),B(300),C(300),BB(300),Z(300),X(300)
C-----  A is the main diagonal, B the lower, and C the upper.
C        B(1) and C(N) are not used, i.e. B goes from 2 to N,
C        C from 1 to N-1.
C        BB is the result vector:  e.g., B(J)X(J-1)+A(J)X(J)+C(J)X(J+1)=BB(J)
C        X is the output vector.

C        STEP 1:
C        The entries of U overwrite C and the entries of L overwrite A.
C        However, the first and last A values do not get changed if C(1)
C        and the last B or C values are 0.
         C(1)=C(1)/A(1)
C        STEP 2:
         DO 10 I=2,N-1
                A(I)=A(I)-B(I)*C(I-1)  ! Ith row of L
10       C(I)=C(I)/A(I)         ! (I+1)st column of U
C        STEP 3:
         A(N)=A(N)-B(N)*C(N-1) ! Nth row of L
C        STEP 4:
         Z(1) = BB(1)/A(1)         ! Steps 4 and 5 solve LZ=BB
C        STEP 5:
         DO 20 I=2,N
20       Z(I)=(BB(I)-B(I)*Z(I-1))/A(I)
```

```
C       STEP 6:
        X(N)=Z(N)   ! Steps 6 and 7 solve UX=Z
C       STEP 7:
        DO 30 II=1,N-1
                I= N-II
30      X(I)=Z(I)-C(I)*X(I+1)
        RETURN
        END
```

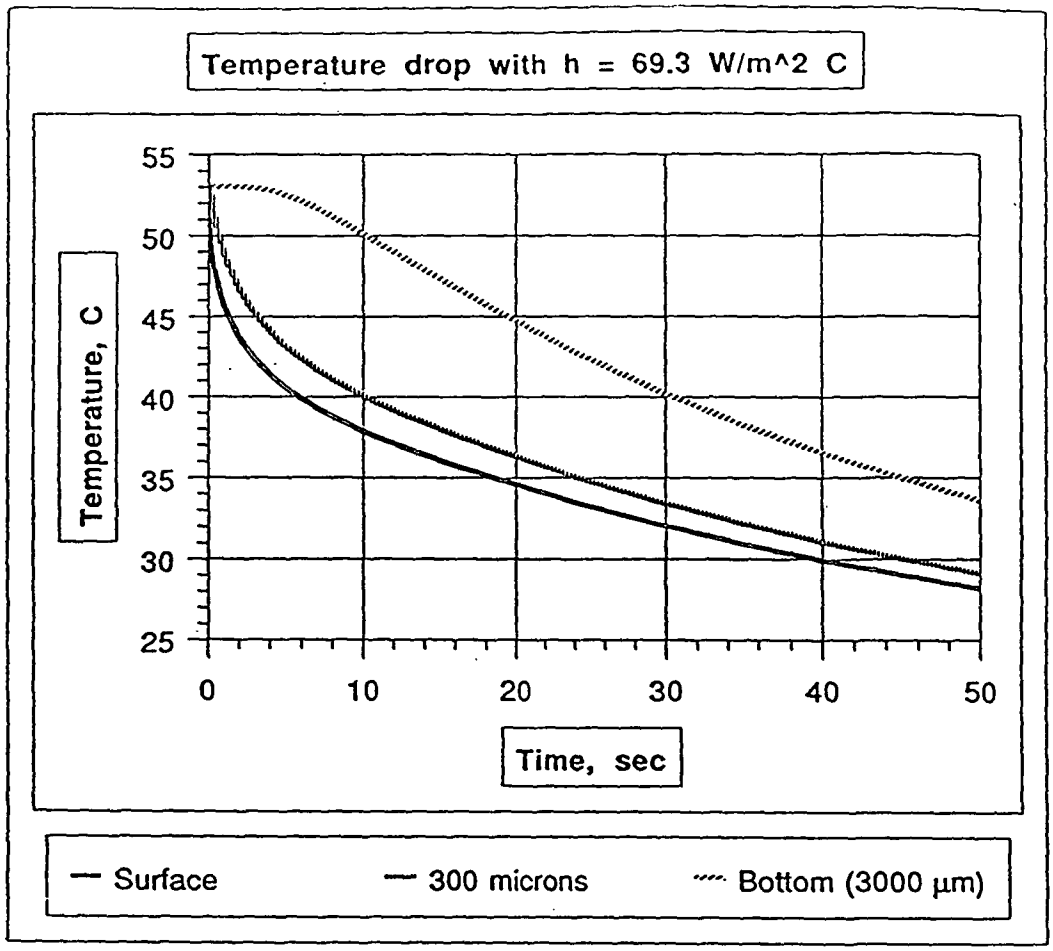


Figure A3.1. Calculated temperature versus time plot for the coated glass-heat transfer coefficient 69 $W/m^{2}°C$

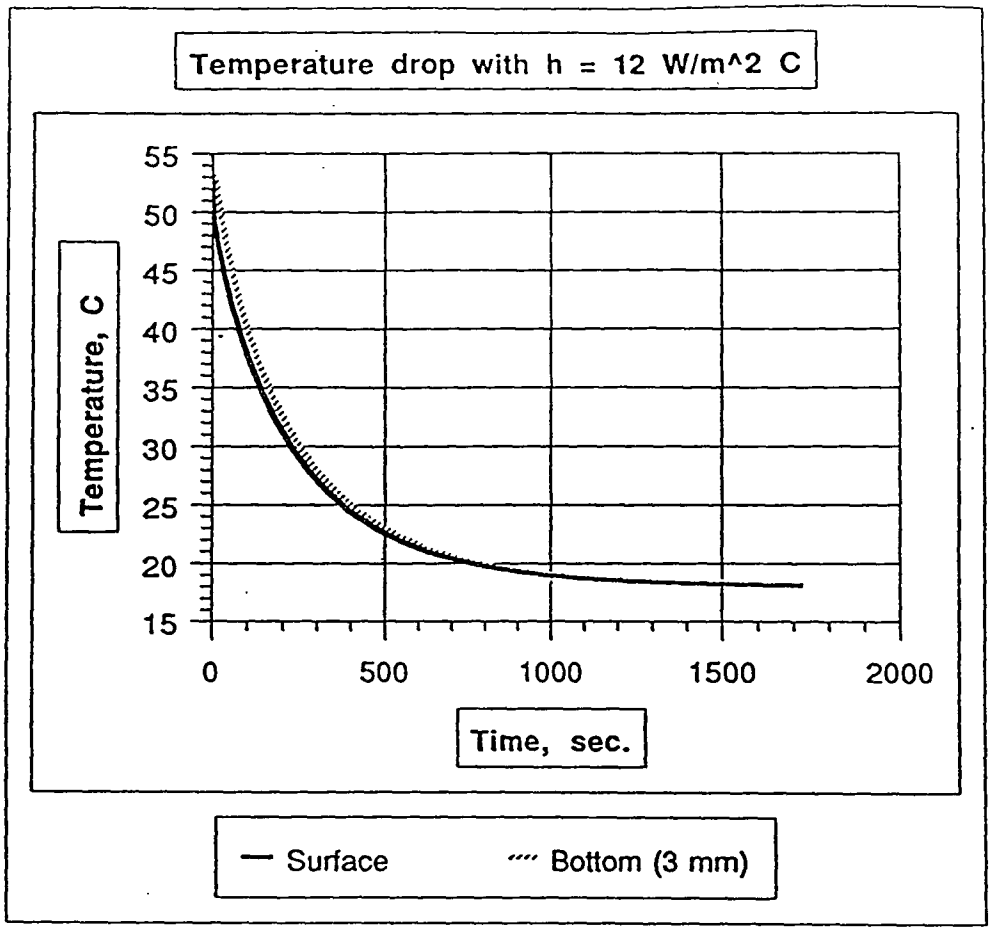


Figure A3.2. Calculated temperature versus time plot for coated glass-heat transfer coefficient 12 W/m$^2$°C

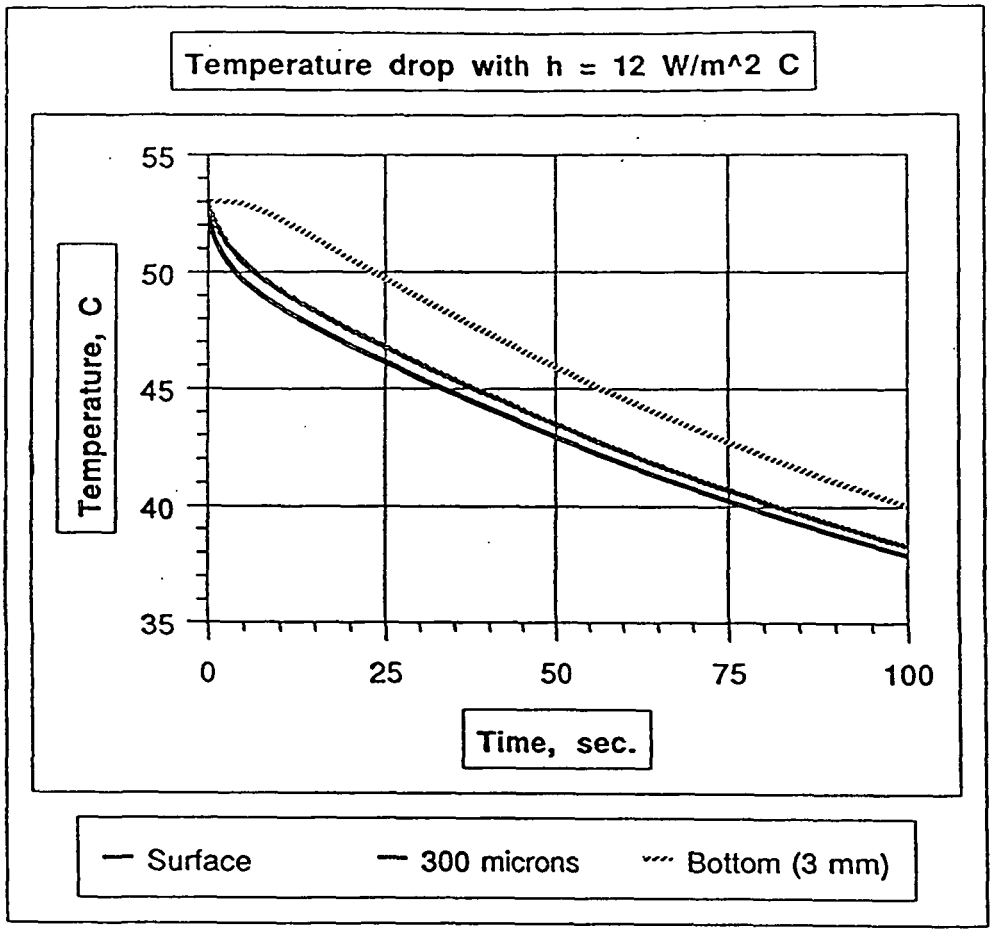


Figure A3.3. Firat 100 seconds of Fig. A3.2 including the temperature at 300 μm into the glass from the coating surface

Biot analysis:

$Bi = hL/k_{coating}$ _ 12 $W/m^2°C$ x 0.03m/0.78 $W/m°C$ = 0.28

Lumped capacitance may not be appropriate. Try it anyway.

Use Heisler Charts, page 192 of Lncropera and Dewitt. use L = 0.01m

$F_o = \alpha t/L^2 = 2.05x10^{-7} m^2/s*t/(0.01m)^2 = 2.05x10^{-3}$ x t $s^{-1}$

$\Theta = (T_{midplane} - T_{air})/(T_{initial} - T_{air})$

Whoops!, $T_{initial} = T_{air}$ Forget it. The whole approach is clearly not appropriate. However, if $T_{initial} = T_{air}$ is not the case and using $B^{-1} = 3$, the Heisler chart indicates that for $\Theta$ to be 0.5, $F_o = 2$ so t = 1000 sec.

That's right! Thousands of seconds are needed to reach thermal equilibrium.

Conclusions:

The rate of temperature decline that you see is reasonable. Based on your data, I'd say h is probably larger than 12 $W/m^2°C$ but less than 69 $W/m^2°C$. Of course, all this was rough and the truth requires better values for physical properties and better knowledge of h and $h_m$. But the values used here are reasonable, and the results make your data look reasonable.

# APPENDIX IV

Temperature response of the coating glass interface with drying at various drying rates.

See Figs. 30 and 31 for locations of resistors A - F and Table VII for parameters used in each trial.

page

Table A4.PT1. Glass plate temperature inserted into drier at 54 C.

| PT1 Ref. Temp. Resistors Time-sec. | 23 A | 23 B | 23 F | 23 C | 23 D | 23 E | Left Edge |
|---|---|---|---|---|---|---|---|
| -11 | 22.83 | 23.00 | 22.78 | 22.87 | 22.81 | 22.94 | |
| -10 | 22.91 | 23.06 | 22.83 | 22.92 | 22.85 | 22.87 | |
| -8 | 22.92 | 23.16 | 22.93 | 22.97 | 22.83 | 23.00 | |
| -6 | 22.98 | 22.86 | 22.98 | 23.02 | 22.98 | 22.94 | |
| -5 | 23.06 | 22.80 | 23.07 | 23.00 | 23.13 | 22.97 | |
| -3 | 23.05 | 22.94 | 23.07 | 23.10 | 23.48 | 23.08 | |
| -1 | 23.18 | 23.11 | 23.24 | 23.05 | 23.74 | 23.13 | |
| 0 | 23.81 | 23.36 | 23.40 | 23.48 | 23.95 | 23.53 | |
| 2 | 25.00 | 24.26 | 23.91 | 24.17 | 24.66 | 24.27 | |
| 4 | 25.66 | 24.68 | 24.09 | 24.80 | 25.01 | 24.81 | |
| 5 | 26.15 | 25.14 | 24.38 | 25.07 | 25.33 | 25.06 | |
| 7 | 26.61 | 25.37 | 24.58 | 25.39 | 25.67 | 25.51 | |
| 9 | 26.92 | 25.71 | 24.74 | 25.58 | 25.89 | 25.62 | |
| 10 | 27.33 | 25.98 | 24.96 | 25.70 | 26.11 | 25.90 | |
| 12 | 27.59 | 26.15 | 25.01 | 26.11 | 26.25 | 26.20 | |
| 14 | 27.87 | 26.44 | 25.19 | 26.26 | 26.42 | 26.36 | |
| 15 | 28.16 | 26.58 | 25.34 | 26.45 | 26.65 | 26.60 | |
| 17 | 28.36 | 26.87 | 25.43 | 26.69 | 26.72 | 26.66 | |
| 18 | 28.67 | 26.98 | 25.62 | 26.77 | 26.98 | 26.92 | |
| 20 | 28.90 | 27.19 | 25.70 | 27.00 | 27.08 | 27.10 | |
| 22 | 29.11 | 27.42 | 25.86 | 27.08 | 27.25 | 27.21 | |
| 23 | 29.34 | 27.55 | 25.89 | 27.33 | 27.40 | 27.45 | |
| 25 | 29.56 | 27.79 | 26.10 | 27.41 | 27.50 | 27.51 | |
| 27 | 29.77 | 27.90 | 26.17 | 27.64 | 27.65 | 27.81 | |
| 28 | 29.97 | 28.15 | 26.29 | 27.77 | 27.74 | 27.86 | |
| 30 | 30.22 | 28.25 | 26.46 | 27.80 | 27.91 | 28.05 | |
| 32 | 30.39 | 28.44 | 26.51 | 28.12 | 27.99 | 28.17 | |
| 55 | 33.06 | 30.57 | 28.09 | 30.02 | 29.70 | 30.24 | |
| 57 | 33.21 | 30.83 | 28.25 | 30.05 | 29.85 | 30.24 | |
| 58 | 33.41 | 30.86 | 28.30 | 30.24 | 29.99 | 30.50 | |
| 61 | 33.66 | 31.14 | 28.49 | 30.24 | 30.22 | 30.66 | |
| 64 | 33.93 | 31.28 | 28.63 | 30.66 | 30.38 | 30.95 | |
| 69 | 34.34 | 31.78 | 28.94 | 31.03 | 30.66 | 31.16 | |
| 74 | 34.91 | 32.29 | 29.35 | 31.32 | 31.08 | 31.66 | |
| 80 | 35.46 | 32.75 | 29.65 | 31.65 | 31.51 | 32.15 | |

| Time sec. | A | B | F | C | D | E | Left Edge |
|---|---|---|---|---|---|---|---|
| 86 | 35.92 | 33.08 | 29.95 | 32.24 | 31.87 | 32.55 | |
| 91 | 36.40 | 33.58 | 30.33 | 32.63 | 32.23 | 32.83 | |
| 97 | 36.85 | 34.11 | 30.72 | 32.91 | 32.61 | 33.21 | |
| 102 | 37.34 | 34.46 | 31.01 | 33.16 | 33.01 | 33.75 | |
| 108 | 37.76 | 34.83 | 31.31 | 33.59 | 33.34 | 34.09 | |
| 114 | 38.15 | 35.26 | 31.66 | 34.07 | 33.61 | 34.36 | |
| 119 | 38.57 | 35.69 | 32.02 | 34.29 | 33.99 | 34.72 | |
| 125 | 38.93 | 36.06 | 32.34 | 34.62 | 34.34 | 35.07 | |
| 131 | 39.33 | 36.36 | 32.62 | 34.94 | 34.65 | 35.51 | |
| 136 | 39.70 | 36.68 | 32.87 | 35.30 | 34.95 | 35.85 | |
| 142 | 40.03 | 37.09 | 33.20 | 35.67 | 35.27 | 36.08 | |
| 147 | 40.38 | 37.49 | 33.56 | 35.89 | 35.60 | 36.38 | |
| 153 | 40.72 | 37.79 | 33.84 | 36.15 | 35.95 | 36.78 | |
| 159 | 41.06 | 38.03 | 34.07 | 36.51 | 36.19 | 37.11 | |
| 164 | 41.34 | 38.43 | 34.42 | 36.88 | 36.44 | 37.33 | |
| 170 | 41.64 | 38.78 | 34.73 | 37.03 | 36.78 | 37.64 | |
| 175 | 41.93 | 39.03 | 34.97 | 37.27 | 37.06 | 37.92 | |
| 181 | 42.18 | 39.25 | 35.18 | 37.66 | 37.29 | 38.27 | |
| 187 | 42.44 | 39.58 | 35.46 | 37.95 | 37.50 | 38.44 | |
| 192 | 42.70 | 39.95 | 35.81 | 38.06 | 37.87 | 38.74 | |
| 198 | 43.00 | 40.10 | 36.03 | 38.38 | 38.11 | 39.13 | |
| 203 | 43.19 | 40.34 | 36.21 | 38.73 | 38.29 | 39.30 | |
| 209 | 43.42 | 40.71 | 36.55 | 38.86 | 38.56 | 39.49 | |
| 215 | 43.67 | 40.95 | 36.81 | 38.98 | 38.85 | 39.84 | |
| 361 | 47.41 | 45.50 | 41.31 | 43.43 | 43.47 | 44.06 | |
| 372 | 47.69 | 45.89 | 41.93 | 43.77 | 43.81 | 44.46 | |
| 389 | 47.97 | 46.29 | 42.54 | 44.13 | 44.25 | 44.92 | |
| 405 | 48.16 | 46.61 | 43.01 | 44.48 | 44.58 | 45.27 | |
| 529 | 49.30 | 48.13 | 45.74 | 46.58 | 46.65 | 47.07 | |
| 688 | 49.98 | 49.78 | 47.90 | 47.93 | 48.03 | 48.46 | |
| 865 | 50.45 | 50.64 | 49.22 | 48.58 | 48.99 | 49.29 | |
| 1049 | 50.63 | 50.83 | 49.57 | 48.87 | 49.41 | 49.53 | |
| 1355 | 50.84 | 50.42 | 50.45 | 49.28 | 49.76 | 49.86 | |
| 1933 | 51.13 | 51.85 | 50.65 | 49.54 | 50.10 | 50.09 | |

Figure A4.PT1a. Glass plate at 23 C inserted into drying air at 54 C.

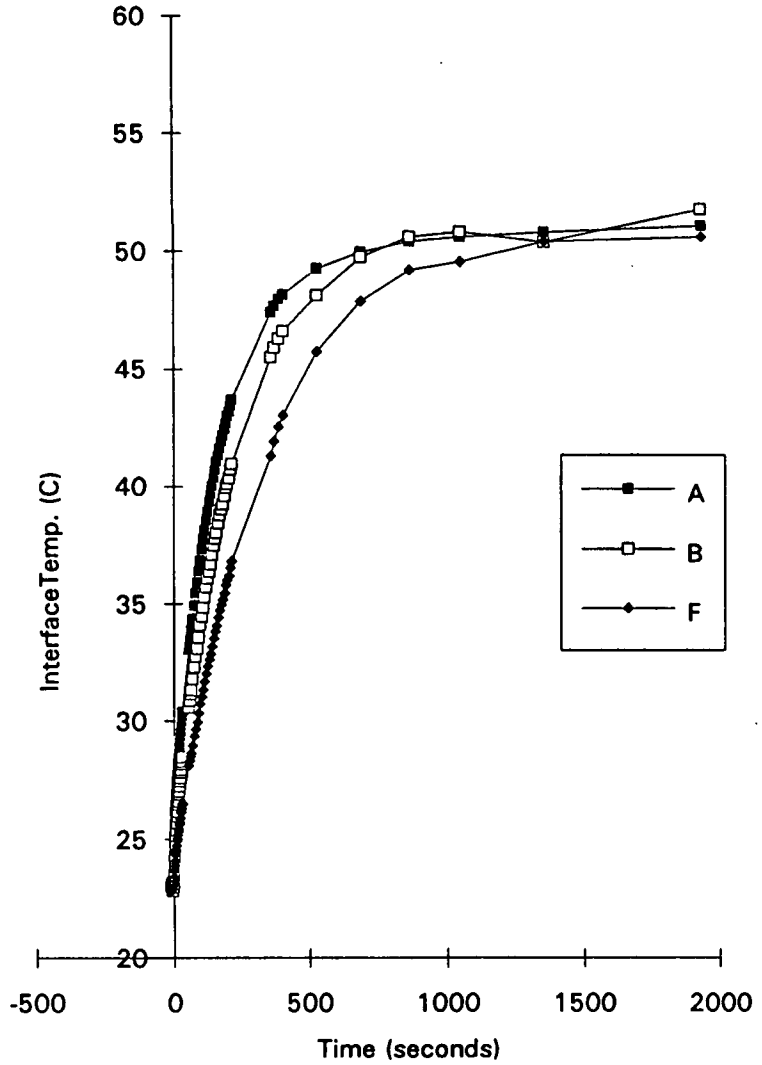


Figure A4.PT1b. Glass plate at 23 C inserted into drying air at 54 C.

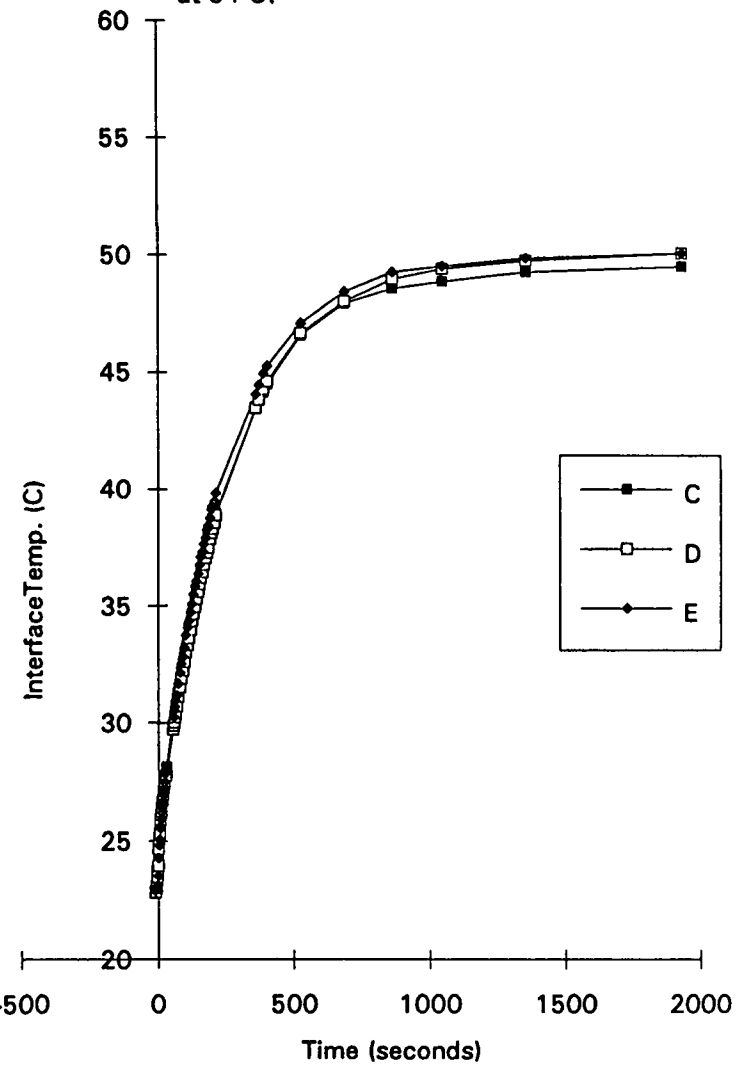

Table A4.PT2. Glass plate temperature inserted into drier at 54 C.

| PT2 Ref. Temp. Resistors Time-sec. | 25 A | 25 B | 25 F | 25 C | 25 D | 25 E | Left Edge |
|---|---|---|---|---|---|---|---|
| -12 | 25.00 | 24.88 | 24.87 | 24.96 | 24.89 | 24.90 | |
| -11 | 25.00 | 24.93 | 24.94 | 24.99 | 24.95 | 24.99 | |
| -9 | 24.98 | 24.91 | 24.98 | 24.96 | 25.01 | 24.98 | |
| -7 | 25.09 | 25.11 | 25.01 | 25.04 | 25.02 | 24.99 | |
| -6 | 24.98 | 25.02 | 25.03 | 25.04 | 25.34 | 25.09 | |
| -4 | 24.91 | 25.08 | 25.03 | 24.86 | 25.04 | 24.98 | |
| -2 | 25.03 | 24.99 | 25.10 | 25.14 | 25.12 | 25.09 | |
| -1 | 25.08 | 25.16 | 25.17 | 25.19 | | 25.06 | |
| 1 | 25.21 | 25.39 | 25.37 | 25.25 | | 25.12 | |
| 3 | 26.24 | 25.90 | 25.56 | 25.76 | | 25.76 | |
| 4 | 27.10 | 26.57 | 25.89 | 26.41 | | 26.40 | |
| 6 | 27.76 | 26.96 | 26.13 | 26.69 | | 26.88 | |
| 8 | 28.16 | 27.35 | 26.28 | 27.18 | | 27.11 | |
| 9 | 28.59 | 27.71 | 26.53 | 27.29 | | 27.39 | |
| 11 | 28.92 | 27.91 | 26.59 | 27.66 | | 27.66 | |
| 13 | 29.24 | 28.29 | 26.92 | 27.82 | | 27.86 | |
| 14 | 29.45 | 28.38 | 26.89 | 27.75 | 27.69 | 28.16 | |
| 16 | 29.81 | 28.63 | 26.99 | 28.17 | 27.81 | 28.27 | |
| 18 | 30.10 | 28.86 | 27.18 | 28.33 | 28.03 | 28.48 | |
| 19 | 30.31 | 29.00 | 27.21 | 28.46 | 28.17 | 28.70 | |
| 21 | 30.56 | 29.26 | 27.40 | 28.67 | 28.34 | 28.82 | |
| 23 | 30.83 | 29.34 | 27.47 | 28.78 | 28.49 | 29.09 | |
| 24 | 31.00 | 29.61 | 27.58 | 29.04 | 28.63 | 29.12 | |
| 26 | 31.31 | 29.73 | 27.73 | 29.05 | 28.81 | 29.33 | |
| 28 | 31.48 | 29.92 | 27.82 | 29.31 | 28.96 | 29.49 | |
| 29 | 31.69 | 30.12 | 27.92 | 29.37 | 29.12 | 29.57 | |
| 31 | 31.86 | 30.20 | 28.02 | 29.55 | 29.22 | 29.81 | |
| 32 | 32.08 | 30.44 | 28.16 | 29.73 | 29.35 | 29.86 | |
| 34 | 32.28 | 30.52 | 28.28 | 29.81 | 29.49 | 30.11 | |
| 36 | 32.43 | 30.70 | 28.35 | 30.08 | 29.59 | 30.21 | |
| 37 | 32.66 | 30.87 | 28.47 | 30.10 | 29.76 | 30.37 | |
| 39 | 32.88 | 30.95 | 28.56 | 30.31 | 29.90 | 30.53 | |
| 41 | 33.14 | 31.22 | 28.70 | 30.43 | 30.10 | 30.73 | |
| 44 | 33.45 | 31.48 | 28.88 | 30.64 | 30.28 | 30.97 | |
| 47 | 33.74 | 31.75 | 29.04 | 30.88 | 30.47 | 31.19 | |

| Time sec. | A | B | F | C | D | E | Left Edge |
|---|---|---|---|---|---|---|---|
| 50 | 34.07 | 32.08 | 29.24 | 31.10 | 30.73 | 31.42 | |
| 56 | 34.68 | 32.47 | 29.55 | 31.38 | 31.15 | 31.94 | |
| 61 | 35.22 | 32.94 | 29.90 | 31.95 | 31.51 | 32.27 | |
| 67 | 35.76 | 33.49 | 30.28 | 32.41 | 31.93 | 32.69 | |
| 72 | 36.34 | 33.91 | 30.61 | 32.67 | 32.37 | 33.27 | |
| 78 | 36.86 | 34.34 | 30.92 | 33.09 | 32.73 | 33.61 | |
| 84 | 37.33 | 34.88 | 31.26 | 33.60 | 33.10 | 33.97 | |
| 89 | 37.83 | 35.32 | 31.66 | 33.84 | 33.50 | 34.40 | |
| 95 | 38.36 | 35.64 | 31.92 | 34.13 | 33.87 | 34.86 | |
| 100 | 38.81 | 36.00 | 32.21 | 34.56 | 34.21 | 35.24 | |
| 106 | 39.17 | 36.49 | 32.54 | 35.06 | 34.50 | 35.49 | |
| 112 | 39.63 | 36.94 | 32.91 | 35.27 | 34.93 | 35.88 | |
| 123 | 40.44 | 37.58 | 33.43 | 36.04 | 35.56 | 36.61 | |
| 128 | 40.80 | 38.08 | 33.83 | 36.32 | 35.87 | 36.87 | |
| 243 | 46.53 | 43.92 | 38.48 | 41.52 | 41.30 | 42.26 | |
| 254 | 47.01 | 44.57 | 39.27 | 42.00 | 41.85 | 42.84 | |
| 265 | 47.35 | 44.94 | 39.76 | 42.48 | 42.22 | 43.26 | |
| 277 | 47.72 | 45.35 | 40.26 | 42.73 | 42.65 | 43.72 | |
| 288 | 47.97 | 45.74 | 40.67 | 43.17 | 42.98 | 44.01 | |
| 300 | 48.31 | 46.09 | 41.11 | 43.46 | 43.39 | 44.45 | |
| 459 | 50.52 | 49.52 | 44.86 | 46.65 | 46.57 | 47.47 | |
| 623 | 51.41 | 50.89 | 46.71 | 48.32 | 48.32 | 48.99 | |
| 804 | 52.23 | 50.27 | 48.99 | 49.81 | 49.88 | 50.37 | |
| 987 | 52.79 | 51.02 | 50.20 | 50.85 | 50.35 | 51.39 | |
| 1154 | 51.60 | 58.35 | 49.50 | 49.96 | 49.38 | 50.35 | |
| 1337 | 51.58 | 58.42 | 49.80 | 49.78 | 49.30 | 50.22 | |
| 1514 | 51.68 | 58.26 | 49.65 | 49.73 | 49.31 | 50.18 | |

Figure A4PT2a. Glass plate at 23 C inserted into drying air at 54 C.

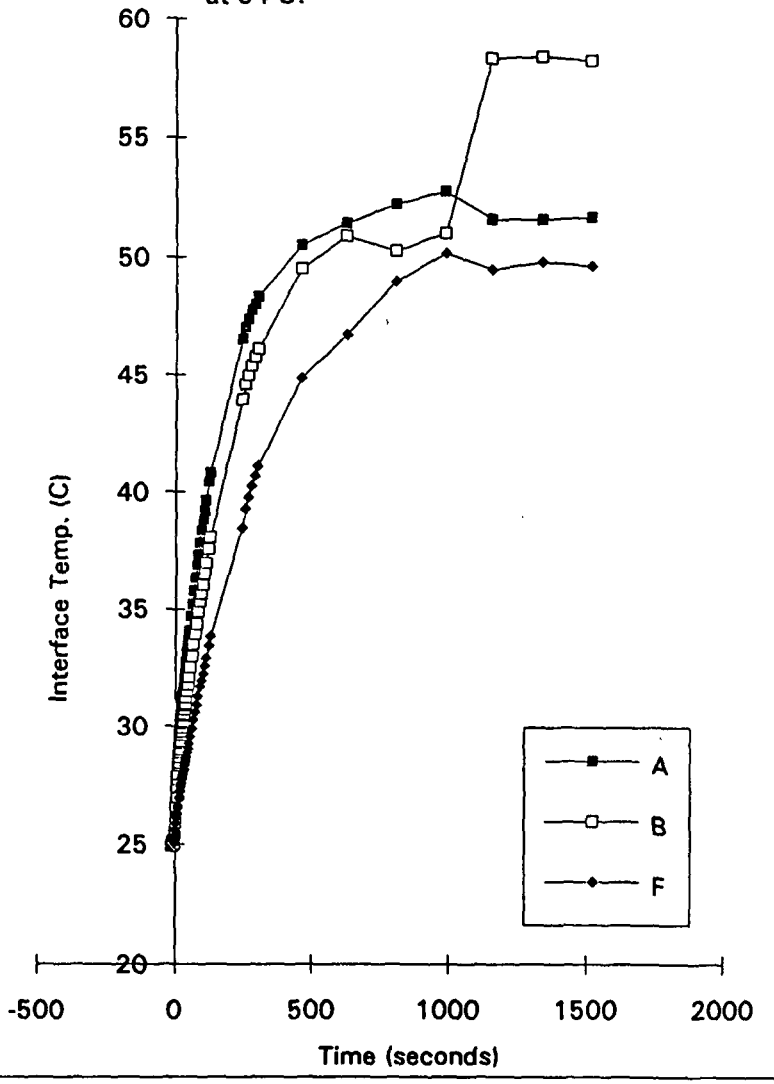


Figure A4.PT2b. Glass plate at 23 C inserted into drying air at 54 C.

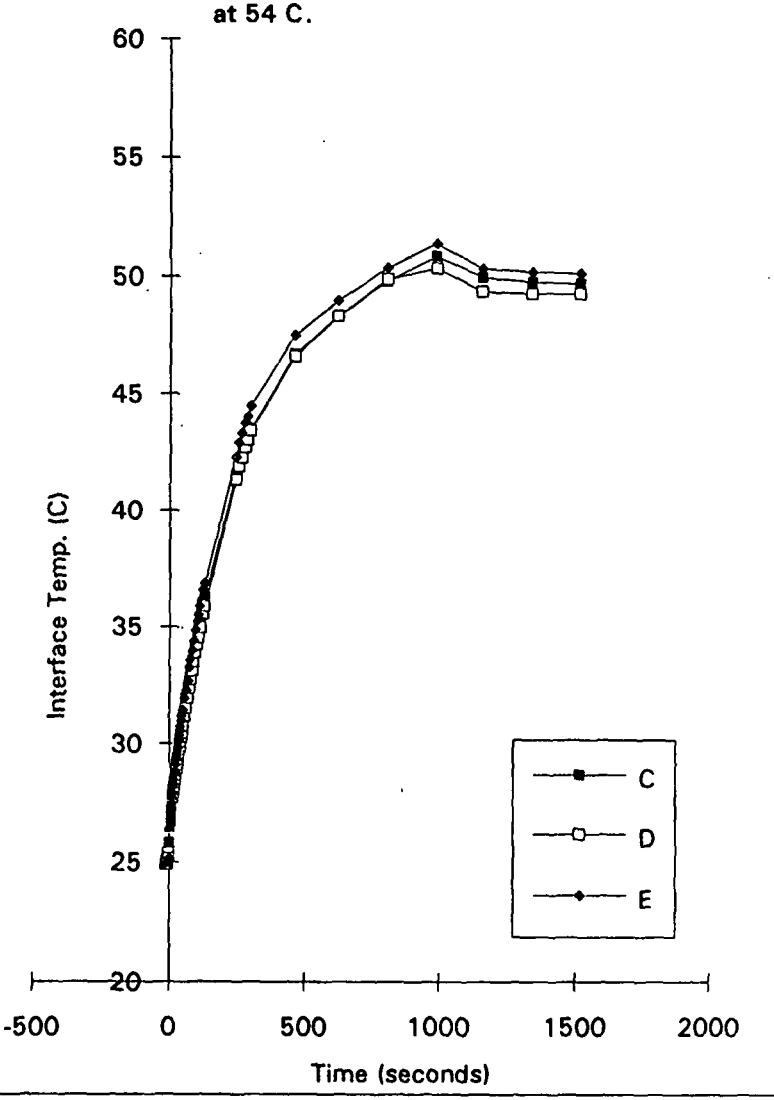

Table A4.PT3. Glass plate temperature inserted into drier at 54 C.

| PT3 Ref. Temp. Resistors Time-sec. | 25 A | 25 B | 25 F | 25 C | 25 D | 25 E | Left Edge |
|---|---|---|---|---|---|---|---|
| -17 | 25.08 | 24.91 | 25.00 | 25.00 | 24.82 | 25.16 | |
| -15 | 25.05 | 24.91 | 25.00 | 25.00 | 24.87 | 25.19 | |
| -14 | 25.10 | 24.96 | 25.00 | 25.00 | 24.91 | 25.16 | |
| -12 | 24.94 | 24.99 | 25.00 | 25.00 | 25.01 | 25.00 | |
| -10 | 24.93 | 25.05 | 24.94 | 24.96 | 25.09 | 24.84 | |
| -9 | 24.94 | 25.03 | 25.04 | 25.04 | 25.09 | 24.84 | |
| -7 | 24.98 | 25.09 | 25.03 | 25.02 | 25.11 | 24.89 | |
| -5 | 25.04 | 25.12 | 24.99 | 25.02 | 25.16 | 24.92 | |
| -4 | 25.13 | 25.22 | 25.18 | 25.12 | 25.24 | 25.02 | |
| -2 | 25.25 | 25.36 | 25.30 | 25.28 | 25.36 | 25.14 | |
| 0 | 25.57 | 25.57 | 25.32 | 25.39 | 25.55 | 25.35 | |
| 1 | 26.75 | 26.57 | 25.87 | 26.43 | 26.21 | 26.18 | |
| 3 | 27.48 | 26.89 | 26.13 | 26.75 | 26.68 | 26.58 | |
| 5 | 27.97 | 27.21 | 26.35 | 27.03 | 26.97 | 26.93 | |
| 6 | 28.49 | 27.60 | 26.49 | 27.40 | 27.26 | 27.21 | |
| 8 | 28.83 | 27.81 | 26.69 | 27.57 | 27.48 | 27.51 | |
| 10 | 29.27 | 28.20 | 26.81 | 27.94 | 27.73 | 27.75 | |
| 11 | 29.50 | 28.40 | 27.06 | 28.13 | 27.93 | 27.97 | |
| 13 | 29.81 | 28.58 | 27.23 | 28.34 | 28.10 | 28.13 | |
| 15 | 30.07 | 28.81 | 27.19 | 28.47 | 28.27 | 28.34 | |
| 17 | 30.30 | 28.96 | 27.47 | 28.66 | 28.44 | 28.52 | |
| 18 | 30.61 | 29.24 | 27.43 | 28.86 | 28.61 | 28.69 | |
| 20 | 30.76 | 29.35 | 27.59 | 28.94 | 28.75 | 28.87 | |
| 22 | 31.06 | 29.59 | 27.78 | 29.19 | 28.90 | 29.03 | |
| 23 | 31.21 | 29.70 | 27.80 | 29.29 | 29.05 | 29.22 | |
| 25 | 31.49 | 29.90 | 28.04 | 29.53 | 29.22 | 29.36 | |
| 26 | 31.72 | 30.08 | 28.00 | 29.66 | 29.34 | 29.52 | |
| 28 | 31.87 | 30.22 | 28.21 | 29.76 | 29.47 | 29.65 | |
| 30 | 32.13 | 30.44 | 28.29 | 29.96 | 29.68 | 29.83 | |
| 31 | 32.24 | 30.53 | 28.36 | 30.01 | 29.76 | 29.97 | |
| 33 | 32.55 | 30.76 | 28.57 | 30.25 | 29.93 | 30.13 | |
| 35 | 32.65 | 30.85 | 28.57 | 30.32 | 30.03 | 30.26 | |
| 37 | 32.96 | 31.08 | 28.77 | 30.55 | 30.21 | 30.50 | |
| 40 | 33.24 | 31.35 | 28.96 | 30.77 | 30.45 | 30.72 | |
| 42 | 33.57 | 31.62 | 29.14 | 31.00 | 30.66 | 30.94 | |

| Time sec. | A | B | F | C | D | E | Left Edge |
|---|---|---|---|---|---|---|---|
| 45 | 33.89 | 31.86 | 29.34 | 31.24 | 30.89 | 31.17 | |
| 48 | 34.21 | 32.15 | 29.47 | 31.46 | 31.10 | 31.42 | |
| 51 | 34.51 | 32.39 | 29.65 | 31.69 | 31.34 | 31.64 | |
| 53 | 34.79 | 32.62 | 29.91 | 31.88 | 31.52 | 31.84 | |
| 56 | 35.09 | 32.92 | 29.95 | 32.11 | 31.72 | 32.09 | |
| 59 | 35.39 | 33.16 | 30.22 | 32.33 | 31.98 | 32.31 | |
| 62 | 35.65 | 33.35 | 30.42 | 32.52 | 32.14 | 32.50 | |
| 64 | 35.94 | 33.62 | 30.57 | 32.79 | 32.37 | 32.74 | |
| 67 | 36.16 | 33.82 | 30.69 | 32.93 | 32.54 | 32.95 | |
| 70 | 36.45 | 34.05 | 30.86 | 33.18 | 32.73 | 33.15 | |
| 73 | 36.72 | 34.26 | 31.08 | 33.38 | 32.96 | 33.36 | |
| 76 | 36.99 | 34.50 | 31.35 | 33.57 | 33.18 | 33.59 | |
| 81 | 37.50 | 34.93 | 31.54 | 33.98 | 33.54 | 33.94 | |
| 87 | 37.97 | 35.39 | 31.84 | 34.33 | 33.91 | 34.36 | |
| 93 | 38.44 | 35.80 | 32.16 | 34.75 | 34.28 | 34.75 | |
| 98 | 38.85 | 36.15 | 32.69 | 35.04 | 34.64 | 35.09 | |
| 188 | 44.39 | 42.82 | 36.91 | 39.87 | 39.49 | 39.79 | |
| 217 | 45.69 | 44.17 | 38.51 | 41.22 | 40.85 | 41.20 | |
| 306 | 48.30 | 46.99 | 41.55 | 44.20 | 43.83 | 43.98 | |
| 320 | 48.65 | 47.40 | 42.20 | 44.63 | 44.29 | 44.43 | |
| 335 | 49.00 | 47.85 | 42.78 | 45.06 | 44.74 | 44.93 | |
| 352 | 49.29 | 48.26 | 43.31 | 45.48 | 45.19 | 45.33 | |
| 435 | 50.49 | 49.95 | 45.29 | 47.23 | 46.96 | 46.90 | |
| 454 | 50.65 | 50.25 | 45.94 | 47.58 | 47.35 | 47.29 | |
| 467 | 50.77 | 50.44 | 46.30 | 47.80 | 47.57 | 47.53 | |
| 546 | 51.59 | 50.71 | 46.83 | 48.84 | 48.44 | 48.39 | |
| 575 | 51.74 | 51.01 | 47.34 | 49.18 | 48.79 | 48.77 | |
| 765 | 52.65 | 51.55 | 48.97 | 50.32 | 49.80 | 49.97 | |
| 909 | 52.73 | 51.83 | 49.43 | 50.72 | 50.26 | 50.21 | |
| 933 | 52.84 | 51.97 | 49.83 | 50.84 | 50.38 | 50.45 | |
| 1350 | 53.02 | 52.58 | 50.92 | 51.16 | 50.98 | 50.93 | |
| 1373 | 52.98 | 52.59 | 51.13 | 51.16 | 50.98 | 51.02 | |

Figure A4.PT3a. Glass plate at 23 C inserted into drying air at 54 C.

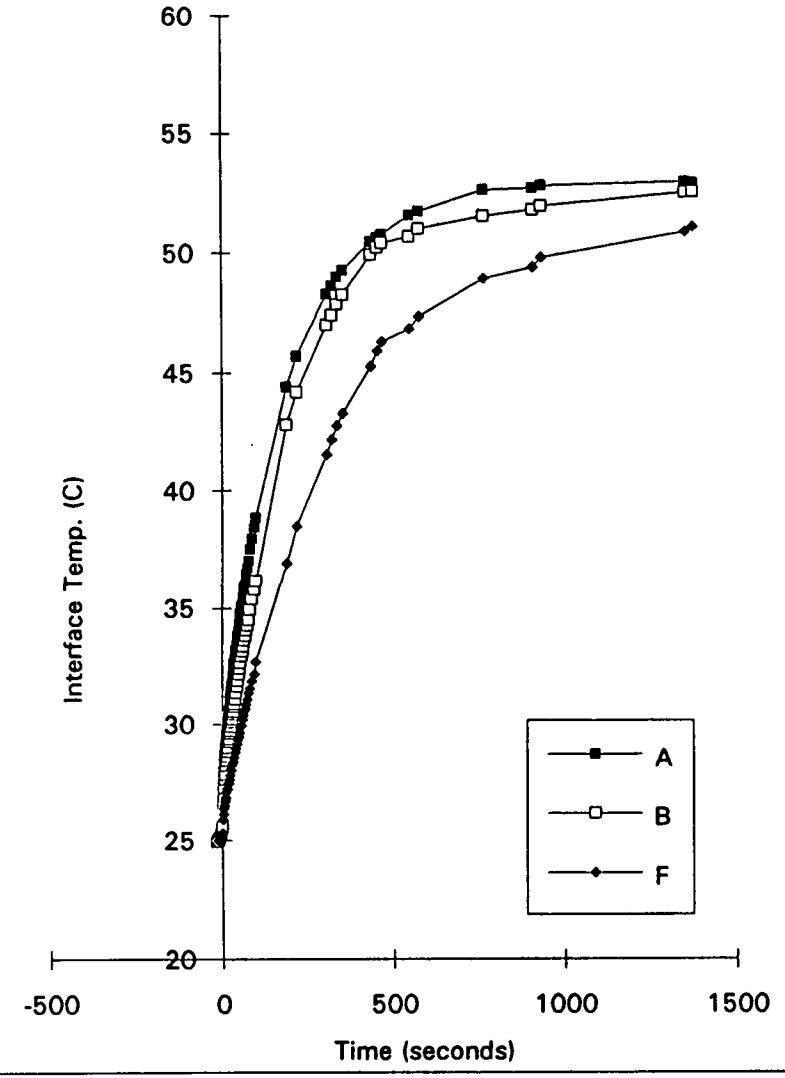


Figure A4.PT3b. Glass plate at 23 C inserted into drying air at 54 C.

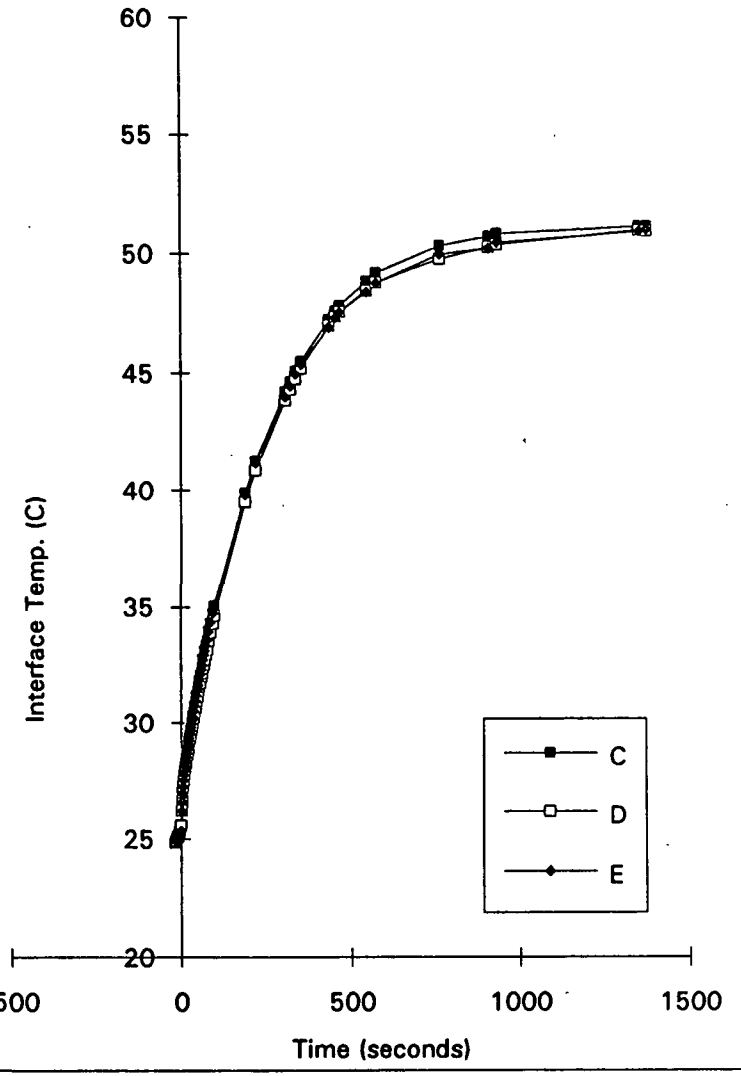

Table A4.PT4. Glass plate temperature inserted into drier at 54 C.

| PT4 Ref. Temp. Resistors Time-sec. | 23 A | 23 B | 23 F | 23 C | 23 D | 23 E | Left Edge |
|---|---|---|---|---|---|---|---|
| -15 | 22.77 | 21.73 | 23.63 | 23.81 | 23.84 | 23.79 | |
| -13 | 22.87 | 21.88 | 23.84 | 23.95 | 23.92 | 23.90 | |
| -11 | 22.93 | 21.91 | 23.89 | 23.93 | 23.94 | 23.95 | |
| -10 | 23.00 | 22.01 | 23.92 | 23.97 | 23.97 | 23.97 | |
| -8 | 23.00 | 21.99 | 24.06 | 24.03 | 23.99 | 24.00 | |
| -7 | 22.99 | 22.02 | 23.99 | 24.00 | 24.04 | 24.01 | |
| -5 | 23.10 | 22.08 | 24.20 | 24.11 | 24.08 | 24.08 | |
| -3 | 23.13 | 22.16 | 24.10 | 24.08 | 24.09 | 24.16 | |
| -2 | 23.20 | 22.22 | 24.39 | 24.19 | 24.23 | 24.27 | |
| 0 | 23.92 | 22.67 | 24.53 | 24.56 | 24.53 | 24.59 | |
| 2 | 24.97 | 23.37 | 24.99 | 25.25 | 25.19 | 25.36 | |
| 3 | 25.71 | 23.94 | 25.25 | 25.83 | 25.62 | 25.77 | |
| 5 | 26.09 | 24.23 | 25.40 | 26.07 | 25.89 | 26.14 | |
| 7 | 26.55 | 24.59 | 25.68 | 26.42 | 26.19 | 26.44 | |
| 8 | 26.92 | 24.83 | 25.71 | 26.68 | 26.41 | 26.67 | |
| 10 | 27.23 | 25.03 | 26.04 | 26.82 | 26.60 | 26.89 | |
| 12 | 27.56 | 25.37 | 26.06 | 27.13 | 26.82 | 27.11 | |
| 13 | 27.81 | 25.49 | 26.32 | 27.22 | 27.00 | 27.32 | |
| 15 | 28.07 | 25.75 | 26.38 | 27.45 | 27.19 | 27.51 | |
| 17 | 28.39 | 26.00 | 26.54 | 27.75 | 27.39 | 27.72 | |
| 19 | 28.56 | 26.15 | 26.64 | 27.80 | 27.49 | 27.88 | |
| 20 | 28.93 | 26.37 | 26.78 | 28.08 | 27.68 | 28.09 | |
| 22 | 29.02 | 26.51 | 26.88 | 28.12 | 27.81 | 28.25 | |
| 24 | 29.35 | 26.70 | 27.11 | 28.36 | 27.97 | 28.39 | |
| 25 | 29.50 | 26.89 | 27.09 | 28.49 | 28.10 | 28.57 | |
| 27 | 29.68 | 27.01 | 27.37 | 28.62 | 28.25 | 28.68 | |
| 29 | 29.90 | 27.21 | 27.31 | 28.80 | 28.39 | 28.81 | |
| 30 | 30.08 | 27.30 | 27.54 | 28.88 | 28.49 | 28.97 | |
| 32 | 30.34 | 27.53 | 27.62 | 29.12 | 28.66 | 29.11 | |
| 34 | 30.50 | 27.66 | 27.71 | 29.15 | 28.78 | 29.31 | |
| 35 | 30.79 | 27.84 | 27.86 | 29.44 | 28.93 | 29.43 | |
| 37 | 30.80 | 27.92 | 27.92 | 29.41 | 29.05 | 29.56 | |
| 39 | 31.11 | 28.15 | 28.10 | 29.62 | 29.22 | 29.76 | |
| 42 | 31.45 | 28.42 | 28.30 | 29.85 | 29.44 | 29.98 | |
| 45 | 31.74 | 28.66 | 28.47 | 30.10 | 29.67 | 30.24 | |

| Time sec. | A | B | F | C | D | E | Left Edge |
|---|---|---|---|---|---|---|---|
| 47 | 32.05 | 28.93 | 28.63 | 30.30 | 29.90 | 30.43 | |
| 50 | 32.31 | 29.18 | 28.81 | 30.52 | 30.08 | 30.67 | |
| 53 | 32.55 | 29.41 | 28.92 | 30.72 | 30.28 | 30.90 | |
| 56 | 32.90 | 29.65 | 29.18 | 30.94 | 30.48 | 31.10 | |
| 58 | 33.14 | 29.89 | 29.33 | 31.16 | 30.69 | 31.35 | |
| 63 | 33.55 | 30.22 | 29.53 | 31.50 | 30.97 | 31.65 | |
| 68 | 34.08 | 30.70 | 29.84 | 31.85 | 31.36 | 32.07 | |
| 74 | 34.54 | 31.01 | 30.38 | 32.23 | 31.75 | 32.45 | |
| 80 | 35.14 | 31.57 | 30.51 | 32.72 | 32.16 | 32.86 | |
| 85 | 35.59 | 32.01 | 30.87 | 33.07 | 32.51 | 33.27 | |
| 153 | 40.24 | 36.39 | 34.39 | 37.00 | 36.44 | 37.21 | |
| 175 | 41.43 | 37.59 | 35.65 | 38.13 | 37.57 | 38.40 | |
| 252 | 44.37 | 40.86 | 38.77 | 41.18 | 40.68 | 41.42 | |
| 275 | 45.07 | 41.72 | 39.74 | 42.00 | 41.51 | 42.27 | |
| 357 | 46.83 | 43.85 | 42.01 | 44.04 | 43.69 | 44.31 | |
| 380 | 47.23 | 44.41 | 42.74 | 44.60 | 44.29 | 44.94 | |
| 461 | 48.46 | 46.25 | 44.23 | 45.99 | 45.79 | 46.27 | |
| 484 | 48.58 | 46.61 | 44.85 | 46.37 | 46.20 | 46.64 | |
| 611 | 49.15 | 47.67 | 46.54 | 47.62 | 47.48 | 47.74 | |
| 634 | 49.27 | 47.93 | 46.95 | 47.88 | 47.72 | 47.99 | |
| 911 | 50.45 | 48.80 | 48.61 | 49.33 | 48.89 | 48.95 | |
| 934 | 50.48 | 48.87 | 48.94 | 49.38 | 48.97 | 49.11 | |
| 1212 | 50.38 | 49.29 | 49.46 | 49.41 | 49.22 | 49.45 | |
| 1234 | 50.45 | 49.42 | 49.58 | 49.49 | 49.33 | 49.58 | |
| 1392 | 50.30 | 50.09 | 49.36 | 49.41 | 49.35 | 49.37 | |
| 1415 | 50.27 | 50.12 | 49.61 | 49.43 | 49.35 | 49.43 | |

Figure A4.PT4a. Glass plate at 23 C inserted into drying air at 54 C.

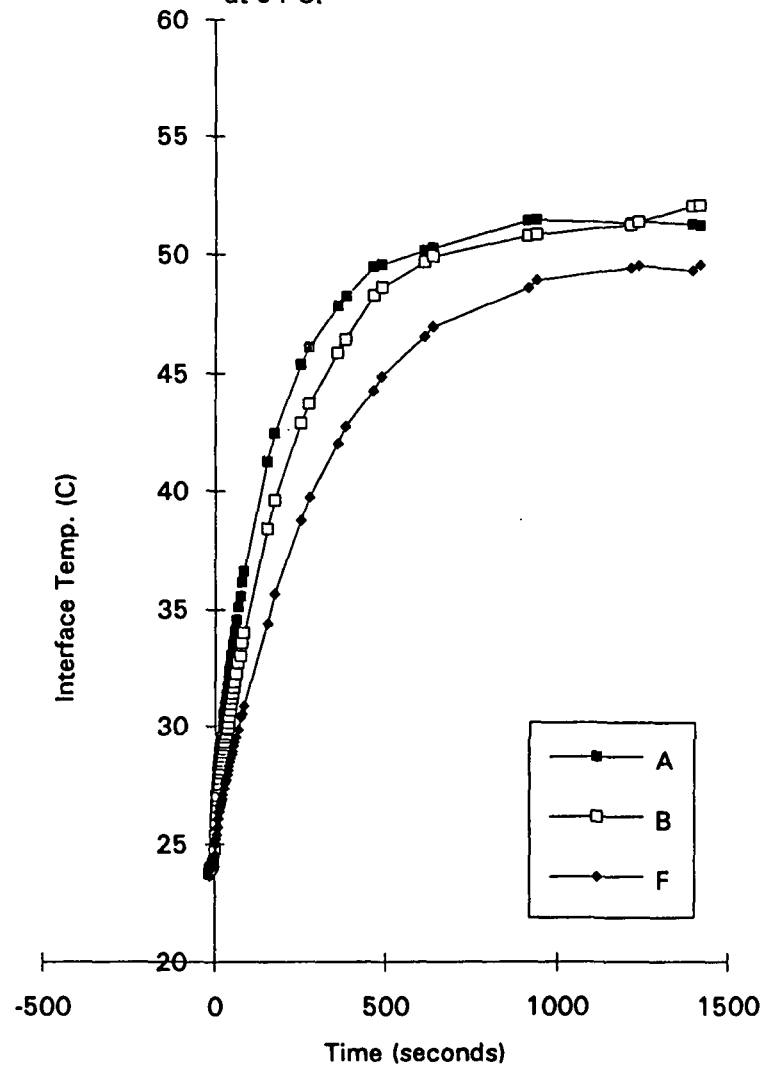


Figure A4.PT4b. Glass plate at 23 C inserted into drying air at 54 C.

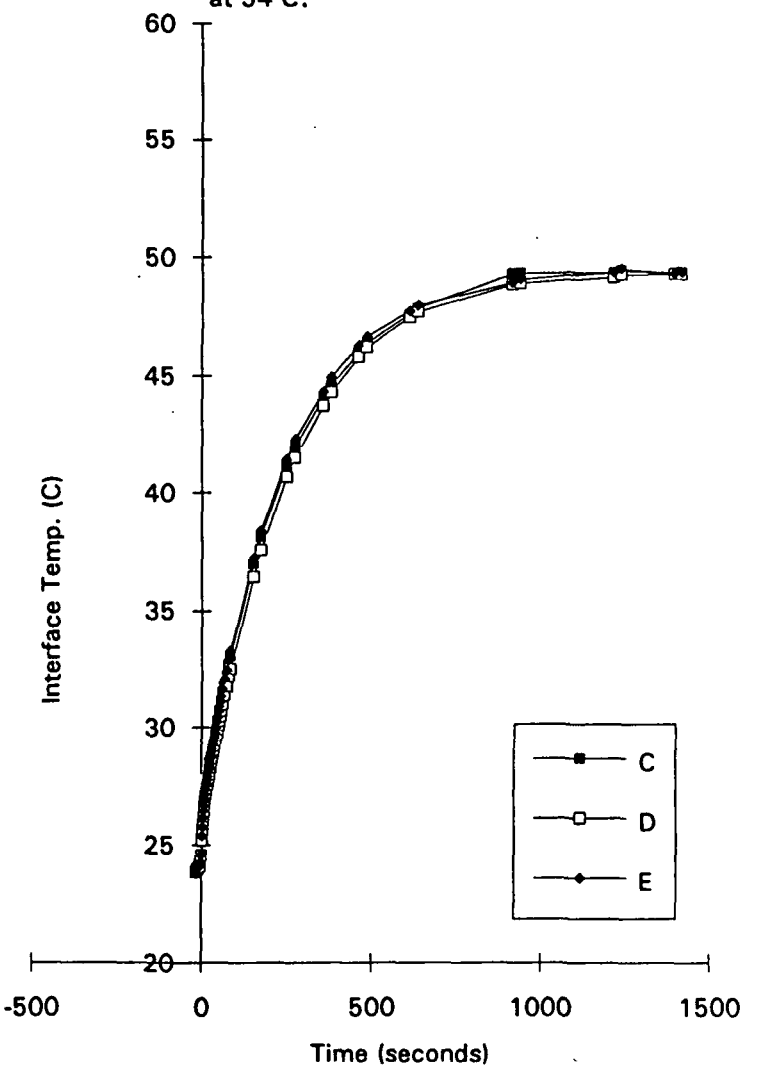

Table A4.PT5. Glass plate temperature at 58 C inserted into drier at 54 C.

| PT5 Ref. Temp. Resistors Time-sec. | 58 A | 58 B | 58 F | 58 C | 58 D | 58 E | Left Edge |
|---|---|---|---|---|---|---|---|
| -21 | 57.78 | 57.78 | 57.74 | 57.80 | 57.79 | 57.82 | |
| -19 | 57.80 | 57.81 | 57.83 | 57.83 | 57.79 | 57.85 | |
| -18 | 57.94 | 57.84 | 57.88 | 79.89 | 57.86 | 57.78 | |
| -16 | 57.82 | 57.67 | 59.22 | 68.67 | 57.45 | 57.27 | |
| -14 | 57.59 | 57.55 | 57.64 | 57.63 | 57.50 | 57.67 | |
| -13 | 57.31 | 57.32 | 57.40 | 56.90 | 57.28 | 57.42 | |
| -11 | 56.86 | 57.31 | 57.37 | | 57.28 | 2.40 | |
| -9 | 57.17 | 57.20 | 57.23 | | 57.08 | 56.90 | |
| -8 | 57.05 | 56.95 | 57.74 | | 57.01 | 2.16 | |
| -6 | 56.79 | 56.72 | 59.00 | | 56.56 | 89.22 | |
| -5 | 56.74 | 56.54 | 57.25 | | 56.78 | 34.73 | |
| -3 | 56.83 | 56.63 | 57.16 | | 56.81 | 56.50 | |
| -1 | 56.86 | 56.72 | 57.16 | | 56.88 | 56.66 | |
| 0 | 56.82 | 56.71 | 57.35 | | 57.05 | 56.78 | |
| 2 | 56.66 | 56.75 | 57.16 | | 56.69 | 56.84 | |
| 4 | 56.46 | 56.88 | 57.16 | | 56.57 | 56.72 | |
| 5 | 56.56 | 56.94 | 57.09 | | 56.71 | 56.62 | |
| 7 | 56.51 | 56.94 | 57.07 | | 56.81 | 56.63 | |
| 9 | 56.48 | 56.86 | 57.07 | | 56.71 | 56.65 | |
| 10 | 56.45 | 56.81 | 57.01 | | 56.76 | 56.58 | |
| 12 | 56.42 | 56.78 | 57.02 | | 56.67 | 56.62 | |
| 14 | 56.43 | 56.78 | 56.87 | | 56.64 | 56.52 | |
| 15 | 56.31 | 56.74 | 57.13 | | 56.73 | 56.60 | |
| 17 | 56.31 | 56.61 | 56.85 | | 56.57 | 56.43 | |
| 19 | 56.33 | 56.72 | 56.85 | | 56.67 | 56.63 | |
| 20 | 56.08 | 56.52 | 56.73 | | 56.51 | 56.44 | |
| 22 | 56.30 | 56.66 | 56.52 | | 56.59 | 56.39 | |
| 24 | 56.06 | 61.28 | 56.51 | | 55.86 | 55.00 | |
| 25 | 56.10 | 56.51 | 56.18 | | 56.44 | 56.23 | |
| 27 | 55.99 | 56.49 | 56.76 | | 56.61 | 56.65 | |
| 29 | 54.47 | 57.52 | 56.08 | | 56.27 | 1.62 | |
| 30 | 58.00 | 54.34 | 55.37 | | 56.27 | 89.22 | |
| 32 | 55.77 | 53.97 | 55.87 | | 55.81 | -2.80 | |
| 34 | 55.71 | 56.37 | 56.27 | | 56.29 | 89.22 | |
| 37 | 55.62 | 56.15 | 56.07 | | 56.37 | 89.22 | |

| Time sec. | A | B | F | C | D | E | Left Edge |
|---|---|---|---|---|---|---|---|
| 39 | 54.85 | 56.06 | 56.19 | | 56.15 | 89.22 | |
| 42 | 55.03 | 56.03 | 56.53 | | 56.21 | 55.17 | |
| 45 | 55.55 | 56.59 | 56.00 | | 56.07 | 23.12 | |
| 48 | 55.47 | 55.91 | 55.96 | | 56.07 | 55.75 | |
| 51 | 55.37 | 55.82 | 55.92 | | 56.05 | 55.80 | |
| 53 | 55.32 | 55.72 | 55.88 | | 55.97 | 55.72 | |
| 56 | 55.21 | 55.62 | 55.82 | | 55.93 | 55.69 | |
| 59 | 55.18 | 55.58 | 55.74 | | 55.83 | 55.57 | |
| 62 | 55.12 | 55.49 | 55.67 | | 55.80 | 55.56 | |
| 64 | 55.06 | 55.44 | 55.60 | | 55.68 | 55.47 | |
| 67 | 55.00 | 55.40 | 55.53 | | 55.65 | 55.43 | |
| 70 | 54.97 | 55.33 | 55.48 | | 55.59 | 55.39 | |
| 73 | 54.93 | 55.31 | 55.45 | | 55.54 | 55.39 | |
| 75 | 54.86 | 55.23 | 55.36 | | 55.48 | 55.33 | |
| 78 | 54.81 | 55.18 | 55.27 | | 55.43 | 55.25 | |
| 81 | 54.80 | 55.16 | 55.18 | | 55.35 | 55.13 | |
| 84 | 54.72 | 55.06 | 55.18 | | 55.34 | 55.14 | |
| 86 | 54.64 | 55.00 | 55.16 | | 55.37 | 55.18 | |
| 89 | 54.61 | 54.92 | 55.09 | | 55.30 | 55.11 | |
| 184 | 53.23 | 53.33 | 52.72 | | 53.78 | 53.43 | |
| 279 | 52.48 | 52.31 | 51.31 | | 52.75 | 52.35 | |
| 444 | 51.58 | 50.90 | 49.69 | | 51.23 | 51.07 | |
| 624 | 51.50 | 50.50 | 49.27 | | 50.67 | 50.43 | |
| 924 | 51.37 | 50.38 | 48.71 | | 50.51 | 50.10 | |
| 1216 | 51.07 | 50.10 | 48.12 | | 50.03 | 49.68 | |

Figure A4.PT5a. Glass plate at 58 C inserted into drying air at 54 C.

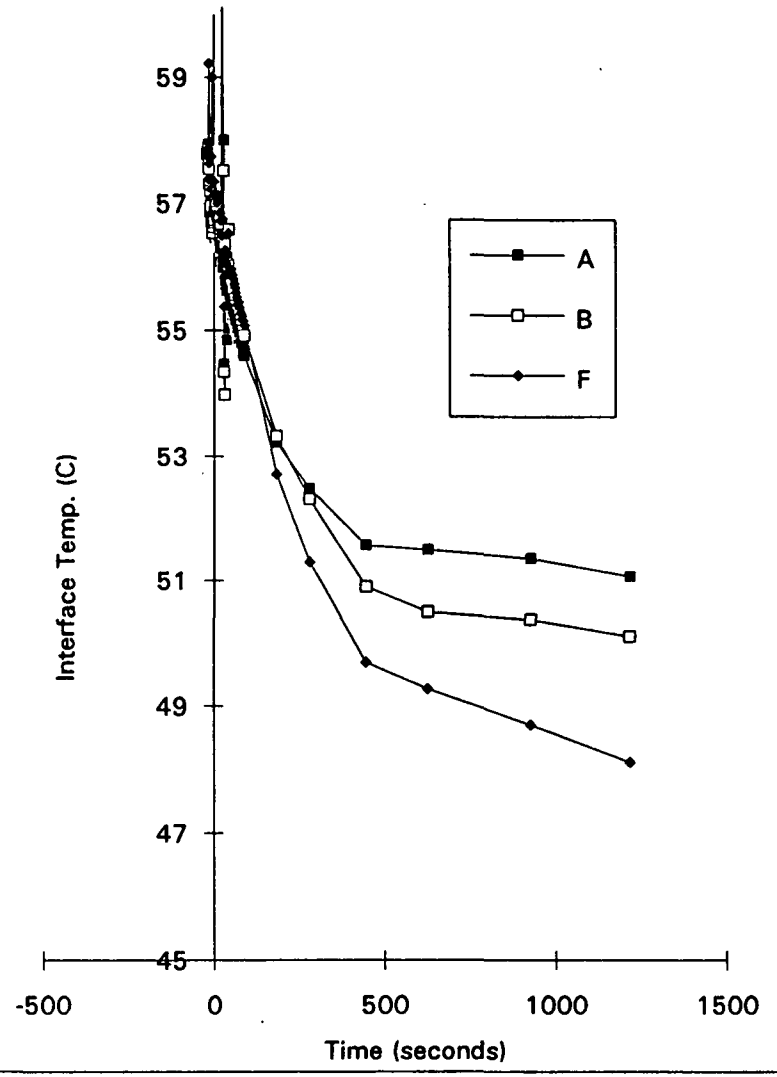


Figure A4.PT5b. Glass plate at 58 C inserted into drying air at 54 C.

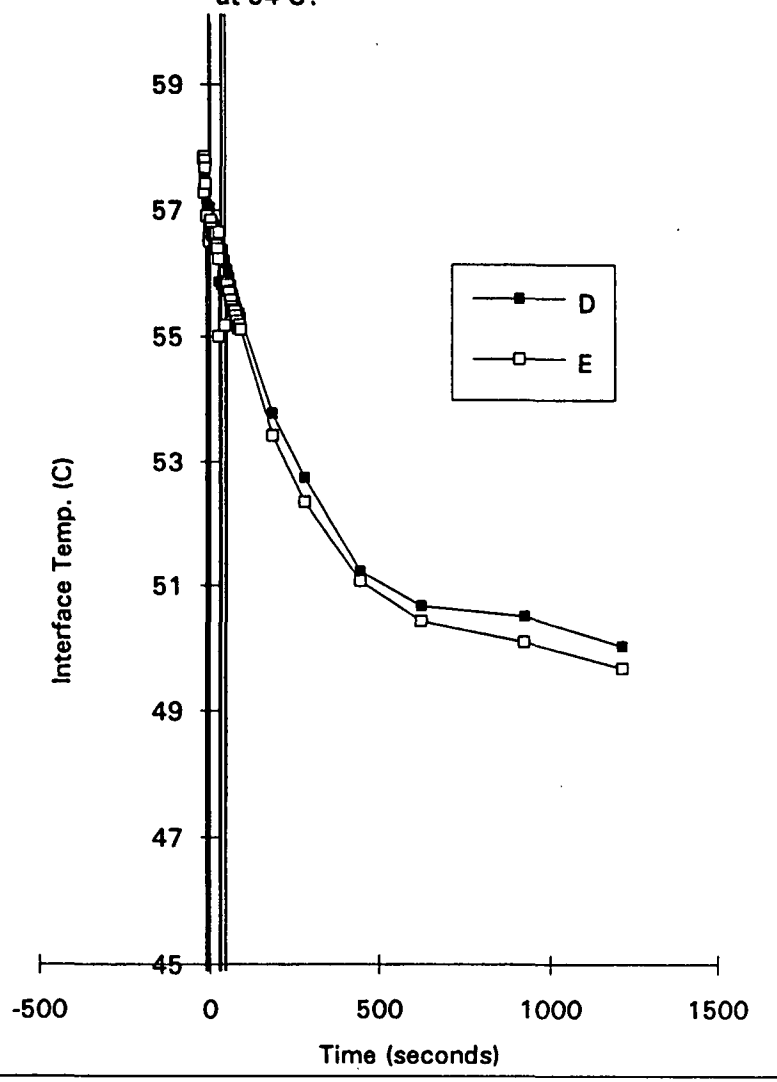

Table A4.PT6. Glass plate temperature at 58 C inserted into drier at 54 C.

| PT6 Ref. Temp. Resistors Time-sec. | 23 A | 23 B | 23 F | 23 C | 23 D | 23 E | Left Edge |
|---|---|---|---|---|---|---|---|
| -21 | 58.05 | 58.06 | 58.14 | 58.08 | 58.10 | 58.09 | |
| -20 | 58.07 | 58.05 | 58.02 | 58.08 | 58.06 | 58.06 | |
| -18 | 67.43 | 58.02 | 57.97 | 57.98 | 57.98 | 57.95 | |
| -16 | 57.82 | 57.79 | 57.79 | 57.77 | 57.79 | 57.83 | |
| -15 | 57.71 | 57.73 | 57.74 | 57.71 | 57.71 | 57.77 | |
| -13 | 57.59 | 57.60 | 57.67 | 57.58 | 57.59 | 57.69 | |
| -11 | 57.50 | 57.53 | 57.59 | 57.52 | 57.52 | 57.56 | |
| -10 | 57.82 | 59.55 | 57.50 | 55.01 | 57.37 | 57.59 | |
| -8 | 66.01 | 57.23 | 57.71 | 57.69 | 57.23 | 2.16 | |
| -6 | 57.27 | 57.05 | 57.62 | 57.58 | 57.00 | 57.34 | |
| -5 | 57.18 | 57.10 | 57.71 | 57.48 | 57.11 | 57.21 | |
| -3 | 57.19 | 57.13 | 57.76 | 57.47 | 57.15 | 57.21 | |
| -2 | 57.27 | 57.16 | 57.78 | 57.36 | 57.06 | 57.31 | |
| 2 | 57.07 | 56.99 | 57.79 | 57.36 | 57.15 | 57.21 | |
| 3 | 57.08 | 57.02 | 57.78 | 57.28 | 57.08 | 57.21 | |
| 5 | 56.99 | 56.99 | 57.83 | 57.47 | 57.23 | 57.18 | |
| 7 | 56.99 | 56.93 | 57.69 | 57.12 | 56.94 | 57.13 | |
| 8 | 57.01 | 56.96 | 57.69 | 57.26 | 57.16 | 57.15 | |
| 10 | 56.82 | 56.83 | 57.69 | 57.20 | 57.01 | 57.02 | |
| 12 | 56.87 | 56.82 | 57.54 | 56.94 | 56.91 | 57.00 | |
| 13 | 56.76 | 56.76 | 57.66 | 57.21 | 57.06 | 56.95 | |
| 15 | 56.67 | 56.63 | 57.50 | 56.96 | 56.83 | 56.89 | |
| 17 | 56.72 | 56.67 | 57.47 | 56.92 | 56.83 | 56.92 | |
| 18 | 56.59 | 56.60 | 57.57 | 57.12 | 56.98 | 56.88 | |
| 20 | 56.59 | 56.56 | 57.35 | 56.71 | 56.66 | 56.81 | |
| 22 | 56.56 | 56.54 | 57.40 | 56.94 | 56.89 | 56.81 | |
| 23 | 56.53 | 56.47 | 57.24 | 56.62 | 56.61 | 56.70 | |
| 25 | 56.38 | 56.39 | 57.21 | 56.60 | 56.56 | 56.72 | |
| 27 | 56.39 | 56.39 | 57.29 | 56.91 | 56.84 | 56.65 | |
| 28 | 56.32 | 56.27 | 57.11 | 56.49 | 56.44 | 56.56 | |
| 30 | 56.32 | 56.33 | 57.11 | 56.65 | 56.57 | 56.54 | |
| 32 | 56.18 | 56.20 | 57.07 | 56.59 | 56.52 | 56.46 | |
| 34 | 56.16 | 56.14 | 56.99 | 56.46 | 56.42 | 56.40 | |
| 37 | 56.08 | 56.07 | 56.96 | 56.50 | 56.39 | 56.35 | |
| 39 | 56.02 | 56.00 | 56.87 | 56.42 | 56.35 | 56.27 | |

| Time sec. | A | B | F | C | D | E | Left Edge |
|---|---|---|---|---|---|---|---|
| 42 | 55.93 | 55.91 | 56.80 | 56.36 | 56.26 | 56.17 | |
| 45 | 55.87 | 55.82 | 56.73 | 56.29 | 56.17 | 56.09 | |
| 48 | 55.81 | 55.81 | 56.63 | 56.11 | 56.06 | 56.08 | |
| 50 | 55.79 | 55.77 | 56.60 | 56.15 | 56.10 | 56.04 | |
| 53 | 55.67 | 55.67 | 56.57 | 56.18 | 56.11 | 55.98 | |
| 56 | 55.60 | 55.60 | 56.46 | 56.00 | 55.92 | 55.90 | |
| 59 | 55.53 | 55.54 | 56.43 | 56.03 | 55.95 | 55.86 | |
| 62 | 55.46 | 55.48 | 56.41 | 55.94 | 55.93 | 55.80 | |
| 67 | 55.45 | 55.43 | 56.37 | 55.93 | 55.90 | 55.72 | |
| 73 | 55.23 | 55.26 | 56.22 | 55.93 | 55.86 | 55.55 | |
| 79 | 54.97 | 54.99 | 55.99 | 55.70 | 55.50 | 55.37 | |
| 84 | 54.77 | 54.80 | 55.74 | 55.31 | 55.18 | 55.19 | |
| 89 | 54.67 | 54.67 | 55.64 | 55.22 | 55.08 | 55.10 | |
| 166 | 52.87 | 53.30 | 52.99 | 54.00 | 53.68 | 53.25 | |
| 240 | 52.13 | 53.03 | 51.68 | 52.66 | 52.54 | 52.11 | |
| 315 | 51.55 | 52.21 | 50.42 | 51.98 | 51.85 | 51.26 | |
| 405 | 51.01 | 51.74 | 49.38 | 50.82 | 51.03 | 50.48 | |
| 495 | 51.02 | 51.63 | 48.44 | 50.13 | 50.67 | 50.06 | |
| 615 | 50.90 | 51.50 | 48.01 | 49.80 | 50.28 | 49.77 | |
| 915 | 50.77 | 51.03 | 47.60 | 49.92 | 49.79 | 49.16 | |
| 1215 | 50.75 | 50.55 | 48.18 | 49.96 | 49.93 | 49.27 | |

Figure A4.PT6a. Glass plate at 58 C inserted into drying air at 54 C.

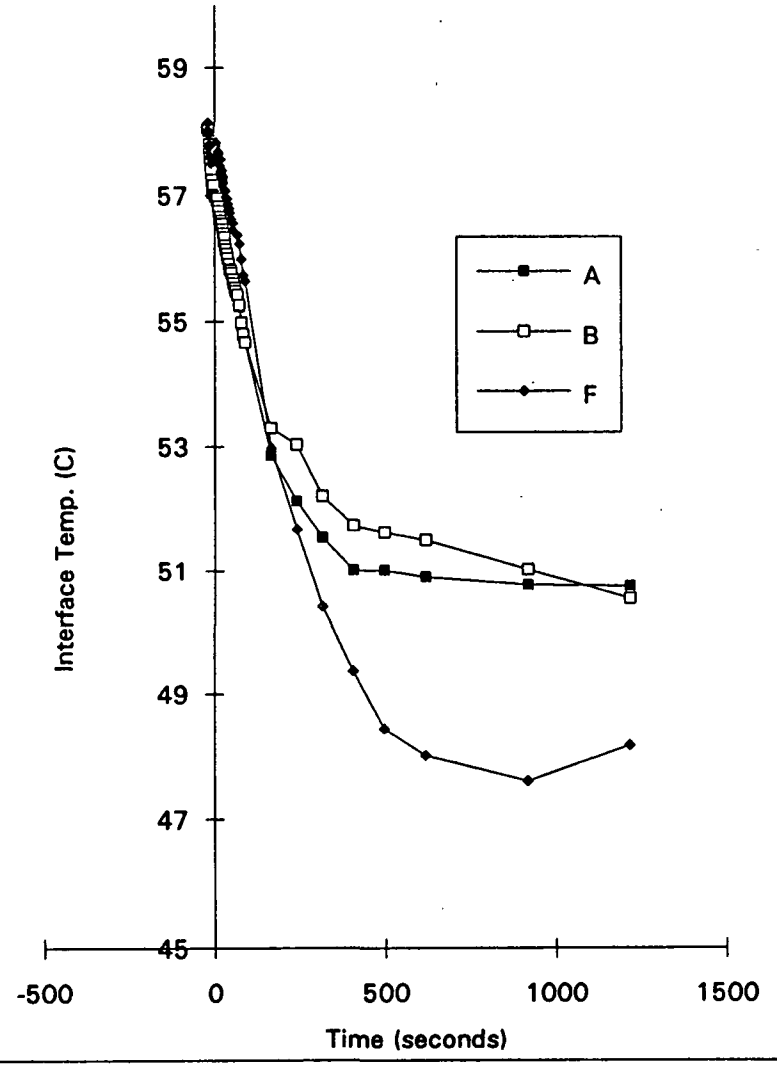


Figure A4.PT6b. Glass plate at 58 C inserted into drying air at 54 C.

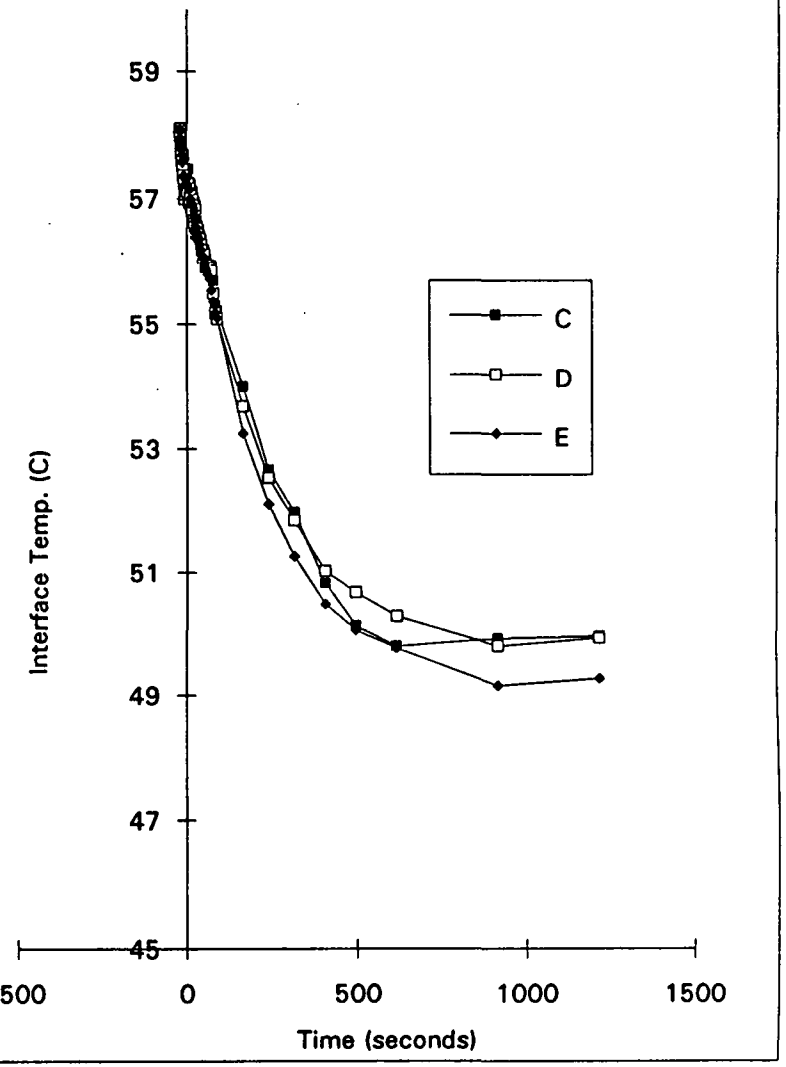

Table A4.PT7. Glass plate temperature during coating and Drying at 53 C and 15%RH.

| PT7 Ref. Temp. Resistors Time-sec. | 57 A | 57 B | 57 F | 57 C | 57 D | 57 E | Left Edge |
|---|---|---|---|---|---|---|---|
| -51 | 56.98 | 57.00 | 55.48 | 57.07 | 57.13 | 56.99 | |
| -48 | 57.04 | 57.06 | 56.89 | 57.04 | 56.87 | 57.04 | |
| -45 | 56.93 | 56.86 | 59.00 | 56.78 | 49.48 | 56.92 | |
| -41 | 56.75 | 56.66 | 57.70 | 56.63 | 54.69 | 56.73 | |
| -38 | 56.60 | 56.01 | 54.79 | 56.31 | 55.11 | 56.62 | |
| -35 | 56.36 | 56.29 | 54.86 | 56.11 | 56.3 | 56.3 | |
| -31 | 56.13 | 56.12 | 54.53 | 55.83 | 56.18 | 56.2 | |
| -28 | 55.98 | 55.89 | 54.39 | 55.64 | 56.04 | 55.93 | |
| -24 | 55.76 | 55.61 | 54.26 | 55.38 | 55.79 | 55.68 | |
| -21 | 55.45 | 55.40 | 53.98 | 55.14 | 55.62 | 55.49 | |
| -18 | 47.95 | 52.17 | 30.44 | 28.97 | 35.4 | 29.69 | |
| -14 | 48.21 | 52.11 | 36.90 | 12.89 | 17.74 | -2.96 | |
| -11 | 47.87 | 51.80 | 40.89 | 19.09 | 27.94 | -1.97 | |
| -8 | 47.46 | 51.39 | 42.52 | 24.36 | 19.77 | 2.004 | |
| -4 | 47.47 | 51.05 | 43.00 | 26.46 | 23.41 | 8.048 | |
| -1 | 47.67 | 51.16 | 43.54 | 27.13 | 28.72 | 9.983 | |
| 2 | 47.53 | 51.17 | 43.85 | 31.37 | 31.16 | 13.53 | |
| 6 | 47.64 | 51.28 | 44.43 | 35.17 | 32.02 | 17.43 | |
| 9 | 47.72 | 51.34 | 44.62 | 36.7 | 32.32 | 19.14 | |
| 13 | 47.70 | 51.34 | 45.10 | 38.38 | 32.53 | 19.51 | |
| 16 | 47.64 | 51.28 | 45.64 | 39.57 | 32.63 | 20.61 | |
| 19 | 47.52 | 51.16 | 46.15 | 40.33 | 32.44 | 22.29 | |
| 23 | 47.24 | 50.91 | 45.96 | 40.01 | 32.34 | 24.37 | |
| 26 | 47.12 | 50.77 | 45.79 | 40.1 | 32.27 | 26.1 | |
| 29 | 47.12 | 50.77 | 45.89 | 40.84 | 32.22 | 27.11 | |
| 33 | 47.05 | 50.69 | 46.00 | 41.27 | 32.22 | 27.86 | |
| 36 | 47.07 | 50.68 | 45.55 | 41.47 | 32.21 | 28.21 | |
| 40 | 47.04 | 50.65 | 45.48 | 41.76 | 32.22 | 28.48 | |

| Time sec. | A | B | F | C | D | E | Left Edge |
|---|---|---|---|---|---|---|---|
| 43 | 47.02 | 50.59 | 45.72 | 42.28 | 32.24 | 28.74 | |
| 46 | 46.89 | 50.48 | 45.88 | 42.59 | 32.17 | 29.12 | |
| 50 | 46.68 | 50.26 | 45.58 | 41.72 | 32.41 | 29.04 | |
| 54 | 46.64 | 50.18 | 45.52 | 41.95 | 34.03 | 29.37 | |
| 60 | 46.60 | 50.12 | 44.91 | 42 | 34.96 | 29.45 | |
| 65 | 46.60 | 50.07 | 44.83 | 42.46 | 35.61 | 29.66 | |
| 70 | 46.48 | 49.99 | 44.98 | 42.6 | 35.78 | 29.84 | |
| 73 | 46.40 | 49.94 | 44.96 | 42.85 | 35.97 | 29.93 | |
| 79 | 46.21 | 49.73 | 44.75 | 42.31 | 36.13 | 30 | |
| 84 | 46.24 | 49.74 | 44.32 | 42.54 | 36.45 | 29.85 | |
| 107 | 45.98 | 49.56 | 42.40 | 36.21 | 33.76 | 25.99 | |
| 145 | 45.52 | 49.41 | 42.38 | 38.59 | 34.87 | 27.55 | |
| 231 | 44.98 | 48.81 | 40.49 | 41.49 | 36.14 | 30.08 | |
| 334 | 44.53 | 50.48 | 38.36 | 43.54 | 36.47 | 29.86 | |
| 416 | 44.71 | 49.50 | 37.47 | 45.53 | 36.9 | 30.31 | |
| 616 | 43.88 | 51.44 | 37.11 | 46.3 | 38.51 | 30.51 | |

Figure A4.PT7a. Glass coated with clay coating and dried in an air stream at 53 C and low RH.

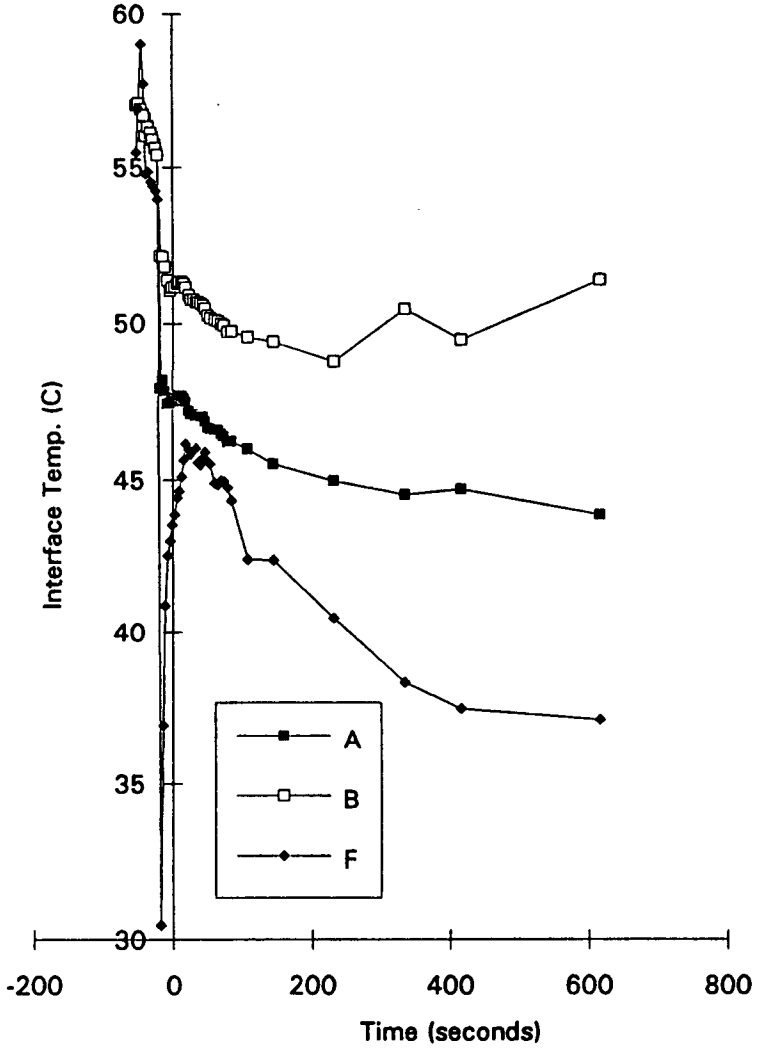


Figure A4.PT7b. Glass coated with clay coating and dried in an air stream at 53 C and low RH.

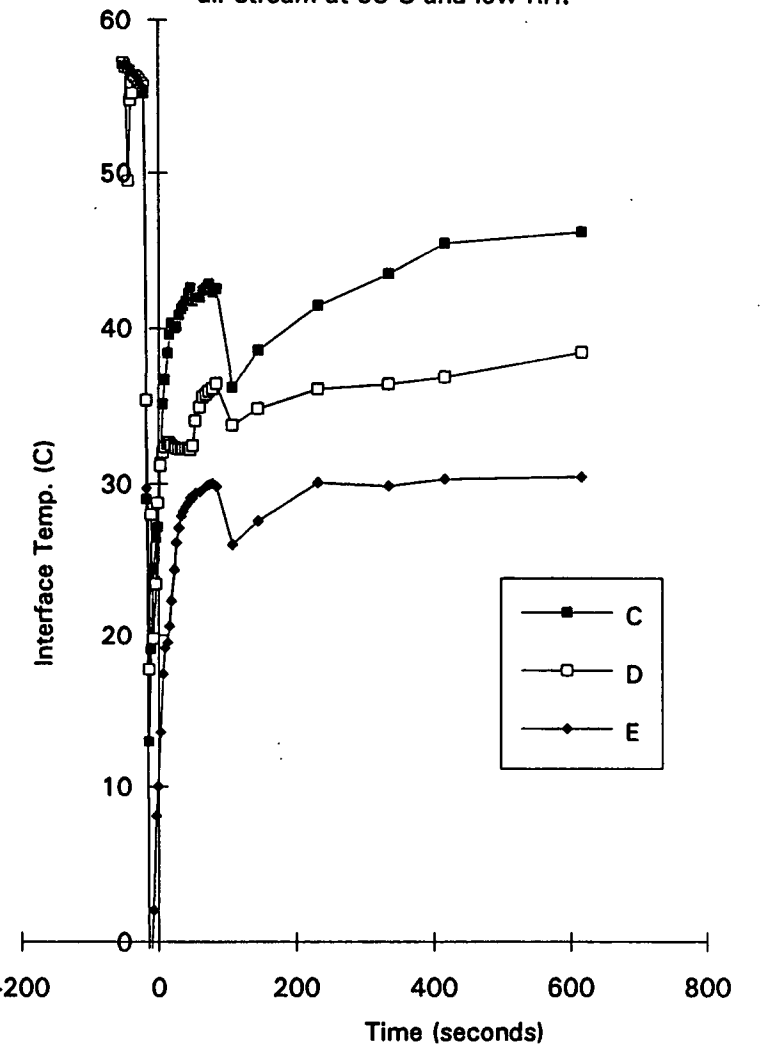

Table A4.PT8. Glass plate temperature during coating and Drying at 53 C and 15%RH.

| PT8 Ref. Temp. Resistors Time-sec. | 57 A | 57 B | 57 F | 57 C | 57 D | 57 E | Left Edge |
|---|---|---|---|---|---|---|---|
| -58 | 57.99 | 58.10 | 58.15 | 57.94 | 57.98 | 57.98 | 52.07 |
| -53 | 57.85 | 57.87 | 57.91 | 57.70 | 57.71 | 57.77 | 51.95 |
| -49 | 57.80 | 57.62 | 57.67 | 57.48 | 57.49 | 57.55 | 52.10 |
| -44 | 57.25 | 57.30 | 56.45 | 57.27 | 57.91 | 57.29 | 52.07 |
| -39 | 56.91 | 56.91 | 57.07 | 56.95 | 56.83 | 56.92 | 52.10 |
| -35 | 56.55 | 56.65 | 56.86 | 56.68 | 56.56 | 56.65 | 52.10 |
| -30 | 56.37 | 56.37 | 56.50 | 56.48 | 56.28 | 56.46 | 52.38 |
| -29 | 56.28 | 56.28 | 56.55 | 56.44 | 56.23 | 56.36 | 52.38 |
| -27 | 56.09 | 56.14 | 56.34 | 56.29 | 56.08 | 56.07 | 52.48 |
| -26 | 55.95 | 56.05 | 56.24 | 56.00 | 55.93 | 55.98 | 51.92 |
| -24 | 55.91 | 55.91 | 56.29 | 56.00 | 55.78 | 56.03 | 52.85 |
| -23 | 55.72 | 55.86 | 56.14 | 56.00 | 55.78 | 55.88 | 52.38 |
| -21 | 55.63 | 55.73 | 56.03 | 55.86 | 55.68 | 55.98 | 52.38 |
| -19 | 55.44 | 55.54 | 56.03 | 55.86 | 55.62 | 55.79 | 52.38 |
| -18 | 52.39 | 51.15 | 55.88 | 55.76 | 55.52 | 55.74 | 52.38 |
| -16 | 52.21 | 52.58 | 55.41 | 18.93 | 49.84 | 55.21 | 51.92 |
| -15 | 51.88 | 52.53 | 54.90 | 21.16 | 50.14 | 54.68 | 51.92 |
| -13 | 51.65 | 52.16 | 54.69 | 21.81 | 49.79 | 54.35 | 52.38 |
| -12 | 51.37 | 52.16 | 54.33 | 24.94 | 49.48 | 54.20 | 52.48 |
| -10 | 51.14 | 51.89 | 54.02 | 26.10 | 49.33 | 53.82 | 52.38 |
| -9 | 50.68 | 51.47 | 53.56 | 27.11 | 49.13 | 53.29 | 51.92 |
| -7 | 50.73 | 51.19 | 53.35 | 27.83 | 48.72 | 53.25 | 52.38 |
| -6 | 50.77 | 51.19 | 53.25 | 28.17 | 48.72 | 52.96 | 52.38 |
| -4 | 50.63 | 51.29 | 53.35 | 28.46 | 48.52 | 53.39 | 52.38 |
| -3 | 51.00 | 51.52 | 53.45 | 28.89 | 48.47 | 53.53 | 51.92 |
| -1 | 51.00 | 51.56 | 53.56 | 29.42 | 48.52 | 53.68 | 51.92 |
| 0 | 51.10 | 51.66 | 53.56 | 29.71 | 48.52 | 53.68 | 51.92 |
| 2 | 50.82 | 51.24 | 53.40 | 31.30 | 49.03 | 53.34 | 53.77 |
| 4 | 50.73 | 50.96 | 52.99 | 34.24 | 49.48 | 52.67 | 50.99 |
| 5 | 50.54 | 50.78 | 52.58 | 35.39 | 49.58 | 52.29 | 50.62 |
| 7 | 50.54 | 50.59 | 52.32 | 36.07 | 49.48 | 51.90 | 51.09 |
| 8 | 50.45 | 50.45 | 52.11 | 36.45 | 49.38 | 51.81 | 50.53 |
| 10 | 50.26 | 50.22 | 51.70 | 36.84 | 49.23 | 51.47 | 50.06 |
| 11 | 50.17 | 50.08 | 51.70 | 37.08 | 49.13 | 51.23 | 50.06 |
| 13 | 50.22 | 50.04 | 51.60 | 36.93 | 49.13 | 51.23 | 49.23 |

| Time sec. | A | B | F | C | D | E | Left Edge |
|---|---|---|---|---|---|---|---|
| 14 | 50.22 | 49.90 | 51.44 | 36.84 | 48.98 | 50.94 | 49.13 |
| 16 | 50.17 | 49.71 | 51.34 | 36.84 | 48.77 | 50.89 | 48.77 |
| 17 | 50.13 | 49.48 | 51.39 | 37.17 | 48.67 | 50.65 | 48.67 |
| 19 | 50.03 | 49.34 | 51.44 | 37.42 | 48.57 | 50.70 | 48.67 |
| 20 | 50.08 | 49.25 | 51.49 | 37.70 | 48.57 | 50.51 | 48.67 |
| 22 | 50.26 | 49.30 | 51.39 | 37.90 | 48.42 | 50.51 | 48.30 |
| 23 | 50.26 | 49.11 | 51.39 | 38.33 | 48.26 | 50.51 | 48.77 |
| 25 | 50.26 | 49.02 | 51.39 | 38.91 | 48.16 | 50.51 | 48.67 |
| 27 | 50.17 | 48.88 | 51.39 | 39.49 | 48.01 | 50.37 | 47.74 |
| 28 | 50.26 | 48.84 | 51.54 | 40.16 | 48.06 | 50.61 | 48.21 |
| 30 | 50.26 | 48.79 | 51.49 | 40.55 | 47.96 | 50.61 | 48.67 |
| 31 | 50.22 | 48.70 | 51.49 | 41.17 | 47.91 | 50.61 | 48.30 |
| 33 | 50.31 | 48.65 | 51.49 | 41.46 | 47.81 | 50.61 | 48.21 |
| 34 | 50.17 | 48.51 | 51.39 | 42.04 | 47.66 | 50.61 | 48.21 |
| 36 | 50.17 | 48.51 | 51.44 | 42.37 | 47.66 | 50.61 | 48.30 |
| 37 | 50.22 | 48.47 | 51.34 | 42.66 | 47.55 | 50.56 | 48.21 |
| 39 | 50.17 | 48.42 | 51.34 | 42.95 | 47.55 | 50.70 | 48.30 |
| 40 | 50.31 | 48.42 | 51.34 | 42.95 | 47.50 | 50.65 | 48.21 |
| 43 | 50.28 | 48.31 | 51.30 | 43.18 | 47.39 | 50.64 | 48.36 |
| 48 | 50.33 | 48.27 | 51.32 | 43.21 | 47.37 | 50.73 | 48.70 |
| 53 | 50.33 | 48.17 | 51.34 | 43.23 | 47.33 | 50.78 | 48.52 |
| 57 | 50.45 | 48.16 | 51.23 | 43.07 | 47.28 | 50.77 | 48.36 |
| 62 | 50.40 | 48.08 | 51.25 | 43.15 | 47.22 | 50.81 | 48.70 |
| 67 | 50.57 | 48.10 | 51.18 | 42.97 | 47.22 | 50.80 | 49.20 |
| 72 | 50.57 | 48.08 | 51.13 | 43.07 | 47.18 | 50.86 | 48.86 |
| 78 | 50.62 | 48.05 | 51.04 | 43.07 | 47.15 | 50.77 | 48.86 |
| 81 | 50.60 | 48.00 | 51.06 | 43.21 | 47.17 | 50.83 | 49.05 |
| 85 | 50.62 | 48.03 | 50.99 | 43.31 | 47.17 | 50.73 | 48.67 |
| 115 | 51.07 | 48.29 | 50.65 | 44.00 | 47.48 | 50.72 | 49.10 |
| 166 | 51.76 | 48.67 | 50.05 | 45.28 | 48.03 | 50.70 | 49.41 |
| 275 | 52.35 | 50.19 | 49.60 | 46.91 | 48.91 | 50.79 | 49.85 |
| 436 | 52.72 | 51.23 | 49.37 | 48.26 | 49.82 | 50.74 | 49.99 |
| 646 | 52.84 | 51.70 | 49.64 | 48.88 | 50.26 | 50.85 | 50.19 |

Figure A4.PT8a. Glass plate coated with clay coating and dried in an air stream at 53 (C) and low RH.

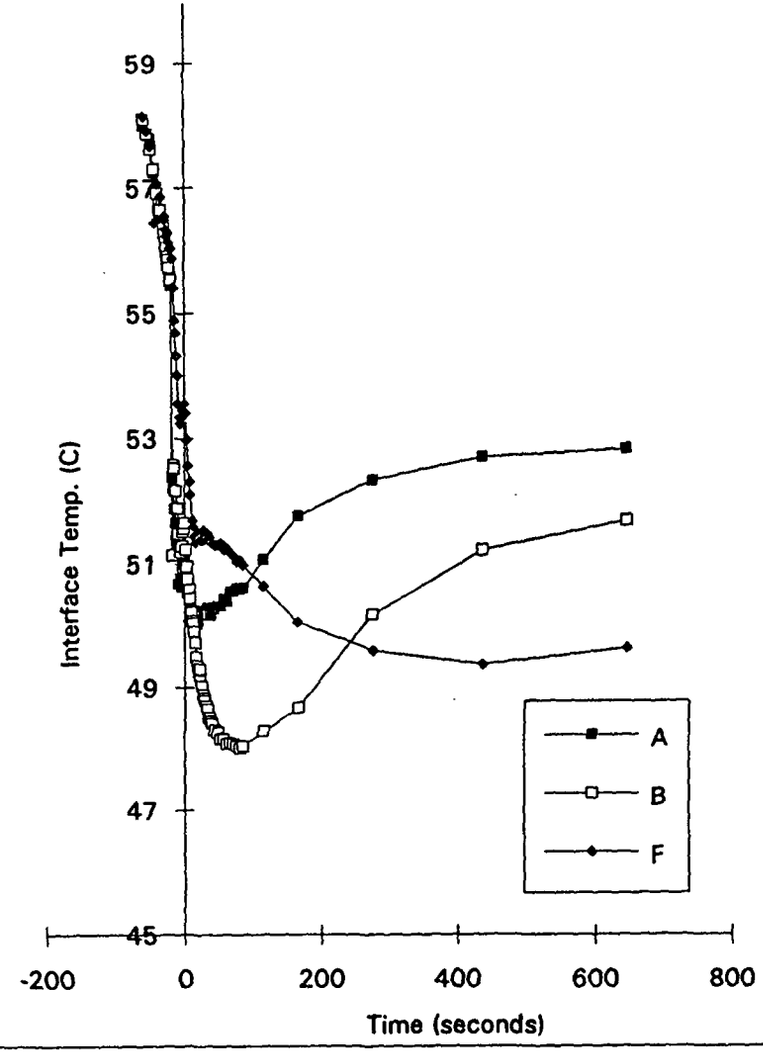


Figure A4.PT8b. Glass plate coated with clay coating and dried in an air stream at 53 (C) and low RH.

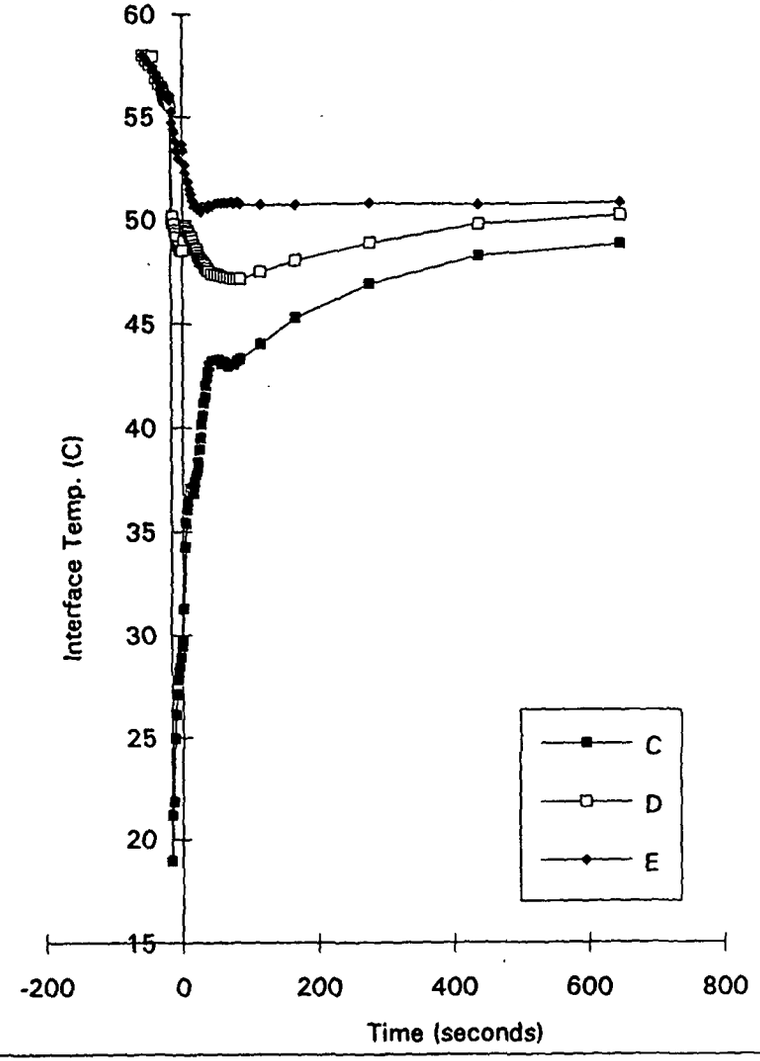

Table A4.PT9. Glass plate temperature at 23 C inserted into drier at 32 C.

| PT9 Ref. Temp. Resistors Time-sec. | 23 A | 23 B | 23 F | 23 C | 23 D | 23 E | Left Edge |
|---|---|---|---|---|---|---|---|
| -13 | 22.97 | 22.90 | 22.88 | 22.95 | 22.92 | 22.92 | |
| -11 | 23.03 | 22.96 | 22.99 | 22.96 | 23.02 | 22.99 | |
| -9 | 22.98 | 23.01 | 23.00 | 23.01 | 23.00 | 23.00 | |
| -7 | 22.97 | 23.06 | 23.07 | 23.04 | 23.08 | 23.03 | |
| -6 | 23.03 | 23.09 | 23.12 | 23.04 | 23.02 | 23.10 | |
| -4 | 23.01 | 23.20 | 23.11 | 23.09 | 23.08 | 23.11 | |
| -2 | 23.03 | 23.12 | 23.28 | 23.04 | 23.12 | 23.18 | |
| -1 | 23.01 | 23.01 | 23.02 | 23.32 | 23.10 | 22.99 | |
| 1 | 23.41 | 23.64 | 23.43 | 22.77 | 23.32 | 23.48 | |
| 2 | 23.44 | 23.20 | 23.71 | 24.01 | 23.47 | 23.64 | |
| 4 | 24.01 | 24.01 | 23.30 | 23.20 | 23.52 | 23.59 | |
| 6 | 23.75 | 23.50 | 24.07 | 23.97 | 23.69 | 24.01 | |
| 7 | 24.18 | 23.95 | 23.42 | 23.83 | 23.71 | 23.71 | |
| 9 | 24.23 | 24.09 | 24.05 | 23.72 | 23.86 | 24.14 | |
| 11 | 24.16 | 23.72 | 23.81 | 24.42 | 23.91 | 24.01 | |
| 12 | 24.53 | 24.44 | 23.93 | 23.65 | 23.98 | 24.20 | |
| 14 | 24.43 | 24.10 | 24.14 | 24.18 | 24.03 | 24.27 | |
| 16 | 24.83 | 24.44 | 23.47 | 23.99 | 24.00 | 24.03 | |
| 17 | 24.66 | 24.45 | 24.57 | 24.02 | 24.24 | 24.63 | |
| 19 | 24.76 | 24.38 | 23.71 | 24.49 | 24.08 | 24.09 | |
| 21 | 24.93 | 24.75 | 24.21 | 23.81 | 24.25 | 24.60 | |
| 22 | 24.73 | 24.22 | 24.17 | 24.83 | 24.27 | 24.44 | |
| 24 | 25.15 | 24.78 | 23.76 | 24.26 | 24.27 | 24.35 | |
| 26 | 24.73 | 24.29 | 24.74 | 24.78 | 24.44 | 24.78 | |
| 27 | 25.12 | 24.75 | 24.36 | 24.57 | 24.40 | 24.62 | |
| 29 | 25.41 | 25.16 | 24.19 | 24.02 | 24.46 | 24.73 | |
| 31 | 25.10 | 24.53 | 24.40 | 25.02 | 24.47 | 24.67 | |
| 32 | 25.35 | 24.88 | 24.09 | 24.54 | 24.52 | 24.65 | |
| 34 | 25.19 | 24.73 | 25.02 | 24.92 | 24.62 | 25.03 | |
| 36 | 25.42 | 24.76 | 23.83 | 25.03 | 24.51 | 24.47 | |
| 37 | 25.42 | 25.02 | 24.86 | 24.73 | 24.71 | 25.06 | |
| 39 | 25.58 | 25.01 | 24.02 | 24.99 | 24.61 | 24.65 | |
| 41 | 25.67 | 25.28 | 24.66 | 24.73 | 24.76 | 25.08 | |
| 42 | 25.49 | 24.85 | 24.79 | 25.35 | 24.83 | 25.08 | |
| 44 | 25.93 | 25.50 | 24.29 | 24.78 | 24.76 | 24.94 | |

| Time sec. | A | B | F | C | D | E | Left Edge |
|---|---|---|---|---|---|---|---|
| 45 | 25.73 | 25.33 | 25.15 | 24.92 | 24.98 | 25.37 | |
| 47 | 25.82 | 25.19 | 24.33 | 25.26 | 24.84 | 24.89 | |
| 49 | 25.90 | 25.56 | 25.00 | 24.81 | 25.03 | 25.38 | |
| 50 | 25.78 | 25.11 | 24.93 | 25.66 | 24.98 | 25.11 | |
| 52 | 26.11 | 25.59 | 24.52 | 25.02 | 25.01 | 25.14 | |
| 54 | 25.87 | 25.30 | 25.29 | 25.39 | 25.18 | 25.54 | |
| 55 | 26.19 | 25.62 | 24.52 | 25.26 | 25.08 | 25.10 | |
| 57 | 26.19 | 25.70 | 25.38 | 25.05 | 25.27 | 25.66 | |
| 59 | 26.15 | 25.45 | 25.02 | 25.66 | 25.20 | 25.35 | |
| 61 | 26.54 | 26.16 | 25.34 | 24.83 | 25.32 | 25.74 | |
| 64 | 26.22 | 25.64 | 25.91 | 25.68 | 25.49 | 25.90 | |
| 67 | 26.78 | 26.34 | 25.96 | 25.03 | 25.54 | 26.09 | |
| 71 | 26.28 | 25.51 | 24.74 | 26.22 | 25.45 | 25.46 | |
| 74 | 26.51 | 25.67 | 24.55 | 26.16 | 25.42 | 25.35 | |
| 78 | 26.96 | 26.36 | 24.79 | 25.47 | 25.50 | 25.61 | |
| 81 | 27.11 | 26.53 | 25.43 | 25.44 | 25.66 | 25.98 | |
| 84 | 27.33 | 26.80 | 26.19 | 25.37 | 25.88 | 26.42 | |
| 88 | 27.30 | 26.80 | 26.41 | 25.56 | 25.98 | 26.55 | |
| 166 | 28.81 | 28.56 | 26.95 | 27.11 | 27.28 | 27.61 | |
| 557 | 31.21 | 31.67 | 30.18 | 30.51 | 30.59 | 30.57 | |
| 676 | 31.30 | 32.09 | 30.65 | 30.89 | 30.75 | 30.85 | |
| 916 | 31.74 | 32.63 | 31.50 | 31.11 | 31.43 | 31.42 | |
| 1216 | 31.79 | 32.72 | 31.32 | 31.65 | 31.61 | 31.39 | |

Figure A4.PT9a. Glass plate at room temperature inserted into drying system with air at 32 C and low RH.

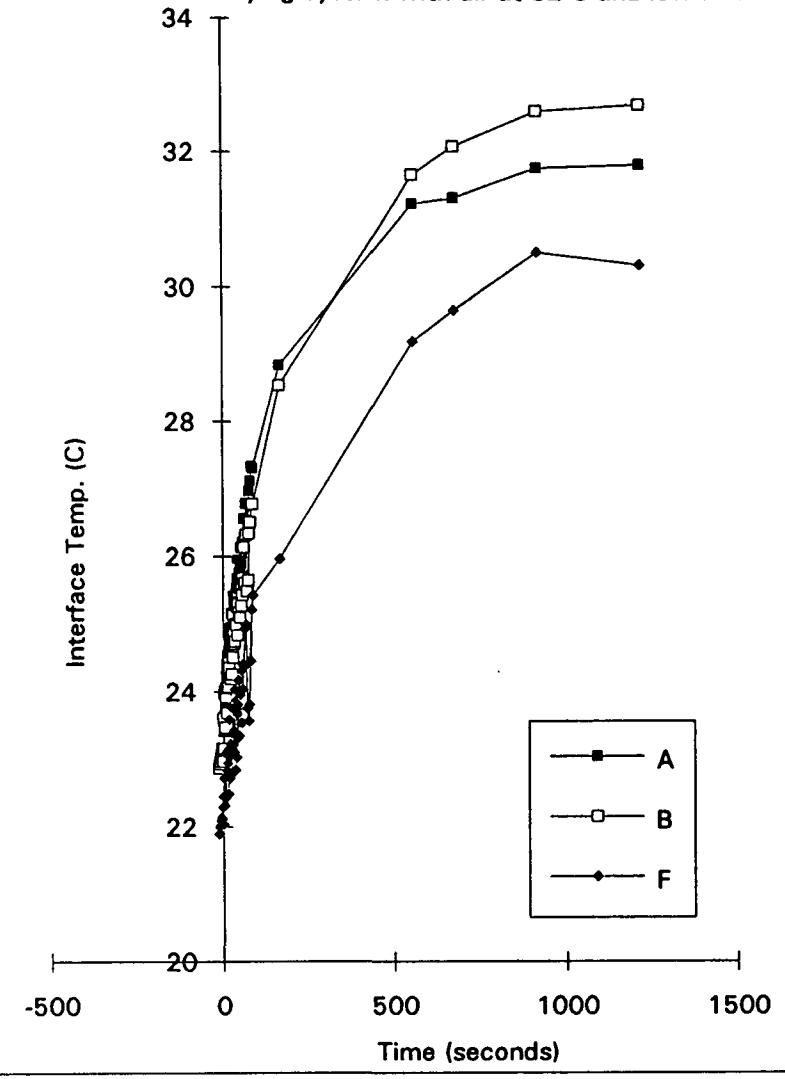


Figure A4.PT9b. Glass plate at room temperature inserted into drying system with air at 32 C and low RH.

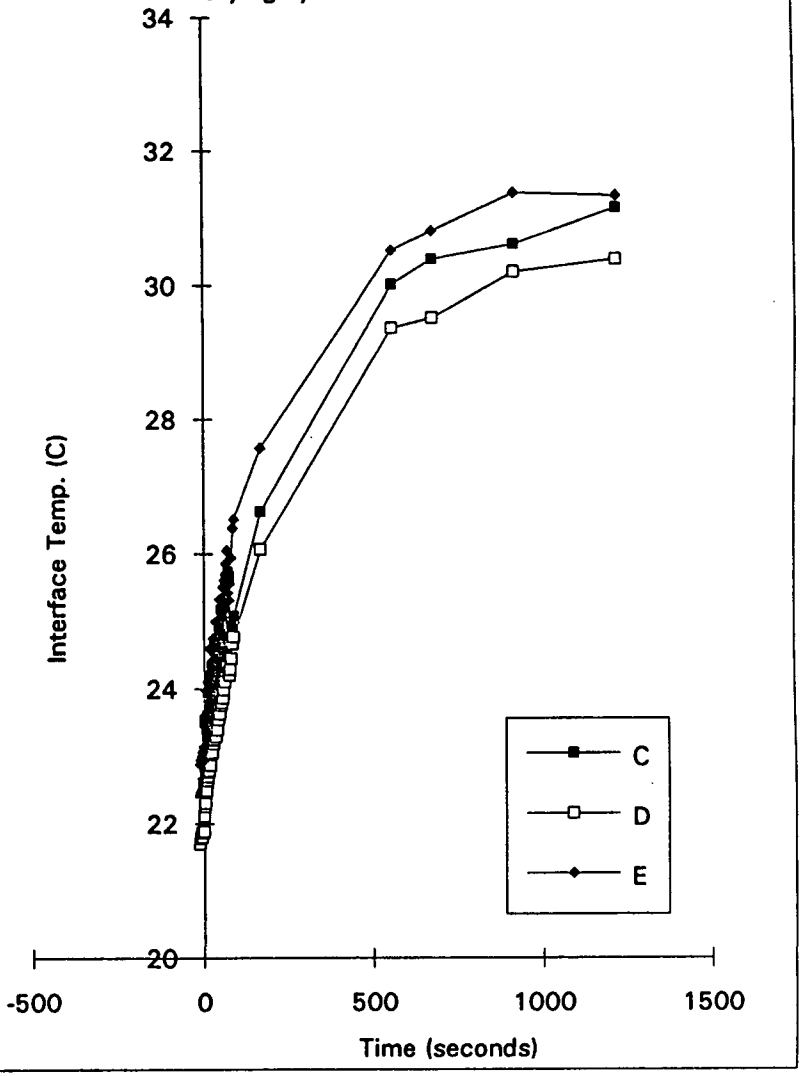

Table A4.PT10. Glass plate temperature at 23 C inserted into drier at 32 C.

| PT10 Ref. Temp. Resistors Time-sec. | 23 A | 23 B | 23 F | 23 C | 23 D | 23 E | Left Edge |
|---|---|---|---|---|---|---|---|
| -20 | 22.95 | 22.89 | 22.87 | 22.94 | 22.95 | 22.86 | |
| -18 | 22.98 | 22.98 | 22.95 | 22.99 | 22.96 | 22.96 | |
| -17 | 23.03 | 23.03 | 23.00 | 23.01 | 23.01 | 23.00 | |
| -15 | 23.00 | 23.00 | 23.09 | 23.02 | 23.00 | 23.02 | |
| -13 | 23.04 | 23.09 | 23.09 | 23.04 | 23.08 | 23.16 | |
| -12 | 23.07 | 23.08 | 23.16 | 23.04 | 23.01 | 23.00 | |
| -10 | 23.20 | 23.18 | 23.21 | 23.15 | 23.05 | 23.18 | |
| -8 | 23.10 | 23.17 | 23.24 | 23.13 | 23.17 | 23.16 | |
| -7 | 22.94 | 23.02 | 23.69 | 23.47 | 23.23 | 23.37 | |
| -5 | 23.33 | 23.41 | 23.00 | 23.07 | 23.03 | 23.05 | |
| -3 | 23.12 | 23.26 | 23.74 | 23.33 | 23.33 | 23.45 | |
| -2 | 23.20 | 23.18 | 23.33 | 23.17 | 23.13 | 23.21 | |
| 0 | 23.44 | 23.61 | 23.61 | 23.30 | 23.39 | 23.51 | |
| 2 | 23.66 | 23.37 | 23.49 | 23.50 | 23.42 | 23.48 | |
| 3 | 23.99 | 23.94 | 23.49 | 23.52 | 23.50 | 23.64 | |
| 5 | 23.92 | 23.74 | 23.98 | 23.81 | 23.76 | 23.95 | |
| 7 | 24.26 | 23.97 | 23.31 | 23.60 | 23.54 | 23.63 | |
| 8 | 24.16 | 23.89 | 24.12 | 24.00 | 23.94 | 24.07 | |
| 10 | 24.33 | 23.97 | 23.71 | 23.87 | 23.77 | 23.93 | |
| 12 | 24.47 | 24.27 | 23.97 | 23.97 | 23.98 | 24.15 | |
| 13 | 24.38 | 23.88 | 24.16 | 24.16 | 24.03 | 24.23 | |
| 15 | 24.72 | 24.44 | 23.78 | 24.02 | 23.94 | 24.11 | |
| 17 | 24.49 | 24.17 | 24.40 | 24.27 | 24.16 | 24.39 | |
| 18 | 24.79 | 24.34 | 23.67 | 24.05 | 23.99 | 24.11 | |
| 20 | 24.79 | 24.52 | 24.26 | 24.27 | 24.25 | 24.46 | |
| 21 | 24.76 | 24.26 | 24.35 | 24.39 | 24.25 | 24.43 | |
| 23 | 25.05 | 24.63 | 23.81 | 24.24 | 24.16 | 24.33 | |
| 25 | 24.85 | 24.38 | 24.50 | 24.50 | 24.40 | 24.60 | |
| 26 | 25.10 | 24.72 | 24.16 | 24.37 | 24.30 | 24.49 | |
| 28 | 25.02 | 24.66 | 24.72 | 24.68 | 24.57 | 24.89 | |
| 30 | 25.10 | 24.60 | 24.50 | 24.56 | 24.40 | 24.60 | |
| 31 | 25.25 | 24.93 | 24.48 | 24.61 | 24.59 | 24.84 | |
| 33 | 25.19 | 24.64 | 24.41 | 24.66 | 24.54 | 24.75 | |
| 35 | 25.56 | 25.12 | 24.12 | 24.55 | 24.45 | 24.62 | |
| 36 | 25.24 | 24.64 | 24.81 | 24.84 | 24.72 | 24.99 | |

| Time sec. | A | B | F | C | D | E | Left Edge |
|---|---|---|---|---|---|---|---|
| 38 | 25.59 | 25.07 | 24.12 | 24.58 | 24.49 | 24.67 | |
| 40 | 25.45 | 25.07 | 24.78 | 24.87 | 24.79 | 25.07 | |
| 41 | 25.52 | 24.89 | 24.60 | 24.84 | 24.67 | 24.87 | |
| 43 | 25.73 | 25.35 | 24.43 | 24.77 | 24.67 | 24.92 | |
| 45 | 25.56 | 24.95 | 24.91 | 24.98 | 24.84 | 25.15 | |
| 46 | 25.87 | 25.38 | 24.48 | 24.85 | 24.77 | 24.99 | |
| 48 | 25.67 | 25.20 | 25.15 | 25.14 | 25.01 | 25.37 | |
| 50 | 25.79 | 25.20 | 24.72 | 24.98 | 24.89 | 25.10 | |
| 51 | 25.95 | 25.47 | 24.86 | 25.08 | 25.04 | 25.34 | |
| 53 | 25.79 | 25.06 | 24.93 | 25.19 | 25.04 | 25.26 | |
| 55 | 26.10 | 25.61 | 24.71 | 25.08 | 25.01 | 25.24 | |
| 56 | 25.93 | 25.40 | 25.39 | 25.40 | 25.23 | 25.55 | |
| 58 | 26.16 | 25.56 | 24.74 | 25.13 | 25.01 | 25.26 | |
| 60 | 26.05 | 25.56 | 25.14 | 25.32 | 25.23 | 25.53 | |
| 63 | 26.30 | 25.72 | 24.81 | 25.16 | 25.18 | 25.34 | |
| 67 | 26.14 | 25.41 | 25.03 | 25.64 | 25.37 | 25.58 | |
| 70 | 26.53 | 25.93 | 25.14 | 25.30 | 25.25 | 25.48 | |
| 73 | 26.73 | 26.22 | 25.58 | 25.48 | 25.53 | 25.90 | |
| 77 | 26.62 | 26.13 | 25.89 | 25.80 | 25.75 | 26.04 | |
| 80 | 26.90 | 26.36 | 25.95 | 25.78 | 25.79 | 26.17 | |
| 83 | 26.68 | 26.07 | 26.03 | 26.01 | 25.86 | 26.18 | |
| 87 | 26.70 | 25.95 | 25.38 | 25.93 | 25.72 | 25.95 | |
| 166 | 28.25 | 28.05 | 26.09 | 27.20 | 26.71 | 27.15 | 28.02 |
| 241 | 29.05 | 31.47 | 27.00 | 27.96 | 27.42 | 27.91 | 28.88 |
| 315 | 30.03 | 30.17 | 28.40 | 29.05 | 28.42 | 29.10 | 29.50 |
| 406 | 30.30 | 31.15 | 29.10 | 29.56 | 29.02 | 29.63 | 30.08 |
| 480 | 30.67 | 31.18 | 30.12 | 30.19 | 29.58 | 30.17 | 30.41 |
| 615 | 31.14 | 31.18 | 30.62 | 30.69 | 30.17 | 30.75 | 30.76 |
| 915 | 31.37 | 31.62 | 31.30 | 31.13 | 30.82 | 31.39 | 31.13 |
| 1215 | 31.47 | 31.12 | 29.79 | 30.69 | 30.13 | 31.85 | 31.18 |

Figure A4.PT10a. Glass plate at 23C inserted into drying air at 32 C.

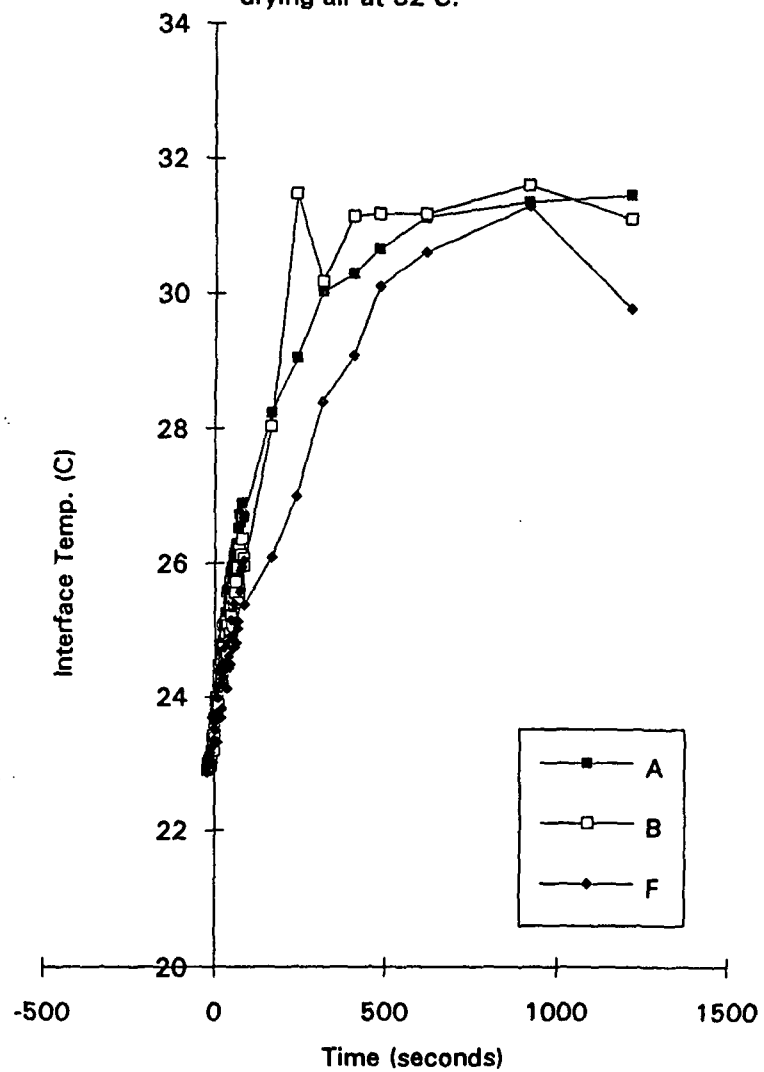


Figure A$.PT10b. Glass plate at 23 C inserted into drying air at 32 C.

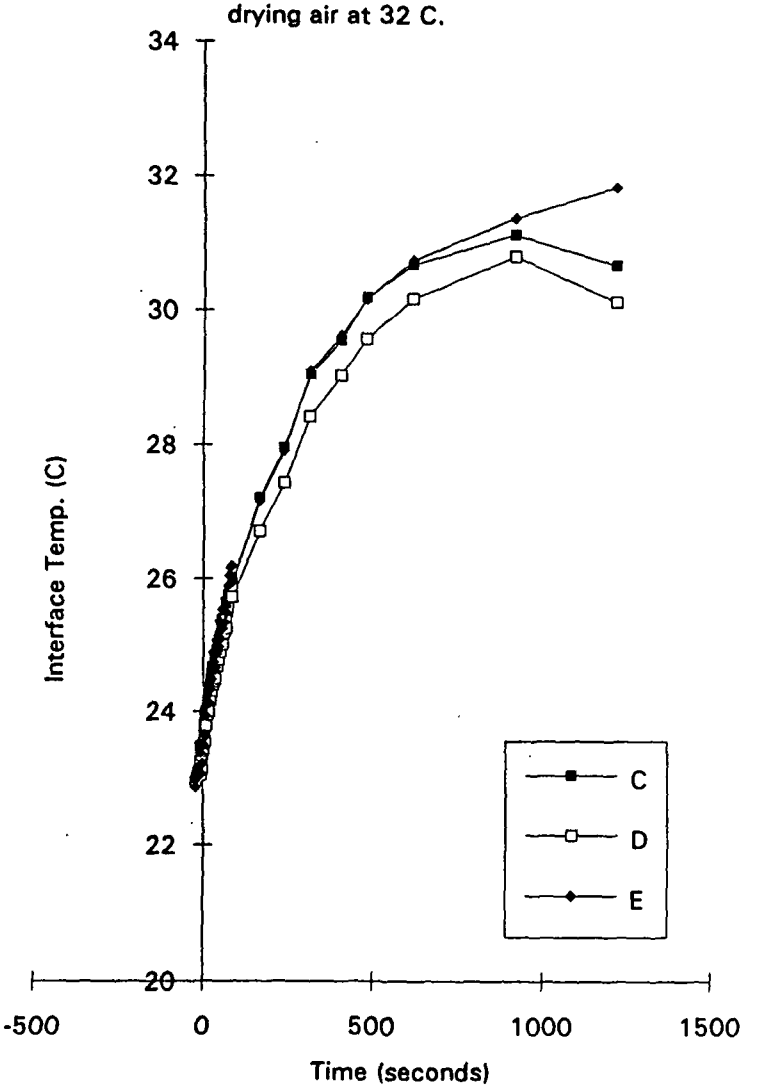

Table A4.PT11. Glass plate temperature at 23 C inserted into drier at 32 C.

| PT11 Ref. Temp. Resistors Time-sec. | 23 A | 23 B | 23 F | 23 C | 23 D | 23 E | Left Edge |
|---|---|---|---|---|---|---|---|
| -20 | 22.93 | 22.92 | 22.87 | 22.99 | 22.93 | 22.90 | |
| -18 | 23.18 | 22.98 | 22.97 | 23.01 | 22.96 | 22.90 | |
| -16 | 23.01 | 23.03 | 23.01 | 23.01 | 23.03 | 23.04 | |
| -14 | 23.04 | 22.98 | 23.03 | 22.96 | 23.00 | 23.03 | |
| -13 | 22.99 | 23.06 | 23.09 | 23.02 | 23.10 | 23.11 | |
| -11 | 23.05 | 23.03 | 23.15 | 23.04 | 23.03 | 23.01 | |
| -10 | 23.13 | 23.15 | 23.15 | 23.04 | 23.06 | 23.14 | |
| -8 | 23.08 | 23.10 | 23.22 | 23.04 | 23.13 | 23.09 | |
| -6 | 23.16 | 23.16 | 23.23 | 23.28 | 23.10 | 23.11 | |
| -5 | 23.18 | 23.21 | 23.30 | 23.12 | 23.22 | 23.19 | |
| -3 | 23.15 | 23.16 | 23.42 | 23.18 | 23.15 | 23.22 | |
| -1 | 23.25 | 23.32 | 23.25 | 23.26 | 23.20 | 23.25 | |
| 0 | 23.32 | 23.27 | 23.49 | 23.26 | 23.32 | 23.31 | |
| 2 | 23.75 | 23.61 | 23.52 | 23.54 | 23.42 | 23.51 | |
| 4 | 23.84 | 23.70 | 23.58 | 23.46 | 23.62 | 23.68 | |
| 5 | 23.96 | 23.75 | 23.66 | 23.71 | 23.67 | 23.71 | |
| 7 | 24.14 | 23.93 | 23.68 | 23.81 | 23.71 | 23.81 | |
| 9 | 24.18 | 23.89 | 23.85 | 23.89 | 23:81 | 23.91 | |
| 10 | 24.36 | 24.05 | 23.75 | 24.00 | 23.82 | 23.99 | |
| 12 | 24.39 | 24.09 | 23.87 | 23.96 | 23.96 | 24.02 | |
| 14 | 24.45 | 24.12 | 23.94 | 24.13 | 23.99 | 24.10 | |
| 15 | 24.59 | 24.25 | 23.87 | 24.08 | 24.03 | 24.13 | |
| 17 | 24.57 | 24.21 | 24.08 | 24.20 | 24.08 | 24.19 | |
| 19 | 24.71 | 24.33 | 23.99 | 24.29 | 24.06 | 24.26 | |
| 20 | 24.73 | 24.36 | 24.11 | 24.18 | 24.20 | 24.32 | |
| 22 | 24.80 | 24.32 | 24.11 | 24.45 | 24.18 | 24.27 | |
| 24 | 24.90 | 24.52 | 24.11 | 24.28 | 24.28 | 24.43 | |
| 25 | 24.90 | 24.44 | 24.25 | 24.44 | 24.28 | 24.40 | |
| 27 | 25.05 | 24.61 | 24.09 | 24.50 | 24.33 | 24.48 | |
| 28 | 25.00 | 24.55 | 24.30 | 24.44 | 24.43 | 24.51 | |
| 30 | 25.16 | 24.70 | 24.30 | 24.68 | 24.37 | 24.58 | |
| 32 | 25.19 | 24.75 | 24.28 | 24.48 | 24.50 | 24.63 | |
| 33 | 25.22 | 24.70 | 24.40 | 24.65 | 24.48 | 24.63 | |
| 36 | 25.30 | 24.81 | 24.34 | 24.69 | 24.58 | 24.72 | |
| 38 | 25.40 | 24.91 | 24.44 | 24.75 | 24.59 | 24.81 | |

| Time sec. | A | B | F | C | D | E | Left Edge |
|---|---|---|---|---|---|---|---|
| 41 | 25.46 | 24.97 | 24.55 | 24.84 | 24.70 | 24.82 | |
| 44 | 25.58 | 25.03 | 24.57 | 24.93 | 24.72 | 24.96 | |
| 47 | 25.67 | 25.13 | 24.65 | 24.94 | 24.85 | 24.98 | |
| 49 | 25.76 | 25.22 | 24.67 | 25.06 | 24.83 | 25.05 | |
| 52 | 25.85 | 25.26 | 24.76 | 25.07 | 24.94 | 25.15 | |
| 55 | 25.93 | 25.33 | 24.79 | 25.20 | 24.95 | 25.19 | |
| 58 | 25.97 | 25.39 | 24.86 | 25.21 | 25.05 | 25.22 | |
| 60 | 26.07 | 25.48 | 24.94 | 25.28 | 25.13 | 25.34 | |
| 65 | 26.15 | 25.52 | 24.95 | 25.45 | 25.11 | 25.37 | |
| 70 | 26.35 | 25.68 | 25.03 | 25.64 | 25.23 | 25.53 | |
| 76 | 26.61 | 25.94 | 25.20 | 25.55 | 25.47 | 25.68 | |
| 82 | 26.63 | 25.96 | 25.44 | 25.54 | 25.63 | 25.79 | |
| 87 | 26.78 | 26.08 | 25.40 | 25.90 | 25.59 | 25.90 | |
| 152 | 27.90 | 27.55 | 26.20 | 26.79 | 26.67 | 26.73 | |
| 211 | 28.72 | 28.49 | 27.02 | 27.58 | 27.54 | 27.53 | |
| 286 | 29.54 | 29.51 | 28.17 | 28.36 | 28.47 | 28.38 | |
| 361 | 29.94 | 30.38 | 28.75 | 28.82 | 29.03 | 28.94 | |
| 436 | 30.43 | 30.01 | 29.56 | 29.48 | 29.61 | 29.58 | |
| 616 | 30.93 | 30.74 | 30.19 | 30.27 | 30.25 | 30.35 | |
| 916 | 31.17 | 31.40 | 30.87 | 30.80 | 30.74 | 30.81 | |
| 1216 | 31.27 | 31.70 | 31.19 | 30.91 | 31.06 | 31.03 | |

Figure A4.PT11a. Glass plate at 23 C inserted into drying air at 32 C.

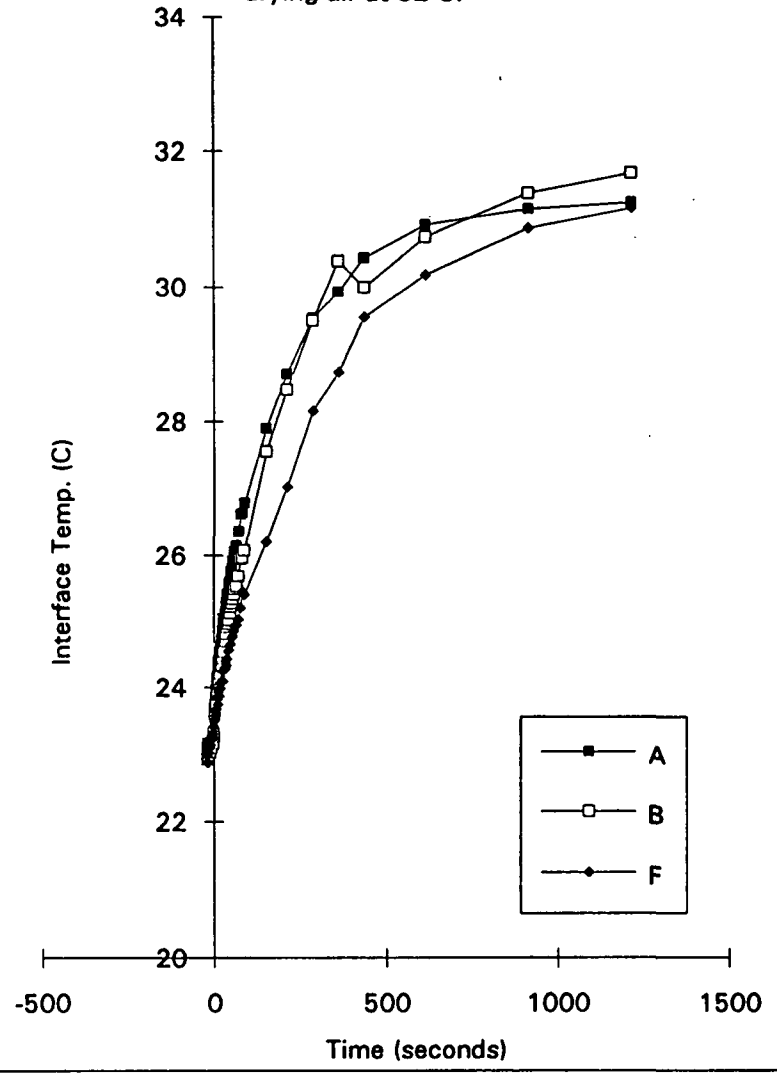


Figure A4.PT11b. Glass plate at 23 C inserted into drying air at 32 C.

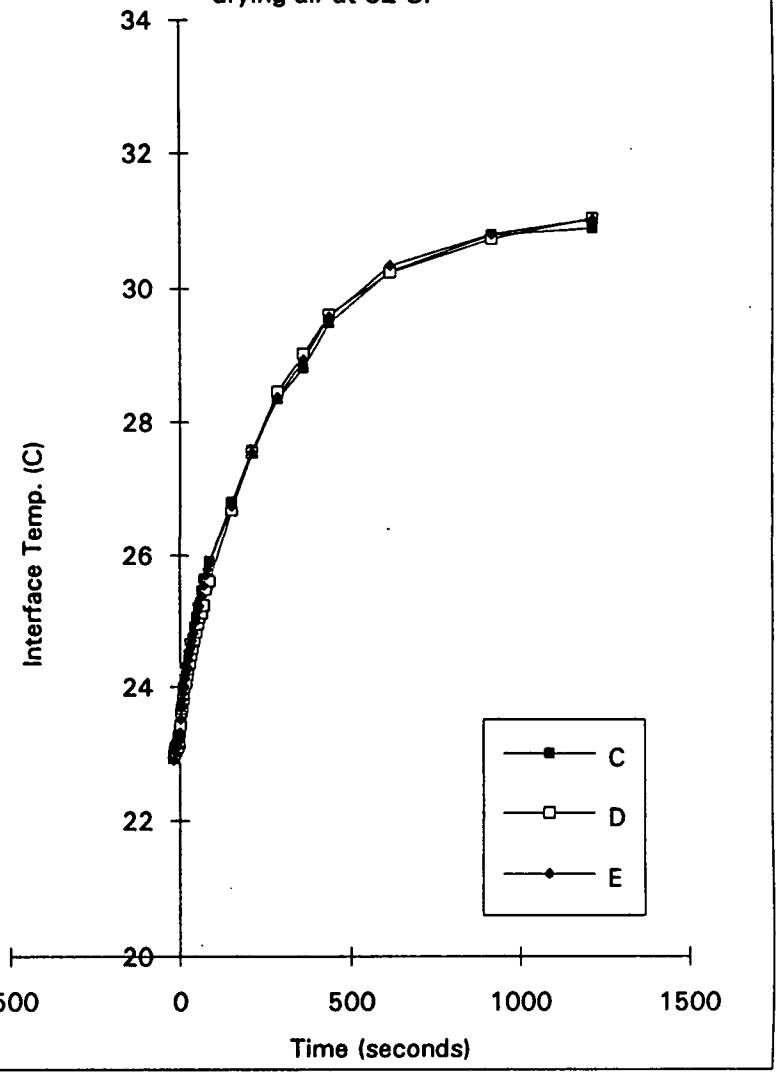

Table A4.PT12. Glass plate temperature at 38 C inserted into drier at 32 C.

| PT12 Ref. Temp. Resistors Time-sec. | 38 A | 38 B | 38 F | 38 C | 38 D | 38 E | Left Edge |
|---|---|---|---|---|---|---|---|
| -34 | 38.01 | 37.98 | 38.00 | 37.99 | 38.02 | 38.02 | 32.02 |
| -31 | 38.05 | 38.02 | 38.00 | 38.04 | 38.03 | 38.06 | 31.55 |
| -26 | 37.96 | 38.01 | 38.01 | 37.99 | 37.97 | 37.96 | 31.70 |
| -22 | 37.82 | 37.86 | 37.93 | 37.91 | 37.81 | 37.86 | 31.55 |
| -17 | 37.65 | 37.69 | 37.86 | 37.67 | 37.63 | 37.77 | 31.86 |
| -13 | 37.71 | 37.72 | 37.84 | 37.64 | 37.66 | 37.78 | 31.55 |
| -8 | 37.58 | 37.70 | 37.86 | 37.75 | 37.75 | 37.69 | 31.86 |
| -3 | 37.56 | 37.69 | 37.86 | 37.72 | 37.70 | 37.75 | 31.86 |
| 1 | 37.25 | 37.43 | 37.67 | 37.54 | 37.51 | 37.50 | 33.29 |
| 6 | 36.98 | 37.15 | 37.77 | 37.37 | 37.32 | 37.32 | 35.03 |
| 10 | 36.87 | 37.01 | 37.67 | 37.19 | 37.17 | 37.16 | 35.66 |
| 15 | 36.58 | 36.87 | 37.63 | 37.01 | 37.12 | 37.11 | 36.12 |
| 20 | 36.44 | 36.75 | 37.46 | 36.87 | 36.98 | 36.92 | 36.12 |
| 24 | 36.29 | 36.67 | 37.43 | 36.72 | 36.92 | 36.95 | 36.12 |
| 29 | 36.06 | 36.41 | 37.29 | 36.80 | 36.76 | 36.70 | 35.97 |
| 33 | 35.92 | 36.32 | 37.19 | 36.68 | 36.66 | 36.54 | 36.12 |
| 38 | 35.87 | 36.21 | 37.08 | 36.50 | 36.54 | 36.47 | 35.66 |
| 43 | 35.81 | 36.12 | 36.96 | 36.37 | 36.41 | 36.46 | 35.81 |
| 47 | 35.66 | 36.03 | 36.89 | 36.24 | 36.36 | 36.30 | 35.97 |
| 52 | 35.47 | 35.88 | 36.84 | 36.26 | 36.31 | 36.19 | 35.66 |
| 56 | 35.38 | 35.78 | 36.74 | 36.13 | 36.16 | 36.14 | 35.66 |
| 61 | 35.26 | 35.71 | 36.74 | 36.05 | 36.14 | 36.01 | 35.81 |
| 66 | 35.10 | 35.52 | 36.57 | 36.05 | 36.00 | 35.85 | 35.66 |
| 70 | 35.04 | 35.48 | 36.45 | 35.92 | 35.94 | 35.80 | 35.50 |
| 75 | 34.97 | 35.43 | 36.46 | 35.79 | 35.92 | 35.74 | 35.35 |
| 79 | 34.92 | 35.32 | 36.33 | 35.71 | 35.73 | 35.71 | 35.35 |
| 84 | 34.83 | 35.28 | 36.33 | 35.60 | 35.75 | 35.64 | 35.19 |
| 89 | 34.67 | 35.12 | 36.19 | 35.60 | 35.63 | 35.48 | 35.03 |
| 93 | 34.63 | 35.08 | 36.15 | 35.49 | 35.60 | 35.48 | 35.03 |
| 98 | 34.50 | 34.91 | 36.02 | 35.47 | 35.48 | 35.34 | 35.19 |
| 102 | 34.46 | 34.88 | 35.97 | 35.38 | 35.45 | 35.31 | 34.88 |
| 107 | 34.47 | 34.85 | 35.86 | 35.22 | 35.34 | 35.29 | 34.88 |
| 112 | 34.31 | 34.74 | 35.86 | 35.23 | 35.33 | 35.11 | 34.72 |
| 116 | 34.23 | 34.66 | 35.69 | 35.12 | 35.21 | 35.10 | 34.72 |
| 195 | 33.10 | 33.41 | 34.39 | 34.06 | 34.15 | 33.88 | 33.78 |

| Time sec. | A | B | F | C | D | E | Left Edge |
|---|---|---|---|---|---|---|---|
| 269 | 32.55 | 32.68 | 33.54 | 33.42 | 33.37 | 33.20 | 33.14 |
| 345 | 32.10 | 32.13 | 32.89 | 32.91 | 32.84 | 32.65 | 32.71 |
| 434 | 31.75 | 31.64 | 32.28 | 32.46 | 32.34 | 32.11 | 32.22 |
| 614 | 31.42 | 31.17 | 31.49 | 31.93 | 31.81 | 31.58 | 31.70 |
| 914 | 31.17 | 30.78 | 30.72 | 31.50 | 31.42 | 31.12 | 31.56 |
| 1214 | 31.16 | 30.80 | 30.54 | 31.48 | 31.36 | 31.08 | 31.43 |

Figure A4.PT12a. Glass plate at 38 C inserted into drying air at 32C.

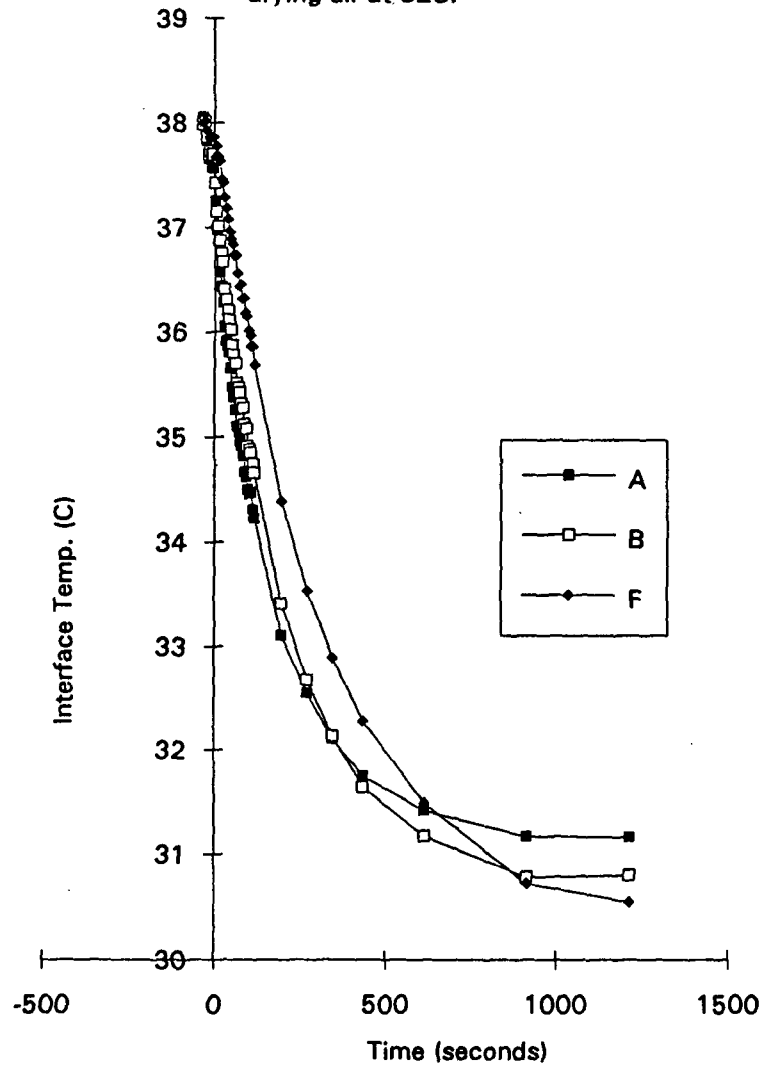


Figure A4.PT12b. Glass plate at 38 C inserted into drying air at 32 C.

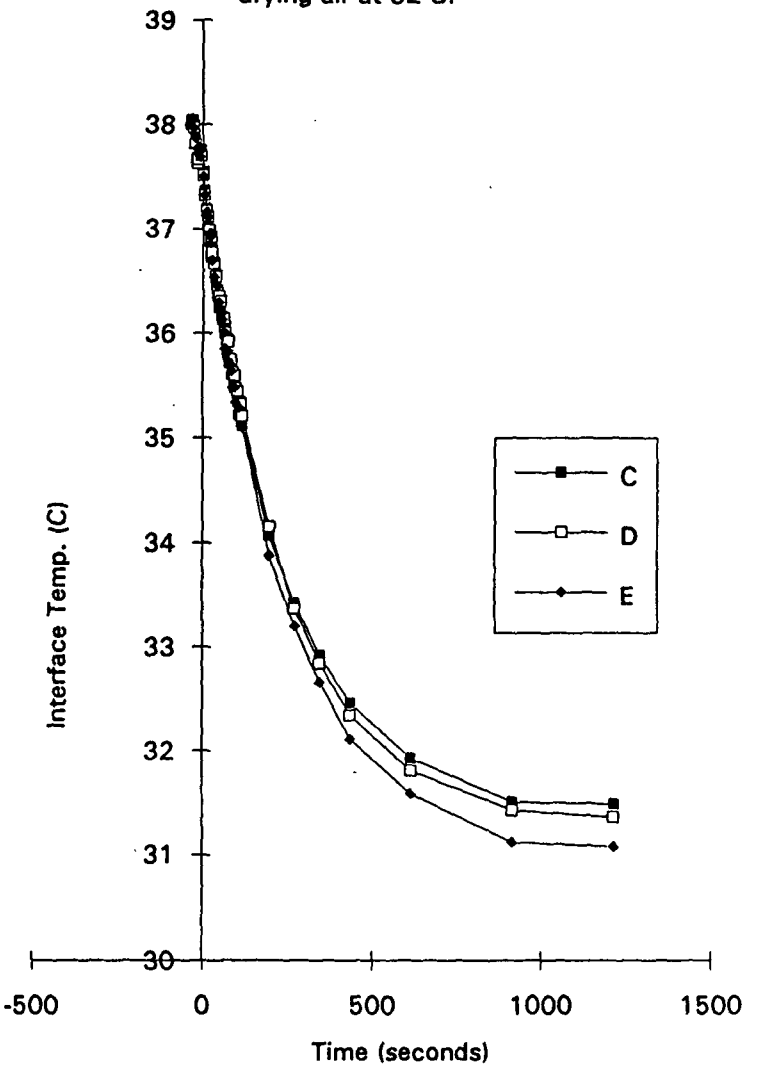

Table A4.PT13. Glass plate temperature at 36 C inserted into drier at 32 C.

| PT13 Ref. Temp. Resistors Time-sec. | 36 A | 36 B | 36 F | 36 C | 36 D | 36 E | Left Edge |
|---|---|---|---|---|---|---|---|
| -38 | 35.48 | 35.49 | 35.45 | 35.53 | 35.54 | 35.47 | 31.70 |
| -34 | 35.52 | 35.51 | 35.52 | 35.51 | 35.51 | 35.50 | 31.70 |
| -29 | 35.50 | 35.51 | 35.52 | 35.46 | 35.45 | 35.53 | 31.39 |
| -24 | 35.33 | 35.34 | 35.54 | 35.35 | 35.35 | 35.34 | 31.70 |
| -20 | 35.41 | 35.26 | 35.45 | 35.17 | 35.27 | 35.24 | 31.55 |
| -15 | 35.18 | 35.23 | 35.30 | 35.14 | 35.15 | 35.28 | 31.70 |
| -10 | 35.13 | 35.21 | 35.26 | 35.00 | 35.18 | 35.16 | 31.55 |
| -6 | 35.16 | 35.17 | 35.33 | 35.32 | 35.17 | 35.26 | 31.86 |
| -1 | 35.10 | 35.18 | 35.28 | 34.82 | 35.15 | 35.18 | 31.86 |
| 3 | 34.92 | 35.04 | 35.21 | 34.98 | 35.01 | 35.16 | 32.97 |
| 8 | 34.67 | 34.81 | 35.01 | 34.50 | 34.88 | 34.89 | 33.61 |
| 13 | 34.49 | 34.69 | 34.99 | 34.72 | 34.81 | 34.83 | 34.40 |
| 17 | 34.43 | 34.57 | 35.02 | 34.80 | 34.73 | 34.75 | 34.72 |
| 22 | 34.30 | 34.49 | 34.87 | 34.29 | 34.63 | 34.72 | 34.72 |
| 26 | 34.24 | 34.40 | 34.80 | 34.76 | 34.56 | 34.64 | 34.40 |
| 31 | 34.12 | 34.32 | 34.68 | 34.08 | 34.51 | 34.49 | 34.56 |
| 36 | 34.06 | 34.23 | 34.77 | 34.34 | 34.42 | 34.51 | 34.40 |
| 40 | 33.96 | 34.20 | 34.75 | 34.10 | 34.36 | 34.44 | 34.40 |
| 45 | 33.89 | 34.11 | 34.66 | 33.92 | 34.30 | 34.38 | 34.40 |
| 49 | 33.78 | 34.00 | 34.47 | 34.56 | 34.24 | 34.28 | 34.40 |
| 54 | 33.73 | 33.89 | 34.32 | 34.19 | 34.15 | 34.16 | 34.24 |
| 59 | 33.66 | 33.82 | 34.47 | 33.91 | 34.08 | 34.20 | 34.24 |
| 63 | 33.55 | 33.80 | 34.25 | 33.62 | 34.03 | 34.05 | 34.40 |
| 68 | 33.50 | 33.71 | 34.39 | 33.66 | 33.97 | 33.98 | 34.08 |
| 72 | 33.44 | 33.63 | 34.23 | 33.92 | 33.90 | 33.98 | 33.93 |
| 77 | 33.37 | 33.54 | 34.16 | 34.15 | 33.85 | 33.92 | 34.24 |
| 82 | 33.30 | 33.48 | 34.13 | 34.00 | 33.81 | 33.84 | 34.08 |
| 86 | 33.23 | 33.46 | 33.92 | 33.49 | 33.76 | 33.76 | 34.24 |
| 91 | 33.18 | 33.39 | 33.97 | 33.49 | 33.71 | 33.73 | 33.77 |
| 95 | 33.12 | 33.32 | 33.97 | 33.36 | 33.70 | 33.69 | 33.73 |
| 100 | 33.04 | 33.29 | 34.03 | 33.47 | 33.61 | 33.63 | 33.77 |
| 105 | 33.03 | 33.23 | 33.94 | 33.46 | 33.54 | 33.60 | 33.61 |
| 109 | 32.95 | 33.17 | 33.72 | 33.63 | 33.53 | 33.55 | 33.77 |
| 114 | 32.87 | 33.14 | 33.80 | 33.41 | 33.44 | 33.50 | 33.61 |
| 118 | 32.81 | 33.06 | 33.63 | 33.44 | 33.44 | 33.41 | 33.77 |

| Time sec. | A | B | F | C | D | E | Left Edge |
|---|---|---|---|---|---|---|---|
| 182 | 32.23 | 32.40 | 32.83 | 32.73 | 32.80 | 32.72 | 33.01 |
| 257 | 31.78 | 31.83 | 32.18 | 32.29 | 32.26 | 32.17 | 32.64 |
| 332 | 31.47 | 31.43 | 31.48 | 31.97 | 31.96 | 31.76 | 32.21 |
| 422 | 31.22 | 31.06 | 30.89 | 31.47 | 31.55 | 31.38 | 31.99 |
| 617 | 31.01 | 30.68 | 30.27 | 30.99 | 31.16 | 30.95 | 31.54 |
| 917 | 30.79 | 30.37 | 29.72 | 30.85 | 30.85 | 30.62 | 31.34 |
| 1217 | 30.79 | 30.37 | 29.61 | 30.78 | 30.70 | 30.53 | 31.25 |

Figure A4.PT13a. Glass plate at 36 C inserted into drying air at 32 C.

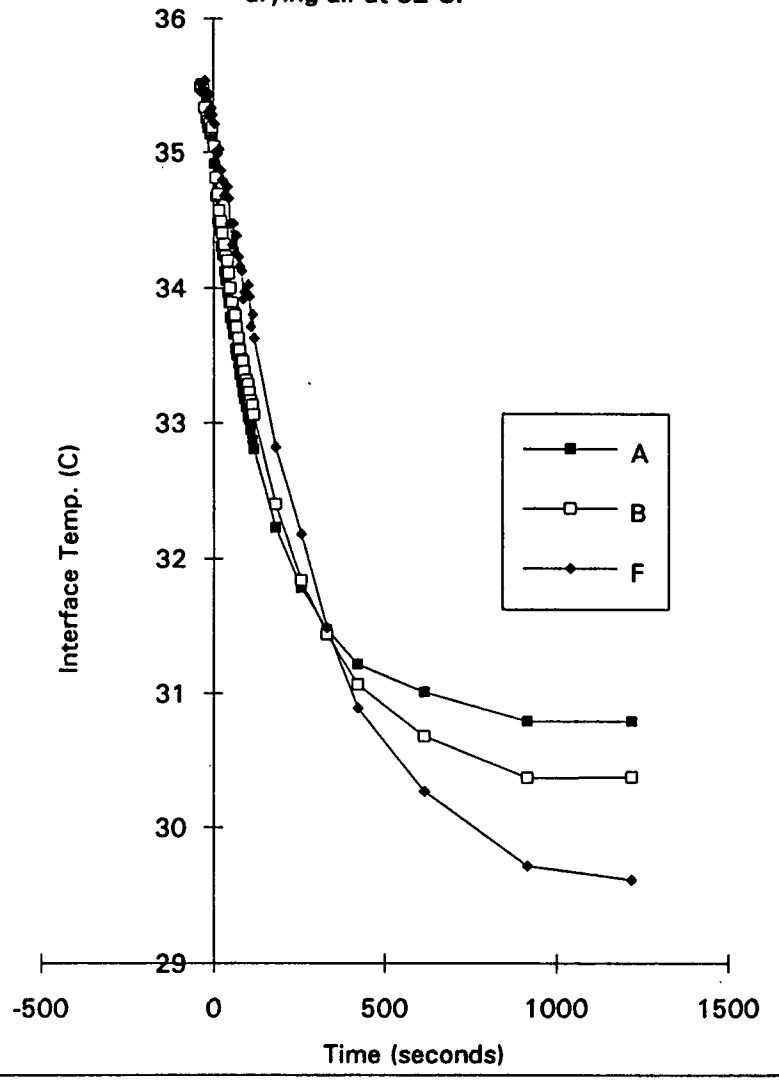


Figure A4.PT13b. Glass plate at 36 C inserted into drying air at 32 C.

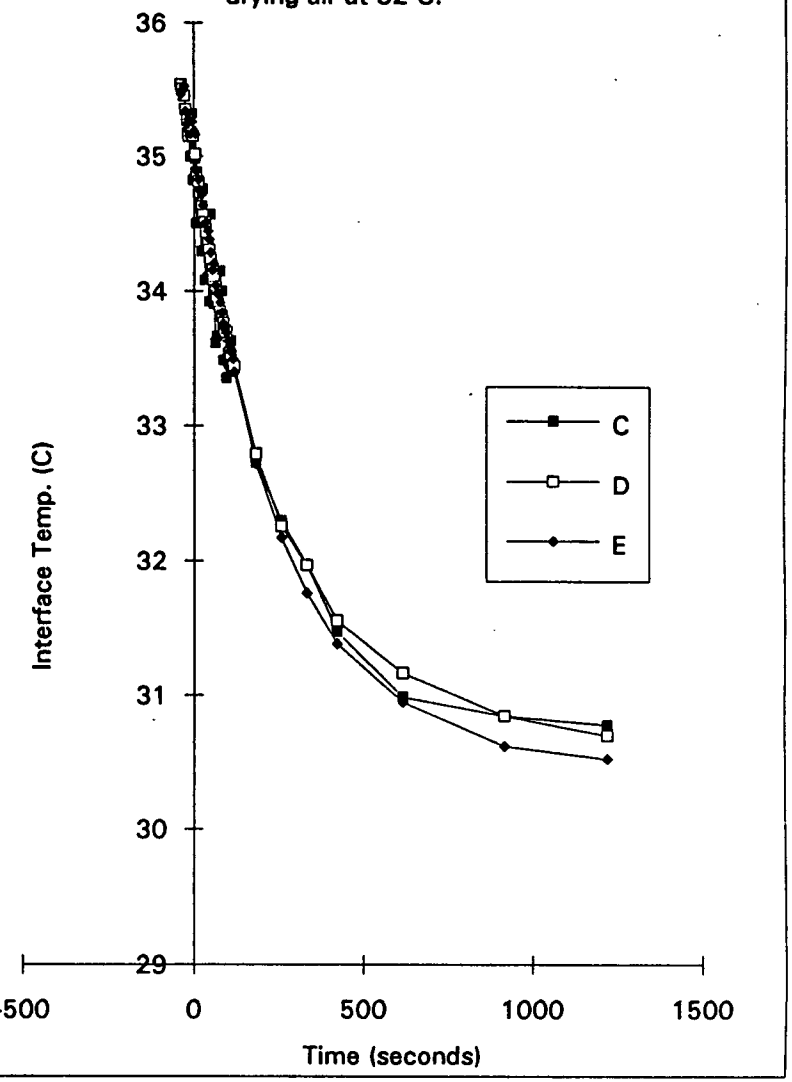

Table A4.PT14. Glass plate temperature at 32 C inserted into drier at 32 C.

| PT14 Ref. Temp. Resistors Time-sec. | 36 A | 36 B | 36 F | 36 C | 36 D | 36 E | Left Edge |
|---|---|---|---|---|---|---|---|
| -38 | 31.98 | 31.95 | 31.90 | 32.00 | 31.99 | 31.93 | 31.80 |
| -34 | 32.06 | 32.02 | 31.99 | 32.03 | 32.06 | 32.04 | 31.86 |
| -29 | 32.04 | 32.03 | 31.99 | 32.00 | 32.02 | 32.02 | 31.99 |
| -25 | 31.96 | 32.02 | 32.04 | 31.97 | 31.97 | 32.01 | 31.86 |
| -20 | 31.80 | 31.89 | 32.15 | 31.97 | 31.90 | 31.90 | 32.18 |
| -15 | 31.73 | 31.91 | 32.15 | 31.90 | 31.90 | 31.94 | 31.86 |
| -11 | 31.78 | 31.92 | 32.15 | 32.08 | 31.92 | 31.98 | 31.67 |
| -6 | 31.84 | 32.02 | 32.42 | 31.82 | 31.94 | 32.02 | 31.86 |
| -1 | 31.81 | 31.89 | 31.94 | 32.19 | 31.84 | 31.88 | 32.02 |
| 3 | 31.80 | 31.87 | 32.32 | 32.02 | 31.89 | 31.99 | 32.46 |
| 8 | 31.81 | 31.84 | 32.08 | 32.05 | 31.85 | 31.90 | 32.18 |
| 12 | 31.93 | 32.18 | 32.42 | 31.57 | 31.97 | 32.04 | 31.55 |
| 17 | 31.96 | 32.07 | 31.80 | 31.89 | 31.85 | 31.86 | 32.02 |
| 22 | 31.96 | 32.07 | 32.13 | 31.84 | 31.90 | 31.94 | 31.86 |
| 26 | 31.81 | 31.79 | 31.97 | 32.10 | 31.89 | 31.93 | 31.70 |
| 31 | 31.81 | 31.92 | 32.33 | 31.68 | 31.94 | 32.04 | 31.70 |
| 35 | 31.73 | 31.70 | 32.03 | 32.19 | 31.84 | 31.94 | 31.55 |
| 40 | 31.83 | 31.95 | 32.33 | 31.66 | 31.92 | 32.02 | 31.39 |
| 45 | 31.84 | 31.82 | 31.85 | 31.97 | 31.80 | 31.83 | 31.55 |
| 49 | 31.78 | 31.99 | 32.40 | 31.57 | 31.97 | 32.09 | 31.39 |
| 54 | 31.83 | 31.87 | 32.23 | 31.73 | 31.90 | 31.96 | 31.70 |
| 58 | 31.73 | 31.66 | 31.77 | 32.13 | 31.75 | 31.83 | 31.39 |
| 63 | 31.81 | 31.91 | 32.16 | 31.71 | 31.85 | 31.98 | 31.70 |
| 68 | 31.66 | 31.58 | 32.01 | 32.11 | 31.80 | 31.86 | 31.23 |
| 72 | 31.86 | 31.91 | 31.90 | 31.70 | 31.82 | 31.88 | 31.55 |
| 77 | 31.75 | 31.68 | 32.06 | 31.94 | 31.82 | 31.91 | 31.55 |
| 81 | 31.86 | 31.82 | 31.89 | 31.86 | 31.80 | 31.82 | 31.70 |
| 86 | 31.83 | 31.97 | 32.40 | 31.50 | 31.87 | 32.06 | 31.55 |
| 91 | 31.72 | 31.66 | 32.20 | 31.81 | 31.85 | 31.94 | 31.39 |
| 95 | 31.66 | 31.66 | 32.18 | 31.87 | 31.87 | 31.98 | 31.39 |
| 100 | 31.83 | 31.74 | 32.09 | 31.86 | 31.82 | 31.88 | 31.23 |
| 104 | 31.69 | 31.60 | 31.92 | 31.94 | 31.82 | 31.88 | 31.23 |
| 109 | 31.90 | 31.81 | 31.80 | 31.86 | 31.74 | 31.78 | 31.39 |
| 114 | 31.70 | 31.66 | 32.08 | 31.87 | 31.84 | 31.94 | 31.39 |
| 118 | 31.81 | 31.79 | 31.85 | 31.78 | 31.80 | 31.85 | 31.23 |

| Time sec. | A | B | F | C | D | E | Left Edge |
|---|---|---|---|---|---|---|---|
| 182 | 31.75 | 31.59 | 31.54 | 31.67 | 31.61 | 31.69 | 31.58 |
| 257 | 31.73 | 31.55 | 31.52 | 31.65 | 31.68 | 31.70 | 31.39 |
| 332 | 31.64 | 31.39 | 31.34 | 31.73 | 31.57 | 31.57 | 31.22 |
| 407 | 31.93 | 31.53 | 31.64 | 31.57 | 31.58 | 31.60 | 31.18 |
| 497 | 31.72 | 31.13 | 31.16 | 31.83 | 31.18 | 31.44 | 31.26 |
| 617 | 31.86 | 31.30 | 31.31 | 31.84 | 31.34 | 31.55 | 31.22 |
| 917 | 31.90 | 31.29 | 31.13 | 32.00 | 31.43 | 31.49 | 31.22 |
| 1216 | 31.90 | 31.58 | 31.52 | 32.05 | 31.57 | 31.50 | 31.30 |

Figure A4.PT14a. Glass plate at 32 C inserted into drying air at 32 C.

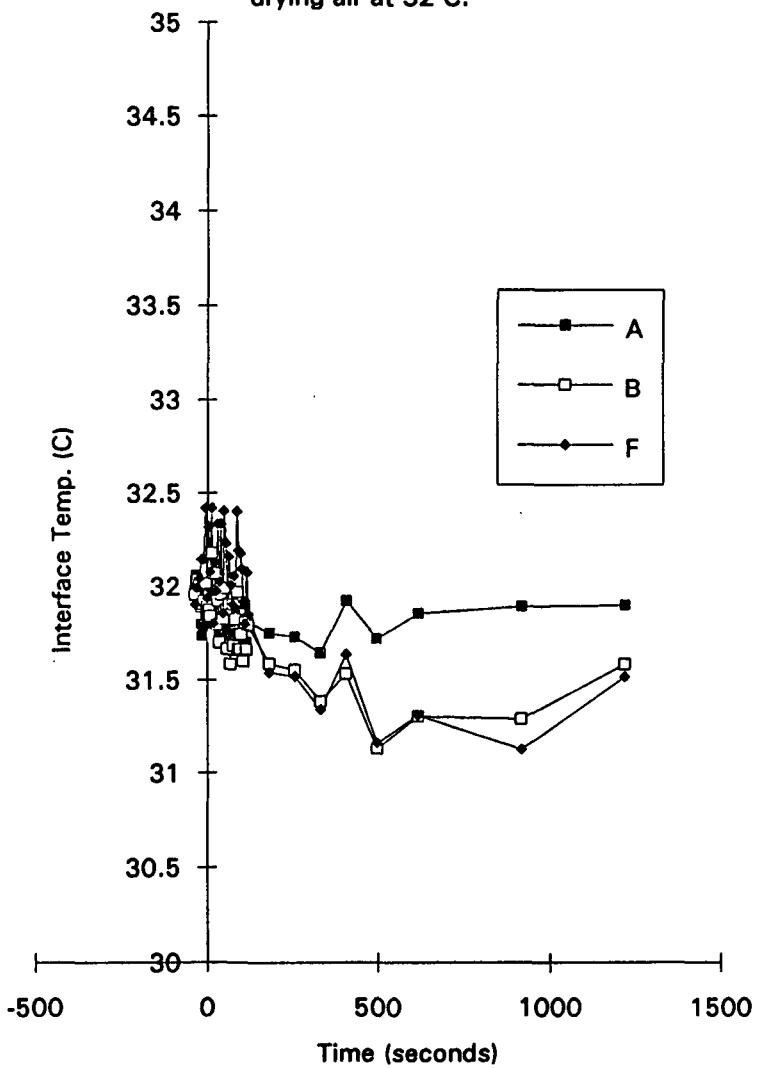


Figure A4.PT14b. Glass plate at 32 C inserted into drying air at 32 C.

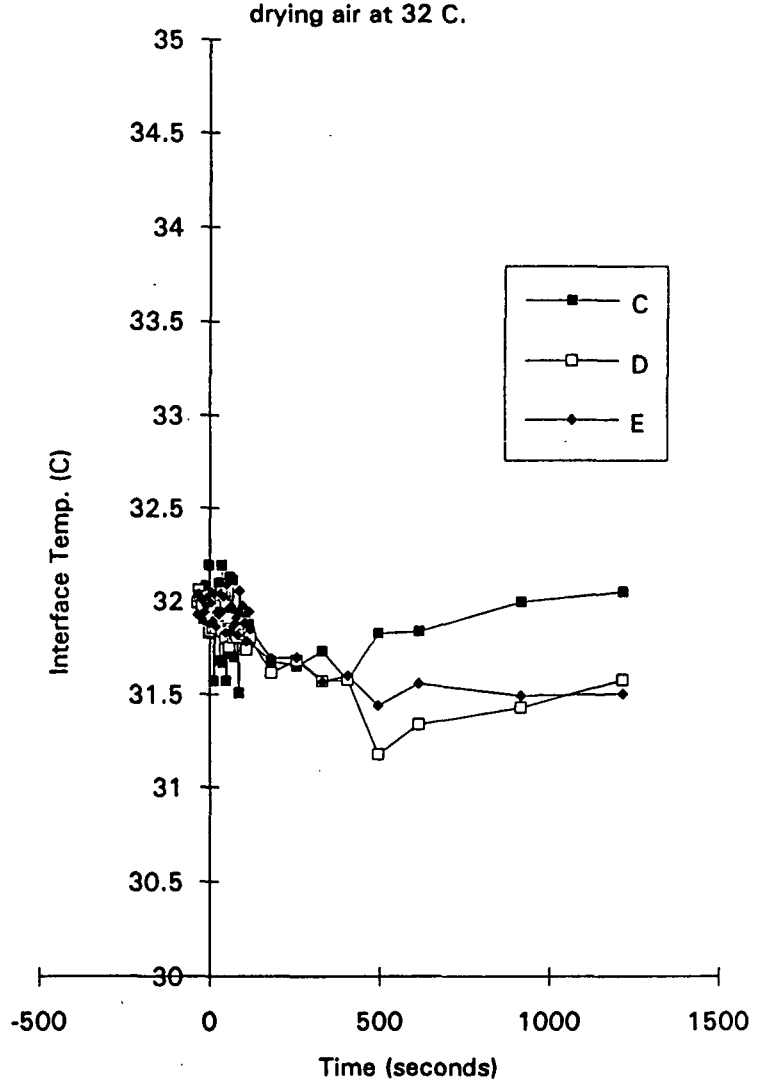

Table A4.PT15. Glass plate temperature during coating and drying at 32 C and 15% RH.

| PT15 Ref. Temp. Resistors Time-sec. | 33 A | 33 B | 33 F | 33 C | 33 D | 33 E | Left Edge |
|---|---|---|---|---|---|---|---|
| -54 | 33.18 | 33.20 | 33.28 | 33.19 | 33.30 | 33.19 | |
| -53 | 33.21 | 33.25 | 33.31 | 33.22 | 33.25 | 33.25 | |
| -51 | 33.41 | 33.32 | 33.26 | 33.35 | 33.34 | 33.25 | |
| -49 | 33.40 | 33.32 | 33.28 | 33.38 | 33.30 | 33.35 | |
| -47 | 33.37 | 33.34 | 33.31 | 33.33 | 33.29 | 33.32 | |
| -46 | 33.28 | 33.29 | 33.29 | 33.30 | 33.29 | 33.32 | |
| -44 | 33.31 | 33.29 | 33.31 | 33.30 | 33.34 | 33.30 | |
| -43 | 33.29 | 33.31 | 33.31 | 33.27 | 33.29 | 33.35 | |
| -41 | 33.25 | 33.38 | 33.36 | 33.35 | 33.30 | 33.38 | |
| -39 | 33.25 | 33.34 | 33.40 | 33.32 | 33.32 | 33.24 | |
| -38 | 33.18 | 33.32 | 33.34 | 33.24 | 33.24 | 33.35 | |
| -36 | 33.18 | 33.23 | 33.29 | 33.41 | 33.25 | 33.30 | |
| -34 | 33.14 | 33.23 | 33.28 | 33.32 | 33.20 | 33.25 | |
| -33 | 33.11 | 33.23 | 33.24 | 33.35 | 33.25 | 33.20 | |
| -31 | 33.05 | 33.12 | 33.26 | 33.27 | 33.17 | 33.20 | |
| -29 | 33.03 | 33.17 | 33.21 | 33.27 | 33.15 | 33.24 | |
| -28 | 33.00 | 33.12 | 33.24 | 33.22 | 33.12 | 33.12 | |
| -26 | 33.00 | 33.12 | 33.14 | 33.16 | 33.07 | 33.14 | |
| -24 | 32.97 | 33.12 | 33.12 | 33.14 | 33.03 | 33.14 | |
| -23 | 32.91 | 33.05 | 33.10 | 33.09 | 33.00 | 33.08 | |
| -21 | 32.85 | 33.05 | 33.09 | 33.13 | 33.03 | 33.14 | |
| -19 | 30.82 | 32.06 | 33.12 | 33.11 | 33.02 | 33.01 | |
| -18 | 30.37 | 30.79 | 29.71 | 10.67 | 7.59 | 10.77 | |
| -16 | 30.34 | 31.54 | 26.77 | 4.36 | -0.93 | 11.30 | |
| -14 | 30.44 | 31.51 | 27.58 | 6.14 | -0.55 | 15.12 | |
| -13 | 30.42 | 31.43 | 26.39 | 7.76 | -0.55 | 16.64 | |
| -11 | 30.32 | 31.20 | 27.29 | 8.90 | 1.02 | 17.70 | |
| -9 | 30.77 | 31.19 | 27.68 | 9.74 | 1.92 | 19.05 | |
| -8 | 30.65 | 31.08 | 27.91 | 10.32 | 2.48 | 19.90 | |
| -6 | 30.64 | 30.99 | 27.91 | 10.89 | 3.20 | 20.38 | |
| -5 | 30.37 | 30.77 | 28.01 | 11.39 | 4.22 | 20.77 | |
| -3 | 30.44 | 30.82 | 27.96 | 11.70 | 4.52 | 21.15 | |
| -1 | 30.44 | 30.83 | 27.92 | 11.84 | 4.93 | 21.28 | |
| 0 | 30.31 | 30.74 | 28.03 | 12.13 | 5.05 | 21.55 | |
| 2 | 29.81 | 30.42 | 27.75 | 12.64 | 4.98 | 21.68 | |

| Time sec. | A | B | F | C | D | E | Left Edge |
|---|---|---|---|---|---|---|---|
| 4 | 29.42 | 30.05 | 27.72 | 12.85 | 5.24 | 21.66 | |
| 5 | 29.16 | 29.84 | 27.53 | 13.30 | 5.25 | 21.63 | |
| 7 | 28.90 | 29.62 | 27.39 | 13.03 | 5.39 | 21.53 | |
| 9 | 28.78 | 29.45 | 27.25 | 13.48 | 5.29 | 21.50 | |
| 10 | 28.58 | 29.36 | 27.12 | 13.46 | 5.34 | 21.36 | |
| 12 | 28.49 | 29.27 | 27.06 | 13.35 | 5.42 | 21.31 | |
| 14 | 28.35 | 29.18 | 26.96 | 13.65 | 5.39 | 21.16 | |
| 15 | 28.26 | 29.13 | 26.77 | 13.45 | 5.47 | 21.15 | |
| 17 | 28.21 | 28.99 | 26.81 | 13.67 | 5.51 | 21.15 | |
| 19 | 28.10 | 28.92 | 26.62 | 13.59 | 5.57 | 21.02 | |
| 20 | 28.04 | 28.82 | 26.65 | 13.69 | 5.62 | 20.99 | |
| 22 | 28.01 | 28.78 | 26.46 | 13.91 | 5.56 | 20.94 | |
| 24 | 27.93 | 28.69 | 26.44 | 13.67 | 5.74 | 20.86 | |
| 25 | 27.90 | 28.61 | 26.38 | 14.01 | 5.68 | 20.78 | |
| 27 | 27.86 | 28.53 | 26.24 | 13.70 | 5.81 | 20.75 | |
| 29 | 27.81 | 28.42 | 26.24 | 13.86 | 5.81 | 20.70 | |
| 30 | 27.79 | 28.39 | 26.00 | 13.85 | 5.84 | 20.61 | |
| 32 | 27.79 | 28.27 | 26.05 | 13.96 | 5.91 | 20.61 | |
| 34 | 27.81 | 28.24 | 25.86 | 14.07 | 5.90 | 20.56 | |
| 35 | 27.78 | 28.12 | 25.89 | 13.90 | 5.98 | 20.54 | |
| 37 | 27.81 | 28.06 | 25.81 | 14.18 | 5.93 | 20.49 | |
| 39 | 27.76 | 27.98 | 25.76 | 13.85 | 6.10 | 20.40 | |
| 40 | 27.79 | 27.89 | 25.70 | 14.18 | 6.00 | 20.40 | |
| 42 | 27.79 | 27.83 | 25.64 | 13.94 | 6.11 | 20.38 | |
| 43 | 27.78 | 27.72 | 25.67 | 14.20 | 6.10 | 20.32 | |
| 45 | 27.84 | 27.70 | 25.50 | 14.18 | 6.06 | 20.29 | |
| 47 | 27.78 | 27.61 | 25.57 | 14.09 | 6.17 | 20.27 | |
| 48 | 27.86 | 27.56 | 25.36 | 14.33 | 6.11 | 20.19 | |
| 50 | 27.81 | 27.46 | 25.46 | 14.17 | 6.22 | 20.17 | |
| 52 | 27.87 | 27.44 | 25.38 | 14.47 | 6.13 | 20.21 | |
| 53 | 27.87 | 27.36 | 25.40 | 14.31 | 6.20 | 20.17 | |
| 55 | 27.92 | 27.32 | 25.36 | 14.62 | 6.08 | 20.14 | |
| 57 | 27.92 | 27.30 | 25.26 | 14.36 | 6.13 | 20.11 | |
| 58 | 27.96 | 27.21 | 25.34 | 14.63 | 6.05 | 20.06 | |
| 60 | 28.01 | 27.20 | 25.15 | 14.62 | 6.03 | 20.08 | |

Table A4.PT15. Glass plate temperature during coating and drying at 32 C and 15% RH.

Continued

| PT15 Ref. Temp. Resistors Time-sec. | 36 A | 36 B | 36 F | 36 C | 36 D | 36 E | Left Edge | Time sec. | A | B | F | C | D | E | Left Edge |
|---|---|---|---|---|---|---|---|---|---|---|---|---|---|---|---|
| 62 | 28.04 | 27.15 | 25.31 | 14.71 | 6.06 | 20.08 | | | | | | | | | |
| 63 | 28.07 | 27.12 | 25.21 | 14.97 | 6.06 | 20.05 | | | | | | | | | |
| 65 | 28.10 | 27.06 | 25.22 | 14.83 | 6.20 | 20.00 | | | | | | | | | |
| 67 | 28.16 | 27.06 | 25.17 | 15.16 | 6.22 | 20.06 | | | | | | | | | |
| 68 | 28.19 | 27.01 | 25.15 | 15.00 | 6.37 | 20.00 | | | | | | | | | |
| 70 | 28.27 | 26.98 | 25.14 | 15.44 | 6.28 | 20.03 | | | | | | | | | |
| 72 | 28.27 | 26.95 | 25.07 | 15.26 | 6.42 | 19.98 | | | | | | | | | |
| 73 | 28.30 | 26.90 | 25.10 | 15.40 | 6.44 | 20.03 | | | | | | | | | |
| 75 | 28.35 | 26.90 | 25.02 | 15.53 | 6.49 | 19.98 | | | | | | | | | |
| 77 | 28.36 | 26.84 | 25.12 | 15.52 | 6.62 | 20.03 | | | | | | | | | |
| 78 | 28.42 | 26.84 | 25.02 | 15.58 | 6.64 | 20.03 | | | | | | | | | |
| 80 | 28.45 | 26.80 | 25.02 | 15.61 | 6.76 | 20.03 | | | | | | | | | |
| 81 | 28.49 | 26.78 | 24.98 | 15.92 | 6.77 | 20.09 | | | | | | | | | |
| 84 | 28.49 | 26.73 | 24.95 | 15.73 | 6.96 | 20.09 | | | | | | | | | |
| 87 | 28.56 | 26.73 | 24.79 | 16.14 | 7.10 | 20.14 | | | | | | | | | |
| 167 | 30.03 | 27.51 | 23.02 | 22.03 | 16.23 | 22.83 | | | | | | | | | |
| 241 | 30.82 | 28.65 | 24.69 | 25.26 | 19.78 | 25.78 | | | | | | | | | |
| 316 | 31.35 | 29.59 | 26.37 | 27.75 | 19.76 | 27.64 | | | | | | | | | |
| 391 | 31.73 | 30.29 | 27.55 | 29.63 | 21.06 | 28.83 | | | | | | | | | |
| 466 | 31.97 | 30.84 | 28.33 | 30.30 | 23.59 | 29.59 | | | | | | | | | |
| 616 | 32.28 | 31.53 | 29.72 | 31.08 | 27.98 | 30.58 | | | | | | | | | |
| 916 | 32.48 | 32.09 | 30.92 | 31.77 | 29.30 | 31.38 | | | | | | | | | |
| 1216 | 32.51 | 32.14 | 31.29 | 31.84 | 29.67 | 31.58 | | | | | | | | | |

Figure A4.PT15a. Clay coating dried on glass plate in drying air at 32 C and low RH.

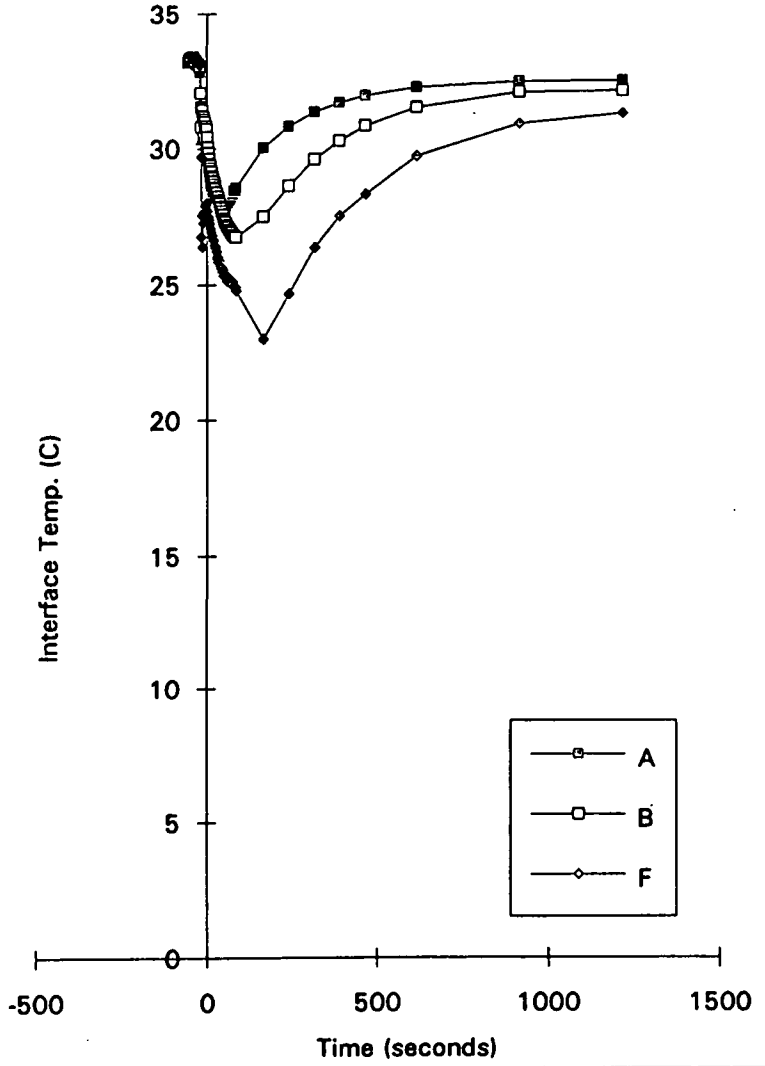


Figure A4.PT15b. Clay coating dried on glass plate in drying air at 32 C and low RH.

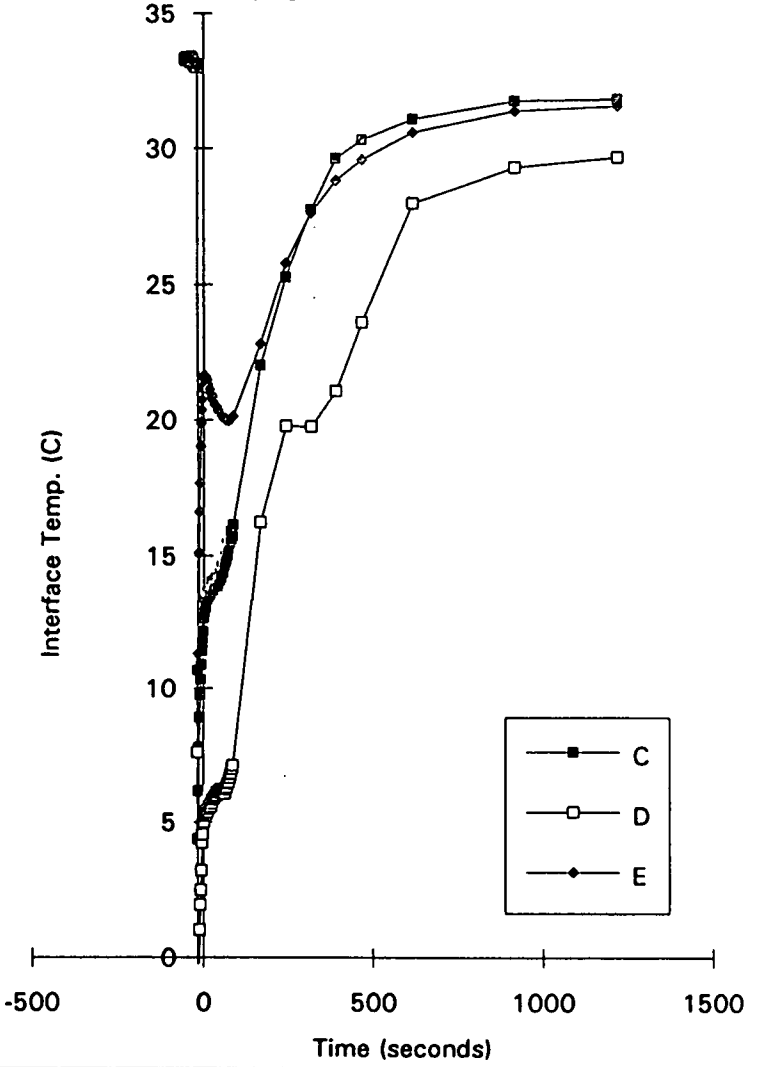

Table A4.PT16. Glass plate temperature during coating and drying at 32 C and 15% RH.

| PT16 Ref. Temp. Resistors Time-sec. | 33 A | 33 B | 33 F | 33 C | 33 D | 33 E | Left Edge |
|---|---|---|---|---|---|---|---|
| -66 | 33.23 | 33.23 | 33.10 | 33.28 | 33.24 | 33.20 | 31.67 |
| -63 | 33.31 | 33.32 | 33.24 | 33.35 | 33.32 | 33.33 | 31.86 |
| -58 | 33.34 | 33.35 | 33.36 | 33.36 | 33.37 | 33.31 | 32.02 |
| -53 | 33.33 | 33.35 | 33.38 | 33.36 | 33.29 | 33.39 | 32.18 |
| -49 | 33.34 | 33.37 | 33.01 | 33.32 | 33.46 | 33.36 | 31.86 |
| -44 | 33.19 | 33.22 | 33.31 | 33.19 | 33.17 | 33.21 | 32.02 |
| -40 | 33.25 | 33.14 | 32.48 | 33.16 | 33.75 | 33.23 | 31.70 |
| -35 | 32.99 | 33.06 | 33.20 | 33.06 | 33.05 | 33.10 | 31.86 |
| -30 | 32.90 | 33.05 | 33.13 | 32.98 | 32.98 | 33.10 | 31.86 |
| -26 | 32.77 | 32.94 | 33.08 | 32.95 | 32.90 | 32.99 | 32.18 |
| -21 | 28.67 | 29.98 | 33.05 | 24.70 | 22.75 | 24.84 | 31.99 |
| -17 | 29.12 | 27.47 | 29.26 | 9.38 | 2.81 | 23.30 | 32.02 |
| -12 | 29.01 | 27.80 | 25.44 | 12.90 | 4.46 | 21.24 | 31.55 |
| -7 | 28.61 | 28.12 | 25.08 | 13.75 | 6.46 | 21.67 | 31.86 |
| -3 | 28.90 | 28.81 | 25.05 | 14.63 | 7.79 | 21.83 | 31.86 |
| 2 | 28.60 | 28.79 | 24.86 | 14.71 | 7.98 | 21.35 | 32.02 |
| 6 | 27.46 | 27.90 | 23.65 | 13.86 | 7.42 | 20.02 | 30.46 |
| 11 | 26.85 | 27.33 | 23.22 | 13.62 | 7.42 | 19.32 | 28.57 |
| 16 | 26.62 | 27.03 | 22.78 | 13.62 | 7.57 | 18.86 | 27.98 |
| 20 | 26.46 | 26.66 | 22.36 | 13.56 | 7.72 | 18.41 | 27.98 |
| 25 | 26.35 | 26.41 | 21.93 | 13.44 | 7.81 | 18.07 | 27.20 |
| 29 | 26.54 | 26.40 | 21.59 | 13.65 | 7.98 | 17.82 | 27.20 |
| 34 | 26.46 | 26.09 | 21.40 | 13.56 | 8.10 | 17.56 | 27.20 |
| 39 | 26.55 | 26.06 | 21.50 | 13.72 | 8.28 | 17.42 | 26.88 |
| 43 | 26.46 | 25.75 | 21.13 | 13.77 | 8.33 | 17.24 | 26.41 |
| 48 | 26.54 | 25.69 | 21.04 | 13.97 | 8.35 | 17.10 | 26.09 |
| 52 | 26.49 | 25.48 | 21.16 | 14.10 | 8.28 | 17.07 | 25.93 |
| 57 | 26.57 | 25.37 | 21.06 | 14.12 | 7.66 | 16.92 | 25.77 |
| 62 | 26.63 | 25.23 | 20.99 | 14.20 | 7.08 | 16.84 | 25.61 |
| 66 | 26.62 | 24.95 | 20.75 | 14.05 | 6.83 | 16.73 | 25.77 |
| 71 | 26.72 | 24.82 | 20.63 | 14.10 | 6.74 | 16.70 | 25.42 |
| 76 | 26.92 | 24.99 | 20.63 | 14.47 | 6.74 | 16.75 | 25.30 |
| 80 | 26.89 | 24.79 | 20.49 | 14.39 | 6.79 | 16.70 | 24.95 |
| 85 | 27.06 | 24.76 | 20.32 | 14.57 | 7.01 | 16.73 | 24.98 |
| 89 | 27.17 | 24.91 | 20.66 | 14.89 | 7.35 | 16.73 | 24.79 |

| Time sec. | A | B | F | C | D | E | Left Edge |
|---|---|---|---|---|---|---|---|
| 94 | 27.15 | 24.71 | 20.61 | 14.73 | 7.23 | 16.73 | 24.82 |
| 99 | 27.14 | 24.60 | 20.57 | 14.71 | 7.18 | 16.70 | 24.82 |
| 103 | 27.17 | 24.56 | 20.68 | 14.66 | 7.30 | 16.71 | 24.82 |
| 108 | 27.14 | 24.46 | 20.40 | 14.58 | 7.66 | 16.78 | 24.50 |
| 112 | 27.31 | 24.59 | 20.42 | 14.68 | 8.23 | 16.83 | 24.50 |
| 117 | 27.41 | 24.77 | 20.73 | 15.02 | 8.94 | 16.86 | 24.19 |
| 122 | 27.43 | 24.71 | 20.63 | 14.95 | 9.64 | 16.83 | 24.19 |
| 126 | 27.66 | 25.02 | 20.80 | 15.37 | 10.45 | 17.00 | 24.03 |
| 131 | 27.66 | 25.02 | 20.87 | 15.40 | 11.24 | 16.97 | 24.03 |
| 135 | 27.71 | 25.11 | 21.09 | 15.68 | 12.11 | 17.03 | 24.35 |
| 140 | 27.81 | 25.19 | 21.19 | 16.11 | 12.94 | 17.18 | 24.50 |
| 145 | 27.61 | 24.91 | 20.92 | 16.17 | 13.63 | 17.29 | 24.66 |
| 149 | 27.74 | 25.02 | 21.04 | 16.69 | 14.41 | 17.47 | 24.82 |
| 211 | 28.47 | 26.03 | 22.43 | 21.79 | 19.01 | 21.06 | 25.79 |
| 286 | 28.87 | 27.02 | 24.27 | 24.43 | 19.28 | 23.39 | 26.81 |
| 361 | 28.90 | 27.38 | 24.95 | 26.10 | 20.35 | 25.16 | 28.23 |
| 436 | 29.14 | 27.90 | 25.89 | 27.10 | 23.13 | 27.04 | 29.24 |
| 616 | 29.36 | 28.76 | 27.33 | 28.36 | 27.57 | 29.12 | 30.45 |
| 917 | 29.54 | 29.35 | 28.61 | 29.23 | 28.91 | 30.19 | 30.94 |
| 1216 | 29.67 | 29.47 | 29.07 | 29.56 | 29.27 | 30.56 | 31.22 |

Figure A4.PT16a. Clay coating dried on glass plate in drying air at 32 C and low RH.

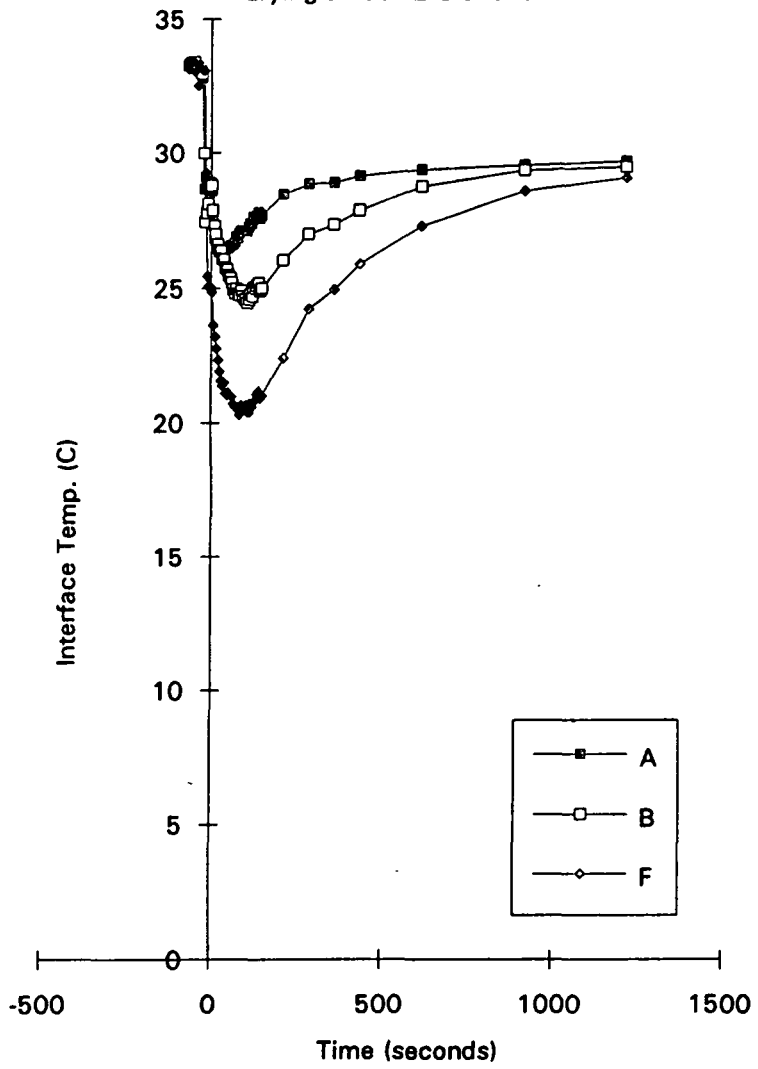


Figure A4.PT16b. Clay coating dried on glass plate in drying air at 32 C and low RH.

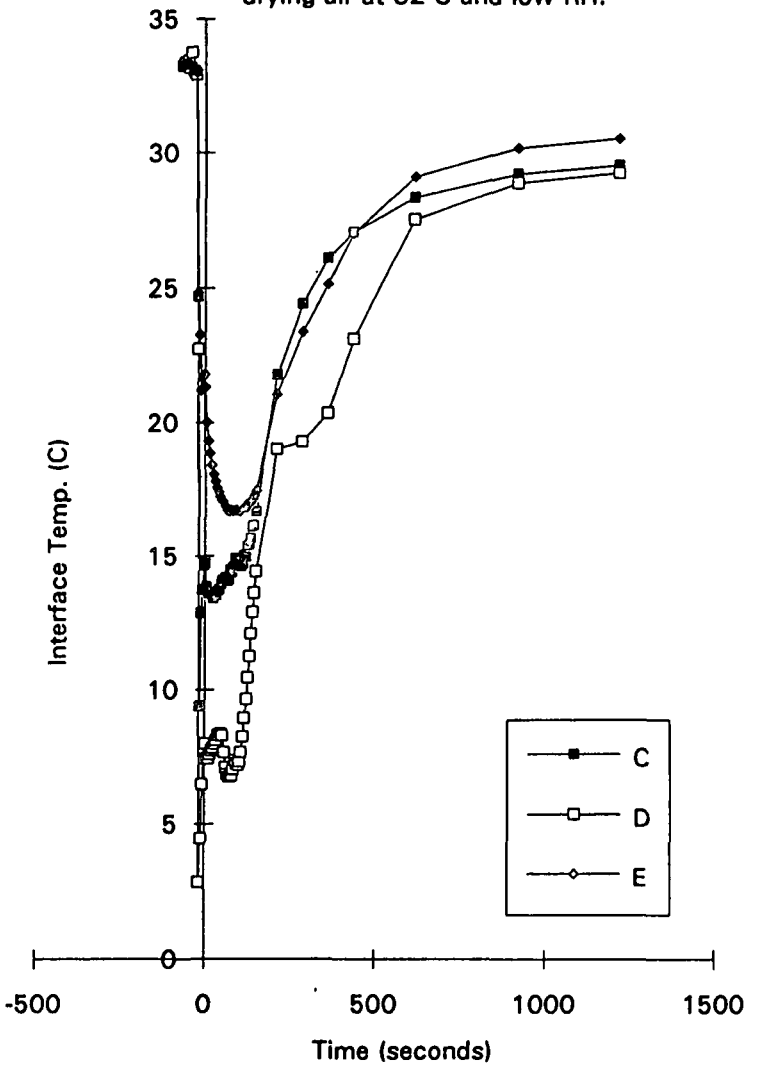

Table A4.PT17. Glass plate temperature during coating and drying at 54 C and 15% RH.

| PT17 Ref. Temp. Resistors Time-sec. | 54 A | 54 B | 54 F | 54 C. | 54 D | 54 E | Left Edge |
|---|---|---|---|---|---|---|---|
| -78 | 53.99 | 54.02 | 54.00 | 54.01 | 53.98 | 53.99 | 54.08 |
| -70 | 54.02 | 54.01 | 54.05 | 54.01 | 54.03 | 53.99 | 54.015 |
| -65 | 53.85 | 53.87 | 53.72 | 53.83 | 53.86 | 53.87 | 54.167 |
| -60 | 53.68 | 53.71 | 53.67 | 53.64 | 53.71 | 53.67 | 54.015 |
| -55 | 53.54 | 53.59 | 53.45 | 53.51 | 53.56 | 53.59 | 54.167 |
| -51 | 53.28 | 53.33 | 53.26 | 53.29 | 53.32 | 53.29 | 54.167 |
| -46 | 53.08 | 53.12 | 53.05 | 53.13 | 53.17 | 53.13 | 54.167 |
| -42 | 52.91 | 52.90 | 52.90 | 53.03 | 52.95 | 52.89 | 54.62 |
| -37 | 52.65 | 52.66 | 52.47 | 52.78 | 52.64 | 52.59 | 54.318 |
| -32 | 52.25 | 52.27 | 52.25 | 52.42 | 52.31 | 52.27 | 54.318 |
| -28 | 51.99 | 52.00 | 51.85 | 52.15 | 52.00 | 51.99 | 54.167 |
| -23 | 51.65 | 51.69 | 51.63 | 51.84 | 51.53 | 51.64 | 54.012 |
| -18 | 51.21 | 50.92 | 50.78 | 51.33 | 50.90 | 51.05 | 54.015 |
| -14 | 49.50 | 49.26 | 49.35 | 50.11 | 49.43 | 49.69 | 54.015 |
| -9 | 48.21 | 47.85 | 47.34 | 48.91 | 48.06 | 48.25 | 54.318 |
| -4 | 48.06 | 47.36 | 46.96 | 48.18 | 47.50 | 47.63 | 54.048 |
| 0 | 46.31 | 46.38 | 46.81 | 47.30 | 46.81 | 46.59 | 50.452 |
| 5 | 42.44 | 43.15 | 44.81 | 44.53 | 44.17 | 43.76 | 41.645 |
| 9 | 41.23 | 41.91 | 43.80 | 43.37 | 43.05 | 42.66 | 40.718 |
| 14 | 41.46 | 41.17 | 43.14 | 42.58 | 42.36 | 41.94 | 39.635 |
| 19 | 43.58 | 40.51 | 42.47 | 42.07 | 41.65 | 41.44 | 39.017 |
| 23 | 44.99 | 40.85 | 42.01 | 41.48 | 41.12 | 40.88 | 38.553 |
| 28 | 45.62 | 42.08 | 41.46 | 41.04 | 40.48 | 40.52 | 37.934 |
| 32 | 45.97 | 43.09 | 40.91 | 40.54 | 40.68 | 40.07 | 37.471 |
| 37 | 46.23 | 43.55 | 40.51 | 40.19 | 41.97 | 39.75 | 37.316 |
| 42 | 46.39 | 43.89 | 40.80 | 39.85 | 42.88 | 39.59 | 36.698 |
| 46 | 46.57 | 44.10 | 41.78 | 40.01 | 43.46 | 39.86 | 36.543 |
| 51 | 46.75 | 44.35 | 42.39 | 40.51 | 43.88 | 40.36 | 35.77 |
| 55 | 46.82 | 44.41 | 42.61 | 41.17 | 44.00 | 40.95 | 35.77 |
| 60 | 46.89 | 44.49 | 42.73 | 41.78 | 44.13 | 41.47 | 35.149 |
| 65 | 47.05 | 44.59 | 42.89 | 42.17 | 44.32 | 41.87 | 35.614 |
| 69 | 47.18 | 44.67 | 42.97 | 42.53 | 44.37 | 42.23 | 36.234 |
| 74 | 47.31 | 44.84 | 43.09 | 42.76 | 44.56 | 42.45 | 37.007 |
| 78 | 47.42 | 44.92 | 43.14 | 42.97 | 44.66 | 42.67 | 37.625 |
| 85 | 47.46 | 44.99 | 43.18 | 43.24 | 44.64 | 42.90 | 38.553 |

| Time sec. | A | B | F | C | D | E | Left Edge |
|---|---|---|---|---|---|---|---|
| 94 | 47.72 | 45.21 | 43.37 | 43.50 | 44.93 | 43.15 | 39.513 |
| 104 | 47.97 | 45.44 | 43.44 | 43.82 | 45.12 | 43.47 | 39.977 |
| 113 | 48.21 | 45.65 | 43.56 | 44.08 | 45.27 | 43.73 | 40.506 |
| 123 | 48.47 | 45.91 | 43.71 | 44.30 | 45.50 | 43.97 | 41.027 |
| 132 | 48.61 | 46.05 | 43.90 | 44.61 | 45.66 | 44.24 | 41.523 |
| 142 | 48.80 | 46.25 | 43.99 | 44.85 | 45.77 | 44.53 | 41.645 |
| 151 | 49.00 | 46.45 | 44.07 | 45.09 | 45.94 | 44.78 | 42.264 |
| 161 | 49.10 | 46.59 | 44.21 | 45.34 | 46.05 | 45.04 | 42.573 |
| 170 | 49.33 | 46.76 | 44.45 | 45.57 | 46.28 | 45.23 | 42.882 |
| 180 | 49.53 | 47.00 | 44.50 | 45.76 | 46.43 | 45.47 | 43.566 |
| 189 | 49.63 | 47.10 | 44.59 | 46.02 | 46.45 | 45.73 | 43.534 |
| 199 | 49.70 | 47.20 | 44.74 | 46.27 | 46.57 | 45.94 | 43.81 |
| 208 | 49.84 | 47.33 | 44.97 | 46.47 | 46.77 | 46.11 | 44.307 |
| 218 | 49.99 | 47.51 | 44.98 | 46.61 | 46.96 | 46.29 | 44.738 |
| 227 | 50.13 | 47.68 | 45.05 | 46.79 | 47.03 | 46.51 | 44.893 |
| 237 | 50.24 | 47.76 | 45.28 | 47.03 | 47.21 | 46.69 | 45.234 |
| 246 | 50.36 | 47.88 | 45.29 | 47.19 | 47.26 | 46.89 | 45.356 |
| 256 | 50.44 | 47.99 | 45.48 | 47.41 | 47.42 | 47.05 | 45.511 |
| 265 | 50.61 | 48.14 | 45.54 | 47.54 | 47.53 | 47.23 | 45.82 |
| 275 | 50.67 | 48.25 | 45.60 | 47.69 | 47.64 | 47.41 | 46.162 |
| 284 | 50.75 | 48.39 | 45.71 | 47.86 | 47.70 | 47.55 | 46.317 |
| 294 | 50.78 | 48.39 | 45.91 | 48.06 | 47.82 | 47.69 | 46.593 |
| 406 | 51.64 | 49.40 | 46.82 | 49.37 | 48.86 | 49.15 | 48.432 |
| 585 | 52.18 | 50.25 | 47.93 | 50.74 | 49.88 | 50.50 | 49.9 |
| 765 | 52.48 | 50.82 | 48.63 | 51.40 | 50.55 | 51.18 | 50.431 |
| 946 | 52.65 | 50.97 | 48.93 | 51.61 | 50.74 | 51.50 | 51.093 |
| 1186 | 52.92 | 51.41 | 49.33 | 52.00 | 51.17 | 51.87 | 51.139 |

Figure A4.PT17a. Clay coating dried on glass plate in drying air at 54 C and low RH.

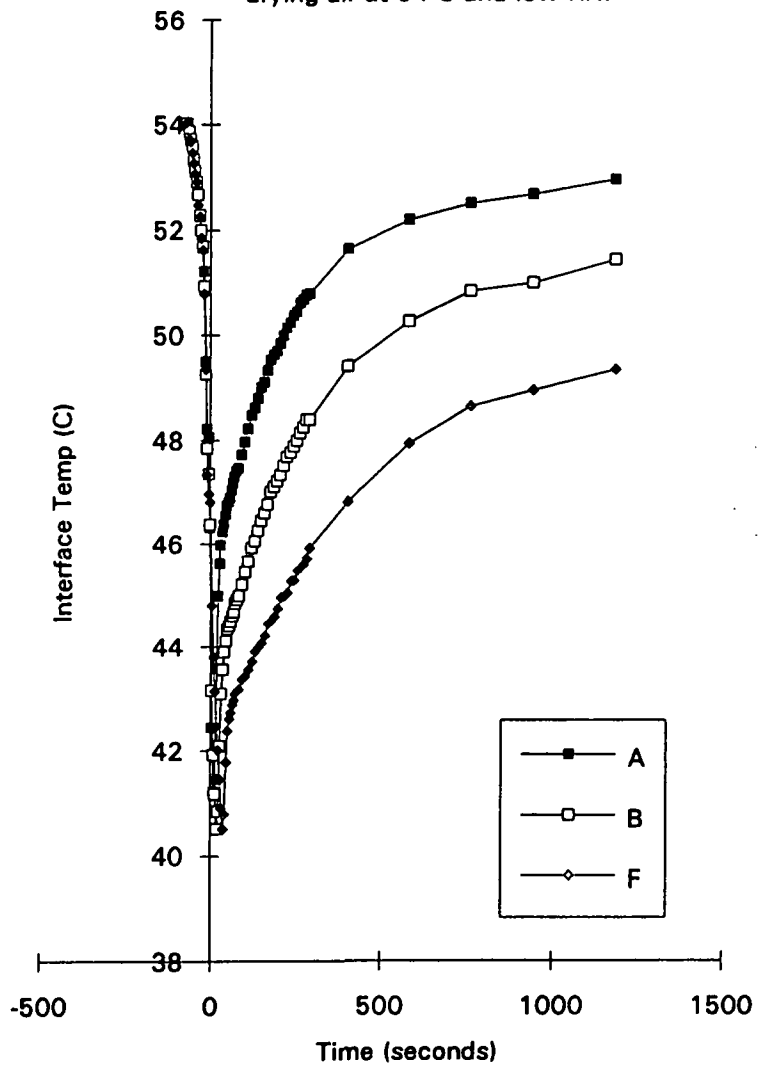


Figure A4.PT17b. Clay coating dried on glass plate in drying air at 54 C and low RH.

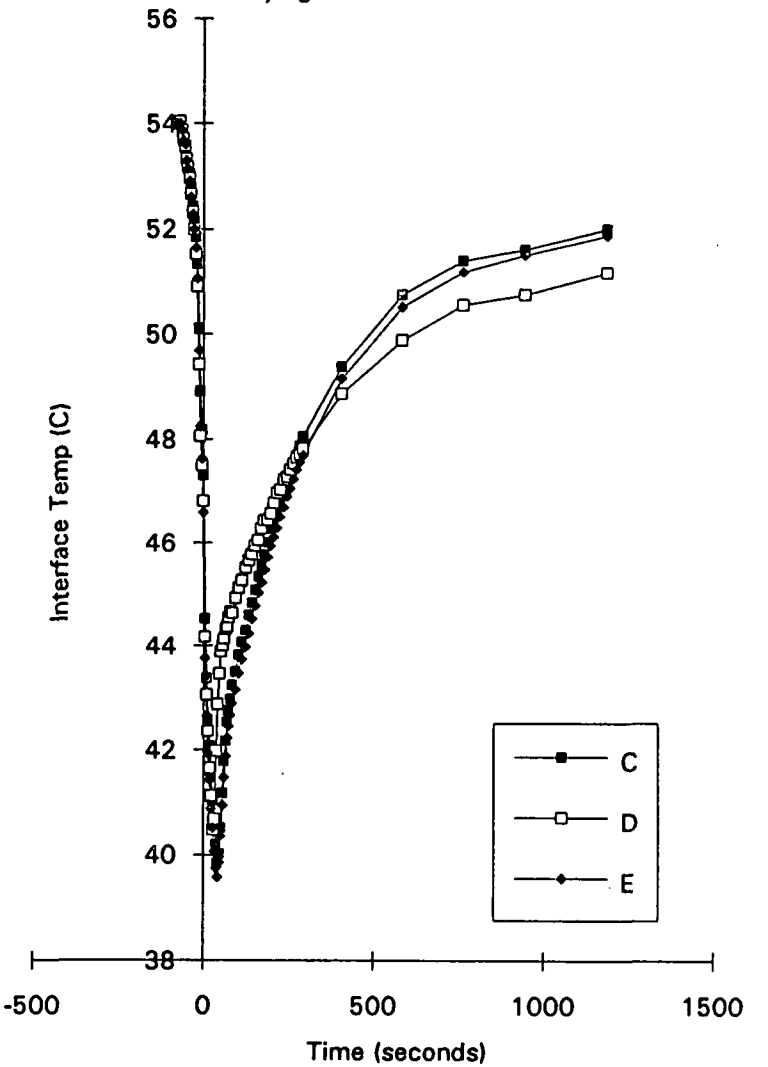

Table A4.PT18. Glass plate temperature during coating and drying at 55 C and 15% RH.

| PT18 Ref. Temp. Resistors Time-sec. | 54 A | 54 B | 54 F | 54 C | 54 D | 54 E | Left Edge |
|---|---|---|---|---|---|---|---|
| -75 | 54.00 | 54.00 | 54.03 | 53.98 | 54.00 | 54.00 | 54.78 |
| -70 | 54.00 | 54.00 | 53.97 | 54.02 | 54.00 | 54.00 | 54.56 |
| -65 | 53.80 | 53.77 | 53.80 | 53.82 | 53.81 | 53.82 | 54.56 |
| -60 | 53.69 | 53.63 | 53.70 | 53.65 | 53.70 | 53.71 | 54.56 |
| -56 | 53.55 | 53.49 | 53.53 | 53.48 | 53.51 | 53.50 | 54.75 |
| -51 | 53.23 | 53.22 | 53.23 | 53.16 | 53.20 | 53.26 | 54.72 |
| -46 | 53.06 | 52.97 | 53.10 | 53.03 | 53.02 | 53.06 | 55.02 |
| -42 | 52.76 | 52.71 | 52.72 | 52.76 | 52.65 | 52.74 | 54.75 |
| -37 | 52.40 | 52.31 | 52.44 | 52.48 | 52.31 | 52.42 | 54.72 |
| -33 | 52.11 | 51.94 | 51.72 | 52.16 | 51.80 | 51.91 | 54.56 |
| -28 | 51.73 | 51.57 | 51.41 | 51.84 | 51.46 | 51.41 | 54.41 |
| -23 | 51.14 | 50.62 | 49.86 | 50.97 | 50.26 | 50.48 | 54.72 |
| -19 | 49.81 | 49.04 | 48.80 | 49.96 | 49.11 | 49.28 | 54.56 |
| -14 | 48.55 | 48.00 | 48.09 | 48.86 | 48.01 | 47.94 | 54.41 |
| -10 | 47.50 | 47.18 | 47.18 | 48.41 | 47.42 | 47.54 | 54.41 |
| -5 | 47.11 | 47.00 | 46.71 | 47.88 | 46.96 | 47.09 | 54.56 |
| 0 | 44.99 | 45.34 | 45.89 | 46.40 | 45.83 | 46.10 | 48.39 |
| 4 | 41.79 | 42.71 | 44.32 | 44.20 | 43.70 | 43.66 | 41.12 |
| 9 | 40.86 | 41.56 | 43.32 | 43.14 | 42.73 | 42.73 | 39.89 |
| 13 | 41.01 | 41.07 | 42.91 | 42.80 | 42.21 | 42.12 | 39.11 |
| 18 | 42.79 | 40.38 | 42.26 | 41.97 | 41.63 | 41.59 | 38.34 |
| 23 | 44.13 | 39.94 | 41.71 | 41.44 | 41.19 | 41.15 | 38.19 |
| 27 | 44.77 | 40.70 | 41.19 | 40.99 | 40.74 | 40.79 | 37.72 |
| 32 | 45.37 | 42.21 | 40.88 | 40.94 | 40.85 | 40.41 | 37.57 |
| 36 | 45.45 | 42.82 | 40.59 | 40.25 | 41.97 | 40.07 | 37.57 |
| 41 | 45.77 | 43.37 | 41.02 | 40.16 | 43.04 | 39.95 | 36.80 |
| 46 | 45.83 | 43.51 | 41.78 | 39.87 | 43.49 | 40.03 | 36.49 |
| 55 | 46.05 | 43.82 | 42.52 | 40.65 | 43.95 | 40.86 | 36.12 |
| 64 | 46.52 | 44.28 | 43.01 | 42.08 | 44.37 | 41.88 | 36.40 |
| 74 | 46.84 | 44.59 | 43.10 | 42.85 | 44.63 | 42.60 | 37.67 |
| 83 | 46.98 | 44.74 | 43.13 | 43.08 | 44.81 | 43.02 | 39.06 |
| 93 | 47.20 | 44.93 | 43.46 | 43.53 | 45.08 | 43.40 | 39.95 |
| 102 | 47.61 | 45.34 | 43.48 | 43.94 | 45.27 | 43.70 | 40.14 |
| 112 | 47.78 | 45.48 | 43.50 | 44.02 | 45.44 | 43.99 | 41.07 |
| 121 | 48.01 | 45.69 | 43.65 | 44.28 | 45.63 | 44.23 | 41.34 |

| Time sec. | A | B | F | C | D | E | Left Edge |
|---|---|---|---|---|---|---|---|
| 131 | 48.33 | 46.03 | 44.06 | 44.87 | 45.88 | 44.52 | 41.38 |
| 140 | 48.67 | 46.34 | 44.13 | 45.28 | 46.12 | 44.79 | 41.81 |
| 150 | 48.84 | 46.52 | 44.25 | 45.44 | 46.30 | 45.05 | 42.31 |
| 159 | 48.92 | 46.58 | 44.37 | 45.52 | 46.39 | 45.30 | 42.92 |
| 169 | 49.13 | 46.88 | 44.67 | 45.95 | 46.61 | 45.56 | 43.08 |
| 178 | 49.39 | 47.11 | 44.67 | 46.26 | 46.81 | 45.81 | 43.51 |
| 188 | 49.55 | 47.29 | 44.72 | 46.32 | 46.89 | 46.02 | 43.82 |
| 197 | 49.64 | 47.38 | 45.03 | 46.59 | 47.10 | 46.28 | 44.01 |
| 207 | 49.88 | 47.69 | 45.29 | 47.04 | 47.30 | 46.44 | 44.62 |
| 216 | 50.02 | 47.84 | 45.35 | 47.15 | 47.44 | 46.71 | 45.06 |
| 226 | 50.16 | 48.01 | 45.47 | 47.41 | 47.60 | 46.92 | 45.09 |
| 236 | 50.30 | 48.13 | 45.58 | 47.60 | 47.74 | 47.16 | 45.36 |
| 405 | 51.92 | 50.15 | 47.51 | 50.27 | 49.81 | 49.95 | 48.76 |
| 585 | 52.56 | 51.21 | 48.74 | 51.63 | 50.95 | 51.40 | 50.43 |
| 765 | 52.91 | 51.76 | 49.69 | 52.38 | 51.56 | 52.04 | 51.29 |
| 945 | 53.06 | 52.01 | 49.96 | 52.57 | 51.83 | 52.42 | 51.47 |
| 1185 | 52.91 | 51.90 | 50.02 | 52.61 | 51.91 | 52.43 | 51.43 |

Figure A4.PT18a. Clay coating dried on glass plate in drying air at 55 C and low RH.

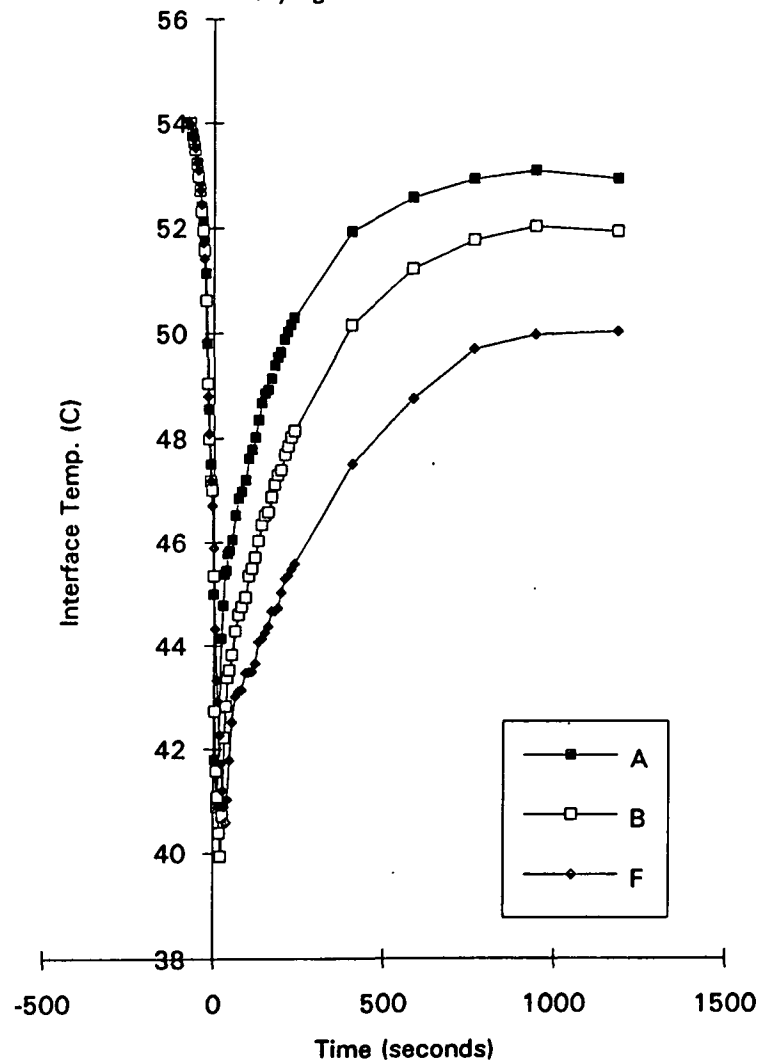


Figure A4.PT18b. Clay coating dried on glass plate in drying air at 55 C and low RH.

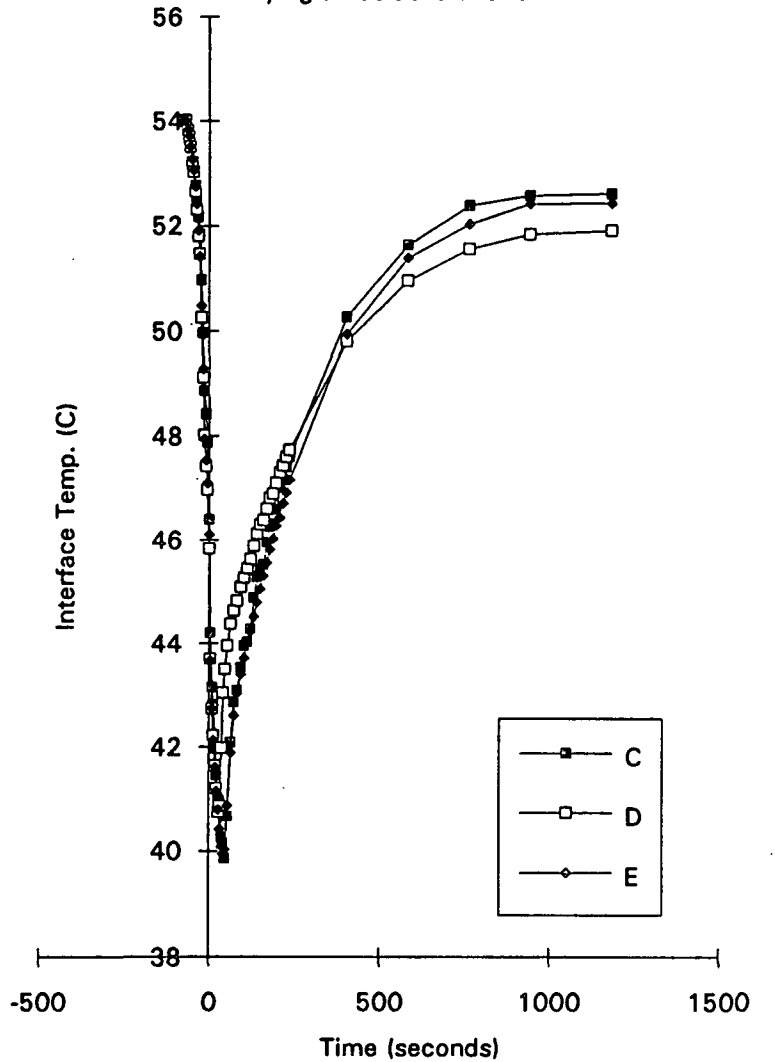

Table A4.PT19. Glass plate temperature during coating and drying at 55 C and 15% RH.

| PT19 Ref. Temp. Resistors Time-sec. | 54 A | 54 B | 54 F | 54 C | 54 D | 54 E | Left Edge |
|---|---|---|---|---|---|---|---|
| -70 | 54.04 | 54.03 | 54.05 | 54.04 | 54.02 | 54.02 | 55.23 |
| -61 | 53.98 | 54.00 | 54.01 | 54.01 | 54.02 | 54.00 | 55.23 |
| -56 | 53.80 | 53.82 | 53.72 | 53.80 | 53.80 | 53.84 | 54.93 |
| -52 | 53.67 | 53.65 | 53.60 | 53.64 | 53.66 | 53.68 | 54.90 |
| -47 | 53.47 | 53.40 | 53.31 | 53.42 | 53.44 | 53.49 | 54.75 |
| -43 | 53.20 | 53.13 | 52.96 | 53.14 | 53.20 | 53.17 | 54.93 |
| -38 | 53.01 | 52.96 | 52.72 | 52.98 | 52.97 | 53.08 | 54.75 |
| -33 | 52.78 | 52.67 | 52.55 | 52.79 | 52.83 | 52.79 | 54.78 |
| -29 | 52.48 | 52.37 | 52.10 | 52.52 | 52.51 | 52.52 | 54.60 |
| -24 | 52.28 | 52.04 | 51.81 | 52.34 | 52.00 | 52.09 | 54.63 |
| -20 | 51.72 | 51.02 | 50.42 | 51.52 | 50.99 | 51.09 | 55.08 |
| -15 | 50.51 | 49.86 | 49.47 | 50.53 | 49.94 | 49.98 | 54.93 |
| -10 | 49.53 | 48.80 | 48.63 | 49.60 | 49.06 | 49.06 | 54.78 |
| -6 | 48.79 | 47.74 | 47.72 | 48.54 | 48.03 | 48.22 | 54.90 |
| -1 | 48.05 | 47.58 | 47.82 | 48.39 | 47.96 | 48.25 | 54.33 |
| 3 | 43.59 | 44.04 | 45.48 | 45.29 | 45.05 | 45.15 | 42.89 |
| 8 | 42.02 | 42.62 | 44.21 | 43.86 | 43.80 | 43.77 | 41.01 |
| 13 | 41.64 | 41.76 | 43.50 | 43.14 | 43.02 | 43.00 | 40.30 |
| 17 | 43.48 | 41.17 | 42.85 | 42.45 | 42.50 | 42.37 | 39.61 |
| 22 | 45.17 | 40.95 | 42.42 | 42.08 | 41.92 | 41.92 | 38.94 |
| 27 | 45.95 | 42.13 | 41.85 | 41.62 | 41.38 | 41.52 | 38.41 |
| 31 | 46.36 | 43.39 | 41.31 | 41.15 | 41.53 | 41.09 | 37.91 |
| 36 | 46.67 | 44.14 | 40.83 | 40.70 | 42.77 | 40.69 | 38.29 |
| 40 | 46.86 | 44.47 | 40.85 | 40.53 | 43.85 | 40.37 | 37.45 |
| 45 | 47.02 | 44.62 | 41.88 | 41.09 | 44.37 | 40.41 | 37.17 |
| 50 | 47.16 | 44.85 | 42.61 | 41.73 | 44.68 | 40.89 | 36.40 |
| 54 | 47.30 | 44.94 | 43.05 | 42.53 | 44.88 | 41.52 | 36.21 |
| 59 | 47.45 | 45.13 | 43.24 | 42.98 | 44.98 | 42.17 | 36.59 |
| 68 | 47.67 | 45.27 | 43.47 | 43.54 | 45.20 | 42.94 | 37.24 |
| 78 | 47.95 | 45.51 | 43.65 | 43.96 | 45.41 | 43.47 | 39.09 |
| 87 | 48.18 | 45.76 | 43.74 | 44.23 | 45.61 | 43.82 | 40.49 |
| 97 | 48.42 | 45.99 | 43.96 | 44.51 | 45.91 | 44.12 | 40.80 |
| 106 | 48.64 | 46.22 | 44.14 | 44.80 | 46.08 | 44.41 | 41.57 |
| 116 | 48.91 | 46.46 | 44.27 | 45.04 | 46.20 | 44.73 | 41.88 |
| 125 | 49.14 | 46.59 | 44.41 | 45.34 | 46.30 | 44.97 | 42.50 |

| Time sec. | A | B | F | C | D | E | Left Edge |
|---|---|---|---|---|---|---|---|
| 135 | 49.33 | 46.82 | 44.65 | 45.60 | 46.57 | 45.26 | 42.96 |
| 144 | 49.54 | 47.02 | 44.76 | 45.82 | 46.71 | 45.53 | 43.11 |
| 154 | 49.76 | 47.23 | 44.93 | 46.13 | 46.86 | 45.82 | 43.58 |
| 163 | 49.99 | 47.48 | 45.00 | 46.27 | 47.05 | 46.03 | 43.89 |
| 173 | 50.13 | 47.66 | 45.17 | 46.47 | 47.27 | 46.25 | 44.35 |
| 182 | 50.26 | 47.81 | 45.36 | 46.71 | 47.44 | 46.49 | 44.66 |
| 192 | 50.43 | 47.98 | 45.44 | 46.95 | 47.54 | 46.70 | 44.97 |
| 201 | 50.59 | 48.11 | 45.60 | 47.20 | 47.66 | 46.95 | 45.28 |
| 211 | 50.65 | 48.18 | 45.77 | 47.48 | 47.77 | 47.13 | 45.59 |
| 221 | 50.82 | 48.37 | 45.91 | 47.64 | 47.96 | 47.34 | 45.74 |
| 230 | 50.94 | 48.52 | 46.06 | 47.81 | 48.16 | 47.55 | 46.21 |
| 406 | 52.60 | 50.58 | 47.99 | 50.59 | 50.18 | 50.32 | 49.41 |
| 586 | 53.27 | 51.55 | 49.18 | 52.07 | 51.35 | 51.63 | 50.61 |
| 766 | 53.45 | 51.91 | 49.86 | 52.64 | 51.91 | 52.25 | 51.34 |
| 946 | 53.38 | 51.97 | 50.19 | 52.63 | 51.97 | 52.52 | 51.86 |
| 1186 | 53.48 | 52.14 | 50.42 | 52.89 | 52.23 | 52.65 | 51.83 |

Figure A4.PT19a. Clay coating dried on glass plate in drying air at 55 C and low RH.

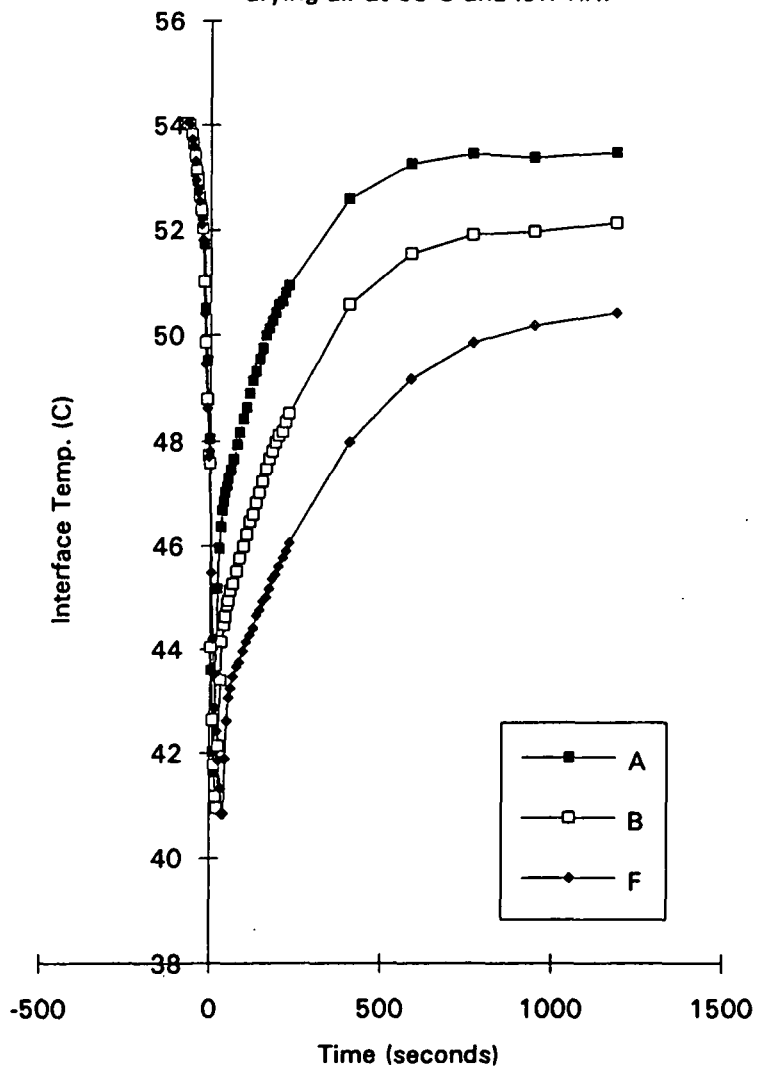


Figure A4.PT19b. Clay coating dried on glass plate in drying air at 55 C and low RH.

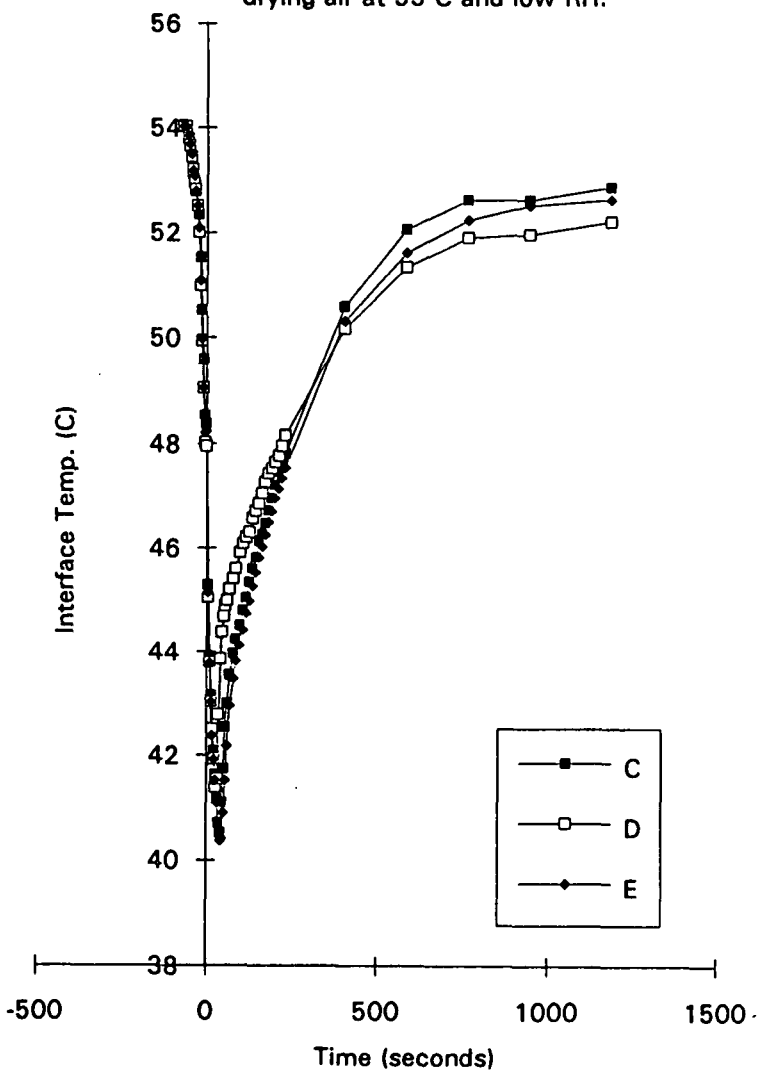

Table A4.PT20. Glass plate temperature during coating and drying at 55 C and 25% RH.

| PT20 Ref. Temp. Resistors Time-sec. | 54 A | 54 B | 54 F | 54 C | 54 D | 54 E | Left Edge |
|---|---|---|---|---|---|---|---|
| -72 | 54.00 | 54.04 | 54.03 | 54.03 | 54.03 | 54.03 | 54.11 |
| -63 | 54.02 | 53.99 | 53.99 | 54.00 | 54.01 | 54.01 | 54.11 |
| -58 | 53.98 | 53.97 | 53.98 | 53.97 | 53.96 | 53.96 | 53.92 |
| -53 | 53.83 | 53.82 | 53.74 | 53.74 | 53.77 | 53.77 | 53.61 |
| -49 | 53.63 | 53.56 | 53.67 | 53.53 | 53.59 | 53.58 | 53.92 |
| -44 | 53.36 | 53.34 | 53.93 | 53.31 | 53.35 | 53.29 | 53.61 |
| -40 | 53.12 | 53.10 | 53.03 | 53.09 | 53.13 | 53.15 | 53.77 |
| -35 | 52.94 | 52.96 | 52.81 | 52.89 | 52.93 | 52.94 | 53.77 |
| -30 | 52.68 | 52.56 | 52.58 | 52.65 | 52.67 | 52.70 | 53.77 |
| -26 | 52.37 | 52.29 | 52.29 | 52.35 | 52.25 | 52.27 | 53.61 |
| -21 | 52.03 | 51.87 | 51.74 | 52.01 | 51.79 | 51.72 | 53.92 |
| -17 | 50.71 | 50.21 | 50.07 | 50.58 | 50.22 | 50.32 | 53.92 |
| -12 | 49.82 | 49.41 | 49.21 | 49.83 | 49.41 | 49.36 | 53.92 |
| -7 | 48.83 | 48.48 | 48.21 | 48.88 | 48.28 | 48.61 | 53.80 |
| -3 | 48.41 | 48.00 | 47.51 | 48.53 | 47.82 | 48.14 | 54.07 |
| 2 | 47.17 | 47.31 | 47.53 | 48.21 | 47.60 | 47.79 | 51.28 |
| 6 | 44.50 | 44.81 | 46.13 | 45.81 | 45.57 | 45.65 | 43.41 |
| 11 | 43.80 | 43.95 | 45.48 | 45.03 | 44.79 | 44.87 | 42.48 |
| 16 | 43.60 | 43.58 | 45.06 | 44.63 | 44.42 | 44.43 | 41.89 |
| 20 | 43.68 | 43.21 | 44.67 | 44.34 | 44.06 | 44.13 | 41.89 |
| 25 | 44.73 | 42.87 | 44.27 | 44.05 | 43.78 | 43.87 | 41.74 |
| 29 | 45.95 | 42.75 | 44.07 | 43.81 | 43.59 | 43.65 | 41.12 |
| 34 | 46.51 | 42.78 | 43.76 | 43.60 | 43.35 | 43.41 | 40.93 |
| 39 | 46.89 | 43.35 | 43.53 | 43.39 | 43.18 | 43.20 | 40.63 |
| 43 | 47.18 | 44.10 | 43.33 | 43.23 | 43.06 | 42.98 | 40.63 |
| 48 | 47.24 | 44.45 | 42.95 | 43.04 | 43.13 | 42.85 | 40.19 |
| 52 | 47.50 | 44.82 | 42.81 | 42.86 | 43.72 | 42.63 | 40.38 |
| 57 | 47.54 | 44.93 | 42.59 | 42.67 | 44.27 | 42.52 | 40.32 |
| 62 | 47.75 | 45.19 | 42.71 | 42.60 | 44.72 | 42.37 | 40.23 |
| 66 | 47.86 | 45.28 | 42.90 | 42.65 | 44.89 | 42.34 | 40.04 |
| 71 | 48.01 | 45.42 | 43.24 | 42.86 | 45.11 | 42.32 | 39.70 |
| 80 | 48.20 | 45.61 | 43.55 | 43.37 | 45.37 | 42.58 | 39.54 |
| 89 | 48.40 | 45.73 | 43.71 | 43.94 | 45.55 | 43.11 | 39.14 |
| 99 | 48.60 | 45.91 | 43.88 | 44.37 | 45.70 | 43.67 | 39.02 |
| 108 | 48.79 | 46.11 | 44.10 | 44.71 | 45.92 | 44.10 | 39.61 |

| Time sec. | A | B | F | C | D | E | Left Edge |
|---|---|---|---|---|---|---|---|
| 118 | 49.04 | 46.37 | 44.26 | 45.03 | 46.16 | 44.40 | 40.72 |
| 127 | 49.27 | 46.67 | 44.32 | 45.28 | 46.30 | 44.72 | 41.46 |
| 137 | 49.49 | 46.80 | 44.51 | 45.54 | 46.47 | 45.01 | 42.42 |
| 146 | 49.64 | 47.00 | 44.69 | 45.77 | 46.65 | 45.27 | 43.01 |
| 184 | 50.13 | 47.71 | 44.48 | 46.57 | 47.36 | 46.21 | 44.56 |
| 194 | 50.24 | 47.86 | 44.77 | 46.79 | 47.55 | 46.48 | 44.71 |
| 203 | 50.42 | 47.97 | 44.91 | 47.07 | 47.70 | 46.67 | 44.95 |
| 213 | 50.45 | 48.12 | 45.05 | 47.13 | 47.63 | 46.86 | 45.48 |
| 222 | 50.61 | 48.22 | 45.20 | 47.39 | 47.90 | 47.07 | 45.79 |
| 232 | 50.64 | 48.37 | 45.37 | 47.52 | 47.92 | 47.30 | 45.83 |
| 407 | 51.87 | 49.99 | 47.21 | 49.91 | 49.62 | 49.71 | 48.86 |
| 587 | 52.47 | 50.73 | 48.22 | 51.13 | 50.69 | 50.85 | 50.25 |
| 767 | 52.76 | 51.23 | 48.82 | 51.71 | 51.27 | 51.46 | 50.77 |
| 947 | 52.67 | 51.35 | 48.99 | 51.83 | 51.29 | 51.66 | 50.71 |
| 1187 | 52.80 | 51.42 | 49.39 | 52.23 | 51.68 | 51.72 | 50.65 |

Figure A4.PT20a. Clay coating dried on glass plate in drying air at 55 C and high RH.

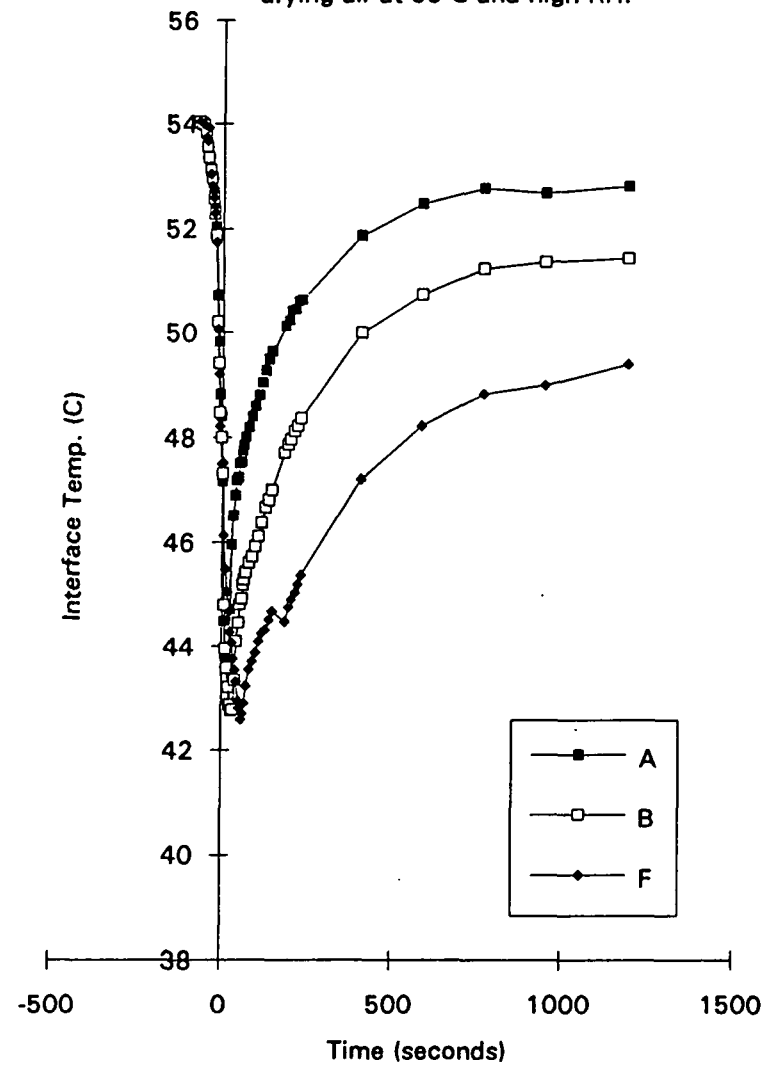


Figure A4.PT20b. Clay coating dried on glass plate in drying air at 55 C and low RH.

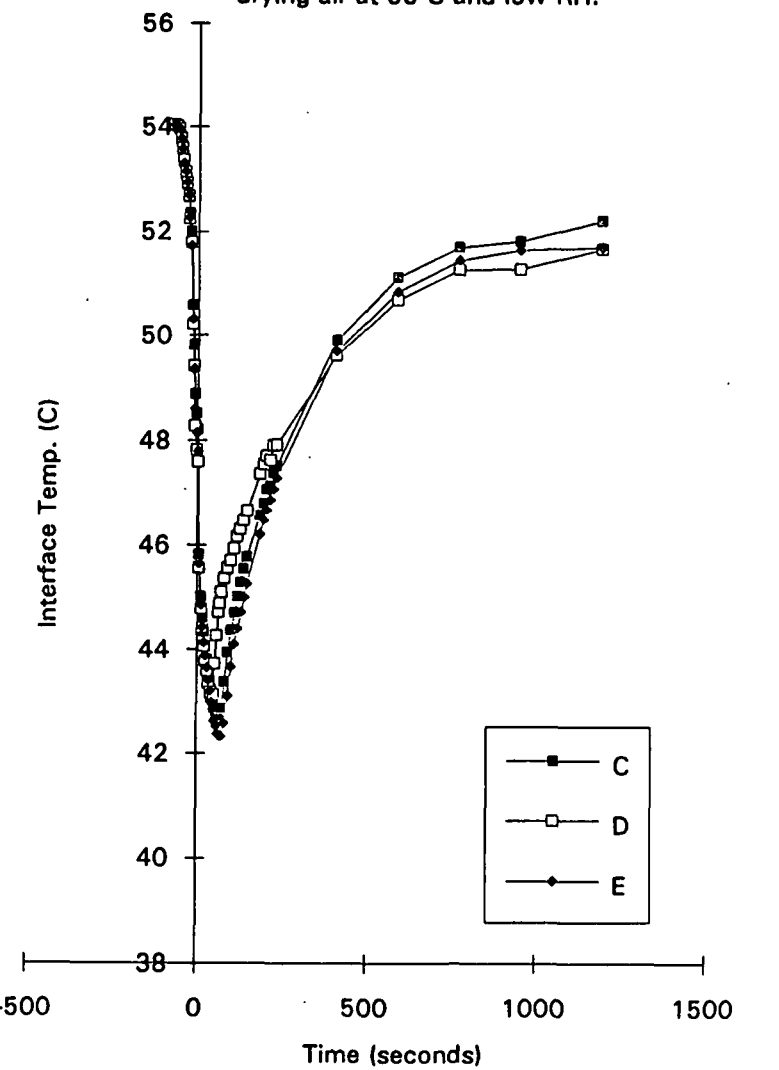

Table A4.PT21. Glass plate temperature during coating and drying at 55 C and 85% RH.

| PT21 Ref. Temp. Resistors Time-sec. | 54 A | 54 B | 54 F | 54 C | 54 D | 54 E | Left Edge |
|---|---|---|---|---|---|---|---|
| -60 | | 53.99 | 54.02 | 54.02 | 54.00 | 54.01 | 53.78 |
| -54 | | 53.92 | 53.92 | 53.92 | 53.94 | 53.90 | 53.94 |
| -49 | | 53.63 | 53.58 | 53.68 | 53.68 | 53.73 | 53.63 |
| -44 | | 53.49 | 53.44 | 53.50 | 53.50 | 53.50 | 53.94 |
| -40 | | 53.10 | 52.94 | 53.17 | 53.16 | 53.23 | 53.78 |
| -35 | | 52.92 | 52.94 | 53.00 | 53.02 | 53.10 | 53.63 |
| -30 | | 52.58 | 52.70 | 52.72 | 52.80 | 52.75 | 53.63 |
| -26 | | 52.20 | 52.36 | 52.35 | 52.26 | 52.40 | 53.94 |
| -21 | | 51.87 | 51.49 | 51.96 | 51.58 | 51.85 | 53.78 |
| -17 | | 49.82 | 50.00 | 50.61 | 50.21 | 50.27 | 53.78 |
| -12 | | 49.02 | 49.05 | 49.78 | 49.28 | 49.20 | 53.78 |
| -7 | | 47.56 | 47.85 | 48.48 | 48.22 | 48.03 | 53.78 |
| -3 | | 46.79 | 46.99 | 48.06 | 47.90 | 48.11 | 53.94 |
| 2 | | 47.27 | 47.54 | 48.48 | 48.35 | 48.37 | 49.14 |
| 6 | | 46.95 | 47.37 | 48.11 | 48.10 | 47.97 | 46.70 |
| 11 | | 46.90 | 47.21 | 48.00 | 48.00 | 47.92 | 45.62 |
| 16 | | 46.72 | 46.99 | 47.79 | 47.84 | 47.71 | 44.04 |
| 20 | | 46.70 | 46.87 | 47.72 | 47.79 | 47.62 | 43.77 |
| 25 | | 46.45 | 46.59 | 47.53 | 47.59 | 47.47 | 42.50 |
| 29 | | 46.49 | 46.51 | 47.48 | 47.54 | 47.31 | 41.29 |
| 34 | | 46.26 | 46.23 | 47.27 | 47.35 | 47.22 | 40.36 |
| 39 | | 46.22 | 46.09 | 47.18 | 47.29 | 47.04 | 39.44 |
| 43 | | 46.15 | 45.95 | 47.11 | 47.22 | 46.96 | 38.82 |
| 48 | | 45.95 | 45.71 | 46.94 | 47.03 | 46.87 | 38.32 |
| 52 | | 45.96 | 45.70 | 46.91 | 47.02 | 46.74 | 38.20 |
| 57 | | 45.90 | 45.56 | 46.83 | 47.00 | 46.61 | 38.17 |
| 62 | | 45.78 | 45.46 | 46.71 | 46.88 | 46.55 | 38.04 |
| 66 | | 45.64 | 45.28 | 46.63 | 46.78 | 46.45 | 37.43 |
| 71 | | 45.70 | 45.25 | 46.60 | 46.76 | 46.40 | 36.96 |
| 75 | | 45.53 | 45.03 | 46.49 | 46.63 | 46.29 | 37.08 |
| 80 | | 45.66 | 45.08 | 46.49 | 46.58 | 46.18 | 36.93 |
| 85 | | 45.46 | 44.80 | 46.33 | 46.39 | 46.18 | 36.96 |
| 89 | | 45.59 | 44.77 | 46.26 | 46.31 | 46.10 | 37.27 |
| 94 | | 45.72 | 44.66 | 46.26 | 46.24 | 46.00 | 36.93 |
| 99 | | 45.99 | 44.66 | 46.28 | 46.32 | 45.94 | 37.08 |

| Time sec. | A | B | F | C | D | E | Left Edge |
|---|---|---|---|---|---|---|---|
| 103 | | 45.92 | 44.48 | 46.13 | 46.12 | 45.91 | 37.08 |
| 108 | | 46.22 | 44.54 | 46.17 | 46.22 | 45.78 | 37.74 |
| 113 | | 46.29 | 44.39 | 46.05 | 46.15 | 45.79 | 38.35 |
| 117 | | 46.49 | 44.42 | 46.05 | 46.27 | 45.76 | 39.28 |
| 122 | | 46.58 | 44.35 | 46.05 | 46.31 | 45.81 | 40.49 |
| 130 | | 46.73 | 44.35 | 45.99 | 46.53 | 45.76 | 41.32 |
| 139 | | 46.98 | 44.25 | 45.91 | 46.76 | 45.67 | 41.72 |
| 149 | | 47.05 | 44.27 | 45.78 | 46.95 | 45.79 | 41.98 |
| 158 | | 47.28 | 44.48 | 45.85 | 47.32 | 45.89 | 41.72 |
| 168 | | 47.51 | 44.51 | 45.94 | 47.47 | 46.10 | 41.72 |
| 178 | | 47.58 | 44.61 | 46.07 | 47.66 | 46.34 | 41.94 |
| 187 | | 47.62 | 44.78 | 46.22 | 47.78 | 46.63 | 41.67 |
| 197 | | 47.93 | 44.84 | 46.52 | 47.96 | 46.80 | 41.79 |
| 206 | | 47.91 | 45.03 | 46.76 | 48.10 | 47.04 | 41.91 |
| 216 | | 48.17 | 45.18 | 47.02 | 48.32 | 47.19 | 42.68 |
| 225 | | 48.25 | 45.34 | 47.26 | 48.47 | 47.36 | 42.99 |
| 235 | | 48.31 | 45.35 | 47.42 | 48.47 | 47.57 | 43.68 |
| 244 | | 48.48 | 45.51 | 47.64 | 48.67 | 47.68 | 44.23 |
| 254 | | 48.67 | 45.59 | 47.85 | 48.76 | 47.81 | 44.54 |
| 263 | | 48.60 | 45.80 | 47.96 | 48.83 | 47.99 | 44.85 |
| 273 | | 48.91 | 45.97 | 48.22 | 49.10 | 48.15 | 45.07 |
| 282 | | 48.90 | 46.01 | 48.33 | 49.08 | 48.27 | 45.34 |
| 292 | | 49.13 | 46.21 | 48.54 | 49.38 | 48.40 | 45.65 |
| 407 | | 50.18 | 47.39 | 50.29 | 50.42 | 49.84 | 48.10 |
| 587 | | 51.13 | 48.58 | 52.04 | 51.54 | 51.27 | 49.64 |
| 767 | | 51.57 | 49.15 | 52.83 | 52.20 | 51.99 | 50.20 |
| 947 | | 51.84 | 49.55 | 53.01 | 52.42 | 52.24 | 50.52 |
| 1187 | | 51.68 | 49.59 | 53.08 | 52.43 | 52.30 | 50.57 |

Figure A4.PT21a. Clay coating dried on glass plate in drying air at 55 C and high RH

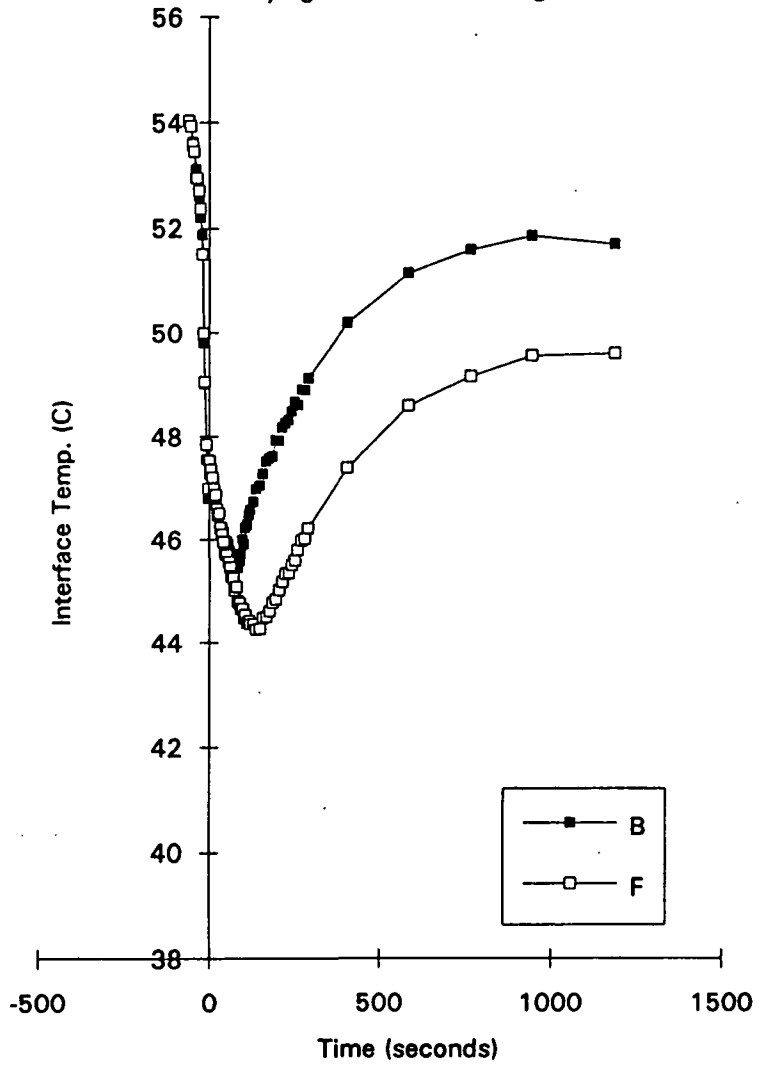


Figure A4.PT21b. Clay coating dried on glass plate in drying air at 55 C and high RH.

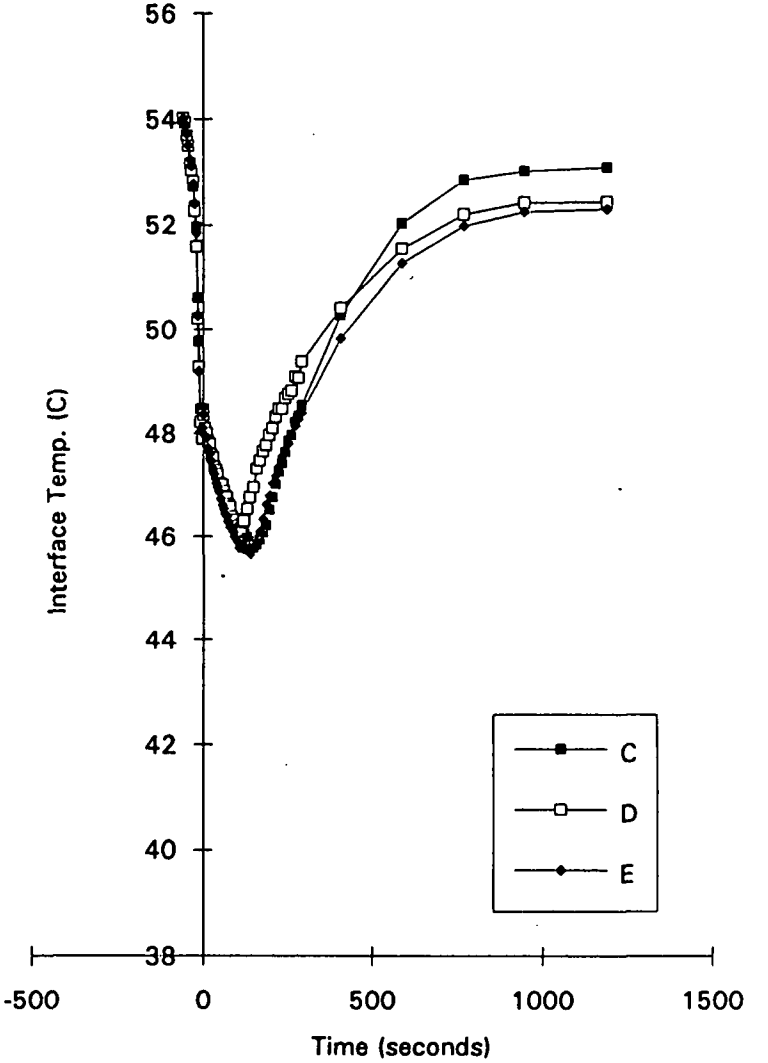

Table A4.PT22. Glass plate temperature during coating and drying at 34 C and 15% RH.

| PT22 Ref. Temp. Resistors Time-sec. | 35 A | 35 B | 35 F | 35 C | 35 D | 35 E | Left Edge |
|---|---|---|---|---|---|---|---|
| -57 | 35.05 | 35.07 | 35.19 | 35.08 | 35.07 | 35.06 | 34.42 |
| -52 | 35.03 | 35.03 | 35.14 | 35.02 | 35.03 | 35.03 | 34.39 |
| -47 | 34.97 | 34.96 | 35.03 | 34.96 | 34.98 | 34.98 | 34.45 |
| -43 | 34.95 | 34.94 | 34.64 | 34.94 | 34.92 | 34.92 | 34.23 |
| -38 | 34.79 | 34.82 | 34.40 | 34.78 | 34.81 | 34.84 | 34.42 |
| -33 | 34.75 | 34.73 | 34.54 | 34.75 | 34.78 | 34.79 | 34.58 |
| -29 | 34.72 | 34.71 | 34.40 | 34.72 | 34.76 | 34.63 | 34.26 |
| -24 | 34.54 | 34.57 | 34.36 | 34.62 | 34.66 | 34.42 | 34.14 |
| -20 | 34.09 | 34.02 | 33.49 | 34.25 | 34.19 | 33.70 | 34.45 |
| -15 | 33.59 | 33.59 | 33.25 | 33.75 | 33.75 | 33.67 | 34.26 |
| -10 | 33.20 | 33.16 | 32.69 | 33.40 | 33.38 | 33.21 | 34.45 |
| -6 | 33.10 | 32.81 | 33.37 | 33.22 | 33.09 | 33.03 | 34.61 |
| -1 | 33.05 | 32.73 | 32.66 | 32.74 | 32.87 | 32.94 | 34.61 |
| 3 | 31.15 | 31.43 | 32.26 | 31.57 | 31.89 | 31.72 | 33.69 |
| 8 | 29.86 | 30.23 | 31.32 | 30.65 | 30.92 | 30.86 | 31.75 |
| 13 | 29.44 | 29.84 | 31.32 | 30.14 | 30.58 | 30.35 | 30.51 |
| 17 | 28.92 | 29.34 | 30.68 | 29.85 | 30.11 | 30.04 | 27.88 |
| 22 | 28.80 | 29.15 | 30.60 | 29.58 | 29.87 | 29.79 | 27.60 |
| 26 | 28.47 | 28.79 | 30.25 | 29.37 | 29.59 | 29.58 | 27.19 |
| 31 | 28.38 | 28.66 | 30.13 | 29.21 | 29.40 | 29.39 | 26.90 |
| 36 | 28.29 | 28.62 | 30.11 | 29.02 | 29.23 | 29.20 | 26.81 |
| 40 | 28.08 | 28.26 | 29.72 | 28.81 | 28.96 | 29.05 | 26.58 |
| 45 | 28.14 | 28.37 | 29.75 | 28.73 | 28.84 | 28.92 | 26.43 |
| 49 | 27.84 | 27.94 | 29.44 | 28.55 | 28.60 | 28.75 | 26.11 |
| 54 | 28.01 | 28.14 | 29.41 | 28.54 | 28.47 | 28.67 | 26.11 |
| 59 | 27.89 | 27.89 | 29.18 | 28.39 | 28.30 | 28.48 | 25.98 |
| 63 | 28.06 | 27.91 | 29.17 | 28.28 | 28.18 | 28.36 | 25.82 |
| 68 | 28.17 | 27.71 | 29.03 | 28.12 | 28.06 | 28.27 | 25.79 |
| 72 | 28.31 | 27.42 | 28.70 | 27.99 | 27.86 | 28.14 | 25.60 |
| 77 | 28.72 | 27.57 | 28.75 | 27.93 | 27.79 | 28.01 | 25.76 |
| 82 | 28.86 | 27.39 | 28.41 | 27.81 | 27.64 | 27.90 | 25.54 |
| 86 | 29.29 | 27.73 | 28.60 | 27.76 | 27.57 | 27.81 | 25.38 |
| 94 | 29.41 | 27.74 | 28.29 | 27.64 | 27.40 | 27.61 | 25.54 |
| 103 | 29.81 | 28.02 | 28.12 | 27.38 | 27.25 | 27.36 | 24.91 |
| 113 | 29.79 | 28.02 | 27.84 | 27.27 | 27.03 | 27.39 | 24.91 |

| Time sec. | A | B | F | C | D | E | Left Edge |
|---|---|---|---|---|---|---|---|
| 122 | 30.04 | 28.19 | 27.53 | 27.06 | 27.03 | 27.25 | 24.75 |
| 132 | 30.24 | 28.48 | 27.52 | 27.03 | 27.22 | 27.15 | 24.75 |
| 141 | 30.56 | 28.77 | 27.38 | 26.88 | 27.56 | 26.97 | 24.75 |
| 151 | 30.85 | 29.15 | 27.34 | 26.85 | 27.88 | 26.85 | 24.75 |
| 160 | 30.92 | 28.98 | 26.84 | 26.66 | 28.05 | 26.83 | 24.43 |
| 170 | 31.07 | 29.20 | 26.74 | 26.75 | 28.25 | 26.88 | 24.43 |
| 180 | 31.27 | 29.41 | 26.83 | 26.96 | 28.42 | 26.89 | 24.43 |
| 189 | 31.45 | 29.49 | 26.78 | 27.03 | 28.60 | 26.97 | 24.27 |
| 199 | 31.73 | 29.92 | 27.14 | 27.28 | 28.79 | 27.07 | 23.80 |
| 208 | 31.79 | 29.92 | 27.34 | 27.52 | 28.91 | 27.34 | 24.11 |
| 218 | 31.96 | 30.12 | 27.62 | 27.85 | 29.08 | 27.57 | 23.80 |
| 227 | 31.99 | 30.15 | 27.71 | 28.05 | 29.20 | 27.90 | 23.95 |
| 237 | 32.21 | 30.46 | 28.01 | 28.31 | 29.40 | 28.05 | 23.80 |
| 406 | 33.70 | 32.40 | 30.72 | 31.10 | 31.40 | 31.11 | 29.16 |
| 587 | 34.49 | 33.66 | 32.31 | 32.83 | 32.63 | 32.95 | 31.61 |
| 767 | 34.83 | 34.25 | 33.17 | 33.67 | 33.31 | 33.78 | 32.41 |
| 947 | 35.00 | 34.57 | 33.74 | 34.16 | 33.77 | 34.36 | 32.98 |
| 1187 | 35.17 | 34.80 | 34.18 | 34.45 | 34.08 | 34.66 | 33.40 |

Figure A4.PT22a. Clay coating dried on glass plate in drying air at 34 C and low RH.

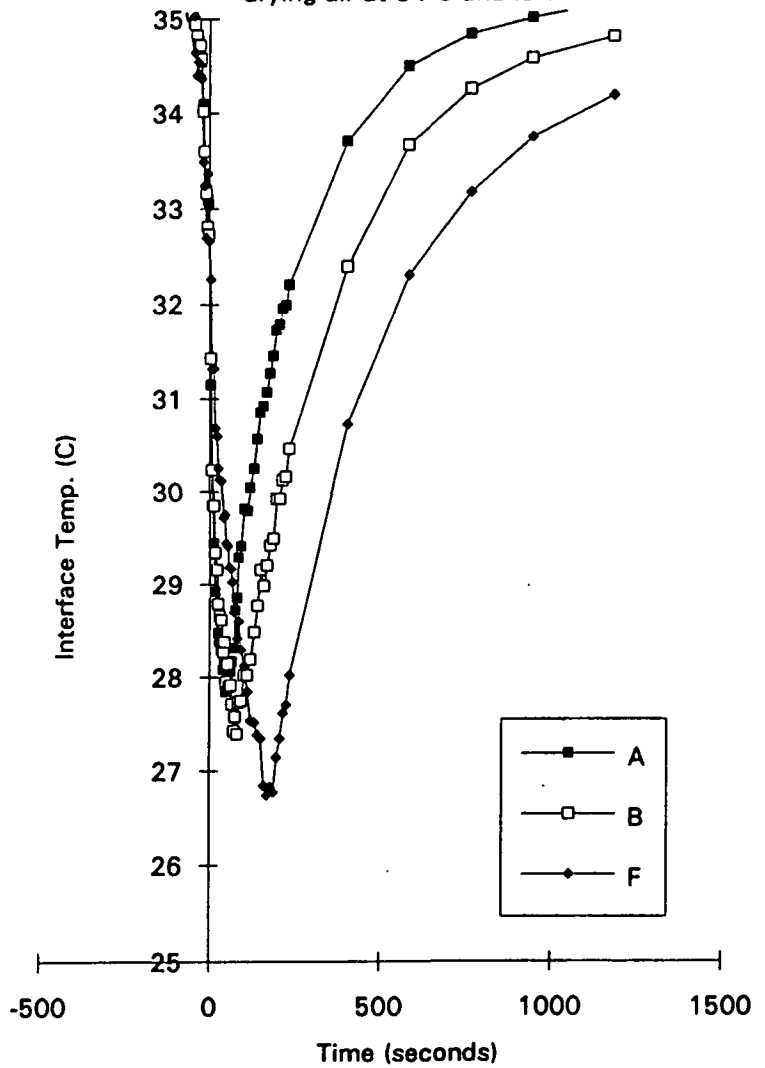


Figure A4.PT22b. Clay coating dried on glass plate in drying air at 34 C and low RH.

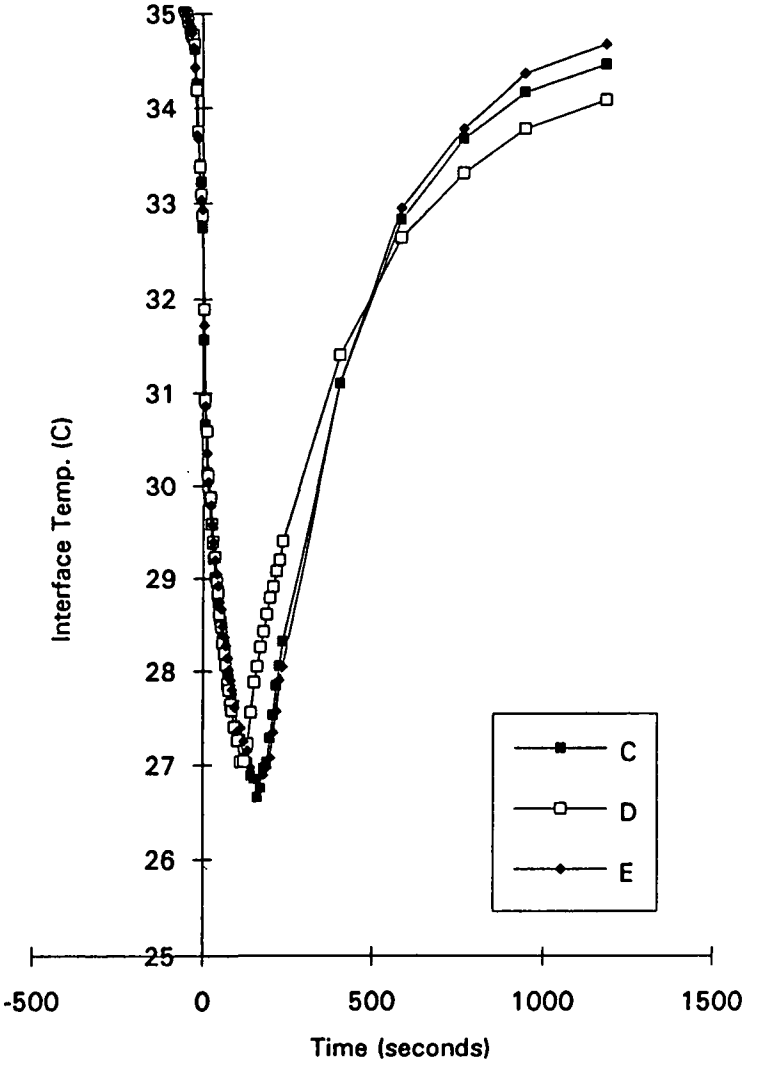

Table A4.PT23. Glass plate temperature during coating and drying at 35 C and 15% RH.

| PT23 Ref. Temp. Resistors Time-sec. | 35 A | 35 B | 35 F | 35 C | 35 D | 35 E | Left Edge |
|---|---|---|---|---|---|---|---|
| -62 | 34.98 | 35.00 | 35.02 | 34.99 | 35.00 | 35.00 | 34.96 |
| -54 | 35.03 | 35.00 | 34.99 | 34.99 | 35.00 | 34.99 | 35.43 |
| -49 | 34.96 | 34.95 | 34.92 | 35.01 | 34.99 | 34.97 | 35.28 |
| -44 | 34.90 | 34.83 | 34.85 | 34.94 | 34.92 | 34.89 | 35.28 |
| -40 | 34.72 | 34.69 | 35.09 | 34.75 | 34.78 | 34.76 | 35.43 |
| -35 | 34.70 | 34.65 | 34.86 | 34.74 | 34.75 | 34.70 | 35.12 |
| -31 | 34.60 | 34.57 | 34.80 | 34.62 | 34.61 | 34.63 | 35.28 |
| -26 | 34.55 | 34.49 | 34.66 | 34.54 | 34.55 | 34.46 | 35.09 |
| -21 | 34.43 | 34.32 | 34.40 | 34.48 | 34.43 | 34.39 | 34.96 |
| -17 | 33.77 | 33.54 | 33.75 | 33.87 | 33.78 | 33.58 | 35.12 |
| -12 | 33.28 | 33.11 | 33.44 | 33.39 | 33.45 | 33.29 | 35.12 |
| -8 | 32.83 | 32.42 | 32.80 | 32.71 | 32.82 | 32.80 | 35.28 |
| -3 | 32.91 | 32.60 | 32.66 | 32.83 | 32.89 | 32.83 | 35.12 |
| 2 | 30.79 | 31.04 | 32.28 | 31.56 | 31.74 | 31.56 | 34.01 |
| 6 | 29.21 | 29.50 | 31.20 | 30.15 | 30.30 | 30.25 | 31.01 |
| 11 | 28.65 | 28.93 | 30.70 | 29.54 | 29.91 | 29.66 | 29.76 |
| 15 | 28.07 | 28.47 | 30.34 | 29.09 | 29.42 | 29.18 | 29.30 |
| 20 | 27.90 | 28.14 | 30.01 | 28.81 | 29.15 | 28.96 | 28.84 |
| 25 | 27.58 | 27.80 | 29.74 | 28.52 | 28.76 | 28.64 | 28.49 |
| 29 | 27.46 | 27.55 | 29.46 | 28.33 | 28.45 | 28.43 | 28.06 |
| 34 | 27.44 | 27.40 | 29.27 | 28.09 | 28.40 | 28.21 | 28.06 |
| 38 | 27.32 | 27.17 | 29.03 | 27.90 | 28.15 | 28.03 | 27.91 |
| 43 | 27.16 | 26.92 | 28.76 | 27.71 | 27.85 | 27.79 | 27.60 |
| 48 | 27.30 | 26.75 | 28.52 | 27.55 | 27.57 | 27.63 | 27.28 |
| 52 | 27.67 | 26.59 | 28.36 | 27.40 | 27.47 | 27.50 | 26.97 |
| 57 | 28.02 | 26.46 | 28.19 | 27.22 | 27.30 | 27.31 | 26.81 |
| 62 | 28.41 | 26.37 | 28.02 | 27.06 | 27.27 | 27.14 | 26.49 |
| 66 | 28.55 | 26.26 | 27.79 | 26.92 | 26.98 | 26.99 | 26.65 |
| 71 | 28.87 | 26.28 | 27.60 | 26.81 | 26.76 | 26.93 | 26.33 |
| 75 | 28.95 | 26.46 | 27.43 | 26.65 | 26.66 | 26.72 | 26.18 |
| 80 | 29.18 | 26.69 | 27.23 | 26.53 | 26.53 | 26.66 | 26.18 |
| 85 | 29.16 | 26.94 | 27.07 | 26.39 | 26.42 | 26.51 | 25.86 |
| 94 | 29.42 | 27.26 | 26.73 | 26.18 | 26.31 | 26.27 | 25.70 |
| 104 | 29.51 | 27.45 | 26.52 | 26.04 | 26.56 | 26.14 | 25.38 |
| 113 | 29.78 | 27.66 | 26.14 | 25.84 | 26.95 | 25.90 | 25.70 |

| Time sec. | A | B | F | C | D | E | Left Edge |
|---|---|---|---|---|---|---|---|
| 123 | 29.90 | 27.81 | 25.90 | 25.76 | 27.27 | 25.81 | 25.54 |
| 132 | 30.22 | 27.98 | 25.66 | 25.81 | 27.68 | 25.71 | 24.91 |
| 142 | 30.42 | 28.14 | 25.51 | 25.97 | 27.74 | 25.63 | 24.91 |
| 151 | 30.40 | 28.23 | 25.69 | 26.33 | 27.76 | 25.81 | 24.75 |
| 161 | 30.59 | 28.40 | 26.04 | 26.61 | 27.95 | 26.00 | 24.43 |
| 170 | 30.82 | 28.55 | 26.26 | 26.90 | 28.17 | 26.26 | 24.11 |
| 180 | 30.94 | 28.72 | 26.47 | 27.16 | 28.25 | 26.50 | 24.11 |
| 189 | 31.00 | 28.80 | 26.73 | 27.40 | 28.32 | 26.80 | 24.15 |
| 199 | 31.23 | 28.98 | 26.92 | 27.61 | 28.57 | 27.04 | 23.95 |
| 208 | 31.28 | 29.07 | 27.11 | 27.83 | 28.67 | 27.26 | 24.66 |
| 218 | 31.40 | 29.23 | 27.33 | 28.01 | 28.91 | 27.50 | 25.73 |
| 227 | 31.54 | 29.41 | 27.41 | 28.14 | 28.96 | 27.65 | 26.18 |
| 237 | 31.73 | 29.53 | 27.60 | 28.30 | 29.15 | 27.87 | 26.49 |
| 404 | 32.80 | 31.17 | 29.72 | 30.79 | 30.77 | 30.50 | 30.91 |
| 586 | 33.27 | 32.05 | 31.03 | 32.25 | 31.78 | 32.02 | 32.80 |
| 766 | 33.51 | 32.58 | 31.96 | 32.96 | 32.38 | 32.75 | 33.35 |
| 946 | 33.68 | 32.84 | 32.38 | 33.29 | 32.75 | 33.14 | 33.79 |
| 1185 | 33.58 | 32.83 | 32.55 | 33.30 | 32.81 | 33.21 | 33.70 |

Figure A4.PT23a. Clay coating dried on glass plate in drying air at 35 C and low RH.

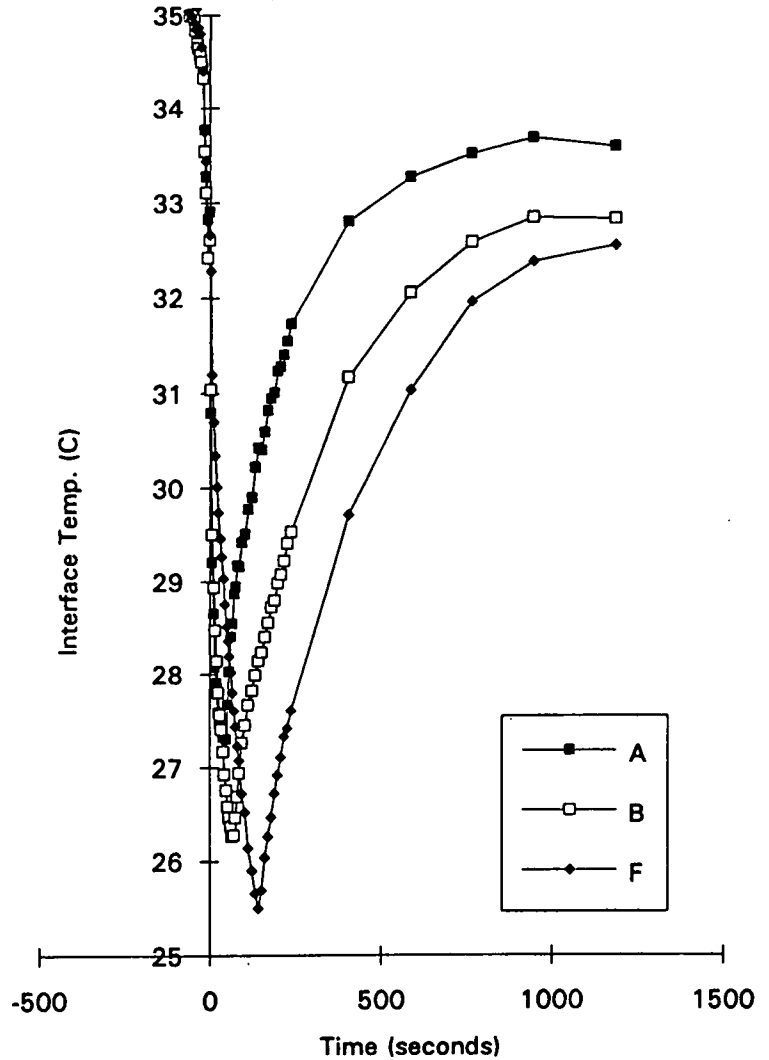


Figure A4.PT23b. Clay coating dried on glass plate in drying air at 35 C and low RH.

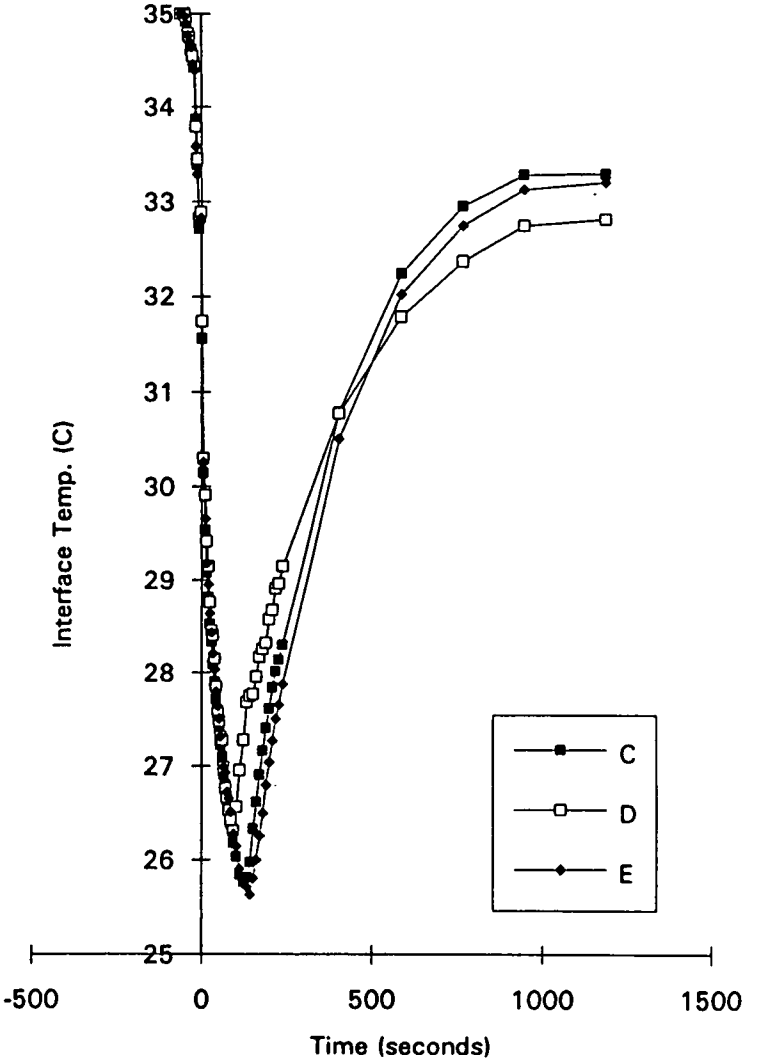

Table A4.PT24. Glass plate temperature during coating and drying at 35 C and 15% RH.

| PT24 Ref. Temp. Resistors Time-sec. | 36 A | 36 B | 36 F | 36 C | 36 D | 36 E | Left Edge |
|---|---|---|---|---|---|---|---|
| -71 | 36.02 | 36.03 | 36.04 | 36.04 | 36.06 | 36.07 | 35.25 |
| -65 | 36.00 | 36.04 | 36.02 | 35.99 | 36.01 | 36.00 | 35.22 |
| -60 | 35.99 | 35.96 | 35.95 | 35.98 | 35.96 | 35.96 | 35.28 |
| -56 | 35.94 | 35.89 | 35.90 | 35.95 | 35.92 | 35.92 | 35.44 |
| -51 | 35.89 | 35.86 | 36.11 | 35.87 | 35.82 | 35.94 | 35.13 |
| -46 | 35.71 | 35.63 | 35.66 | 35.70 | 35.72 | 35.73 | 35.37 |
| -42 | 35.60 | 35.55 | 35.56 | 35.62 | 35.59 | 35.62 | 35.37 |
| -37 | 35.57 | 35.53 | 35.39 | 35.53 | 35.53 | 35.52 | 35.37 |
| -33 | 35.46 | 35.40 | 35.32 | 35.50 | 35.45 | 35.51 | 35.44 |
| -28 | 35.33 | 35.26 | 35.21 | 35.38 | 35.35 | 35.33 | 35.37 |
| -23 | 34.97 | 34.81 | 34.63 | 34.93 | 34.93 | 34.82 | 35.22 |
| -19 | 34.34 | 34.20 | 34.10 | 34.57 | 34.50 | 34.28 | 35.56 |
| -14 | 32.81 | 35.00 | 33.46 | | 33.44 | 31.93 | 35.13 |
| -10 | 31.63 | 36.12 | 32.74 | | 32.32 | 31.43 | 35.41 |
| -5 | 33.78 | 33.80 | 33.99 | 33.79 | 34.00 | 33.92 | 35.41 |
| 0 | 33.16 | 33.39 | 33.84 | 33.60 | 33.71 | 33.62 | 35.28 |
| 4 | 30.52 | 31.11 | 32.50 | 31.72 | 31.88 | 31.80 | 32.53 |
| 9 | 29.60 | 30.21 | 31.82 | 30.86 | 31.09 | 30.98 | 29.43 |
| 13 | 29.18 | 29.76 | 31.43 | 30.41 | 30.63 | 30.58 | 29.12 |
| 18 | 28.86 | 29.38 | 31.12 | 30.07 | 30.31 | 30.22 | 28.81 |
| 23 | 28.54 | 29.06 | 30.79 | 29.85 | 30.02 | 29.93 | 28.41 |
| 27 | 28.49 | 28.87 | 30.55 | 29.61 | 29.78 | 29.77 | 28.04 |
| 32 | 28.29 | 28.59 | 30.24 | 29.46 | 29.51 | 29.54 | 27.70 |
| 36 | 28.23 | 28.47 | 30.10 | 29.25 | 29.36 | 29.35 | 27.54 |
| 41 | 28.08 | 28.24 | 29.81 | 29.04 | 29.11 | 29.14 | 27.26 |
| 46 | 28.14 | 28.10 | 29.64 | 28.90 | 28.95 | 29.00 | 27.30 |
| 50 | 28.23 | 27.87 | 29.40 | 28.75 | 28.75 | 28.78 | 27.07 |
| 55 | 28.68 | 27.80 | 29.30 | 28.59 | 28.65 | 28.68 | 26.94 |
| 59 | 29.03 | 27.67 | 29.05 | 28.45 | 28.46 | 28.52 | 26.79 |
| 64 | 29.31 | 27.60 | 28.90 | 28.30 | 28.29 | 28.39 | 26.43 |
| 69 | 29.54 | 27.64 | 28.76 | 28.21 | 28.16 | 28.26 | 26.31 |
| 73 | 29.77 | 27.73 | 28.56 | 28.11 | 28.01 | 28.17 | 26.31 |
| 78 | 29.89 | 27.98 | 28.42 | 27.98 | 27.92 | 28.04 | 26.15 |
| 83 | 30.03 | 28.15 | 28.26 | 27.84 | 27.77 | 27.91 | 25.99 |
| 92 | 30.26 | 28.46 | 27.95 | 27.65 | 27.72 | 27.71 | 25.83 |

| Time sec. | A | B | F | C | D | E | Left Edge |
|---|---|---|---|---|---|---|---|
| 97 | 30.46 | 28.66 | 27.87 | 27.57 | 27.84 | 27.64 | 25.32 |
| 105 | 30.57 | 28.75 | 27.59 | 27.42 | 28.04 | 27.48 | 25.64 |
| 114 | 30.80 | 28.93 | 27.32 | 27.28 | 28.43 | 27.32 | 25.64 |
| 124 | 30.98 | 29.04 | 27.11 | 27.26 | 28.70 | 27.18 | 25.32 |
| 133 | 31.26 | 29.24 | 26.83 | 27.31 | 28.87 | 27.02 | 25.17 |
| 143 | 31.32 | 29.32 | 26.71 | 27.60 | 29.05 | 27.05 | 24.88 |
| 152 | 31.53 | 29.55 | 26.89 | 27.86 | 29.24 | 27.07 | 24.85 |
| 162 | 31.76 | 29.72 | 27.14 | 28.10 | 29.38 | 27.13 | 24.69 |
| 172 | 31.84 | 29.81 | 27.45 | 28.39 | 29.53 | 27.35 | 24.37 |
| 181 | 32.02 | 29.99 | 27.63 | 28.61 | 29.66 | 27.50 | 24.21 |
| 191 | 32.16 | 30.13 | 27.78 | 28.82 | 29.78 | 27.77 | 24.05 |
| 200 | 32.21 | 30.24 | 28.06 | 29.09 | 29.95 | 28.09 | 23.90 |
| 210 | 32.44 | 30.38 | 28.19 | 29.28 | 30.07 | 28.26 | 24.37 |
| 219 | 32.50 | 30.44 | 28.38 | 29.51 | 30.17 | 28.57 | 24.85 |
| 229 | 32.65 | 30.64 | 28.57 | 29.69 | 30.32 | 28.76 | 25.01 |
| 238 | 32.70 | 30.76 | 28.78 | 29.86 | 30.46 | 28.97 | 25.64 |
| 406 | 34.15 | 32.62 | 31.13 | 32.31 | 32.24 | 31.74 | 30.54 |
| 586 | 34.87 | 33.71 | 32.56 | 33.75 | 33.40 | 33.43 | 32.42 |
| 766 | 35.04 | 34.09 | 33.30 | 34.38 | 33.94 | 34.21 | 33.36 |
| 946 | 35.17 | 34.31 | 33.63 | 34.69 | 34.23 | 34.59 | 33.75 |
| 1185 | 35.31 | 34.54 | 33.99 | 34.96 | 34.51 | 34.82 | 34.14 |

Figure A4.PT24a. Clay coating dried on glass plate in drying air at 35 C and low RH.

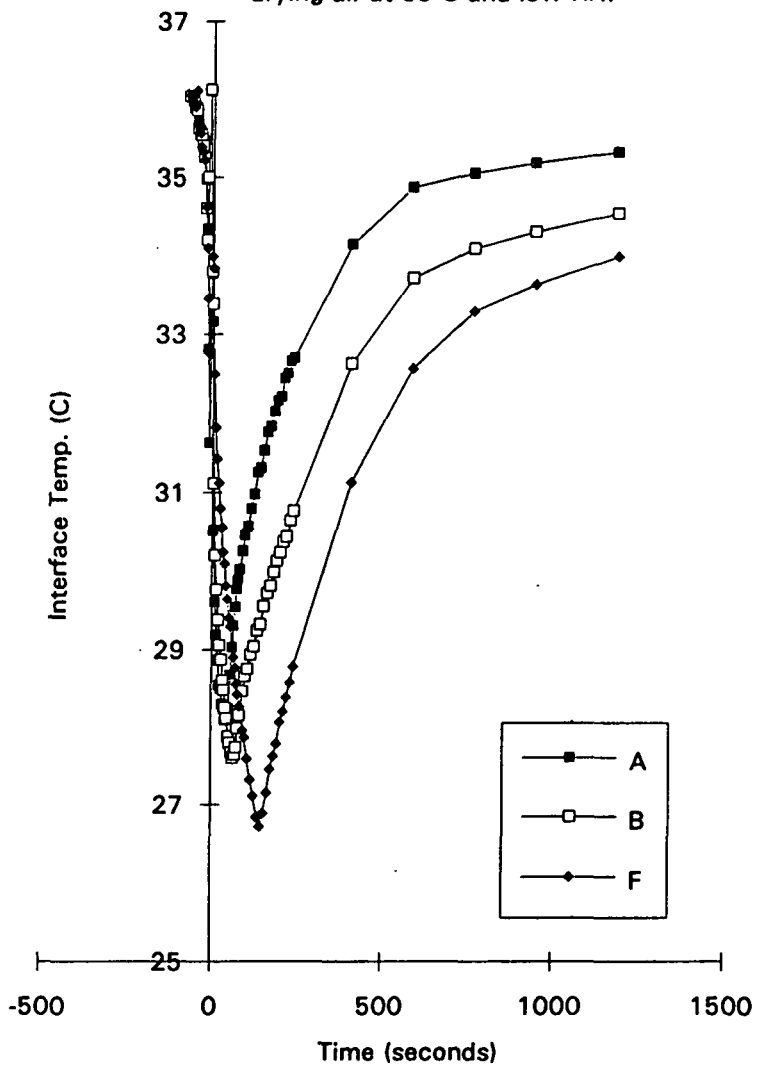


Figure A4.PT24b. Clay coating dried on glass plate in drying air at 35 C and low RH.

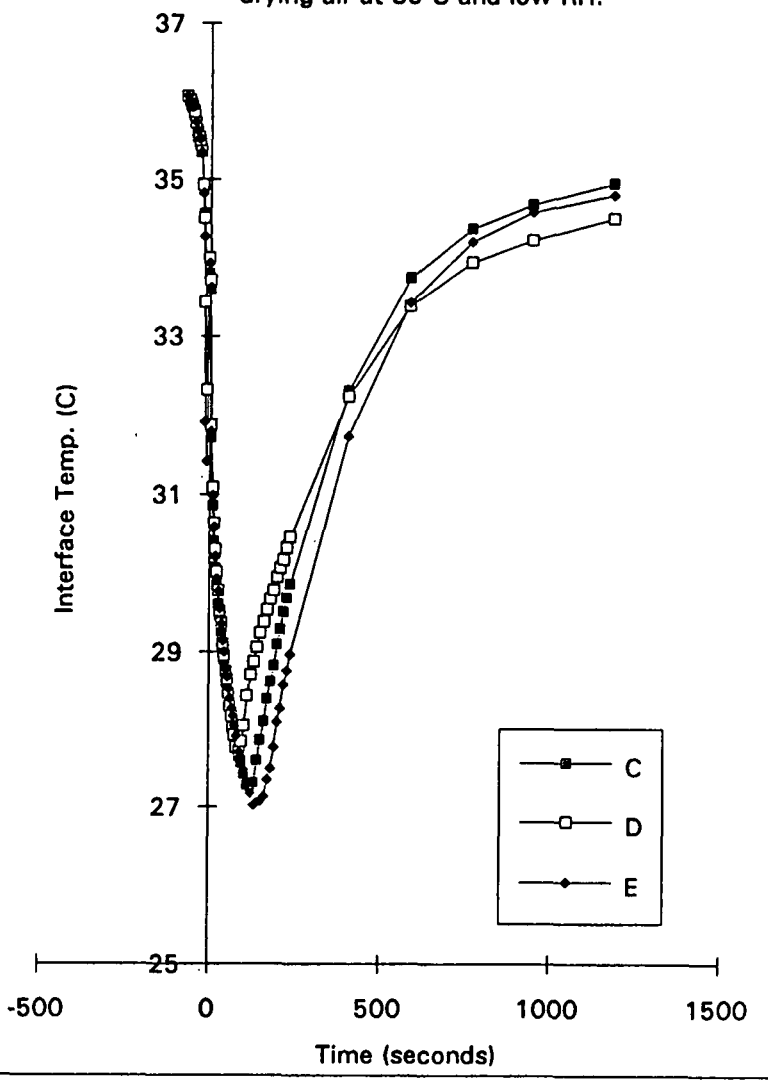

Table A4.PT25. Glass plate temperature during coating and drying at 35 C and 85% RH.

| PT25 Ref. Temp. Resistors Time-sec. | 36 A | 36 B | 36 F | 36 C | 36 D | 36 E | Left Edge |
|---|---|---|---|---|---|---|---|
| -81 | 36.00 | 36.01 | 35.99 | 35.98 | 34.99 | 36.00 | 35.44 |
| -71 | 36.01 | 36.03 | 36.03 | 36.03 | 35.04 | 36.01 | 35.28 |
| -65 | 36.01 | 36.01 | 36.06 | 36.03 | 35.02 | 36.04 | 35.53 |
| -60 | 36.00 | 35.96 | 35.96 | 35.98 | 34.97 | 35.98 | 35.41 |
| -55 | 35.92 | 35.92 | 35.84 | 35.90 | 34.94 | 35.90 | 35.56 |
| -51 | 35.80 | 35.80 | 35.79 | 35.80 | 34.82 | 35.84 | 35.25 |
| -46 | 35.72 | 35.70 | 35.61 | 35.71 | 34.72 | 35.72 | 35.59 |
| -41 | 35.69 | 35.63 | 35.70 | 35.66 | 34.67 | 35.71 | 35.37 |
| -37 | 35.55 | 35.52 | 35.63 | 35.55 | 34.58 | 35.61 | 35.53 |
| -32 | 35.44 | 35.46 | 35.55 | 35.48 | 34.48 | 35.40 | 35.25 |
| -28 | 35.29 | 35.30 | 35.39 | 35.29 | 34.24 | 35.23 | 35.41 |
| -23 | 34.71 | 34.28 | 34.65 | 34.57 | 33.48 | 34.54 | 35.59 |
| -18 | 34.05 | 33.77 | 34.32 | 34.28 | 33.13 | 34.01 | 35.56 |
| -14 | 33.43 | 33.25 | 33.67 | 33.84 | 32.62 | 33.65 | 35.53 |
| -9 | 32.42 | 32.82 | 32.64 | 33.49 | 32.06 | 33.17 | 35.37 |
| -5 | 31.77 | 32.42 | 32.50 | 33.11 | 31.69 | 32.99 | 35.53 |
| 0 | 31.45 | 32.43 | 32.67 | 33.20 | 31.76 | 33.01 | 35.25 |
| 5 | 30.76 | 31.91 | 32.36 | 32.82 | 31.42 | 32.59 | 32.84 |
| 9 | 30.38 | 31.67 | 32.21 | 32.67 | 31.28 | 32.40 | 32.21 |
| 14 | 30.19 | 31.42 | 32.04 | 32.46 | 31.20 | 32.16 | 32.24 |
| 18 | 29.87 | 31.19 | 31.90 | 32.37 | 30.94 | 32.03 | 31.92 |
| 23 | 29.65 | 30.99 | 31.73 | 32.22 | 30.82 | 31.86 | 31.76 |
| 28 | 29.38 | 30.73 | 31.52 | 32.01 | 30.50 | 31.66 | 31.57 |
| 32 | 29.10 | 30.51 | 31.42 | 31.90 | 30.37 | 31.49 | 31.45 |
| 37 | 28.93 | 30.38 | 31.28 | 31.74 | 30.37 | 31.34 | 31.45 |
| 41 | 28.64 | 30.15 | 31.12 | 31.61 | 30.11 | 31.18 | 31.01 |
| 46 | 28.56 | 30.05 | 30.99 | 31.48 | 30.13 | 31.04 | 30.98 |
| 51 | 28.35 | 29.82 | 30.87 | 31.42 | 29.96 | 30.90 | 30.67 |
| 55 | 28.10 | 29.64 | 30.76 | 31.31 | 29.64 | 30.80 | 30.63 |
| 60 | 28.03 | 29.50 | 30.57 | 31.18 | 29.61 | 30.59 | 30.55 |
| 64 | 27.86 | 29.32 | 30.45 | 31.10 | 29.34 | 30.50 | 30.55 |
| 69 | 27.84 | 29.16 | 30.26 | 30.89 | 29.30 | 30.32 | 30.39 |
| 74 | 27.69 | 29.04 | 30.16 | 30.81 | 29.15 | 30.19 | 30.27 |
| 80 | 27.53 | 28.81 | 29.97 | 30.70 | 28.88 | 30.00 | 29.93 |
| 90 | 27.41 | 28.55 | 29.75 | 30.49 | 28.68 | 29.74 | 29.77 |

| Time sec. | A | B | F | C | D | E | Left Edge |
|---|---|---|---|---|---|---|---|
| 99 | 27.34 | 28.35 | 29.58 | 30.23 | 28.68 | 29.52 | 29.58 |
| 109 | 27.27 | 28.15 | 29.32 | 30.06 | 28.46 | 29.30 | 29.43 |
| 118 | 27.37 | 27.98 | 29.11 | 29.93 | 28.17 | 29.11 | 29.34 |
| 128 | 27.55 | 27.83 | 28.87 | 29.72 | 28.05 | 28.90 | 28.84 |
| 137 | 27.86 | 27.72 | 28.61 | 29.64 | 27.76 | 28.75 | 28.84 |
| 147 | 28.13 | 27.66 | 28.41 | 29.49 | 27.56 | 28.53 | 28.84 |
| 156 | 28.36 | 27.75 | 28.18 | 29.33 | 27.32 | 28.34 | 28.53 |
| 166 | 28.55 | 27.89 | 27.98 | 29.21 | 27.15 | 28.16 | 28.23 |
| 175 | 28.73 | 28.09 | 27.82 | 29.04 | 27.10 | 28.02 | 28.41 |
| 185 | 28.87 | 28.23 | 27.61 | 28.84 | 27.19 | 27.79 | 27.79 |
| 194 | 29.09 | 28.36 | 27.46 | 28.68 | 27.41 | 27.62 | 27.79 |
| 204 | 29.19 | 28.50 | 27.25 | 28.60 | 27.53 | 27.44 | 27.48 |
| 213 | 29.32 | 28.62 | 27.15 | 28.58 | 27.75 | 27.31 | 27.33 |
| 223 | 29.53 | 28.78 | 27.01 | 28.69 | 27.98 | 27.20 | 27.45 |
| 232 | 29.67 | 28.96 | 27.00 | 28.80 | 28.22 | 27.04 | 27.61 |
| 242 | 29.78 | 29.10 | 26.93 | 29.06 | 28.19 | 26.96 | 27.48 |
| 252 | 29.95 | 29.25 | 27.00 | 29.21 | 28.42 | 26.84 | 27.33 |
| 261 | 29.99 | 29.35 | 27.05 | 29.43 | 28.41 | 26.69 | 27.33 |
| 271 | 30.13 | 29.42 | 27.27 | 29.56 | 28.63 | 26.61 | 27.64 |
| 280 | 30.13 | 29.52 | 27.39 | 29.69 | 28.73 | 26.52 | 27.95 |
| 290 | 30.30 | 29.64 | 27.61 | 29.82 | 28.96 | 26.53 | 28.23 |
| 298 | 30.44 | 29.75 | 27.77 | 30.02 | 29.04 | 26.60 | 28.72 |
| 405 | 31.12 | 30.78 | 33.01 | 31.42 | 30.13 | 29.48 | 30.74 |
| 585 | 31.95 | 31.99 | 34.19 | 32.88 | 31.44 | 31.95 | 32.65 |
| 765 | 32.39 | 32.69 | 35.12 | 33.77 | 32.10 | 33.05 | 33.47 |
| 945 | 32.51 | 32.99 | 36.11 | 34.20 | 32.61 | 33.50 | 34.23 |
| 1185 | 32.60 | 33.14 | 37.33 | 34.46 | 32.86 | 33.80 | 34.39 |

Figure A4.PT25a. Clay coating dried on glass plate in drying air at 35 C and high RH.

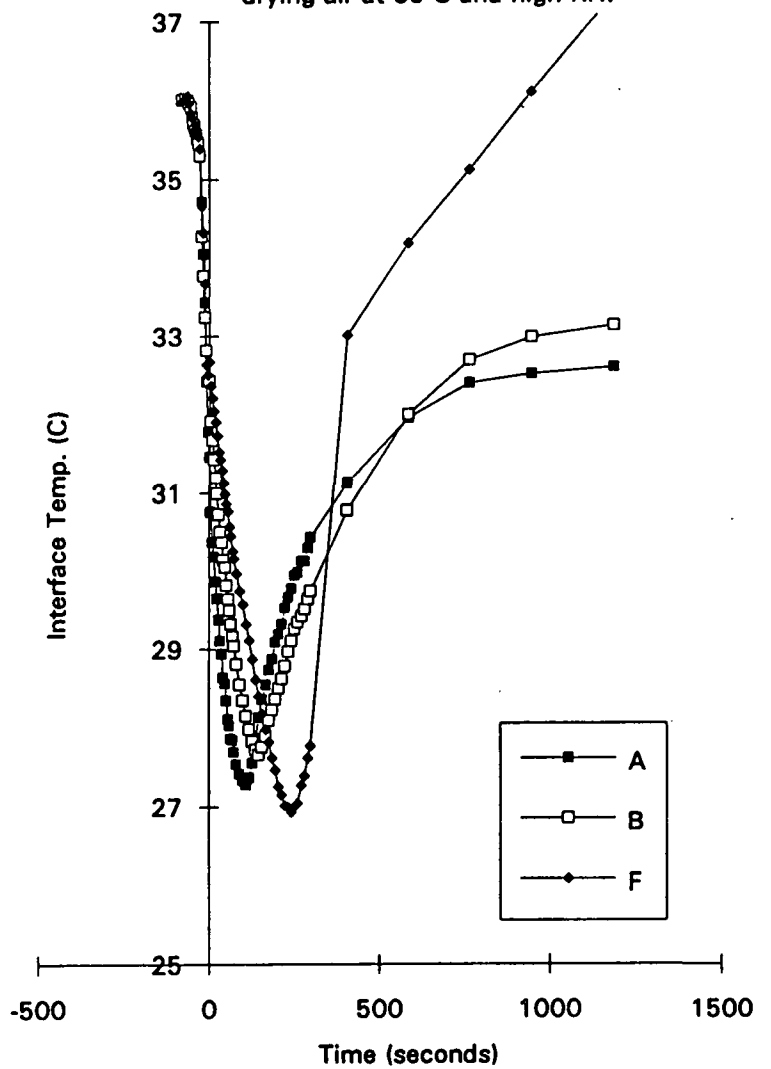


Figure A4.PT25b. Clay coating dried on glass plate in drying air at 35 C and high RH.

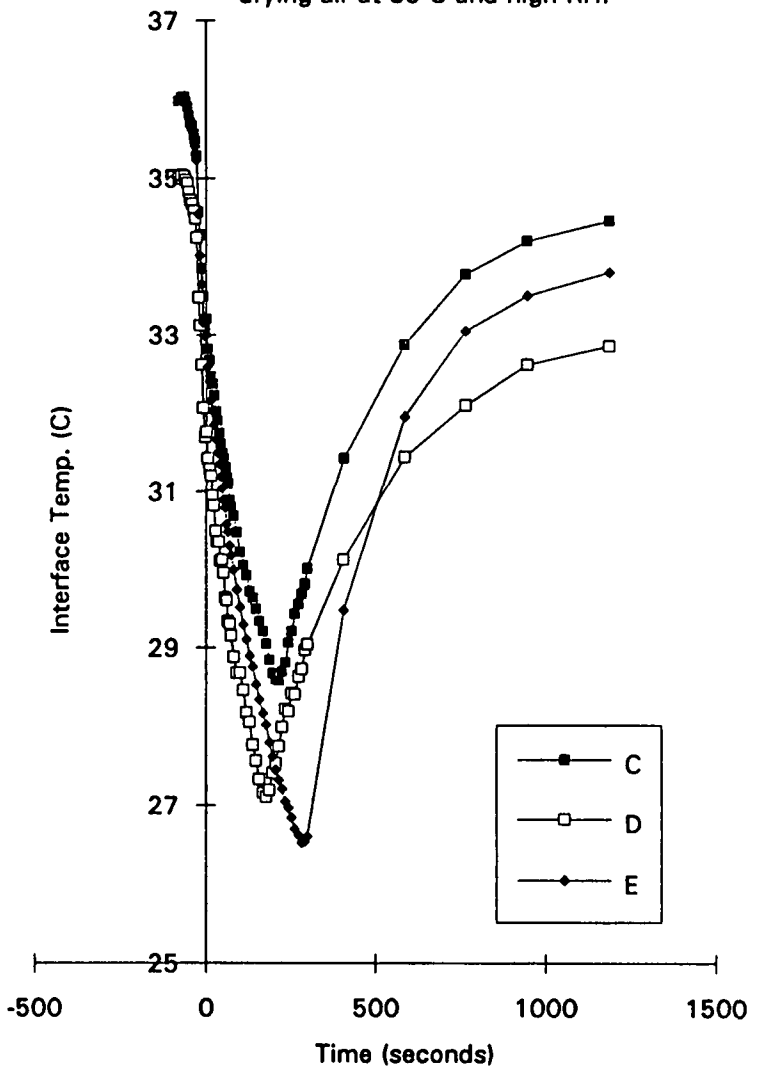

Table A4.PT26. Glass plate temperature during coating and drying at 35 C and 85% RH.

| PT26 Ref. Temp. Resistors Time-sec. | 36 A | 36 B | 36 F | 36 C | 36 D | 36 E | Left Edge | Time sec. | A | B | F | C | D | E | Left Edge |
|---|---|---|---|---|---|---|---|---|---|---|---|---|---|---|---|
| -68 | 36.03 | 36.01 | 36.02 | 36.02 | 36.02 | 35.98 | 35.50 | 97 | 31.75 | 29.96 | 30.40 | 30.08 | 29.44 | 30.47 | 30.61 |
| -60 | 36.02 | 36.01 | 36.01 | 36.00 | 35.99 | 36.05 | 35.50 | 101 | 31.58 | 29.84 | 30.24 | 30.00 | 29.51 | 30.29 | 30.30 |
| -55 | 35.95 | 35.98 | 35.97 | 35.98 | 35.99 | 35.97 | 35.35 | 106 | 31.65 | 29.79 | 30.16 | 29.88 | 29.29 | 30.24 | 30.45 |
| -51 | 35.89 | 35.92 | 35.87 | 35.87 | 35.84 | 35.86 | 35.50 | 111 | 31.58 | 29.71 | 30.05 | 29.85 | 29.31 | 30.13 | 30.14 |
| -46 | 35.85 | 35.83 | 35.95 | 35.79 | 35.82 | 35.81 | 35.50 | 115 | 31.61 | 29.67 | 29.95 | 29.71 | 29.02 | 30.07 | 30.14 |
| -41 | 35.66 | 35.66 | 35.71 | 35.66 | 35.67 | 35.70 | 35.19 | 120 | 31.55 | 29.55 | 29.86 | 29.63 | 29.02 | 29.94 | 29.99 |
| -37 | 35.63 | 35.55 | 35.70 | 35.65 | 35.57 | 35.60 | 35.19 | 124 | 31.47 | 29.50 | 29.79 | 29.63 | 28.98 | 29.88 | 29.68 |
| -32 | 35.48 | 35.44 | 35.51 | 35.50 | 35.23 | 35.41 | 35.50 | 129 | 31.42 | 29.36 | 29.66 | 29.44 | 28.90 | 29.75 | 29.84 |
| -28 | 35.40 | 35.30 | 35.33 | 35.37 | 34.96 | 35.30 | 35.50 | 134 | 31.52 | 29.32 | 29.57 | 29.39 | 28.68 | 29.72 | 29.84 |
| -23 | 34.86 | 34.64 | 34.46 | 34.74 | 34.30 | 34.58 | 35.35 | 138 | 31.42 | 29.21 | 29.47 | 29.35 | 28.83 | 29.57 | 29.68 |
| -18 | 34.11 | 33.92 | 34.39 | 34.12 | 34.20 | 34.08 | 35.19 | 143 | 31.47 | 29.15 | 29.38 | 29.23 | 28.68 | 29.51 | 29.68 |
| -14 | 33.85 | 33.86 | 34.10 | 34.09 | 36.23 | 35.20 | 35.19 | 147 | 31.52 | 29.05 | 29.24 | 29.11 | 28.58 | 29.40 | 29.53 |
| -9 | 35.09 | 35.30 | 34.01 | 34.86 | 35.73 | 35.02 | 35.50 | 152 | 31.69 | 28.99 | 29.23 | 28.95 | 28.36 | 29.35 | 29.37 |
| -5 | 32.07 | 31.70 | 33.85 | 34.07 | 31.32 | 31.83 | 35.35 | 157 | 31.67 | 28.93 | 29.11 | 29.00 | 28.43 | 29.24 | 29.22 |
| 0 | 33.76 | 33.46 | 33.68 | 33.27 | 33.55 | 33.67 | 35.35 | 161 | 31.84 | 28.92 | 29.02 | 28.94 | 28.39 | 29.19 | 29.22 |
| 5 | 33.11 | 32.76 | 33.25 | 32.74 | 32.81 | 33.15 | 34.40 | 166 | 31.88 | 28.89 | 28.93 | 28.86 | 28.36 | 29.08 | 29.09 |
| 9 | 32.78 | 32.37 | 32.94 | 32.44 | 32.59 | 32.82 | 33.29 | 170 | 32.02 | 28.90 | 28.90 | 28.74 | 28.14 | 29.06 | 29.06 |
| 14 | 32.62 | 32.16 | 32.75 | 32.21 | 32.30 | 32.64 | 33.29 | 175 | 32.01 | 28.90 | 28.78 | 28.76 | 28.24 | 28.97 | 28.94 |
| 18 | 32.44 | 31.96 | 32.58 | 32.10 | 32.20 | 32.45 | 33.13 | 180 | 32.13 | 28.99 | 28.69 | 28.55 | 27.97 | 28.92 | 28.91 |
| 23 | 32.44 | 31.82 | 32.44 | 31.81 | 31.74 | 32.35 | 32.81 | 184 | 32.13 | 29.01 | 28.64 | 28.58 | 28.05 | 28.85 | 28.75 |
| 28 | 32.25 | 31.60 | 32.22 | 31.70 | 31.66 | 32.18 | 32.81 | 189 | 32.18 | 29.07 | 28.54 | 28.41 | 27.95 | 28.74 | 28.60 |
| 32 | 32.16 | 31.47 | 32.07 | 31.59 | 31.54 | 32.05 | 32.50 | 193 | 32.24 | 29.16 | 28.50 | 28.41 | 27.94 | 28.74 | 28.44 |
| 37 | 32.12 | 31.33 | 31.96 | 31.38 | 31.34 | 31.91 | 32.66 | 198 | 32.28 | 29.21 | 28.40 | 28.30 | 27.92 | 28.65 | 28.44 |
| 42 | 32.10 | 31.22 | 31.79 | 31.36 | 31.20 | 31.78 | 32.34 | 203 | 32.44 | 29.27 | 28.37 | 28.12 | 27.70 | 28.65 | 28.13 |
| 46 | 32.04 | 31.08 | 31.65 | 31.18 | 31.03 | 31.62 | 32.02 | 207 | 32.39 | 29.28 | 28.25 | 28.01 | 27.77 | 28.50 | 28.29 |
| 51 | 32.04 | 30.99 | 31.55 | 31.10 | 30.86 | 31.57 | 31.70 | 212 | 32.47 | 29.33 | 28.21 | 28.04 | 27.90 | 28.49 | 28.17 |
| 55 | 32.01 | 30.87 | 31.36 | 30.93 | 30.81 | 31.35 | 31.86 | 221 | 32.55 | 29.39 | 28.07 | 27.91 | 27.90 | 28.37 | 28.17 |
| 60 | 32.07 | 30.76 | 31.33 | 30.83 | 30.47 | 31.32 | 31.55 | 230 | 32.70 | 29.53 | 27.94 | 27.69 | 27.87 | 28.25 | 28.23 |
| 65 | 32.01 | 30.61 | 31.17 | 30.70 | 30.44 | 31.16 | 31.39 | 240 | 32.79 | 29.61 | 27.80 | 27.62 | 28.22 | 28.12 | 28.05 |
| 69 | 31.99 | 30.50 | 31.05 | 30.57 | 30.32 | 31.03 | 31.23 | 249 | 32.87 | 29.67 | 27.71 | 27.62 | 28.46 | 28.02 | 27.70 |
| 74 | 31.93 | 30.39 | 30.90 | 30.46 | 30.12 | 30.93 | 31.07 | 259 | 33.04 | 29.82 | 27.54 | 27.48 | 28.39 | 27.91 | 27.92 |
| 78 | 31.98 | 30.33 | 30.86 | 30.45 | 29.95 | 30.87 | 30.76 | 268 | 33.16 | 29.90 | 27.42 | 27.44 | 28.65 | 27.83 | 27.86 |
| 83 | 31.88 | 30.19 | 30.71 | 30.32 | 29.85 | 30.71 | 30.92 | 278 | 33.19 | 29.98 | 27.37 | 27.54 | 28.78 | 27.83 | 27.58 |
| 88 | 31.79 | 30.11 | 30.57 | 30.25 | 29.81 | 30.56 | 30.92 | 287 | 33.27 | 30.07 | 27.35 | 27.78 | 28.88 | 27.89 | 27.24 |
| 92 | 31.73 | 29.99 | 30.45 | 30.14 | 29.66 | 30.50 | 30.92 | 297 | 33.36 | 30.16 | 27.35 | 27.93 | 28.93 | 27.94 | 27.11 |

Table A4.PT26. Glass plate temperature during coating and drying at 35 C and 85% RH.

Continued

| PT26 Ref. Temp. Resistors Time-sec. | 36 A | 36 B | 36 F | 36 C | 36 D | 36 E | Left Edge | Time sec. | A | B | F | C | D | E | Left Edge |
|---|---|---|---|---|---|---|---|---|---|---|---|---|---|---|---|
| 407 | 34.13 | 31.18 | 29.03 | 30.03 | 30.10 | 29.46 | 27.95 | | | | | | | | |
| 527 | 34.65 | 32.06 | 30.33 | 31.44 | 31.08 | 30.89 | 30.54 | | | | | | | | |
| 767 | 35.17 | 33.04 | 31.84 | 32.91 | 32.17 | 32.66 | 32.99 | | | | | | | | |
| 947 | 35.35 | 33.36 | 32.37 | 33.35 | 32.56 | 33.19 | 33.71 | | | | | | | | |
| 1186 | 35.40 | 33.54 | 32.79 | 33.62 | 32.84 | 33.52 | 33.97 | | | | | | | | |

Figure A4.PT26a. Clay coating dried on glass plate in drying air at 35 C and high RH.

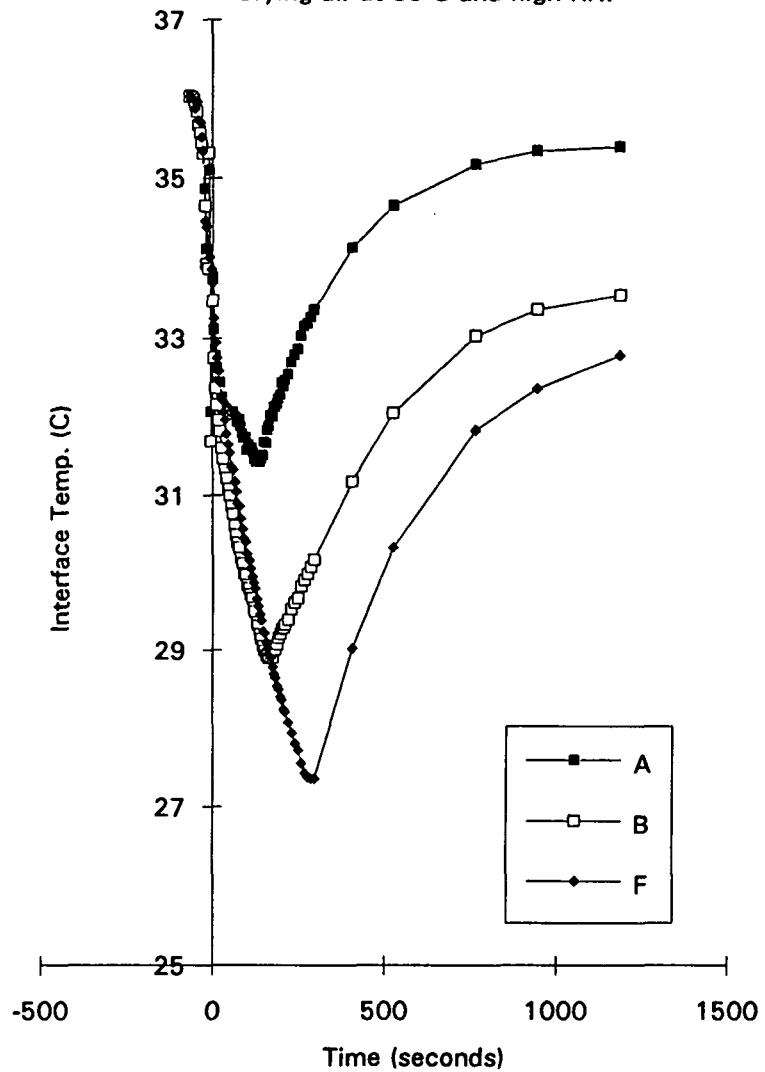


Figure A4.PT26b. Clay coating dried on glass plate in drying air at 35 C and high RH.

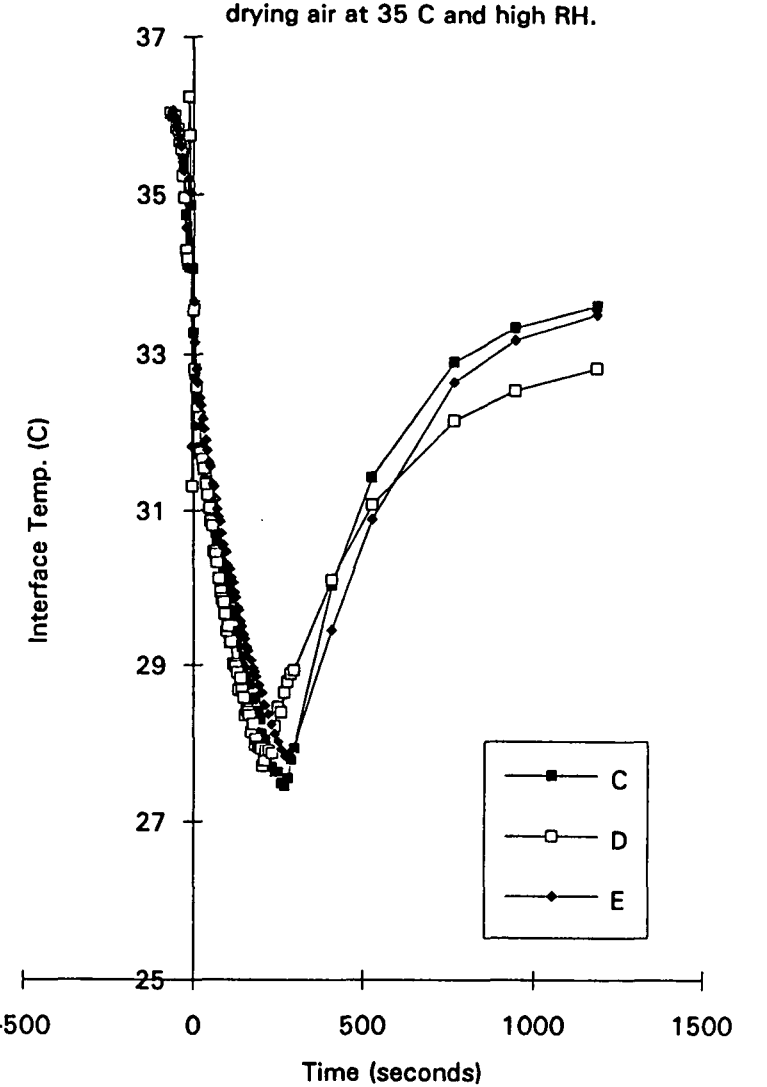

Table A4.PT27. Glass plate temperature during coating and drying at 35 C and 85% RH.

| PT27 Ref. Temp. Resistors Time-sec. | 36 A | 36 B | 36 F | 36 C | 36 D | 36 E | Left Edge |
|---|---|---|---|---|---|---|---|
| -74 | 35.99 | 36.00 | 36.07 | 36.02 | 36.01 | 36.00 | 35.33 |
| -69 | 36.05 | 36.11 | 36.13 | 36.07 | 36.06 | 36.08 | 35.49 |
| -64 | 36.02 | 36.01 | 35.99 | 36.05 | 36.05 | 36.03 | 35.49 |
| -60 | 35.95 | 35.92 | 35.88 | 35.91 | 35.95 | 35.93 | 35.49 |
| -55 | 35.95 | 35.92 | 35.82 | 35.92 | 35.89 | 35.90 | 35.64 |
| -50 | 35.86 | 35.83 | 34.92 | 35.84 | 36.33 | 35.77 | 35.33 |
| -46 | 35.76 | 35.71 | 33.61 | 35.75 | 37.42 | 35.74 | 35.49 |
| -41 | 35.66 | 35.65 | 35.09 | 35.75 | 36.27 | 35.71 | 35.49 |
| -37 | 35.56 | 35.54 | 35.49 | 35.60 | 35.61 | 35.56 | 35.33 |
| -32 | 35.43 | 35.42 | 35.37 | 35.52 | 35.42 | 35.48 | 35.33 |
| -27 | 35.29 | 35.29 | 35.28 | 35.44 | 35.25 | 35.34 | 35.64 |
| -23 | 34.81 | 34.42 | 34.35 | 34.54 | 34.69 | 34.62 | 35.64 |
| -18 | 34.24 | 34.22 | 34.40 | 34.32 | 34.30 | 34.33 | 35.49 |
| -14 | 33.80 | 33.65 | 33.91 | 33.84 | 33.83 | 33.92 | 35.33 |
| -9 | 33.46 | 33.31 | 33.34 | 33.50 | 33.58 | 33.63 | 35.49 |
| -4 | 33.81 | 33.77 | 33.89 | 33.77 | 33.85 | 34.03 | 35.33 |
| 0 | 33.77 | 33.70 | 33.84 | 33.74 | 33.80 | 33.98 | 35.33 |
| 5 | 33.21 | 33.08 | 33.39 | 33.32 | 33.32 | 33.52 | 32.96 |
| 10 | 33.06 | 32.87 | 33.25 | 33.05 | 33.02 | 33.29 | 32.16 |
| 14 | 32.86 | 32.64 | 33.08 | 32.95 | 32.90 | 33.10 | 31.69 |
| 19 | 32.81 | 32.54 | 32.98 | 32.76 | 32.71 | 32.99 | 31.53 |
| 23 | 32.63 | 32.38 | 32.80 | 32.66 | 32.58 | 32.86 | 31.37 |
| 28 | 32.63 | 32.24 | 32.72 | 32.50 | 32.41 | 32.77 | 31.37 |
| 33 | 32.52 | 32.07 | 32.53 | 32.36 | 32.26 | 32.54 | 30.90 |
| 37 | 32.49 | 31.95 | 32.43 | 32.25 | 32.16 | 32.43 | 30.90 |
| 42 | 32.54 | 31.85 | 32.36 | 32.14 | 31.95 | 32.37 | 30.90 |
| 46 | 32.46 | 31.71 | 32.17 | 32.05 | 31.87 | 32.18 | 30.75 |
| 51 | 32.55 | 31.61 | 32.12 | 31.93 | 31.73 | 32.14 | 30.59 |
| 56 | 32.46 | 31.45 | 31.96 | 31.80 | 31.61 | 31.98 | 30.44 |
| 60 | 32.51 | 31.39 | 31.91 | 31.67 | 31.48 | 31.90 | 30.44 |
| 65 | 32.45 | 31.24 | 31.76 | 31.62 | 31.38 | 31.78 | 30.13 |
| 69 | 32.55 | 31.16 | 31.69 | 31.57 | 31.26 | 31.73 | 30.13 |
| 74 | 32.51 | 31.05 | 31.57 | 31.41 | 31.16 | 31.58 | 29.97 |
| 79 | 32.46 | 30.96 | 31.39 | 31.30 | 31.04 | 31.50 | 29.82 |
| 83 | 32.46 | 30.89 | 31.29 | 31.14 | 30.92 | 31.39 | 29.82 |

| Time sec. | A | B | F | C | D | E | Left Edge |
|---|---|---|---|---|---|---|---|
| 88 | 32.37 | 30.73 | 31.12 | 31.09 | 30.84 | 31.23 | 29.67 |
| 92 | 32.31 | 30.66 | 31.03 | 31.06 | 30.79 | 31.17 | 29.51 |
| 97 | 32.32 | 30.59 | 30.95 | 30.95 | 30.68 | 31.09 | 29.82 |
| 102 | 32.35 | 30.53 | 30.89 | 30.88 | 30.55 | 31.02 | 29.20 |
| 106 | 32.28 | 30.49 | 30.81 | 30.77 | 30.46 | 30.94 | 29.51 |
| 111 | 32.19 | 30.35 | 30.67 | 30.69 | 30.43 | 30.86 | 29.05 |
| 115 | 32.12 | 30.27 | 30.60 | 30.66 | 30.35 | 30.75 | 29.05 |
| 120 | 32.15 | 30.26 | 30.57 | 30.48 | 30.24 | 30.66 | 29.05 |
| 125 | 32.12 | 30.13 | 30.41 | 30.50 | 30.18 | 30.61 | 28.74 |
| 129 | 32.17 | 30.13 | 30.38 | 30.35 | 30.13 | 30.51 | 28.74 |
| 134 | 32.14 | 30.06 | 30.31 | 30.32 | 30.06 | 30.45 | 28.74 |
| 138 | 32.17 | 29.98 | 30.21 | 30.21 | 29.96 | 30.32 | 28.74 |
| 143 | 32.23 | 29.93 | 30.12 | 30.14 | 29.91 | 30.26 | 28.58 |
| 148 | 32.32 | 29.89 | 30.07 | 30.10 | 29.85 | 30.22 | 28.74 |
| 152 | 32.43 | 29.87 | 29.95 | 30.00 | 29.80 | 30.18 | 28.27 |
| 157 | 32.55 | 29.86 | 29.88 | 29.95 | 29.75 | 30.10 | 28.43 |
| 161 | 32.71 | 29.92 | 29.90 | 29.84 | 29.65 | 30.05 | 28.27 |
| 167 | 32.80 | 29.90 | 29.78 | 29.79 | 29.63 | 29.98 | 28.27 |
| 177 | 32.98 | 30.01 | 29.59 | 29.66 | 29.58 | 29.87 | 28.22 |
| 186 | 33.20 | 30.21 | 29.42 | 29.47 | 29.43 | 29.73 | 28.22 |
| 196 | 33.32 | 30.30 | 29.33 | 29.42 | 29.41 | 29.67 | 27.88 |
| 205 | 33.48 | 30.43 | 29.23 | 29.33 | 29.38 | 29.57 | 27.75 |
| 215 | 33.66 | 30.58 | 29.12 | 29.18 | 29.45 | 29.46 | 27.75 |
| 224 | 33.89 | 30.75 | 29.04 | 28.96 | 29.62 | 29.38 | 27.75 |
| 234 | 34.03 | 30.87 | 28.93 | 28.84 | 29.82 | 29.31 | 27.75 |
| 243 | 34.14 | 31.01 | 28.78 | 28.75 | 30.06 | 29.27 | 27.25 |
| 253 | 34.35 | 31.13 | 28.62 | 28.62 | 30.24 | 29.19 | 27.13 |
| 262 | 34.40 | 31.21 | 28.56 | 28.68 | 30.43 | 29.31 | 27.44 |
| 272 | 34.61 | 31.41 | 28.47 | 28.59 | 30.55 | 29.31 | 27.28 |
| 282 | 34.72 | 31.50 | 28.49 | 28.64 | 30.70 | 29.44 | 27.13 |
| 291 | 34.81 | 31.62 | 28.54 | 28.73 | 30.85 | 29.59 | 27.06 |
| 298 | 34.84 | 31.68 | 28.56 | 28.90 | 30.97 | 29.74 | 26.84 |
| 407 | 35.57 | 32.86 | 30.44 | 31.17 | 32.20 | 31.43 | 29.34 |
| 587 | 36.40 | 34.24 | 32.37 | 33.48 | 33.66 | 33.44 | 32.35 |
| 766 | 36.73 | 34.86 | 33.49 | 34.61 | 34.45 | 34.51 | 33.55 |

Figure A4.PT27a. Clay coating dried on glass plate in drying air at 35 C and high RH.

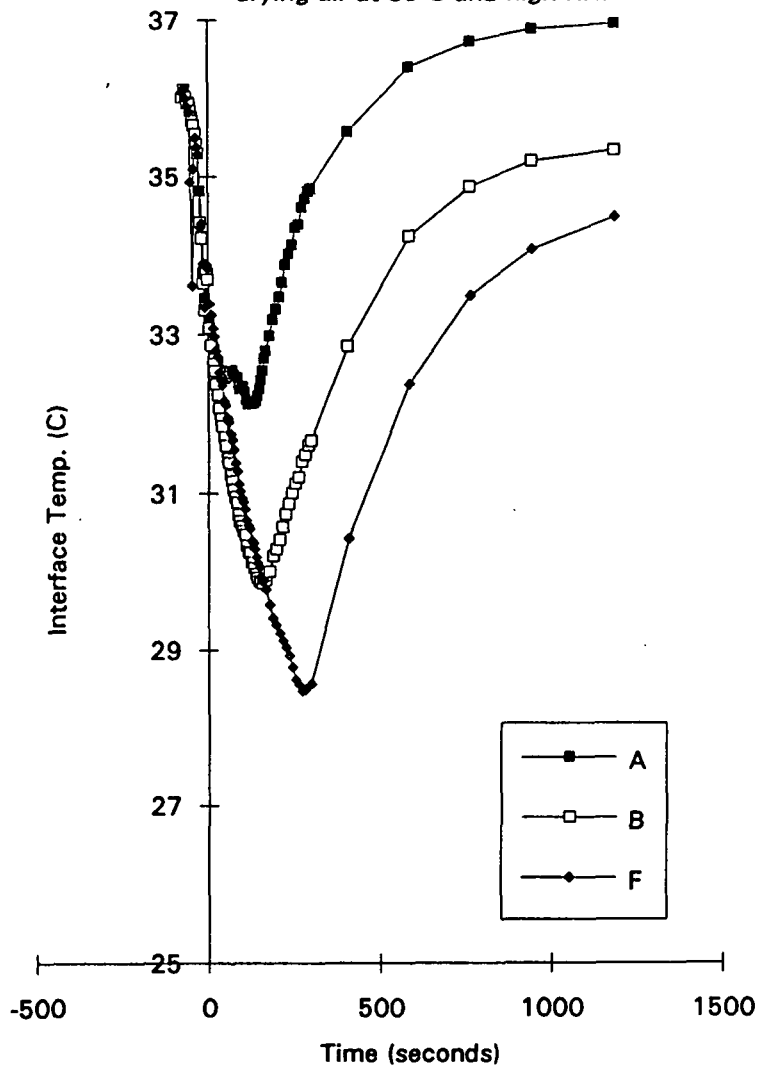


Figure A4.PT27b. Clay coating dried on glass plate in drying air at 35 C and high RH.

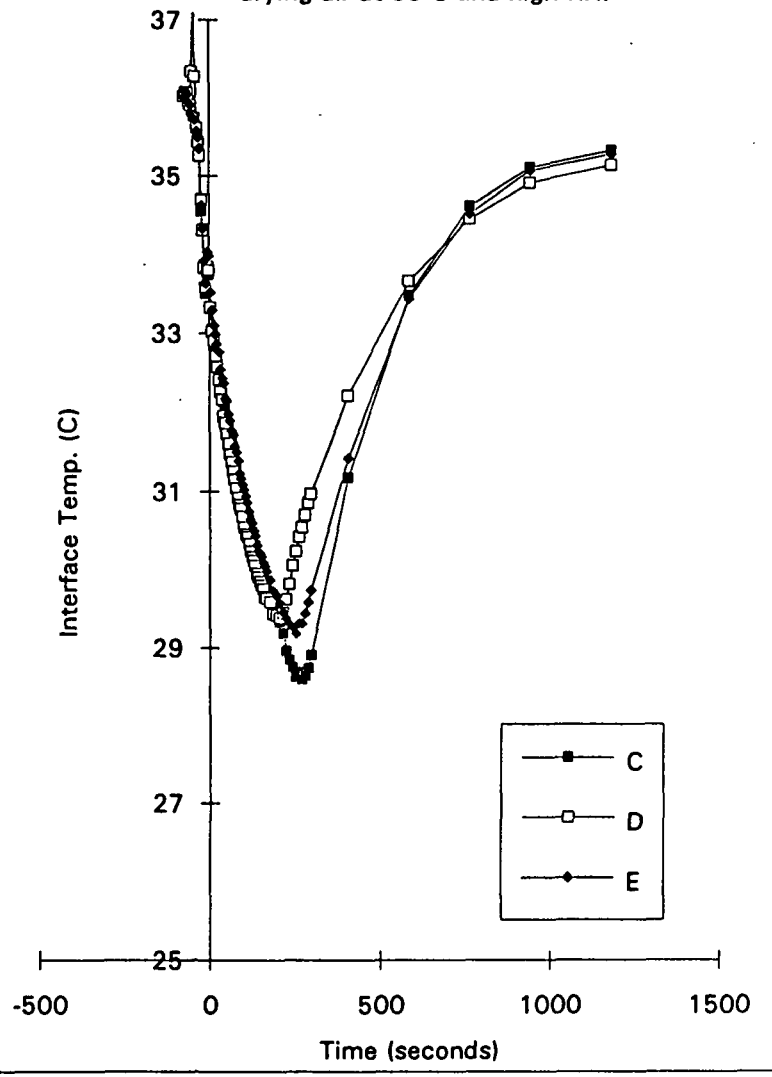

Table A4.PT28. Glass plate temperature during coating and drying at 35 C and 55% RH.

| PT28 Ref. Temp. Resistors Time-sec. | 35 A | 35 B | 35 F | 35 C | 35 D | 35 E | Left Edge |
|---|---|---|---|---|---|---|---|
| -70 | 35.03 | 35.04 | 34.92 | 35.04 | 35.04 | 35.05 | 34.80 |
| -65 | 34.98 | 35.03 | 35.01 | 35.00 | 35.04 | 35.02 | 35.12 |
| -60 | 35.01 | 34.98 | 35.06 | 35.00 | 34.98 | 35.02 | 34.80 |
| -55 | 34.95 | 34.90 | 34.87 | 34.92 | 34.90 | 34.88 | 34.96 |
| -51 | 34.83 | 34.79 | 35.08 | 34.81 | 34.88 | 34.81 | 34.80 |
| -46 | 34.69 | 34.66 | 34.04 | 34.65 | 34.63 | 34.67 | 34.96 |
| -41 | 34.61 | 34.56 | 34.01 | 34.62 | 34.56 | 34.64 | 34.80 |
| -37 | 34.46 | 34.47 | 33.96 | 34.49 | 34.48 | 34.52 | 34.96 |
| -32 | 34.40 | 34.33 | 33.80 | 34.38 | 34.31 | 34.35 | 35.12 |
| -28 | 34.24 | 34.23 | 33.68 | 34.27 | 34.14 | 34.27 | 35.12 |
| -23 | 33.66 | 33.63 | 32.91 | 33.62 | 33.65 | 33.69 | 34.80 |
| -18 | 33.08 | 32.97 | 32.36 | 33.08 | 33.07 | 33.04 | 35.28 |
| -14 | 32.51 | 32.54 | 32.96 | 32.61 | 32.55 | 32.65 | 34.77 |
| -9 | 32.46 | 32.49 | 32.31 | 32.42 | 32.24 | 32.38 | 34.96 |
| -5 | 32.69 | 32.71 | 32.13 | 32.56 | 32.48 | 32.68 | 34.96 |
| 0 | 31.06 | 31.48 | 31.43 | 31.63 | 31.50 | 31.81 | 34.96 |
| 5 | 28.79 | 29.48 | 30.28 | 29.85 | 29.86 | 30.09 | 33.22 |
| 9 | 27.99 | 28.67 | 29.73 | 29.10 | 29.15 | 29.39 | 29.61 |
| 14 | 27.44 | 28.07 | 29.21 | 28.55 | 28.66 | 28.88 | 28.84 |
| 18 | 27.07 | 27.67 | 28.87 | 28.17 | 28.34 | 28.48 | 28.53 |
| 23 | 26.83 | 27.36 | 28.57 | 27.91 | 27.95 | 28.19 | 28.22 |
| 28 | 26.61 | 27.06 | 28.26 | 27.62 | 27.64 | 27.90 | 27.60 |
| 32 | 26.47 | 26.81 | 28.02 | 27.43 | 27.35 | 27.71 | 27.60 |
| 37 | 26.34 | 26.58 | 27.73 | 27.14 | 27.08 | 27.44 | 27.44 |
| 41 | 26.34 | 26.32 | 27.49 | 26.90 | 26.88 | 27.15 | 26.65 |
| 46 | 26.78 | 26.07 | 27.25 | 26.67 | 26.58 | 26.96 | 26.65 |
| 51 | 27.32 | 25.86 | 26.99 | 26.48 | 26.32 | 26.72 | 26.49 |
| 55 | 27.78 | 25.67 | 26.77 | 26.32 | 26.20 | 26.51 | 26.33 |
| 60 | 28.09 | 25.67 | 26.53 | 26.13 | 25.90 | 26.37 | 25.86 |
| 64 | 28.35 | 25.84 | 26.34 | 25.92 | 25.73 | 26.21 | 25.70 |
| 69 | 28.45 | 26.15 | 26.06 | 25.71 | 25.59 | 25.99 | 25.54 |
| 74 | 28.64 | 26.50 | 25.92 | 25.49 | 25.53 | 25.87 | 25.19 |
| 78 | 28.70 | 26.73 | 25.67 | 25.28 | 25.53 | 25.63 | 25.06 |
| 83 | 28.85 | 26.93 | 25.51 | 25.10 | 25.65 | 25.54 | 24.75 |
| 91 | 29.01 | 27.13 | 25.20 | 24.88 | 26.15 | 25.28 | 24.75 |

| Time sec. | A | B | F | C | D | E | Left Edge |
|---|---|---|---|---|---|---|---|
| 100 | 29.22 | 27.33 | 24.75 | 24.62 | 26.56 | 25.03 | 24.43 |
| 110 | 29.42 | 27.49 | 24.34 | 24.59 | 26.90 | 24.93 | 23.80 |
| 119 | 29.59 | 27.61 | 24.15 | 24.84 | 27.07 | 25.09 | 23.80 |
| 129 | 29.70 | 27.75 | 24.60 | 25.31 | 27.24 | 25.41 | 23.48 |
| 138 | 29.88 | 27.89 | 25.01 | 25.77 | 27.37 | 25.75 | 23.32 |
| 148 | 30.07 | 28.07 | 25.27 | 26.14 | 27.56 | 26.08 | 23.32 |
| 157 | 30.17 | 28.19 | 25.48 | 26.47 | 27.69 | 26.35 | 23.00 |
| 167 | 30.37 | 28.36 | 25.61 | 26.77 | 27.90 | 26.59 | 23.48 |
| 177 | 30.53 | 28.55 | 25.82 | 27.06 | 28.05 | 26.82 | 24.27 |
| 186 | 30.73 | 28.75 | 25.98 | 27.27 | 28.23 | 27.01 | 24.91 |
| 196 | 30.80 | 28.87 | 26.15 | 27.44 | 28.30 | 27.22 | 25.70 |
| 205 | 30.96 | 28.99 | 26.32 | 27.64 | 28.44 | 27.41 | 25.86 |
| 215 | 31.14 | 29.19 | 26.51 | 27.85 | 28.61 | 27.55 | 26.33 |
| 224 | 31.25 | 29.28 | 26.65 | 28.02 | 28.72 | 27.78 | 26.65 |
| 234 | 31.34 | 29.39 | 26.80 | 28.17 | 28.81 | 27.92 | 26.97 |
| 404 | 32.61 | 31.10 | 29.04 | 30.73 | 30.51 | 30.54 | 30.88 |
| 585 | 33.30 | 32.13 | 30.32 | 32.11 | 31.64 | 31.90 | 32.78 |
| 764 | 33.49 | 32.55 | 31.04 | 32.78 | 32.20 | 32.63 | 33.31 |
| 945 | 33.64 | 32.80 | 31.46 | 33.14 | 32.52 | 32.96 | 33.88 |
| 1185 | 33.75 | 32.96 | 31.73 | 33.37 | 32.81 | 33.16 | 33.93 |

Figure A4.PT28a. Clay coating dried on glass plate in drying air at 35 C and med. RH.

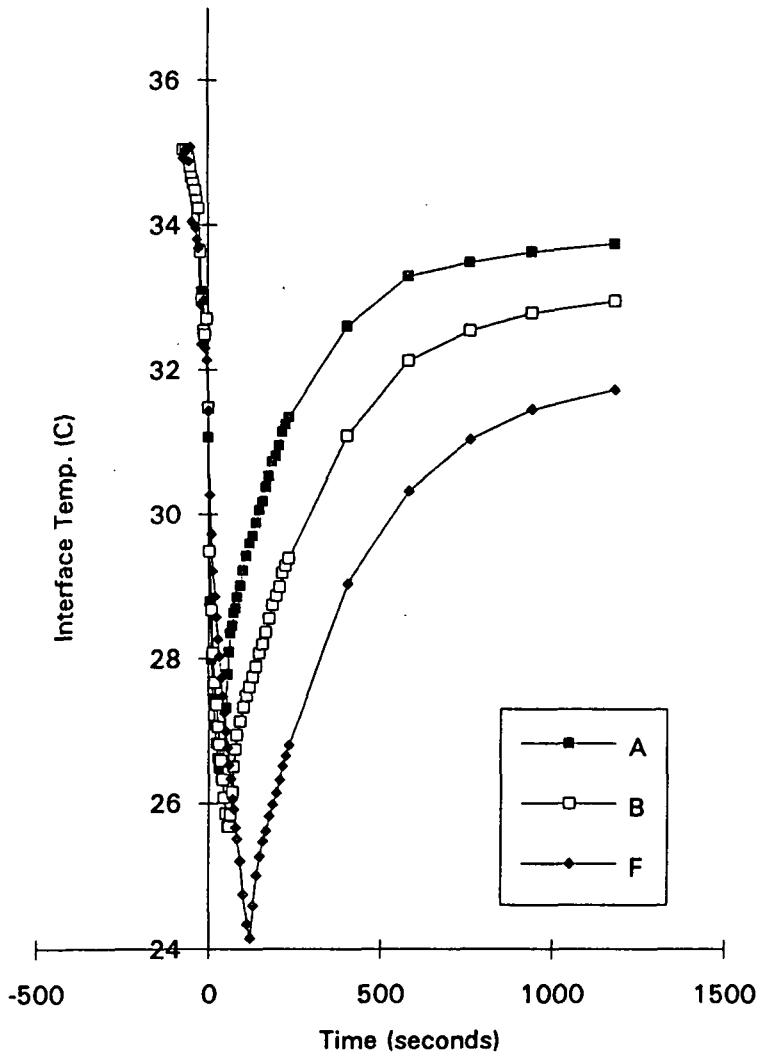


Figure A4.PT28b. Clay coating dried on glass plate in drying air at 35 C and med. RH.

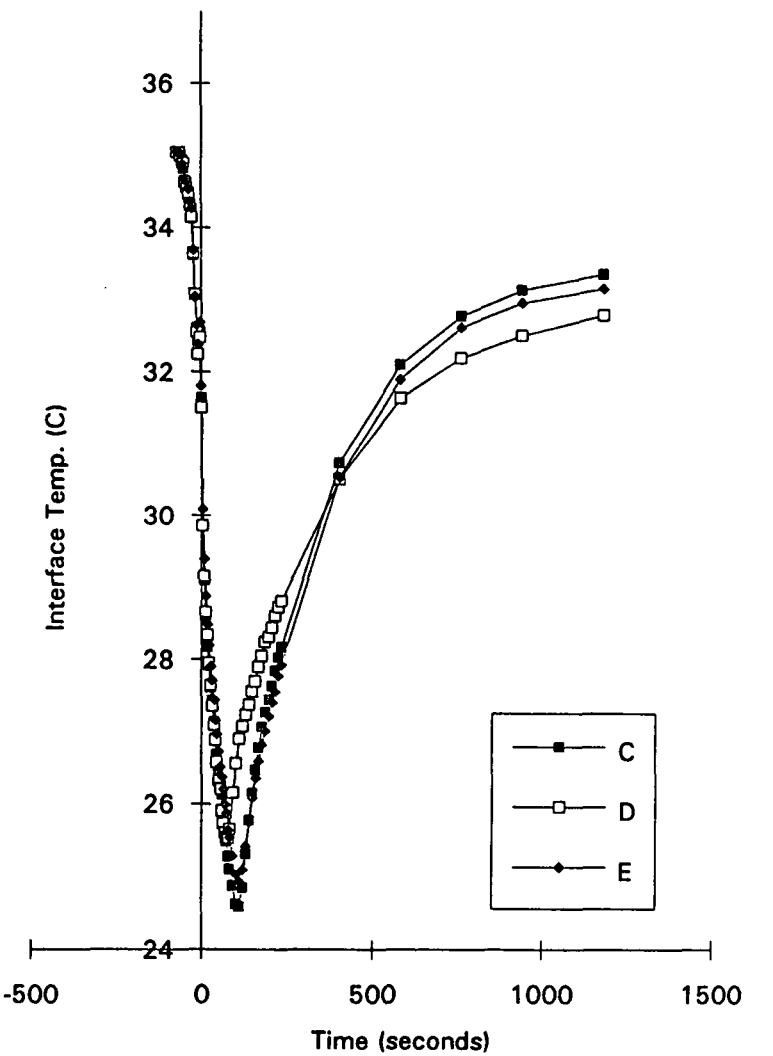

# APPENDIX V

## SUMMARIZED DATA FROM PORE VOLUME ANALYSIS

This appendix contains summaries of pore volume analysis for individual cross-sections for each drying condition used in the experimental drier (Fig. 25).

The first line of the first column of each table is trial code. Table VIII in the Material and Methods section contains the parameters for the trial codes. The remainder of the first column is the depth within the coating form which the data was obtained. The depth was measured in micrometer increments from the surface toward the substrate.

The next seven columns in each table are labeled with a sheet number and a direction code. The sheet number indicates which coating from a particular trial condition was used. The direction code indicates the orientation of the sample with respect to the coating direction and the number of embedded sample it was obtained from.

x - sample cut perpendicular to the coating direction.

y - sample cut parallel to the coating direction.

45 - Sample cut 45° to the coating direction.

The values on these columns are the relative pore volumes for each section with respect to depth into the coating.

The column labeled "overall total area analyzed" is the sum of the areas, in $\mu m^2$, analyzed from each section. The total pore area column is the corresponding total area occupied by pores for the seven sections. These values are used to calculate the composite relative pore area for each micrometer in depth.

The last two columns contain the average relative pore volume per section per coating depth and the standard deviation of the average respectively.

Finally below each column is the average and in some cases the standard deviation for each of the columns in the table. Following each table is a graph of the relative pore volume versus coating thickness. Low values of thickness are near the coating surface and high values are near the substrate.

## Pore Volume Profiles for Each of the Drying Conditions Employed to Dry Clay Films on Mylar

Table A5.1. Pore volume data for coating trial T35R15.

| Depth (microns) | Sheet 3 X1 | Sheet 1 X2 | Sheet 2 Y1 | Sheet 2 Y2 | Sheet 4 Y3 | Sheet 4 A45 | Sheet 3 B45 | OVERALL Total Area Analyzed | Total Pore Area | Relative Pore Area | Average Pore Vol. per sample | Std. Dev. |
|---|---|---|---|---|---|---|---|---|---|---|---|---|
| 1 | 42.25% | 42.06% | 41.90% | 41.31% | 42.06% | 41.83% | 42.06% | 56.45 | 23.66 | 42.07% | 0.419 | 0.0030 |
| 2 | 41.20% | 40.91% | 41.63% | 42.04% | 41.20% | 41.38% | 42.04% | 60.16 | 24.94 | 41.25% | 0.415 | 0.0044 |
| 3 | 40.77% | 40.18% | 40.32% | 40.73% | 40.73% | 40.50% | 40.73% | 74.71 | 30.32 | 40.44% | 0.406 | 0.0024 |
| 4 | 39.66% | 39.27% | 39.44% | 39.86% | 39.27% | 39.97% | 39.66% | 79.35 | 31.40 | 39.46% | 0.396 | 0.0027 |
| 5 | 38.90% | 39.04% | 39.22% | 39.64% | 39.22% | 39.51% | 39.51% | 79.00 | 31.04 | 39.05% | 0.393 | 0.0027 |
| 6 | 39.76% | 38.96% | 39.37% | 39.79% | 39.79% | 39.57% | 39.37% | 84.55 | 33.42 | 39.36% | 0.395 | 0.0031 |
| 7 | 39.41% | 39.42% | 39.56% | 39.98% | 39.41% | 39.42% | 39.98% | 84.64 | 33.51 | 39.47% | 0.396 | 0.0027 |
| 8 | 40.00% | 39.37% | 39.31% | 39.73% | 39.31% | 39.73% | 39.31% | 84.81 | 33.51 | 39.54% | 0.395 | 0.0028 |
| 9 | 38.63% | 39.42% | 40.01% | 40.42% | 39.42% | 39.31% | 39.31% | 74.95 | 29.61 | 39.38% | 0.395 | 0.0057 |
| 10 | 40.85% | 39.98% | 40.78% | 41.20% | 40.85% | 40.01% | 40.85% | 67.35 | 27.35 | 40.51% | 0.406 | 0.0047 |
| 11 | 41.22% | 40.70% | 41.88% | 41.65% | 41.65% | 40.21% | 40.70% | 66.32 | 27.26 | 41.22% | 0.411 | 0.0062 |
| 12 | 42.19% | 40.99% | 41.62% | 42.03% | 40.99% | 41.92% | 42.19% | 70.34 | 29.34 | 41.57% | 0.417 | 0.0053 |
| 13 | 42.52% | 41.25% | 42.35% | 42.76% | 42.35% | 41.50% | 41.25% | 71.83 | 30.17 | 42.07% | 0.420 | 0.0064 |
| 14 | 43.02% | 42.08% | 42.86% | 43.27% | 43.27% | 42.11% | 43.27% | 75.82 | 32.51 | 42.70% | 0.428 | 0.0053 |
| 15 | 43.81% | 42.89% | 44.13% | 44.54% | 43.81% | 42.97% | 43.81% | 77.14 | 33.76 | 43.70% | 0.437 | 0.0059 |
| 16 | 44.20% | 43.58% | 43.99% | 44.96% | 43.99% | 43.53% | 44.20% | 77.03 | 33.97 | 43.94% | 0.441 | 0.0048 |
| 17 | 44.89% | 44.11% | 44.66% | 45.06% | 44.11% | 44.77% | 44.77% | 77.83 | 34.75 | 44.58% | 0.446 | 0.0037 |
| 18 | 45.21% | 45.29% | 45.60% | 46.00% | 45.21% | 45.00% | 45.60% | 74.63 | 33.90 | 45.36% | 0.454 | 0.0034 |
| 19 | 45.74% | 45.37% | 45.82% | 46.22% | 46.22% | 45.62% | 46.22% | 73.43 | 33.68 | 45.61% | 0.459 | 0.0034 |
| 20 | 46.07% | 45.71% | 46.01% | 46.41% | 45.71% | 46.22% | 46.01% | 71.47 | 32.87 | 45.88% | 0.460 | 0.0025 |
| 21 | 46.16% | 45.95% | 46.45% | 46.74% | 46.45% | 46.23% | 46.23% | 77.30 | 35.78 | 46.15% | 0.463 | 0.0025 |
| 22 | 45.74% | 46.07% | 46.57% | 47.29% | 47.29% | 46.80% | 47.29% | 74.41 | 34.74 | 46.14% | 0.467 | 0.0063 |
| 23 | 45.80% | 46.43% | 46.34% | 46.85% | 45.80% | 46.16% | 46.43% | 80.19 | 37.11 | 46.21% | 0.463 | 0.0038 |
| 24 | 46.04% | 46.18% | 46.90% | 46.71% | 46.90% | 46.57% | 46.04% | 78.20 | 36.36 | 46.41% | 0.465 | 0.0039 |
| 25 | 46.73% | 46.38% | 47.13% | 47.12% | 46.38% | 47.01% | 46.38% | 85.19 | 39.83 | 46.77% | 0.467 | 0.0036 |
| 26 | 45.92% | 46.70% | 46.31% | 46.70% | 45.92% | 47.09% | 46.70% | 83.60 | 38.85 | 46.28% | 0.465 | 0.0044 |
| 27 | 45.71% | 46.26% | 46.10% | 46.50% | 46.50% | 46.94% | 46.50% | 74.76 | 34.66 | 46.01% | 0.464 | 0.0039 |
| 28 | 46.05% | 46.09% | 46.44% | 46.83% | 46.09% | 46.07% | 46.05% | 76.61 | 35.43 | 46.20% | 0.462 | 0.0030 |
| 29 | 44.84% | 45.91% | 45.22% | 45.62% | 45.22% | 45.91% | 45.91% | 83.43 | 38.00 | 45.38% | 0.455 | 0.0043 |
| 30 | 45.48% | 45.23% | 45.86% | 46.26% | 46.26% | 45.78% | 45.86% | 80.70 | 36.96 | 45.50% | 0.458 | 0.0038 |
| 31 | 44.70% | 44.98% | 45.13% | 45.53% | 44.70% | 45.12% | 45.53% | 76.99 | 34.71 | 44.95% | 0.451 | 0.0034 |
| 32 | 43.95% | 44.00% | 44.67% | 45.07% | 44.67% | 44.00% | 44.67% | 69.10 | 30.70 | 44.20% | 0.444 | 0.0044 |
| 33 | 43.31% | 44.21% | 43.27% | 43.67% | 44.00% | 43.68% | 43.68% | 69.03 | 30.17 | 43.64% | 0.437 | 0.0034 |
| 34 | 42.62% | 43.16% | 43.15% | 43.55% | 42.69% | 42.99% | 42.69% | 64.96 | 27.92 | 43.01% | 0.430 | 0.0034 |
| 35 | 42.19% | 42.44% | 41.67% | 42.07% | 41.95% | 41.55% | 42.44% | 55.87 | 23.48 | 42.09% | 0.420 | 0.0035 |
| Average | 43.36% | 43.33% | 43.53% | 43.94% | 43.19% | 43.46% | 43.54% | 74.63 | 32.45 | 43.48% | 0.434 | 0.0040 |
| Std. Dev. | | | | | | | | 7.55 | 4.06 | Total PoreVolume | 0.026 | 0.0012 |

**Figure A5.1. Pore Volume Profile For Trial T35R15.**

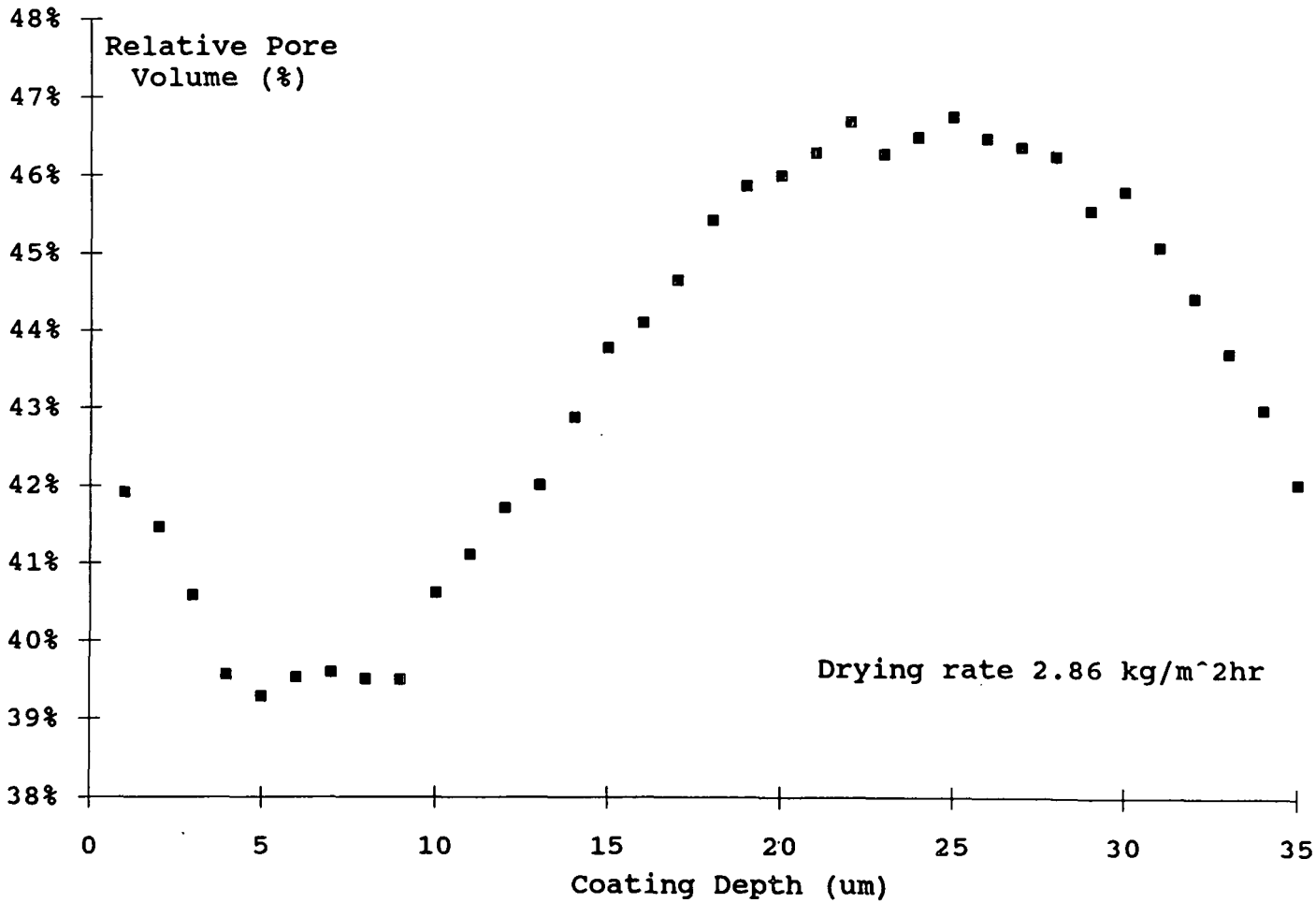

Table A5.2. Pore volume data for coating trial T35R55.

| Depth | Sheet 2 X1 | Sheet 3 X2 | Sheet 2 X3 | Sheet 4 Y1 | Sheet 1 A45 | Sheet 1 B45 | Sheet 2 C45 | OVERALL Total Area Analyzed | Total Pore Area | Relative Pore Area | Average Pore Vol. per sample | Std. Dev. |
|---|---|---|---|---|---|---|---|---|---|---|---|---|
| 1 | 41.92% | 41.42% | 41.65% | 41.65% | 41.84% | 42.74% | 42.00% | 45.28 | 18.94 | 41.83% | 0.419 | 0.0044 |
| 2 | 41.10% | 40.89% | 41.11% | 41.11% | 41.35% | 40.25% | 40.53% | 53.38 | 21.88 | 41.00% | 0.410 | 0.0043 |
| 3 | 40.32% | 40.02% | 40.24% | 40.24% | 39.95% | 40.15% | 40.05% | 63.30 | 25.45 | 40.20% | 0.402 | 0.0021 |
| 4 | 39.76% | 39.46% | 39.68% | 39.68% | 39.61% | 39.51% | 39.61% | 70.66 | 28.04 | 39.68% | 0.397 | 0.0021 |
| 5 | 39.41% | 38.49% | 39.77% | 38.70% | 39.44% | 39.51% | 39.00% | 68.68 | 27.00 | 39.31% | 0.393 | 0.0042 |
| 6 | 39.77% | 39.68% | 39.90% | 39.90% | 39.61% | 39.15% | 39.28% | 64.84 | 25.64 | 39.54% | 0.395 | 0.0036 |
| 7 | 39.74% | 40.00% | 40.22% | 40.22% | 40.15% | 39.57% | 39.41% | 60.42 | 24.03 | 39.76% | 0.397 | 0.0042 |
| 8 | 39.75% | 39.81% | 40.03% | 40.03% | 39.68% | 39.84% | 39.37% | 54.88 | 21.80 | 39.72% | 0.397 | 0.0021 |
| 9 | 39.64% | 39.67% | 39.89% | 39.89% | 39.74% | 39.54% | 39.45% | 63.75 | 25.27 | 39.64% | 0.396 | 0.0014 |
| 10 | 40.46% | 39.91% | 40.13% | 40.13% | 40.78% | 40.57% | 40.17% | 60.70 | 24.52 | 40.40% | 0.404 | 0.0032 |
| 11 | 40.88% | 40.91% | 41.14% | 41.14% | 41.01% | 40.61% | 40.29% | 60.73 | 24.73 | 40.73% | 0.407 | 0.0033 |
| 12 | 41.26% | 41.33% | 41.56% | 41.56% | 41.66% | 40.83% | 40.75% | 63.05 | 25.96 | 41.18% | 0.412 | 0.0036 |
| 13 | 41.94% | 42.19% | 42.42% | 42.42% | 41.72% | 41.52% | 41.08% | 64.95 | 27.15 | 41.80% | 0.418 | 0.0045 |
| 14 | 42.08% | 41.76% | 41.99% | 41.99% | 41.86% | 42.57% | 41.99% | 63.36 | 26.65 | 42.06% | 0.421 | 0.0028 |
| 15 | 42.85% | 42.38% | 42.61% | 42.61% | 42.72% | 43.28% | 42.37% | 59.43 | 25.38 | 42.71% | 0.427 | 0.0031 |
| 16 | 43.23% | 43.60% | 43.84% | 43.84% | 43.34% | 43.00% | 42.81% | 58.70 | 25.45 | 43.36% | 0.434 | 0.0040 |
| 17 | 43.66% | 43.83% | 44.07% | 44.07% | 43.62% | 44.61% | 43.53% | 63.26 | 27.73 | 43.84% | 0.439 | 0.0037 |
| 18 | 44.18% | 44.57% | 44.82% | 44.82% | 44.09% | 44.21% | 44.11% | 67.05 | 29.69 | 44.28% | 0.443 | 0.0028 |
| 19 | 44.50% | 44.11% | 44.35% | 44.35% | 44.07% | 44.86% | 44.60% | 67.17 | 29.83 | 44.40% | 0.444 | 0.0028 |
| 20 | 44.69% | 44.91% | 45.16% | 45.16% | 45.12% | 45.25% | 44.68% | 61.01 | 27.45 | 44.98% | 0.450 | 0.0023 |
| 21 | 45.08% | 45.41% | 45.66% | 45.66% | 45.33% | 45.62% | 45.08% | 60.39 | 27.40 | 45.37% | 0.454 | 0.0023 |
| 22 | 45.58% | 44.98% | 45.23% | 45.23% | 44.94% | 45.21% | 45.57% | 59.28 | 26.91 | 45.39% | 0.454 | 0.0046 |
| 23 | 45.62% | 45.67% | 45.92% | 45.92% | 45.88% | 45.67% | 45.69% | 60.03 | 27.52 | 45.83% | 0.458 | 0.0026 |
| 24 | 45.81% | 45.38% | 45.63% | 45.63% | 45.77% | 45.83% | 45.62% | 62.00 | 28.35 | 45.72% | 0.457 | 0.0020 |
| 25 | 46.18% | 45.92% | 46.17% | 46.17% | 45.29% | 46.00% | 45.61% | 63.68 | 29.15 | 45.78% | 0.458 | 0.0040 |
| 26 | 45.81% | 45.44% | 46.60% | 45.69% | 46.41% | 46.10% | 45.70% | 63.99 | 29.46 | 46.03% | 0.460 | 0.0041 |
| 27 | 45.85% | 46.01% | 46.26% | 46.26% | 46.33% | 45.18% | 45.33% | 62.42 | 28.59 | 45.81% | 0.458 | 0.0044 |
| 28 | 45.54% | 45.70% | 45.95% | 45.95% | 45.17% | 45.44% | 45.42% | 63.07 | 28.69 | 45.49% | 0.455 | 0.0029 |
| 29 | 45.04% | 45.46% | 45.71% | 45.71% | 45.52% | 44.67% | 45.45% | 61.20 | 27.71 | 45.27% | 0.453 | 0.0037 |
| 30 | 45.01% | 45.61% | 45.86% | 45.86% | 45.92% | 44.83% | 44.91% | 64.16 | 29.05 | 45.28% | 0.453 | 0.0050 |
| 31 | 44.35% | 45.17% | 45.42% | 45.42% | 44.41% | 43.61% | 44.19% | 60.14 | 26.72 | 44.42% | 0.445 | 0.0062 |
| 32 | 43.46% | 44.44% | 44.68% | 44.68% | 43.57% | 43.08% | 43.68% | 52.98 | 23.17 | 43.74% | 0.438 | 0.0057 |
| 33 | 42.72% | 43.17% | 43.41% | 43.41% | 42.15% | 42.15% | 42.53% | 49.07 | 20.92 | 42.62% | 0.426 | 0.0052 |
| 34 | 42.30% | 42.33% | 42.56% | 42.56% | 41.78% | 42.67% | 42.08% | 44.88 | 18.90 | 42.10% | 0.421 | 0.0049 |
| Average | 42.93% | 42.93% | 43.22% | 43.17% | 42.94% | 42.87% | 42.70% | 60.64 | 26.0326194 | 0.42926866 | 0.4292061 | 0.0036 |
| Stdev. | | | | | | | | 5.87 | 2.90 | Total Pore Volume | 0.023 | 0.0011 |

**Figure A5.2. Pore Volume Profile For Trial T35R55.**

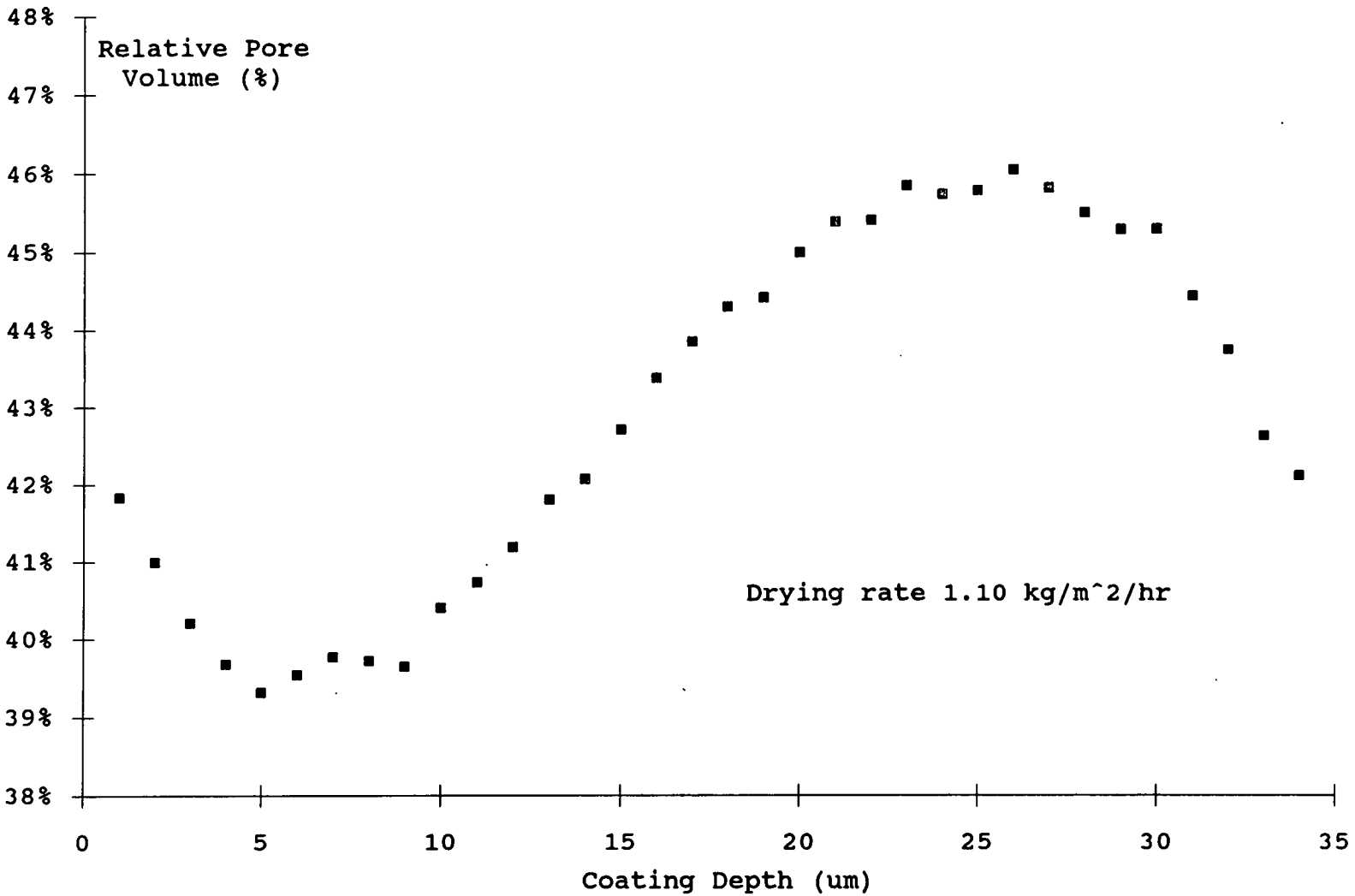

Table A5.3. Pore volume data for coating trial T35R85.

| Depth (microns) | Sheet 3 X1 | Sheet 1 X2 | Sheet 2 X3 | Sheet 2 Y1 | Sheet 4 Y2 | Sheet 4 A45 | Sheet 3 B45 | OVERALL Total Area Analyzed | Total Pore Area | Relative Pore Area | Average Pore Vol. per Sample | Std. Dev. |
|---|---|---|---|---|---|---|---|---|---|---|---|---|
| 1 | 41.84% | 42.11% | 42.28% | 41.25% | 41.71% | 42.73% | 41.54% | 61.37 | 25.74 | 41.93% | 0.419 | 0.0050 |
| 2 | 41.66% | 41.03% | 40.92% | 40.31% | 41.07% | 40.39% | 40.35% | 87.51 | 35.75 | 40.85% | 0.408 | 0.0050 |
| 3 | 40.36% | 40.18% | 40.34% | 39.36% | 39.79% | 40.77% | 39.63% | 115.92 | 46.45 | 40.07% | 0.401 | 0.0049 |
| 4 | 39.86% | 39.87% | 40.14% | 39.41% | 39.85% | 40.82% | 39.68% | 112.03 | 44.77 | 39.96% | 0.399 | 0.0044 |
| 5 | 39.81% | 39.66% | 39.82% | 38.84% | 39.28% | 40.24% | 39.12% | 98.06 | 38.79 | 39.56% | 0.395 | 0.0048 |
| 6 | 40.54% | 40.21% | 40.00% | 39.18% | 39.61% | 40.79% | 39.66% | 102.02 | 40.84 | 40.03% | 0.400 | 0.0056 |
| 7 | 39.32% | 39.73% | 39.92% | 39.94% | 39.37% | 40.44% | 40.18% | 105.04 | 41.90 | 39.89% | 0.398 | 0.0041 |
| 8 | 39.86% | 40.00% | 40.02% | 39.95% | 39.03% | 40.46% | 40.37% | 106.36 | 42.53 | 39.99% | 0.400 | 0.0046 |
| 9 | 40.73% | 39.87% | 39.91% | 39.57% | 40.03% | 40.21% | 39.00% | 85.51 | 34.11 | 39.89% | 0.399 | 0.0053 |
| 10 | 40.22% | 40.50% | 40.66% | 39.67% | 40.11% | 41.09% | 39.94% | 65.73 | 26.51 | 40.32% | 0.403 | 0.0048 |
| 11 | 40.55% | 40.84% | 41.00% | 40.00% | 40.45% | 41.43% | 40.28% | 67.85 | 27.59 | 40.66% | 0.406 | 0.0048 |
| 12 | 40.92% | 41.87% | 41.13% | 40.52% | 40.26% | 41.00% | 40.27% | 63.65 | 26.01 | 40.86% | 0.409 | 0.0057 |
| 13 | 40.79% | 41.12% | 41.28% | 40.34% | 40.67% | 41.27% | 40.50% | 68.19 | 27.86 | 40.86% | 0.409 | 0.0038 |
| 14 | 41.07% | 42.13% | 41.55% | 40.53% | 40.98% | 41.98% | 40.81% | 71.56 | 29.56 | 41.30% | 0.413 | 0.0061 |
| 15 | 42.13% | 43.11% | 42.61% | 41.57% | 41.05% | 42.05% | 41.08% | 72.37 | 30.34 | 41.93% | 0.419 | 0.0077 |
| 16 | 41.75% | 43.04% | 43.12% | 42.00% | 42.95% | 42.27% | 41.24% | 70.72 | 29.97 | 42.37% | 0.423 | 0.0073 |
| 17 | 42.57% | 43.23% | 42.96% | 42.28% | 42.69% | 43.50% | 41.54% | 69.36 | 29.60 | 42.68% | 0.427 | 0.0065 |
| 18 | 43.00% | 43.06% | 43.21% | 42.17% | 42.72% | 43.56% | 42.74% | 78.55 | 33.72 | 42.93% | 0.429 | 0.0044 |
| 19 | 43.00% | 43.37% | 43.45% | 42.36% | 43.07% | 43.70% | 42.90% | 77.72 | 33.52 | 43.13% | 0.431 | 0.0044 |
| 20 | 43.22% | 43.78% | 43.59% | 43.73% | 43.22% | 43.47% | 42.73% | 78.89 | 34.23 | 43.39% | 0.434 | 0.0037 |
| 21 | 43.93% | 44.18% | 43.64% | 44.34% | 43.95% | 44.37% | 42.71% | 73.60 | 32.29 | 43.87% | 0.439 | 0.0058 |
| 22 | 44.25% | 45.12% | 44.91% | 44.34% | 43.99% | 45.22% | 43.41% | 77.44 | 34.43 | 44.47% | 0.445 | 0.0066 |
| 23 | 45.21% | 45.56% | 44.54% | 44.46% | 44.13% | 45.84% | 44.94% | 78.73 | 35.41 | 44.98% | 0.450 | 0.0062 |
| 24 | 45.00% | 45.32% | 45.51% | 44.39% | 44.89% | 45.99% | 44.70% | 69.04 | 31.16 | 45.13% | 0.451 | 0.0053 |
| 25 | 45.47% | 45.79% | 45.98% | 44.86% | 45.36% | 46.47% | 45.17% | 69.32 | 31.61 | 45.60% | 0.456 | 0.0054 |
| 26 | 45.14% | 45.79% | 46.73% | 44.96% | 45.03% | 45.98% | 45.03% | 69.24 | 31.52 | 45.53% | 0.455 | 0.0067 |
| 27 | 45.22% | 45.53% | 45.75% | 44.60% | 45.10% | 46.20% | 44.91% | 65.81 | 29.84 | 45.34% | 0.453 | 0.0054 |
| 28 | 44.53% | 45.90% | 45.00% | 44.13% | 44.39% | 45.47% | 44.20% | 61.29 | 27.47 | 44.82% | 0.448 | 0.0068 |
| 29 | 44.47% | 44.41% | 44.43% | 44.80% | 44.49% | 44.98% | 44.09% | 72.10 | 32.11 | 44.53% | 0.445 | 0.0029 |
| 30 | 43.90% | 44.01% | 43.44% | 44.56% | 44.06% | 44.26% | 45.41% | 74.97 | 33.16 | 44.23% | 0.442 | 0.0062 |
| 31 | 43.65% | 43.06% | 42.72% | 44.23% | 43.80% | 43.99% | 44.32% | 74.44 | 32.48 | 43.63% | 0.437 | 0.0059 |
| 32 | 42.31% | 41.68% | 42.06% | 42.43% | 42.85% | 43.08% | 43.17% | 78.87 | 33.52 | 42.50% | 0.425 | 0.0055 |
| 33 | 40.82% | 41.16% | 41.33% | 42.41% | 42.47% | 41.83% | 42.32% | 82.81 | 34.54 | 41.72% | 0.418 | 0.0067 |
| 34 | 41.00% | 41.22% | 41.18% | 40.88% | 42.55% | 42.52% | 42.48% | 84.72 | 35.26 | 41.62% | 0.417 | 0.0078 |
| Average | 42.30% | 42.57% | 42.50% | 42.01% | 42.20% | 42.89% | 42.07% | 79.14 | 33.37 | 42.13% | 0.4236453 | 0.0055 |
| Std. Dev. | | | | | | | | 14.62 | 5.21 | Total Pore Volume | 0.020 | 0.0012 |

**Figure A5.3. Pore Volume Profile For Trial T35R85.**

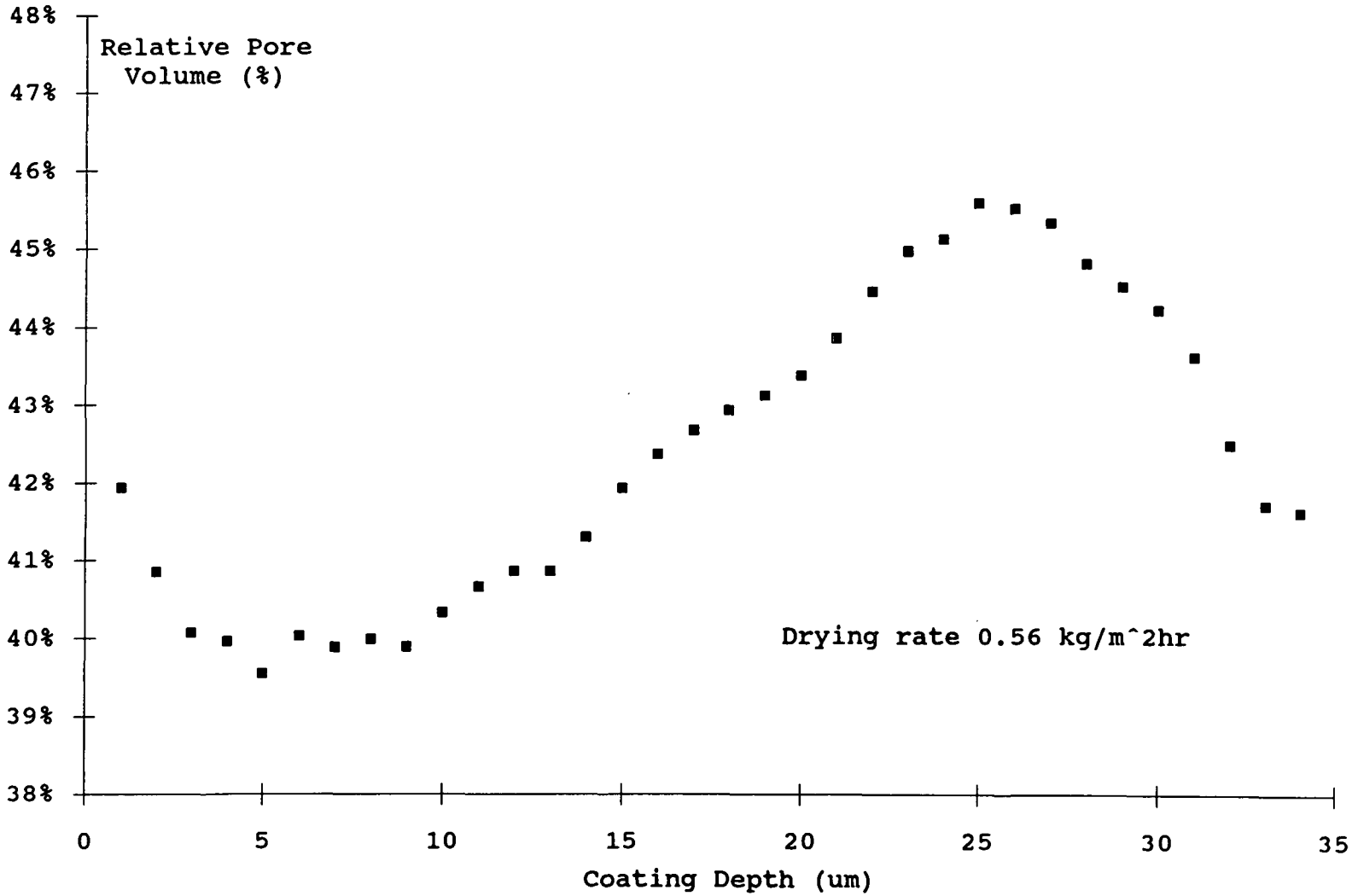

Table A5.4. Pore volume data for coating trial T55R15.

| Depth (microns) | Sheet 1 X1 | Sheet 2 X2 | Sheet 2 Y1 | Sheet 3 Y2 | Sheet 1 Y3 | Sheet 1 A45 | Sheet 2 B45 | OVERALL Total Area Analyzed | Total Pore Area | Relative Pore Area | Average Pore Vol. per Sample | Std. Dev. |
|---|---|---|---|---|---|---|---|---|---|---|---|---|
| 1 | 42.05% | 41.50% | 41.52% | 42.15% | 41.61% | 42.38% | 42.08% | 53.79 | 22.53 | 41.89% | 0.419 | 0.0035 |
| 2 | 41.41% | 40.89% | 41.06% | 40.92% | 40.67% | 41.38% | 40.56% | 59.49 | 24.40 | 41.02% | 0.410 | 0.0033 |
| 3 | 40.32% | 40.67% | 40.00% | 40.45% | 40.06% | 40.37% | 40.15% | 63.59 | 25.62 | 40.29% | 0.403 | 0.0024 |
| 4 | 39.52% | 40.24% | 39.31% | 39.67% | 39.55% | 39.98% | 39.42% | 67.45 | 26.77 | 39.68% | 0.397 | 0.0033 |
| 5 | 39.19% | 39.25% | 38.67% | 39.12% | 39.25% | 39.56% | 39.51% | 71.87 | 28.18 | 39.21% | 0.392 | 0.0029 |
| 6 | 39.21% | 39.46% | 38.75% | 38.99% | 39.46% | 39.30% | 39.15% | 78.06 | 30.59 | 39.19% | 0.392 | 0.0026 |
| 7 | 39.82% | 39.15% | 39.37% | 38.17% | 39.33% | 39.46% | 39.26% | 77.44 | 30.37 | 39.22% | 0.392 | 0.0051 |
| 8 | 40.19% | 39.67% | 39.88% | 39.57% | 39.71% | 40.51% | 39.48% | 75.92 | 30.28 | 39.88% | 0.399 | 0.0037 |
| 9 | 40.33% | 41.00% | 40.14% | 40.33% | 40.49% | 40.81% | 40.67% | 74.27 | 30.11 | 40.54% | 0.405 | 0.0030 |
| 10 | 41.05% | 40.36% | 40.67% | 41.25% | 41.37% | 40.99% | 41.13% | 70.22 | 28.77 | 40.98% | 0.410 | 0.0035 |
| 11 | 41.82% | 40.99% | 41.49% | 42.80% | 42.19% | 41.31% | 41.26% | 67.74 | 28.27 | 41.73% | 0.417 | 0.0063 |
| 12 | 42.47% | 41.56% | 41.93% | 43.17% | 43.67% | 41.89% | 42.67% | 64.71 | 27.52 | 42.53% | 0.425 | 0.0076 |
| 13 | 42.91% | 42.90% | 42.65% | 43.68% | 43.71% | 44.02% | 43.91% | 64.65 | 28.04 | 43.38% | 0.434 | 0.0056 |
| 14 | 43.69% | 43.33% | 43.34% | 44.28% | 43.89% | 44.63% | 44.26% | 66.12 | 29.01 | 43.88% | 0.439 | 0.0050 |
| 15 | 44.54% | 43.97% | 43.92% | 44.93% | 44.09% | 44.89% | 44.87% | 69.65 | 30.94 | 44.43% | 0.445 | 0.0046 |
| 16 | 44.90% | 44.67% | 44.87% | 45.28% | 44.67% | 45.02% | 45.66% | 69.86 | 31.41 | 44.96% | 0.450 | 0.0036 |
| 17 | 45.35% | 45.75% | 45.06% | 45.77% | 45.37% | 45.73% | 46.09% | 71.15 | 32.42 | 45.57% | 0.456 | 0.0035 |
| 18 | 45.93% | 46.19% | 45.38% | 46.03% | 46.18% | 45.74% | 46.84% | 72.73 | 33.46 | 46.00% | 0.460 | 0.0045 |
| 19 | 46.43% | 46.61% | 45.69% | 46.82% | 46.27% | 46.05% | 46.59% | 73.15 | 33.90 | 46.34% | 0.464 | 0.0038 |
| 20 | 46.73% | 46.57% | 46.13% | 46.72% | 46.66% | 47.09% | 46.82% | 71.51 | 33.38 | 46.68% | 0.467 | 0.0029 |
| 21 | 46.89% | 46.80% | 46.81% | 46.91% | 46.83% | 47.26% | 47.00% | 70.39 | 33.03 | 46.93% | 0.469 | 0.0016 |
| 22 | 47.05% | 46.99% | 46.37% | 47.03% | 46.99% | 46.73% | 47.09% | 68.71 | 32.23 | 46.90% | 0.469 | 0.0026 |
| 23 | 46.80% | 47.35% | 47.00% | 47.32% | 47.03% | 47.40% | 47.23% | 68.83 | 32.46 | 47.16% | 0.472 | 0.0022 |
| 24 | 47.03% | 47.02% | 46.75% | 47.49% | 47.25% | 47.86% | 47.15% | 70.74 | 33.40 | 47.22% | 0.472 | 0.0036 |
| 25 | 47.06% | 47.15% | 46.60% | 47.11% | 47.37% | 47.52% | 46.49% | 70.73 | 33.29 | 47.06% | 0.470 | 0.0038 |
| 26 | 46.83% | 47.31% | 46.59% | 47.03% | 46.87% | 47.40% | 47.35% | 69.20 | 32.56 | 47.05% | 0.471 | 0.0031 |
| 27 | 46.80% | 46.25% | 46.22% | 46.82% | 46.91% | 46.61% | 47.05% | 68.84 | 32.10 | 46.63% | 0.467 | 0.0032 |
| 28 | 46.73% | 46.71% | 46.51% | 46.85% | 46.73% | 47.10% | 46.60% | 67.04 | 31.34 | 46.75% | 0.467 | 0.0019 |
| 29 | 46.20% | 46.01% | 45.94% | 46.18% | 46.55% | 46.91% | 46.51% | 70.89 | 32.84 | 46.32% | 0.463 | 0.0035 |
| 30 | 45.83% | 45.23% | 45.37% | 45.61% | 45.70% | 45.73% | 46.02% | 70.58 | 32.20 | 45.62% | 0.456 | 0.0027 |
| 31 | 45.13% | 45.27% | 44.99% | 44.54% | 44.31% | 45.62% | 44.82% | 71.97 | 32.34 | 44.94% | 0.450 | 0.0044 |
| 32 | 44.31% | 44.67% | 44.58% | 43.50% | 43.67% | 45.02% | 44.67% | 69.78 | 30.92 | 44.32% | 0.443 | 0.0056 |
| 33 | 43.50% | 43.10% | 43.63% | 42.97% | 42.75% | 43.31% | 44.28% | 63.78 | 27.65 | 43.35% | 0.434 | 0.0051 |
| 34 | 42.69% | 42.80% | 42.21% | 42.15% | 42.26% | 42.48% | 43.88% | 59.16 | 25.21 | 42.61% | 0.426 | 0.0060 |
| 35 | 41.99% | 41.53% | 41.69% | 41.83% | 42.38% | 42.32% | 42.99% | 51.76 | 21.78 | 42.07% | 0.421 | 0.0050 |
| Average | 43.79% | 43.68% | 43.46% | 43.81% | 43.77% | 44.01% | 43.99% | 68.45 | 29.98 | 43.80% | 0.438 | 0.0038 |
| Std. Dev. | | | | | | | | 5.74 | 3.23 | Total Pore Volume | 0.028 | 0.0013 |

**Figure A5.4. Pore Volume Profile For Trial T55R15.**

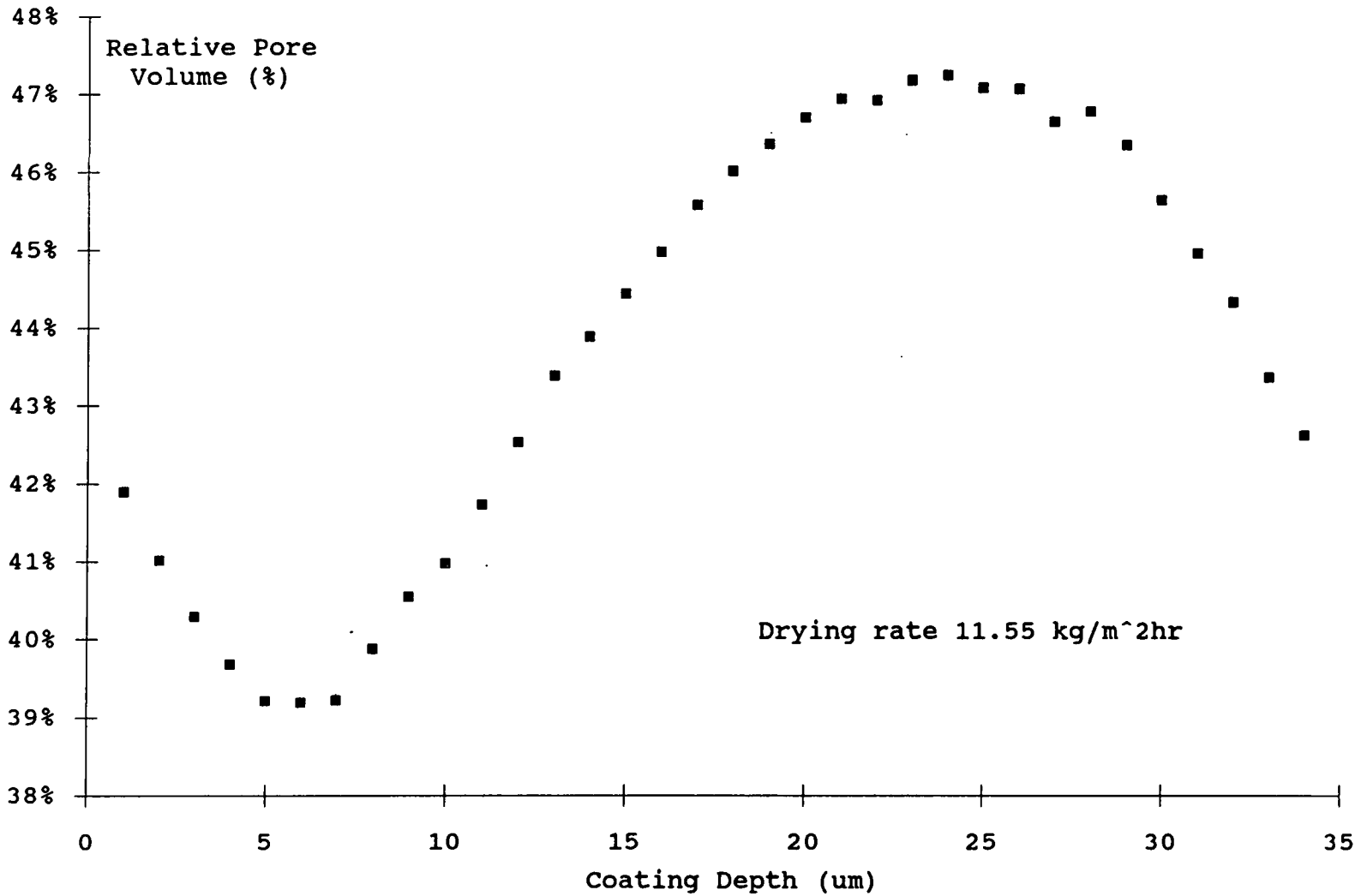

Table A5.5. Pore volume data for coating trial T55R55.

| Depth (microns) | Sheet 1 X1 | Sheet 1 X2 | Sheet 3 X3 | Sheet 2 Y1 | Sheet 3 Y2 | Sheet 4 A45 | Sheet 4 B45 | OVERALL Total Area Analyzed | Total Pore Area | Relative Pore Area | Average Pore Vol. per Sample | Std. Dev. |
|---|---|---|---|---|---|---|---|---|---|---|---|---|
| 1 | 41.88% | 40.20% | 41.56% | 40.58% | 41.25% | 41.56% | 42.15% | 49.26 | 20.37 | 41.36% | 0.413 | 0.0070 |
| 2 | 41.23% | 40.52% | 40.37% | 40.65% | 41.37% | 40.16% | 40.91% | 52.10 | 21.23 | 40.74% | 0.407 | 0.0045 |
| 3 | 40.39% | 39.50% | 39.85% | 40.23% | 40.11% | 40.01% | 40.00% | 54.33 | 21.75 | 40.03% | 0.400 | 0.0029 |
| 4 | 39.62% | 38.24% | 39.76% | 40.00% | 40.08% | 39.82% | 39.67% | 59.42 | 23.56 | 39.65% | 0.396 | 0.0062 |
| 5 | 39.30% | 38.25% | 39.61% | 39.87% | 39.87% | 39.54% | 39.82% | 70.87 | 28.00 | 39.51% | 0.395 | 0.0058 |
| 6 | 39.53% | 38.67% | 39.57% | 39.56% | 39.72% | 39.40% | 39.64% | 83.29 | 32.85 | 39.44% | 0.394 | 0.0035 |
| 7 | 39.68% | 39.07% | 39.79% | 39.74% | 39.81% | 39.39% | 39.72% | 85.05 | 33.68 | 39.60% | 0.396 | 0.0027 |
| 8 | 39.61% | 39.15% | 39.52% | 39.66% | 39.70% | 39.81% | 39.51% | 84.27 | 33.34 | 39.56% | 0.396 | 0.0021 |
| 9 | 39.57% | 39.64% | 40.28% | 39.93% | 40.65% | 39.99% | 39.89% | 83.07 | 33.22 | 39.99% | 0.400 | 0.0037 |
| 10 | 40.50% | 40.05% | 40.39% | 40.26% | 41.52% | 40.62% | 40.38% | 72.26 | 29.30 | 40.55% | 0.405 | 0.0047 |
| 11 | 40.92% | 40.59% | 41.66% | 40.86% | 41.06% | 40.67% | 40.91% | 56.67 | 23.22 | 40.98% | 0.410 | 0.0035 |
| 12 | 41.44% | 40.23% | 41.40% | 41.18% | 41.75% | 41.32% | 41.62% | 53.03 | 21.91 | 41.32% | 0.413 | 0.0050 |
| 13 | 41.90% | 41.38% | 41.87% | 41.62% | 42.29% | 41.96% | 42.38% | 65.79 | 27.57 | 41.91% | 0.419 | 0.0035 |
| 14 | 42.47% | 41.90% | 42.54% | 41.88% | 42.67% | 42.63% | 43.17% | 71.17 | 30.17 | 42.40% | 0.425 | 0.0045 |
| 15 | 43.24% | 42.52% | 43.99% | 42.60% | 43.32% | 43.08% | 43.59% | 58.40 | 25.24 | 43.22% | 0.432 | 0.0052 |
| 16 | 43.73% | 42.96% | 43.86% | 43.15% | 43.51% | 43.66% | 44.30% | 54.30 | 23.68 | 43.61% | 0.436 | 0.0045 |
| 17 | 44.24% | 43.50% | 44.21% | 43.63% | 43.30% | 44.10% | 44.81% | 55.43 | 24.37 | 43.97% | 0.440 | 0.0052 |
| 18 | 44.85% | 43.78% | 45.19% | 44.05% | 44.06% | 44.23% | 44.97% | 56.84 | 25.28 | 44.48% | 0.444 | 0.0055 |
| 19 | 45.13% | 44.05% | 45.67% | 45.38% | 44.51% | 45.37% | 45.39% | 70.10 | 31.62 | 45.10% | 0.451 | 0.0058 |
| 20 | 45.49% | 44.66% | 45.92% | 45.16% | 44.65% | 45.68% | 45.27% | 81.67 | 36.97 | 45.27% | 0.453 | 0.0048 |
| 21 | 45.83% | 45.00% | 46.28% | 45.33% | 44.73% | 45.82% | 45.88% | 84.89 | 38.67 | 45.56% | 0.456 | 0.0055 |
| 22 | 46.04% | 45.93% | 46.35% | 45.70% | 45.80% | 46.37% | 46.15% | 78.54 | 36.17 | 46.05% | 0.460 | 0.0026 |
| 23 | 46.05% | 46.80% | 46.82% | 46.02% | 46.09% | 46.02% | 46.20% | 68.27 | 31.60 | 46.29% | 0.463 | 0.0036 |
| 24 | 46.11% | 46.84% | 46.15% | 46.58% | 45.81% | 46.11% | 46.37% | 63.53 | 29.37 | 46.24% | 0.463 | 0.0034 |
| 25 | 46.26% | 46.53% | 46.40% | 46.39% | 45.72% | 46.00% | 46.11% | 68.52 | 31.64 | 46.18% | 0.462 | 0.0028 |
| 26 | 46.25% | 45.28% | 46.02% | 46.51% | 46.00% | 45.96% | 46.34% | 76.88 | 35.38 | 46.02% | 0.461 | 0.0040 |
| 27 | 46.08% | 45.10% | 46.15% | 46.44% | 46.11% | 46.17% | 45.98% | 84.89 | 39.05 | 46.00% | 0.460 | 0.0042 |
| 28 | 45.87% | 45.06% | 46.22% | 45.99% | 46.28% | 45.73% | 46.01% | 84.42 | 38.72 | 45.87% | 0.459 | 0.0041 |
| 29 | 45.41% | 44.58% | 45.76% | 44.31% | 45.81% | 45.22% | 45.51% | 74.17 | 33.57 | 45.26% | 0.452 | 0.0058 |
| 30 | 45.54% | 45.37% | 45.03% | 44.56% | 44.99% | 44.96% | 44.80% | 65.06 | 29.32 | 45.07% | 0.450 | 0.0033 |
| 31 | 44.75% | 44.29% | 44.70% | 44.40% | 44.65% | 44.51% | 44.12% | 62.70 | 27.92 | 44.54% | 0.445 | 0.0023 |
| 32 | 44.08% | 43.15% | 44.16% | 43.61% | 43.90% | 43.82% | 43.53% | 57.28 | 25.10 | 43.81% | 0.438 | 0.0035 |
| 33 | 43.17% | 42.60% | 43.29% | 43.12% | 42.26% | 42.66% | 43.10% | 53.97 | 23.14 | 42.88% | 0.429 | 0.0038 |
| 34 | 42.54% | 41.37% | 41.22% | 42.59% | 41.95% | 41.83% | 42.28% | 47.12 | 19.76 | 41.95% | 0.420 | 0.0054 |
| Average | 43.20% | 42.55% | 43.28% | 42.99% | 43.10% | 43.06% | 43.25% | 67.28 | 29.02 | 43.14% | 0.431 | 0.0043 |
| Std. Dev. | | | | | | | | 12.17 | 5.72 | Total Pore Volume | 0.025 | 0.0012 |

**Figure A5.5. Pore Volume Profile For Trial T55R55.**

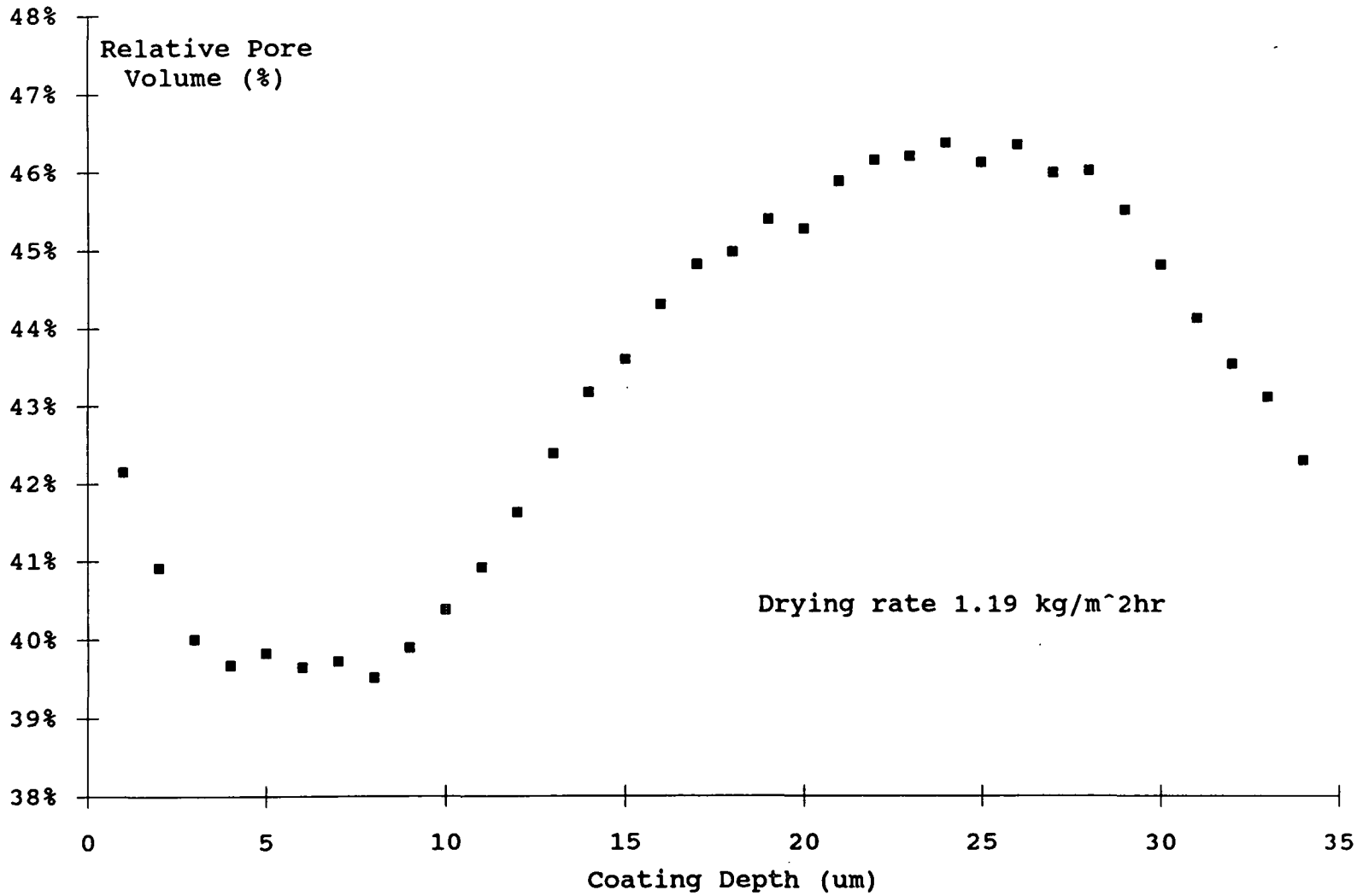

Table A5.6. Pore volume data for coating trial T55R85.

| Depth (microns) | Sheet 1 X1 | Sheet 2 X2 | Sheet 2 X3 | Sheet 4 Y1 | Sheet 3 Y2 | Sheet3 Y3 | Sheet 4 A45 | OVERALL Total Area Analyzed | Total Pore Area | Relative Pore Area | Average Pore Vol. per Sample | Std. Dev |
|---|---|---|---|---|---|---|---|---|---|---|---|---|
| 1 | 41.88% | 42.18% | 41.06% | 41.31% | 42.19% | 41.61% | 41.15% | 47.78 | 19.89 | 41.63% | 0.416 | 0.0047 |
| 2 | 40.92% | 41.16% | 40.46% | 40.58% | 40.47% | 40.63% | 40.08% | 57.63 | 23.40 | 40.60% | 0.406 | 0.0035 |
| 3 | 40.14% | 40.57% | 40.52% | 39.65% | 40.15% | 40.37% | 39.64% | 60.72 | 24.39 | 40.17% | 0.401 | 0.0038 |
| 4 | 39.82% | 40.27% | 39.75% | 39.37% | 40.29% | 39.88% | 39.25% | 60.33 | 24.00 | 39.78% | 0.398 | 0.0040 |
| 5 | 39.43% | 40.19% | 39.20% | 39.24% | 38.86% | 39.38% | 38.95% | 64.99 | 25.52 | 39.28% | 0.393 | 0.0044 |
| 6 | 38.74% | 39.88% | 39.46% | 39.51% | 39.17% | 39.50% | 39.41% | 64.29 | 25.30 | 39.35% | 0.394 | 0.0035 |
| 7 | 39.83% | 39.61% | 39.42% | 39.47% | 39.33% | 39.57% | 38.24% | 77.74 | 30.58 | 39.33% | 0.394 | 0.0052 |
| 8 | 39.85% | 39.70% | 39.68% | 39.52% | 40.30% | 39.22% | 39.15% | 79.75 | 31.61 | 39.64% | 0.396 | 0.0039 |
| 9 | 39.77% | 40.08% | 39.84% | 38.33% | 40.10% | 40.00% | 39.84% | 71.86 | 28.50 | 39.66% | 0.397 | 0.0062 |
| 10 | 40.18% | 40.59% | 39.90% | 39.80% | 40.58% | 40.56% | 40.08% | 70.12 | 28.22 | 40.25% | 0.402 | 0.0034 |
| 11 | 40.69% | 40.99% | 40.60% | 40.32% | 41.45% | 41.13% | 40.15% | 63.76 | 25.98 | 40.74% | 0.408 | 0.0046 |
| 12 | 41.02% | 41.56% | 40.88% | 40.67% | 41.57% | 40.94% | 40.55% | 59.38 | 24.34 | 40.99% | 0.410 | 0.0040 |
| 13 | 41.33% | 41.82% | 41.23% | 40.80% | 40.82% | 41.65% | 40.97% | 70.12 | 28.86 | 41.15% | 0.412 | 0.0040 |
| 14 | 41.68% | 42.19% | 41.44% | 41.03% | 41.70% | 42.06% | 41.25% | 71.41 | 29.68 | 41.57% | 0.416 | 0.0042 |
| 15 | 42.32% | 42.67% | 41.79% | 41.56% | 41.57% | 42.28% | 41.66% | 66.66 | 27.97 | 41.96% | 0.420 | 0.0044 |
| 16 | 42.86% | 42.66% | 42.46% | 41.87% | 42.47% | 42.01% | 42.29% | 71.58 | 30.34 | 42.39% | 0.424 | 0.0035 |
| 17 | 43.11% | 42.69% | 43.28% | 41.93% | 43.48% | 43.01% | 42.37% | 65.24 | 27.98 | 42.88% | 0.428 | 0.0055 |
| 18 | 43.61% | 43.50% | 43.09% | 42.28% | 43.10% | 42.82% | 43.67% | 67.09 | 28.91 | 43.09% | 0.432 | 0.0050 |
| 19 | 43.76% | 44.11% | 43.77% | 43.15% | 43.78% | 43.55% | 43.98% | 61.45 | 26.82 | 43.65% | 0.437 | 0.0031 |
| 20 | 44.19% | 44.54% | 43.86% | 43.78% | 44.55% | 43.95% | 44.08% | 63.71 | 28.11 | 44.12% | 0.441 | 0.0031 |
| 21 | 44.62% | 44.96% | 43.97% | 44.11% | 44.12% | 44.83% | 44.67% | 65.43 | 29.07 | 44.43% | 0.445 | 0.0040 |
| 22 | 44.93% | 45.18% | 44.23% | 44.42% | 44.94% | 45.23% | 45.03% | 63.55 | 28.50 | 44.84% | 0.449 | 0.0038 |
| 23 | 45.40% | 45.23% | 44.71% | 44.80% | 44.66% | 45.48% | 45.30% | 59.81 | 26.98 | 45.11% | 0.451 | 0.0035 |
| 24 | 45.43% | 46.08% | 45.23% | 44.97% | 44.90% | 45.51% | 45.55% | 64.65 | 29.34 | 45.38% | 0.454 | 0.0040 |
| 25 | 45.69% | 45.97% | 45.21% | 45.16% | 45.98% | 46.07% | 45.87% | 64.45 | 29.46 | 45.71% | 0.457 | 0.0038 |
| 26 | 45.78% | 46.08% | 45.55% | 45.35% | 45.56% | 46.32% | 46.13% | 67.41 | 30.90 | 45.84% | 0.458 | 0.0036 |
| 27 | 45.92% | 45.62% | 45.50% | 45.27% | 45.35% | 46.24% | 45.65% | 74.48 | 34.03 | 45.69% | 0.457 | 0.0034 |
| 28 | 44.93% | 45.73% | 45.23% | 45.97% | 45.48% | 45.80% | 45.32% | 83.71 | 38.08 | 45.49% | 0.455 | 0.0036 |
| 29 | 45.22% | 44.44% | 44.79% | 45.11% | 45.25% | 45.38% | 45.09% | 73.88 | 33.32 | 45.09% | 0.450 | 0.0032 |
| 30 | 44.53% | 44.30% | 43.95% | 44.01% | 44.77% | 44.60% | 44.11% | 67.84 | 30.07 | 44.32% | 0.443 | 0.0032 |
| 31 | 44.14% | 43.95% | 44.00% | 43.38% | 43.53% | 43.27% | 43.67% | 62.32 | 27.22 | 43.67% | 0.437 | 0.0033 |
| 32 | 42.88% | 43.70% | 43.25% | 42.96% | 43.20% | 44.34% | 42.85% | 57.50 | 24.93 | 43.36% | 0.433 | 0.0054 |
| 33 | 42.17% | 42.93% | 42.42% | 42.10% | 43.12% | 43.15% | 42.62% | 53.75 | 22.91 | 42.62% | 0.426 | 0.0044 |
| 34 | 41.86% | 42.54% | 41.71% | 41.35% | 42.52% | 42.51% | 41.98% | 45.96 | 19.31 | 42.02% | 0.421 | 0.0047 |
| Average | 42.61% | 42.87% | 42.40% | 42.15% | 42.63% | 42.73% | 42.37% | 65.30 | 27.78 | 42.52% | 0.425 | 0.0040 |
| Std. Dev | | | | | | | | 8.02 | 3.79 | Total Pore Volume | 0.022 | 0.0008 |

**Figure A5.6. Pore Volume Profile For Trial T55R85.**

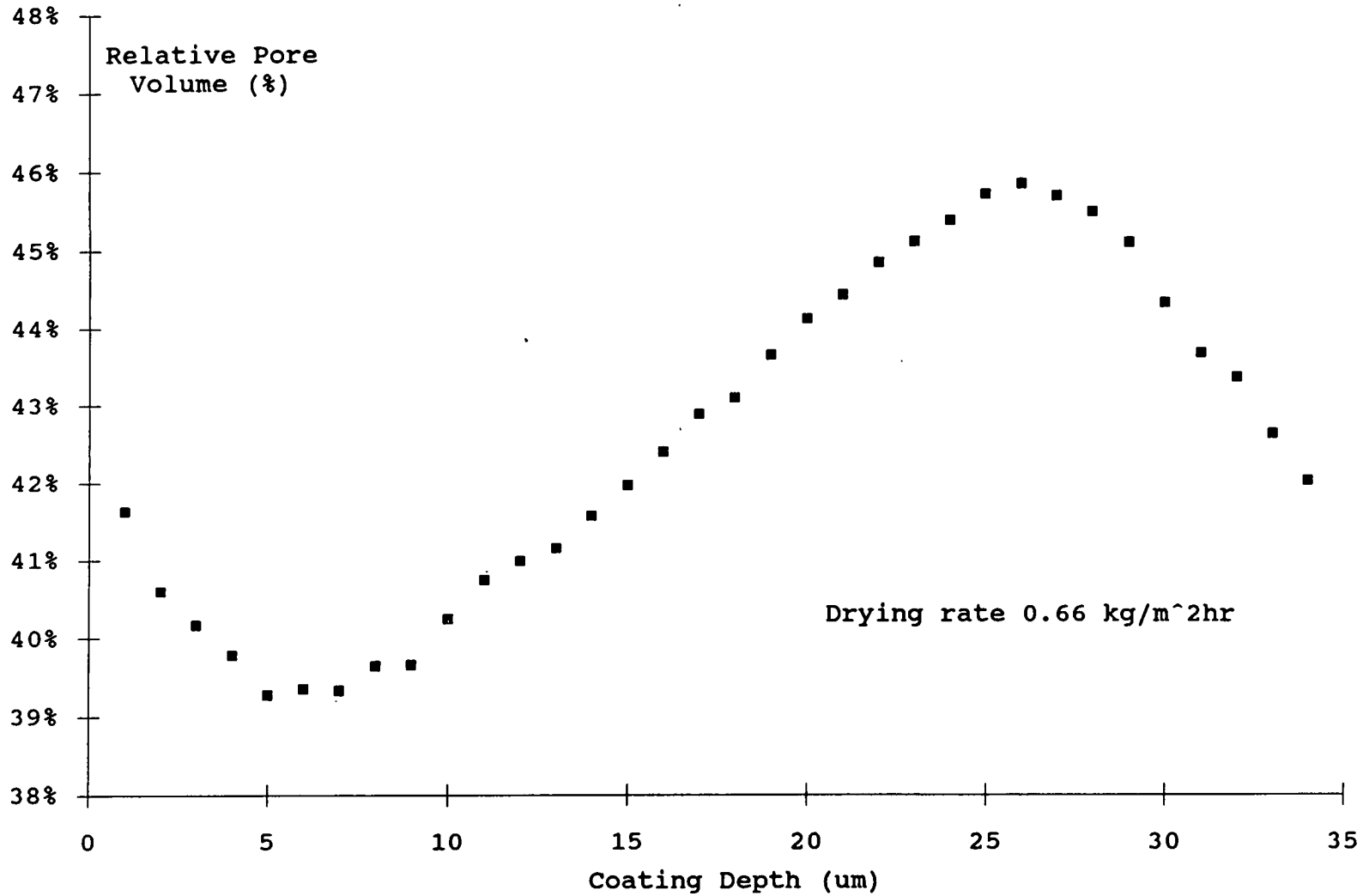

Table A5.7. Pore volume data for coating trial T75R15.

| Depth (microns) | Sheet 1 X1 | Sheet 2 X2 | Sheet 2 X3 | Sheet 1 Y1 | Sheet 1 Y2 | Sheet 4 Y3 | Sheet 3 A45 | OVERALL Total Area Analyzed | Total Pore Area | Relative Pore Volume | Average Pore Vol. per sample | Stdev. |
|---|---|---|---|---|---|---|---|---|---|---|---|---|
| 1 | 42.04% | 42.55% | 42.08% | 42.14% | 41.90% | 42.34% | 42.14% | 51.85 | 21.87 | 42.18% | 0.422 | 0.0021 |
| 2 | 41.45% | 41.20% | 41.17% | 41.30% | 41.15% | 41.63% | 41.74% | 60.71 | 25.12 | 41.37% | 0.414 | 0.0024 |
| 3 | 39.88% | 40.44% | 39.98% | 39.86% | 40.01% | 40.17% | 40.14% | 67.45 | 27.03 | 40.07% | 0.401 | 0.0020 |
| 4 | 40.18% | 38.32% | 39.73% | 40.28% | 39.27% | 39.75% | 38.59% | 71.48 | 28.22 | 39.48% | 0.394 | 0.0076 |
| 5 | 39.22% | 38.70% | 39.21% | 39.10% | 38.89% | 39.40% | 39.16% | 74.19 | 29.01 | 39.10% | 0.391 | 0.0023 |
| 6 | 38.95% | 38.79% | 38.90% | 38.88% | 39.05% | 38.32% | 39.22% | 73.14 | 28.44 | 38.89% | 0.389 | 0.0028 |
| 7 | 39.37% | 40.25% | 40.05% | 40.35% | 40.00% | 39.98% | 40.26% | 76.04 | 30.44 | 40.04% | 0.400 | 0.0033 |
| 8 | 40.72% | 40.51% | 41.14% | 40.82% | 40.83% | 41.05% | 41.12% | 75.43 | 30.83 | 40.88% | 0.409 | 0.0023 |
| 9 | 40.38% | 41.22% | 41.69% | 41.32% | 40.98% | 41.39% | 41.51% | 79.16 | 32.59 | 41.16% | 0.412 | 0.0043 |
| 10 | 41.18% | 41.44% | 41.67% | 41.54% | 41.27% | 41.60% | 41.89% | 71.00 | 29.46 | 41.50% | 0.415 | 0.0024 |
| 11 | 41.86% | 42.33% | 43.15% | 41.96% | 42.44% | 42.92% | 43.21% | 74.30 | 31.60 | 42.54% | 0.426 | 0.0055 |
| 12 | 42.58% | 43.19% | 43.69% | 43.56% | 42.99% | 43.14% | 43.86% | 65.19 | 28.19 | 43.24% | 0.433 | 0.0044 |
| 13 | 43.90% | 43.46% | 44.17% | 43.57% | 43.78% | 43.80% | 44.24% | 66.59 | 29.17 | 43.81% | 0.438 | 0.0029 |
| 14 | 44.20% | 44.12% | 45.15% | 44.23% | 44.51% | 44.73% | 44.51% | 71.37 | 31.76 | 44.50% | 0.445 | 0.0036 |
| 15 | 45.30% | 45.18% | 45.22% | 45.41% | 45.02% | 45.38% | 45.73% | 76.39 | 34.61 | 45.30% | 0.453 | 0.0022 |
| 16 | 45.01% | 45.83% | 45.74% | 45.94% | 45.62% | 45.67% | 46.15% | 73.86 | 33.76 | 45.70% | 0.457 | 0.0036 |
| 17 | 45.53% | 46.11% | 46.25% | 46.12% | 45.93% | 46.28% | 46.25% | 71.05 | 32.72 | 46.05% | 0.461 | 0.0027 |
| 18 | 45.95% | 46.23% | 46.98% | 46.06% | 46.51% | 47.02% | 46.27% | 67.81 | 31.49 | 46.43% | 0.464 | 0.0042 |
| 19 | 46.74% | 47.06% | 47.19% | 47.05% | 46.85% | 46.93% | 47.26% | 68.35 | 32.12 | 46.99% | 0.470 | 0.0018 |
| 20 | 47.07% | 47.45% | 47.29% | 47.56% | 47.67% | 47.45% | 48.00% | 65.39 | 31.03 | 47.46% | 0.475 | 0.0029 |
| 21 | 47.44% | 47.23% | 48.07% | 47.35% | 47.68% | 47.26% | 47.57% | 66.27 | 31.48 | 47.50% | 0.475 | 0.0029 |
| 22 | 46.85% | 47.63% | 47.72% | 46.97% | 47.14% | 47.71% | 48.04% | 66.65 | 31.59 | 47.40% | 0.474 | 0.0045 |
| 23 | 47.26% | 47.21% | 47.37% | 47.33% | 47.39% | 47.34% | 47.44% | 72.50 | 34.31 | 47.33% | 0.473 | 0.0008 |
| 24 | 47.44% | 47.78% | 47.76% | 47.62% | 47.15% | 47.28% | 47.95% | 74.37 | 35.38 | 47.57% | 0.476 | 0.0029 |
| 25 | 47.48% | 47.23% | 47.53% | 47.60% | 46.92% | 47.23% | 47.60% | 75.57 | 35.79 | 47.36% | 0.474 | 0.0025 |
| 26 | 47.05% | 47.38% | 47.27% | 47.13% | 47.06% | 47.01% | 47.38% | 75.11 | 35.44 | 47.19% | 0.472 | 0.0016 |
| 27 | 47.14% | 47.13% | 47.18% | 47.25% | 47.41% | 46.93% | 47.58% | 74.83 | 35.35 | 47.23% | 0.472 | 0.0021 |
| 28 | 46.71% | 47.37% | 47.05% | 47.49% | 47.02% | 47.17% | 47.71% | 76.07 | 35.91 | 47.21% | 0.472 | 0.0033 |
| 29 | 46.48% | 46.54% | 47.08% | 46.60% | 46.90% | 47.00% | 47.23% | 74.06 | 34.70 | 46.85% | 0.468 | 0.0029 |
| 30 | 45.64% | 45.66% | 46.21% | 45.77% | 45.72% | 46.03% | 45.96% | 74.51 | 34.17 | 45.86% | 0.459 | 0.0022 |
| 31 | 44.51% | 45.22% | 45.09% | 44.95% | 45.02% | 45.59% | 45.91% | 72.58 | 32.79 | 45.17% | 0.452 | 0.0046 |
| 32 | 43.96% | 44.04% | 44.40% | 44.07% | 44.27% | 44.02% | 44.58% | 66.60 | 29.43 | 44.19% | 0.442 | 0.0023 |
| 33 | 42.71% | 43.48% | 43.39% | 43.26% | 43.56% | 42.98% | 43.78% | 66.78 | 28.90 | 43.28% | 0.433 | 0.0036 |
| 34 | 42.41% | 42.01% | 43.09% | 42.12% | 42.79% | 42.06% | 42.35% | 60.90 | 25.83 | 42.41% | 0.424 | 0.0040 |
| 35 | 41.59% | 42.20% | 42.23% | 42.31% | 41.60% | 41.60% | 42.29% | 51.44 | 21.59 | 41.96% | 0.420 | 0.0036 |
| Average | 43.85% | 44.17% | 44.39% | 44.26% | 44.14% | 44.26% | 44.24% | 69.97 | 30.92 | 44.19% | 0.442 | 0.0031 |
| Stdev | | | | | | | | 6.43 | 3.68 | Total Pore Volume | 0.029 | 0.0013 |

**Figure A5.7. Pore Volume Profile For Trial T75R15.**

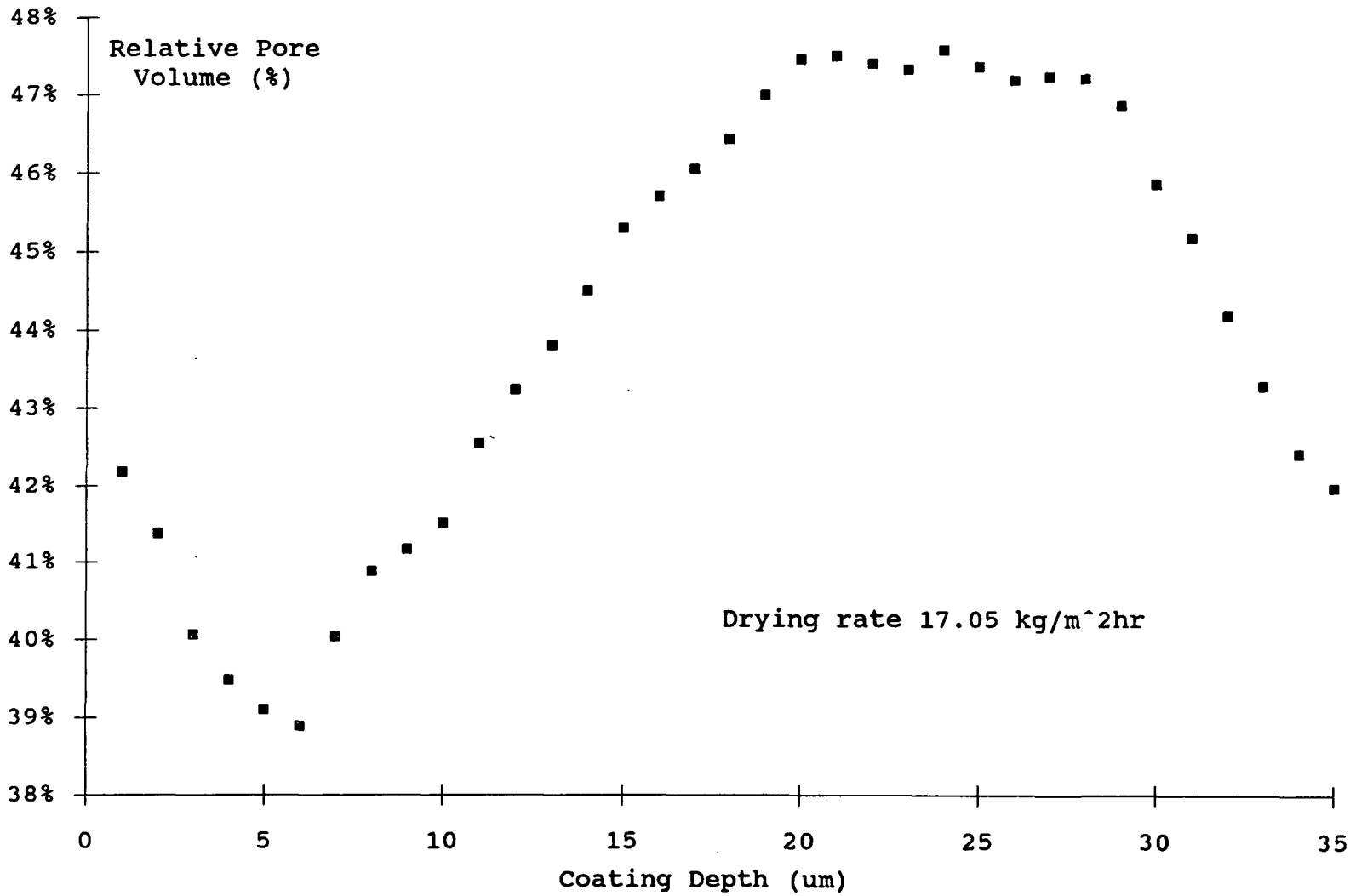

Table A5.8. Pore volume data for coating trial T75R85.

| Depth (microns) | Sheet 3 X1 | Sheet 3 X2 | Sheet 1 Y1 | Sheet 2 Y2 | Sheet 4 Y3 | Sheet 3 A45 | Sheet 4 B45 | OVERALL Total Area Analyzed | Total Pore Area | Relative Pore Area | Average Pore Vol. per Sample | Std. Dev. |
|---|---|---|---|---|---|---|---|---|---|---|---|---|
| 1 | 41.80% | 40.96% | 41.52% | 40.00% | 41.59% | 40.86% | 40.98% | 52.99 | 21.78 | 41.10% | 0.411 | 0.0061 |
| 2 | 41.10% | 40.45% | 40.39% | 40.43% | 40.77% | 40.35% | 40.96% | 65.33 | 26.57 | 40.68% | 0.406 | 0.0030 |
| 3 | 40.15% | 40.19% | 39.94% | 39.34% | 40.59% | 40.49% | 39.97% | 71.02 | 28.47 | 40.09% | 0.401 | 0.0041 |
| 4 | 39.81% | 39.63% | 39.66% | 39.12% | 40.42% | 39.56% | 39.58% | 74.46 | 29.56 | 39.70% | 0.397 | 0.0039 |
| 5 | 39.10% | 39.34% | 39.62% | 39.73% | 39.96% | 39.17% | 39.45% | 77.68 | 30.67 | 39.49% | 0.395 | 0.0031 |
| 6 | 39.64% | 39.37% | 39.51% | 39.02% | 39.15% | 38.84% | 39.72% | 83.00 | 32.67 | 39.36% | 0.393 | 0.0033 |
| 7 | 39.66% | 39.39% | 39.44% | 38.60% | 38.79% | 38.69% | 39.12% | 81.65 | 31.93 | 39.10% | 0.391 | 0.0041 |
| 8 | 39.78% | 39.53% | 39.38% | 39.74% | 38.83% | 39.68% | 39.52% | 87.02 | 34.34 | 39.46% | 0.395 | 0.0032 |
| 9 | 39.73% | 40.39% | 39.00% | 39.85% | 39.23% | 39.09% | 39.38% | 81.58 | 32.25 | 39.53% | 0.395 | 0.0050 |
| 10 | 40.32% | 40.09% | 39.82% | 39.05% | 39.37% | 39.99% | 39.71% | 74.87 | 29.77 | 39.76% | 0.398 | 0.0044 |
| 11 | 40.71% | 40.42% | 40.90% | 39.92% | 39.57% | 40.32% | 40.36% | 69.09 | 27.85 | 40.32% | 0.403 | 0.0045 |
| 12 | 41.01% | 40.72% | 40.61% | 40.21% | 40.36% | 40.91% | 40.58% | 62.41 | 25.36 | 40.63% | 0.406 | 0.0028 |
| 13 | 41.27% | 41.10% | 40.82% | 40.83% | 40.43% | 40.33% | 40.86% | 65.89 | 26.89 | 40.82% | 0.408 | 0.0034 |
| 14 | 41.64% | 41.45% | 41.35% | 41.53% | 40.21% | 41.25% | 41.34% | 67.19 | 27.72 | 41.25% | 0.413 | 0.0048 |
| 15 | 42.20% | 41.88% | 41.88% | 42.23% | 40.89% | 42.12% | 41.93% | 66.66 | 27.91 | 41.87% | 0.419 | 0.0046 |
| 16 | 42.71% | 42.37% | 42.06% | 42.64% | 41.93% | 42.57% | 42.90% | 65.14 | 27.66 | 42.46% | 0.425 | 0.0035 |
| 17 | 43.13% | 42.71% | 42.67% | 42.90% | 42.27% | 42.16% | 43.24% | 78.00 | 33.32 | 42.72% | 0.427 | 0.0041 |
| 18 | 43.44% | 43.13% | 43.06% | 42.81% | 43.82% | 43.33% | 43.67% | 80.86 | 35.05 | 43.34% | 0.433 | 0.0035 |
| 19 | 43.73% | 43.07% | 43.74% | 43.32% | 43.71% | 43.50% | 44.01% | 82.19 | 35.82 | 43.58% | 0.436 | 0.0031 |
| 20 | 44.16% | 43.85% | 43.81% | 44.38% | 43.78% | 43.74% | 44.53% | 82.21 | 36.21 | 44.05% | 0.440 | 0.0032 |
| 21 | 44.56% | 44.18% | 44.61% | 44.26% | 44.58% | 44.07% | 45.11% | 75.34 | 33.51 | 44.49% | 0.445 | 0.0035 |
| 22 | 44.90% | 44.63% | 44.35% | 44.68% | 44.14% | 44.79% | 45.13% | 72.71 | 32.47 | 44.65% | 0.447 | 0.0033 |
| 23 | 45.32% | 44.95% | 44.66% | 44.92% | 44.65% | 44.80% | 45.47% | 72.52 | 32.62 | 44.98% | 0.450 | 0.0032 |
| 24 | 45.41% | 45.15% | 45.02% | 45.43% | 45.03% | 44.91% | 45.95% | 69.21 | 31.33 | 45.27% | 0.453 | 0.0036 |
| 25 | 45.70% | 45.31% | 45.31% | 44.92% | 45.18% | 44.81% | 45.76% | 72.18 | 32.68 | 45.28% | 0.453 | 0.0036 |
| 26 | 45.80% | 45.54% | 45.11% | 44.67% | 45.01% | 45.56% | 45.76% | 75.55 | 34.24 | 45.32% | 0.454 | 0.0043 |
| 27 | 45.61% | 45.33% | 45.67% | 44.53% | 45.38% | 45.27% | 45.81% | 79.49 | 36.02 | 45.31% | 0.454 | 0.0042 |
| 28 | 45.17% | 44.90% | 45.56% | 45.29% | 45.47% | 45.15% | 45.82% | 77.89 | 35.31 | 45.33% | 0.453 | 0.0030 |
| 29 | 44.97% | 44.62% | 45.13% | 44.95% | 45.32% | 44.75% | 45.50% | 78.36 | 35.29 | 45.03% | 0.450 | 0.0031 |
| 30 | 44.61% | 44.49% | 44.85% | 44.69% | 44.04% | 44.38% | 45.15% | 75.41 | 33.63 | 44.59% | 0.446 | 0.0035 |
| 31 | 43.91% | 43.93% | 44.09% | 44.28% | 44.08% | 43.57% | 44.59% | 71.82 | 31.65 | 44.07% | 0.441 | 0.0032 |
| 32 | 43.20% | 43.39% | 43.39% | 43.77% | 44.00% | 42.81% | 43.47% | 66.74 | 28.98 | 43.43% | 0.434 | 0.0038 |
| 33 | 42.32% | 42.85% | 42.17% | 43.29% | 43.47% | 42.15% | 42.74% | 62.41 | 26.66 | 42.72% | 0.427 | 0.0053 |
| 34 | 41.91% | 42.06% | 41.52% | 42.45% | 43.03% | 41.67% | 42.06% | 59.61 | 25.11 | 42.12% | 0.421 | 0.0051 |
| Average | 42.60% | 42.39% | 42.37% | 42.29% | 42.32% | 42.23% | 42.65% | 72.90 | 30.92 | 42.42% | 0.424 | 0.0038 |
| Std. Dev. | | | | | | | | 7.72 | 3.67 | Total Pore Volume | 0.022 | 0.0008 |

**Figure A5.8. Pore Volume Profile For Trial T75R85.**